USGS
science for a changing world

Prepared in cooperation with the
U.S. Department of Energy
Office of Environmental Management, National Nuclear Security Administration, Nevada Site Office,
under Interagency Agreement DE-AI52-01NV13944, and
Office of Repository Development,
under Interagency Agreement DE-AI08-02RW12167

Death Valley Regional Ground-Water Flow System, Nevada and California—Hydrogeologic Framework and Transient Ground-Water Flow Model

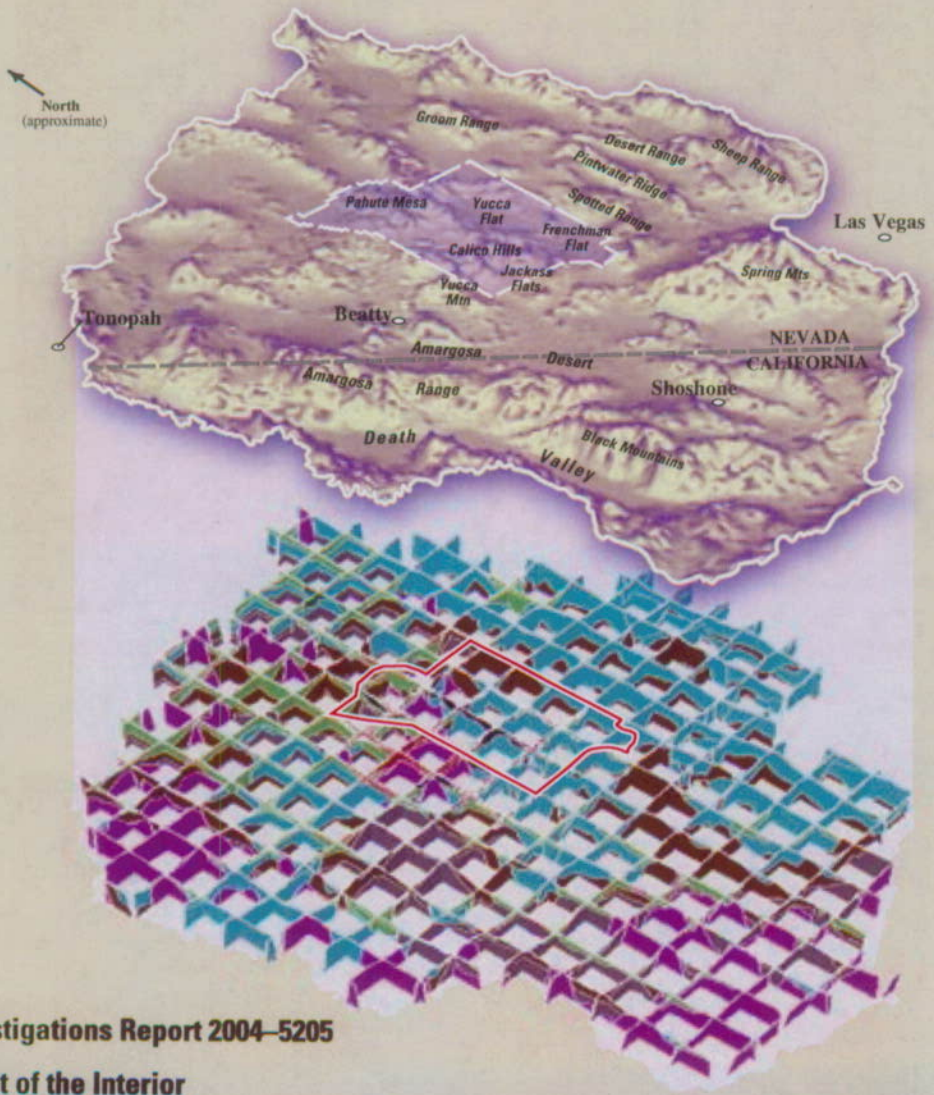

Scientific Investigations Report 2004–5205

U.S. Department of the Interior
U.S. Geological Survey

125 years of science for America ★ ★ ★ ★ ★ *1879–2004*

Death Valley Regional Ground-Water Flow System, Nevada and California—Hydrogeologic Framework and Transient Ground-Water Flow Model

Edited by Wayne R. Belcher

Prepared in cooperation with the
U.S. Department of Energy
Office of Environmental Management, National Nuclear Security Administration, Nevada Site Office,
under Interagency Agreement DE–AI52–01NV13944, and
Office of Repository Development,
under Interagency Agreement DE–AI08–02RW12167

Scientific Investigations Report 2004–5205

U.S. Department of the Interior
U.S. Geological Survey

U.S. Department of the Interior
Gale A. Norton, Secretary

U.S. Geological Survey
Charles G. Groat, Director

U.S. Geological Survey, Reston, Virginia: 2004

For more information about the USGS and its products:
Telephone: 1-888-ASK-USGS
World Wide Web: http://www.usgs.gov/

This report and any updates to it are available online at:
http://pubs.water.usgs.gov/sir2004-5205/

Suggested citation:
Belcher, W.R., ed., 2004, Death Valley regional ground-water flow system, Nevada and California—Hydrogeologic framework and transient ground-water flow model: U.S. Geological Survey Scientific Investigations Report 2004–5205, 408 p.

Acknowledgments

The Death Valley regional ground-water flow system project would not have been possible without the financial support of the U.S. Department of Energy–National Nuclear Security Administration–Nevada Site Office and the U.S. Department of Energy–Office of Civilian Radioactive Waste Management–Office of Repository Development. Funding to develop a model for their specific uses made possible the development of a tool that can be used to assess regional water-resource issues. Many other agencies also contributed financially to this work, including Nye County in Nevada, Inyo County in California, the National Park Service, the U.S. Fish and Wildlife Service, and the U.S. Air Force.

The authors would like to acknowledge the support and encouragement of Robert W. Craig, U.S. Geological Survey (USGS), Las Vegas, Yucca Mountain Project Branch, Technical Program Officer; and Bonnie K. Thompson (USGS, Las Vegas), National Nuclear Security Administration Program Manager. We also would like to thank Kelly L. Ashton-Reis (USGS, Las Vegas) for her tireless support and cheerful demeanor as the project assistant, and Joyce L. (Golos) Lum (USGS, Las Vegas) for aid, encouragement, and financial management. Douglas A. Trudeau (USGS, Tampa) helped to initiate and launch the project, and Devin L. Galloway (USGS, Sacramento) provided interim leadership and technical guidance.

As the editor, I have not worked with a finer team——the authors, supporting scientists, technical staff, and publications staff. Over the many years of this project, the efforts of many people have contributed to this final report. The teamwork of authors, scientists, and technical staff from many disciplines; 20 report reviewers, including Chester Zenone with a final review; and the publications staff has enabled the completion of this final report on the Death Valley regional ground-water flow system. A few lines from Tennyson's "Ulysses" express my deep gratitude for the hard work and dedication of all of the people involved over the years of this project:

> Tho' much is taken, much abides; and tho'
> We are not now that strength which in the old days
> Moved earth and heaven; that which we are, we are;
> One equal-temper of heroic hearts,
> Made weak by time and fate, but strong in will
> To strive, to seek, to find, and not to yield.

Contents

Plates

Conversion Factors, Datums, and Abbreviations

Multiply	By	To obtain
millimeter (mm)	0.03937	inch
meter (m)	3.281	foot
kilometer (km)	0.6214	mile
square kilometer (km^2)	0.3861	square mile
cubic meter (m^3)	35.31	cubic foot
million cubic meters (Mm^3)	35.31	million cubic feet
meter per day (m/d)	3.281	foot per day
millimeter per year (mm/yr)	0.03937	inch per year
meter per year (m/yr)	3.281	foot per year
meter squared per day (m^2/d)	10.76	square foot per day
cubic meter per day (m^3/d)	35.31	cubic foot per day
cubic meter per day (m^3/d)	264.2	gallon per day
cubic meter per year (m^3/yr)	35.31	cubic foot per year
meter per day per meter (m/d/m)	1	foot per day per foot

Temperature in degrees Celsius (°C) may be converted to degrees Fahrenheit (°F) as follows:

$$°F = (1.8 \times °C) + 32$$

Vertical coordinate information is referenced to the North American Vertical Datum of 1988 (NAVD 88). Horizontal coordinate information is referenced to the North American Datum of 1927 (NAD 27). Altitude, as used in this report, refers to distance above the vertical datum.

Abbreviations and Acronyms

2D	Two-dimensional
3D	Three-dimensional
AA	Alluvial aquifer
ACU	Alluvial confining unit
BRU	Belted Range unit
CAU	Corrective Action Unit
CFBCU	Crater Flat–Bullfrog confining unit
CFPPA	Crater Flat–Prow Pass aquifer
CFTA	Crater Flat–Tram aquifer
CHVU	Calico Hills volcanic-rock unit
CSS	Composite scaled sensitivity
CV	Coefficient of variation
DEM	Digital elevation model
DOE	U.S. Department of Energy
DOE/NV	U.S. Department of Energy, Nevada Operations Office
DRN	Drain
DSS	Dimensionless scaled sensitivity
DVRFS	Death Valley regional ground-water flow system
ECU	Eleana confining unit
EM	Office of Environmental Management
ERD	Environmental Restoration Division

ET	Evapotranspiration
EWDP	Early Warning Drilling Program
FWS	U.S. Fish and Wildlife Service
Ga	Giga-annum (billion years ago)
GFM	Geologic framework model
GIS	Geographic information system
GPS	Global positioning system
GWSI	Ground-Water Site Inventory
HFB	Horizontal flow barrier
HFM	Hydrogeologic framework model
HG	Hydrograph
HGU	Hydrogeologic unit
HRMP	Hydrologic Resource Management Program
HUF	Hydrogeologic-unit flow
ICU	Intrusive-rock confining unit
K	Hydraulic conductivity
ka	Thousand years ago
K-Ar	Potassium-argon
LA	Limestone aquifer
LCA	Lower carbonate-rock aquifer
LCA_T1	Lower carbonate-rock thrust
LCCU	Lower clastic-rock confining unit
LCCU_T1	Lower clastic-rock confining unit thrust
LFU	Lava-flow unit
LOTR	Line of transient regression
LVVSZ	Las Vegas Valley shear zone
LVVWD	Las Vegas Valley Water District
Ma	Mega-annum (million years ago)
MNW	Multi-node well
Mvs	Mesozoic volcanics and sedimentary rock unit
NAD 27	North American Datum of 1927
NAVD 88	North American Vertical Datum of 1988
NDWR	Nevada Division of Water Resources
NNSA	National Nuclear Security Administration
Nobs	Number of observations
NPS	National Park Service
NSO	Nevada Site Office
NTS	Nevada Test Site
NWIS	National Water Information System
OAA	Older alluvial aquifer
OACU	Older alluvial confining unit
OCRWM	Office of Civilian Radioactive Waste Management
ORD	Office of Repository Development
OVU	Older volcanic-rock unit
P1	Lower clastic confining unit

P2	Regional carbonate aquifer
PCC	Parameter correlation coefficient
PMOV	Pahute Mesa–Oasis Valley
PVA	Paintbrush volcanic-rock aquifer
SCCC	Silent Canyon caldera complex
SCU	Sedimentary-rock confining unit
sd	Standard deviation
SOSWR	Sum of squared weighted residuals
SWNVF	Southwestern Nevada volcanic field
TBA	Belted Range aquifer
TBCU	Basal confining unit
TBQ	Basal aquifer
TC	Paintbrush/Calico Hills tuff cone unit
TCB	Bullfrog confining unit
TMA	Timber Mountain aquifer
TMCC	Timber Mountain caldera complex
TMVA	Thirsty Canyon–Timber Mountain volcanic-rock aquifer
TSDVS	Tertiary sediments–Death Valley sediments
Tv	Tertiary volcanic-rock unit
UCA	Upper carbonate-rock aquifer
UCCU	Upper clastic-rock confining unit
UGTA	Underground Test Area
USGS	U.S. Geological Survey
UTM	Universal Transverse Mercator
VA	Volcanic-rock aquifer
VCU	Volcanic-rock confining unit
VSU	Volcanic- and sedimentary-rock unit
VU	Volcanic rocks undifferentiated
WVU	Wahmonie volcanic-rock confining unit
XCU	Crystalline-rock confining unit
YAA	Younger alluvial aquifer
YACU	Younger alluvial confining unit
YMP	Yucca Mountain Project
YVU	Younger volcanic-rock unit

Death Valley Regional Ground-Water Flow System, Nevada and California—Hydrogeologic Framework and Transient Ground-Water Flow Model

Edited by Wayne R. Belcher

Abstract

A numerical three-dimensional (3D) transient ground-water flow model of the Death Valley region was developed by the U.S. Geological Survey for the U.S. Department of Energy programs at the Nevada Test Site and at Yucca Mountain, Nevada. Decades of study of aspects of the ground-water flow system and previous less extensive ground-water flow models were incorporated and reevaluated together with new data to provide greater detail for the complex, digital model.

A 3D digital hydrogeologic framework model (HFM) was developed from digital elevation models, geologic maps, borehole information, geologic and hydrogeologic cross sections, and other 3D models to represent the geometry of the hydrogeologic units (HGUs). Structural features, such as faults and fractures, that affect ground-water flow also were added. The HFM represents Precambrian and Paleozoic crystalline and sedimentary rocks, Mesozoic sedimentary rocks, Mesozoic to Cenozoic intrusive rocks, Cenozoic volcanic tuffs and lavas, and late Cenozoic sedimentary deposits of the Death Valley regional ground-water flow system (DVRFS) region in 27 HGUs.

Information from a series of investigations was compiled to conceptualize and quantify hydrologic components of the ground-water flow system within the DVRFS model domain and to provide hydraulic-property and head-observation data used in the calibration of the transient-flow model. These studies reevaluated natural ground-water discharge occurring through evapotranspiration (ET) and spring flow; the history of ground-water pumping from 1913 through 1998; ground-water recharge simulated as net infiltration; model boundary inflows and outflows based on regional hydraulic gradients and water budgets of surrounding areas; hydraulic conductivity and its relation to depth; and water levels appropriate for regional simulation of prepumped and pumped conditions within the DVRFS model domain. Simulation results appropriate for the regional extent and scale of the model were provided by acquiring additional data, by reevaluating existing data using current technology and concepts, and by refining earlier interpretations to reflect the current understanding of the regional ground-water flow system.

Ground-water flow in the Death Valley region is composed of several interconnected, complex ground-water flow systems. Ground-water flow occurs in three subregions in relatively shallow and localized flow paths that are superimposed on deeper, regional flow paths. Regional ground-water flow is predominantly through a thick Paleozoic carbonate rock sequence affected by complex geologic structures from regional faulting and fracturing that can enhance or impede flow. Spring flow and ET are the dominant natural ground-water discharge processes. Ground water also is withdrawn for agricultural, commercial, and domestic uses.

Ground-water flow in the DVRFS was simulated using MODFLOW-2000, a 3D finite-difference modular ground-water flow modeling code that incorporates a nonlinear least-squares regression technique to estimate aquifer parameters. The DVRFS model has 16 layers of defined thickness, a finite-difference grid consisting of 194 rows and 160 columns, and uniform cells 1,500 meters (m) on each side.

Prepumping conditions (before 1913) were used as the initial conditions for the transient-state calibration. The model uses annual stress periods with discrete recharge and discharge components. Recharge occurs mostly from infiltration of precipitation and runoff on high mountain ranges and from a small amount of underflow from adjacent basins. Discharge occurs primarily through ET and spring discharge (both simulated as drains) and water withdrawal by pumping and, to a lesser amount, by underflow to adjacent basins, also simulated by drains. All parameter values estimated by the regression are reasonable and within the range of expected values. The simulated hydraulic heads of the final calibrated transient model generally fit observed heads reasonably well (residuals with absolute values less than 10 m) with two exceptions: in most areas of nearly flat hydraulic gradient the fit is considered moderate (residuals with absolute values of 10 to 20 m), and in areas of steep hydraulic gradient, such as Indian Springs, western Yucca Flat, and the southern part of the Bullfrog Hills, the fit is poor (residuals with absolute values greater than 20 m). Ground-water discharge residuals are fairly random, with as many areas where simulated flows are less than observed flows as areas where simulated flows are greater. The highest unweighted ground-water discharge residuals occur at Death

Valley and Ash Meadows. High weighted discharge residuals were computed in the Pahrump Valley, possibly indicating a poor definition of hydraulic properties or discharge estimates in that area.

The model represents the large and complex ground-water flow system of the Death Valley region at a greater degree of refinement and accuracy than has been possible previously. The representation of detail provided by the 3D digital hydrogeologic framework model and the numerical ground-water flow model enabled greater spatial accuracy in every model parameter. The lithostratigraphy and structural effects of the hydrogeologic framework; recharge estimates from simulated net infiltration; discharge estimates from ET, spring flow, and pumping; and boundary inflow and outflow estimates all were reevaluated, some additional data were collected, and accuracy was improved. Uncertainty in the results of the flow model simulations can be reduced by improving on the quality, interpretation, and representation of the water-level observations used to calibrate the model and improving on the representation of the HGU geometries, the spatial variability of HGU material properties, the flow model physical framework, and the hydrologic conditions.

View from Mount Stirling (2,506 m) in the Spring Mountains to the northeast toward the Pintwater, Desert, and Sheep Ranges. The Las Vegas Valley shear zone runs across the middle of the photograph between the Spring Mountains and the mountain ranges to the north. Playas are visible in Indian Springs Valley (toward the west or left side of the photograph) and in Three Lakes Valley (to the east or the right side of the photograph). Indian Springs Air Force Base is visible in the center foreground, at the base of the Pintwater Range. Photograph by Nancy A. Damar, U.S. Geological Survey.

Introduction

By Wayne R. Belcher, Frank A. D'Agnese, and Grady M. O'Brien

Chapter A of

Death Valley Regional Ground-Water Flow System, Nevada and California—Hydrogeologic Framework and Transient Ground-Water Flow Model

Edited by Wayne R. Belcher

Prepared in cooperation with the
U.S. Department of Energy
Office of Environmental Management, National Nuclear Security Administration, Nevada Site Office,
under Interagency Agreement DE–AI52–01NV13944, and
Office of Repository Development,
under Interagency Agreement DE–AI08–02RW12167

Scientific Investigations Report 2004–5205

U.S. Department of the Interior
U.S. Geological Survey

Contents

Figures

CHAPTER A. Introduction

By Wayne R. Belcher, Frank A. D'Agnese, and Grady M. O'Brien

In the early 1990's, two numerical models of the Death Valley regional ground-water flow system (DVRFS) were developed by the U.S. Department of Energy (DOE) to support investigations at the Nevada Test Site (NTS), where nuclear tests were conducted from 1951 to 1992, and at Yucca Mountain, Nev., the proposed geologic repository for high-level radioactive waste and spent nuclear fuel for the U.S. (fig. A–1). The model developed for the National Nuclear Security Administration/Nevada Site Office (NNSA/NSO) Underground Test Area (DOE/NV-UGTA) project of the Office of Environmental Management (EM) is designated the DOE/NV-UGTA model (IT Corporation, 1996a). The second model was developed collaboratively for the Office of Civilian Radioactive Waste Management's (OCRWM) Yucca Mountain Project (YMP) and the NNSA/NSO Hydrologic Resource Management Program (HRMP) and is designated the YMP/HRMP model (D'Agnese and others, 1997).

The DOE/NV-UGTA flow model (IT Corporation, 1996a) was developed by the EM support services contractor, HSI/GeoTrans Inc., using MODFLOW (McDonald and Harbaugh, 1988) to evaluate the transport of radionuclides from underground nuclear weapons test sites on the NTS. The YMP/HRMP model (D'Agnese and others, 1997) was developed by the U.S. Geological Survey (USGS) using MODFLOWP (Hill, 1992) to characterize the regional ground-water flow system with respect to the potential release of radionuclides from the proposed geologic high-level radioactive waste repository at Yucca Mountain.

In general, the two models were based on the same hydrologic data set. However, the models differed somewhat in the details of their particular interpretations of the regional hydrogeology. Firstly, these differences were the result of the fact that the DOE/NV-UGTA model had 20 layers and encompassed areas in, adjacent to, and downgradient from the UGTAs of the NTS, whereas the YMP/HRMP model had only three layers but encompassed much of the DVRFS region. Secondly, differences between the two hydrogeologic frameworks occurred where different data sets were used or data were sparse and the results were highly interpretive. Thirdly, the hydrogeologic units used in each framework differed, especially in the Cenozoic volcanic rocks. Finally, estimates of recharge were highly interpretive and differed significantly for each flow model domain. Together, these differences likely resulted in the different ground-water flow path and flux results from the two models.

In 1998, DOE requested that the USGS begin a 5-year project to develop an improved ground-water flow model of the DVRFS to support NNSA/NSO and YMP programs. This work was done by the U.S. Geological Suvey in cooperation with the U.S. Department of Energy under Interagency Agreements DE–AI52–01NV13944 and DE–AI08–02RW12167. Newly available data and modeling tools were used and the data and results of the previous two regional-scale models were integrated to produce a single regional-scale flow model. During this effort, the USGS cooperated with other Federal, State, and local entities in the region, including the National Park Service (NPS), the Fish and Wildlife Service (FWS), the Bureau of Land Management (BLM), and county governments in Nevada and California, in order to benefit from their expertise. Many of these entities also contributed funds to this project.

Interest in the regional flow system is driven by the need to: (1) understand the ground-water flow paths and travel times associated with potential movement of radioactive material from the NTS; (2) characterize the ground-water system in the vicinity of the proposed high-level radioactive waste repository at Yucca Mountain, Nev. (Hanks and others, 1999); and (3) address a variety of potential effects on users downgradient from the NTS and Yucca Mountain, including the agricultural communities in the Amargosa Desert, the Death Valley National Park, and Native American interests.

The initial objectives of the DVRFS project included the construction and calibration of a steady-state model that represents prepumping conditions for the DVRFS. This model was intended to (1) provide a starting point for calibration of the transient ground-water flow model, (2) characterize regional three-dimensional (3D) ground-water flow paths, (3) define discharge and recharge locations, (4) estimate the magnitude of subsurface flux, and (5) represent the effects of regional geologic structural features on regional flow. The digital 3D hydrogeologic framework model (HFM) and steady-state prepumping numerical flow model are documented, respectively, in Belcher and others (2002) and D'Agnese and others (2002).

The ultimate objective of the DVRFS model project, and the subject of the chapters in this volume, is the construction and calibration of a transient model that simulates the ground-water conditions of the model domain through time. Over the long term, this model is intended to be used to (1) provide the boundary conditions for the site-scale models at Yucca Mountain and the UGTA Corrective Action Units

Abbreviations

AF = Amargosa Farms
AM = Ash Meadows
BB = Busted Butte
BM = Bare Mountain
CF = Crater Flat
DVNP=Death Valley National Park
EM = Eagle Mountain
FC = Fluorspar Canyon
FW = Fortymile Wash
GWR = Greenwater Range
IH = Ibex Hills
JF = Jackass Flats
MM = Mt. Montgomery, Montgomery Mountains
MP = Mormon Point
MQM = Mesquite Mountains
PV = Pahranagat Valley
RSR = Resting Spring Range
RV = Rock Valley
SH/LSM = Striped Hills/ Little Skull Mtn
SPH = Sperry Hills
SR = Specter Range
STV = Stewart Valley
SV = Shadow Valley
YM = Yucca Mountain

50,000-meter grid based on Universal Transverse Mercator projection, Zone 11
Shaded-relief base from 1:250,000-scale Digital Elevation Model; sun illumination from northwest at 30 degrees above horizon

EXPLANATION

- Death Valley regional ground-water flow system model boundary
- Prepumping Death Valley regional ground-water flow system model boundary (D'Agnese and others, 2002)
- Yucca Mountain Project ground-water flow model boundary (D'Agnese and others, 1997)
- Underground Test Area ground-water flow model boundary (IT Corporation, 1996a)
- Nevada Test Site boundary
- Desert boundary
- Populated location

Figure A–1. Geographic and prominent topographic features of the Death Valley regional ground-water flow system region, Nevada and California.

(CAUs) on the NTS, (2) evaluate the impacts of changes in system flux, regardless of whether the changes are natural or human induced, (3) provide a technical basis for decisions on the quantity of water available for defense and economic development activities on the NTS, (4) determine the potential effects of increased offsite water use on NTS water supplies, (5) provide a framework for determining effective source plume, ambient trend, and point-of-use ground-water-quality monitoring locations, and (6) facilitate the development of a cooperative, regional Death Valley ground-water management district.

Purpose and Scope

This report presents the hydrogeology, the conceptual hydrologic model, the hydrologic system inputs and outputs of the DVRFS region, and how this information is used to construct an HFM and a transient numerical ground-water flow model. The ground-water flow model simulates transient conditions from 1913 through 1998 using the modular ground-water flow model, MODFLOW-2000 (Harbaugh and others, 2000), and a simulated steady-state head distribution representing prepumping conditions (the initial conditions of the model). Transient stresses imposed on the regional ground-water flow system include ground-water pumpage that occurred from 1913 through 1998, and flows from springs affected by pumping; simulated areal recharge was held constant at average annual values.

The current understanding of regional ground-water flow in the Great Basin came from the basin studies done under the U.S. Geological Survey and the State of Nevada cooperative ground-water program. Maxey and Eakin (1949) compared recharge and discharge estimates of individual basins and realized that many basins were not closed to ground-water transfer to or from adjacent basins. Eakin (1966) identified a system of interconnected basins of the White River and Muddy River springs area. The water budget imbalances within and between basins was useful in discerning interbasin flow and defining the basins of the Colorado River flow system (formerly the White River flow system) to the east of the DVRFS. The concept of interbasin flow into the Death Valley region was first suggested by Hunt and Robinson (1960).

The DVRFS is a major regional flow system in which ground water flows between recharge areas in the mountains of central and southern Nevada and discharge areas of wet playas and springs, south and west of the NTS and in Death Valley, Calif. (Rush, 1968; Harrill and others, 1988). Ground-water flow in the region is strongly influenced by the complex geologic framework of the DVRFS region. Numerical modeling of the regional ground-water flow system must incorporate the 3D distribution of the principal aquifers and confining units, as well as the principal geologic structures that may affect subsurface flow.

The scope of this study can be summarized as follows:

1. The study is limited to the DVRFS region, specified as the model domain (fig. A–1).

2. The details of the hydrogeologic framework are limited to a particular interpretation of regional hydrogeologic conditions.

3. The period of simulation consists of a steady-state prepumping condition (prior to 1913) and transient condition (1913 to 1998).

4. The scale of investigation is regional, simulating features and processes that are appropriate at a 1:250,000 scale.

This report consists of six chapters that describe various aspects of the geology, hydrology, and transient simulation of the DVRFS region. Chapter A (this chapter) introduces the DVRFS transient flow modeling effort, describes the site, and outlines previous regional-scale simulations in this area. Chapter B describes the geologic and hydrogeologic framework of the DVRFS region, detailing the geologic history, the geologic and hydrogeologic units present in the region, and structural features that control regional ground-water flow. Chapter C describes various hydrologic evaluations and the basic hydrologic data of the regional ground-water flow system, including studies of recharge, evapotranspiration, spring discharge, pumpage rate, and hydraulic properties of the hydrogeologic units. Chapter D describes the hydrologic conceptual model of the region. The discussion includes the flow-system boundaries and subregions within the model area, occurrence of ground water and surface water, and paleohydrology. Chapter E describes the construction of the HFM using the stratigraphic and structural data presented in Chapter B. Finally, chapter F describes the construction and calibration of the numerical transient ground-water flow model of the DVRFS, from prepumping conditions (before 1913) to transient conditions from 1913 to 1998.

Site Description

In this report, the DVRFS region encompasses approximately 100,000 km^2 in Nevada and California and is bounded by latitudes 35°00'N and 38°15'N and by longitudes 115°00'W and 118°00'W. The DVRFS boundary has been variably defined and named in the past by several investigators (Harrill and others, 1988; Bedinger and others, 1989; D'Agnese and others, 1997; Harrill and Prudic, 1998; Bedinger and Harrill, Appendix 1, this volume) (fig. A–2). Comparison of figures A–1 and A–2 shows that the DVRFS model boundary depicted on figure A–1 differs slightly from the flow system boundaries depicted on figure A–2. Because of the various definitions of the DVRFS boundary, the simulated area is referred to as the "model domain." The region surrounding the model domain, inclusive of the model domain, is referred to as the "DVRFS region." The DVRFS is approximately that area depicted on figure A–1.

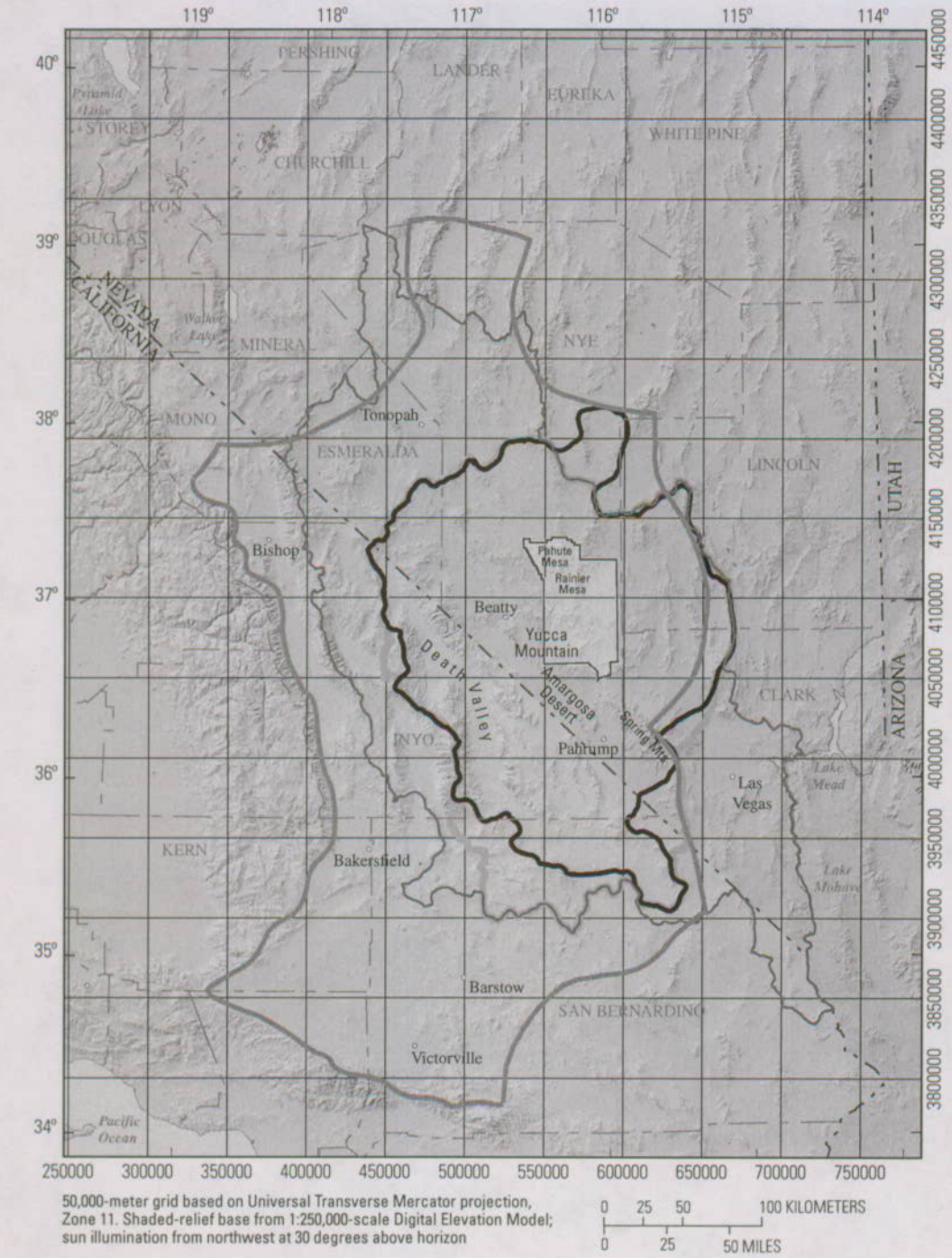

EXPLANATION

- Area contributing flow to the Death Valley regional ground-water flow system (Bedinger and Harrill, Appendix 1, this volume)
- Death Valley region (Bedinger and others, 1989)
- Death Valley regional flow system (Harrill and others, 1988; Harrill and Prudic, 1998)
- Death Valley regional flow system (D'Agnese and others, 1997)
- Nevada Test Site boundary
- Populated location

Figure A–2. Delineations of the Death Valley regional ground-water flow system.

Physiography

The DVRFS region is in the southern Great Basin, a subprovince of the Basin and Range physiographic province (Fenneman, 1931). The DVRFS region (fig. A–1) includes several large valleys, including the Amargosa Desert, Pahrump Valley, and Death Valley. The region also includes several major mountain ranges including the Spring Mountains and the Panamint, Sheep, Amargosa, Kawich, Kingston, Pahranagat, Timpahute, and Last Chance Ranges. Late Cenozoic tectonic activity accounts for much of the observed topographic relief across the DVRFS region (Grose and Smith, 1989). Altitudes range from 86 meters (m) below sea level at Death Valley to 3,600 m above sea level at Charleston Peak in the Spring Mountains. The maximum relief, 3,500 m, occurs on the west side of Death Valley. The relief between valleys and adjoining mountains locally exceeds 1,500 m (Bedinger and others, 1989). Mountain ranges in the northern one-half of the model domain trend north-south typical of the Basin and Range province, whereas principal mountain ranges in the southern one-half of the model domain trend northwest-southeast. Throughout the model domain the trends of intermediate-scale topographic features are quite variable.

Mountain ranges in the Basin and Range province typically occupy an area of about 25 percent of the total province (Peterson, 1981). The remainder is occupied by broad intermontane basins and, in the central part of the DVRFS region, a broad volcanic plateau. The basins are filled with sediment and some interbedded volcanic deposits that gently slope from the valley floors to the bordering mountain ranges (Peterson, 1981).

The valley floors are local depositional centers that usually contain playas that act as catchments for surface-water runoff (Grose and Smith, 1989). The Amargosa River (fig. A–1), an intermittent stream whose drainage basin encompasses about 15,000 km^2, discharges into the south end of the Death Valley saltpan, the largest playa in the DVRFS region (Hunt and others, 1966). Most of the basins seldom contain perennial surface water. Playas and alluvial flats lying within these intermontane basins constitute about 10 percent of the region (Bedinger and others, 1989). Many playas contain saline deposits that indicate the evaporation of surface water and(or) shallow ground water from the playa surface. Some of the playas that have been deformed by Quaternary faulting contain springs where ground water is forced to the surface by juxtaposed lacustrine and basin-fill deposits (Bedinger and others, 1989). The Amargosa Desert contains several spring pools and human-engineered reservoirs that are supported by regional ground-water discharge.

Climate

Climatic conditions in the DVRFS region vary significantly and are primarily controlled by altitude. The northern part of the region, including the Cactus, Kawich, and Timpahute Ranges (fig. A–1), forms part of the Great Basin Desert and is characterized by warm, dry summers and cold, dry winters. The southern part of the region, including Death Valley and the eastern Mojave Desert, is characterized by hot, dry summers and warm, dry winters (Benson and Darrow, 1981). The central area around the NTS has been called the Transition Desert (Beatley, 1976), which represents a mixing of the two climates (fig. A–3).

Precipitation in the region is influenced by two distinct storm patterns, one occurring in the winter and the other in the summer. Winter precipitation (dominantly snow in the mountains and rain in the valleys) tends to be of low intensity and long duration and covers great areas. In contrast, most summer rains, resulting from local convective thunderstorms, are of high intensity and short duration (Hales, 1972, 1974).

Quiring (1965) and French (1983) analyzed the distribution of precipitation resulting from the winter and summer weather regimes across southern Nevada. Quiring (1965) concluded that the two sources of precipitation (fig. A–4) affect regions south of latitude 38°30'N and primarily are orographically controlled (especially by the Sierra Nevada, fig. A–1). Because of these rain shadows, some areas of southern Nevada receive excess precipitation while other areas receive a precipitation deficit relative to mean precipitation (French, 1983).

Soils and Vegetation

The soils and vegetation of the DVRFS region are controlled to a substantial degree by climatic, geomorphic, and hydrologic factors and are highly variable and complex. Soils in the DVRFS region typically include soils weathered from bedrock (lithosols) on the mountains, medium- to coarse-textured soils on alluvial fans and terraces, and fine-grained, alluvial soils on the valley floors. In general, the soils of the mountains and hills are thin and coarse textured, with little moisture-holding capacity. The soils of the alluvial fans on the upper bajadas also are coarse textured but are thicker, so that infiltration rates are relatively high. Infiltration rates of the alluvial basin soils are low because the downward movement of water commonly is impeded by calcium-carbonate-cemented layers (pedogenic carbonate), fine-grained playa deposits, and less commonly, silicified hardpans that form within the soils over time (Beatley, 1976).

Vegetation distributions in the DVRFS region are influenced by water availability and temperature and vary by latitude and altitude. Thus, vegetation communities in the region demonstrate both topographic and geographic patterns. Mixing of the cold, northern Great Basin Desert climate with the warm, southern Mojave Desert climate results in a heterogeneous distribution of plant associations (Beatley, 1976).

Land Management and Water Use

Most of the land in the DVRFS region is owned by the U.S. Government and is administered by numerous Federal agencies. Privately owned land is scattered throughout the region, but most private ownership is concentrated near the

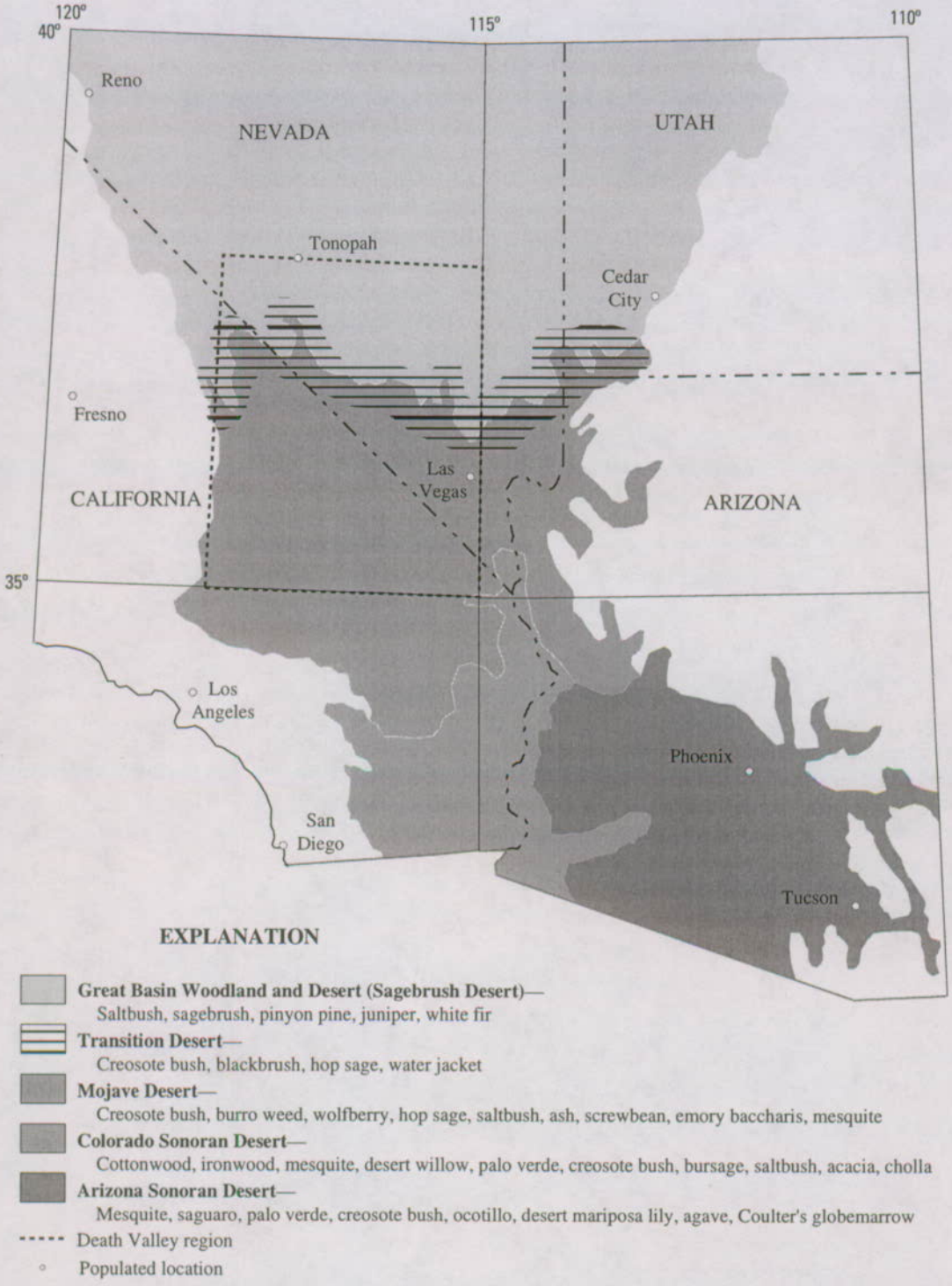

Figure A–3. Desert climatic zones of the Death Valley regional ground-water flow system region.

agricultural centers of Amargosa Desert and Pahrump Valley, the mining community of Beatty, Nev., and the towns of Shoshone, Tecopa, and Baker, Calif. (fig. A–1).

The major land-use activities in the region are agriculture, livestock ranching, recreation, and mining. Water within the DVRFS region is used mostly for domestic, commercial, agricultural, livestock, military, and mining purposes. Water resources in the Amargosa Desert support biological communities protected by the National Park Service in Death Valley and by the U.S. Fish and Wildlife Service at Ash Meadows National Wildlife Refuge, such as the Devils Hole pupfish (*Cyprinidon diabolis*), whose continued existence depends on naturally occurring spring discharges and stable pool levels in Devils Hole.

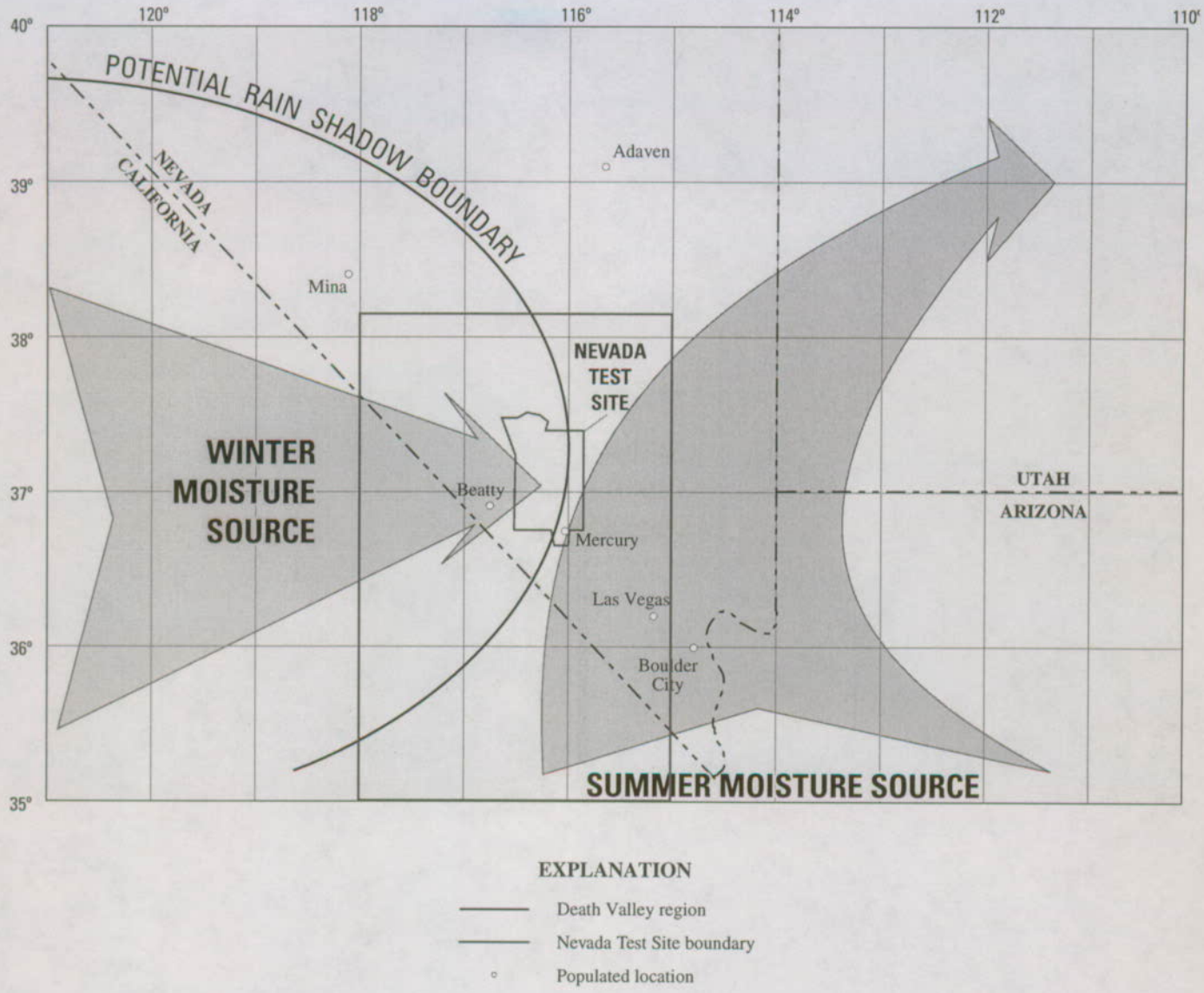

Figure A–4. Weather regimes of the Death Valley regional ground-water flow system region (Quiring, 1965).

Previous Work

Regional-scale ground-water flow models developed over the last 2 decades have provided new insights into ground-water flow in the DVRFS region. The NNSA/NSO and YMP have supported the construction of several such models to evaluate ground-water flow in the DVRFS. Successive models incorporated additional hydrogeologic complexity and computational sophistication in an effort to address increasingly complex water-resource issues in the region. Each of these studies attempted to model the complex hydrology and hydrogeologic framework, but the heterogeneity of the flow system was oversimplified because practical methods for representing the complex hydrogeologic framework were not available. With each model, investigators refined the understanding of the 3D nature of the DVRFS.

Early numerical ground-water modeling efforts were based on simplified conceptual models of the geology and hydrology known to exist in the region. Two- and three-dimensional ground-water flow models developed in the 1980's contained considerable abstractions of the natural hydrogeologic conditions and depended on lumped system parameters (Waddell, 1982; Czarnecki and Waddell, 1984; Rice, 1984; Czarnecki, 1985; Sinton, 1987). Although these models were considered adequate for their intended purposes, the results of these investigations indicated that lumped-parameter representations do not necessarily adequately depict vertical ground-water flow components, subbasin ground-water flux, steep hydraulic gradients, and physical subbasin boundaries.

In contrast, the more complex ground-water flow models developed in recent investigations allow for the examination of the spatial and process complexities of the 3D hydrogeologic system (Prudic and others, 1995; IT Corporation,

1996a; D'Agnese and others, 1997; D'Agnese and others, 2002). These more geologically and hydrologically representative flow models usually require a 3D HFM to define the complexities of the hydrogeologic unit (HGU) geometry and structure.

Early Ground-Water Flow Models

Waddell (1982) used a 2D, finite-element model to simulate the ground-water system of the NTS. Data from two wells [USW G–2 (USGS Site ID 365322116273501) and USW WT–24 (USGS Site ID 365301116271301)] drilled after the completion of Waddell's model defined steep hydraulic gradients in the vicinity of Yucca Mountain and contradicted the results of the simulation. Waddell (1982) noted several model shortcomings:

1. The simulation was inaccurate in the eastern part of the Pahute Mesa area, possibly because of the limited amount of data available for the eastern and northeastern parts of the NTS.

2. Structural controls of ground-water flow were poorly represented.

3. Vertical flow components were ignored.

4. Estimation of transmissivity values from potentiometric data had large uncertainty.

Czarnecki and Waddell (1984) used a 2D, finite-element model to simulate and evaluate steady-state conditions in a subregional ground-water flow system in the Amargosa Desert. Parameter-estimation techniques using nonlinear regression were applied to head and flux data to estimate transmissivities within this flow system. Numerous simplifications were used to describe the flow system. As a result, the simulation did not adequately reproduce observed head values in areas where vertical-flow components and steep hydraulic gradients occurred. Sensitivity analyses indicated that rates of discharge and recharge provided important constraints on defining the ground-water flow system. Czarnecki (1985) improved on this model by adding a low-permeability zone that more accurately reproduced observed head values in the Amargosa Desert.

Rice (1984) developed a preliminary, 2D regional ground-water flow model of the NTS and vicinity using an approach similar to that used by Czarnecki and Waddell (1984). Although Rice's model contained detailed estimates of recharge and discharge, it ignored 3D heterogeneity. Because the model was developed primarily to assess flux, Rice assumed that using transmissivity values eliminated the need for detailed hydrogeologic framework characterization. Ultimately this 2D modeling approach prevented adequate simulation of vertical ground-water flow in Pahute Mesa and resulted in calibration difficulties. Rice (1984) recommended that a 3D model be constructed to correct this problem.

Sinton (1987) used a more sophisticated, quasi-3D, steady-state approach to characterize the regional ground-water flow system for the NTS. This model included two transmissive layers that represented the NTS flow system more accurately than did earlier models. The uppermost layer represented a shallow aquifer composed of volcanic rocks, basin-fill deposits, and lacustrine carbonate rocks. The lowermost layer represented a deep aquifer composed of carbonate and volcanic rocks. Horizontal flow was simulated within aquifer layers and vertical flow was simulated between layers and controlled using a vertical conductance term. The sensitivity analysis implied that the primary controls on ground-water flow were (1) the spatial distribution of low-permeability HGUs, (2) the distribution and magnitude of discharge and recharge locations, and (3) the rates of discharge and recharge. The analysis also revealed that small adjustments in recharge or discharge rates commonly produced substantial changes in the simulated magnitude and direction of ground-water flow. As a consequence, Sinton recommended that the following aspects of the flow system be investigated further:

1. The interaction between the lower carbonate aquifer and the overlying volcanic units,

2. The discharge rates at Ash Meadows, Death Valley, Alkali Flat, and other areas, and

3. The potential for recharge along Fortymile Wash and Fortymile Canyon.

Prudic and others (1995) developed a regional-scale numerical model of the carbonate-rock province of the Great Basin. This model simulated a conceptualized ground-water flow system containing a relatively shallow component in which water moved from mountain ranges to basin-fill deposits beneath adjacent valleys, as well as a deeper component in which water moved primarily through the carbonate rocks. This conceptual model is the basis of subsequent numerical models that describe regional ground-water flow in the DVRFS region. The calibrated numerical model indicated that:

1. The transmissivity values for basin-fill deposits and carbonate rocks in the upper layer are greater than those for other consolidated rocks.

2. The transmissivity values in the lower layer are greater in areas of regional springs.

3. Ground-water flow is relatively shallow, moving from recharge areas in mountain ranges to discharge areas in valleys.

4. Ground water discharges at deep regional springs or in areas with greater evapotranspiration rates.

5. Interbasin ground-water flow to larger regional springs occurs through carbonate rocks.

Recent Hydrogeologic Framework and Ground-Water Flow Models

The 3D ground-water flow models developed in recent investigations allow for the examination of the spatial and process complexities of the hydrogeologic system. These more geologically and hydrologically representative flow models are based on 3D HFMs to define the intricacies of the HGU geometry and structure. A digital HFM provides a computer-based description of the geometry and composition of the HGUs. Digital models defining the geometry and composition of the HGUs were constructed for several of the regional-scale ground-water flow models completed in the 1990's and early 2000's as part of the UGTA program at the NTS, and the YMP. These include the DOE/NV-UGTA model (IT Corporation, 1996b) for the UGTA Phase I work, the YMP/HRMP model (D'Agnese and others, 1997), and the merged YMP/HRMP and DOE/NV-UGTA framework model (Belcher and others, 2002). Figure A–5 presents the boundaries of each of these HFMs.

Underground Test Area (DOE/NV-UGTA) Model

The DOE/NV-UGTA HFM is a 3D geologic model that describes the hydrogeologic framework for the regional ground-water flow system around the NTS (IT Corporation, 1996b). The detailed hydrogeologic framework was required for the systematic estimation of hydrologic and radionuclide attenuation properties of the rocks through which any radionuclides related to nuclear weapons testing might migrate. The framework also was constructed to assess the regional distribution and thickness of aquifers and confining units as well as to determine the depth to the base of the ground-water flow system in a complex geologic terrane. The geologic model has constant grid-cell spacing of 2,000 m on a side and variable vertical thickness, extends from land surface to 7,600 m below sea level, and encompasses approximately 17,700 km^2. Twenty HGUs were modeled, including thrusted bedrock units. The DOE/NV-UGTA geologic model domain is centered on the NTS and extends from Death Valley to east of the East Pahranagat Range, and from the Black Mountains to north of Penoyer and the southern part of Railroad Valleys (fig. A–5). This model was developed on the basis of information from geologic reports, maps, measured stratigraphic sections, cross sections, well data, and geophysical interpretations. Fifty-four regional interpretive cross sections and approximately 700 lithologic well logs were used in constructing the HFM.

The DOE/NV-UGTA flow model is a regional 3D, steady-state flow model of the NTS and surrounding areas (IT Corporation, 1996a). This 20-layer model is designed to provide a basis for predicting the movement of contaminants from the underground nuclear weapons testing areas on a regional scale. The model is used for estimating the amount of water moving through the ground-water system, evaluating uncertainty in these predictions, and supplying boundary conditions for more detailed models of the underground testing areas.

The calibrated DOE/NV-UGTA model accurately simulates several observed hydrologic features on the NTS:

1. The steep hydraulic gradients between Emigrant Valley and Yucca Flat and north of the Yucca Mountain area,

2. The shape of the potentiometric surface in the western part of Yucca Flat,

3. A moderately flat hydraulic gradient beneath Timber Mountain, steepening to the north beneath Pahute Mesa,

4. The trough in the potentiometric surface located in Area 20 on the western part of Pahute Mesa, and

5. Water budgets generally within expected ranges.

Yucca Mountain Project/Hydrologic Resource Management Program (YMP/HRMP) Model

The YMP/HRMP HFM is a 3D geologic model that describes the hydrogeologic framework for the regional ground-water flow system around Yucca Mountain (D'Agnese and others, 1997). The purpose of the model was to provide a description of the geometry, composition, and hydraulic properties that control regional ground-water flow for use in a regional steady-state ground-water flow model of the present-day system. The model grid is 1,500 m on a side with variable vertical thickness, extends from land surface to 10,000 m below sea level, and encompasses approximately 70,000 km^2. The model cells are attributed to define both the HGU and faulting conditions. Ten HGUs were modeled. The model domain is centered on Yucca Mountain and the NTS and extends from Death Valley to the East Pahranagat Range and from the Avawatz Mountains to Cactus Flat (fig. A–5). Development of the HFM was based on digital elevation models (DEM), geologic maps and sections, and lithologic well logs. Thirty-two regional cross sections, and approximately 700 lithologic well logs provided subsurface control for the HFM. Although thousands of faults have been mapped in the region, only 300 were used in constructing the HFM (D'Agnese and others, 1997).

The YMP/HRMP flow model is a 3D steady-state simulation of the present-day (pumped) DVRFS region (D'Agnese and others, 1997). The 3-layer model used a non-linear least-squares regression technique to estimate aquifer-system variables (or parameters). The 3D simulation supported the analysis of interactions between the relatively shallow local and subregional flow paths and the deeper, dominant regional flow paths controlled by the regional carbonate-rock aquifer.

50,000-meter grid based on Universal Transverse Mercator projection, Zone 11
Shaded-relief base from 1:250,000-scale Digital Elevation Model; sun illumination from northwest at 30 degrees above horizon

EXPLANATION

- Death Valley regional ground-water flow system hydrogeologic framework model boundary (Belcher and others, 2002)
- Yucca Mountain Project hydrogeologic framework ground-water flow model boundary (D'Agnese and others, 1997)
- Underground Test Area geologic model boundary (IT Corporation, 1996b)
- Nevada Test Site boundary

Figure A–5. Delineations of regional hydrogeologic framework models of the Death Valley regional ground-water flow system region.

Values of hydraulic head, spring flow, hydraulic conductivity, and water-budget components derived from the calibrated model were assessed for accuracy (D'Agnese and others, 1997). This assessment revealed that:

1. Simulated hydraulic heads matched observed conditions closely in nearly flat hydraulic-gradient areas and relatively well in steep hydraulic-gradient areas.

2. Simulated spring-flow volumes were generally less than observed values.

3. All estimated parameter values were within expected ranges.

4. Given the uncertainty, simulated water budgets were within the expected ranges for the flow system.

5. Weighted residuals were not entirely random, indicating some model error.

Death Valley Regional Ground-Water Flow System Prepumping Model

Belcher and others (2002) merged the two regional framework models constructed for YMP/HRMP (D'Agnese and others, 1997) and DOE/NV-UGTA (IT Corporation, 1996b) to produce a single, integrated HFM for use with a steady-state prepumping ground-water flow model (D'Agnese and others, 2002). Because of project-scope limitations, few interpretations were made where these two framework models disagree (mostly with respect to the HGUs defined for each HFM), and the hydrogeologic representation of the flow system is limited. During the merging process, the Cenozoic volcanic HGUs of the YMP/HRMP framework model were replaced by the Cenozoic volcanic HGUs of the DOE/NV-UGTA framework model. The more detailed Cenozoic basin-fill HGUs from the DOE/NV-UGTA framework model were used, augmented by the playa-deposits HGU from the YMP/HRMP model.

The DVRFS steady-state prepumping flow model (D'Agnese and others, 2002) simulated the flow system using a 3D steady-state model that incorporated a nonlinear least-squares regression technique to estimate aquifer-system parameters. This model had a vertical discretization that resulted in 15 model layers.The accuracy of the final calibrated DVRFS steady-state model was tested by comparing measured (observed) and expected values for heads, ground-water discharges, and parameter values, such as hydraulic conductivity, with simulated values (D'Agnese and others, 2002). The analysis resulted in the following observations:

1. A good fit between simulated and observed hydraulic heads generally was achieved in areas of low hydraulic gradients; a moderate fit to observed heads was achieved in the remainder of the nearly flat hydraulic-gradient areas; a poorer fit to observed heads was achieved in steep hydraulic-gradient areas; and the poorest fit to observed hydraulic heads was achieved in the vicinity of Indian Springs, the western part of Yucca Flat, and the southern part of the Bullfrog Hills. Most of the discrepancies can be attributed to (a) insufficient representation of the hydrogeology in the HFM, (b) misinterpretation of water levels, and (c) model error associated with grid-cell size.

2. Ground-water discharge residuals between simulated and observed values were generally interpreted to be random.

3. All resulting parameter values were within the range of expected values.

Overall evaluation of the model indicates that the steady-state prepumping DVRFS model reasonably represents the prepumping conditions for the DVRFS. Although the model is an improvement over previous representations of the flow system, important uncertainties and model errors remain. These uncertainties and errors include the quality of interpretation and representation of: (1) flow-model observations, (2) geometry and spatial variability of hydrogeologic materials and structures in the hydrogeologic-framework and ground-water flow models, and (3) physical framework and the hydrologic conditions in the flow model (D'Agnese and others, 2002). Furthermore, it is unclear whether the model of D'Agnese and others (2002) adequately simulates the DVRFS because the water table was simulated substantially below the uppermost layer of the model, and the flow system was simulated as confined (Richard K. Waddell, GeoTrans, written commun., 2002).

Summary

The hydrogeology, conceptual hydrologic model, and the hydrologic system inputs and outputs of the Death Valley regional ground-water flow system (DVRFS) region are used in this report to construct a hydrogeologic framework model and a transient numerical ground-water flow model. The ground-water flow model simulates transient conditions from 1913 through 1998 using the modular ground-water flow model, MODFLOW-2000, and a simulated steady-state head distribution representing prepumping conditions. Transient stresses imposed on the regional ground-water flow system include ground-water pumpage that occurred from 1913 through 1998, and flows from springs affected by pumping; simulated areal recharge was held constant at average annual values. The DVRFS region encompasses approximately 100,000 square kilometers in Nevada and California and is bounded by latitudes 35°00'N and 38°15'N and by longitudes 115°00'W and 118°00'W.

More than 20 years of ground-water flow modeling in the Death Valley region has produced a succession of models that are increasingly more realistic representations of the hydrogeologic framework and ground-water flow system. The current transient simulation, described in the following chapters, builds upon this substantial body of previous work and provides the most refined model of the DVRFS region to date.

References Cited

Beatley, J.C., 1976, Vascular plants of the Nevada Test Site and central-southern Nevada—Ecologic and geographic distributions: Technical Information Center, Office of Technical Information, Energy Research and Development Administration, Springfield, Va., 308 p.

Bedinger, M.S., Langer, W.H., and Reed, J.E., 1989, Groundwater hydrology, *in* Bedinger, M.S., Sargent, K.A., and Langer, W.H., eds., Studies of geology and hydrology in the Basin and Range Province, southwestern United States, for isolation of high-level radioactive waste—Characterization of the Death Valley Region, Nevada and California: U.S. Geological Survey Professional Paper 1370–F, p. 28–35.

Belcher, W.R., Faunt, C.C., and D'Agnese, F.A., 2002, Three-dimensional hydrogeologic framework model for use with a steady-state numerical ground-water flow model of the Death Valley regional flow system, Nevada and California: U.S. Geological Survey Water-Resources Investigations Report 01–4254, 87 p.

Benson, Lyman, and Darrow, R.A., 1981, Trees and shrubs of the southwestern deserts: Tucson, University of Arizona Press, 416 p.

Czarnecki, J.B., 1985, Simulated effects of increased recharge on the ground-water flow system of Yucca Mountain and vicinity, Nevada-California: U.S. Geological Survey Water-Resources Investigations Report 84–4344, 33 p.

Czarnecki, J.B., and Waddell, R.K., 1984, Finite-element simulation of ground-water flow in the vicinity of Yucca Mountain, Nevada-California: U.S. Geological Survey Water-Resources Investigations Report 84–4349, 38 p.

D'Agnese, F.A., Faunt, C.C., Turner, A.K., and Hill, M.C., 1997, Hydrogeologic evaluation and numerical simulation of the Death Valley regional ground-water flow system, Nevada and California: U.S. Geological Survey Water-Resources Investigations Report 96–4300, 124 p.

D'Agnese, F.A., O'Brien, G.M., Faunt, C.C., Belcher, W.R., and San Juan, Carma, 2002, A three-dimensional numerical model of predevelopment conditions in the Death Valley regional ground-water flow system, Nevada and California: U.S. Geological Survey Water-Resources Investigations Report 02–4102, 114 p. Accessed September 22, 2004, at *http://pubs.water.usgs.gov/wri024102/.*

Eakin, T.E., 1966, A regional interbasin groundwater system in the White River area, southeastern Nevada: Water Resources Research, v. 2, no. 2, p. 251–271.

Fenneman, N.M., 1931, Physiography of western United States: New York, McGraw-Hill Book Company, Inc., 534 p.

French, R.H., 1983, A preliminary analysis of precipitation in southern Nevada: Water Resources Center, Desert Research Institute, DOE/NV/10162–10, 42 p.

Grose, T.L., and Smith, G.I., 1989, Geology, *in* Bedinger, M.S., Sargent, K.A., and Langer, W.H., eds., Studies of geology and hydrology in the Basin and Range Province, southwestern United States, for isolation of high-level radioactive waste: U.S. Geological Survey Professional Paper 1370–F, p. 5–19.

Hales, J.R., Jr., 1972, Surges of maritime tropical air northward over the Gulf of California: Monthly Weather Review, v. 100, p. 298–306.

Hales, J.R., Jr., 1974, Southwestern United States summer monsoon source—Gulf of Mexico or Pacific Ocean?: Journal of Applied Meteorology, v. 13, p. 331–342.

Hanks, T.C., Winograd, I.J., Anderson, R.E., Reilly, T.E., and Weeks, E.P., 1999, Yucca Mountain as a radioactive-waste repository: U.S. Geological Survey Circular C1184, 19 p.

Harbaugh, J.W., Banta, E.R., Hill, M.C., and McDonald, M.G., 2000, MODFLOW-2000, The U.S. Geological Survey's modular ground-water flow model—User guide to modularization concepts and the ground-water flow process: U.S. Geological Survey Open-File Report 00–92, 121 p.

Harrill, J.R., Gates, J.S., and Thomas, J.M., 1988, Major ground-water flow systems in the Great Basin region of Nevada, Utah, and adjacent States: U. S. Geological Survey Hydrologic Investigations Atlas HA–694–C, 2 sheets.

Harrill, J.R., and Prudic, D.E., 1998, Aquifer systems in the Great Basin region of Nevada, Utah, and adjacent States: U.S. Geological Survey Professional Paper 1409–A, 66 p.

Hill, M.C., 1992, A computer program (MODFLOWP) for estimating parameters of a transient three-dimensional, ground-water flow model using nonlinear regression: U.S. Geological Survey Open-File Report 91–484, 358 p.

Hunt, C.B. and Robinson, T.W., 1960, Possible interbasin circulation of ground water in the southern part of the Great Basin: U.S. Geological Survey Professional Paper 400–B, p. B273–274.

Hunt, C.B., Robinson, T.W., Bowles, W.A., and Washburn, A.L., 1966, Hydrologic basin, Death Valley, California: U.S. Geological Survey Professional Paper 494–B, 138 p.

IT Corporation, 1996a, Underground test area subproject, Phase I, Data analysis task, volume VI—Groundwater flow model data documentation package: Las Vegas, Nev., Report ITLV/10972–181 prepared for the U.S. Department of Energy, 8 volumes, various pagination.

IT Corporation, 1996b, Underground test area subproject, Phase I, Data analysis task, volume I—Geologic model data documentation package: Las Vegas, Nev., Report ITLV/10972–181 prepared for the U.S. Department of Energy, 8 volumes, various pagination.

Maxey, G.B., and Eakin, T.E., 1949, Ground water in White River Valley, White Pine, Nye, and Lincoln Counties, Nevada: Nevada State Engineer, Water Resources Bulletin Number 8, 59 p.

McDonald, M.G., and Harbaugh, A.W., 1988, A modular three-dimensional finite-difference ground-water flow model: U.S. Geological Survey Techniques of Water-Resources Investigations, book 6, chap. A1, 576 p.

Peterson, F.F., 1981, Landforms of the Basin and Range province defined for soil survey: Nevada Agricultural Bulletin No. 28, Max C. Fleischmann College of Agriculture, University of Nevada, Reno, Nev., 53 p.

Prudic, D.E., Harrill, J.R., and Burbey, T.J., 1995, Conceptual evaluation of regional ground-water flow in the carbonate-rock province of the Great Basin, Nevada, Utah, and adjacent States: U.S. Geological Survey Professional Paper 1409–D, 102 p.

Quiring, R.F., 1965, Annual precipitation amount as a function of elevation in Nevada south of 38-1/2 degree latitude, Las Vegas, Nevada: U.S. Weather Bureau Research Statistics, 14 p.

Rice, W.A., 1984, Preliminary two-dimensional regional hydrologic model of the Nevada Test Site and vicinity: Albuquerque, N. Mex., Sandia National Laboratories Report SAND83–7466, 89 p.

Rush, F.E., 1968, Index of hydrographic areas in Nevada: Carson City, Nevada Department of Conservation and Water Resources, Water Resources Reconnaissance Series Report 54, 25 p.

Sinton, P.O., 1987, Three-dimensional, steady-state, finite-difference model of the ground-water flow system in the Death Valley ground-water basin, Nevada-California: Golden, Colorado School of Mines, Master's thesis, 145 p.

Waddell, R.K., 1982, Two-dimensional, steady-state model of ground-water flow, Nevada Test site and vicinity, Nevada-California: U.S. Geological Survey Water-Resources Investigations Report 84–4267, 72 p.

Geology and Hydrogeology

By Donald S. Sweetkind, Wayne R. Belcher, Claudia C. Faunt, and
Christopher J. Potter

Chapter B of

Death Valley Regional Ground-Water Flow System, Nevada and California—Hydrogeologic Framework and Transient Ground-Water Flow Model

Edited by Wayne R. Belcher

Prepared in cooperation with the
U.S. Department of Energy
Office of Environmental Management, National Nuclear Security Administration, Nevada Site Office,
under Interagency Agreement DE–AI52–01NV13944, and
Office of Repository Development,
under Interagency Agreement DE–AI08–02RW12167

Scientific Investigations Report 2004–5205

U.S. Department of the Interior
U.S. Geological Survey

Contents

Figures

Tables

CHAPTER B. Geology and Hydrogeology

By Donald S. Sweetkind, Wayne R. Belcher, Claudia C. Faunt, and Christopher J. Potter

Introduction

The geology of the Death Valley regional ground-water flow system (DVRFS) region, consisting of many types of rocks that have been subjected to a variety of structural disruptions, is stratigraphically and structurally complex. These rocks form a complex, three-dimensional (3D) framework that can be subdivided into aquifers and confining units on the basis of their ability to store and transmit water. The principal aquifer is a thick sequence of Paleozoic carbonate rock that extends throughout the subsurface of much of central and southeastern Nevada (Dettinger, 1989; Harrill and Prudic, 1998) and crops out in the eastern one-half of the DVRFS region (fig. B–1). Fractured Cenozoic volcanic rocks in the vicinity of the Nevada Test Site (NTS) and permeable Cenozoic basin fill throughout the DVRFS region (fig. B–1) locally are important aquifers that interact with the regional flow through the underlying Paleozoic carbonate rocks (Blankennagel and Weir, 1973; Winograd and Thordarson, 1975; Harrill and others, 1988, sheet 2; Dettinger, 1989). Proterozoic to Early Cambrian metamorphic and siliciclastic rocks and Paleozoic siliciclastic rocks are the primary regional confining units; they are associated with abrupt changes in the potentiometric surface. Zeolitically altered and nonwelded tuffs within the Cenozoic volcanic rocks and fine-grained parts of the Cenozoic basin fill form locally important confining units (Blankennagel and Weir, 1973; Winograd and Thordarson, 1975). Stratigraphic units in the DVRFS region are disrupted by large-magnitude offset thrust, strike-slip, and normal faults. Combinations of normal, reverse, and strike-slip faulting and folding episodes (Carr, 1984) have resulted in a complex distribution of rocks. Consequently, diverse rock types, ages, and deformational structures are juxtaposed, creating variable and complex subsurface conditions. These faults juxtapose units with different hydraulic properties that may disrupt regional flow paths. Broader zones of distributed deformation may enhance permeability through the creation of secondary (fracture) permeability (Carr, 1984). Understanding the ground-water flow system in Death Valley or in any area depends on understanding the geologic framework of the area, especially in stratigraphically and structurally complex areas.

More than 20 years of ground-water flow modeling of the DVRFS has produced a succession of models that represent the regional hydrogeologic framework and ground-water flow system. Different approaches were taken, however, in incorporating the geologic framework in the models with different geologic data sets or subsurface interpretations. In general, the models have used increasing levels of geologic detail, which has resulted in better model calibration. The increase in computing power and advances in modeling routines over time has allowed the incorporation of more geologic detail in framework and flow models. The data and descriptions presented in this chapter attempt to (1) integrate and resolve different geologic interpretations used in the two most recent regional flow models (IT Corporation, 1996a; D'Agnese and others, 1997; see discussion in Chapter A, this volume); and (2) incorporate abundant new data that were developed during or following the construction of the two models.

This chapter describes the geologic and hydrogeologic framework of the DVRFS region, summarizes the stratigraphic and structural settings, and discusses the major structures that affect ground-water flow. The hydrogeologic units and stratigraphic and structural data are discussed that are used as input for the 3D hydrogeologic framework model (HFM) (Chapter E, this volume) and used in the transient ground-water flow model (Chapter F, this volume).

Stratigraphic and Structural Setting

Stratigraphic Setting

In Late Proterozoic to Devonian time, the southwestern part of the United States was largely characterized by deposition of marine sedimentary rocks at the continental margin. The Paleozoic shelf province in the DVRFS region is bounded on the southeast by the westward limit of cratonal sections and on the northwest by facies transitions to rocks interpreted to have been deposited in deeper water (fig. B–1). In the DVRFS region, Late Proterozoic and Early Cambrian rocks form a westward-thickening wedge of predominantly quartzites and siltstones that record deposition on the early shelf edge of western North America (Stewart and Poole, 1974; Poole and others, 1992). These rocks are overlain by a thick succession of predominantly continental shelf-facies carbonate rocks deposited throughout most of the eastern and central parts of the DVRFS region during Paleozoic (Middle Cambrian through Devonian) time. These carbonate rocks and calcareous

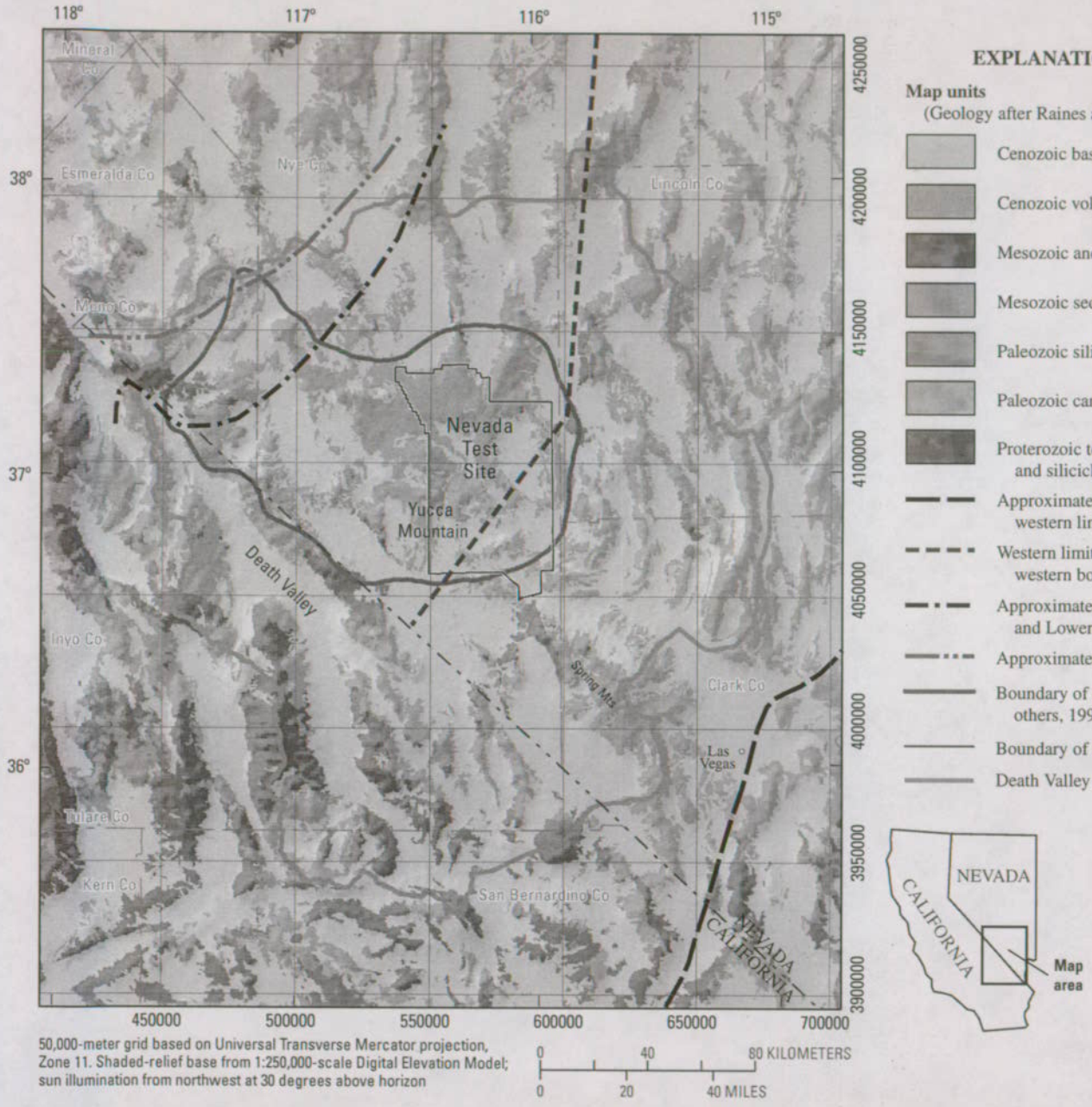

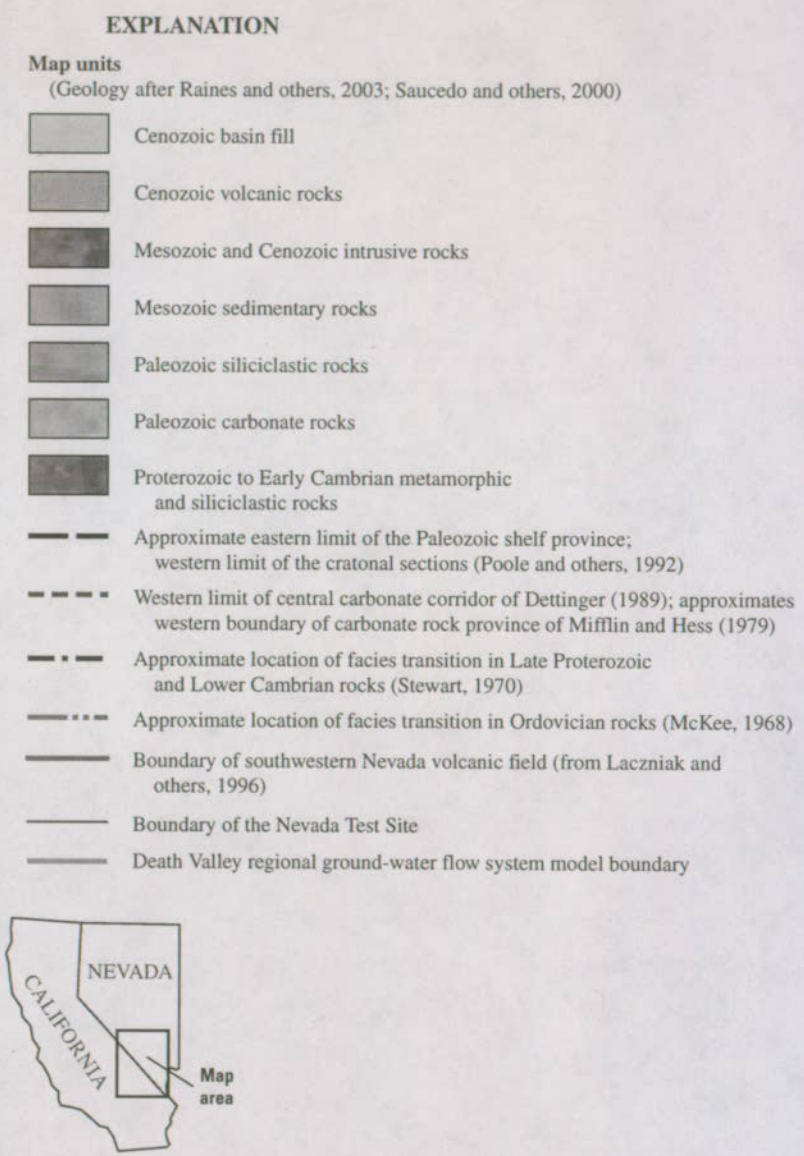

Figure B–1. Generalized geology within and surrounding the area of the Death Valley regional ground-water flow system.

shales form a westward-thickening carbonate- and clastic-rock section up to 4,500 m thick (Burchfiel, 1964) (fig. B–2). In the western and northwestern parts of the DVRFS region, Middle Cambrian through Devonian strata consist of slope-facies carbonate rocks intermixed with siliciclastic and volcanic rocks (Stewart, 1980). To the east of the DVRFS region, Middle Cambrian through Devonian strata form a relatively thin (hundreds of meters) cratonic sequence; to the west and northwest of the DVRFS region, these rocks represent deeper water facies (figs. B–1 and B–2). In the eastern and central parts of the DVRFS region, carbonate sedimentation was interrupted by two periods of siliciclastic rock deposition that resulted from periods of Paleozoic orogenesis.

In the vicinity of the NTS, deposition of marine carbonate rocks was interrupted during Late Devonian to Mississippian time (Poole and Sandberg, 1977; Poole, 1981; Trexler and others, 1996). Siliciclastic sediments were shed from uplifts to the north and west of the DVRFS region and deposited in a northeast-to-southwest-trending foreland basin. This basin dominantly consists of relatively low permeability argillites and shales and is now defined by the location of the Chainman Shale. Deposition of shelf-type carbonate rocks continued during Mississippian time in the southeastern part of the DVRFS region. By Pennsylvanian time, shallow marine carbonate rocks were deposited over much of the eastern and southern parts of the DVRFS region. During late Paleozoic and Mesozoic time, the Paleozoic stratigraphic sequence was deformed by regional thrust faulting (Armstrong, 1968; Barnes and Poole, 1968) of the older Late Proterozoic to Lower Cambrian siliciclastic section over the younger Paleozoic carbonate rock section.

Only minor amounts of Mesozoic sedimentary rocks are preserved in most of the DVRFS region (fig. B–1). Mesozoic cratonic sedimentary rocks are exposed east of the DVRFS region in the Las Vegas area and in the Spring Mountains; Mesozoic metasedimentary and metavolcanic rocks are sparsely exposed in the western part of the DVRFS region. Mesozoic plutonic rocks associated with the Sierra Nevada batholith are abundant immediately south and west of the DVRFS model area.

The distribution and character of Cenozoic volcanic and sedimentary rocks of the DVRFS region are influenced by two factors: (1) the general southward and westward sweep of volcanism across this area in Oligocene and Miocene time (fig. B–3) (Best and others, 1989; McKee, 1996; Dickinson, 2002); and (2) the timing, location, and magnitude of extension and the formation of basin-and-range topography. For the purposes of the regional ground-water flow model, the volcanic rocks of the region can be categorized into four groups: (1) Cenozoic volcanic centers and volcanic rocks north of the NTS, mostly older than volcanic rocks at the NTS (Ekren and others, 1971, 1977; Best and others, 1989; McKee, 1996); (2) the southwestern Nevada volcanic field (SWNVF), characterized in part by a thick section of regionally distributed welded tuffs that were derived from a central complex of nested calderas (Byers, Carr, Orkild, and others, 1976; Sawyer and others, 1994); (3) the central Death Valley volcanic field that is composed of a series of lava flows and nonwelded tuffs that were derived from localized volcanic centers rather than climactic caldera-forming eruptions (Wright and others, 1991); and (4) local, mostly younger extrusive rocks, both rhyolite flows and basaltic centers (fig. B–3). Eruptions of the SWNVF began about 16 Ma, peaked between 13.5 and 11 Ma, and then declined with time as the focus of volcanism migrated generally westward, largely moving out of the region about 5 Ma (fig. B–3).

Changes in sedimentation patterns of Cenozoic continental sedimentary rocks reflect the Cenozoic tectonic evolution of the DVRFS region. Relatively quiescent alluvial to lacustrine sedimentation of Oligocene to Early Miocene age gives way to post-Middle Miocene sedimentary rocks deposited in relatively small intermontane basins with local sediment sources as basin-range topography developed in the DVRFS region. Post-Miocene alluvial basins have progressively filled with as much as 1,500 m of coarse gravel and sand and locally fine-grained playa-lake deposits of silt and clay. In many basins, coarse synorogenic clastic sediments filled opening basins, later to be supplanted by alluvial fan, playa, and local channel deposits in Neogene time. Basin-range topography first developed in the DVRFS region from about 14 to about 12 Ma, and it is still actively evolving in the southwesternmost part of the region and to the west. Areas of thick Cenozoic rocks, both sedimentary and volcanic (fig. B–4), are interpreted on the basis of low-density gravity anomalies and depth-to-basement modeling (Jachens and Moring, 1990; Saltus and Jachens, 1995; Blakely and others, 1998, 1999, 2001).

More detailed stratigraphic descriptions are found in geologic compilations of the DVRFS region or parts of the region by Wahl and others (1997), Slate and others (2000), and Workman, Menges, Page, Taylor, and others (2002).

Structural Setting

The oldest deformation of hydrologic significance in the DVRFS region was the formation of regional thrust belts in late Paleozoic and Mesozoic time. Thrust faults are exposed in mountain ranges throughout the central and southern parts of the DVRFS region, from the Pahranagat Range, Sheep Range, and Spring Mountains on the east to the Funeral, Grapevine, and Cottonwood Mountains on the west (fig. B–5; see also map compilations of Workman, Menges, Page, Taylor, and others, 2002, and Workman, Menges, Page, Ekren, and others, 2002, and references cited therein). The northern part of the DVRFS region is largely covered by volcanic rocks and Cenozoic sediments, making the projection of thrusts northward uncertain.

Individual thrust faults that are exposed in separated range blocks have been interpreted to be regionally continuous Paleozoic and Mesozoic structures that were disrupted by Cenozoic extensional and strike-slip faulting (Armstrong, 1968; Barnes and Poole, 1968; Longwell, 1974; Stewart, 1988; Wernicke and others, 1988; Caskey and Schweickert, 1992; Snow, 1992; Serpa and Pavlis, 1996; Cole and Cashman, 1999;

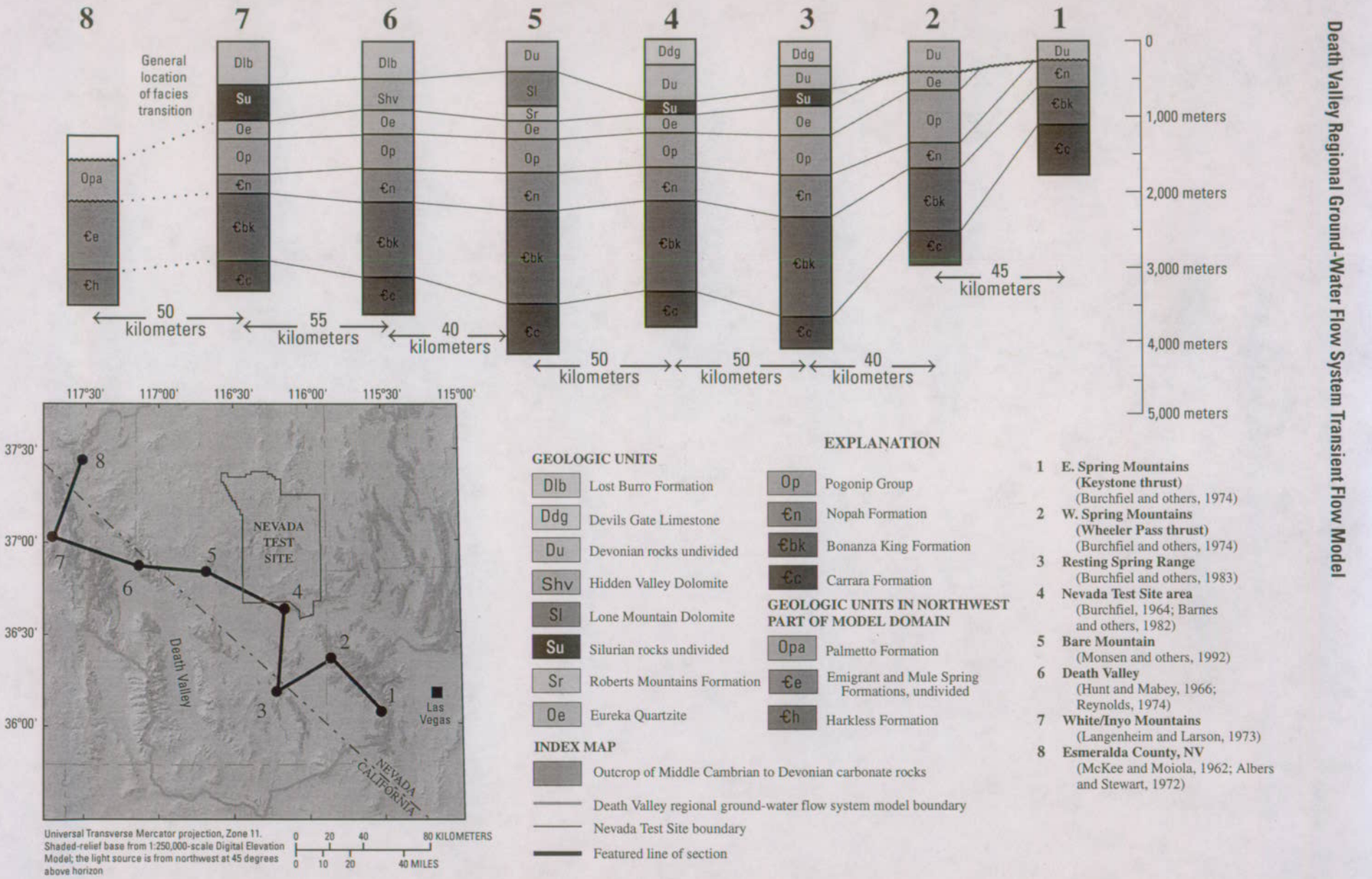

Figure B–2. Stratigraphic diagram of Paleozoic carbonate-rock units.

Figure B–3. Volcanic features of the Death Valley regional ground-water flow system region.

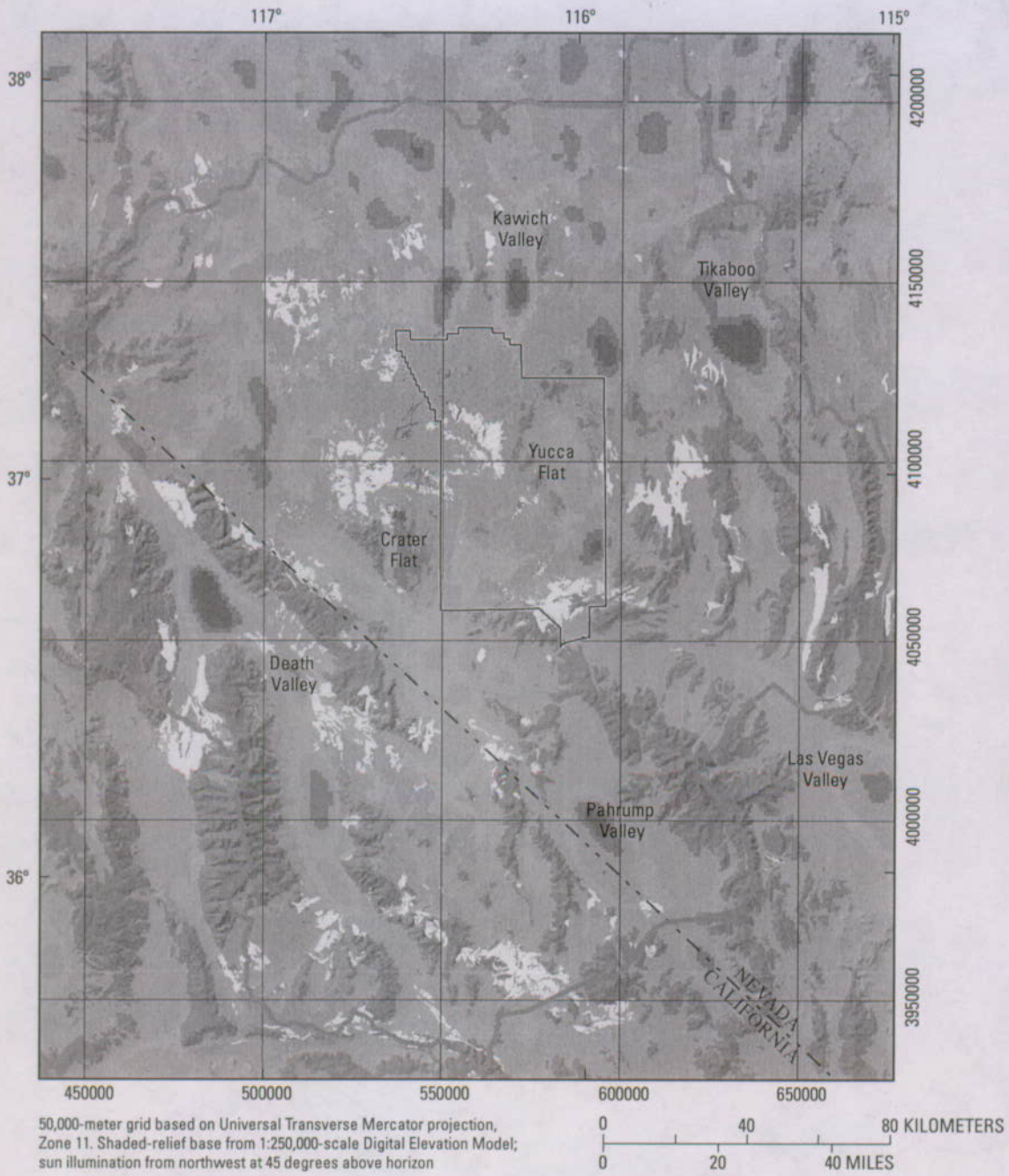

Figure B–4. Basins of the Death Valley regional ground-water flow system region.

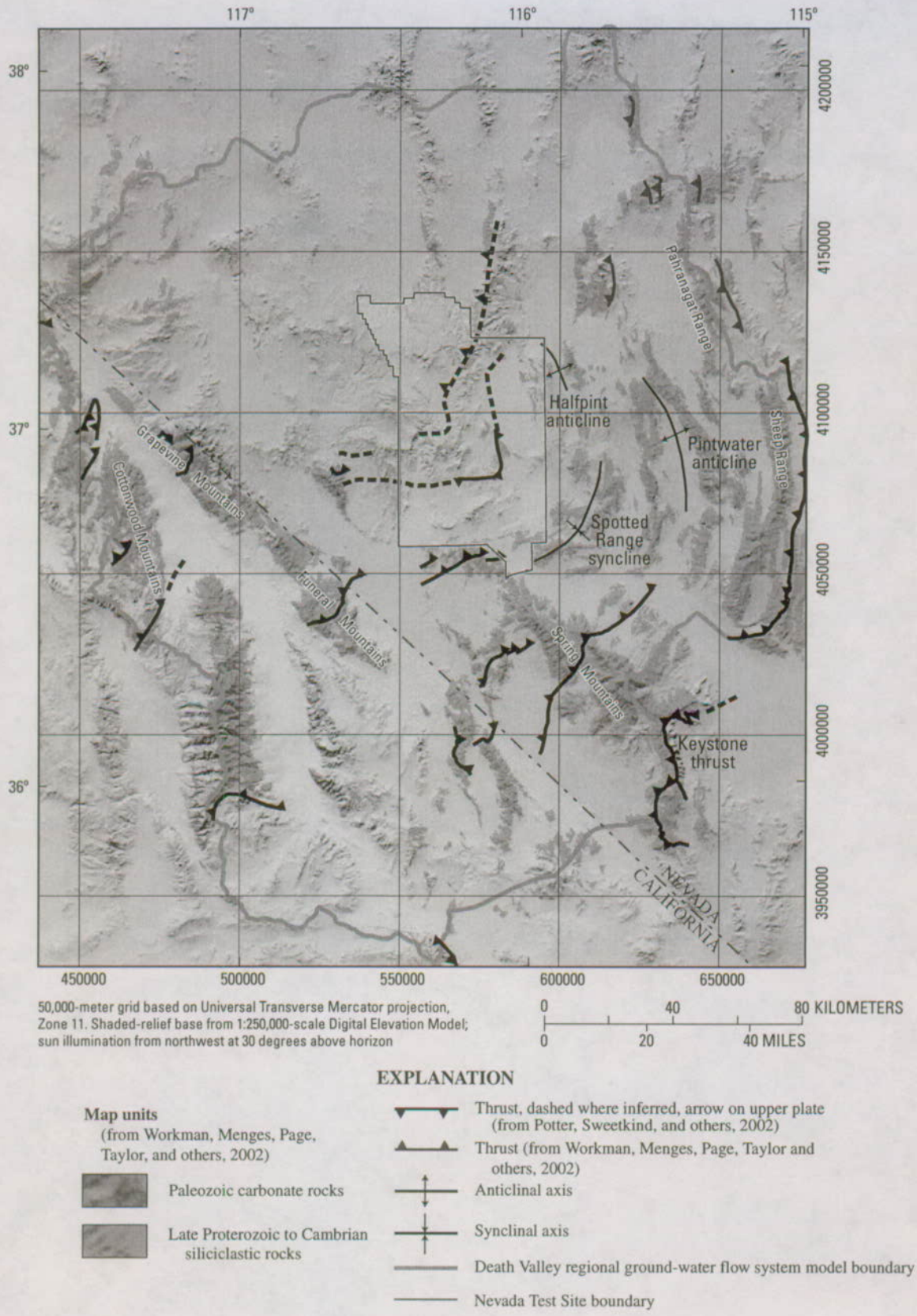

Figure B–5. Thrust faults of the Death Valley regional ground-water flow system region.

Snow and Wernicke, 2000). Individual thrusts and folds have been correlated throughout the DVRFS region on the basis of stratigraphic throw, sense of vergence, relative position, spacing, and style (Burchfiel and others, 1983; Wernicke and others, 1988, Snow and Wernicke, 1989; Snow, 1992; Caskey and Schweickert, 1992; Serpa and Pavlis, 1996). Regardless of specific correlation, mapped thrusts have been projected beneath Cenozoic cover on the basis of regional geologic relations and available outcrop and borehole control (Wernicke and others, 1988; Snow and Wernicke, 1989; Cole, 1997; Cole and Cashman, 1999; Potter, Sweetkind, and others, 2002).

Associated with the Paleozoic and Mesozoic regional thrusting are regional thrust-related folds (fig. B–5). West of the Sheep Range, the Pintwater anticline (Longwell and others, 1965) and the Spotted Range syncline (Barnes and others, 1982) are a regional, north-trending fold pair. Proterozoic and Paleozoic rocks in the eastern part of the NTS area are exposed in the Halfpint anticline, which has a core of Late Proterozoic siliciclastic rocks (Cole, 1997).

Cenozoic deformation of the region is characterized by a variety of structural patterns that overlap in space and time: (1) basin-range extension, (2) local extreme extension along detachment faults that currently have gentle dips, (3) development of discrete strike-slip faults and transtensional basins in the Walker Lane belt, and (4) Cenozoic volcanism that both preceded and accompanied regional extension. The magnitude of late Cenozoic extensional deformation varied spatially in the Death Valley region, with greatly extended domains alternating with lesser extended domains (Wernicke and others, 1984; Guth, 1981; Wernicke, 1992) (fig. B–6). In the northern part of the DVRFS region, late Cenozoic extensional deformation was dominated by movement along north- to northeast-striking normal faults related to development of the characteristic basin and range structure and associated topography of the southern Great Basin (Stewart, 1980). There, the north-south-trending basins such as Tikaboo Valley and Kawich Valley generally have asymmetric cross sections, with dominant normal faults producing a half-graben geometry. These normal faults generally dip 50° to 65° and have as much as 3,000 m of displacement. Gravity data (Healey and others, 1981) indicate that some of the larger faults are concealed beneath surficial deposits in the basins between the exposed range-front faults.

In the southern part of the DVRFS region, extension is spatially variable but in general of greater magnitude than in the northern part of the DVRFS region (fig. B–6). Tracts of east-dipping, rotated range blocks are bounded by west-side-down normal faults that are inferred to flatten and converge at depth into a deep detachment zone (Guth, 1981, 1990; Wernicke and others, 1984). In other parts of the DVRFS region, such as at Yucca Mountain, closely spaced north-striking normal faults apparently do not merge into a gently dipping detachment at depth (Brocher and others, 1998). Local large-magnitude extension is expressed as detachment-related core complexes. In these areas, gently to moderately dipping, large-offset extensional detachment faults expose broadly domed metamorphic complexes in the lower plates of the faults. The upper plates commonly are highly extended and tilted along normal faults that merge into the detachment faults. Although these detachment faults generally have gentle dips, the fault surfaces locally have dips of 50° to 60°. Strike-slip faults of both northwest and northeast strike may have transferred extensional strain between individual extensional domains (Wernicke and others, 1984).

The northwest-trending Walker Lane belt (Stewart, 1988; Stewart and Crowell, 1992) transects the DVRFS region (fig. B–7). The Walker Lane belt is a complex structural zone that is dominated by large right-lateral faults with northwest orientations, such as the Pahrump-Stewart Valley fault zone and the Las Vegas Valley shear zone (LVVSZ) (fig. B–7). The belt also contains a variety of structures that are discontinuous and appear to interact complexly in accommodating an overall mixed right-shear and extensional strain field (Stewart, 1988; Stewart and Crowell, 1992). The Walker Lane belt has been subdivided into a series of structural blocks according to their style of deformation (Stewart, 1988; Stewart and Crowell, 1992) (fig. B–7). In the northwestern part of the DVRFS region, the Goldfield block is notable for its lack of through-going strike-slip faults and relative lack of normal faults (fig. B–6). The Spotted Range–Mine Mountain block is characterized by east-northeast-trending, left-lateral strike-slip faults, such as the Rock Valley fault zone and the Cane Spring and Mine Mountain faults (fig B–7). The Spring Mountains block is a relatively intact block that is bounded by the Pahrump-Stewart Valley fault zone and the LVVSZ. The Inyo-Mono block (redefined as part of the Basin and Range province of eastern California by Workman, Menges, Page, Ekren, and others, 2002) features large, northwest-striking right-lateral faults, such as the Furnace Creek fault zone and the southern Death Valley fault zone and also features major extensional detachment faults (fig. B–7). Most of the deformation in the Walker Lane belt may have occurred during Middle Miocene time (Hardyman and Oldow, 1991; Dilles and Gans, 1995), although deformation in the vicinity of Death Valley continued into Late Miocene time (Wright and others, 1999; Snow and Wernicke, 2000). Some structures in the belt, such as the Rock Valley fault zone, continue to be active (Rogers and others, 1987; von Seggern and Brune, 2000).

Hydrogeologic Units

The rocks and deposits forming the hydrostratigraphic framework for a ground-water flow system are termed hydrogeologic units (HGUs). An HGU has considerable lateral extent and has reasonably distinct hydrologic properties because of its physical (geological and structural) characteristics.

Previous Use

The basic pre-Cenozoic hydrostratigraphic setting for the DVRFS region, particularly in the vicinity of the NTS, was established by Winograd and Thordarson (1975). The pre-Cenozoic sedimentary rocks were grouped into four HGUs:

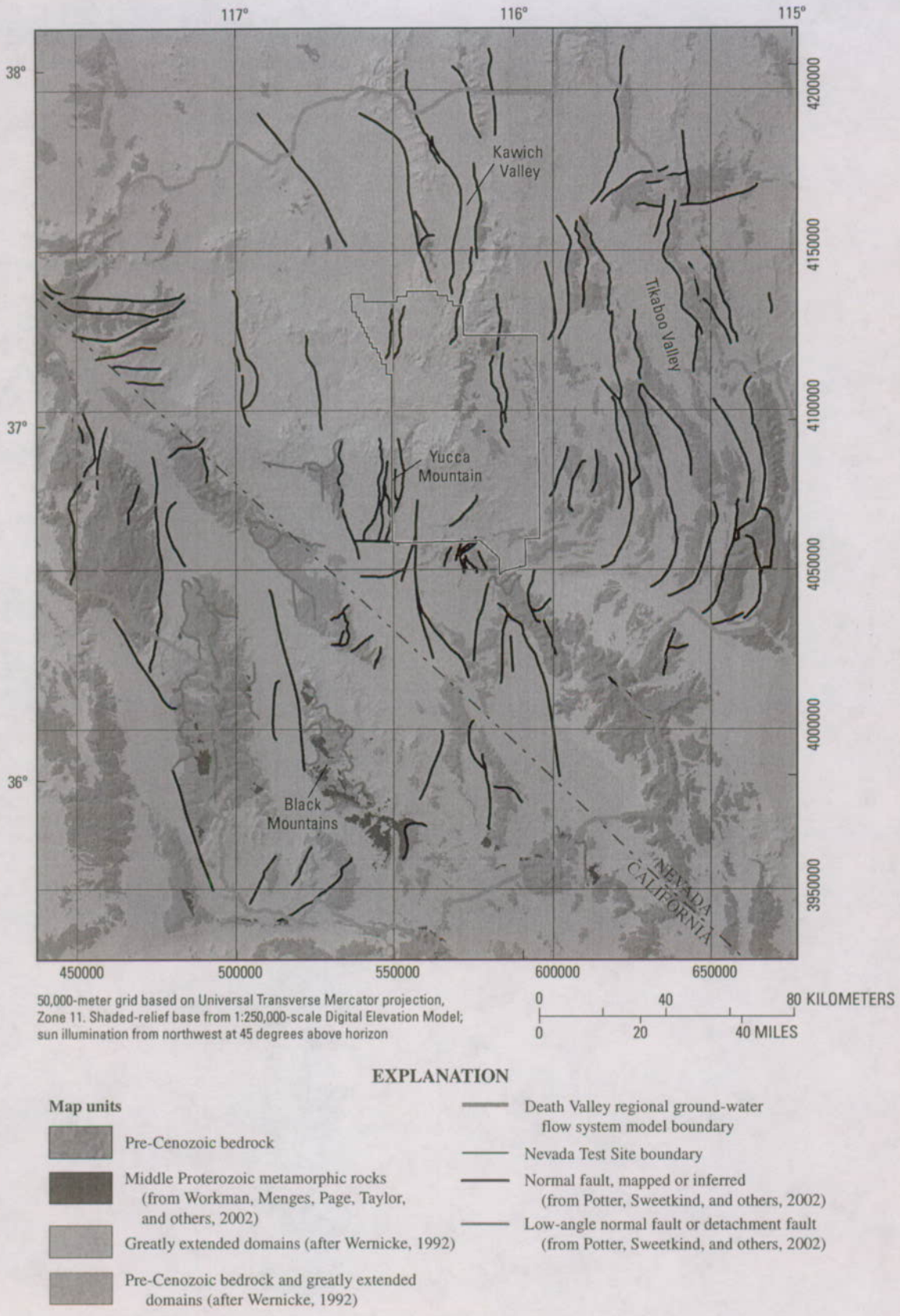

Figure B–6. Normal faults and greatly extended domains of the Death Valley regional ground-water flow system region.

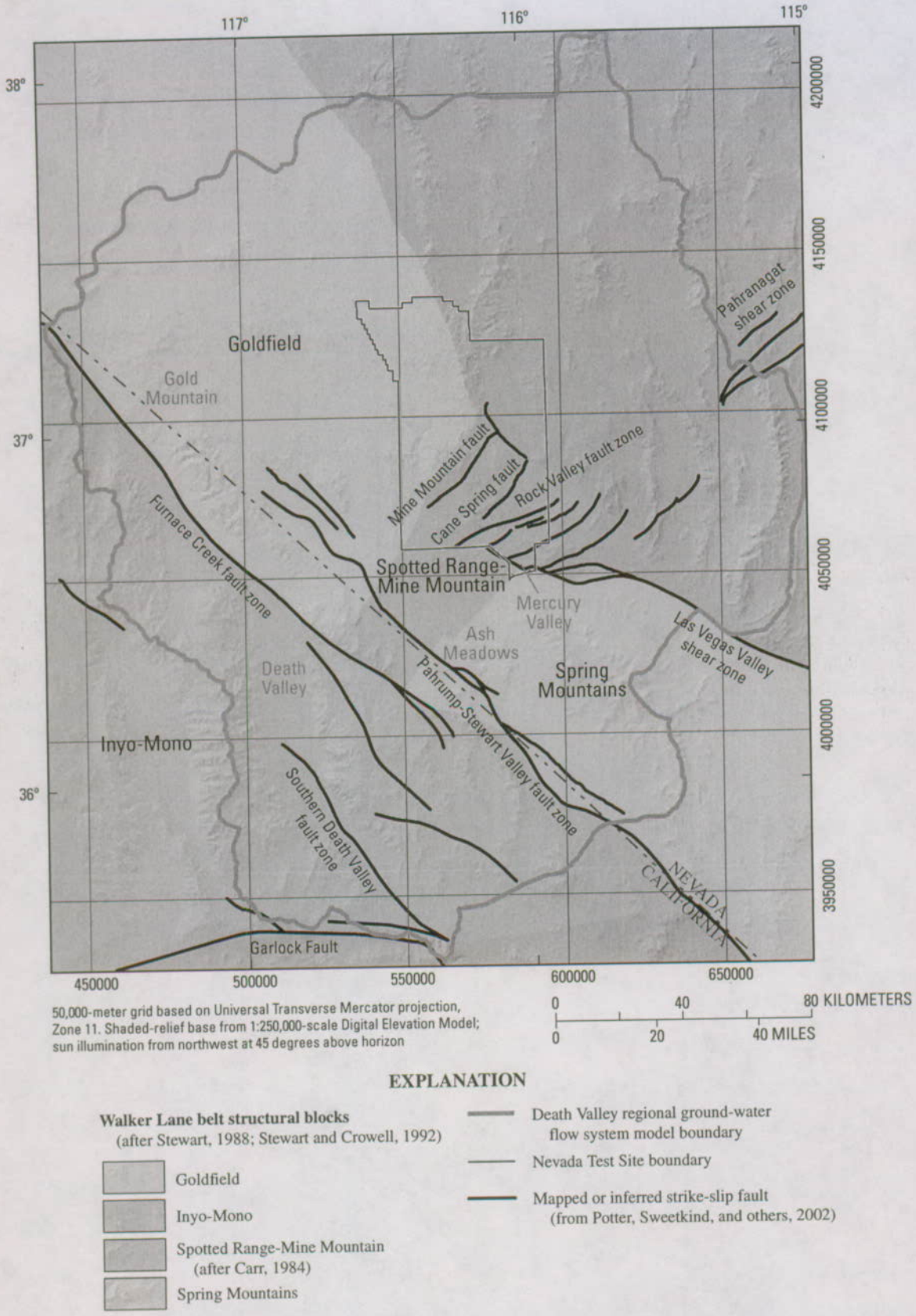

Figure B–7. The Walker Lane belt and strike-slip faults of the Death Valley regional ground-water flow system region.

the lower clastic aquitard (confining unit), composed of Late Proterozoic through Middle Cambrian siliciclastic rocks; the lower carbonate aquifer, composed of Middle Cambrian through Devonian mostly carbonate rocks; the upper clastic aquitard, composed of Devonian and Mississippian siliciclastic rocks; and the upper carbonate-rock aquifer, composed of Pennsylvanian and Permian carbonate rocks which, in the vicinity of the NTS, overlie the rocks of the upper clastic aquitard. Most subsequent tabulations of HGUs and ground-water flow models of the region (Waddell, 1982; Luckey and others, 1996; Laczniak and others, 1996; IT Corporation, 1996a; D'Agnese and others, 1997) have honored these HGU subdivisions of the pre-Cenozoic sedimentary section. For example, table B–1 shows similar treatment of these units in the two recent regional ground-water flow models (IT Corporation, 1996b; D'Agnese and others, 1997).

In contrast to the general consistency in the treatment of the pre-Cenozoic section, a number of approaches have been taken to subdividing the Cenozoic section into HGUs, particularly the volcanic rocks at the NTS. Past approaches have differed in the number of HGUs used and in the treatment of spatially variable material properties in the volcanic-rock units. Winograd and Thordarson (1975; their table 1) assigned the volcanic rocks at the NTS to HGUs based upon lithology and inferred hydrologic significance—for example, tuff aquitard, bedded tuff aquifer, welded tuff aquifer, lava flow aquifer. The geologic units described and their stratigraphic position, however, were based upon older 1960's-era geologic mapping, and the designations did not necessarily account for spatial variability of properties in an HGU. Laczniak and others (1996; their table 1) extended the work of Winograd and Thordarson (1975) to produce a more detailed description of volcanic-rock HGUs in the area around the NTS. The updated designations were based on new volcanic-rock stratigraphic unit assignments (Sawyer and others, 1994); each formation was assigned as a welded tuff aquifer, lava flow aquifer, or tuff confining unit and also designated as to where on the NTS the units were important aquifers or confining units. Both of these studies provided essential descriptions of the volcanic-rock HGUs; however, neither study was sufficiently detailed to define the stratigraphic complexities throughout the DVRFS region and model domain.

The two recent regional ground-water flow models (IT Corporation, 1996a; D'Agnese and others, 1997) differ significantly in how the Cenozoic section of the DVRFS region has been grouped into HGUs, both in terms of the number of units and in how the spatial variability of material properties in the volcanic units is addressed (table B–1, fig. B–8). The volcanic rock HGUs in the YMP/HRMP model (D'Agnese and others, 1997) were based on a hydrogeologic map compilation (Faunt

Table B–1. Hydrogeologic units used in previous U.S. Department of Energy ground-water flow models in the Death Valley region.

[---, unit not used in model]

DOE/NV-UGTA model units (IT Corporation, 1996b)	YMP/HRMP model units (D'Agnese and others, 1997)	Description of geologic unit
AA	QTvf	Basin-fill deposits
AA	QTvf	Playa deposits
AA	QTvf	Lacustrine limestone and spring deposits
VA, VCU, VU	QTv, Tv	Younger Tertiary volcanic rocks
VCU, TSDVS, VU	Tvs	Younger Tertiary sedimentary rocks
TMA, VA	QTv, Tv	Timber Mountain Group
TC, VA	QTv, Tv	Paintbrush Group
TC	QTv, Tv	Calico Hills Formation
VA	QTv, Tv	Wahmonie Formation
TBCU	QTv, Tv	Prow Pass Tuff, Crater Flat Group
TCB	QTv, Tv	Bullfrog Tuff, Crater Flat Group
TBCU	QTv, Tv	Tram Tuff, Crater Flat Group
TBA	QTv, Tv	Belted Range Group
TBCU, TBQ, VCU, VU	QTv, Tv	Older Tertiary volcanic rocks (pre-Belted Range Group)
VCU, TSDVS	Tvs	Older Tertiary sedimentary rocks
---	Mvs	Mesozoic volcanic and sedimentary rocks
LCA3	---	Upper Paleozoic carbonate rocks
UCCU	ECU	Mississippian and Devonian siliciclastic rocks (Eleana Formation and Chainman Shale)
LCA, LCA1	P2	Middle Cambrian through Devonian mostly carbonate rocks
LCCU	P1	Late Proterozoic through Middle Cambrian siliciclastic rocks
LCCU	PCgm	Metamorphic and igneous rocks
---	TJg	Intrusive rocks, undifferentiated

A YMP/HRMP model (D'Agnese and others, 1997)

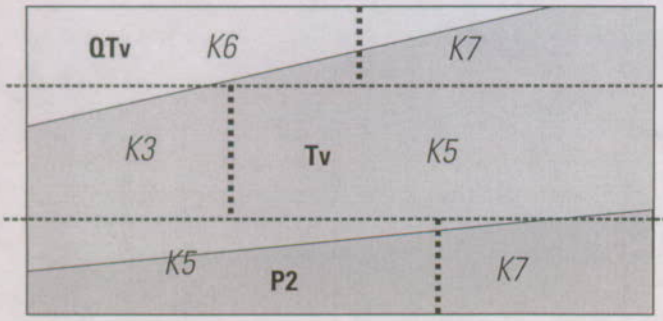

Abbreviations: QTv, Quaternary and Tertiary volcanic rocks; Tv, Tertiary volcanic rocks; P2, Paleozoic carbonate-rock aquifer

HGUs from 3D framework model are discretized into the three layers of the flow model. To approximate the hydrologic effects of spatially varying material properties, different hydraulic conductivities (K3, K5,...) were applied to specific parts of each model layer during flow modeling.

B DOE/NV-UGTA model (IT Corporation, 1996b)

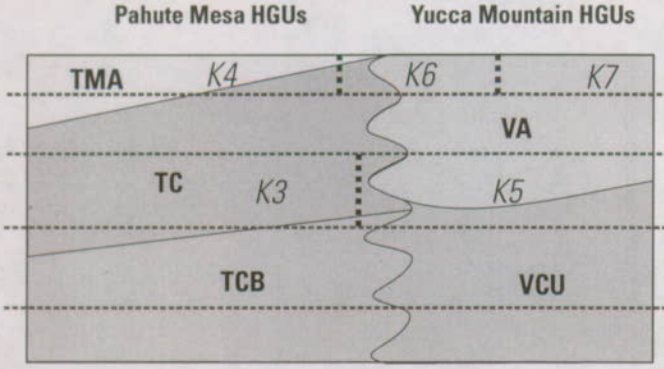

Abbreviations: TMA, Timber Mountain aquifer; TC, Paintbrush tuff cone; TCB, Bullfrog confining unit; VA, volcanic aquifer; VCU, volcanic confining unit

HGUs change for different geographic regions represented in the 3D framework model based on stratigraphic changes in the volcanic section. To approximate the hydrologic effects of spatially varying material properties, different hydraulic conductivities (K3, K4,...) were applied to specific parts of each model layer during flow modeling.

C Current model

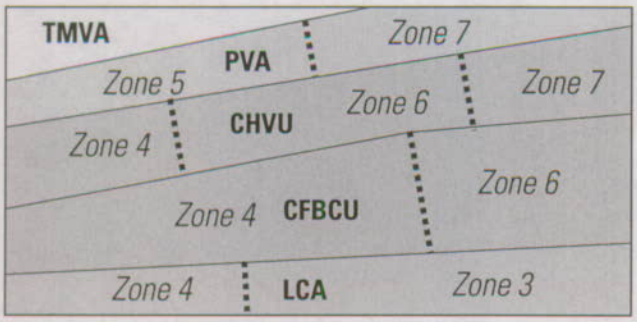

Abbreviations: TMVA, Timber Mountain volcanic aquifer; PVA, Paintbrush volcanic aquifer; CHVU, Calico Hills volcanic unit; CFBCU, Crater Flat–Bullfrog confining unit; LCA, Lower carbonate-rock aquifer

HGUs remain consistently named throughout the 3D framework model and are referenced to geologic map units, geologic cross sections, and borehole logs. Spatially varying material properties based upon geologic judgment are derived for each HGU (zone 1, zone 2...). Assignment of hydraulic conductivities and modification of geologically based zonations are discussed in Chapter F.

Figure B–8. Treatment of hydrogeologic units and spatially varying material properties in previous and current regional models.

and others, 1997) and geologic cross sections (Grose, 1983) in which all volcanic rocks were designated as Tertiary volcanic rocks (Tv) or Tertiary-Quaternary volcanic rocks (QTv) (table B–1). Spatial variability in hydrologic properties in the volcanic-rock section was addressed using zones of variable hydraulic conductivity in the flow model (D'Agnese and others, 1997, 2002) (fig. B–8). The volcanic rock HGUs in the DOE/NV-UGTA model (IT Corporation, 1996b) were based on abundant borehole data from the NTS and are considerably more detailed (table B–1). Spatial variation in the volcanic units was handled in part by developing different HGU schemes for specific parts of the NTS (fig. B–8), with specific aquifers (primarily lava flow and welded tuff) and confining units assigned for each geographic area. Belcher and others (2002) merged these two HGU schemes in the creation of a 3D HFM for the DVRFS region by using the DOE/NV-UGTA model (IT Corporation, 1996b) HGUs in the immediate vicinity of the NTS and the volcanic-rock HGUs of the YMP/HRMP model (D'Agnese and others, 1997) outside of the NTS. This HFM was used as input for a steady-state prepumping ground-water flow model of the DVRFS region (D'Agnese and others, 2002).

Volcanic-rock HGUs for the current model (fig. B–8) remain consistently named throughout the entire HFM and are defined by group-level stratigraphic designations that are based on recent geologic map compilations (Slate and others, 2000; Workman, Menges, Page, Taylor, and others, 2002), geologic cross sections (Sweetkind, Dickerson, and others, 2001), and borehole lithologic data. The spatial variability of material properties is defined for each volcanic-rock HGU on geologic grounds, discussed herein.

Description of Hydrogeologic Units

The unconsolidated sediments and consolidated rocks of the DVRFS region have been subdivided into 25 HGUs (table B–2). These HGUs are based primarily on the work of Laczniak and others (1996). Lithologically similar HGUs are discussed together in this section. In general, HGUs whose abbreviated names end in the letter "A", such as LCA, are considered aquifer units; those names ending in "CU" are considered confining units, and those ending in "U" are units that can function either as aquifers or confining units. These designations are only generally applicable because almost all of the HGUs have spatially varying material and hydraulic properties throughout the DVRFS region.

Unconsolidated Cenozoic Basin-Fill Sediments and Local Young Volcanic Rocks

Unconsolidated Cenozoic basin-fill sediments consist of coarse-grained alluvial and colluvial deposits, fine-grained basin axis deposits, and local lacustrine limestones and spring discharge deposits and are divided into six HGUs. Relatively local basaltic- and rhyolitic-lava flows and tuffs form another HGU. All seven of these HGUs are defined on the basis of geologic map data from a 1:250,000-scale geologic compilation of the DVRFS region (Workman, Menges, Page, Taylor, and others, 2002) (fig. B–9). The age terms "younger" and "older" in the names of the alluvial aquifer and confining unit HGUs refer to the relative ages of mapped surficial-deposit units, as described by Workman, Menges, Page, Taylor, and others (2002).

Younger and Older Alluvial Aquifers (YAA and OAA)

Coarse-grained surficial units are included in the younger alluvial aquifer (YAA) and the older alluvial aquifer (OAA). The YAA and OAA consist of Holocene to Pliocene alluvium, colluvium, and minor eolian and debris-flow sediments associated with alluvial geomorphic surfaces (Swan and others, 2001; Potter, Dickerson and others, 2002). In general, fluvial deposits are predominant sandy gravel with interbedded gravelly sand and sand, whereas alluvial fans have a more gradational decrease in grain size from proximal to distal fan. Local eolian accumulations consist of Holocene sand sheets or dune fields or relict upper to middle Pleistocene sand-ramp deposits that are banked along the flanks of some ranges. Sediments generally are not cemented but are more indurated with increasing depth. These HGUs tend to be aquifers, but finer grained sediments and intercalated volcanic rocks locally can impede ground-water movement.

Younger and Older Alluvial Confining Units (YACU and OACU)

The alluvial confining units (YACU and OACU) consist of Holocene to Pliocene fine-grained basin-axis deposits. These units consist of late Holocene playa and (or) salt-pan deposits that are commonly underlain by older playa or lacustrine sequences of middle to early Holocene and Pleistocene age. These rocks typically are mixtures of moderately to well stratified silt, clay, and fine sand. The thickness is poorly constrained but may range from 1 to 10 m for Holocene deposits and may be greater than 300 m for the older deposits (Workman, Menges, Page, Taylor, and others, 2002).

Limestone Aquifer (LA)

The limestone aquifer (LA) consists of Holocene to Pliocene lacustrine and spring deposits that are interfingered with the alluvial basin-fill units. Typically, these are dense, crystalline deposits of limestone or travertine. The hydrologic properties of these deposits can differ greatly over short distances because of abrupt changes in grain size, fracturing, and consolidation. These deposits can be productive local aquifers, such as in parts of the Amargosa Desert. In general, the LA does not crop out and is identified only from drill holes in the basin-filling units.

Table B–2. Geologic and hydrogeologic units of the Death Valley regional ground-water flow system (DVRFS) model.

[SWNVF, southwestern Nevada volcanic field]

Hydrogeologic unit abbreviation and name	Age and description of geologic units
Unconsolidated Cenozoic basin-fill sediments and local younger volcanic rocks	
YAA; Younger alluvial aquifer	Pliocene to Holocene coarse-grained basin-fill deposits
YACU; Younger alluvial confining unit	Pliocene to Holocene playa and fine-grained basin-fill deposits
OAA; Older alluvial aquifer	Pliocene to Holocene coarse-grained basin-fill deposits
OACU; Older alluvial confining unit	Pliocene to Holocene playa and fine-grained basin-fill deposits
LA; Limestone aquifer	Cenozoic limestone, undivided
LFU; Lava-flow unit	Cenozoic basalt cones and flows and surface outcrops of rhyolite-lava flows
YVU; Younger volcanic-rock unit	Cenozoic volcanic rocks that overlie the Thirsty Canyon Group
Consolidated Cenozoic basin-fill deposits	
Upper VSU; Volcanic- and sedimentary-rock unit (upper)	Cenozoic volcanic and sedimentary rocks, undivided, that overlie volcanic rocks of SWNVF
Lower VSU; Volcanic- and sedimentary-rock unit (lower)	Cenozoic volcanic and sedimentary rocks, undivided; where named Cenozoic volcanic rocks exist, lower VSU underlies them.
Cenozoic volcanic rocks of the southwestern Nevada volcanic field	
TMVA; Thirsty Canyon–Timber Mountain volcanic-rock aquifer	Miocene Thirsty Canyon and Timber Mountain Groups, plus Stonewall Mountain tuff, undivided
PVA; Paintbrush volcanic-rock aquifer	Miocene Paintbrush Group
CHVU; Calico Hills volcanic-rock unit	Miocene Calico Hills Formation
WVU; Wahmonie volcanic-rock unit	Miocene Wahmonie and Salyer Formations
CFPPA; Crater Flat–Prow Pass aquifer	Miocene Crater Flat Group, Prow PassTuff
CFBCU; Crater Flat–Bullfrog confining unit	Miocene Crater Flat Group, Bullfrog Tuff
CFTA; Crater Flat–Tram aquifer	Miocene Crater Flat Group, Tram Tuff
BRU; Belted Range unit	Miocene Belted Range Group
OVU; Older volcanic-rock unit	Oligocene to Miocene; near the Nevada Test Site consists of all volcanic rocks older than the Belted Range Group. Elsewhere, consists of all tuffs that originated outside of the SWNVF.
Hydrogeologic units associated with Mesozoic, Paleozoic and Late Proterozoic sedimentary rocks	
SCU; Sedimentary-rock confining unit	Paleozoic and Mesozoic sedimentary and volcanic rocks
UCA; Upper carbonate-rock aquifer	Paleozoic carbonate rocks (UCA only used where UCCU exists, otherwise UCA is lumped with LCA)
UCCU; Upper clastic-rock confining unit	Upper Devonian to Mississippian Eleana Formation and Chainman Shale
LCA; Lower carbonate-rock aquifer	Cambrian through Devonian predominantly carbonate rocks
LCCU; Lower clastic-rock confining unit	Late Proterozoic through Lower Cambrian primarily siliciclastic rocks (including the Pahrump Group and Noonday Dolomite)
Hydrogeologic units associated with crystalline metamorphic rocks and plutons	
XCU; Crystalline-rock confining unit	Early Proterozoic metamorphic and igneous rocks and metamorphosed Middle and Late Proterozoic sedimentary rocks
ICU; Intrusive-rock confining unit	All intrusive rocks, regardless of age

Lava-Flow Unit (LFU)

The lava-flow unit (LFU) consists of local Neogene (generally 11 Ma and younger) basalt- and rhyolite-lava flows in the DVRFS region. Pliocene and Pleistocene volcanism on the NTS is expressed by isolated, relatively small basaltic cinder cones and associated lava flows. The eruptive style and chemical composition of the basalts is typical of Pliocene and Pleistocene basalts throughout most of the western part of the Basin and Range province (Hedge and Noble, 1971). They probably represent the waning stages of regional volcanism that peaked around 11 Ma.

Basalts of about 10 Ma in the vicinity of the NTS include lava flows on Skull Mountain and Little Skull Mountain, the southern part of Crater Flat, Black Mountain and to the west of the NTS (fig. B–9). Basalts of similar ages are part of the Funeral Formation in the Furnace Creek basin (Cemen and others, 1985; Greene, 1997; Wright and others, 1999). The LFU also includes volcanic rocks of the Towne Pass area and west of the model domain in the Darwin plateau. Younger basalts in the Amargosa Desert and in the southeast part of Crater Flat include an approximately 3.7-Ma event (Crowe and others, 1995) that is characterized by basalt-lava flows and exposed dikes along a north-trending

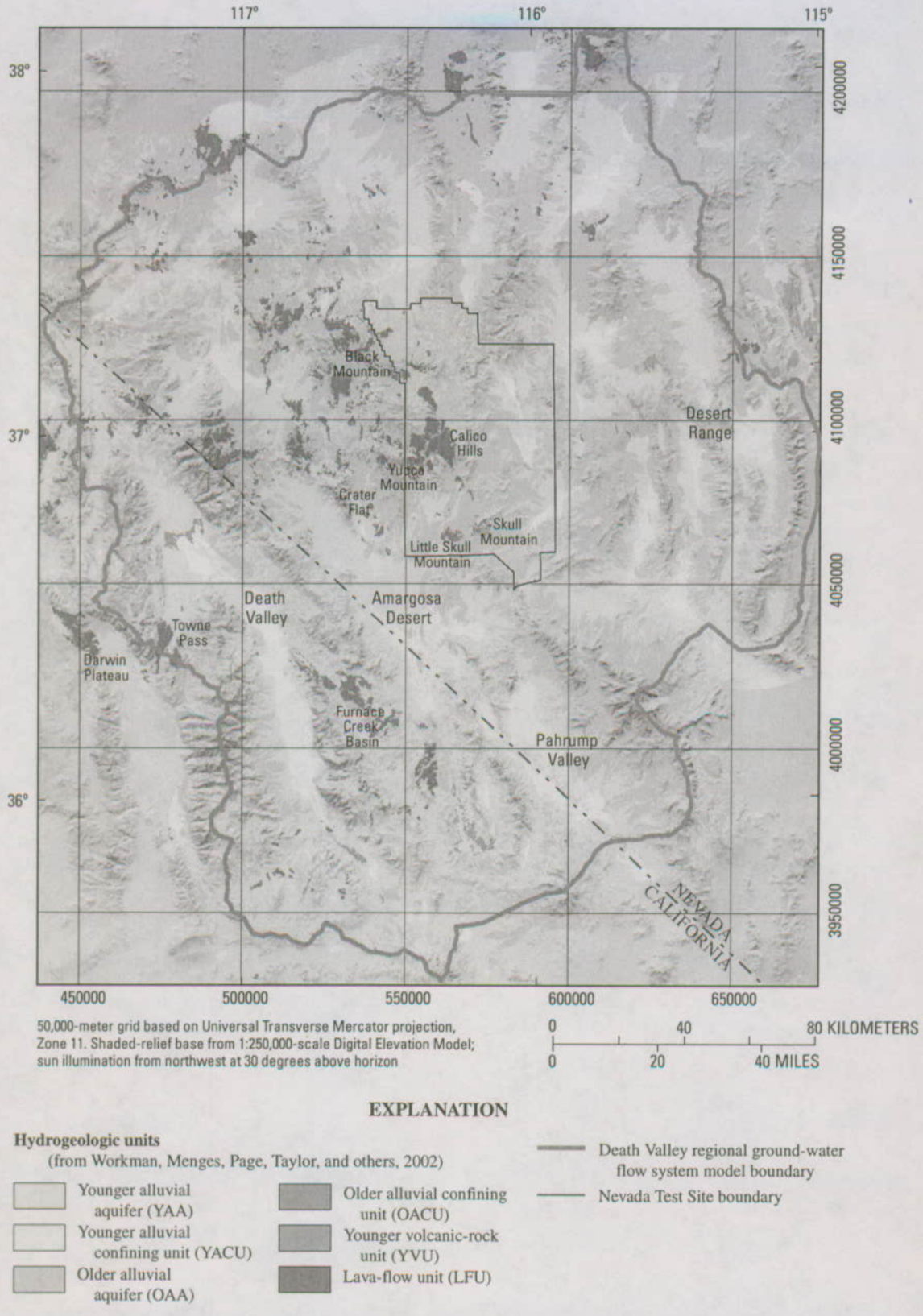

Figure B–9. Outcrop distribution of hydrogeologic units associated with alluvial sediments and local young volcanic rocks.

alignment of vents, four 1.0-Ma cinder cones that form a slightly curved north-northeast alignment in Crater Flat, and a single cinder cone (Lathrop Wells cone, 77.76 ka, Heizler and others, 1999) at the southern end of Yucca Mountain. Aeromagnetic anomalies and local basaltic float are evidence for shallowly buried basalt flows at several locations in the northern part of Amargosa Desert (O'Leary and others, 2002).

The LFU also includes Miocene rhyolite-lava flows in the northern part of Yucca Mountain and the Calico Hills, where they form extensive surface outcrops (fig. B–9). Individual lava flows are not laterally extensive. Because the LFU is typically above the water table, the unit is not a regional aquifer.

Younger Volcanic-Rock Unit (YVU)

The younger volcanic-rock unit (YVU) consists of Neogene (mostly 15 to 11 Ma) tuffs and other volcanic rocks that are not associated with sources in the SWNVF. Individual units are not laterally extensive, such as the isolated exposures of Kane Wash Tuff to the north of the Desert Range (fig. B–9); these are outliers of much more extensive volcanic outcrops that lie to the northeast of the model domain (Ekren and others, 1977). Most of the unit lies above the water table and is thought to have limited influence on ground-water flow in the DVRFS region.

Consolidated Cenozoic Basin-Fill Deposits—Volcanic- and Sedimentary-Rock Unit (VSU)

The volcanic- and sedimentary-rock unit (VSU) (fig. B–10) consists of all Cenozoic basin-filling sedimentary and volcanic rocks, except for the named volcanic-rock units in the vicinity of the SWNVF and the alluvial HGUs discussed previously. Consolidated Cenozoic basin-fill units of the DVRFS region range from late Eocene to Pliocene in age and generally underlie the more recent alluvial sediments assigned to the alluvial aquifers and confining units described herein. They consist of a broad range of both volcanic and sedimentary rocks including lavas, welded and nonwelded tuffs, and alluvial, fluvial, colluvial, eolian, paludal, and lacustrine sediments. Cenozoic volcanic and sedimentary rocks in the DVRFS region may be generalized into three sequences according to their relation to the tectonic evolution of the region (Snow and Lux, 1999): (1) an early extensional sequence that generally predates the formation of basin-range topography; (2) a synextensional and synvolcanic sequence that corresponds to the major period of formation of basin-range topography in this region and to the peak of volcanic activity in the southwestern Nevada and central Death Valley volcanic fields; and (3) a 6-Ma to present, late extensional to post-extensional sequence. This general subdivision is similar to that used by Ekren and others (1977) and Workman, Menges, Page, Taylor, and others (2002) and is more clearly documented in Fridrich and others (2000).

Rocks in the early extensional sequence are late Eocene to Miocene in age and have variable thickness and facies, and their distribution is discontinuous, probably because they were deposited on the irregular pre-Cenozoic erosional surface. Many of these rocks were deposited in a fluvio-lacustrine regime. Included in this sequence are the Titus Canyon Formation along the east side of the Funeral and Grapevine Mountains (Reynolds, 1974; Wright and Troxel, 1993), sedimentary rocks informally called the "rocks of Winapi Wash" that occur in and near the NTS, 25- to 14-Ma sedimentary strata including the Rocks of Pavits Spring in the vicinity of the NTS (Slate and others, 2000), and unnamed units widely exposed in and around the Grapevine Mountains and the Funeral Mountains.

Rocks in the synextensional and synvolcanic sequence are middle Miocene in age and include such units as the Artist Drive Formation in the Furnace Creek Basin and similar sedimentary rocks that probably underlie parts of the Amargosa Desert, Pahrump Valley, and Death Valley. Middle Miocene synextensional sedimentary rocks consist of coarse, tuffaceous clastic types, locally derived megabreccias, and tuffaceous sandstone locally interbedded with lavas that range in composition from basalt through rhyolite. The geology and stratigraphic relations of these middle Miocene rocks are discussed by Cemen and others (1985), Greene (1997), and Wright and others (1999).

Also included in the synextensional and synvolcanic sequence are the volcanic rocks of the central Death Valley volcanic field and volcanic rocks around the margins of the SWNVF that have not been correlated to a specific unit. Volcanic rocks of the central Death Valley volcanic field consist of predominantly silicic- to intermediate-composition lava flows and associated fallout tephra (Wright and others, 1991). Only one relatively widespread welded ash-flow tuff, the Rhodes Tuff, is recognized in the volcanic field (Wright and others, 1991); most of the volcanic-rock units appear to be associated with local source areas and have limited areal distribution (Wright and others, 1991). The general absence of strong magnetic anomalies in the vicinity of the Amargosa Desert between the SWNVF and the central Death Valley volcanic field implies that strongly magnetic volcanic rocks from either volcanic field are thin or absent (Carr, 1990; Blakely and others, 2000).

Rocks of the late extensional to post-extensional sequence include units such as the Funeral Formation of the Furnace Creek Basin that were deposited mostly in restricted, intermontane basins that developed as extension progressed (Snow and Lux, 1999). Synextensional sedimentary rocks were deposited during this time in the Nova basin on the western side of the Panamint Mountains (Hodges and others, 1989).

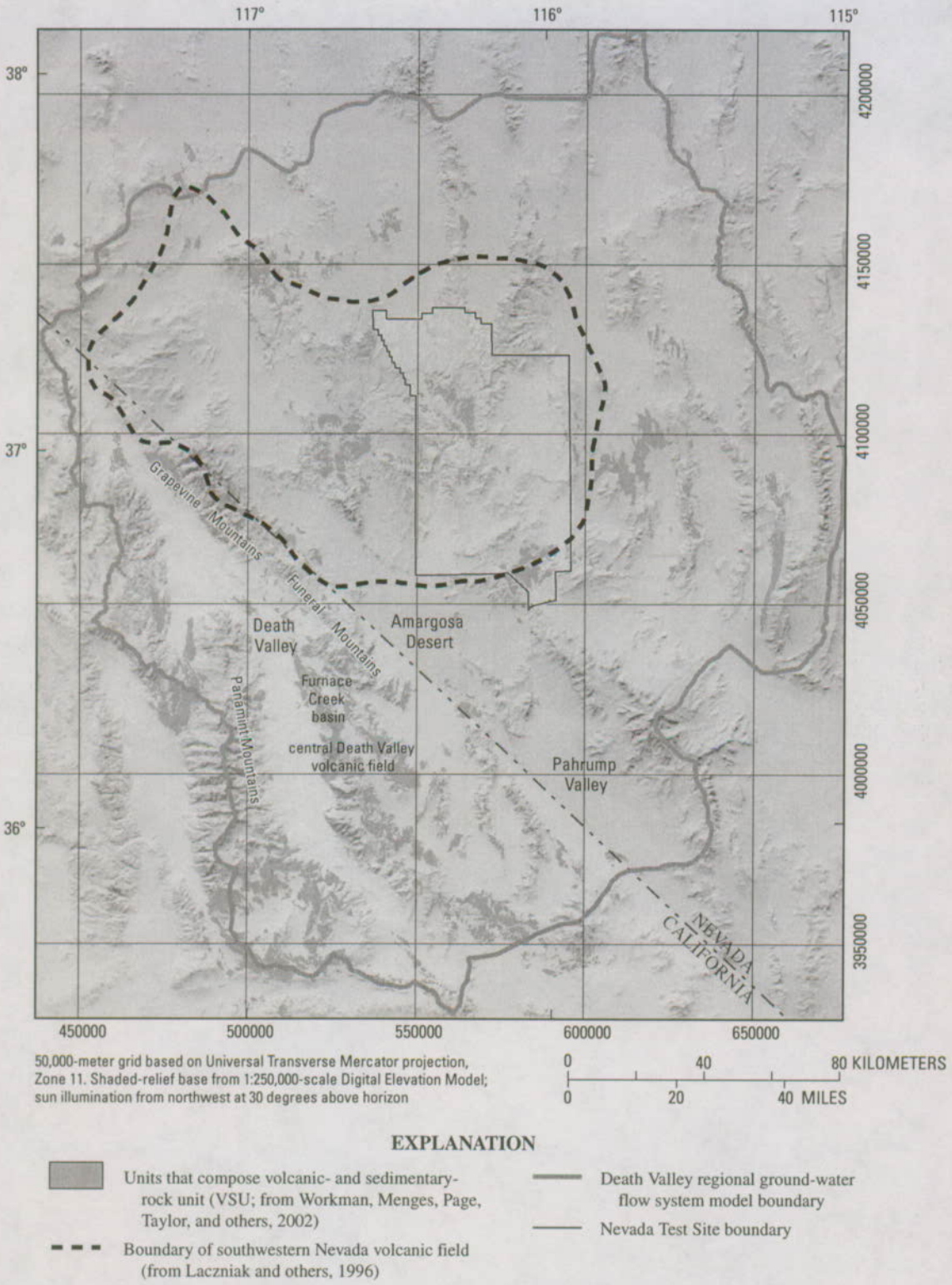

Figure B–10. Outcrop distribution of the volcanic- and sedimentary-rock unit (VSU).

The VSU is lithologically diverse and rock types are complexly interfingered. For example, interpreted lithologic data from boreholes in the southern part of the Amargosa Desert (fig. B–11) reveal a heterogeneous basinfill with few lithologically similar intervals that can be correlated between adjacent boreholes. Interpolation of lithologic data between boreholes indicates complex interfingering of basin-fill lithologies (Oatfield and Czarnecki, 1989). In order to generalize the basin-fill lithologic diversity for use in a regional model, Sweetkind, Fridrich, and Taylor (2001) delineated regional facies trends on the basis of borehole and outcrop data. Five zones of potential hydrologic significance were defined on the basis of the relative amounts of coarse- and fine-grained sedimentary rocks compared to volcanic rocks at each locality (fig. B–12). Mapped zones (fig. B–12) do not imply the existence of the VSU throughout the region; rather, they are a guide to which set of material properties applies where the VSU exists in the 3D HFM (Chapter E, this volume).

In order for units to stack correctly when constructing a 3D HFM of the DVRFS region (Chapter E, this volume), the VSU was divided into two units. The lower VSU consists of those rocks that underlie these named volcanic rocks (table B–3); the upper VSU consists of those rocks that overlie the named volcanic rocks of the SWNVF (table B–4). Outside of the SWNVF, the boundary between the two units is arbitrary. Upper VSU hydrogeologic zones are delineated by their relation to aquifer and confining units in the overlying basin-fill material.

Volcanic Rocks of the Southwestern Nevada Volcanic Field

Volcanic rocks that emanated from the SWNVF are widely distributed in the west-central part of the DVRFS region; associated caldera collapse structures of the SWNVF dominate the northwestern and west-central parts of the NTS (fig. B–13). Volcanism associated with the SWNVF occurred episodically between about 15 and 9 Ma (Byers, Carr, Orkild, and others, 1976; Sawyer and others, 1994). Eruption of voluminous, extensive ash-flow-tuff sheets resulted in the collapse of at least seven known calderas, two of which overlapped to form the Silent Canyon caldera complex (SCCC), and three of them overlapped or were nested to form the Timber Mountain caldera complex (TMCC) and the Claim Canyon caldera. The sources of many of the older ash-flow tuffs remain uncertain because associated calderas have been buried or destroyed by younger calderas. Volumetrically subordinate, but related, silicic-lava flows and minor pyroclastic flows were erupted from the calderas and from isolated volcanic vents in the field (Sawyer and others, 1994). Numerous authoritative sources exist for more detailed information on the volcanic rocks (Byers, Carr, Orkild, and others, 1976; Christiansen and others, 1977; Carr, Byers, and Orkild, 1986; Sawyer and Sargent, 1989; Ferguson and others, 1994; Sawyer and others, 1994), and for a number of geologic-map compilations that portray the volcanic rocks at the NTS (Byers, Carr, Christiansen, and others 1976; Frizzell and Shulters, 1990; Wahl and others, 1997; Slate and others, 2000).

The volcanic-rock units of the SWNVF are important hydrogeologic units because they are thick enough in the vicinity of the NTS to be important subregional aquifers, and a number of nuclear weapons tests were conducted in the volcanic rocks at Rainier Mesa and Pahute Mesa at the NTS. The proposed high-level radioactive waste repository at Yucca Mountain on the western edge of the NTS would be located in these volcanic rocks.

Volcanic rocks of the SWNVF consist of the pre-Belted Range Group rocks, the Belted Range and Crater Flat Groups, the Calico Hills and Wahmonie Formations, the Paintbrush, Timber Mountain, and Thirsty Canyon Groups, and the Stonewall Mountain Tuff. The volcanic-rock units are divided at the group level into nine HGUs, except for the Crater Flat Group (table B–2). In order to maintain consistency with the Yucca Mountain 3D geologic framework model (YMP-GFM) (Bechtel SAIC Company, 2002), the Crater Flat Group is subdivided at the formation level with separate HGUs for the Prow Pass, Bullfrog, and Tram Tuffs (table B–2).

Method for Assigning Material Property Variations to Hydrogeologic Units of the Southwestern Nevada Volcanic Field

The Cenozoic volcanic rocks of the SWNVF have varying degrees of both fracture and matrix permeability. Most of the crystallized and densely welded tuffs have very low matrix permeabilities (Montazer and Wilson, 1984); consequently, fracture networks and faults are the primary pathways for gas and water flow through the welded parts of the rock mass. Poorly welded to nonwelded ash-flow tuffs and ash-fall tuff, reworked tuff, and volcaniclastic rocks have higher matrix permeabilities but poorly developed and connected fracture networks. Fracture-dominated flow in the welded portions of the tuffs of the SWNVF changes to matrix-dominated flow in the comparatively unfractured units (Blankennagel and Weir, 1973; Montazer and Wilson, 1984; Laczniak and others, 1996). Alteration of rock-forming minerals to zeolite, clay, carbonate, silica, and other minerals, most prevalent in nonwelded rocks, can reduce permeability.

At the group and formation level, mapped volcanic-rock units commonly display widely variable lithology and degree of welding both vertically and horizontally (fig. B–14). The hydraulic properties of these deposits depend mostly on the mode of eruption and cooling, by the extent of primary and secondary fracturing, and by the degree to which secondary alteration (crystallization of volcanic glass and zeolitic alteration) has affected primary permeability. Fractured rhyolite-lava flows and moderately to densely welded ash-flow tuffs are the principal volcanic-rock aquifers. Rhyolite-lava flows and thick intracaldera welded tuff (fig. B–15*A*) are relatively restricted areally, whereas outflow welded-tuff sheets are more

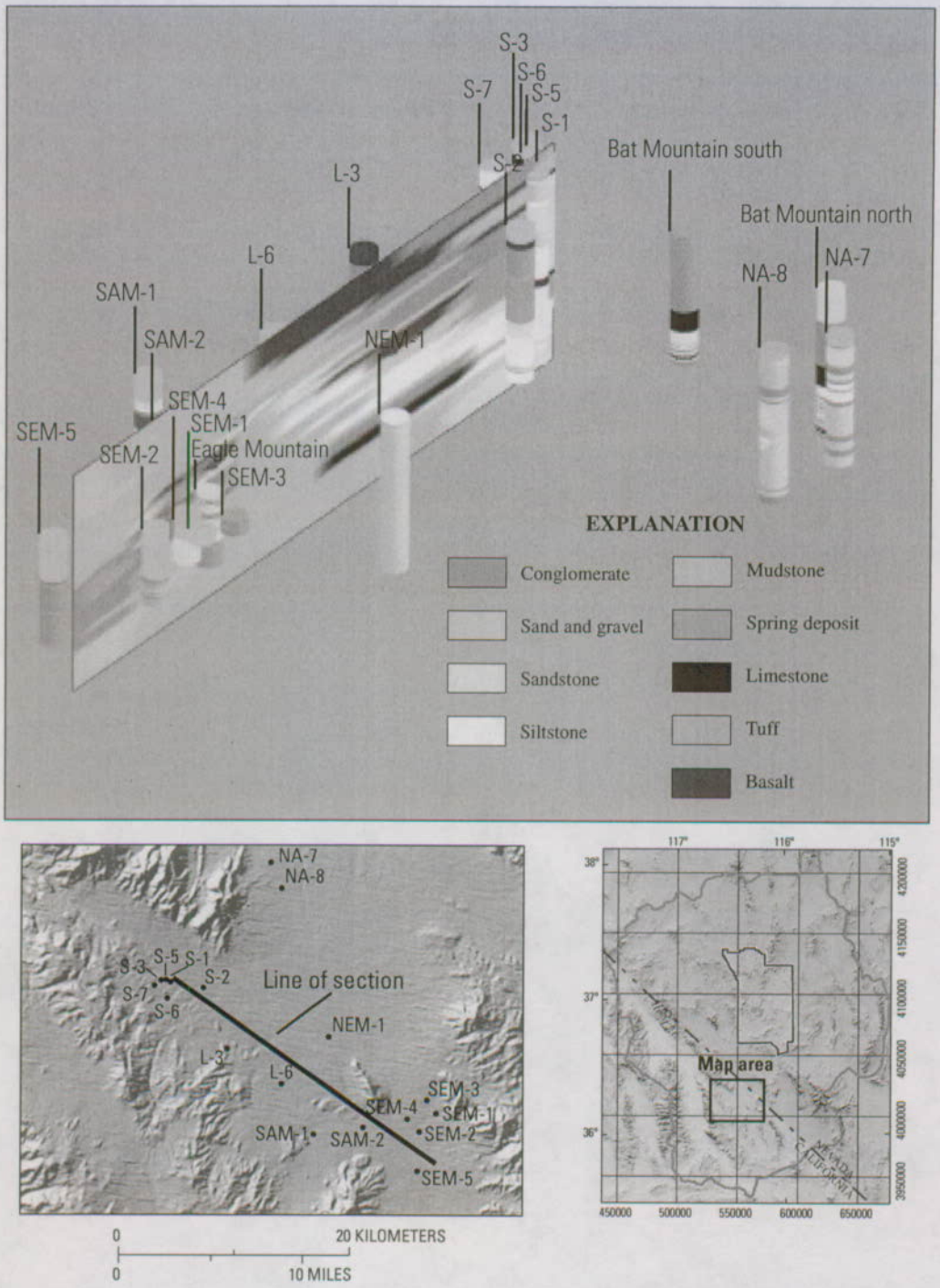

Vertical panel is a slice through a three-dimensional rock properties model of basin-filling deposits corresponding to the lower volcanic- and sedimentary-rock hydrogeologic unit (lower VSU) beneath the Amargosa Desert. Model was created by numerical interpolation of borehole lithologic data from the southern Amargosa Desert. Cylinders represent the location and drilled depth of boreholes; colors represent lithologic units penetrated by the boreholes. View is to the southwest. Cross section panel is approximately 25 kilometers long and 1 kilometer deep. With the exception of thin surficial units, the various lithologic units penetrated by all of the boreholes shown correspond to hydrogeologic unit lower VSU.

Figure B–11. Lithologic variability in the volcanic- and sedimentary-rock unit (VSU).

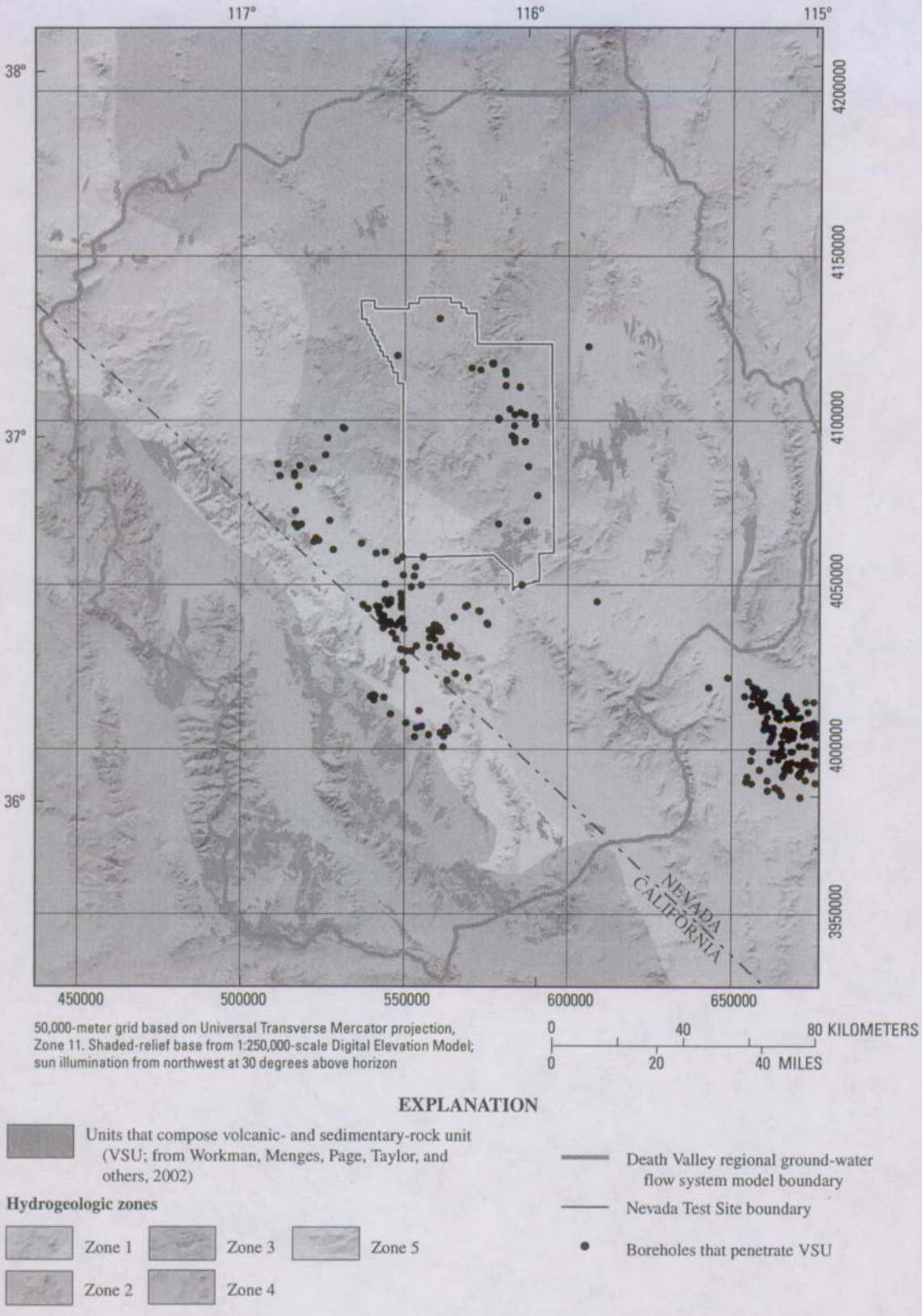

Figure B–12. Hydrogeologic zones in the volcanic- and sedimentary-rock unit (VSU).

Table B–3. Hydrogeologic zones in the lower volcanic- and sedimentary-rock unit (lower VSU).

[SWNVF, southwestern Nevada volcanic field]

Zone number	Description
1	Fluvial and lacustrine sedimentary rocks with few or no volcanic units. Mostly fine-grained deposits.
2	VSU in and to the north of the SWNVF includes Cenozoic sedimentary rocks that may underlie the volcanic section. Volcanic rocks penetrated by boreholes may be lumped with the underlying sedimentary rocks in some places.
3	Coarse gravels and megabreccias.
4	This zone consists of the volcano-sedimentary trough that incorporates the central Death Valley volcanic field and the Furnace Creek Basin. Stratigraphic successions are a mixed assemblage of coarse and fine sedimentary rocks and basalt- and rhyolite-lava flows and minor ash-flow tuff.
5	Stratigraphic successions in this zone are similar only in the diversity of their lithologies. Sedimentary rocks consist of coarse-and fine-grained alluvial deposits, lacustrine and playa deposits, fluvially reworked tuffs, and tuffaceous sedimentary rocks that span an age range from Oligocene to the Pliocene. Volcanic rocks are present in the northeastern and southwestern parts of the zone.

regionally distributed and may provide lateral continuity for water to move through the regional flow system. The confining units are formed generally by nonwelded or partly welded tuff that has low fracture permeability (fig. B–15*B*) and can be zeolitically altered in the older, deeper parts of the volcanic sections (Laczniak and others, 1996). The hydraulic properties of the volcanic rocks underlying Pahute Mesa were described by Blankennagel and Weir (1973); analysis of additional volcanic rock material and hydraulic properties (Belcher and others, 2001) indicates that these concepts may apply throughout the SWNVF.

For each of the volcanic-rock HGUs of the SWNVF, zones of potential enhanced and reduced permeability (termed hydrogeologic zones) were evaluated on the basis of lithologic and material property information available from boreholes (Warren and others, 1999) and surface localities (R.M. Drake, U.S. Geological Survey, written commun., 2001). At each location, the percentage of welded, fractured rock and percentage of altered rock were calculated by dividing the aggregate thickness of brittle (welded-tuff and lava-flow lithologies) or altered rock, respectively, by the total thickness of the HGU (R.M. Drake, written commun., 2001). The brittle rock and alteration data were interpolated and extrapolated from the available data over the modeled spatial extent of each HGU (see Chapter E, this volume) to produce gridded surfaces of these respective properties. Areas with greater than 50 percent brittle rock were considered potential enhanced permeability zones, whereas areas with less than 50 percent brittle rock were considered potential reduced permeability zones (table B–5). Areas with greater than 60 percent altered rock were considered potential reduced permeability zones, while areas with less than 60 percent altered rock were considered potential enhanced permeability zones (table B–5). The brittle rock and alteration characteristics were combined to produce four types of zones: brittle rock that is not altered; brittle, altered rock; nonbrittle rock that is altered; and nonbrittle rock that is unaltered. Zones with a combination of a high percentage of brittle rock and a small degree of alteration are inferred to have enhanced permeability (zone 1, table B–5); zones with a combination of a low percentage of brittle rock and a high degree of alteration are inferred to have reduced permeability (zone 3, table B–5). The combined effects of fracturing and alteration on permeability are less predictable for highly altered brittle rocks (zone 2, table B–5) and unaltered nonbrittle rocks (zone 4, table B–5). Mapped zones do not imply the existence of each HGU throughout the zone; rather, they are a guide to which set of material properties applies where the HGU exists in the 3D HFM (Chapter E, this volume).

Table B–4. Hydrogeologic zones in the upper volcanic- and sedimentary-rock unit (upper VSU).

Zone number	Description
1	Upper VSU underlying the younger alluvial confining unit (YACU) and older alluvial confining unit (OACU)
2	Upper VSU underlying the older alluvial aquifer (OAA) and younger alluvial aquifer (YAA)

Volcanic-Rock Hydrogeologic Units of the Southwestern Nevada Volcanic Field

Thirsty Canyon–Timber Mountain Volcanic-Rock Aquifer (TMVA)

The Thirsty Canyon–Timber Mountain volcanic-rock aquifer (TMVA) is composed of the volcanic rocks of the 11.6- to 11.45-Ma Timber Mountain Group, the 9.4- to 9.15-Ma Thirsty Canyon Group, and the 7.5-Ma Stonewall Flat Tuff (Sawyer and others, 1994; Slate and others, 2000). Volcanic activity in the SWNVF peaked volumetrically with the eruption of the Timber Mountain Group ash-flow tuffs, which were erupted from the TMCC (Christiansen and Lipman, 1965; Byers, Carr, Orkild, and others, 1976; Byers, Carr, Christiansen, and others, 1976; Christiansen and others, 1977; Sawyer and others, 1994). The TMCC consists of the Rainier Mesa caldera, which formed as a result of the eruption of the 11.6-Ma Rainier Mesa Tuff, and the Ammonia Tanks caldera, which formed as a result of the eruption of the 11.45-Ma Ammonia Tanks Tuff (Sawyer and others, 1994;

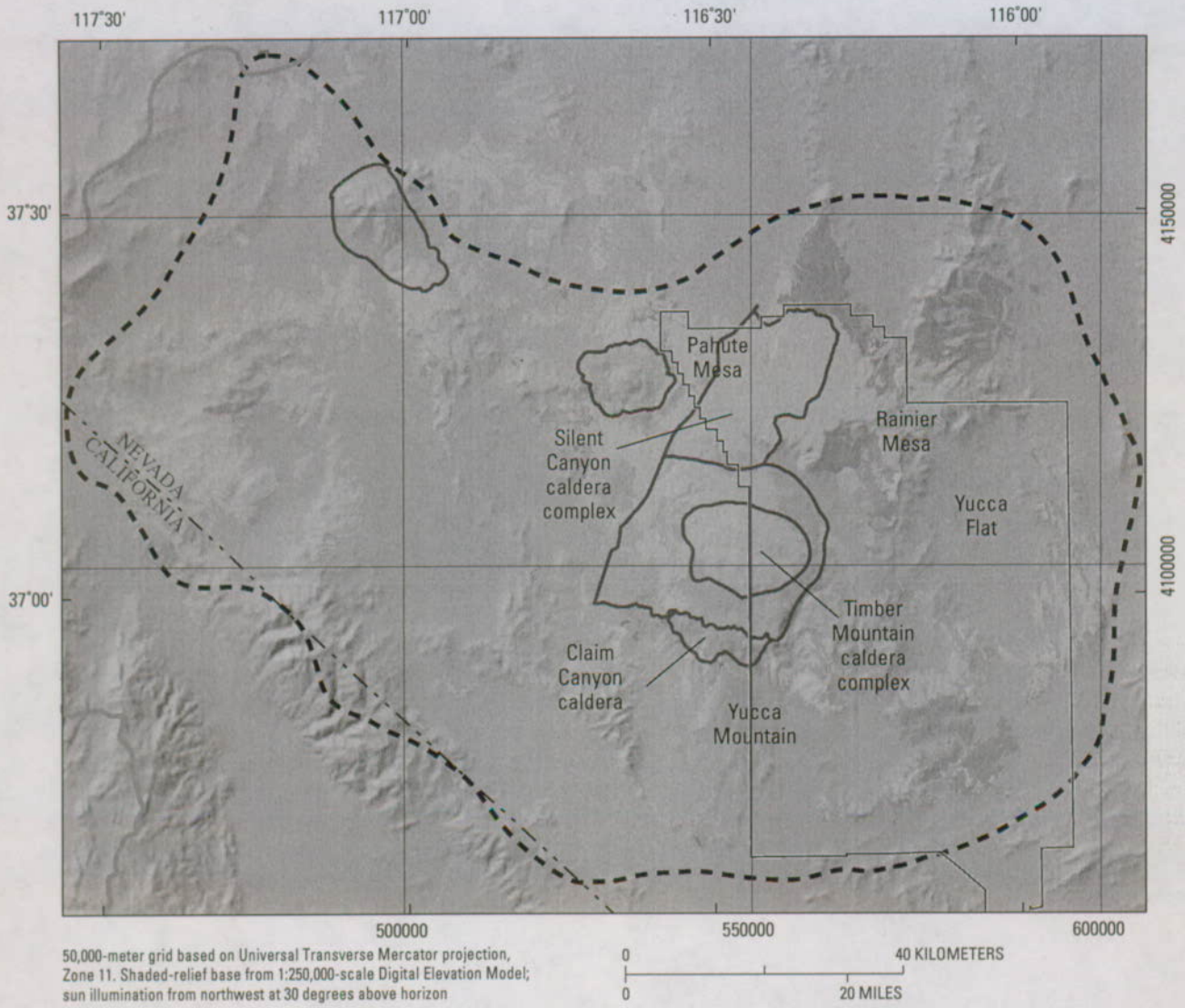

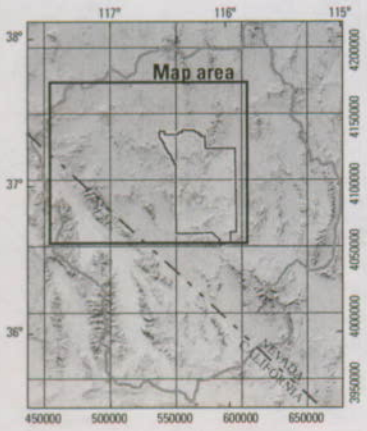

EXPLANATION

Hydrogeologic units
(Workman, Menges, Page, Taylor, and others, 2002)

- Thirsty Canyon–Timber Mountain volcanic-rock aquifer (TMVA)
- Paintbrush volcanic-rock aquifer (PVA)
- Calico Hills volcanic-rock unit (CHVU)
- Wahmonie volcanic-rock unit (WVU)
- Crater Flat–Prow Pass aquifer (CFPPA)
- Crater Flat–Bullfrog confining unit (CFBCU)
- Crater Flat–Tram aquifer (CFTA)
- Belted Range unit (BRU)
- Death Valley regional ground-water flow system model boundary
- Nevada Test Site boundary
- Boundary of southwestern Nevada volcanic field (SNWVF; from Laczniak and others, 1996)
- Caldera boundary—Pre-SWNVF calderas not shown (from Workman, Menges, Page, Ekren, and others, 2002)

Figure B–13. Outcrop distribution of hydrogeologic units associated with volcanic rocks of the southwestern Nevada volcanic field.

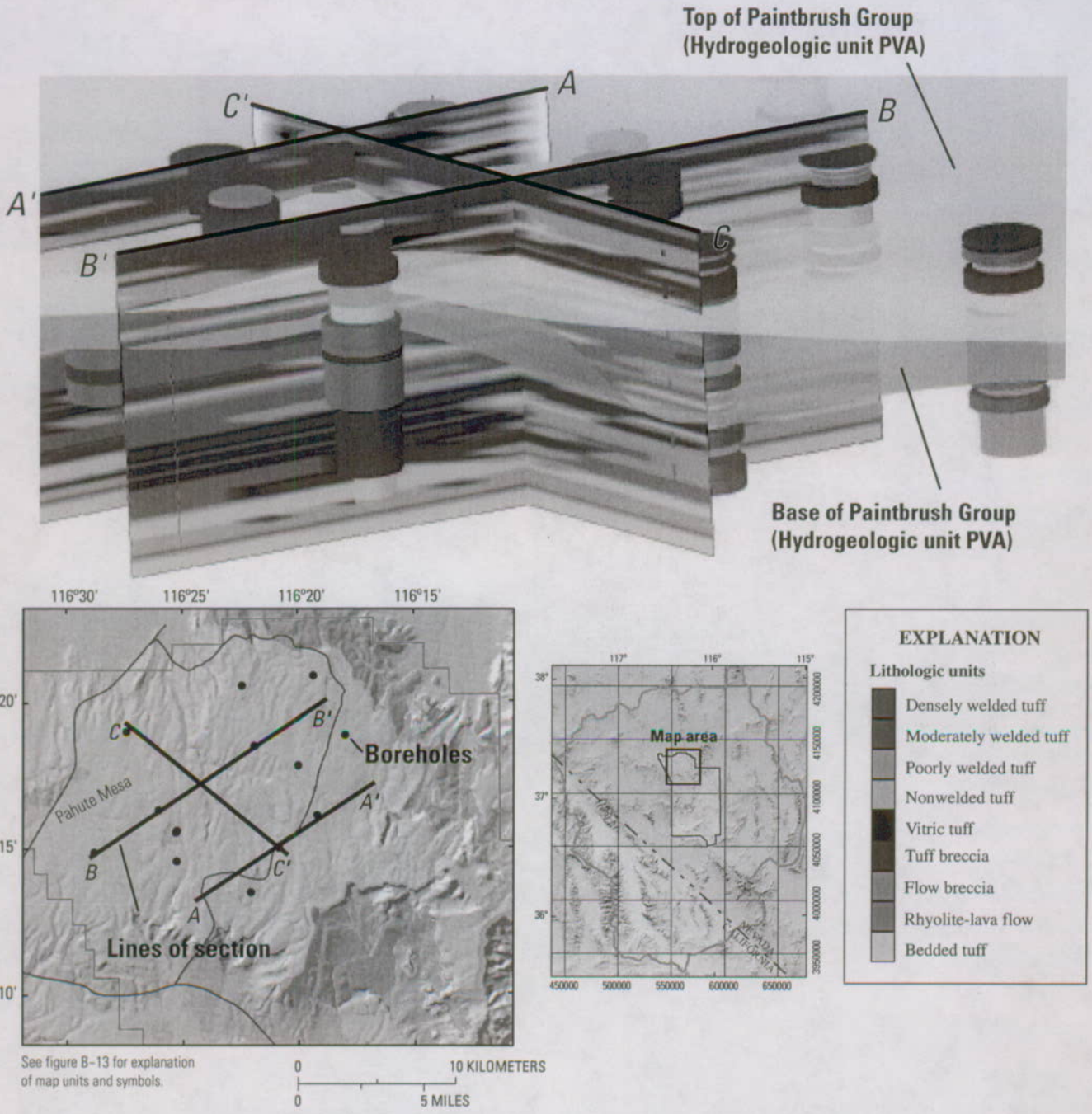

Vertical panels are slices through a three-dimensional rock-properties model of volcanic rocks within the southwestern Nevada volcanic field at Pahute Mesa. Cylinders represent the location and drilled depth of boreholes; colors represent lithologic units and welding variations in the Cenozoic volcanic rocks penetrated by the boreholes. View is from north to the south. Cross-section panels are approximately 20 kilometers long and 1 kilometer deep.

Figure B–14. Variability in lithology and relative degree of welding in volcanic rocks of the southwestern Nevada volcanic field.

A View of the north end of Yucca Mountain, looking WSW

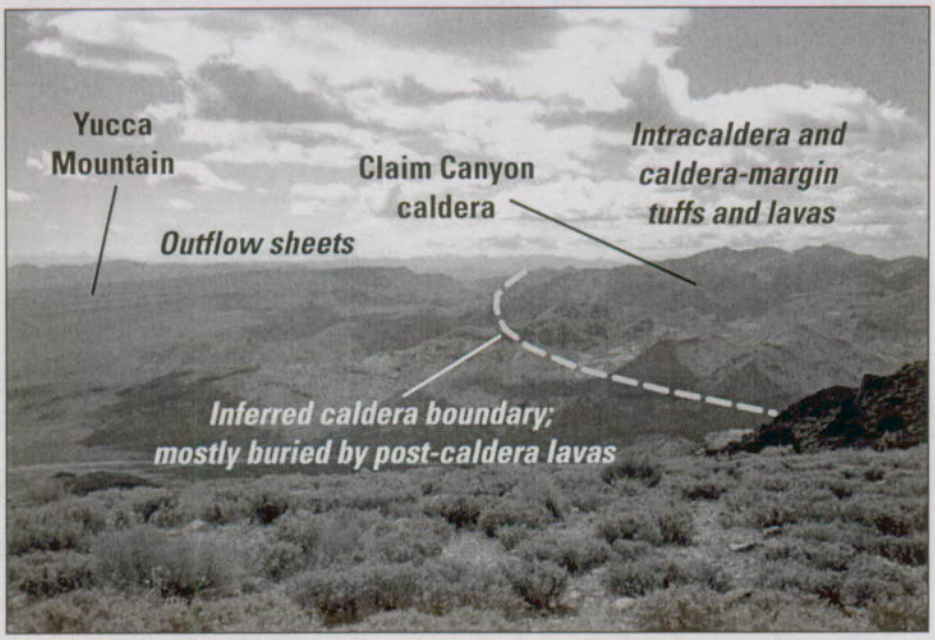

Example of regional-scale lithologic variability associated with calderas of the southwestern Nevada volcanic field. A heterogeneous assemblage of partly to densely welded tuff, volcanic megabreccia, and rhyolite lava flows within the Claim Canyon caldera. The stratigraphic complexity of the intracaldera rocks contrasts with the regionally widespread outflow tuffs exposed at Yucca Mountain. Field of view shown in the photograph is approximately 10 kilometers. Photograph by C.J. Potter, U.S. Geological Survey.

B Tiva Canyon Tuff, Paintbrush Group

Example of welding controls on fracture connectivity in the Tiva Canyon Tuff, Paintbrush Group. Well-developed columnar joints in densely welded tuff terminate abruptly at the transition to partly welded, vitric rock at the base of the ash-flow tuff (approximate contact shown by arrows). The partly welded rock is characterized by short, irregular, poorly connected fractures. Outcrop is approximately 2 meters in height. Photograph by D.S. Sweetkind, U.S. Geological Survey.

Figure B–15. Examples of lithologic and welding variability in volcanic rocks of the southwestern Nevada volcanic field.

Table B–5. Hydrogeologic zones for Cenozoic volcanic-rock hydrogeologic units of the southwestern Nevada volcanic field.

[Zonation applies to most Cenozoic volcanic-rock hydrogeologic units including the Belted Range unit (BRU), Crater Flat–Tram aquifer (CFTA), Crater Flat–Bullfrog confining unit (CFBCU), Crater Flat–Prow Pass aquifer (CFPPA), Wahmonie volcanic-rock unit (WVU), Calico Hills volcanic-rock unit (CHVU), Paintbrush volcanic-rock aquifer (PVA), and Thirsty Canyon–Timber Mountain volcanic-rock aquifer (TMVA)]

Zone number	Description
1	Brittle—Nonaltered: Contains greater than 50 percent brittle (fractured) rock and less than 60 percent altered rock.
2	Brittle—Altered: Contains greater than 50 percent brittle (fractured) rock and greater than 60 percent altered rock.
3	Nonbrittle—Altered: Contains less than 50 percent brittle (fractured) rock and greater than 60 percent altered rock.
4	Nonbrittle—Nonaltered: Contains less than 50 percent brittle (fractured) rock and less than 60 percent altered rock.

Sawyer and others, 1995). Borehole UE–18r, located to the north of Timber Mountain, penetrated up to 1,200 m of Timber Mountain Group rocks (Warren and others, 1999) and provides clear evidence for the structural collapse of both calderas (Christiansen and others, 1977). Timber Mountain Group rocks were deposited in a generally radial pattern surrounding the caldera complex, with some preferential flow to the west (fig. B–16). In addition to the two regionally extensive ash-flow tuffs, the Timber Mountain Group includes minor ash-flow tuffs, rhyolite-lava flows and domes, and intracaldera landslide breccia (Wahl and others, 1997; Slate and others, 2000). Thirsty Canyon Group rocks were erupted from the Black Mountain caldera (Noble and others, 1964; 1984) and cover large areas of the Pahute Mesa area and the northwestern part of the NTS.

Similar to most of the HGUs in the SWNVF, hydrologically significant material properties vary spatially on the basis of the presence of rhyolite-lava flows, the degree of welding of the ash-flow tuffs, and the presence of alteration. Hydrogeologic zones in the TMVA are mapped in fig. B–16.

Paintbrush Volcanic-Rock Aquifer (PVA)

The Paintbrush volcanic-rock aquifer (PVA) is composed of rhyolite tuffs and lavas of the Paintbrush Group, whose source was the Claim Canyon caldera north of Yucca Mountain (Christiansen and Lipman, 1965; Byers, Carr, Christiansen, and others, 1976; Byers, Carr, Orkild and others, 1976; Potter, Dickerson, and others, 2002). The Paintbrush Group includes rhyolite-lava flows and four densely welded tuffs near the Claim Canyon caldera and at the northernmost part of Yucca Mountain. To the south, the Paintbrush Group consists of the densely welded 12.7-Ma Tiva Canyon and 12.8-Ma Topopah Spring Tuffs separated by a comparatively thin interval of mostly nonwelded, vitric pyroclastic deposits and minor bedded tuff units (Sawyer and others, 1994; Buesch and others, 1996). These two densely welded ash-flow tuffs are the thickest stratigraphic units exposed on Yucca Mountain.

Hydrogeologic zones for the PVA are mapped in figure B–17. Paintbrush Group rocks at Yucca Mountain are generally above the water table; alteration in these rocks is primarily local argillic or zeolitic alteration of the nonwelded interval between the Tiva Canyon Tuff and the Topopah Spring Tuff (Moyer and others, 1996). Paintbrush Group rocks lie above the water table in the eastern and central parts of Pahute Mesa, and below the water table in the western part of Pahute Mesa, where they are zeolitically altered locally in downfaulted blocks (Laczniak and others, 1996, plate 4). The Topopah Spring Tuff is zeolitically altered in southern and central Yucca Flat where it approaches its depositional terminus. Paintbrush Group rocks are affected by silicic, argillic, and hematitic alteration in the vicinity of Tram Ridge and in the Calico Hills (Simonds, 1989).

Calico Hills Volcanic-Rock Unit (CHVU)

The Calico Hills Formation is the Calico Hills volcanic-rock unit (CHVU). The 12.9-Ma Calico Hills Formation is a sequence of thick rhyolite-lava flows and intercalated, variably welded ash-flow deposits and nonwelded ash-fall deposits that lie between the Crater Flat Group and Paintbrush Group rocks at Yucca Mountain and Pahute Mesa (Sawyer and others, 1994). Thick lava flows and intercalated tuffs of the Calico Hills Formation are exposed in the Calico Hills and Fortymile Canyon and to the north of Crater Flat and are penetrated in several boreholes at Yucca Mountain (Moyer and Geslin, 1995) and at Pahute Mesa (fig. B–18). Rhyolite lavas in the Calico Hills Formation are common proximal to source vents (Dickerson and Drake, 1998); elsewhere the unit is dominated by nonwelded pyroclastic flows that commonly are zeolitically altered. The rocks were erupted from vents in two spatially distinct volcanic centers—the Calico Hills and Fortymile Canyon area and beneath Pahute Mesa (Sawyer and others, 1994) (fig. B–18).

Hydrogeologic zones of potential enhanced permeability in the CHVU are controlled by the distribution of fractured, vent-proximal, rhyolite-lava flows. For example, the CHVU is an aquifer in the central and western parts of Pahute Mesa (Blankennagel and Weir, 1973; Laczniak and others, 1996, plate 4), where thick accumulations of rhyolite-lava flows function as a single fractured aquifer (brittle, nonaltered zone, fig. B–18). In the northeastern part of Pahute Mesa (nonbrittle, nonaltered zone, fig. B–18) and beneath the southern part of Yucca Mountain (nonbrittle, altered zone, fig. B–18), relatively minor lava flows are isolated between thick intervals of nonwelded ash-flow tuff, and the CHVU functions as a confining unit (Blankennagel and Weir, 1973; Moyer and Geslin, 1995; Laczniak and others, 1996; Prothro and Drellack, 1997).

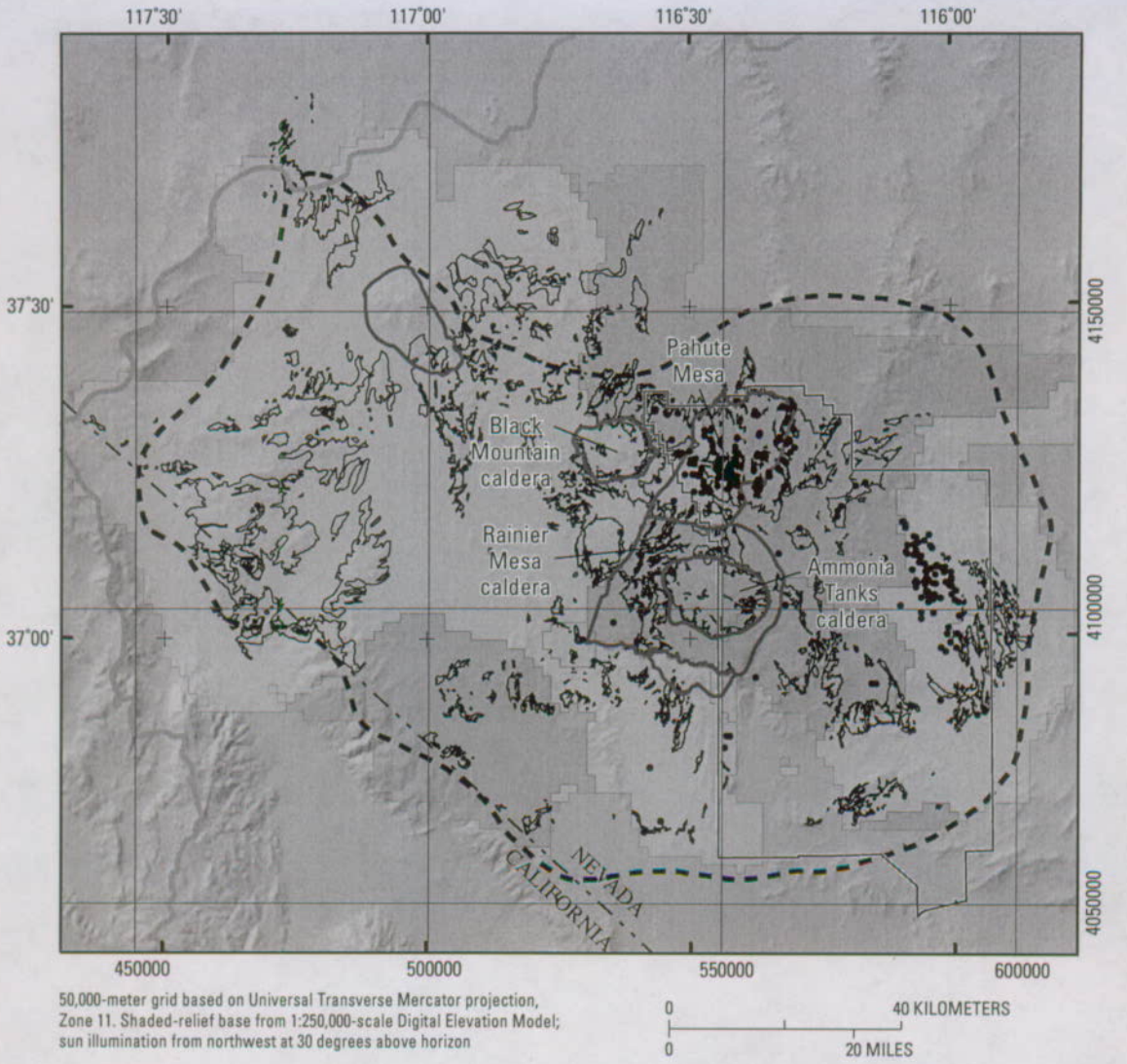

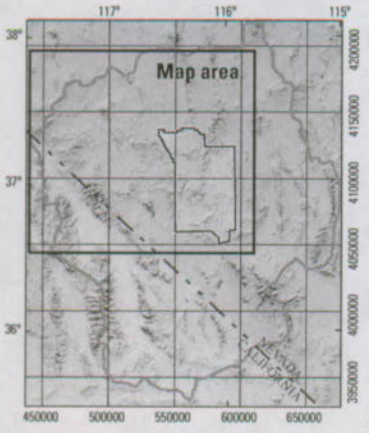

EXPLANATION

Hydrogeologic zones

- Brittle—Nonaltered
- Nonbrittle—Altered
- Brittle—Altered
- Nonbrittle—Nonaltered

- Death Valley regional ground-water flow system model boundary
- Nevada Test Site boundary
- Boundary of southwestern Nevada volcanic field (SWNVF; from Laczniak and others, 1996)
- Caldera boundary—Pre-SWNVF calderas not shown (from Workman, Menges, Page, Ekren, and others, 2002)
- Outcrop of units that compose Thirsty Canyon–Timber Mountain volcanic-rock aquifer (TMVA; from Workman, Menges, Page, Ekren, and others, 2002)
- Boreholes that penetrate TMVA

Figure B–16. Hydrogeologic zones in the Thirsty Canyon–Timber Mountain volcanic-rock aquifer (TMVA).

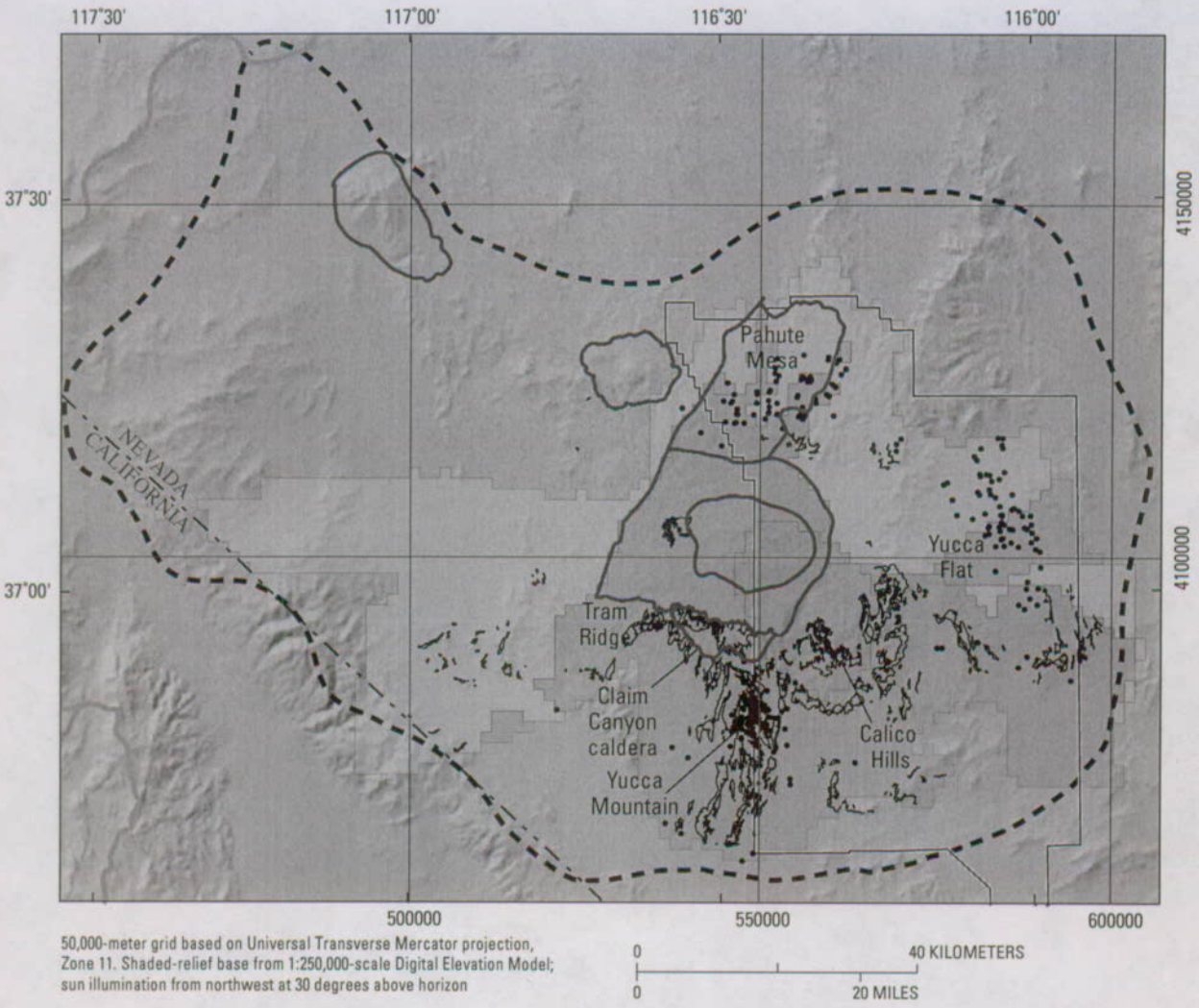

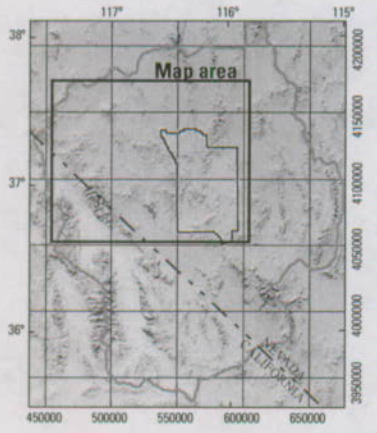

EXPLANATION

Hydrogeologic zones

- Brittle—Nonaltered
- Nonbrittle—Altered
- Brittle—Altered
- Nonbrittle—Nonaltered

- Death Valley regional ground-water flow system model boundary
- Nevada Test Site boundary
- Boundary of southwestern Nevada volcanic field (SWNVF; from Laczniak and others, 1996)
- Caldera boundary—Pre-SWNVF calderas not shown (from Workman, Menges, Page, Ekren, and others, 2002)
- Outcrop of units that compose Paintbrush volcanic-rock aquifer (PVA; from Workman, Menges, Page, Ekren, and others, 2002)
- Boreholes that penetrate PVA

Figure B–17. Hydrogeologic zones in the Paintbrush volcanic-rock aquifer (PVA).

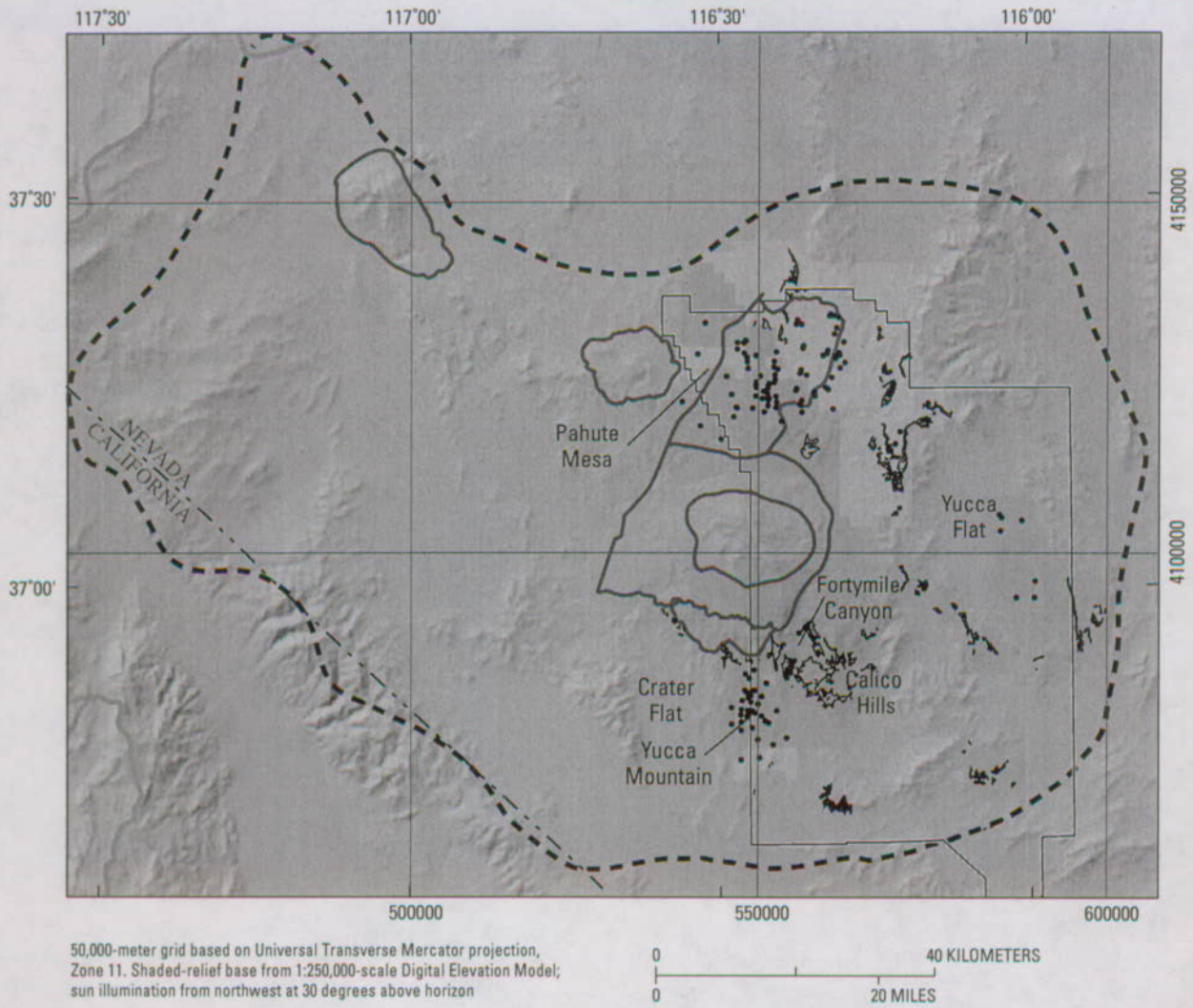

EXPLANATION

Hydrogeologic zones

- Brittle—Nonaltered
- Nonbrittle—Altered
- Brittle—Altered
- Nonbrittle—Nonaltered

- Death Valley regional ground-water flow system model boundary
- Nevada Test Site boundary
- Boundary of southwestern Nevada volcanic field (SWNVF; from Laczniak and others, 1996)
- Caldera boundary—Pre-SWNVF calderas not shown (from Workman, Menges, Page, Ekren, and others, 2002)
- Outcrop of units that compose Calico Hills volcanic-rock unit (CHVU; from Workman, Menges, Page, Ekren, and others, 2002)
- Boreholes that penetrate CHVU

Figure B–18. Hydrogeologic zones in the Calico Hills volcanic-rock unit (CHVU).

Hydrogeologic zones of potential reduced permeability are related to zeolitic and other alteration of nonwelded and bedded tuffs. The nonwelded ash-flow tuffs of the Calico Hills Formation are zeolitically altered throughout most of the southern part of Pahute Mesa (nonbrittle, altered zone, fig. B–18) (Blankennagel and Weir, 1973; Laczniak and others, 1996) and Yucca Flat (Winograd and Thordarson, 1975, IT Corporation, 1996b). Calico Hills Formation tuffs are zeolitically altered beneath the northern part of Yucca Mountain but are locally vitric and classified as nonbrittle and nonaltered (fig. B–18) beneath southern and southwestern parts of Yucca Mountain (Moyer and Geslin, 1995). Brittle facies containing lava flows are pervasively hydrothermally altered in the Calico Hills with argillic alteration, silicification, and pyritization (Simonds, 1989).

Wahmonie Volcanic-Rock Unit (WVU)

The Wahmonie volcanic-rock unit (WVU) is composed of the Wahmonie Formation. The 13.0-Ma (Sawyer and others, 1994) Wahmonie Formation consists of andesitic- and dacitic-lava flows, tephra, and related volcaniclastic deposits that become thinner away from the Wahmonie volcanic center north of Skull Mountain (fig. B–19) (Poole, Carr, and Elston, 1965; Sawyer and others, 1994). The lavas are restricted in extent to the Wahmonie volcanic center, but a distinctive biotite-rich, nonwelded tuff is widespread and forms a marker bed between the Calico Hills Formation and the Crater Flat Group. Regionally, this tuff extends east to Yucca Flat, north to Rainier Mesa, and southwest to Little Skull Mountain and the southern part of Yucca Mountain. The Wahmonie Formation is more than 1,300 m thick in exposures north and east of Skull Mountain (Poole, Carr, and Elston, 1965; Poole, Elston, and Carr, 1965; Ekren and Sargent, 1965).

The criteria for selecting hydrogeologic zones of potential enhanced and reduced permeability (fig. B–19) were similar to those used for the CHVU, a unit that is lithologically similar to the WVU. The distribution of potentially fractured lava flows and the pattern of alteration in the vicinity of the Wahmonie volcanic center is based on surface geologic mapping (Poole, Elston, and Carr, 1965; Ekren and Sargent, 1965).

Crater Flat Group

The Crater Flat Group (Carr, Byers, and Orkild, 1986; Sawyer and others, 1994) consists of three principal units: the Tram Tuff, overlain by the 13.25-Ma Bullfrog Tuff, and the Prow Pass Tuff and two local units, the tuff of Pool, and the rhyolite of Inlet (Sawyer and others, 1994). In order to maintain consistency with the 3D geologic framework model constructed for the proposed geologic repository for high-level radioactive waste at Yucca Mountain (Bechtel SAIC Company, 2002), the Prow Pass, Bullfrog, and Tram Tuffs of the Crater Flat Group are treated as separate HGUs.

The Crater Flat Group rocks are present in the Pahute Mesa area as well as in the vicinity of Yucca Mountain and Crater Flat. A proposed source caldera beneath Crater Flat (Carr, 1982; Carr, Byers, and Orkild, 1986) has been questioned on geologic and geophysical grounds (Scott, 1990; Brocher and others, 1998); a source for the Bullfrog Tuff has been inferred to be the Area 20 caldera (part of the Silent Canyon caldera complex) (Sawyer and others, 1994), but this also has been questioned on geophysical grounds (Hildenbrand and others, 1999).

Crater Flat–Prow Pass Aquifer (CFPPA)

The Crater Flat–Prow Pass aquifer (CFPPA) consists of the Prow Pass Tuff of the Crater Flat Group and local time-equivalent tuffs and rhyolite-lava flows present in the subsurface beneath Pahute Mesa. The Prow Pass Tuff is exposed to the northwest of Yucca Mountain (Moyer and Geslin, 1995) and at the south end of Yucca Mountain (fig. B–20); drilling indicates that it exists in the subsurface in Crater Flat (Carr, Byers, and Orkild, 1986; Moyer and Geslin, 1995). The unit is thickest and most densely welded beneath Yucca Mountain; it thins westward into Crater Flat and southward. Tuffs and rhyolite-lava flows present in the subsurface beneath Pahute Mesa that are equivalent in age to the Prow Pass Tuff include the Andesite of Grimy Gulch, Tuff of Jorum, Rhyolite of Sled, and Rhyolite of Kearsarge (Ferguson and others, 1994).

Hydrogeologic zones for the CFPPA are mapped in figure B–20. Nonwelded to partly welded parts of the unit are zeolitically altered.

Crater Flat–Bullfrog Confining Unit (CFBCU)

The Bullfrog Tuff of the Crater Flat Group composes the Crater Flat–Bullfrog confining unit (CFBCU). The Bullfrog Tuff is widely distributed around the TMCC (Carr, Byers, and Orkild, 1986). The thickness of the outflow tuff is 100 to 150 m in the Bullfrog Hills, at Yucca Mountain, and in Jackass Flats, but it may be greater than 400 m thick in Crater Flat (Carr, Byers, and Orkild, 1986). Maximum thickness in boreholes in intracaldera tuff in the SCCC is about 680 m (Ferguson and others, 1994; Sawyer and others, 1994).

The CFBCU is nonwelded to poorly welded throughout most of the SCCC and Yucca Flat, where it is classified as nonbrittle and altered (fig. B–21) and is a confining unit (Blankennagel and Weir, 1973; Laczniak and others, 1996). In the vicinity of Yucca Mountain, the Bullfrog Tuff forms a compound-cooling unit with variable welding and alteration characteristics (fig. B–21). In general, the unit has a moderately to densely welded and devitrified interior with nonwelded to partly welded margins in the Yucca Mountain area. The Bullfrog Tuff at Yucca Mountain was included in a "lower volcanic aquifer" HGU described by Luckey and others (1996), primarily because of fracture permeability in the interior welded zone.

Crater Flat–Tram Aquifer (CFTA)

The Tram Tuff of the Crater Flat Group constitutes the Crater Flat–Tram aquifer (CFTA). The Tram Tuff is a mostly nonwelded to partially welded, ash-flow tuff (fig. B–22), but

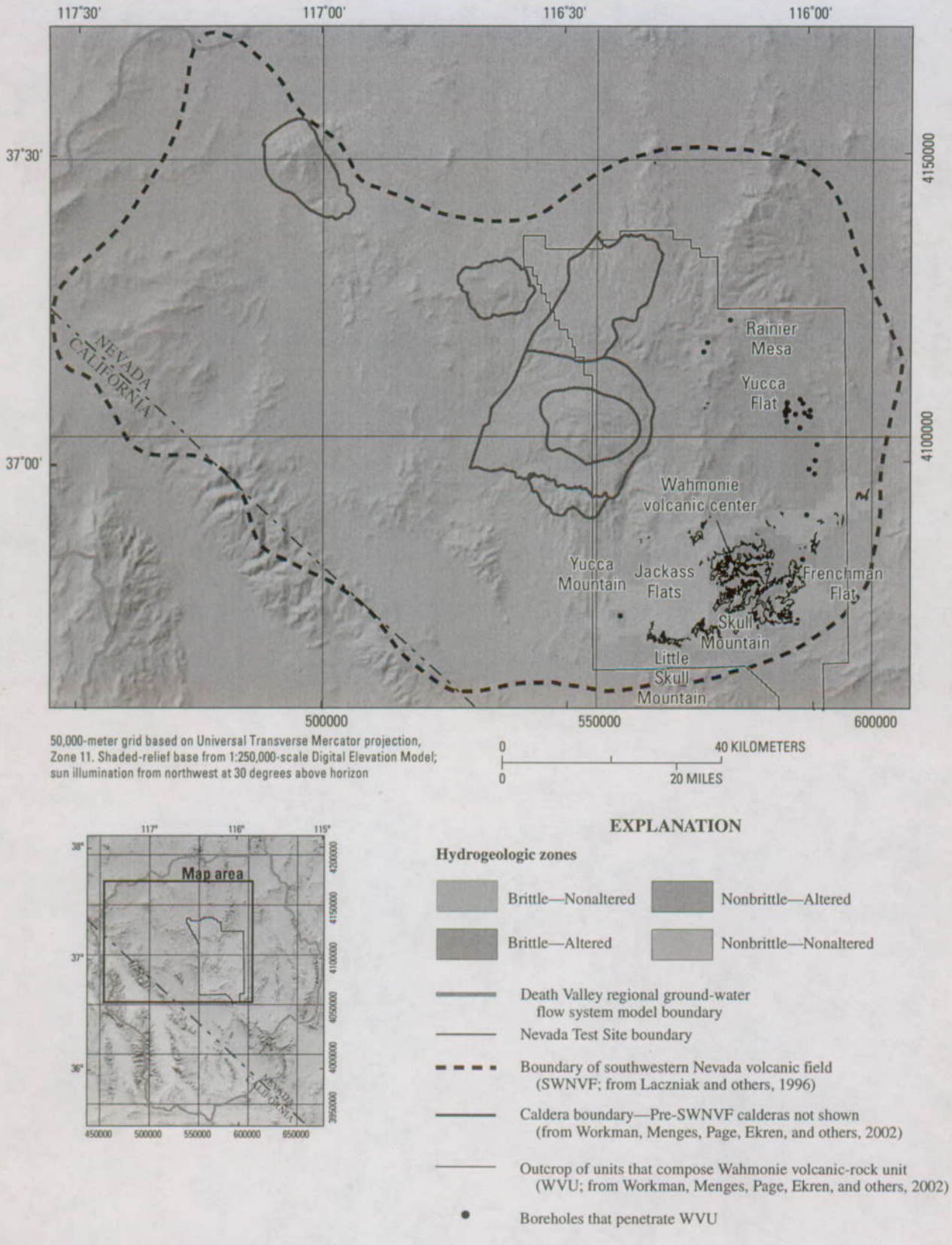

Figure B–19. Hydrogeologic zones in the Wahmonie volcanic-rock unit (WVU).

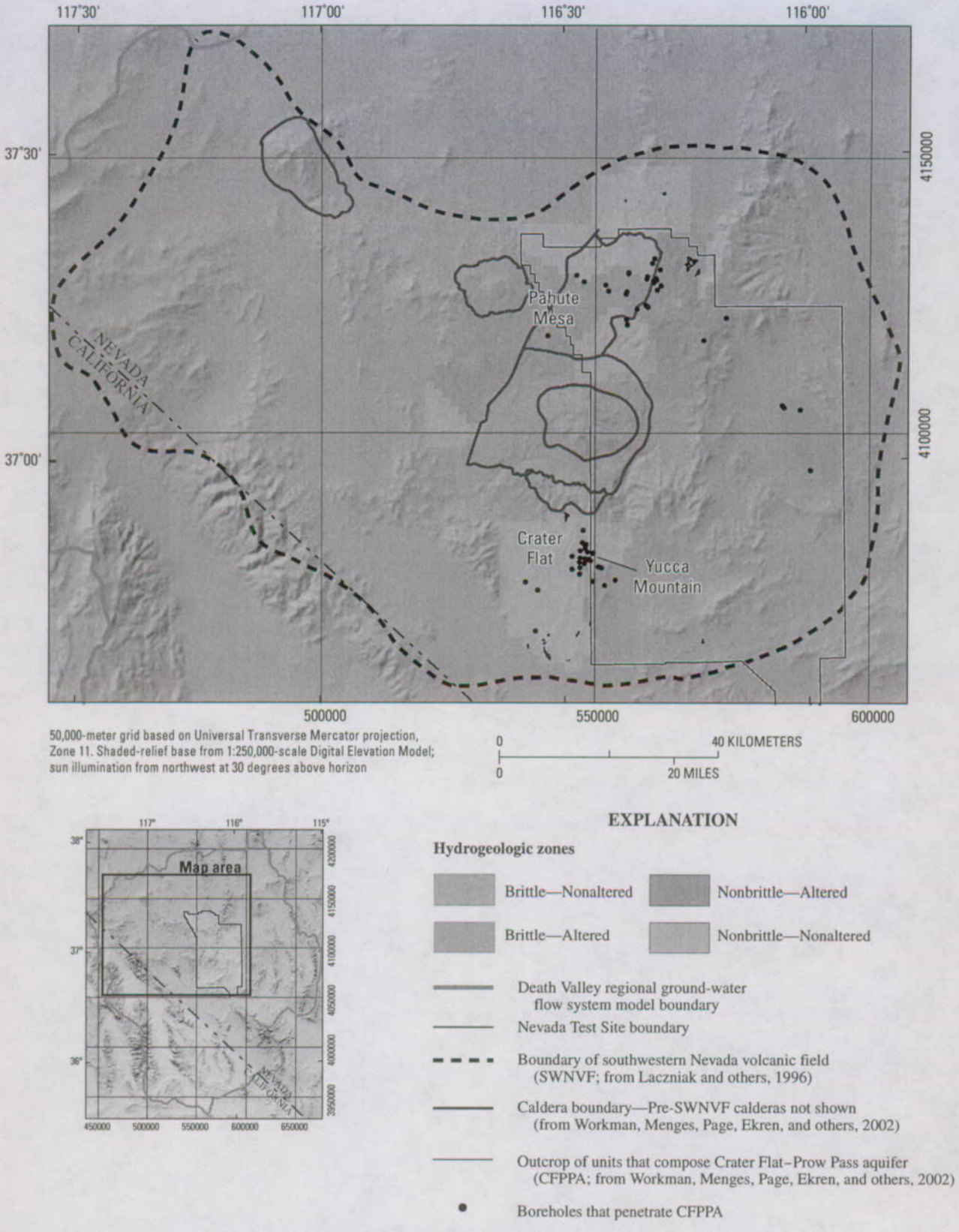

Figure B–20. Hydrogeologic zones in the Crater Flat–Prow Pass aquifer (CFPPA).

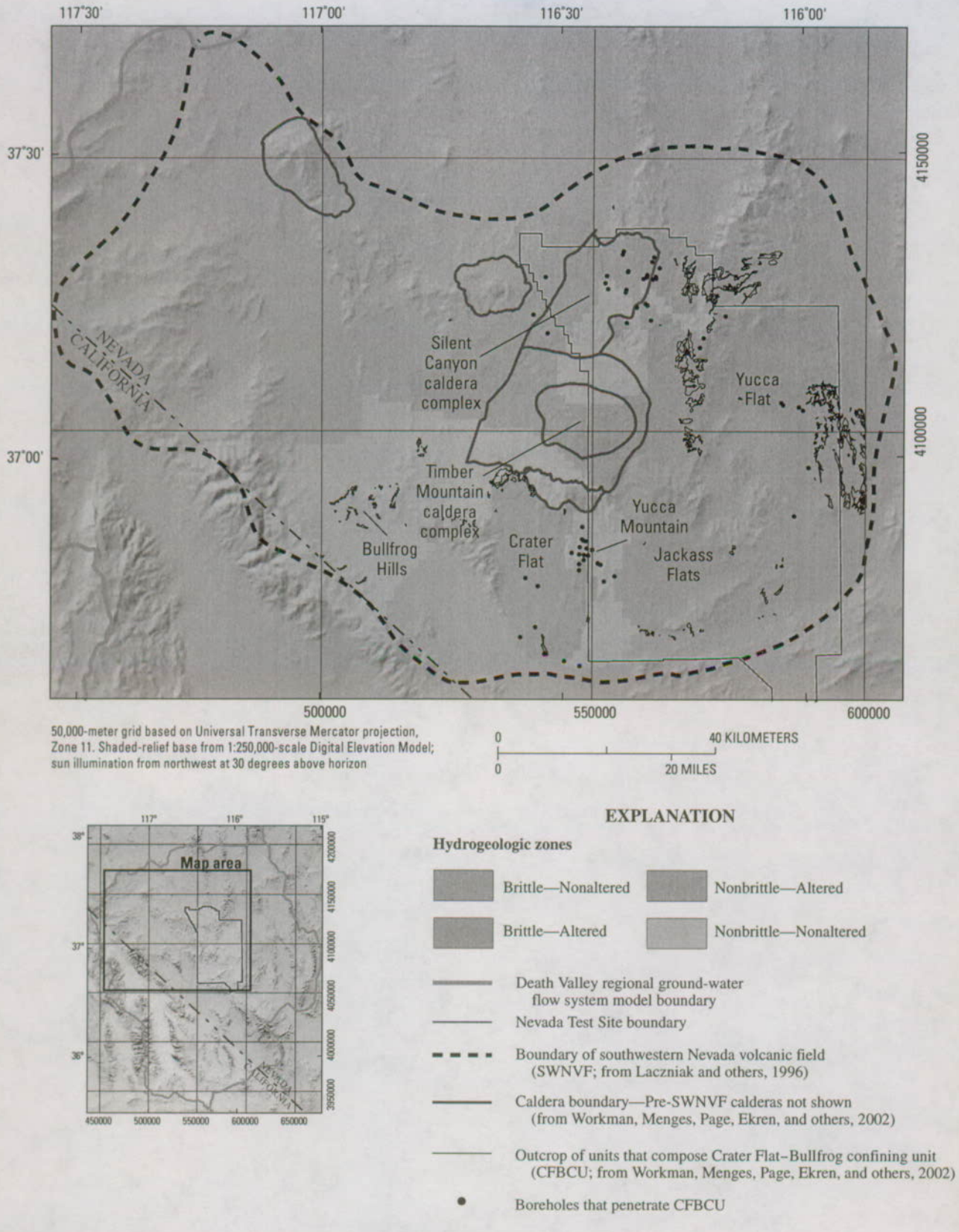

Figure B–21. Hydrogeologic zones in the Crater Flat–Bullfrog confining unit (CFBCU).

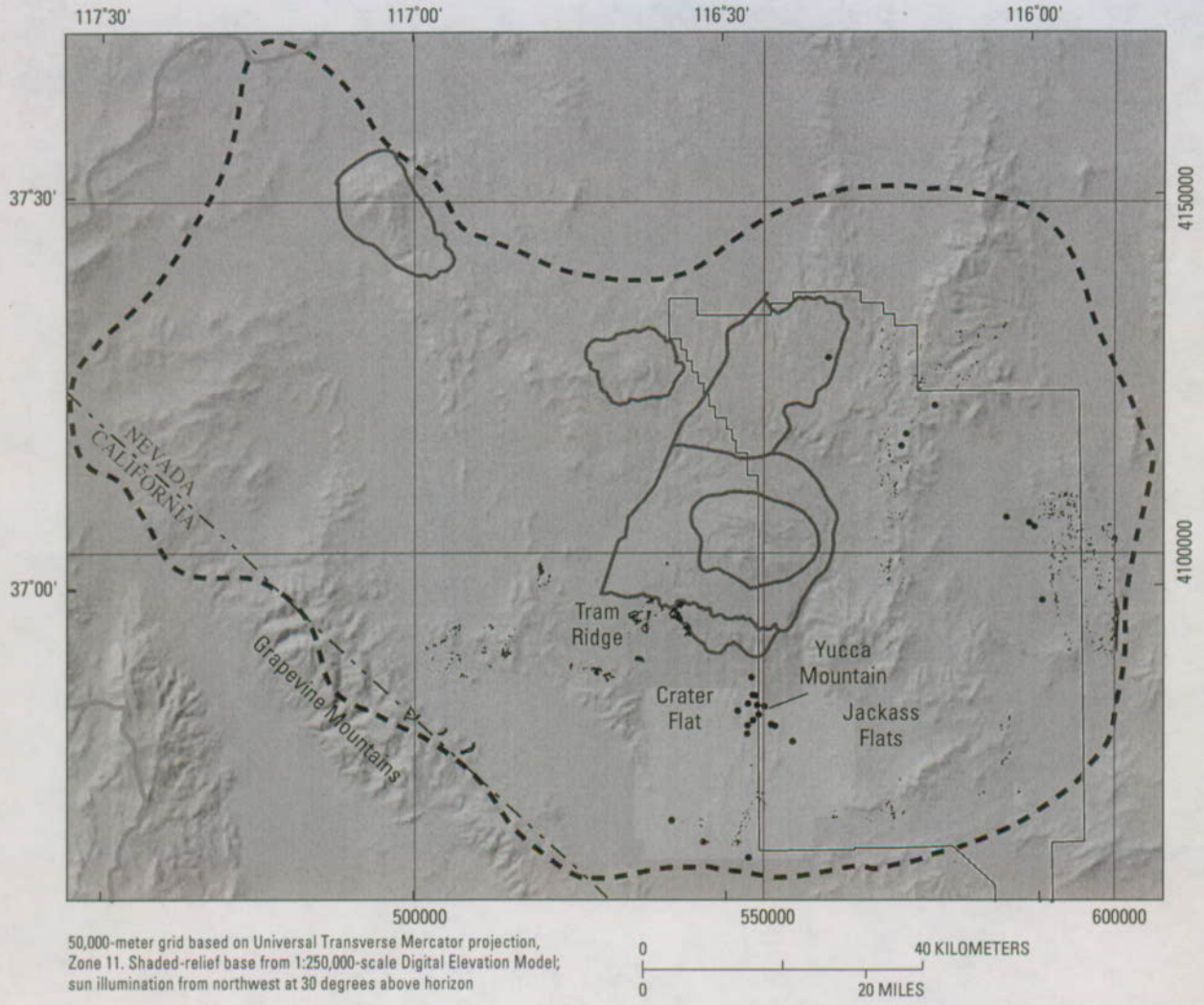

EXPLANATION

Hydrogeologic zones

- Brittle—Nonaltered
- Nonbrittle—Altered
- Brittle—Altered
- Nonbrittle—Nonaltered

- Death Valley regional ground-water flow system model boundary
- Nevada Test Site boundary
- Boundary of southwestern Nevada volcanic field (SWNVF; from Laczniak and others, 1996)
- Caldera boundary—Pre-SWNVF calderas not shown (from Workman, Menges, Page, Ekren, and others, 2002)
- Outcrop of units that compose Crater Flat–Tram aquifer (CFTA; from Workman, Menges, Page, Ekren, and others, 2002)
- Boreholes that penetrate CFTA

Figure B–22. Hydrogeologic zones in the Crater Flat–Tram aquifer (CFTA).

is densely welded at Tram Ridge (Fridrich and others, 1999). It is locally exposed and also encountered in boreholes in the Crater Flat and Yucca Mountain areas (Carr, Byers, and Orkild, 1986). Regionally, the Tram Tuff extends as far west as the Grapevine Mountains and east beneath Jackass Flats (Carr, Byers, and Orkild, 1986). Hydrogeologic zones for the CFTA are mapped in figure B–22.

Belted Range Unit (BRU)

Rocks of the Belted Range Group constitute the Belted Range unit (BRU). The Belted Range Group is composed of the 13.7-Ma Grouse Canyon Tuff and associated pre-caldera lava flows and post-caldera lavas and tuffs of the Dead Horse Flat Formation (Sawyer and others, 1994). Belted Range Group rocks are interpreted to have erupted between 13.85 Ma and 13.5 Ma from the Grouse Canyon caldera, now buried in the SCCC. Syn- and post-collapse volcanic-rock units thicken toward the eastern margin of the caldera, on the basis of borehole data and gravity inversion analysis (Ferguson and others, 1994; Hildenbrand and others, 1999). Thick post-caldera rhyolitic lavas of the Dead Horse Flat Formation accumulated in the eastern and northeastern parts of the caldera (Laczniak and others, 1996, plate 4; McKee and others, 1999). Belted Range Group rocks are not present in the southern parts of the SWNVF, including Yucca Mountain.

Aquifers in the BRU include both thick post-caldera rhyolitic lavas of the Dead Horse Flat Formation and welded Grouse Canyon Tuff. The lavas are highly fractured and form the principal aquifer unit on the eastern part of Pahute Mesa (Blankennagel and Weir, 1973; Prothro and Drellack, 1997; Laczniak and others, 1996, plate 4). The 50-percent brittle rock area (fig. B–23) incorporates all of the thick intracaldera lava flows of the Dead Horse Flat Formation that dominate the deeper parts of the eastern one-half of the SCCC, plus the thickest welded intervals of Grouse Canyon Tuff that are proximal to the SCCC.

Older Volcanic-Rock Unit (OVU)

The older volcanic-rock unit (OVU) consists of Oligocene and early Miocene volcanic rocks that consist of ash-flow tuff, ash-fall tuff, reworked tuff, tuff breccia, lava flows, and volcaniclastic rocks. The OVU may be subdivided into two general groups: (1) those volcanic rocks in and near, and perhaps originating from, the SWNVF, and (2) volcanic rocks that originated from volcanic centers to the north of the SWNVF. Volcanic rocks associated with these two general groups are for the most part separated from each other. The older volcanic rocks of the NTS (almost entirely within the SWNVF) do not extend more than a few tens of kilometers north of the northern boundary of the NTS (Slate and others, 2000), whereas older volcanic rocks derived from outside the SWNVF are common to the north and northeast of the NTS but are known only in the extreme northeastern and northern parts of the NTS (Ekren and others, 1971; Workman, Menges, Page, Taylor, and others, 2002).

Oligocene and lower Miocene volcanic rocks north of the NTS consist predominantly of partly to densely welded ash-flow tuffs that have an aggregate thickness of up to several hundred meters over large parts of western Lincoln County and central Nye County, Nev. (Ekren and others, 1971; Workman, Menges, Page, Taylor, and others, 2002). Regionally distributed, welded ash-flow tuffs include the Monotony Tuff, the Shingle Pass Tuff, the "Tuffs of Antelope Springs," and the Tuff of White Blotch Springs. Proposed source areas for these units are volcanic centers to the north of the SWNVF that include known or inferred calderas in the Cactus Range, the Kawich Range, the Quinn Canyon Range, and the Mt. Helen area (Ekren and others, 1971; Best and others, 1989; McKee, 1996; Workman, Menges, Page, Ekren, and others, 2002).

A locally thick section of 15.5- to 13.8-Ma pre-Belted Range Group volcanic rocks is associated with, and perhaps originated from, the SWNVF. These units are known from limited outcrops at the NTS and from boreholes in Pahute Mesa, Yucca and Frenchman Flats, and Yucca Mountain. Most of these units do not extend more than a few tens of kilometers north of the northern boundary of the NTS. Most of the pre-Belted Range Group volcanic-rock units are nonwelded to partly welded, with the exception of the densely welded Redrock Valley and Tub Spring Tuffs (Sawyer and others, 1995), and the nonwelded tuffs typically are devitrified and zeolitically altered (Drellack, 1997; Prothro and others, 1999).

Because of the large number of volcanic-rock units that are included in this HGU, the OVU has widely varying material properties. The OVU may be subdivided into areas of potentially different material and hydrologic properties on the basis of geography and the presence of calderas (fig. B–24). OVU rocks north of the NTS form a series of regionally extensive ash-flow tuffs that are locally fractured volcanic-rock aquifers throughout a large part of southern Nye County (Plume and Carlton, 1988). OVU rocks to the north of the NTS can be divided into intracaldera and outflow components (fig. B–24), on the basis of caldera boundaries shown in Workman, Menges, Page, Ekren, and others (2002). This zonation is based on the presence of thick intracaldera accumulations of tuff and lavas, regardless of their correlation to specific ash-flow sheets.

In most places in the SWNVF, OVU rocks likely act as a confining unit because they generally are nonwelded to partially welded and zeolitic alteration is widespread (Sawyer and others, 1995; Drellack, 1997; Prothro and others, 1999). Lava flows and densely welded tuffs in this section can form fracture-flow aquifers but are generally too localized or too deep in the section to be significant. The OVU is important in Yucca and Frenchman Flats, where it separates the overlying fractured volcanic-rock aquifers from the underlying regional carbonate-rock aquifer. The OVU is saturated in much of the central part of Yucca Flat, and measured transmissivities are very low (IT Corporation, 1996b).

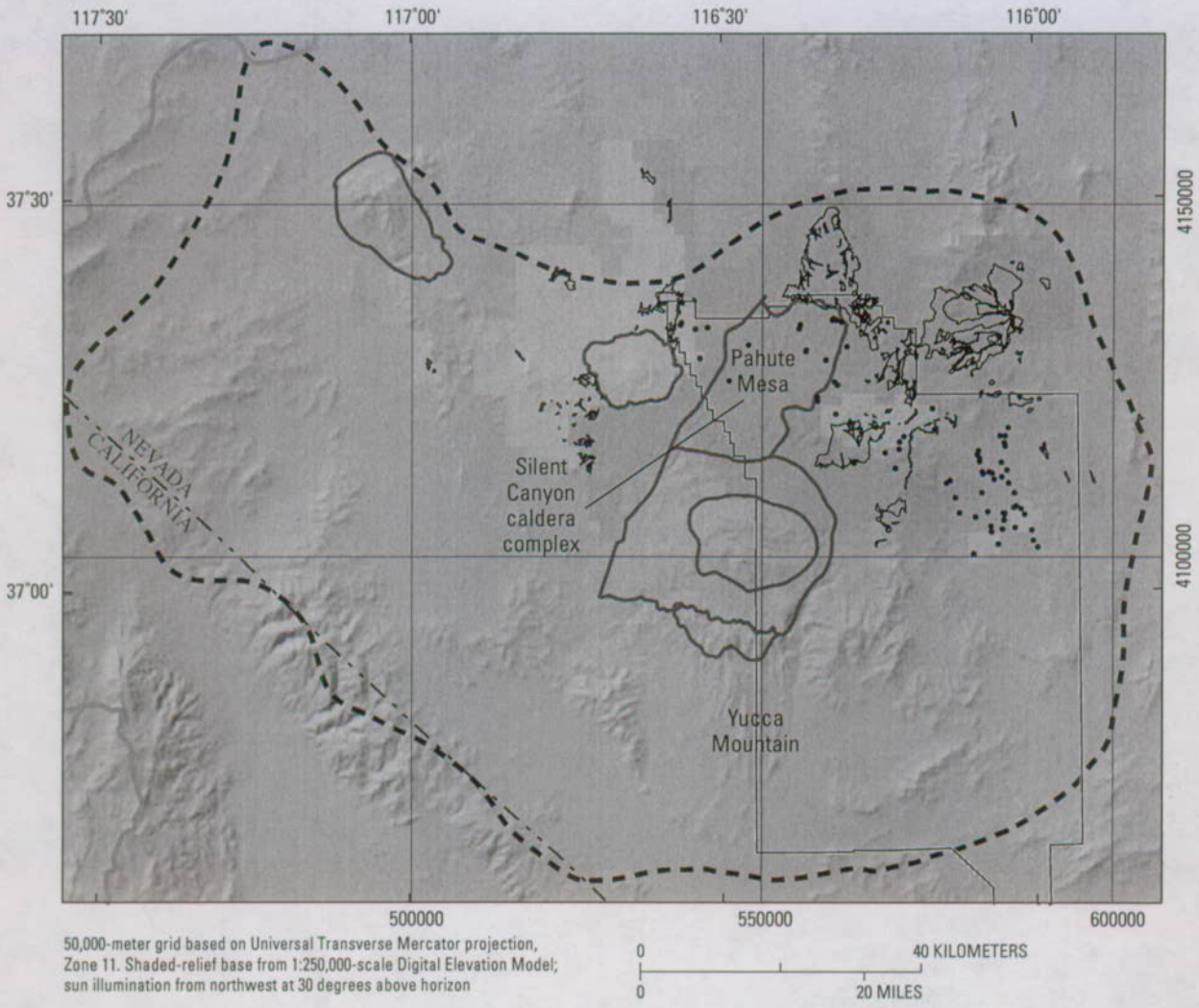

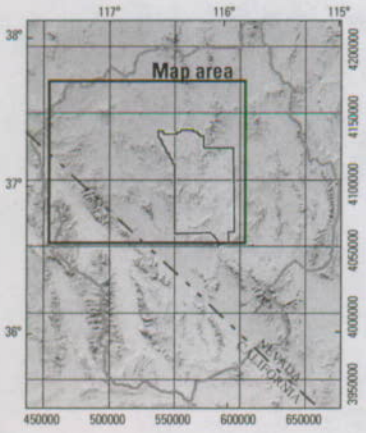

EXPLANATION

Hydrogeologic zones

- Brittle—Nonaltered
- Nonbrittle—Altered
- Brittle—Altered
- Nonbrittle—Nonaltered
- Death Valley regional ground-water flow system model boundary
- Nevada Test Site boundary
- Boundary of southwestern Nevada volcanic field (SWNVF; from Laczniak and others, 1996)
- Caldera boundary—Pre-SWNVF calderas not shown (from Workman, Menges, Page, Ekren, and others, 2002)
- Outcrop of units that compose Belted Range unit (BRU; from Workman, Menges, Page, Ekren, and others, 2002)
- Boreholes that penetrate BRU

Figure B–23. Hydrogeologic zones in the Belted Range unit (BRU).

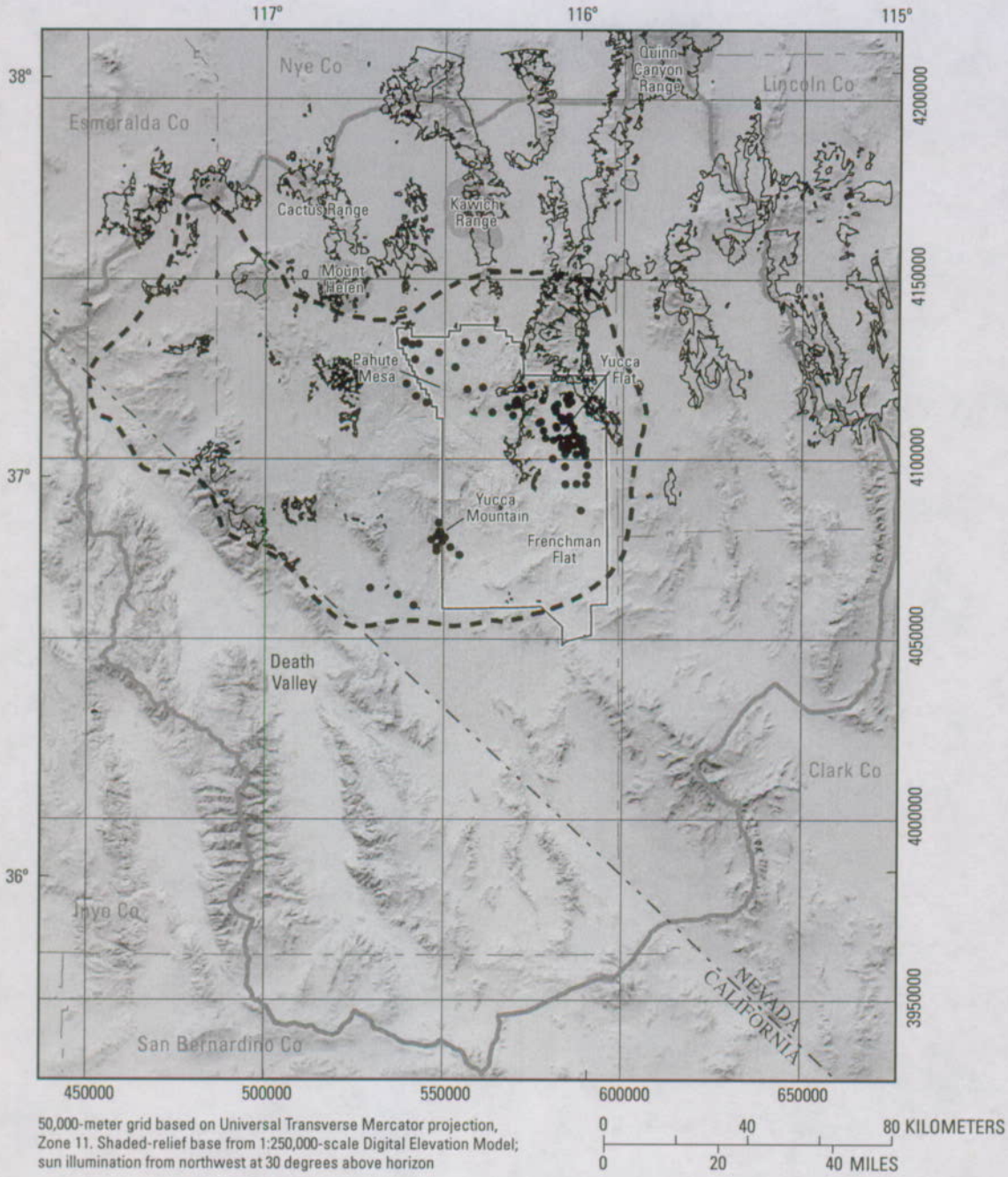

Figure B–24. Hydrogeologic zones in the older volcanic-rock unit (OVU).

Hydrogeologic Units Associated with Mesozoic, Paleozoic, and Late Proterozoic Sedimentary Rocks

The pre-Cenozoic sedimentary rocks of the DVRFS region are grouped into five HGUs: the sedimentary-rock confining unit (SCU), the upper carbonate-rock aquifer (UCA), the upper clastic-rock confining unit (UCCU), the lower carbonate-rock aquifer (LCA), and the lower clastic-rock confining unit (LCCU) (table B–2; fig. B–25). This usage is similar to that established by Winograd and Thordarson (1975), particularly for the vicinity of the NTS.

Sedimentary-Rock Confining Unit (SCU)

The sedimentary-rock confining unit (SCU) consists of unmetamorphosed Mesozoic cratonic sedimentary rocks in the eastern part of the DVRFS region (fig. B–25) and Mesozoic metasedimentary and metavolcanic rocks that are sparsely exposed in the western part of the DVRFS region. Local exposures of Mesozoic sedimentary rocks as young as the Lower Jurassic Aztec Sandstone crop out in the Las Vegas, Nev., area. Triassic rocks (Middle(?) and Lower Triassic Moenkopi Formation and Upper Triassic Chinle Formation) crop out in the Pahrump Valley and Spring Mountains area. These units consist of interbedded conglomerate, sandstone, siltstone, shale, calcareous shale, limestone, and gypsum. Mesozoic metasedimentary and metavolcanic rocks are exposed in the extreme southwestern part of the DVRFS region in the southern Panamint Mountains and Avawatz Mountains.

Hydraulic properties of the SCU vary according to grain size and sorting in the different units. Some of these rocks are regional aquifers on the Colorado Plateau east of the DVRFS region, but most exposures of the SCU either lie outside the boundary of the DVRFS region or are too small or shallow to have significance in the regional ground-water flow system.

Upper Carbonate-Rock Aquifer (UCA)

The upper carbonate-rock aquifer (UCA) includes Pennsylvanian and Mississippian limestone, dolomite, and calcareous shales in the vicinity of the NTS that are stratigraphically above the Eleana Formation and Chainman Shale (Winograd and Thordarson, 1975; Laczniak and others, 1996). Where the Eleana Formation and Chainman Shale are absent to the southeast of the NTS, the Pennsylvanian and Mississippian carbonate rocks are included in the lower carbonate-rock aquifer (LCA). The UCA exists primarily in the area of Yucca Flat (fig. B–25), where Pennsylvanian carbonate rocks are preserved in a syncline at Syncline Ridge. In general, the rocks of the UCA are of only local importance and are not significant in the regional flow system.

Upper Clastic-Rock Confining Unit (UCCU)

The upper clastic-rock confining unit (UCCU) is composed of Upper Devonian through Mississippian synorogenic siliciclastic and carbonate rocks including the Eleana Formation and the Chainman Shale (Laczniak and others, 1996). The Eleana Formation is present in parts of the western and northern part of the DVRFS region and consists of up to 2,000 m of siltstone, argillite, sandstone, conglomerate, and minor limestone deposited as turbidites and debris flows filling the Antler foredeep to the east of the Antler orogenic belt (Poole and others, 1961; Nilsen and Stewart, 1980; Poole, 1981; Trexler and others, 1996). The Eleana Formation grades laterally into and is thrust eastward over the 1,200-m-thick Mississippian Chainman Shale in Yucca Flat and the northern part of Jackass Flats at the NTS (Trexler and others, 1996) (fig. B–25).

The Eleana-Chainman section is a locally important siliciclastic-rock confining unit in the vicinity of the NTS. Steep hydraulic gradients in the area of Yucca Flat are attributed to the low transmissivity values of the Eleana Formation (Winograd and Thordarson, 1975; D'Agnese and others, 1997). Southeast of the NTS in the Spotted Range and in the Indian Springs Valley carbonate platform limestones of Mississippian age are less than 350 m thick (Poole and others, 1961; Barnes and others, 1982). In the Cottonwood Mountains and the Last Chance Range in the western part of the DVRFS region, the Mississippian section is represented by carbonate-dominated units such as the Tin Mountain limestone and the Perdido Group (Stevens and others, 1991; 1996). These Mississippian carbonate rocks that occur outside of the NTS vicinity are not designated as part of the UCCU but instead are considered part of the lower carbonate-rock aquifer (LCA).

Lower Carbonate-Rock Aquifer (LCA)

The lower to middle Paleozoic carbonate-rock succession forms the major regional carbonate-rock aquifer in the eastern two-thirds of the Great Basin (Winograd and Thordarson, 1975; Bedinger and others, 1989a; Dettinger and others, 1995; Harrill and Prudic, 1998). As in previous regional analyses of ground-water flow in the southern Great Basin, these carbonate rocks are treated as a single HGU, the lower carbonate-rock aquifer (LCA) (Winograd and Thordarson, 1975; Laczniak and others, 1996).

The Paleozoic carbonate rocks of the LCA are widely distributed in the eastern part of the DVRFS region (fig. B–25). These rocks consist of a Middle Cambrian through Middle Devonian carbonate-dominated succession, about 4,500 m thick in this region, that includes dolomite, interbedded limestone, and thin but persistent shale, quartzite, and calcareous clastic units (Burchfiel, 1964). The lower part of this carbonate-rock section (Lower and Middle Cambrian Carrara Formation, Middle and Upper Cambrian Bonanza King Formation, Upper Cambrian Nopah Formation, Lower and Middle Ordovician Pogonip Group) is exposed in most of the mountain

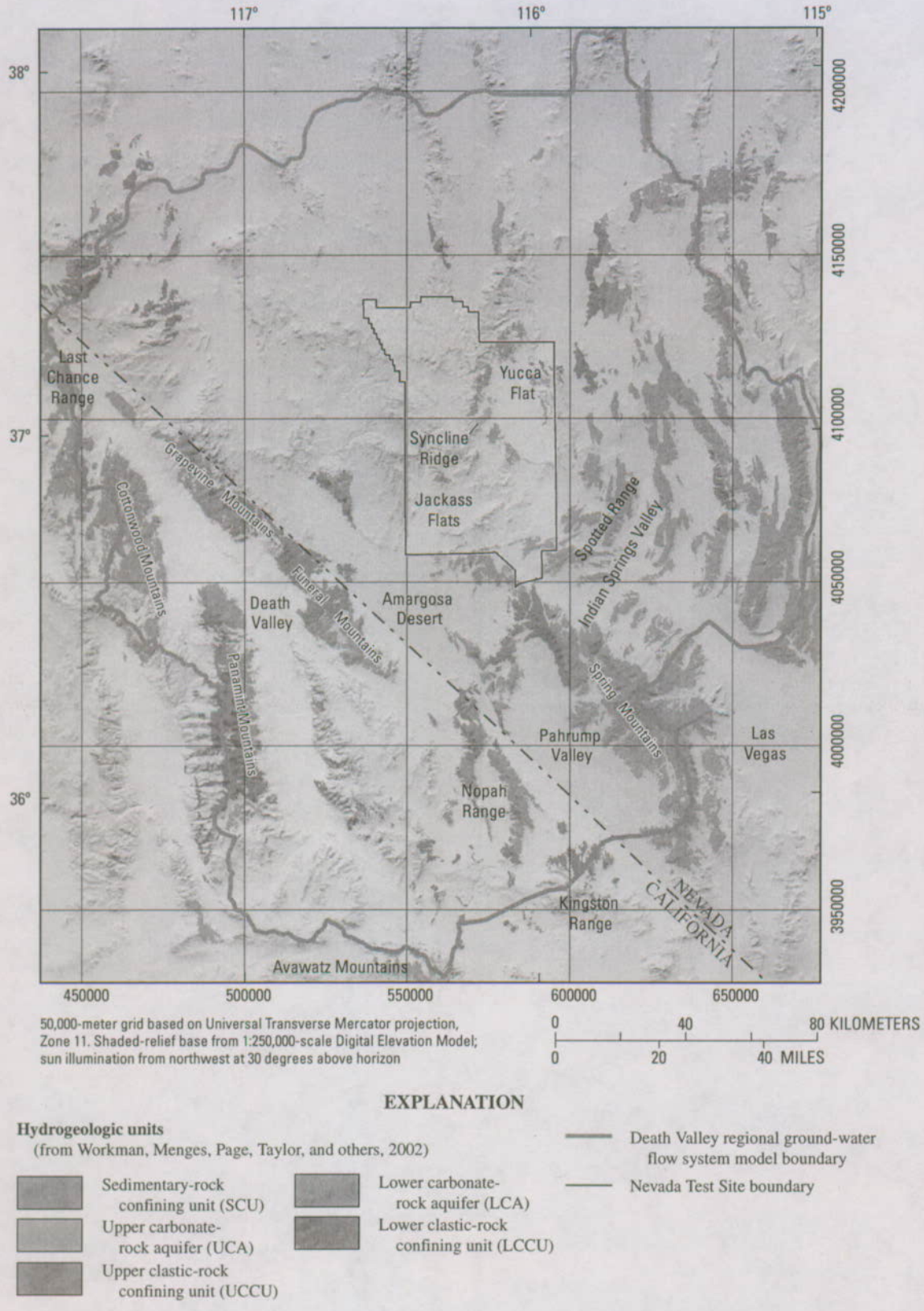

Figure B–25. Outcrop distribution of hydrogeologic units associated with Mesozoic, Paleozoic, and Late Proterozoic sedimentary rocks.

ranges in the central and southern parts of the DVRFS region (fig. B–25). In contrast to the Proterozoic siliciclastic rocks, thickness variations in this interval are generally small across much of the DVRFS region (fig. B–2) (Cornwall, 1972). In the northwestern part of the DVRFS region, the Middle Cambrian through Middle Devonian rocks are somewhat thicker and represent a somewhat deeper-water facies of shale and impure carbonate rocks, including the Campito Formation (Cornwall, 1972; Burchfiel and others, 1982).

Southeast of the NTS, the LCA consists of Mississippian and Pennsylvanian carbonate rocks where the siliciclastic rocks of the UCCU do not separate the Paleozoic carbonate rocks into an upper and lower aquifer. The Bird Spring Formation is nearly 2,000 m thick in the central part of the Spring Mountains (Langenheim and Larson, 1973; Burchfiel and others, 1974). In the west and northwest parts of the DVRFS region, predominantly carbonate rocks of Mississippian, Pennsylvanian, and Permian age are exposed in the Grapevine, Cottonwood, and Panamint Mountains (Workman, Menges, Page, Taylor, and others, 2002).

The LCA carbonate rocks have an aggregate thickness of as much as 8,000 m and are generally the most permeable rocks in the DVRFS region (Bedinger and others, 1989b; Belcher and others, 2001). Where hydraulically connected, they provide a path for interbasinal flow (Dettinger and Schaefer, 1996; D'Agnese and others, 1997; Harrill and Prudic, 1998). Most of the springs in the area are associated with the carbonate rocks (Winograd and Thordarson, 1975). Compared to flow through secondary openings in the carbonate rocks of the LCA, intergranular flow is relatively insignificant. The large hydraulic conductivities reported for rocks of this unit primarily are because of fractures, faults, and solution channels (Winograd and Thordarson, 1975). Hydraulic tests of carbonate-rock aquifers throughout eastern and southern Nevada indicate that faults can increase the carbonate-rock transmissivity by a factor of 25 or more (Dettinger and others, 1995). Areas affected by multiple deformational events are inferred to have potentially greater secondary fracture permeability.

Eleven hydrogeologic zones are defined for the LCA (fig. B–26, table B–6) on the basis of stratigraphic facies, inferred continuity of the aquifer, and degree of structural deformation. As with previous maps, mapped zones do not imply the existence of each HGU throughout the zone; rather, they are a guide to which set of material properties applies where the HGU exists in the 3D HFM (Chapter E, this volume).

In the eastern part of the DVRFS region, shelf sequence rocks of the central carbonate corridor (Dettinger and others, 1995) are differentiated from the basinal facies that exist in the extreme northwestern part of the region (Zone 9, fig. B–26*A* and table B–6). Outcrops of Paleozoic rocks are extremely sparse northwest of the NTS; in this region, the aquifer properties of the LCA are highly uncertain (Zone 10, fig. B–26*A* and table B–6). Paleozoic carbonate rocks are inferred to be absent or highly altered in the vicinity of the calderas of the SWNVF and exist only as tectonically dismembered blocks in a broad belt through the southern part of Death Valley (Zone 5, fig. B–26*A* and table B–6).

Rocks of the central carbonate corridor are subdivided on the basis of the inferred degree of structural disruption (fig. B–26*B*). The magnitude of Cenozoic extension was heterogeneous in the DVRFS region; regions of large-magnitude extension alternated with areas of lesser extension (Wernicke and others, 1984; Wernicke, 1992). Relatively undeformed stable blocks of the Sheep Range and Spring Mountains occupy the eastern part of the DVRFS region (Zone 1, fig. B–26*B* and table B–6). To the west of each of these blocks, the LCA is broken into a series of back-rotated, extended range blocks in the vicinity of the Desert Range and the Nopah Range (Zone 4, fig. B–26*B* and table B–6). Abundant normal faults in these extended blocks may provide potential flow pathways; however, structural thinning could limit the available thickness of the carbonate aquifer (Dettinger and Schaefer, 1996). East of the NTS is a regional syncline (Zone 3, fig. B–26*B* and table B–6). Increased fracture permeability may exist along the axis of this fold. Much of the northeastern and central parts of the DVRFS region have been affected by basin-range faulting (Zone 8, fig. B–26*B* and table B–6). The degree of deformation and amount of extension in these areas is not as high as in the rotated, extended blocks to the southeast. In the western part of the DVRFS region, relatively large blocks have been displaced by extension and by movement on large regional strike-slip faults (Zone 7, fig. B–26*B* and table B–6). These blocks may be isolated from the regional carbonate aquifer (Dettinger and Schaefer, 1996) but may be of local importance.

Three additional types of deformation that potentially increase fracture-related permeability of the LCA are regional shear zones, oroflexural bending associated with regional strike-slip faults, and the presence of brittle detachments (fig. B–26*C*). In addition to major northwest-striking strike-slip faults, the Walker Lane belt includes northeast-striking shear zones that are transverse to the main trend of the belt (Carr, 1984; Stewart, 1988; Stewart and Crowell, 1992). These zones (Zone 2, fig. B–26*C* and table B–6) are characterized by subparallel, northeast-striking faults that accommodate relatively small amounts of sinistral and normal offset across a broad regional zone. Two such zones in the DVRFS region are the Spotted Range–Mine Mountain shear zone in the southern part of the NTS (Carr, 1984; Stewart, 1988) and the Pahranagat shear zone along the eastern boundary of the DVRFS region (Jayko, 1990). Broad areas of oroflexural bending (Albers, 1967) associated with major northwest-striking strike-slip faults have been defined by arcuate trends in the strike of tilted beds and fold axes (Burchfiel, 1965; Guth, 1981; Wernicke and others, 1984) (Zone 6, fig. B–26*C* and table B–6). In the vicinity of the LVVSZ, the clockwise bending appears to be related to the dextral slip and represents a broad zone of shear accommodated by crushing and local vertical axis rotation of blocks on the order of a few kilometers in lateral dimension (Nelson and Jones, 1987; Sonder and others, 1994). Local zones of potential enhanced permeability also are inferred in the upper plates of certain shallow-level, low-angle normal faults in the LCA (Zone 11, fig. B–26*C* and table B–6).

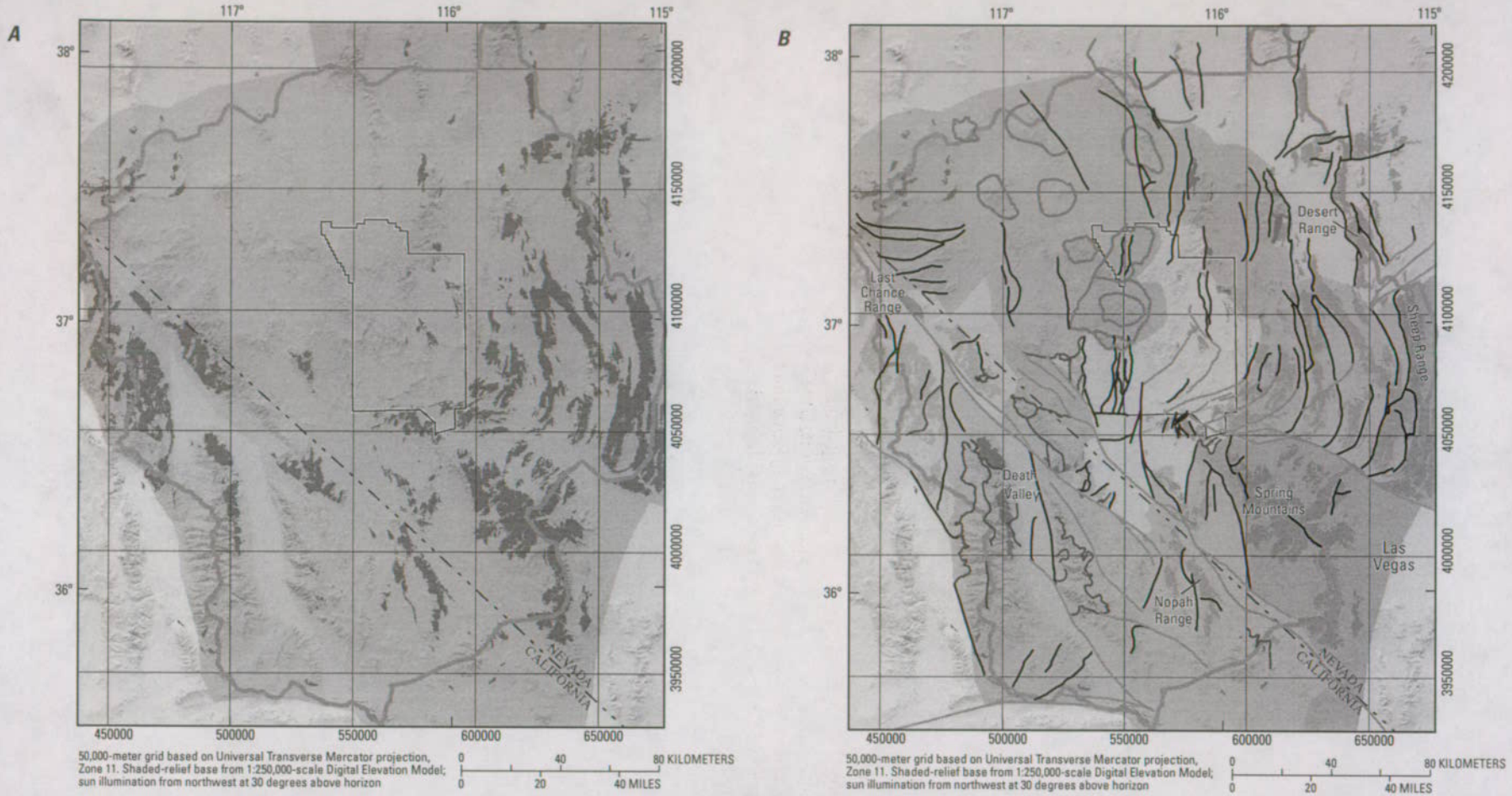

Figure B–26. Hydrogeologic zones in the lower carbonate-rock aquifer (LCA). *A*, Based on facies and continuity. *B*, Addition of zones based on degree of structural disruption. *C*, Addition of zones based on deformation that potentially increases fracture permeability.

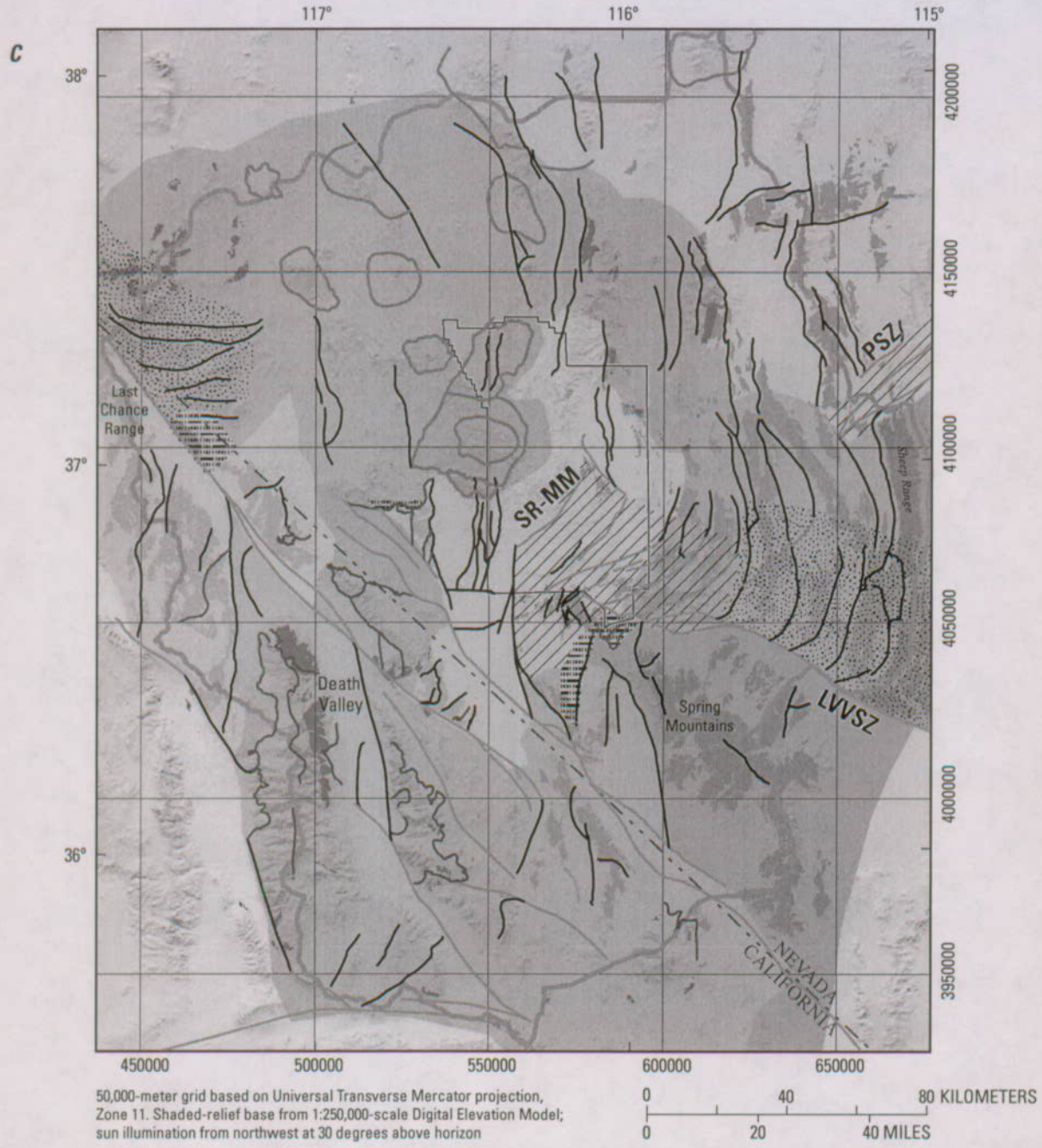

Figure B–26. Hydrogeologic zones in the lower carbonate-rock aquifer (LCA). *A*, Based on facies and continuity. *B*, Addition of zones based on degree of structural disruption. *C*, Addition of zones based on deformation that potentially increases fracture permeability.—Continued

Table B–6. Hydrogeologic zones for the lower carbonate-rock aquifer (LCA).

[SWNVF, southwestern Nevada volcanic field]

Zone	Description
1	Stable block: Relatively unextended and unfaulted blocks of the Spring Mountains and Sheep Range.
2	Regional shear zone: Spotted Range–Mine Mountain and Pahranagat shear zones. High fault/fracture densities associated with numerous minor strike-slip faults.
3	Regional syncline: Spotted Range syncline, a large regional fold; moderate fault/fracture density along axis of fold.
4	Rotated range blocks: Highly extended, rotated range blocks. May be associated with detachment at depth. Moderate to high fault/fracture density.
5	LCA not continuous: LCA is absent (near calderas of the SWNVF) or exists as tectonically dismembered blocks in areas of extreme extension.
6	Oroflexural bending: Associated with major strike-slip faults. High fault and fracture density associated with rotation of kilometer-scale (and smaller) blocks of LCA.
7	Displaced blocks: Relatively intact blocks of carbonate rocks that are involved in regional extension. Mesozoic thrusts reactivated as normal faults; moderate fault/fracture density. May be associated with detachment at depth.
8	Basin-range faulting: LCA that occurs in basin-range fault blocks. Low to moderate fault/fracture density.
9	Basinal facies: Low matrix permeability as carbonate rocks transition to shale in the extreme northwest part of the DVRFS region.
10	Uncertain: Aquifer properties of LCA highly uncertain.
11	Brittle detachment: Upper plate of shallow-level brittle detachment faults. High fault/fracture density.

Lower Clastic-Rock Confining Unit (LCCU)

The lower clastic-rock confining unit (LCCU) consists of Middle Proterozoic to Cambrian siliciclastic rocks and subordinate dolomite, and locally, their metamorphic equivalents. Throughout much of the central part of the DVRFS region, Late Proterozoic to Lower Cambrian strata consist of a westward-thickening wedge of fine- to coarse-grained sandstone, conglomeratic sandstone, siltstone, and minor amounts of carbonate rock (Stewart, 1970). The stratigraphic section includes the Late Proterozoic Johnnie Formation and Stirling Quartzite, the Late Proterozoic to Lower Cambrian Wood Canyon Formation, the Lower Cambrian Zabriskie Quartzite (Stewart, 1970), and the lower one-third of the interbedded carbonate and quartzose rocks of the Lower and Middle Cambrian Carrara Formation (Palmer and Halley, 1979). These rocks are exposed in the northwestern part of the Spring Mountains where they are about 3,000 m thick (Burchfiel, 1964; Stewart, 1970); in the Nopah Range, where the interval is up to 3,300 m thick, to the east of the NTS (Barnes and Christiansen, 1967; Reso, 1963); and in the Panamint Mountains west of Death Valley (Hunt and Mabey, 1966; Diehl, 1974; Wright and others, 1974) where they are about 2,500 m thick; and in the Funeral Mountains (Labotka and others, 1980; Wernicke and others, 1986; Wright and Troxel, 1993). Strata of equivalent age to the east of the DVRFS region are only a few hundred meters thick, mostly Early Cambrian, and are similar to the cratonic sections exposed in the Grand Canyon (Rowland, 1987; Poole and others, 1992).

Stratigraphically underlying the rocks described above are the oldest sedimentary rocks in the DVRFS region, which are exposed in a relatively small area of the southern part of the region. These consist of the Middle and Late Proterozoic carbonate and siliciclastic rocks of the Pahrump Group and the Late Proterozoic Noonday Dolomite. These rocks unconformably overlie the Early Proterozoic basement gneiss and intrusive rocks and are as thick as 2,500 m in an east-west-trending trough that extends from southern Death Valley to the Kingston Range (Wright and others, 1974). Pahrump Group rocks thin to the north, south, and east (Stewart, 1972; Wright and others, 1974). Abrupt stratigraphic pinch-outs and facies changes have been used to infer that these rocks were deposited in a fault-controlled, rift basin setting (Wright and others, 1974). The extent and thickness of Pahrump Group rocks throughout most of the DVRFS region are not known, however, because this stratigraphic unit is not exposed.

In the northwestern part of the DVRFS region, Late Proterozoic and Cambrian strata that correlate with those of the central part of the DVRFS region are thicker and finer grained and contain significant amounts of carbonate rocks. They consist of interbedded siltstone, shale, limestone, dolomite, and fine-grained quartzite (Nelson, 1962; Stewart, 1970; Albers and Stewart, 1972). The stratigraphic section of this region includes the Late Proterozoic Wyman Formation, Reed Dolomite and Deep Spring Formation, and the Lower Cambrian Campito, Poleta, and Harkless Formations. These strata are considered to be the White-Inyo assemblage (Stewart, 1970). They contrast with their more quartzose correlatives to the south—the Death Valley assemblage. Typical exposures are found in the White and Inyo Mountains and Last Chance Range in California (Nelson, 1962; McKee, 1985; Signor and Mount, 1986) and exposures in Esmeralda County, Nev. (McKee and Moiola, 1962; Stewart, 1970; Albers and Stewart, 1972; Nelson, 1978).

The LCCU has long been considered a major confining unit in the DVRFS region (Winograd and Thordarson, 1975) and, along with the crystalline confining unit (XCU),

represents the hydraulic basement for the DVRFS region (D'Agnese and others, 1997). The low hydraulic conductivity of the rock matrix permits negligible ground-water movement, but in many places the rocks are highly fractured and locally brecciated (Winograd and Thordarson, 1975). At shallow depths, the fractures and breccias can be conduits to flow, converting the clastic rocks into locally important shallow aquifers (D'Agnese and others, 1997).

The LCCU has been subdivided into six hydrogeologic zones based on lithology and structural considerations (Sweetkind and White, 2001) (fig. B–27, table B–7). The main facies transition in the Late Proterozoic through Lower Cambrian stratigraphic section of the DVRFS region is from an eastern region dominated by thick intervals of coarse siliciclastic rocks interbedded with shale (Zone 2; fig. B–27 and table B–7) to a more shale-dominated region with significant amounts of carbonate rocks (Zone 3; fig. B–27 and table B–7). Rocks of the LCCU are metamorphosed to medium and high grades where present in the lower plates of major detachment faults in the Panamint and Funeral Mountains (Labotka and others, 1980; Wernicke and others, 1986; Wright and Troxel, 1993) (Zone 5; fig. B–27 and table B–7). In the southernmost part of the DVRFS region, thick sections of Middle and Late Proterozoic carbonate rocks of the Pahrump Group are shallow enough that they could potentially be aquifers (Zone 4; fig. B–27 and table B–7).

Hydrogeologic Units Associated with Crystalline Metamorphic Rocks and Plutons

Intrusive-Rock Confining Unit (ICU)

The rocks of the intrusive-rock confining unit (ICU) include granodiorite, quartz monzonite, granite, and tonalite. Mesozoic and Cenozoic plutonic rocks in the DVRFS region are widely scattered, poorly exposed, and not abundant in the northeastern two-thirds of the DVRFS (fig. B–28). Plutonic rocks are much more common in the southwestern and western parts of the DVRFS region and include both plutons of the Mesozoic Sierran arc and synextensional plutons of the southern DVRFS region (Workman, Menges, Page, Ekren, and others, 2002).

Mesozoic granitic rocks include the Late Triassic to Early Jurassic quartz monzodioritic plutonic rocks underlying most of the Avawatz Mountains, Jurassic (mostly 186–161 Ma) plutons mostly to the west of Death Valley, and Cretaceous (mostly 100–92 Ma) in the Panamint Mountains and Owlshead Mountains. Small exposures of Cretaceous plutonic rocks in the vicinity of the NTS include the Climax stock on the northern side of Yucca Flat, the Gold Meadows stock north of Rainier Mesa, and granitic rocks on the eastern flank of the southern Kawich Range.

Oligocene and Miocene plutonic rocks crop out locally in the vicinity of the NTS, some of which are associated with caldera-related volcanism ranging in age from 32 to 11 Ma (Ekren and others, 1971; Cornwall, 1972; Ekren and others, 1977; Kleinhampl and Ziony, 1985; Slate and others, 2000). To the north of the NTS, a subcaldera pluton has been inferred in the Quinn Canyon Range (Workman, Menges, Page, Ekren, and others, 2002). At the NTS, outcrops of Neogene plutonic rocks include those near Wahmonie Flat and small intrusive bodies mapped in the Calico Hills and near Timber Mountain (Maldonado, 1985; Potter, Dickerson, and others, 2002). Neogene plutonic rocks that are associated with extension crop out in the southern part of Death Valley (Wright and others, 1999). These rocks include the gabbro to diorite intrusive rocks in the Black Mountains (about 10.3 Ma, Holm and others, 1992), the granites of the Kingston Range (12.4 Ma, Fowler and Calzia, 1999), the Little Chief stock in the Panamint Mountains, and other Neogene plutons of the Greenwater Range and central Death Valley volcanic field (Wright and others, 1991).

The ICU unit acts mostly as a confining unit. Although small quantities of water may pass through these intrusive crystalline rocks, where fractures or weathered zones exist, the fractures are poorly connected, and these rocks generally impede ground-water flow (Winograd and Thordarson, 1975).

Crystalline-Rock Confining Unit (XCU)

The crystalline-rock confining unit (XCU) consists of Early Proterozoic (about 1.7 Ga, Wright and Troxel, 1993) quartzofeldspathic schist, augen gneiss, granitic intrusive rocks, and metamorphosed Middle and Late Proterozoic sedimentary rocks. Early Proterozoic rocks are present in scattered exposures in the southern and southwestern parts of the DVRFS region and are rarely exposed throughout most of the rest of the DVRFS region (fig. B–28). These rocks crop out in the central part of the Panamint Mountains (Labotka and others, 1980), in the southern part of the Black Mountains (Holm and others, 1994), in the southern end of the Nopah Range, and in small exposures in the Funeral Mountains (Wright and Troxel, 1993) and the Bullfrog Hills (Hoisch and others, 1997) (fig. B–28). In many of these places, the Early Proterozoic crystalline rocks are in the lower plates of detachment faults. The Early Proterozoic crystalline rocks presumably form a continuous basement beneath most of the DVRFS region; they have been tectonically thickened and thinned and are locally invaded by younger plutons.

Ground water likely is present only locally in the XCU where the rock is fractured. Much of the XCU has gneissic or schistose foliation and lacks a continuous fracture network. Because the fractures are poorly connected, these rocks act mostly as confining units or barriers to flow (D'Agnese and others, 1997).

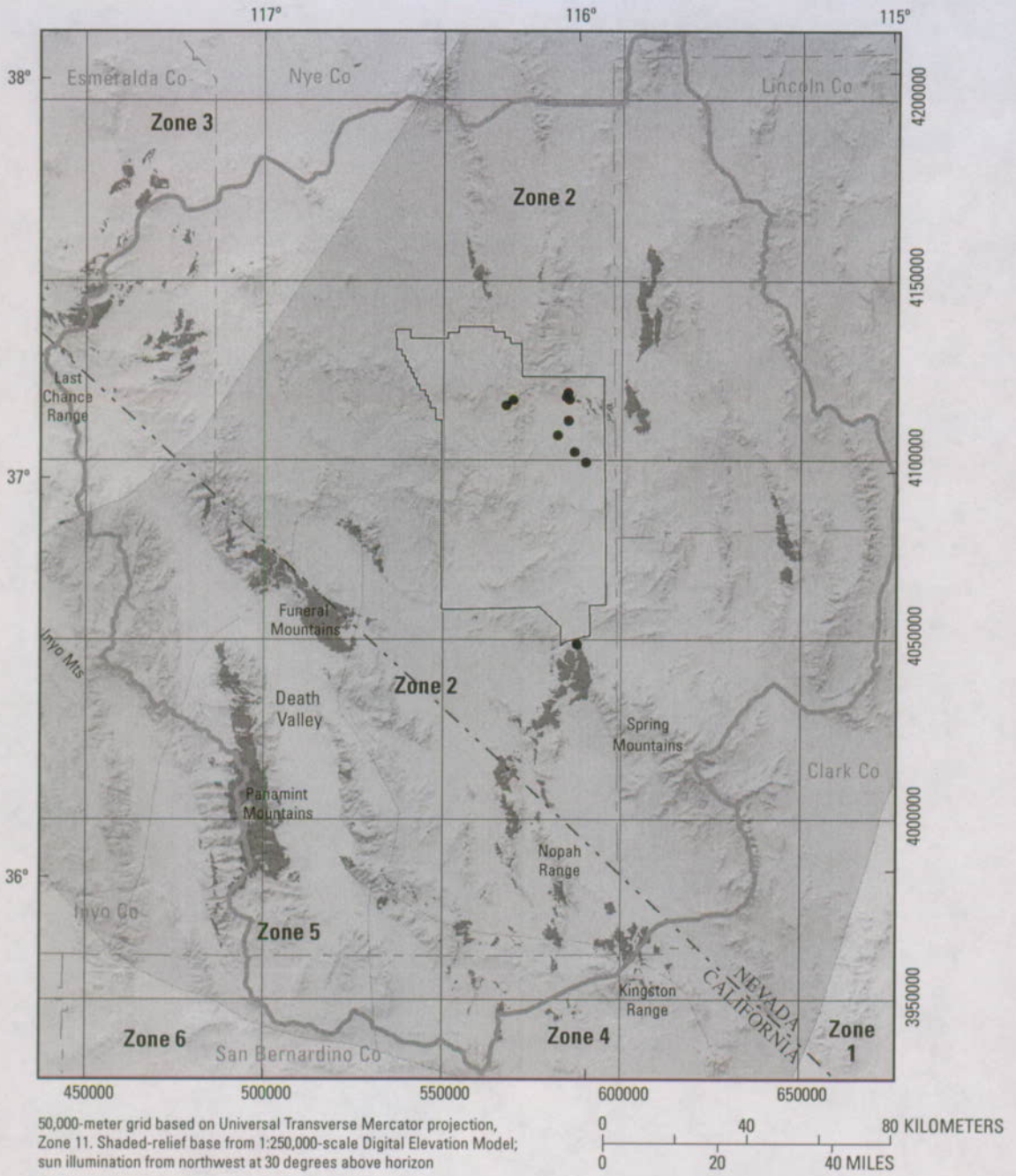

Figure B–27. Hydrogeologic zones in the lower clastic-rock confining unit (LCCU).

Table B–7. Hydrogeologic zones for the lower clastic-rock confining unit (LCCU).

Zone	Description
1	LCCU is very thin (a few hundred meters) and is similar to the cratonic sedimentary interval exposed in the Grand Canyon. Fine-grained siliciclastic rocks that generally act as a confining unit.
2	LCCU forms a westward-thickening wedge (generally 2,000 to 3,000 m thick) of fine- to coarse-grained sandstone, siltstone, conglomeratic sandstone, shale, and minor amounts of carbonate rock. Generally low permeability but may form local aquifer where highly deformed and complexly fractured.
3	LCCU is a thick (greater than 3,000 m) section of interbedded siltstone, limestone, dolomite, and fine-grained sandstone. Generally finer grained and more poorly sorted than rocks in Zone 2; however, interbedded sandstones and carbonate rocks locally may act as aquifers.
4	LCCU includes rocks of the Pahrump Group, a locally thick accumulation of Middle and Late Proterozoic sedimentary rocks. The Pahrump Group includes a significant thickness of dolomite and locally might be important to ground-water flow.
5	LCCU exposed beneath regional detachment structures. In these exposures, metamorphic grade is high, and the rocks are foliated and are of relatively low permeability. Possibly the lowest permeability of the LCCU.
6	LCCU either missing or properties are completely unknown.

Structural Factors Affecting Ground-Water Flow

The hydrogeologic effects of faulting in the DVRFS region result from either fault-caused juxtaposition of HGUs with contrasting hydrologic properties or from the physical characteristics of the fault zones themselves that may cause specific parts of the fault zone to act either as conduits or barriers to flow. Faults can have two effects on ground-water flow: direct effects associated with alterations to flow rates and ground-water velocities within the faulted zone, and indirect effects associated with alterations to the flow field in the area near the faulted zone (Black and others, 1987). Direct effects are related to (1) the physical characteristics of the fault-zone material or the material properties of the rock on either side of the fault that may cause specific parts of the zone to act either as conduits or as barriers to ground-water flow, (2) orientation of a fault with respect to the present stress field that affects dilatancy and possibly influences hydraulic conductivity along the fault zone, and (3) the recency of fault motion or association with contemporary seismicity where active stresses maintain fault openings and enhance permeabilities. Indirect effects are related to (1) fault juxtaposition of HGUs with contrasting hydrologic properties that may cause ground-water discharge and other perturbations in the flow system, and (2) the orientation of the structure with respect to the flow field. Structural controls on ground-water flow in the DVRFS region have long been recognized (Blankennagel and Weir, 1973; Winograd and Thordarson, 1975; Dudley and Larsen, 1976; Laczniak and others, 1996; Dettinger and Schaefer, 1996; McKee and others, 1998). Matrix permeability is low for both the LCA (Winograd and Thordarson, 1975) and for the welded parts of the volcanic-rock aquifers (Blankennagel and Weir, 1973). As such, faults, shear zones, and fractures largely determine the secondary water-transmitting properties of these rocks (McKee, 1997; McKee and others, 1998).

Juxtaposition of Hydrogeologic Units

Fault juxtaposition of hydrogeologic units with contrasting hydraulic and hydrologic properties may result in ground-water discharge and other perturbations in the regional flow system. Regional flow of ground water in the LCA in the DVRFS region is greatly influenced by the structural position of the relatively low permeability clastic-rock confining units (fig. B–29) (Winograd and Thordarson, 1975). Previous ground-water modeling studies (D'Agnese and others, 1997; IT Corporation, 1996a) have inferred that structurally elevated confining units divert ground-water flow in the central Funeral Mountains, the northwestern part of the Spring Mountains, and in the western part of Yucca Flat (fig. B–29). D'Agnese and others (1998) show that steep hydraulic gradients correlate in general with places where relatively low permeability rocks or structures are juxtaposed with aquifers.

The influence of structures and the juxtaposition of HGUs on a ground-water flow system emphasize the importance of subsurface geologic interpretation and the resulting depiction in a 3D digital HFM (Chapter E, this volume). The two recent regional ground-water flow models (IT Corporation, 1996a; D'Agnese and others, 1997) differ substantially in their subsurface structural geologic interpretation of the DVRFS region in terms of level of detail and structural style portrayed and internal consistency of the interpretations. The geologic framework in the YMP/HRMP model (D'Agnese and others, 1997) was based on a regional geologic map compilation (Faunt and others, 1997) and on a set of regional geologic cross sections (Grose, 1983; Grose and Smith, 1989). The cross sections did not include interpretations of large-magnitude extension (Wernicke and others, 1988; Snow, 1992; Snow and Wernicke, 2000) and more recent interpretations of regional thrust correlation (Trexler and others, 1996; Cole and Cashman, 1999). The DOE/NV-UGTA geologic framework model (IT Corporation, 1996b) incorporated recent interpretations of compressional and extensional structures, but cross sections drawn by multiple authors led to some inconsistencies in the geologic interpretations. Further, the cross sections were not referenced to a regional geologic map to guide structural interpretations.

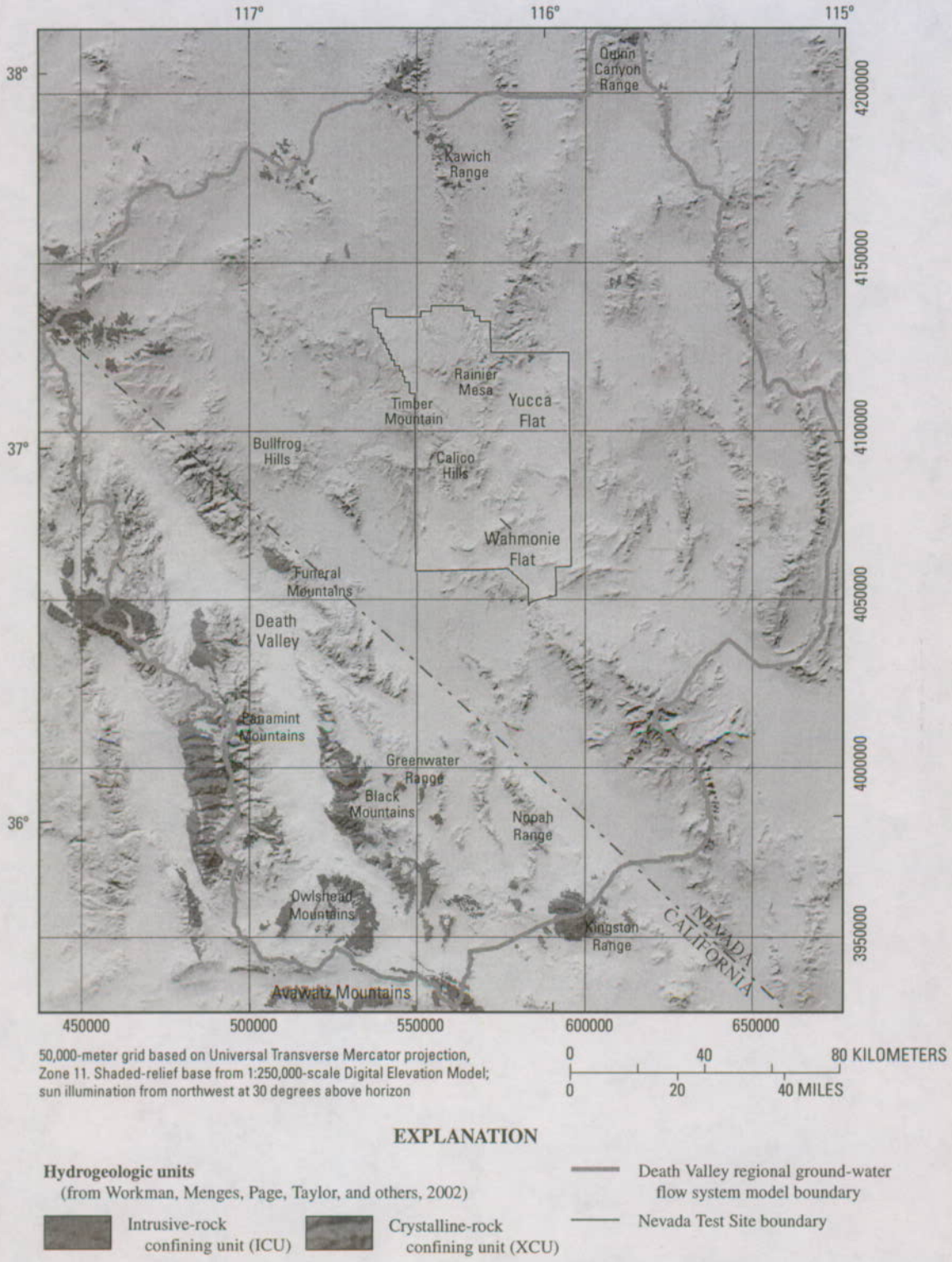

Figure B–28. Outcrop distribution of hydrogeologic units associated with metamorphic rocks and igneous plutons.

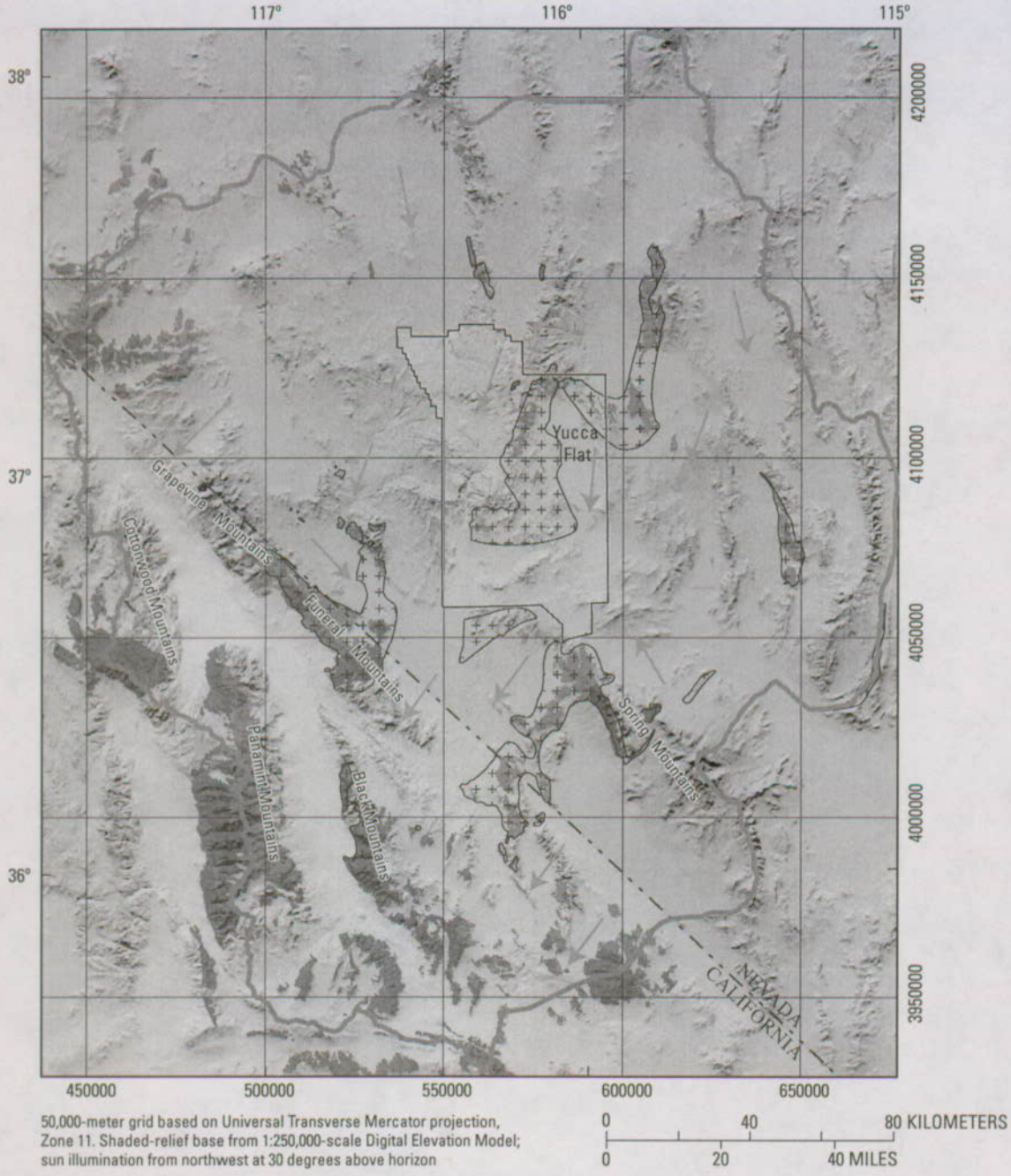

Figure B–29. Outcrop distribution of confining unit hydrogeologic units that potentially influence ground-water flow through juxtaposition of hydrogeologic units.

The current HFM (Chapter E, this volume) incorporates data from an integrated series of geologic investigations to develop a subsurface structural geologic interpretation. A regional geologic map compilation (Workman, Menges, Page, Taylor, and others, 2002) was created using a regionally consistent set of geologic map units and incorporating numerous sources of recent unpublished mapping. An accompanying regional tectonic map (Workman, Menges, Page, Ekren, and others, 2002) was created using regional magnetic and gravity compilations (Ponce and others, 2001; Ponce and Blakely, 2001; Blakely and Ponce, 2001) to interpret buried structures. A derivative regional structural map (Potter, Sweetkind, and others, 2002) interpreted the hydrologic significance of the features on the tectonic map on the basis of the regional potentiometric surface, springs, and structural evidence such as magnitude of fault offset. Subsurface geologic interpretation is depicted on 28 geologic cross sections (Sweetkind, Dickerson, and others, 2001) that were explicitly referenced to the geologic and structural map compilations. Cross-section interpretations used by the previous regional models were incorporated where appropriate.

Juxtaposition of Hydrogeologic Units by Thrust Faults

Thrust faults in the DVRFS region juxtapose hydrogeologic units of contrasting hydrologic properties and complicate the ground-water flow patterns by serving as local barriers (Winograd and Thordarson, 1975; McKee and others, 1998). These thrust faults are capable of causing significant diversion of ground-water flow or steep hydraulic gradients in the DVRFS region (Winograd and Thordarson, 1975; D'Agnese and others, 1998; Potter, Sweetkind, and others, 2002). The major thrust faults of the DVRFS region have stratigraphic offsets of several kilometers and horizontal displacements of up to several tens of kilometers based on offsets in regional facies trends (Fleck, 1970; Snow, 1992). This magnitude of stratigraphic offset typically results (for all thrusts except the frontal Keystone thrust and its equivalents; fig. B–5) in the juxtaposition of the older Late Proterozoic to Lower Cambrian siliciclastic-rock section in the upper plate against the younger Paleozoic Cambrian through Permian, predominantly carbonate-rock section in the lower plate (fig. B–30) (Armstrong, 1968; Fleck, 1970; Burchfiel and others, 1974). A complete description of thrust faults in the area is found in the tectonic map compilation of the DVRFS region (Workman, Menges, Page, Ekren, and others, 2002); thrust faults in the vicinity of the NTS are described by Cole and Cashman (1999). Structural reconstructions based on thrust correlation are summarized in Snow and Wernicke (2000).

To affect regional ground-water flow, thrust faults in the DVRFS region (fig. B–31) must have sufficient stratigraphic offset and along-strike continuity and be at an angle to the regional flow direction. Thrusts in the western part of the DVRFS region in the Funeral, Cottonwood, and Grapevine Mountains are generally subparallel to the regional northeast-to-southwest flow direction and may not influence the flow field except to divert water locally (D'Agnese and others, 1997). To the west of the Spring Mountains, several smaller thrusts are exposed in the rotated range blocks (Burchfiel and others, 1982, 1983; Snow and Wernicke, 2000). These thrusts exist in a tract of LCCU that generally separates Pahrump Valley from the Amargosa Desert, but the thrust plates are, in general, broken by normal faults and may be too discontinuous to be regionally significant. The Spring Mountains preserve two major, regionally extensive thrust faults, the Keystone thrust to the east and the Wheeler Pass thrust to the west (Burchfiel and others, 1974). Although well exposed, these thrusts crop out in the highest part of the DVRFS region; therefore, the large amount of water available as potential recharge may overwhelm bedrock geologic controls from the thrusts (D'Agnese and others, 1998).

The Belted Range thrust is the most northwesterly thrust structure identified in the vicinity of the NTS and is almost completely buried beneath Cenozoic volcanic rocks (fig. B–32). Late Proterozoic to Cambrian siliciclastic rocks in the upper plate of the thrust, part of the LCCU, are exposed only locally at the NTS and are known from borehole data (Cole and Cashman, 1999). In a general sense, the Belted Range thrust and related imbricate thrusts in its footwall juxtapose siliciclastic-rock confining units of the LCCU and UCCU against the Paleozoic carbonate rocks of the LCA. The great permeability contrast between these units is thought to create an effective barrier to ground-water flow (Laczniak and others, 1996) and segregates flow systems in the volcanic rocks of the western part of the NTS from carbonate-rock flow systems of the eastern part of the NTS (fig. B–31). The steep hydraulic gradient along most of the western side of Yucca Flat appears to be related to the combined effects of the Belted Range thrust and its footwall imbricates (Winograd and Thordarson, 1975; D'Agnese and others, 1998). This thrust was not explicitly included in the geologic framework of the YMP/HRMP model (D'Agnese and others, 1997), and a zone of low hydraulic conductivity that approximated the trace of the thrust had to be added during model calibration. The Belted Range thrust was included explicitly in the geologic framework of the DOE/NV-UGTA model (IT Corporation, 1996b) but was generalized as a vertical barrier in this flow model (IT Corporation, 1996a).

The Gass Peak thrust, along the eastern margin of the DVRFS region (fig. B–31), juxtaposes older siliciclastic Late Proterozoic Stirling Quartzite and Late Proterozoic to Lower Cambrian Wood Canyon Formation in its upper plate over highly folded and locally overturned younger Pennsylvanian and Permian carbonate-rock strata in the lower plate (Longwell and others, 1965; Guth, 1981). The thrust extends for at least 100 km along the eastern side of the Sheep Range and southward into the Las Vegas Range and may have greater than 30 km of horizontal displacement (Longwell and others, 1965; Guth, 1981). The siliciclastic rocks above the Gass Peak thrust may compartmentalize regional flow and

A View of north end of the Nopah Range, looking west-southwest

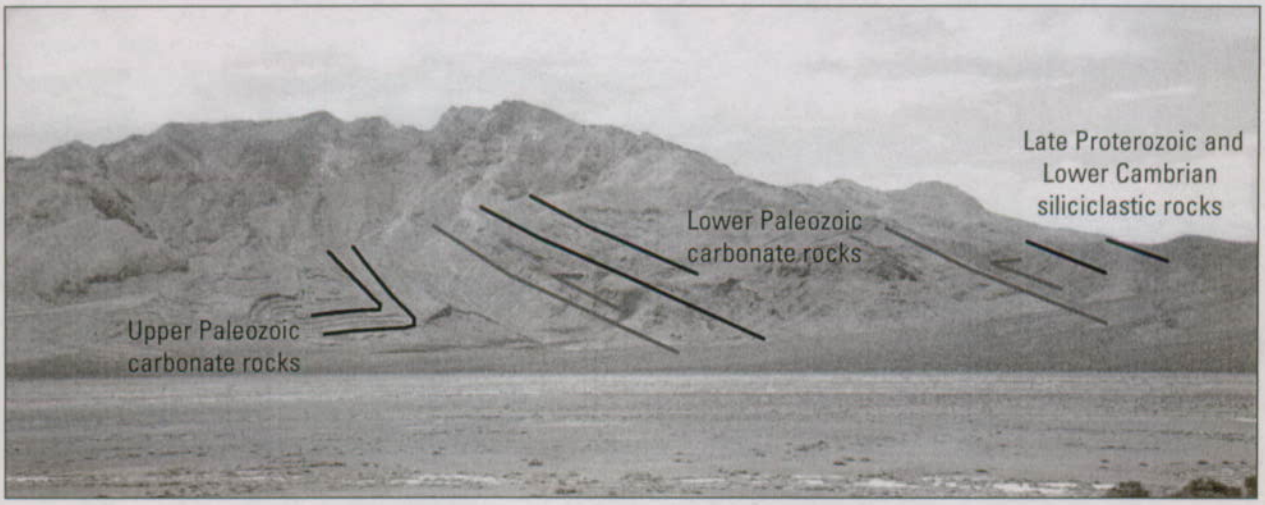

Late Proterozoic and Lower Cambrian siliciclastic rocks of hydrogeologic unit LCCU are thrust over lower Paleozoic carbonate rocks of hydrogeologic unit LCA, which are themselves thrust over younger carbonate rocks. Red lines denote thrust faults with arrow on the upper plate. Black lines portray general attitude of bedding. Geology after Burchfiel and others (1983). Photograph by D.S. Sweetkind, U.S. Geological Survey.

B Baxter thrust fault, Resting Spring Range

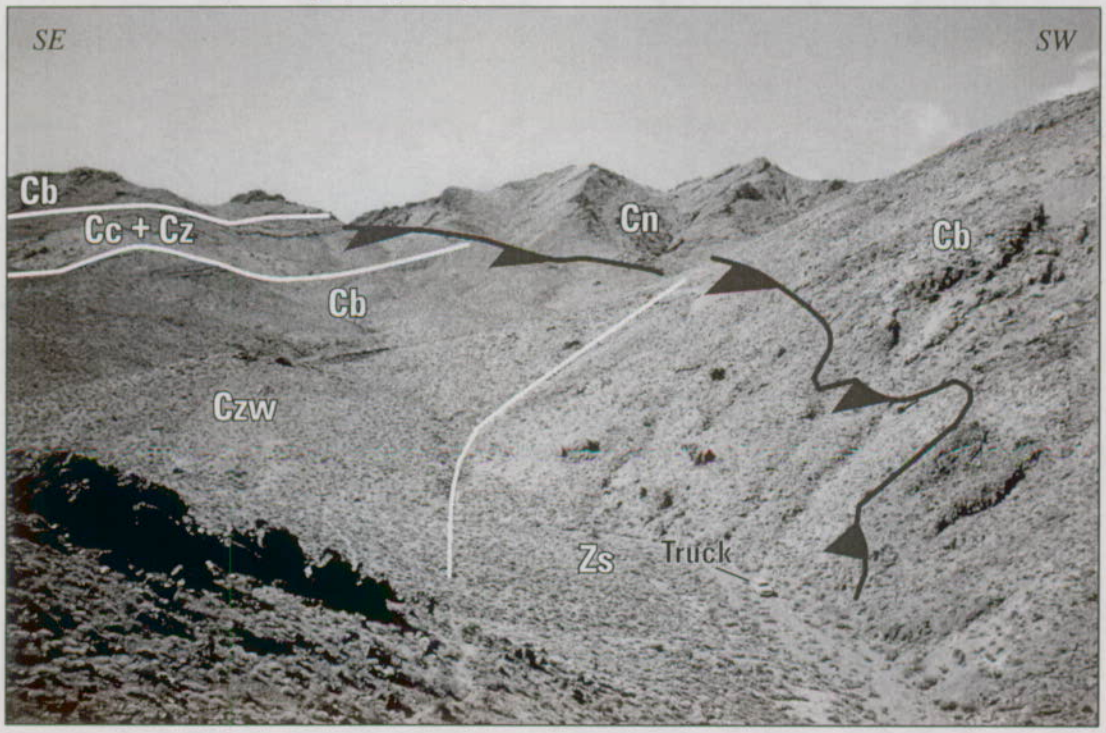

In this photo, the Baxter thrust places older rocks included within hydrogeologic unit LCCU (units Zs, Czw, Cz, and Cc) over younger Paleozoic carbonate rocks of hydrogeologic unit LCA (units Cb and Cn). Red line denotes thrust fault, with barbs on upper plate. Cenozoic deformation has rotated the strata 25 to 40 degrees to the east, exposing the Paleozoic carbonate rocks that lie beneath the thrust. The thrust climbs upsection in both the hanging wall and the footwall, successively truncating younger units. Geology after Burchfiel and others (1983). White truck in wash at lower right for scale. Photograph by D.S. Sweetkind, U.S. Geological Survey.

Figure B–30. Examples of thrust fault relations in the Death Valley regional ground-water flow system region.

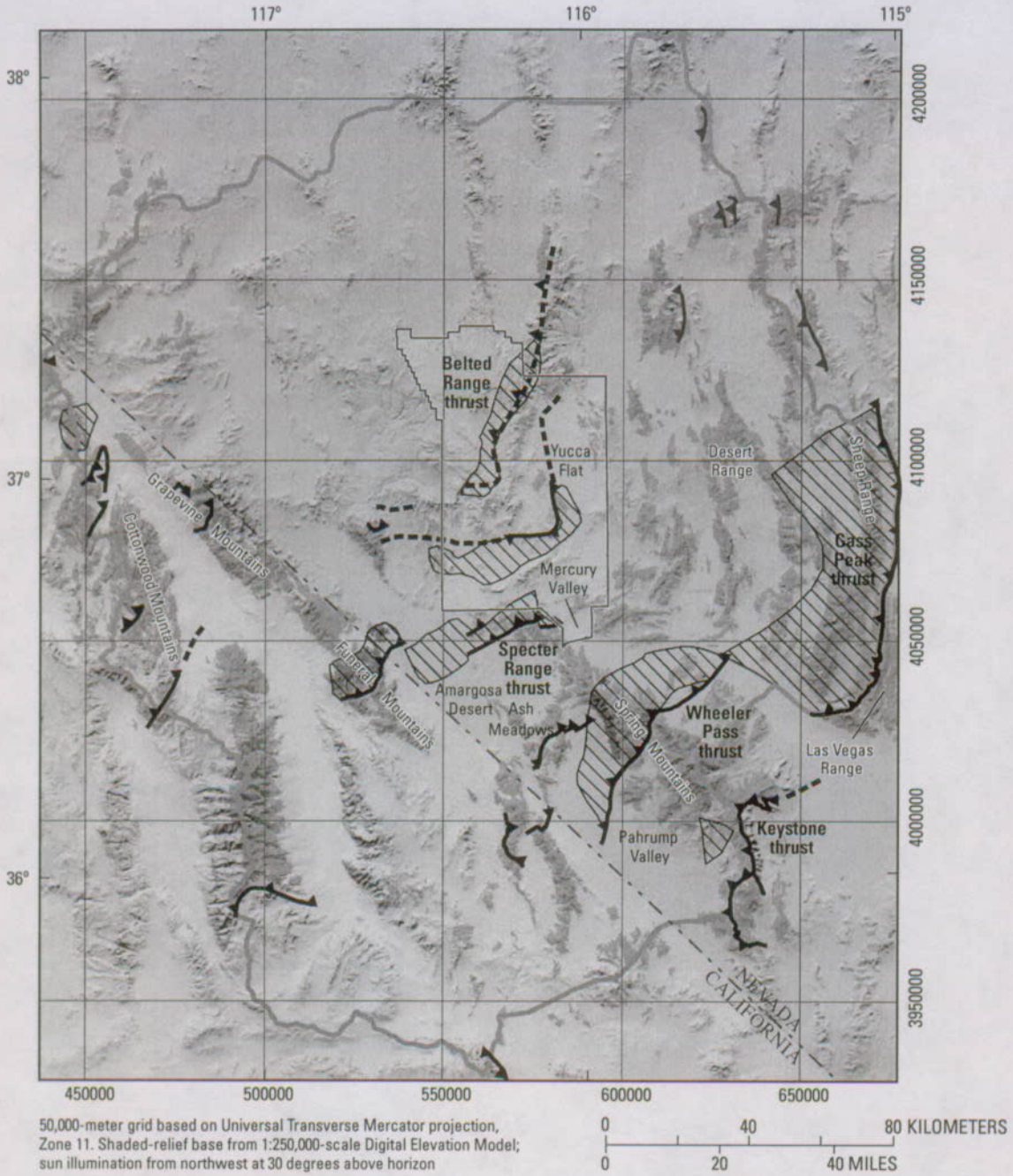

Figure B–31. Juxtaposition of hydrogeologic units by thrust faults in the Death Valley regional ground-water flow system region.

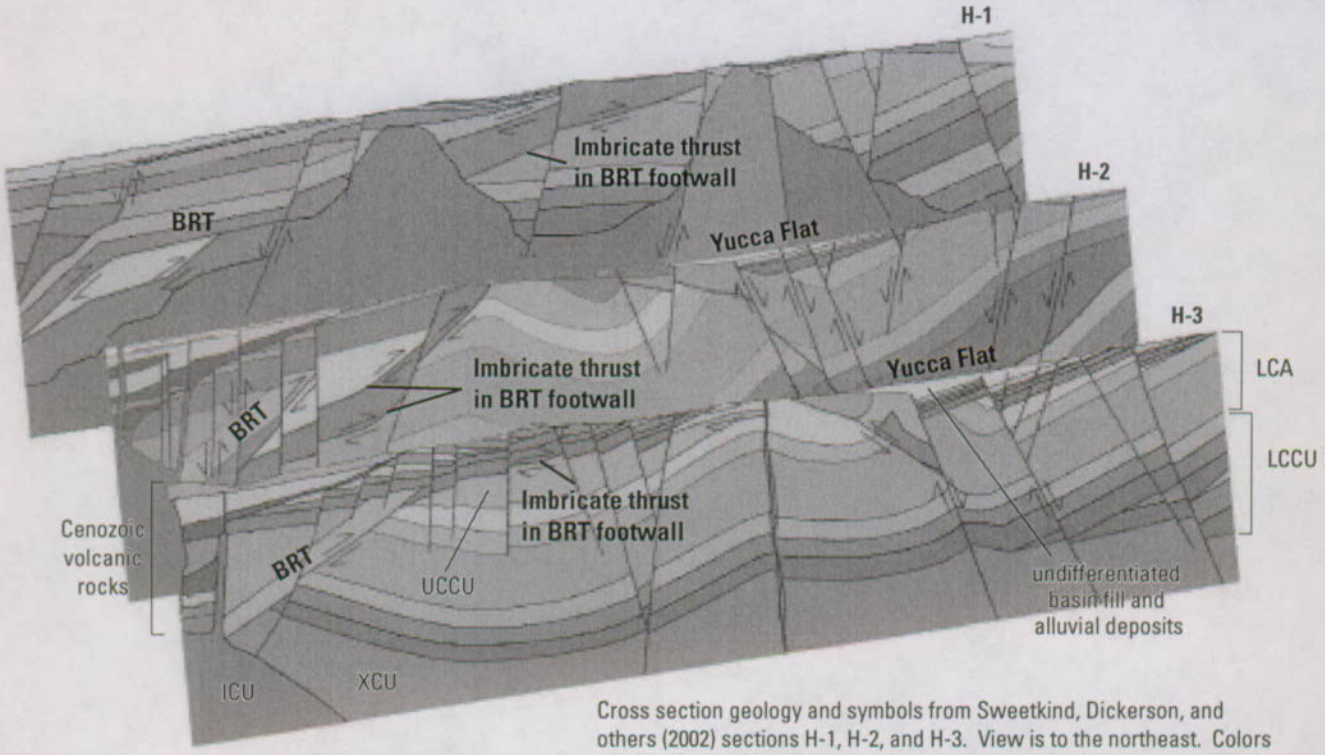

Cross section geology and symbols from Sweetkind, Dickerson, and others (2002) sections H-1, H-2, and H-3. View is to the northeast. Colors on the section correspond to hydrogeologic units as follows: Unit colored gray, XCU; units colored brown or tan, LCCU; units colored in shades of blue, LCA; gray, UCCU; red and pink, ICU; orange and light brown units at west (left) end of each section and beneath Yucca Flat are Cenozoic volcanic rocks; yellow color denotes undifferentiated basin fill and alluvial deposits. BRT, Belted Range thrust.

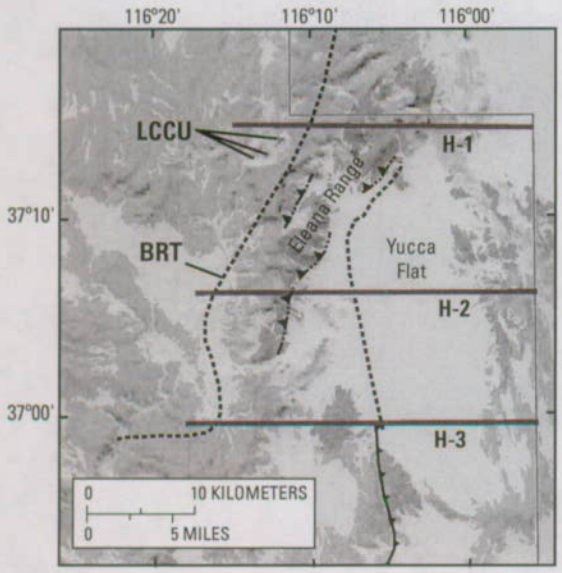

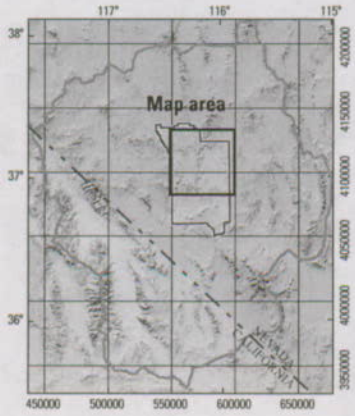

EXPLANATION

Map units
(from Workman, Menges, Page, Taylor, and others, 2002)

- Mississippian dominantly siliciclastic rocks (UCCU)
- Paleozoic carbonate rocks (LCA)
- Late Proterozoic to Cambrian siliciclastic rocks in upper plate of thrust (LCCU)
- Late Proterozoic to Cambrian siliciclastic rocks
- Undifferentiated Cenozoic volcanic rocks
- Undifferentiated Cenozoic basin fill
- Other rocks

- Nevada Test Site boundary
- Mapped thrust (from Potter, Sweetkind and others, 2002)
- Inferred thrust (from Potter, Sweetkind and others, 2002)
- Mapped thrust (after Cole and Cashman, 1999)
- Cross section line

Figure B–32. Interpreted subsurface geology, Belted Range thrust.

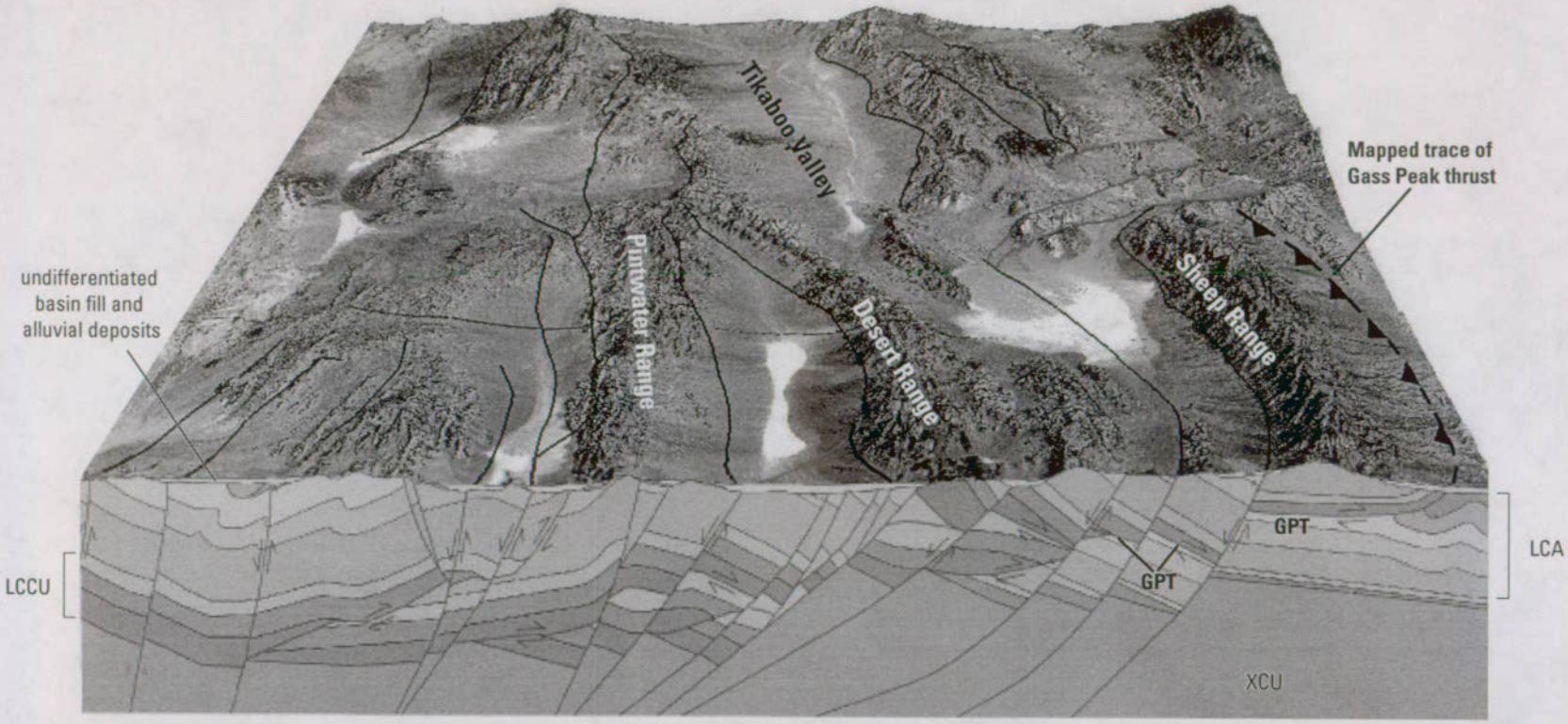

Image is false-color composite combining LANDSAT 6 spectral bands 2, 5, and 7 in RGB (Red-Green-Blue) space. Individual bands were processed to display their full dynamic range. The image was further processed in hue-saturation space to emphasize specific geologic features.

Cross section geology from Sweetkind, Dickerson, and others (2001) section H-5. View is to the north. GPT, Gass Peak thrust

EXPLANATION

Mapped and inferred faults from surface geologic mapping
(from Potter, Sweetkind, and others, 2002)

- Strike-slip fault
- Normal fault
- Thrust fault

Figure B–33. Interpreted subsurface geology, Gass Peak thrust.

separate the DVRFS from the Colorado River flow system to the east (Eakin, 1966). However, Cenozoic normal faults to the west of the Sheep Range have disrupted the continuity of the Gass Peak thrust (Guth, 1981, 1990; Wernicke and others, 1984) (fig. B–33). These faults are part of the Sheep Range detachment, a system of down-to-the-west normal faults that are inferred to flatten and converge at depth into a deep detachment zone, on the basis of significant rotation of bedding in the eastern part of the DVRFS region (Guth, 1981, 1990; Wernicke and others, 1984). These listric faults disrupt the continuity of the upper plate of the Gass Peak thrust and potentially allow connection of the two regional flow systems (fig. B–33). Guth (1981) presents an alternative view in which upper plate LCCU units thicken rapidly westward and effectively prohibit hydraulic connection of carbonate rocks of the upper and lower plate. Structurally elevated LCCU in the Desert Range (fig. B–33) is interpreted as a structural duplex of the Gass Peak thrust plate (Caskey and Schweikert, 1992) that has been subsequently disrupted by regional extension. This area forms a regional high of LCCU that diverts flow coming from the northeastern part of the DVRFS region (Dettinger and others, 1995; Dettinger and Schaefer, 1996).

The Specter Range thrust (fig. B–31) is a southeast-vergent thrust exposed in the Specter Range just south of the southern border of the NTS (Burchfiel, 1965; Sargent and Stewart, 1971). The thrust fault places older Late Proterozoic Stirling Quartzite and Late Proterozoic to Lower Cambrian Wood Canyon Formation (LCCU) over younger folded Ordovician, Silurian, and Devonian, strata (LCA) in the footwall (Burchfiel, 1965). The Specter Range thrust fault climbs upsection and loses stratigraphic throw to the northeast, where it appears to die out beneath Mercury Valley (McKee and others, 1998; Cole and Cashman, 1999). Interpretation of the subsurface extent of this thrust (McKee and others, 1998) indicates that it is a barrier to ground-water flow and channels flow in the regional carbonate aquifer southwestward toward discharge sites at Ash Meadows.

Juxtaposition of Hydrogeologic Units by Detachment and Normal Faults

Structurally high LCCU and XCU hydrogeologic units in the southwest part of the DVRFS region are associated with areas of highly disrupted surface rocks that are underlain by gently dipping extensional detachments that commonly expose a metamorphic core in their lower plates. The ranges bounding Death Valley (including the Panamint, Grapevine, Funeral, and Black Mountains) (fig. B–34) preserve major detachment faults that juxtapose lower plate, midcrustal, medium- and high-grade metamorphic rocks against unmetamorphosed upper-plate rocks across mylonite zones (Hamilton, 1988). The Grapevine and Funeral Mountains preserve the upper and lower plates, respectively, of the Boundary Canyon detachment, a gently dipping fault that juxtaposes amphibolite-grade metamorphic rocks of the lower plate against the unmetamorphosed rocks of the upper plate across a mylonitic zone only a few meters thick (Hamilton, 1988; Wright and Troxel, 1993). A major system of gently inclined normal faults exposes midcrustal metamorphic rocks in the Black Mountains, to the east of Death Valley. Overlying these major, low-angle detachment faults are Cenozoic sedimentary and volcanic rocks (fig. B–35*A*) that are cut by abundant listric normal faults (Greene, 1997). The Panamint Mountains (fig. B–34) are bounded on the east, north, and west sides by extensional structures known as the Tucki Mountain detachment system (Wernicke and others, 1986; McKenna and Hodges, 1990; Andrew, 2000). Exposures of Proterozoic metamorphic and siliciclastic rocks in the Funeral and Black Mountains are associated with a steep hydraulic gradient along the east side of Death Valley (D'Agnese and others, 1997). Regional springs are present in Death Valley only in the northern part of the Grapevine Mountains and the southern part of the Funeral Mountains (Steinkampf and Werrell, 2001), where more permeable rocks allow ground-water flow; no regional springs are present where the confining units are exposed.

The Fluorspar Canyon–Bullfrog Hills detachment system (fig. B–35*B*) separates nonmetamorphosed Cenozoic volcanic strata in the upper plate from the pre-Cenozoic bedrock of the lower plate at Bare Mountain (Monsen and others, 1992; Fridrich and others, 1999). In the southern Bullfrog Hills, complexly faulted upper plate volcanic rocks are disrupted by listric normal faults that merge with the detachment zone, which consists of fault-bounded lenses of nonmetamorphosed Paleozoic strata (fig. B–35*B*) (Maldonado and Hausback, 1990; Maldonado, 1990), all of which overlie a lower plate of amphibolite-grade metamorphic rocks (Hoisch and others, 1997). This fault was not included in the geologic framework of the YMP/HRMP model, and a zone of low hydraulic conductivity that approximated the fault was added during flow-model calibration (D'Agnese and others, 1997). Inverse models of gravity data (fig. B–35*C*) (Ponce and others, 2001) and recent geologic mapping (Monsen and others, 1992; Fridrich and others, 1999) show that Cenozoic volcanic rocks are thin and that pre-Cenozoic rocks lie at shallow depths throughout most of the southern part of the Bullfrog Hills. These data substantiate the existence of the detachment fault in the Bullfrog Hills.

Juxtaposition of contrasting HGUs along large-offset normal faults localizes substantial ground-water discharge at several places in the DVRFS region. Regional northeast-to-southwest flowing ground water is likely diverted to the surface in the eastern Amargosa Desert, where the LCA is juxtaposed against the low-permeability basin-fill materials across the Gravity fault (Winograd and Thordarson, 1975; Dudley and Larsen, 1976). At Oasis Valley, a cluster of springs is localized along the Hogback normal fault (Potter, Sweetkind, and others, 2002). These springs appear to be localized by the juxtaposition of permeable volcanic rocks on the east against LCCU on the west (Grauch and others, 1999; Fridrich and others, 1999). As a result, westward-flowing ground water in the volcanic rocks is forced to the land surface when it contacts the LCCU. Several springs in the central part of the DVRFS region appear to be related to fault juxtaposition of contrasting

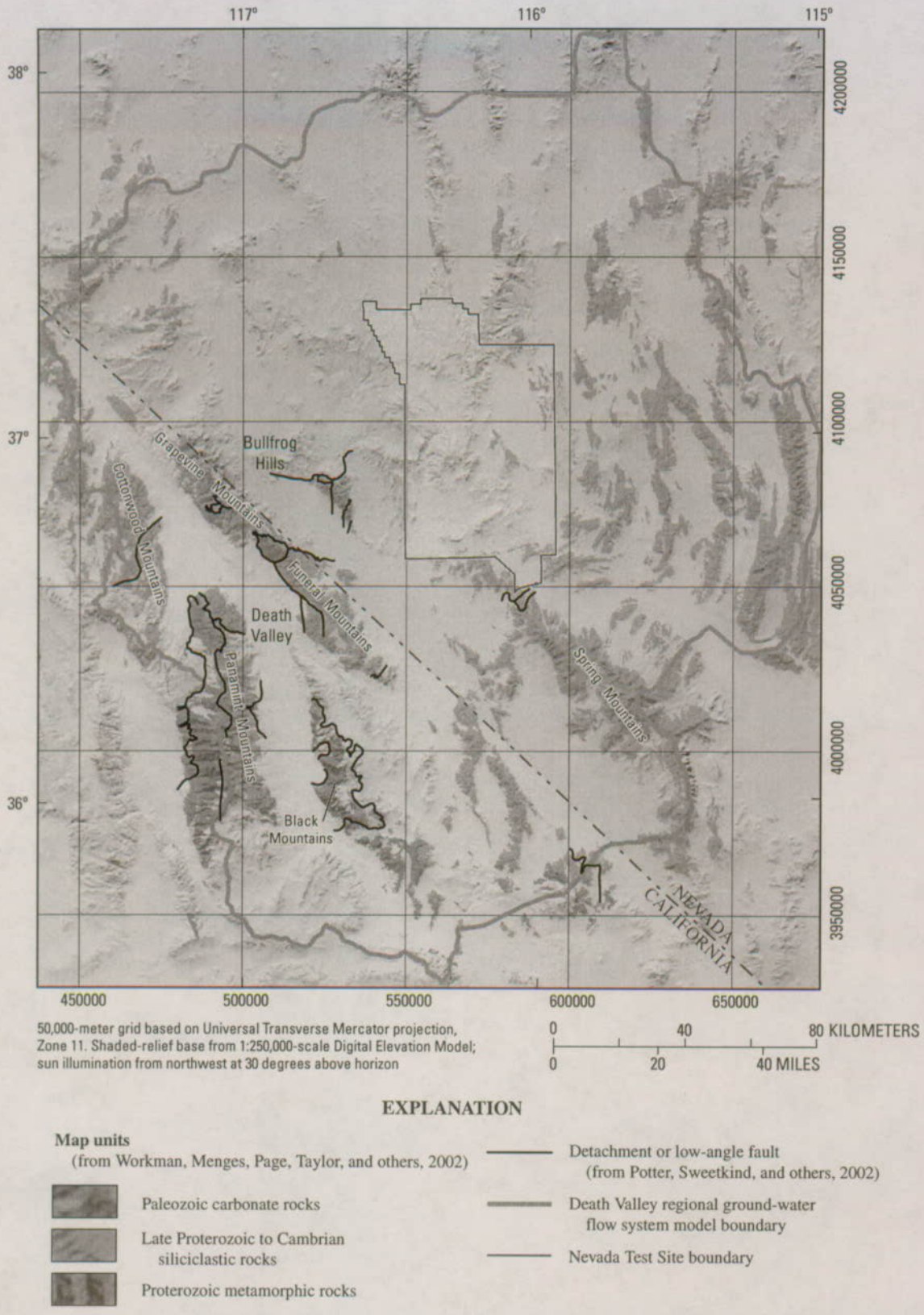

Figure B–34. Juxtaposition of hydrogeologic units by detachment faults in the Death Valley regional ground-water flow system region.

A

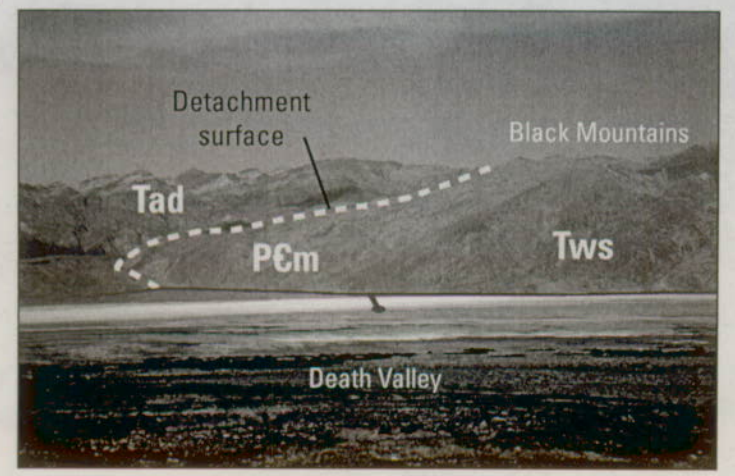

View is to the east from the western side of Death Valley. The crystalline core of the Black Mountains (PCm and Tws on the figure) lie beneath a gently northwest-dipping detachment fault. Upper plate rocks are Cenozoic sedimentary and volcanic rocks (Tad on figure; equivalent to hydrogeologic unit VSU) cut by abundant listric normal faults that flatten and merge with the detachment fault. Normal faults are shown by red lines, with ball and bar on downthrown side.

B

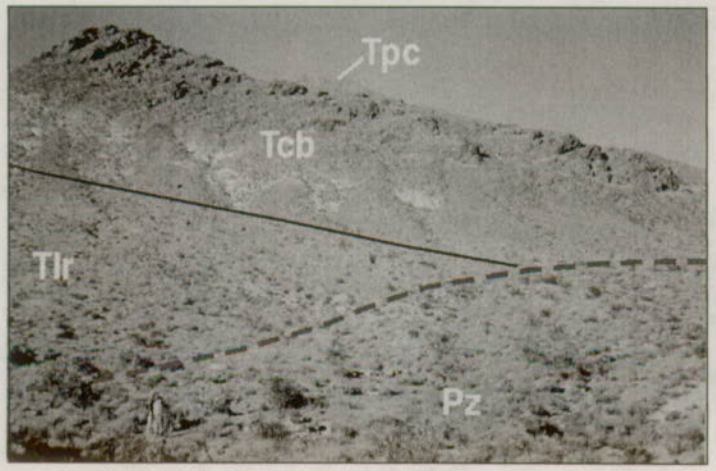

View of Fluorspar Canyon–Bullfrog Hills detachment. Tilted Cenozoic volcanic rocks (Tlr, Tcb, Tpc) are truncated against a subhorizontal detachment fault that locally has complexly faulted Paleozoic strata (Pz in figure) in its lower plate. Geology after Maldonado and Hausback (1990). Inverse models of gravity data (below) show that pre-Cenozoic rocks lie at shallow depths throughout most of the southern part of the Bullfrog Hills.

Photographs by D.S. Sweetkind, U.S. Geological Survey.

C

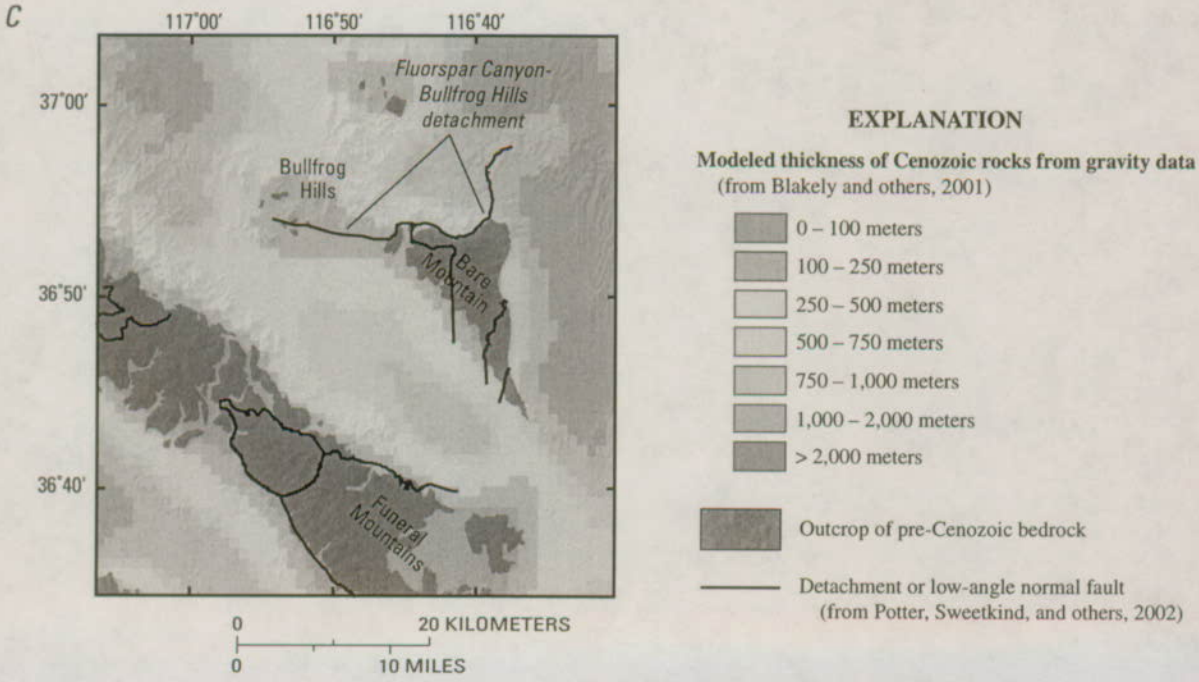

Figure B–35. Examples of detachment fault relations in the Death Valley regional ground-water flow system region.

HGUs near the Furnace Creek fault zone (D'Agnese and others, 1997; Steinkampf and Werrell, 2001). This strike-slip fault zone has a significant component of down-to-the-southwest displacement, juxtaposing the LCA (to the east) against the VSU units (to the west). Southwestward-flowing ground water that bears the chemical signature of regional flow in the LCA (Winograd and Thordarson, 1975; Steinkampf and Werrell, 2001) is diverted to the land surface, most likely because of contrasting hydraulic conductivities across the fault zone. Contrasting water levels and water-chemistry data across faults in the Yucca Mountain–Crater Flat area provide evidence that some normal faults in the volcanic rocks impede ground-water flow (Luckey and others, 1996) and thus compartmentalize the flow system.

Implication of Alternative Interpretations on Magnitude of Regional Extension

Ground-water investigations of the DVRFS region have assumed a relatively continuous Paleozoic carbonate aquifer throughout at least the eastern one-half of the DVRFS region (Winograd and Thordarson, 1975; Prudic and others, 1995; Thomas and others, 1996; Laczniak and others, 1996; D'Agnese and others, 1997, 2002). The Paleozoic carbonate-rock aquifer crops out extensively in the ranges throughout most of the eastern one-half of the DVRFS region; its presence beneath basin-fill sediments in the valleys, however, is subject to interpretation. Regional models of extension (Wernicke, 1992; Snow and Wernicke, 2000) imply discontinuity between range blocks in the carbonate-rock section. Regional estimates of extension based on correlation of thrust faults indicate that many of the carbonate-rock mountain ranges of the DVRFS region lie in a zone of extreme crustal extension, implying that these ranges are thin slivers of crust that detached above a migrating flexure in highly thinned crust (Holm and others, 1992; Wernicke, 1992). In this view, Proterozoic siliciclastic or crystalline rocks might be expected beneath basin-fill sediments in the valleys. In contrast, a number of interpretive geologic cross sections of the region portray a relatively continuous carbonate aquifer beneath basin-fill sediments throughout much of the DVRFS region (Grose, 1983; Grose and Smith, 1989; Laczniak and others, 1996; Sweetkind, Dickerson, and others, 2001).

Pre-Cenozoic bedrock has been identified in boreholes in areas of the DVRFS region that have been interpreted to have been greatly extended (fig. B–36), although the bedrock beneath most of the basins has not been reached by drill holes. Paleozoic carbonate rocks have been identified in borehole UE–25 p#1 (USGS Site ID 364938116252101) to the east of Yucca Mountain (Carr and others, 1986) and in the northern part of the Amargosa Desert (Carr and others, 1995; R.W Spengler, U.S. Geological Survey, written commun., 2002). Boreholes of Paleozoic bedrock in Yucca Flat are numerous enough to construct subsurface geologic maps of specific formations (Cole and others, 1997). Furthermore, hydrochemical data indicate that a number of the major springs in the DVRFS region (fig. B–36) are probably sourced from water that flowed through the carbonate-rock aquifer (Winograd and Thordarson, 1975; Steinkampf and Werrell, 2001). These data indicate at a minimum that some, if not all, of the water from regional springs is flowing through a continuous carbonate-rock aquifer (Winograd and Pearson, 1976). More information on the hydrochemistry and its implications for regional ground-water flow can be found in Chapter D (this volume).

Juxtaposition of Hydrogeologic Units at Caldera Boundaries

The structural and topographic margins of calderas in the SWNVF juxtapose intracaldera and outflow-facies volcanic rocks. Intracaldera rocks differ in their geometry and material properties from equivalent outflow facies in having greater thicknesses of welded material and more complex welding zonation, greater lithologic diversity including megabreccia and thick lava accumulations, and a greater degree of alteration. Fracture patterns in intracaldera rocks tend to be more irregular than those of outflow tuffs (Blankennagel and Weir, 1973), leading to a smaller number of connected flow paths. Outflow tuff sheets, although thinner than intracaldera tuff accumulations, have better connected fracture networks and there is less likelihood of significant alteration (Blankennagel and Weir, 1973). Few boreholes in the SWNVF are located such that the hydraulic significance of juxtaposition at caldera boundaries can be defined.

A caldera model with gently inwardly sloping topographic walls along with near-vertical ring faults defining the structural boundary of caldera subsidence (Lipman, 1984; Lipman 1997) was used as a conceptual basis for simulating all calderas within the SWNVF in the YMP/HRMP model (D'Agnese and others, 1997, p. 15). An alternative conceptual model for the buried calderas of the SCCC and TMCC was used in the geologic framework of the DOE/NV-UGTA model (IT Corporation, 1996b). The alternative model envisions a group of rectilinear fault-block basins formed by caldera collapse localized by preexisting linear normal faults (Ferguson and others, 1994; Warren and others, 2000). An example of such a fault is the Thirsty Canyon lineament (corresponding to feature 14 of Grauch and others, 1999; their figure B–7 and table B–4) that is interpreted from geophysical data to be a preexisting fault zone that was later exploited to form the straight northwestern boundaries (fig. B–13) of the SCCC and TMCC (Grauch and others, 1999). Numerous local fault blocks proposed for this alternative model (Ferguson and others, 1994; Warren and others, 2000) were not used in recent 3D geologic framework models of the Pahute Mesa area (McKee and others, 1999; McKee and others, 2001) because (1) the geophysical data are insufficient to detect the high-angle fault-block basins and (2) the geologic data from boreholes in the upper 900 m define small-offset, high-angle faults (McKee and others, 1999, 2001).

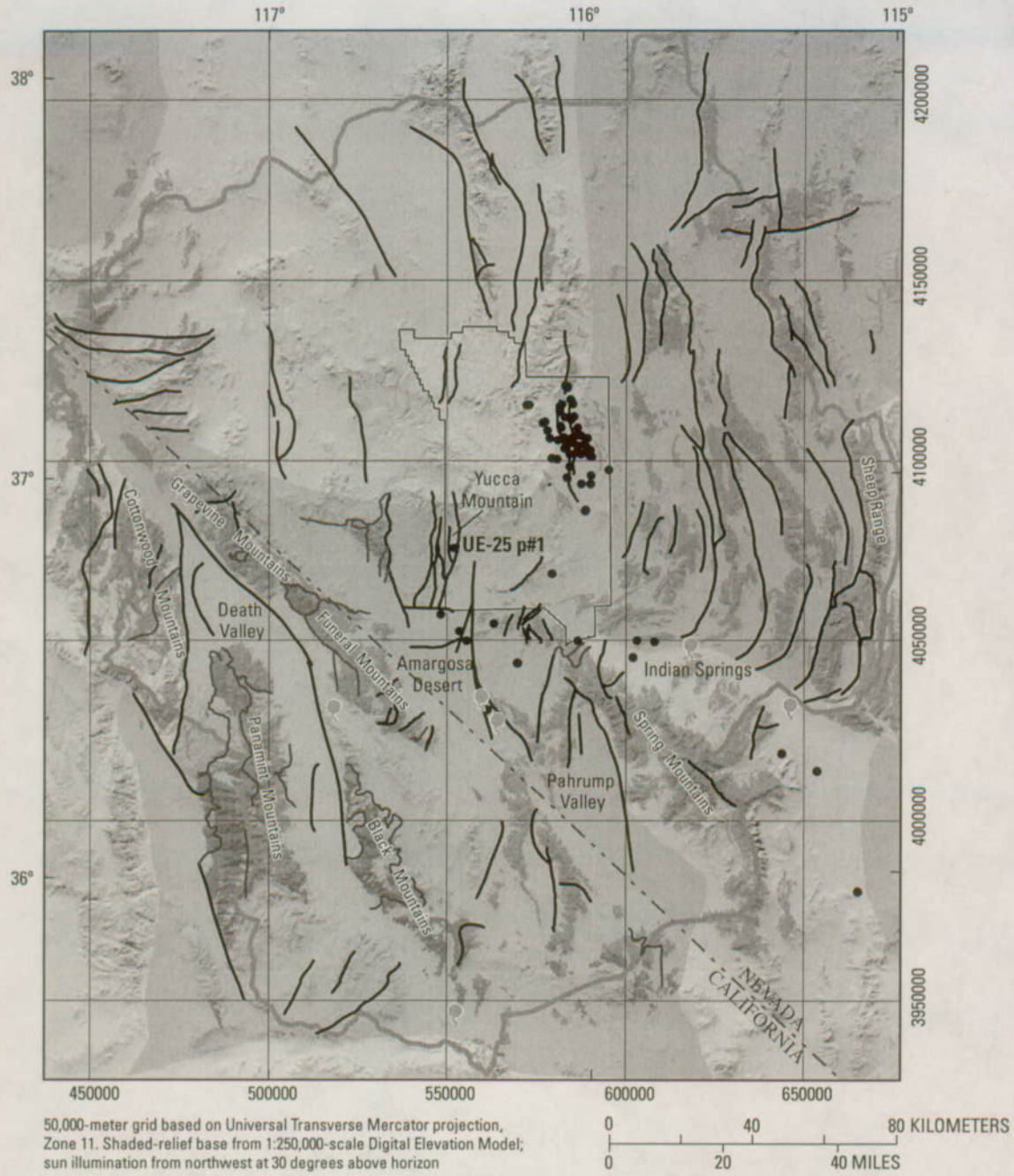

EXPLANATION

Map units
(from Workman, Menges, Page, Taylor, and others, 2002)

- Paleozoic carbonate rocks
- Late Proterozoic to Cambrian siliciclastic rocks
- Proterozoic metamorphic rocks
- Greatly extended domains (after Wernicke, 1992)

- Normal fault (from Potter, Sweetkind, and others, 2002)
- Detachment or low-angle fault (from Potter, Sweetkind and others, 2002)
- Death Valley regional ground-water flow system model boundary
- Nevada Test Site boundary
- Location of borehole that penetrates hydrogeologic unit LCA
- Location of large-volume spring with chemistry consistent with flow through hydrogeologic unit LCA

Figure B–36. Greatly extended domains, faults, boreholes, and regional springs associated with the Paleozoic carbonate-rock aquifer.

Faults as Hydrogeologic Features

Many brittle fault zones contain a narrow core of fine-grained, relatively low-permeability gouge that is the locus of fault displacement (Caine and others, 1996). In many cases, the core will have reduced permeability, relative to that of the original rock or the surrounding damage zone, as a result of progressive grain-size reduction, dissolution, reaction, and mineral precipitation (Caine and others, 1996). The core zone can be flanked by damage zones, a network of subsidiary small faults and fractures that enhance secondary permeability (Caine and others, 1996; Caine and Forster, 1999). Fault cores typically restrict fluid flow across the fault, while the damage zone may conduct ground-water flow parallel to the fault zone. In general, large-displacement faults are characterized by a continuous, relatively low permeability core zone (Chester and Logan, 1986).

Hydraulic Barriers

On the basis of characteristics of the potentiometric surface, the location of springs, and the location of the fault with respect to predominant northeast-to-southwest ground-water flow in the DVRFS region, several of the large strike-slip faults in the DVRFS region, including the LVVSZ, the Pahrump–Stewart Valley fault zone, and the Death Valley–Furnace Creek fault system (fig. B–7), are thought to be potential barriers to ground-water flow. The large strike-slip faults in the southwestern part of the DVRFS region are generally buried beneath Cenozoic sediments, although traces of the faults are commonly defined by Quaternary fault scarps (Anderson and others, 1995; Piety, 1996). Geophysical investigations of the LVVSZ (Langenheim and others, 2001) and the Pahrump–Stewart Valley fault zone (Blakely and others, 1998, 1999) portray a structurally complex pre-Cenozoic surface adjacent to these faults consisting of steep-sided local depressions and ridges that likely are fault-bounded (fig. B–37) and probably represent local compression and extension in the overall strike-slip environment (Wright, 1989).

The LVVSZ extends more than 100 km northwestward from its eastern end near Frenchman Mountain, on the east side of Las Vegas Valley (fig. B–7). The LVVSZ is a complex system of right-lateral faults with several fault strands and associated steep-sided pull-apart subbasins (Langenheim and others, 2001). Right-lateral offset of correlative features across the LVVSZ is estimated to be from 40 to 66 km (Stewart and others, 1968; Longwell, 1974); displacement is thought to have occurred between 14 and 8.5 Ma (Bohannon, 1984; Duebendorfer and Black, 1992). The LVVSZ appears to form a hydraulic barrier in the Indian Springs, Nev., area; spring discharge at Indian Springs (fig. B–36) may reflect upward flow of ground water against a low-permeability fault barrier (Winograd and Thordarson, 1975). The Pahrump–Stewart Valley fault zone (Stewart and others, 1968; Burchfiel and others, 1983; Stewart and Crowell, 1992) is a regionally extensive, right-lateral, strike-slip fault zone that roughly parallels the California-Nevada border through the Stewart and Pahrump Valleys. The fault zone may be as long as 150 km (Schweickert and Lahren, 1997; Blakely and others, 1998) and is estimated to have between 20 and 30 km of right-lateral offset based on offset of Proterozoic and Paleozoic rocks (Stewart and others, 1968), interpreted correlations of thrust sheets, and offsets in regional facies trends (Stevens and others, 1991). The faults are almost everywhere buried by Cenozoic rocks; part of the zone is exposed in the southern Montgomery Mountains (fig. B–38) (as defined by Burchfiel and others, 1983).

The 250-km-long Death Valley–Furnace Creek fault system consists of right-lateral strike-slip and normal faults that cross the entire western part of the DVRFS region (fig. B–7) (Stewart, 1988; Piety, 1996). The southern part of the system is a 50-km-long set of northwest-striking, predominantly right-lateral faults that underlie southern Death Valley (Workman, Menges, Page, Ekren, and others, 2002). The central part of the system is a 60-km-long, north-northwest-trending, primarily oblique normal-slip fault zone that forms the western range front of the Black Mountains (fig. B–6) (Piety, 1996). The northern part of this fault system is an active right-lateral fault zone (Piety, 1996) with a total cumulative right-lateral offset estimated at about 65 to 80 km (Stewart, 1967; Stewart and others, 1968; Snow and Wernicke, 1989). Springs in the northern part of Death Valley may be localized along the northern Death Valley–Furnace Creek fault zone where upward flow of ground water is localized against a low-permeability fault barrier (Winograd and Thordarson, 1975; Potter, Sweetkind, and others, 2002).

Potter, Sweetkind, and others (2002) compiled the locations of principal faults and structural zones in the DVRFS region that may influence ground-water flow. A subset of the mapped faults in DVRFS region was chosen for possible inclusion as hydraulic barriers in the ground-water flow model (fig. B–39). Faults were chosen on the basis of their length, offset, type of slip, orientation, characteristics of the potentiometric surface, and the location of springs. The emphasis was on faults that may have special hydraulic characteristics that may require them to be treated as separate entities in the flow model. Juxtaposition of HGUs with different hydraulic properties was not a primary consideration as these relations are incorporated in the HFM (Chapter E, this volume). Structural features were classified based on a hierarchical approach for possible sequential inclusion into the flow model (table B–8). Initially, northwest-striking faults were separated from faults of other (primarily north-south) orientation (table B–8; fig. B–39). The northwest-striking faults typically are the large-offset strike-slip faults that are oriented approximately perpendicular to the flow direction. These faults are interpreted as being the most likely structural barriers to regional ground-water flow. Second-level subdivision of these faults consists of dividing the northwest-striking faults that involve the regional carbonate-rock aquifer from those that involve other, primarily confining, units. Finally, local segments of strike-slip faults are subdivided; these segments of different orientation from the main fault trace correspond to releasing or restraining bends

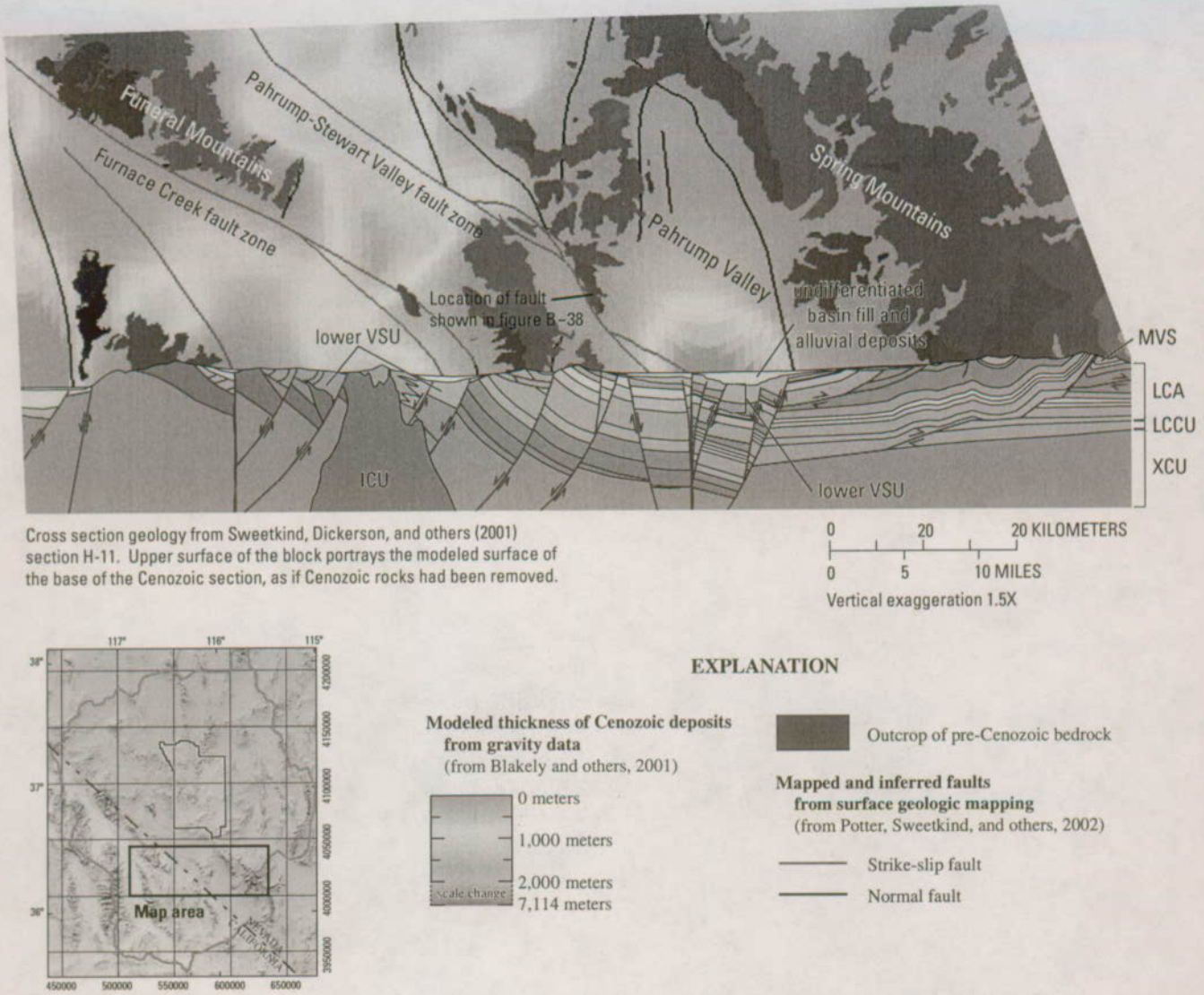

Figure B–37. Interpreted geometry of strike-slip faults, Death Valley regional ground-water flow system region.

that may differ significantly in hydraulic conductivity from other parts of the fault (Potter, Sweetkind and others, 2002). North-south-striking normal faults were subdivided primarily on magnitude of offset, and then by distribution in the DVRFS region (table B–8; fig. B–39).

Hydraulic Conduits

Comparison of the location of large-offset structures with the regional potentiometric surface (Winograd and Thordarson, 1975; D'Agnese and others, 1998) and the results of recent ground-water flow models (IT Corporation, 1996a; D'Agnese and others, 1997) indicates that few of the individual structures are hydraulic conduits on the regional scale. Rather than being associated with single faults, hydraulic conduits in the DVRFS region appear to be spatially associated with broad, northeast-striking zones that are transverse to the main trend of the Walker Lane belt (fig. B–7) (Carr, 1984; Stewart, 1988; Stewart and Crowell, 1992). These zones are characterized by active seismicity associated with subparallel, northeast-striking faults that accommodate relatively small amounts of sinistral and normal offset across a broad zone (Carr, 1984; Potter, Sweetkind, and others, 2002).

In the southern part of the NTS, the Spotted Range–Mine Mountain shear zone (Carr, 1984; Stewart, 1988) includes the Rock Valley, Cane Spring, and Mine Mountain faults (fig. B–7). These faults generally strike north-northeast, have demonstrated left-lateral offset of a few kilometers, have variable sense and amount of normal displacement (Frizzell and Shulters, 1990), and are associated with minor seismic events (Piety, 1996; Potter, Sweetkind, and others, 2002). These strike-slip faults are linked by north-striking normal faults that form local pull-apart basins and create complex map patterns in the south-central part of the Nevada Test Site (Maldonado, 1985; Frizzell and Shulters, 1990). Winograd and Pearson (1976) described a transmissive pathway or "megachannel" between Mercury

A

(A) Outcrop of a splay of the Pahrump–Stewart Valley fault zone exposed east of Stewart Valley. Fault is in Late Proterozoic Sterling Quartzite, part of hydrogeologic unit LCCU. Fault core consists of 10 centimeters of foliated clay-rich fault gouge, surrounded by a zone of brecciated wall rock. Hammer is about 30 centimeters in length.

(B) Looking west from near locality shown in (A) across splay of the Pahrump–Stewart Valley fault zone to Stewart Valley. Fault zone has a northwest strike and is about 250 meters wide. Fault zone consists of fault-bounded lenses of Late Proterozoic Stirling Quartzite; fault contacts are shown as black dashed lines.

Photographs by D.S. Sweetkind, U.S. Geological Survey.

B

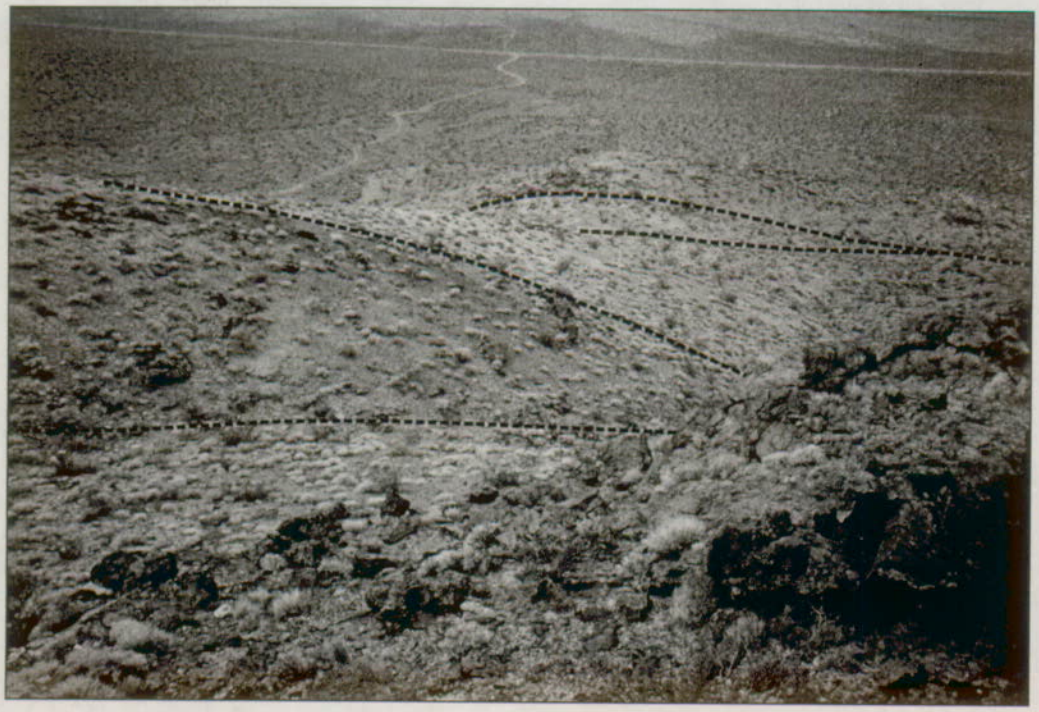

Figure B–38. Examples of strike-slip faults east of Stewart Valley, Death Valley regional ground-water flow system region.

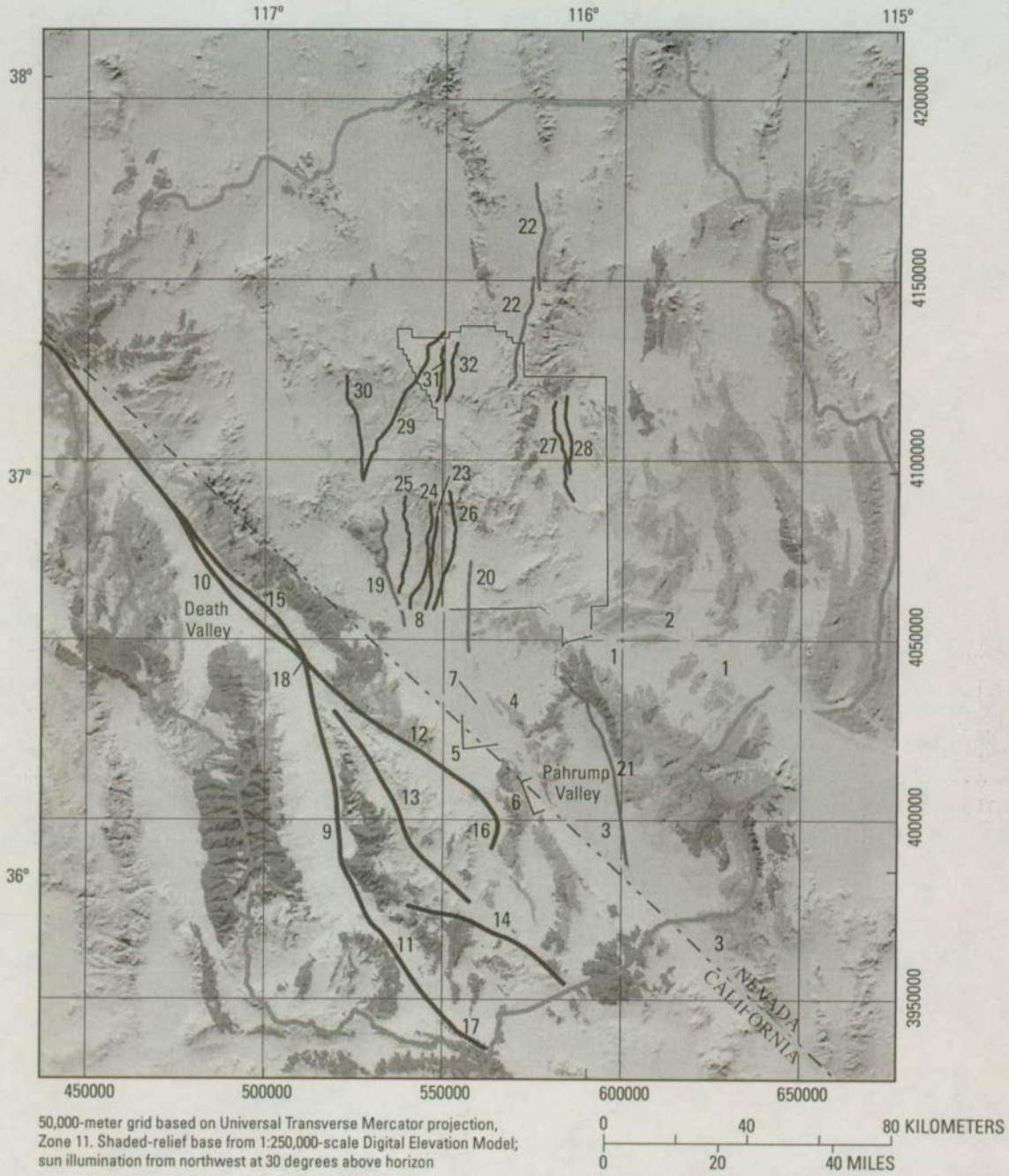

Figure B–39. Structures designated as potential flow barriers in the Death Valley regional ground-water flow system region.

Table B–8. Hierarchical subdivision of faults designated as potential flow barriers in the DVRFS model.

[LCA, lower carbonate-rock aquifer; LVVSZ, Las Vegas Valley shear zone. Numbers in parentheses refer to locations shown on figure B–39]

- **Northwest-striking structures**
  - Faults mainly in LCA
    - LVVSZ
      - Main trace of LVVSZ (1)
      - Indian Spring splay (2)
    - Pahrump–Stewart Valley and Highway 95 faults
      - Pahrump–Stewart Valley fault
        - Northwest-striking segments
          - Pahrump Valley area (3)
          - Ash Meadows area (4)
          - Amargosa Desert area (5)
        - North-striking segments
          - Stewart Valley (6)
          - Southern Gravity fault (7)
      - Highway 95 fault (8)
  - Faults in hydrogeologic unit other than LCA
    - Death Valley–Furnace Creek fault zone, main trace
      - North-striking sections (central Death Valley) (9)
      - Northwest-striking sections
        - Death Valley sections
          - Northern Death Valley section (10)
          - Southern Death Valley section (11)
          - Furnace Creek fault (12)
        - Grandview fault (13)
        - Sheephead fault (14)
        - Keane Wonder fault (15)
    - Death Valley–Furnace Creek fault zone, transition zones and bends
      - Eagle Mountain area (16)
      - Saratoga Springs area (17)
      - Furnace Creek Ranch area (18)
  - Major faults
    - Major faults near Yucca Mountain
      - Bare Mountain fault (19)
      - Northern Gravity fault (20)
    - Other major north-striking faults
      - Western Spring Mountains fault (21)
      - Belted Range fault (22)
  - Minor faults
    - Yucca Mountain or Yucca Flat areas
      - Minor faults near Yucca Mountain
        - Western Yucca Mountain faults
          - Solitario Canyon fault (23)
          - Windy Wash fault (24)
        - Crater Flat fault (25)
        - Paintbrush Canyon fault (26)
      - Minor faults near Yucca Flat
        - Carpetbag fault (27)
        - Yucca fault (28)
    - Pahute Mesa–Oasis Valley features
      - Thirsty Canyon lineament (29)
      - Hogback fault (30)
      - East Box Car fault (31)
      - Almendro fault (32)

Valley and Ash Meadows to explain the carbon-14 content of spring water at Ash Meadows. The Spotted Range–Mine Mountain shear zone (Carr, 1984; Stewart, 1988) is associated with a trough in the regional potentiometric surface, potentially indicating high transmissivity in the Paleozoic carbonate rocks (D'Agnese and others, 1998), and corresponds in part to the "megachannel" defined by Winograd and Pearson (1976). Previous work (Winograd and Thordarson, 1975; D'Agnese and others, 1997; Faunt, 1997) indicates this area has greater permeability associated with highly fractured LCA.

Another zone of minor northeast-striking faults associated with active seismicity, has been inferred to exist in the Gold Mountain area (fig. B-7) northeast of the northern terminus of Death Valley (Albers and Stewart, 1972; Carr, 1984; Potter, Sweetkind, and others, 2002). This region is characterized by highly jointed granite adjacent to the northern Death Valley–Furnace Creek strike-slip fault zone and, to the south, by closely spaced normal faults that cut both the Cenozoic volcanic rocks and the underlying Paleozoic carbonate rocks (Potter, Sweetkind, and others, 2002). This zone corresponds spatially with spring discharge in the northern part of Death Valley; a region of greater transmissivity was added to the YMP/HRMP flow model during calibration (D'Agnese and others, 1997) to simulate this zone.

Although not part of the Walker Lane belt, the Pahranagat shear zone is another northeast-trending system of left-lateral strike-slip faults at the northern end of the Sheep Range (fig. B–7) (Tschanz and Pampeyan, 1970; Jayko, 1990). The fault zone is about 13 km wide, extends for at least 40 km along strike, and consists of several steeply dipping fault strands with oblique left-lateral strike-slip displacement.

Summary

Decades of study in the southern Great Basin have shown that the geologic framework, which is stratigraphically and structurally complex, is important in controlling ground-water flow. Flow within the regional carbonate-rock aquifer and in more localized basin-fill and volcanic-rock aquifers reflects structural and lithologic conditions that produce permeability variations. The hydrogeologic units (HGUs) in the Death Valley regional ground-water flow system (DVRFS) region generally include: Cenozoic basin-fill and playa deposits; as much as 2,000-m-thick sequence of Cenozoic lava flows, welded and nonwelded tuffs; Cenozoic and Mesozoic intrusive rocks; Mesozoic sedimentary and volcanic rocks; as much as 8,000-m-thick Paleozoic carbonate and siliciclastic rocks that are the principal aquifer, and Paleozoic to Late Proterozoic siliclastic rocks and Proterozoic igneous and metamorphic rocks that are the primary regional confining units.

Ground-water flow is affected by faults with kilometers of offset that cause juxtaposition of aquifers and confining units; structural deformation; degree of welding; and facies transitions, lithologic features, and hydrothermal alteration that produce variations in permeability.

Based on characteristics of the potentiometric surface, the location of springs, and the location with respect to predominant northeast-to-southwest ground-water flow in the DVRFS region, the LVVSZ, the Pahrump–Stewart Valley fault zone, and the Death Valley–Furnace Creek fault system strike-slip faults are potential barriers to ground-water flow; broad, northeast-striking zones that are transverse to the main trend of the Walker Lane belt, but not individual faults, are hydraulic conduits.

References Cited

Albers, J.P., 1967, Belt of sigmoidal bending and right-lateral faulting in the western Great Basin: Geological Society of America Bulletin, v. 78, p. 143–156.

Albers, J.P., and Stewart, J.H., 1972, Geology and mineral deposits of Esmeralda County: Nevada Bureau of Mines and Geology Bulletin 78, 80 p.

Anderson, R.E., Crone, A.J., Machette, M.N., Bradley, L.A., and Diehl, S.F., 1995, Characterization of Quaternary and suspected Quaternary faults, Amargosa area, Nevada and California: U.S. Geological Survey Open-File Report 95–613, 41 p.

Andrew, J.E., 2000, Late Cretaceous extension in the Panamint Range, California—Implications for Tertiary Death Valley regional extension: Geological Society of America Abstracts with Programs, v. 32, no. 7, p. 168.

Armstrong, R.L., 1968, Sevier orogenic belt in Nevada and Utah: Geological Society of America Bulletin, v. 79, p. 429–458.

Barnes, Harley, and Christiansen, R.L., 1967, Cambrian and Precambrian rocks of the Groom District Nevada, southern Great Basin: U.S. Geological Survey Bulletin 1244–G, 34 p.

Barnes, Harley, and Poole, F.G., 1968, Regional thrust-fault system in Nevada Test Site and vicinity, *in* Eckel, E.B., ed., Nevada Test Site: Geological Society of America Memoir 110, p. 233–238.

Barnes, Harley, Ekren, E.B., Cleaves, L.R., and Hedlund, D.C., 1982, Geologic and tectonic maps of the Mercury quadrangle, Nye and Clark Counties, Nevada: U.S. Geological Survey Miscellaneous Investigations Series Map I–1197, scale 1:24,000.

Bechtel SAIC Company, 2002, Geologic Framework Model (GFM2000), MDL–NBS–GS–000002 REV 01. Las Vegas, Nevada: Accession No. MOL.20020530.0078.

Bedinger, M.S., Langer, W.H., and Reed, J.E., 1989a, Groundwater hydrology, *in* Bedinger, M.S., Sargent, K.A., and Langer, W.H., eds., Studies of geology and hydrology in the Basin and Range Province, southwestern United States, for isolation of high-level radioactive waste—Characterization of the Death Valley region, Nevada and California: U.S. Geological Survey Professional Paper 1370–F, p. 28–35.

Bedinger, M.S., Langer, W.H., and Reed, J.E., 1989b, Hydraulic properties of rocks in the Basin and Range Province, *in* Bedinger, M.S., Sargent, K.A., Langer, W.H., Sherman, F.B., Reed, J.E., and Brady, B.T., eds., Studies of geology and hydrology in the Basin and Range Province, southwestern United States, for isolation of high-level radioactive waste—Basis of characterization and evaluation: U.S. Geological Survey Professional Paper 1370–A, p. 16–18.

Belcher, W.R., Elliott, P.E., and Geldon, A.L., 2001, Hydraulic-property estimates for use with a transient ground-water flow model for the Death Valley regional ground-water flow system, Nevada and California: U.S. Geological Survey Water-Resources Investigations Report 01–4210, 25 p. Accessed September 1, 2004, at *http://water.usgs.gov/pubs/wri/wri014210.*

Belcher, W.R., Faunt, C.C., and D'Agnese, F.A., 2002, Three-dimensional hydrogeologic framework model for use with a steady-state numerical ground-water flow model of the Death Valley regional flow system, Nevada and California: U.S. Geological Survey Water-Resources Investigations Report 01–4254. Accessed September 1, 2004, at *http://water.usgs.gov/pubs/wri/wri014254/.*

Best, M.G., Christiansen, E.H., Deino, A.L., Gromme, C.S., McKee, E.H., and Noble, D.C., 1989, Eocene through Miocene volcanism in the Great Basin of the western United States, *in* Chapen, C.E., and Zedlik, V., eds., Field excursions to volcanic terranes in the western United States, v. II; Cascades and intermountain west: New Mexico Bureau of Mines and Mineral Resources Memoir 47, p. 91–133.

Black, J.H., Alexander, J., Jackson, P.D., Kimbell, G.S., and Lake, R.D., 1987, The role of faults in the hydrogeological environment: Report of Fluid Processes Research Group, British Geological Survey, 54 p.

Blakely, R.J., Jachens, R.C., Calzia, J.P., and Langenheim, V.E., 1999, Cenozoic basins of the Death Valley extended terrane as reflected in regional gravity anomalies, *in* Wright, L.A., and Troxel, B.W., eds., Cenozoic basins of the Death Valley Region: Geological Society of America Special Paper 333, p. 1–16.

Blakely, R.J., Langenheim, V.E., Ponce, D.A., and Dixon, G.L., 2000, Aeromagnetic survey of the Amargosa Desert, Nevada and California—A tool for understanding near-surface geology and hydrology: U.S. Geological Survey Open-File Report 00–188, 39 p., 2 plates. Accessed September 1, 2004, at *http://geopubs.wr.usgs.gov/open-file/of00-188/.*

Blakely, R.J., Morin, R.L., McKee, E.H., Schmidt, K.M., Langenheim, V.E., and Dixon, G.L., 1998, Three-dimensional model of pre-Cenozoic basement beneath Amargosa Desert and Pahrump Valley, California and Nevada—Implications for tectonic evolution and water resources: U.S. Geological Survey Open-File Report 98–496, 29 p.

Blakely, R.J., and Ponce, D.A., 2001, Map showing depth to pre-Cenozoic basement in the Death Valley ground-water model area, Nevada and California: U.S. Geological Survey Miscellaneous Field Studies Map MF–2381–E, scale 1:250,000.

Blankennagel, R.K., and Weir, J.E., Jr., 1973, Geohydrology of the eastern part of Pahute Mesa, Nevada Test Site, Nye County, Nevada: U.S. Geological Survey Professional Paper 712–B, 35 p.

Bohannon, R.G., 1984, Nonmarine sedimentary rocks of Tertiary age in the Lake Mead region, southeastern Nevada and northwestern Arizona: U.S. Geological Survey Professional Paper 1259, 72 p.

Brocher, T.M., Hunter, W.C., and Langenheim, V.E., 1998, Implications of seismic reflection and potential field geophysical data on the structural framework of the Yucca Mountain-Crater Flat region, Nevada: Geological Society of America Bulletin, v. 110, p. 947–971.

Buesch, D.C., Spengler, R.W., Moyer, T.C., and Geslin, J.K., 1996, Proposed stratigraphic nomenclature and macroscopic identification of lithostratigraphic units of the Paintbrush Group exposed at Yucca Mountain, Nevada: U.S. Geological Survey Open-File Report 94–469, 45 p.

Burchfiel, B.C., 1964, Precambrian and Paleozoic stratigraphy of Specter Range quadrangle, Nye County, Nevada: American Association of Petroleum Geologists Bulletin, v. 48, p. 40–56.

Burchfiel, B.C., 1965, Structural geology of the Specter Range quadrangle, Nevada, and its regional significance: Geological Society of America Bulletin, v. 76, p. 175–192.

Burchfiel, B.C., Fleck, R.J., Secor, D.T., Vincelette, R.R., and Davis, G.A., 1974, Geology of the Spring Mountains: Geological Society of America Bulletin, v. 85, p. 1013–1022.

Burchfiel, B.C., Hamill, G.S., and Wilhelms, D.E., 1982, Stratigraphy of the Montgomery Mountains and the northern half of the Nopah and Resting Springs Ranges, Nevada and California: Geological Society of America Map and Chart Series MC–44, scale 1:62,5000.

Burchfiel, B.C., Hamill, G.S., and Wilhelms, D.E., 1983, Structural geology of the Montgomery Mountains and the northern half of the Nopah and Resting Springs Ranges, Nevada and California: Geological Society of America Bulletin, v. 94, p. 1359–1376.

Byers, F.M., Jr., Carr, W.J., Christiansen, R.L., Lipman, P.W., Orkild, P.P., and Quinlivan, W.D., 1976, Geologic map of the Timber Mountain caldera area, Nye County, Nevada: U.S. Geological Survey Miscellaneous Investigations Series Map I–891, scale 1:48,000, 10 p. text.

Byers, F.M., Jr., Carr, W.J., Orkild, P.P., Quinlivan, W.D., and Sargent, K.A., 1976, Volcanic suites and related cauldrons of the Timber Mountain-Oasis Valley caldera complex, southern Nevada: U.S. Geological Survey Professional Paper 919, 70 p.

Caine, J.S., Evans, J.P., and Forster, C.B., 1996, Fault zone architecture and permeability structure: Geology, v. 24, p. 1025–1028.

Caine, J.S., and Forster, C.B., 1999, Fault zone architecture and fluid flow—Insights from field data and numerical modeling, *in* Haneberg, W.C., Mozley, P.S., Moore, J.C., and Goodwin, L.B., eds., Faults and subsurface fluid flow in the shallow crust: American Geophysical Union Monograph 113, p. 101–127.

Carr, W.J., 1982, Volcano-tectonic history of Crater Flat, southwestern Nevada, as suggested by new evidence from drill hole USW VH–1 and vicinity: U.S. Geological Survey Open-File Report 82–457, 23 p.

Carr, W.J., 1984, Regional structural setting of Yucca Mountain, southeastern Nevada, and late Cenozoic rates of tectonic activity in part of the southwestern Great Basin, Nevada and California: U.S. Geological Survey Open-File Report 84–854, 98 p.

Carr, W.J., 1990, Styles of extension in the Nevada Test Site region, southern Walker Lane Belt—An integration of volcano-tectonic and detachment fault models, *in* Wernicke, B.P., ed., Basin and Range extensional tectonics near the latitude of Las Vegas, Nevada: Geological Society of America Memoir 176, p. 283–303.

Carr, W.J., Byers, F.J., Jr., and Orkild, P.P., 1986, Stratigraphic and volcano-tectonic relations of Crater Flat Tuff and some older volcanic units, Nye County, Nevada: U.S. Geological Survey Professional Paper 1323, 28 p.

Carr, W. J., Keller, S. M., and Grow, J. A., 1995, Lithologic and geophysical logs of drill holes Felderhoff Federal 5-1 and 25-1, Amargosa Desert, Nye County, Nevada: U.S. Geological Survey Open-File Report 95–155, 14 p.

Carr, M.D., Waddell, S.J., Vick, G.S., Stock, J.M., Monsen, S.A., Harris, A.G., Cork, B.W., and Byers, F.M. , Jr., 1986, Geology of drill hole UE25p#1, a test hole into pre-Tertiary rocks near Yucca Mountain, southern Nevada: U.S. Geological Survey Open-File Report 86–175, 87 p.

Caskey, S.J., and Schweickert, R.A., 1992, Mesozoic deformation in the Nevada Test Site and vicinity—Framework of the Cordilleran Fold and Thrust Belt and Tertiary extension north of Las Vegas Valley: Tectonics, v. 11, p. 1314–1331.

Cemen, Ibrahim, Wright, L.A., Drake, R.E., and Johnson, F.C., 1985, Cenozoic sedimentation and sequence of deformational events at the southeastern end of the Furnace Creek strike-slip fault zone, Death Valley region, California, *in* Biddle, K.T., and Christie-Blick, Nicholas, eds., Strike-slip deformation and basin formation: Society of Economic Paleontologists and Mineralogists Special Publication 37, p. 127–141.

Chester, F.M., and Logan, J.M., 1986, Implications for mechanical properties of brittle faults from observations of the Punchbowl fault zones, California: PAGEOPH, v. 124, p. 79–106.

Christiansen, R.L., and Lipman, P.W., 1965, Geologic map of the Topopah Spring NW quadrangle, Nye County, Nevada: U.S. Geological Survey Geologic Quadrangle Map GQ–444, scale 1:24,000.

Christiansen, R.L., Lipman, P.W., Carr, W.J., Byers, F.M., Jr., Orkild, P.P., and Sargent, K.A., 1977, Timber Mountain-Oasis Valley caldera complex of southern Nevada: Geological Society of America Bulletin, v. 88, p. 943–959.

Cole, J.C., 1997, Major structural controls on the distribution of pre-Tertiary rocks, Nevada Test Site vicinity, southern Nevada: U.S. Geological Survey Open-File Report 97–533, 19 p.

Cole, J.C., and Cashman, P.H., 1999, Structural relationships of pre-Tertiary rocks in the Nevada Test Site region, southern Nevada: U.S. Geological Survey Professional Paper 1607, 39 p.

Cole, J.C., Harris, A.G., and Wahl, R.R., 1997, Subcrop geologic map of pre-Tertiary rocks in the Yucca Flat and northern Frenchman Flat areas, Nevada Test Site, southern Nevada: U.S. Geological Survey Open-File Report 97–678, scale 1:48,000, 24 p.

Cornwall, H.R., 1972, Geology and mineral deposits of southern Nye County, Nevada: Nevada Bureau of Mines and Geology Bulletin 77, 49 p.

Crowe, B., Perry, F., Geisman, J., McFadden, L., Wells, S., Murrell, M., Poths, J., Valentine, G.A., Bowker, L., and Finnegan, K., 1995, Status of volcanism studies for the Yucca Mountain site characterization project: Los Alamos National Laboratory Report LA–12908–MS, 379 p.

D'Agnese, F.A., O'Brien, G.M., Faunt, C.C., Belcher, W.R., and San Juan, Carma, 2002, A three-dimensional numerical model of predevelopment conditions in the Death Valley regional ground-water flow system, Nevada and California: U.S. Geological Survey Water-Resources Investigations Report 02–4102, 114 p. Accessed September 22, 2004, at *http://pubs.water.usgs.gov/wri024102/.*

D'Agnese, F.A., Faunt, C.C., and Turner, A.K., 1998, An estimated potentiometric surface of the Death Valley region, Nevada and California, using geographic information systems and automated techniques: U.S. Geological Survey Water-Resources Investigations Report 97–4052, 15 p., 1 plate.

D'Agnese, F.A., Faunt, C.C, Turner, A.K., and Hill, M.C., 1997, Hydrogeologic evaluation and numerical simulation of the Death Valley regional ground-water flow system, Nevada, and California: U.S. Geological Survey Water-Resources Investigations Report 96–4300, 124 p.

Dettinger, M.D., 1989, Distribution of carbonate-rock aquifers in southern Nevada and the potential for their development—Summary of findings, 1985–88: Carson City, Nev., State of Nevada, Program for the Study and Testing of Carbonate-Rock Aquifers in Eastern and Southern Nevada, Summary Report No. 1, 37 p.

Dettinger, M.D., Harrill, J.R., Schmidt, D.L., and Hess, J.W., 1995, Distribution of carbonate-rock aquifers and the potential for their development, southern Nevada and parts of Arizona, California, and Utah: U.S. Geological Survey Water-Resources Investigations Report 91–4146, 100 p.

Dettinger, M.D., and Schaefer, D.H., 1996, Hydrogeology of structurally extended terrain in the eastern Great Basin of Nevada, Utah, and adjacent States, from geologic and geophysical models: U.S. Geological Survey Hydrologic Investigations Atlas HA–694D, 1 plate.

Dickerson, R.P., and Drake, R.M. II, 1998, Geologic map of the Paintbrush Canyon area, Yucca Mountain, Nevada: U.S. Geological Survey Open-File Report 97–783, scale 1:6,000, 25 p. text.

Dickinson, W.R., 2002, The Basin and Range province as a composite extensional domain: International Geology Review, v. 44, p. 1–38.

Diehl, Paul, 1974, Stratigraphy and sedimentology of the Wood Canyon Formation, Death Valley area, *in* Guidebook—Death Valley Region, California and Nevada: Geological Society of America 70th annual meeting of the Cordilleran section Field Trip Number 1, Shoshone, Calif., The Death Valley Publishing Company, p. 37–48.

Dilles, J.H., and Gans, P.B., 1995, The chronology of Cenozoic volcanism and deformation in the Yerington area, western Basin and Range and Walker Lane: Geological Society of America, v. 107, p. 474–486.

Drellack, S.L., Jr., 1997, Selected stratigraphic data for drill holes located in Frenchman Flat, Nevada Test Site, Rev. 1: Las Vegas, Nev., DOE/NV/11718–077, 83 p.

Dudley, W.W., Jr., and Larsen, J.D., 1976, Effect of irrigation pumping on desert pupfish habitats in Ash Meadows, Nye County, Nevada: U.S. Geological Survey Professional Paper 927, 52 p.

Duebendorfer, E.M., and Black, R.A., 1992, Kinematic role of transverse structures in continental extension—An example from the Las Vegas Valley shear zone, Nevada: Geology, v. 20, p. 1107–1110.

Eakin, T.E., 1966, A regional inter-basin ground-water system in the White River area, southwestern Nevada: Water Resources Research, v. 2, p. 251–271.

Ekren, E.B., and Sargent, K.A., 1965, Geologic map of the Skull Mountain quadrangle, Nye County, Nevada: U.S. Geological Survey Geologic Quadrangle Map GQ–387, scale 1:24,000.

Ekren, E.B., Anderson, R.E., Rogers, C.L., and Noble, D.C., 1971, Geology of northern Nellis Air Force Base Bombing and Gunnery Range, Nye County, Nevada: U.S. Geological Survey Professional Paper 651, 91 p.

Ekren, E.B., Orkild, P.P., Sargent, K.A., and Dixon, G.L., 1977, Geologic map of Tertiary rocks, Lincoln County, Nevada: U.S. Geological Survey Miscellaneous Investigations Series Map I–1041, scale 1:250,000.

Faunt, C.C., 1997, Effect of faulting on ground-water movement in the Death Valley region, Nevada and California: U.S. Geological Survey Water-Resources Investigations Report 95–4132, 42 p.

Faunt, C.C., D'Agnese, F.A., and Turner, A.K., 1997, A hydrogeologic map of the Death Valley region, Nevada and California, developed using GIS techniques: U.S. Geological Survey Water-Resources Investigations Report 95–4016, 18 p., one plate.

Ferguson, J.F., Cogbill, A.H., and Warren, R.G., 1994, A geophysical-geological transect of the Silent Canyon caldera complex, Pahute Mesa, Nevada: Journal of Geophysical Research, v. 99, p. 4323–4339.

Fleck, R.J., 1970, Tectonic style, magnitude, and age of deformation in the Sevier orogenic belt in southern Nevada and eastern California: Geological Society of America Bulletin, v. 81, p. 1705–1720.

Fowler, T.K., Jr., and Calzia, J.P., 1999, The Kingston Range detachment fault, southeastern Death Valley region, California—Relation to Tertiary deposits and reconstruction of initial dip, *in* Wright, L.A., and Troxel, B.W., eds., Cenozoic basins of the Death Valley region: Geological Society of America Special Paper 333, p. 245–257.

Fridrich, C.J., Minor, S.A., Ryder, P.L., and Slate, J.L., *with contributions from* Warren, R.G., Hildenbrand, T.G., Sawyer, D.A., and Orkild, P.P., 1999, Geologic map of the Oasis Valley Basin and vicinity, Nye County, Nevada: U.S. Geological Survey Open-File Report 99–533–B, scale 1:62,500.

Fridrich, C.J., Thompson, R.A., Machette, M.N., and Miggins, D.P., 2000, Late Cenozoic stratigraphic record of tectonic evolution, volcanism, and climate change in the Death Valley region, California and Nevada: EOS, Transactions, American Geophysical Union, v. 81, p. F1127.

Frizzell, V.A., Jr., and Shulters, Jacqueline, 1990, Geologic map of the Nevada Test Site, southern Nevada: U.S. Geological Survey Miscellaneous Investigations Series Map I–2046, scale 1:100,000.

Grauch, V.J.S., Sawyer, D.A., Fridrich, C.J., and Hudson, M.R., 1999, Geophysical framework of the southwestern Nevada volcanic field and hydrogeologic implications: U.S. Geological Survey Professional Paper 1608, 39 p.

Greene, R.C., 1997, Geology of the northern Black Mountains, Death Valley, California: U.S. Geological Survey Open-File Report 97–79, 82 p., 3 plates, map scale 1:24,000.

Grose, T.L.T., 1983, Thirty-two geologic cross sections, Clark, Esmeralda, Lincoln, Mineral, and Nye Counties, Nevada, and adjacent areas in California: Nevada Bureau of Mines and Geology Open-File Report 83–13, University of Nevada-Reno, 90 p., 48 plates.

Grose, T.L., and Smith, G.I., 1989, Geology, *in* Bedinger, M.S., Sargent, K.A., and Langer, W.H., eds., Studies of geology and hydrology in the Basin and Range Province, Southwestern United States, for isolation of high-level radioactive waste: U.S. Geological Survey Professional Paper 1370–F, p. 5–19.

Guth, P.L., 1981, Tertiary extension north of the Las Vegas Valley shear zone, Sheep and Desert Ranges, Clark County, Nevada: Geological Society of America Bulletin, v. 92, p. 763–771.

Guth, P.L., 1990, Superposed Mesozoic and Cenozoic deformation, Indian Springs quadrangle, southern Nevada, *in* Wernicke, B.P., ed., Basin and Range extensional tectonics near the latitude of Las Vegas, Nevada: Geological Society of America Memoir 176, p. 237–249.

Hamilton, W.B., 1988, Detachment faulting in the Death Valley region, California and Nevada, *in* Carr, M.D., and Yount, J.C., eds., Geologic and hydrologic investigations of a potential nuclear waste disposal site at Yucca Mountain, southern Nevada: U.S. Geological Survey Bulletin 1790, p. 51–85.

Hardyman, R.F., and Oldow, J.S., 1991, Tertiary tectonic framework and Cenozoic history of the central Walker Lane, Nevada, *in* Raines, G.L., Lisle, R.E., Schafer, R.W., and Wilkinson, W.H., eds., Geology and ore deposits of the Great Basin: Geological Society of Nevada Symposium Proceedings, v. 1, p. 279–301.

Harrill, J.R., Gates, J.S., and Thomas, J.M., 1988, Major ground-water flow systems in the Great Basin region of Nevada, Utah, and adjacent States: U. S. Geological Survey Hydrologic Investigations Atlas HA–694–C, 2 sheets.

Harrill, J.R., and Prudic, D.E., 1998, Aquifer systems in the Great Basin region of Nevada, Utah, and adjacent States—A summary report: U.S. Geological Survey Professional Paper 1409–A, 66 p.

Healey, D.L., Snyder, D.B., Wahl, R.R., and Currey, F.E., 1981, Bouguer gravity map of Nevada, Caliente sheet: Nevada Bureau of Mines and Geology Map 70, scale 1:250,000.

Hedge, C.E., and Noble, D.C., 1971, Upper Cenozoic basalts with high $^{87}Sr/^{86}Sr$ and Sr/Rb ratios, southern Great Basin, Western United States: Geological Society of America Bulletin, v. 82, no. 12, p. 3503–3509.

Heizler, M.T., Perry, F.V., Crowe, B.M., Peters, L., and Appelt, R., 1999, The age of the Lathrop Wells volcanic center—An $^{40}Ar/^{39}Ar$ dating investigation: Journal of Geophysical Research, v. 104, p. 767–804.

Hildenbrand, T.G., Langenheim, V.E., Mankinen, E.A., and McKee, E.H., 1999, Inversion of gravity data to define the pre-Tertiary surface and regional structures possibly influencing ground-water flow in the Pahute Mesa-Oasis Valley region, Nye County, Nevada: U.S. Geological Survey Open-File Report 99–49, 27 p.

Hodges, K.V., McKenna, L.W., Stock, J., Knapp, J., Page, L., Sternlof, K., Silverberg, D., Wust, G., and Walker, J.D., 1989, Evolution of extensional basins and Basin and Range topography west of Death Valley, California: Tectonics, v. 8, p. 453–467, 1 plate.

Hoisch, T.D., Heizler, M.T., and Zartman, R.E., 1997, Timing of detachment faulting in the Bullfrog Hills and Bare Mountain area, southwest Nevada: Inferences from $^{40}Ar/^{39}Ar$, K-Ar, U-Pb, and fission track thermochronology: Journal of Geophysical Research, v. 102, p. 2815–2833.

Holm, D.K., Pavlis, T.L., and Topping, D.J., 1994, Black Mountains crustal section, Death Valley extended terrane, California, *in* McGill, S.F., and Ross, T.M., eds., Geological investigations of an active margin: Geological Society of America, Cordilleran Section Field Trip Guidebook, Trip 2, San Bernardino, Calif., p. 31–54.

Holm, D.K., Snow, J.K., and Lux, D.R., 1992, Thermal and barometric constraints on the intrusive and unroofing history of the Black Mountains—Implications for timing, initial dip, and kinematics of detachment faulting in the Death Valley region, California: Tectonics, v. 11, p. 507–522.

Hunt, C.B., and Mabey, D.R., 1966, Stratigraphy and structure of Death Valley, California: U.S. Geological Survey Professional Paper 494–A, 162 p.

IT Corporation, 1996a, Underground test area subproject phase I, Data analysis task, vol. VI—Groundwater flow model data documentation package: Las Vegas, Nev., Report ITLV/10972–81 prepared for the U.S. Department of Energy, 8 volumes, various pagination.

IT Corporation, 1996b, Underground test area subproject, Phase I, Data analysis task, vol. I—Geologic model data documentation package: Las Vegas, Nev., Report ITLV/10972–81 prepared for the U.S. Department of Energy, 8 volumes, various pagination.

Jachens, R.C., and Moring, D.R., 1990, Maps of thickness of Cenozoic deposits and the isostatic residual gravity over basement for Nevada: U.S. Geological Survey Open-File Report 90–404, scale 1:1,000,000.

Jayko, A.S., 1990, Shallow crustal deformation in the Pahranagat area, southern Nevada, *in* Wernicke, B.P., ed., Basin and Range extensional tectonics near the latitude of Las Vegas, Nevada: Geological Society of America Memoir 176, p. 213–236.

Kleinhampl, F.J., and Ziony, J.I., 1985, Geology of northern Nye County: Nevada Bureau of Mines and Geology Bulletin 99A, 172 p.

Labotka, T.C., Albee, A.L., Lanphere, M.A., and McDowell, S.D., 1980, Stratigraphy, structure and metamorphism in the central Panamint Mountains (Telescope Peak quadrangle), Death Valley area, California: Geological Society of America Bulletin, v. 91, pt. I, p. 125–129, and pt. II, p. 843–933.

Laczniak, R.J., Cole, J.C., Sawyer, D.A., and Trudeau, D.A., 1996, Summary of hydrogeologic controls on groundwater flow at the Nevada Test Site, Nye County, Nevada: U.S. Geological Survey Water-Resources Investigations Report 96–4109, 59 p.

Langenheim, R.L., and Larson, E.R., 1973, Correlation of Great Basin stratigraphic units: Nevada Bureau of Mines and Geology Bulletin 72, 36 p.

Langenheim, V.E., Grow, J.A., Jachens, R.C., Dixon, G.L., and Miller, J.J., 2001, Geophysical constraints on the location and geometry of the Las Vegas Valley shear zone, Nevada: Tectonics, v. 20, p. 189–209.

Lipman, P.W., 1984, The roots of ash flow calderas in western North America—Windows into the tops of granitic batholiths: Journal of Geophysical Research, v. 89, p. 8801–8841.

Lipman, P.W., 1997, Subsidence of ash-flow calderas—Relation to caldera size and magma chamber geometry: Bulletin Volcanologique, v. 59, p. 198–218.

Longwell, C.R., 1974, Measure and date of movement on Las Vegas Valley shear zone, Clark County, Nevada: Geological Society of America Bulletin, v. 85, p. 985–990.

Longwell, C.R., Pampeyan, E.H., Bowyer, Ben, and Roberts, R.J., 1965, Geology and mineral deposits of Clark County, Nevada: Nevada Bureau of Mines and Geology Bulletin 62, 218 p.

Luckey, R.R., Tucci, Patrick, Faunt, C.C., Ervin, E.M., Steinkampf, W.C., D'Agnese, F.A., and Patterson, G.L., 1996, Status of understanding of the saturated-zone ground-water flow system at Yucca Mountain, Nevada as of 1995: U.S. Geological Survey Water-Resources Investigations Report 96–4077, 71 p.

Maldonado, Florian, 1985, Geologic map of the Jackass Flats area, Nye County, Nevada: U.S. Geological Survey Miscellaneous Investigations Series Map I–1519, scale 1:48,000.

Maldonado, Florian, 1990, Structural geology of the upper plate of the Bullfrog Hills detachment fault system, southern Nevada: Geological Society of America Bulletin, v. 102, p. 992–1006.

Maldonado, Florian, and Hausback, B.P., 1990, Geologic map of the northeastern quarter of the Bullfrog 15-minute quadrangle, Nye County Nevada: U.S. Geological Survey Miscellaneous Investigations Series Map I–2049, scale 1:24,000.

McKee, E.H., 1968, Geology of the Magruder Mountain area, Nevada-California: U.S. Geological Survey Bulletin 1251-H, 40 p., 1 plate.

McKee, E.H., 1985, Geologic map of the Magruder Mountain quadrangle, Esmeralda County, Nevada and Inyo County, California: U.S. Geological Survey Geologic Quadrangle Map GQ–1587, scale 1:24,000.

McKee, E.H., 1996, Cenozoic magmatism and mineralization in Nevada, *in* Coyner, A.R. and Fahey, P.L., eds., Geology and ore deposits of the American Cordillera: Geological Society of Nevada Symposium Proceedings, Reno/Sparks, Nevada, April 1995, p. 581–588.

McKee, E.H., 1997, Evaluation of geologic structure guiding ground-water flow south and west of Frenchman Flat, Nevada Test Site: U.S. Geological Survey Open-File Report 97–734, 26 p.

McKee, E.H., Hildenbrand, T.G., Anderson, M.L., Rowley, P.D., and Sawyer, D.A., 1999, The Silent Canyon caldera complex—A three-dimensional model based on drill-hole stratigraphy and gravity inversion: U.S. Geological Survey Open-File Report 99–555, 79 p. Accessed September 1, 2004, at *http://geopubs.wr.usgs.gov/open-file/of99-555/.*

McKee, E.H., and Moiola, R.J., 1962, Precambrian and Cambrian rocks of south-central Esmeralda County, Nevada: American Journal of Science, v. 260, p. 530–538.

McKee, E.H., Phelps, G.A., and Mankinen, E.A., 2001, The Silent Canyon Caldera—A three-dimensional model as part of a Pahute Mesa–Oasis Valley, Nevada, hydrogeologic model: U.S. Geological Survey Open-File Report 01–297, 23 p. Accessed September 1, 2004, at *http://geopubs.wr.usgs.gov/open-file/of01-297/.*

McKee, E.H., Wickham, T.A., and Wheeler, K.L., 1998, Evaluation of faults and their effect on ground-water flow southwest of Frenchman Flat, Nye and Clark Counties, Nevada – A digital database: U.S. Geological Survey Open-File Report 98–580, 16 p., 4 plates.

McKenna, L.W., and Hodges, K.V., 1990, Constraints on the kinematics and timing of late Miocene–Recent extension between the Panamint and Black Mountains, southeastern California, *in* Wernicke, B.P., ed., Basin and Range extensional tectonics near the latitude of Las Vegas, Nevada: Geological Society of America Memoir 176, p. 363–376, map scale 1:5,840.

Mifflin, M.D., and Hess, J.W., 1979, Regional carbonate flow systems in Nevada: Journal of Hydrology, v. 43, p. 217–237.

Monsen, S.A., Carr, M.D., Reheis, M.C., and Orkild, P.P., 1992, Geologic map of Bare Mountain, Nye County, Nevada; U.S. Geological Survey Miscellaneous Investigations Series Map I–2201, scale 1:24,000.

Montazer, Parviz, and Wilson, W.E., 1984, Conceptual hydrologic model of flow in the unsaturated zone, Yucca Mountain, Nevada: U.S. Geological Survey Water-Resources Investigations Report 84–4345, 55 p.

Moyer, T.C., and Geslin, J.K., 1995, Lithostratigraphy of the Calico Hills Formation and the Prow Pass Tuff (Crater Flat Group) at Yucca Mountain, Nevada: U.S. Geological Survey Open-File Report 94–460, 59 p.

Moyer, T.C., Geslin, J.K., and Flint, L.E., 1996, Stratigraphic relations and hydrologic properties of the Paintbrush Tuff nonwelded (PTn) hydrologic unit, Yucca Mountain, Nevada: U.S. Geological Survey Open-File Report 95–397, 151 p.

Nelson, C.A., 1962, Lower Cambrian-Precambrian succession, White-Inyo Mountains, California: Geological Society of America Bulletin v. 73, p. 139–144.

Nelson, C.A., 1978, Late Precambrian–Early Cambrian stratigraphic and faunal succession of eastern California and the Precambrian-Cambrian boundary: Geology, v. 115, p. 121–126.

Nelson, M.R., and Jones, C.H., 1987, Paleomagnetism and crustal rotations along a shear zone, Las Vegas Range, southern Nevada: Tectonics, v. 6, p. 13–33.

Nilsen, T.H., and Stewart, J.H., 1980, The Antler orogeny—Mid-Paleozoic tectonism in western North America (Penrose Conference report): Geology, v. 8, p. 298–302.

Noble, D.C., Anderson, R.E., Ekren, E.B., O'Connor, J.T., 1964, Thirsty Canyon Tuff of Nye and Esmeralda Counties, Nevada, Article 126: Short papers in geology and hydrology, U.S. Geological Survey Professional Paper 475–D, p. 24–27.

Noble, D.C., Vogel, T.A., Weiss, S.I., Erwin, J.W., McKee, E.H., and Younker, L.W., 1984, Stratigraphic relations and source areas of ash-flow sheets of the Black Mountain and Stonewall Mountain volcanic centers, Nevada: Journal of Geophysical Research, v. 89, p. 8593–8602.

Oatfield, W.J., and Czarnecki, J.B., 1989, Hydrogeologic inferences from driller's logs and from gravity and resistivity surveys in the Amargosa Desert, southern Nevada: U.S. Geological Survey Open-File Report 89–234, 296 p.

O'Leary, D.W., Mankinen, E.A., Blakely, R.J., Langenheim, V.E., and Ponce, D.A., 2002, Aeromagnetic expression of buried basaltic volcanoes near Yucca Mountain, Nevada: U.S. Geological Survey Open-File Report 02–020, 52 p. Accessed September 1, 2004, at *http://geopubs.wr.usgs.gov/open-file/of02-020/.*

Palmer, A.R., and Halley, R.B., 1979, Physical stratigraphy and trilobite biostratigraphy of the Carrara Formation (Lower and Middle Cambrian) in the southern Great Basin: U.S. Geological Survey Professional Paper 1047, 131 p.

Piety, L.A., 1996, Compilation of known or suspected Quaternary faults within 100 km of Yucca Mountain, Nevada and California: U.S. Geological Survey Open-File Report 94–112, 404 p., scale 1:250,000.

Plume, R.W., and Carlton, S.M., 1988, Hydrogeology of the Great Basin region of Nevada, Utah, and adjacent States: U.S. Geological Survey Hydrologic Investigations Atlas 694–A, 1 sheet.

Ponce, D.A., and Blakely, R.J., 2001, Aeromagnetic map of the Death Valley ground-water model area, Nevada and California: U.S. Geological Survey Miscellaneous Field Studies Map MF–2381–D, scale 1:250,000.

Ponce, D.A., Blakely, R.J., Morin, R.L., and Mankinen, E.A., 2001, Isostatic gravity map of the Death Valley ground-water model area, Nevada and California: U.S. Geological Survey Miscellaneous Field Studies Map MF–2381–C, scale 1:250,000.

Poole, F.G., 1981, Molasse deposits of the Antler foreland basin in Nevada and Utah: Geological Society of America Abstracts with Programs, v. 13, p. 530–531.

Poole, F.G., Carr, W.J., and Elston, D.P., 1965, Salyer and Wahmonie Formations of southeastern Nye County, Nevada, *in* Cohee, G.V., and West, W.S., eds., Changes in stratigraphic nomenclature by the U.S. Geological Survey 1964: U.S. Geological Survey Bulletin 1224–A, p. A36–A44.

Poole, F.G., Elston, D.P., and Carr, W.J., 1965, Geologic map of the Cane Spring quadrangle, Nye County, Nevada: U.S. Geological Survey Geologic Quadrangle Map GQ–455, scale 1:24,000.

Poole, F.G., Houser, F.N., and Orkild, P.P., 1961, Eleana Formation of Nevada Test Site and vicinity, Nye County, Nevada: U.S. Geological Survey Professional Paper 424–D, p. D104–D111.

Poole, F.G., and Sandberg, C.W., 1977, Mississippian paleogeography and tectonics of the western United States, *in* Stewart, J.H., Stevens, C.H., and Fritsche, A.E., eds., Paleozoic paleogeography of the western United States, Pacific Coast Paleogeography Symposium 1: Society of Economic Paleontologists and Mineralogists, p. 67–85.

Poole, F.G., Stewart, J.H., Palmer, A.R., Sandberg, C.A., Madrid, R.J., Ross, R.J., Jr., Hintze, L.F., Miller, M.M., and Wrucke, C.T., 1992, Latest Precambrian to latest Devonian time; development of a continental margin, *in* Burchfiel, B.C., Lipman, P.W., and Zoback, M.L., eds., The Cordilleran orogen—Conterminous U.S.: Geological Society of America, The Geology of North America, v. G–3, p. 9–54.

Potter, C.J., Dickerson, R.P., Sweetkind, D.S., Drake II, R.M., Taylor, E.M., Fridrich, C.J., San Juan, C.A., and Day, W.C., 2002, Geologic map of the Yucca Mountain region, Nye County, Nevada: U.S. Geological Survey Geologic Investigations Series I–2755, scale 1;50,000, 1 plate with pamphlet.

Potter, C.J., Sweetkind, D.S., Dickerson, R.P. and Killgore, M.L., 2002, Hydrostructural map of the Death Valley ground-water basin, Nevada and California: U.S. Geological Survey Miscellaneous Field Studies Map MF–2372 scale 1:350,000, 2 plates with pamphlet. Accessed September 1, 2004, at *http://pubs.usgs.gov/mf/2002/mf-2372/.*

Prothro, L.B., and Drellack, S.L., Jr., 1997, Nature and extent of lava-flow aquifers beneath Pahute Mesa, Nevada Test Site: Las Vegas, Nev., DOE/NV/11718–156, 50 p.

Prothro, L.B., Drellack, S.L., Jr., Allen, B.M., 1999, Lithology and stratigraphy of holes drilled in LANL-use areas of the Nevada Test Site: Las Vegas, Nev., DOE/NV/11718–254, 152 p.

Prudic, D.E., Harrill, J.R., and Burbey, T.J., 1995, Conceptual evaluation of regional ground-water flow in the carbonate-rock province of the Great Basin, Nevada, Utah, and adjacent States: U.S. Geological Survey Professional Paper 1409–D, 102 p.

Reso, Anthony, 1963, Composite columnar section of exposed Paleozoic and Cenozoic rocks in the Pahranagat Range, Lincoln County, Nevada: Geological Society of America Bulletin, v. 74, p. 901–918.

Reynolds, M.W., 1974, Geology of the Grapevine Mountains, Death Valley, California—A summary, *in* Guidebook—Death Valley Region, California and Nevada: Geological Society of America 70th annual meeting of the Cordilleran Section Field Trip Number 1: Shoshone, Calif., The Death Valley Publishing Company, p. 92–99.

Rogers, A.M., Harmsen, S.C., and Meremonte, M.E., 1987, Evaluation of the seismicity of southern Great Basin and its relationship to the tectonic framework of the region: U.S. Geological Survey Open-File Report 87–408, 196 p.

Rowland, S.M., 1987, Paleozoic stratigraphy of Frenchman Mountain, Clark County, Nevada: Boulder, Colo., Geological Society of America Centennial Field Guide—Cordilleran Section, p. 53–56.

Saltus, R.W., and Jachens, R.C., 1995, Gravity and basin-depth maps of the Basin and Range Province, western United States: U.S. Geological Survey Geophysical Investigations Map 1012, scale 1:250,000.

Sargent, K.A., and Stewart, J.H., 1971, Geologic map of the Specter Range NW quadrangle, Nye County, Nevada: U.S. Geological Survey Geologic Quadrangle Map GQ–884, scale 1:24,000.

Saucedo, G.J., Bedford, D.R., Raines, G.L., Miller, R.J. and Wentworth, C.M., 2000, Digital Data for the Geologic Map of California: Sacramento, California Department of Conservation, California Geological Survey CD 2000–06.

Sawyer, D.A., Fleck, R.J., Lanphere, M.A., Warren, R.G., Broxton, D.E., and Hudson, M.R., 1994, Episodic caldera volcanism in the Miocene southwestern Nevada volcanic field—Revised stratigraphic framework, $^{40}Ar/^{39}Ar$ geochronology, and implications for magmatism and extension: Geological Society of America Bulletin, v. 106, p. 1304–1318.

Sawyer, D.A., and Sargent, K.A., 1989, Petrologic evolution of divergent peralkaline magmas from the Silent Canyon caldera complex, southwestern Nevada volcanic field: Journal of Geophysical Research, v. 94, no. B5, p. 6021–6040.

Sawyer, D.A., Wahl, R.R., Cole, J.C., Minor, S.A., Laczniak, R.J., Warren, R.G., Engle, C.M., and Vega, R.G., 1995, Preliminary digital geological map database of the Nevada Test Site area, Nevada: U.S. Geological Survey Open-File Report 95–567, 43 p, scale 1:130,000.

Schweickert, R.A., and Lahren, M.M., 1997, Strike-slip fault system in Amargosa Valley and Yucca Mountain, Nevada: Tectonophysics, v. 272, p. 25–41.

Scott, R.B., 1990, Tectonic setting of Yucca Mountain, southwest Nevada, *in* Wernicke, B.P., ed., Basin and Range extensional tectonics near the latitude of Las Vegas, Nevada: Geological Society of America Memoir 176, p. 251–282.

Serpa, Laura, and Pavlis, T.L., 1996, Three-dimensional model of the late Cenozoic history of the Death Valley region, southeastern California: Tectonics, v. 15, p. 1113–1128.

Signor, P.W., and Mount, J.F., 1986, Position of the Lower Cambrian boundary in the White-Inyo Mountains of California and in Esmeralda County, Nevada: Newsletters in Stratigraphy, v. 16, p. 9–18.

Simonds, F.W., 1989, Geology and hydrothermal alteration in the Calico Hills, southern Nevada: Boulder, University of Colorado, Master's thesis, 136 p.

Slate, J.L, Berry, M.E., Rowley, P.D., Fridrich, C.J., Morgan, K.S., Workman, J.B., Young, O.D., Dixon, G.L., Williams, V.S., McKee, E.H., Ponce, D.A., Hildenbrand, T.G., Swadley, W.C., Lundstrom, S.C., Ekren, E.B., Warren, R.G., Cole, J.C., Fleck, R.J., Lanphere, M.A., Sawyer, D.A., Minor, S.A., Grunwald, D.J., Laczniak, R.J., Menges, C.M., Yount, J.C., and Jayko, A.S., 2000, Digital geologic map of the Nevada Test Site and vicinity, Nye, Lincoln, and Clark Counties, Nevada, and Inyo County, California: U.S. Geological Survey Open-File Report 99–554A, 53 p, scale 1:120,000. Accessed September 1, 2004, at *http://pubs.usgs.gov/of/1999/ofr-99-0554/.*

Snow, J.K., 1992, Large-magnitude Permian shortening and continental-margin tectonics in the southern Cordillera: Geological Society of America Bulletin, v. 104, p. 80–105.

Snow, J.K., and Lux, D.R., 1999, Tectono-sequence stratigraphy of Tertiary rocks in the Cottonwood Mountains and northern Death Valley area, *in* Wright, L.A., and Troxel, B.W., eds., Cenozoic basins of the Death Valley region: Geological Society of America Special Paper 333, p. 17–64.

Snow, J.K., and Wernicke, B.P., 1989, Uniqueness of geological correlations—An example from the Death Valley extended terrain: Geological Society of America Bulletin, v. 101, p. 1351–1362.

Snow, J.K., and Wernicke, B.P., 2000, Cenozoic tectonism in the central Basin and Range—Magnitude, rate, and distribution of upper crustal strain: American Journal of Science, v. 300, p. 659–719.

Sonder, L.J., Jones, C.H., Salyards, S.L., and Murphy, K.M., 1994, Vertical axis rotations in the Las Vegas Valley shear zone, southern Nevada—Paleomagnetic constraints on kinematics and dynamics of block rotations: Tectonics, v. 13, p. 769–788.

Steinkampf, W.C., and Werrell, W.L., 2001, Ground-water flow to Death Valley, as inferred from the chemistry and geohydrology of selected springs in Death Valley National Park, California and Nevada: U.S. Geological Survey Water-Resources Investigations Report 98–4114, 37 p.

Stevens, C.H., Klingman, D.S., Sandberg, C.A., Stone, P., Belasky, P., Poole, F.G., and Snow, J.K., 1996, Mississippian stratigraphic framework of east-central California and southern Nevada with revision of Upper Devonian and Mississippian stratigraphic units in Inyo County, California: U.S. Geological Survey Bulletin 1988–J, 39 p.

Stevens, C.H., Stone, Paul, and Belasky, Paul, 1991, Paleogeographic and structural significance of an upper Mississippian facies boundary in southern Nevada and east-central California: Geological Society of America Bulletin, v. 103, p. 876–885.

Stewart, J.H., 1967, Possible large right-lateral displacement along fault and shear zones in Death Valley-Las Vegas area, California and Nevada: Geological Society of America Bulletin, v. 78, no. 2, p. 131–142.

Stewart, J.H., 1970, Upper Precambrian and Lower Cambrian strata in the southern Great Basin, California and Nevada: U.S. Geological Survey Professional Paper 620, 206 p.

Stewart, J.H., 1972, Initial deposits in the Cordilleran geosyncline—Evidence of a late Precambrian (< 850 m.y.) continental separation: Geological Society of America Bulletin, v. 83, p. 1345–1360.

Stewart, J.H., 1980, Geology of Nevada, a discussion to accompany the geologic map of Nevada: Nevada Bureau of Mines and Geology, Special Publication 4, 136 p.

Stewart, J.H., 1988, Tectonics of the Walker Lane belt, western Great Basin Mesozoic and Cenozoic deformation in a zone of shear, *in* Ernst, W.G., ed., Metamorphism and crustal evolution of the western United States (Ruby Volume 7): Englewood Cliffs, N.J., Prentice-Hall, p. 683–713.

Stewart, J.H., Albers, J.P., and Poole, F.G., 1968, Summary of regional evidence for right-lateral displacement in the western Great Basin: Geological Society of America Bulletin, v. 79, p. 1407–1413.

Stewart, J.H., and Crowell, J.C., 1992, Strike-slip tectonics in the Cordillera region, western United States, *in* Burchfiel, B.C., Lipman, P.W., and Zoback, M.L., eds., The Cordilleran orogen in conterminous U.S.: Geological Society of America, Geology of North America, v. H–3, p. 609–628.

Stewart, J.H. and Poole, F.G., 1974, Lower Paleozoic and uppermost Precambrian Cordilleran miogeocline, Great Basin, western United States, *in* Dickinson, W.R., ed., Tectonics and sedimentation: Society of Economic Paleontologist and Mineralogists Special Publication 22, p. 28–57.

Swan, F., Wesling, J., Angel, M., Thomas, A., Whitney, J., Gibson, J., 2001, Evaluation of the location and recency of faulting near prospective surface facilities in Midway Valley, Nye County, Nevada: U.S. Geological Survey Open-File Report, 01–055, 1 disc.

Sweetkind, D.S., Dickerson, R.P., Blakely, R., and Denning, P.D., 2001, Interpretive geologic cross sections for the Death Valley regional flow system and surrounding areas, Nevada and California: U.S. Geological Survey Miscellaneous Field Studies Map MF–2370, 3 plates, 32 pages of explanatory text. Accessed September 1, 2004, at *http://pubs.usgs.gov/mf/2001/mf-2370/.*

Sweetkind, D.S., Fridrich. C.J., and Taylor, E., 2001, Facies analysis of Tertiary basin-filling rocks of the Death Valley regional ground-water system and surrounding areas, Nevada and California: U.S. Geological Survey Open-File Report 01–400, 55 p. Accessed September 1, 2004, at *http://pubs.usgs.gov/of/2001/ofr-01-0400/.*

Sweetkind, D.S., and White, D.K., 2001, Facies analysis of Late Proterozoic through Lower Cambrian clastic rocks of the Death Valley regional ground-water system and surrounding areas, Nevada and California: U.S. Geological Survey Open-File Report 01–351, 13 p. Accessed September 1, 2004, at *http://pubs.usgs.gov/of/2001/ofr-01-0351/.*

Thomas, J.M., Welch, A.H., and Dettinger, M.D., 1996, Geochemistry and isotope hydrology of representative aquifers in the Great Basin region of Nevada, Utah, and adjacent States: U.S. Geological Survey Professional Paper 1409–C, 100 p.

Trexler, J.H., Jr., Cole, J.C., and Cashman, P.H., 1996, Middle Devonian through Mississippian stratigraphy on and near the Nevada Test Site—Implications for hydrocarbon potential: American Association of Petroleum Geologists Bulletin, v. 80, p. 1736–1762.

Tschanz, C.M., and Pampeyan, E.H., 1970, Geology and mineral deposits of Lincoln County, Nevada: Nevada Bureau of Mines and Geology Bulletin 73, 188 p.

von Seggern, D.H. and Brune, J.N., 2000, Seismicity in the Southern Great Basin, 1868–1992: U.S. Geological Survey Digital Data Series 58, Chapter J, 15 p.

Waddell, R.K., 1982, Two-dimensional, steady-state model of ground-water flow, Nevada Test site and vicinity, Nevada-California: U.S. Geological Survey Water-Resources Investigations Report 84–4267, 72 p.

Wahl, R.R., Sawyer, D.A., Minor, S.A., Carr, M.D., Cole, J.C., Swadley, W.C, Laczniak, R.J., Warren, R.G., Green, K.S., and Engle, C.M., 1997, Digital geologic map of the Nevada Test Site area, Nevada; U.S. Geological Survey Open-File Report 97–140, scale 1:120,000. Accessed September 1, 2004, at *http://pubs.usgs.gov/of/1997/ofr-97-0140/.*

Warren, R.G., Cole, G.L. and D. Walther, 2000, A structural block model for the three-dimensional geology of the southwestern Nevada volcanic field: Los Alamos National Laboratory Report LA–UR–00–5866, 82 p.

Warren, R.G., Sawyer, D.A., Byers, F.M., Jr., and Cole, G.L., 1999, A petrographic/geochemical database and structural framework for the southwestern Nevada volcanic field. Accessed September 1, 2004, at *http://queeg.ngdc.noaa.gov/seg/geochem/swnuf/.*

Wernicke, B.P., 1992, Cenozoic extensional tectonics of the U.S. Cordillera, *in* Burchfiel, B.C., Lipman, P.W., and Zoback, M.L., eds., The Cordilleran orogen, The geology of North America, conterminous U.S.: Geological Society of America, v. G–3, p. 553–581.

Wernicke, B.P., Axen, G.J., and Snow, J.K., 1988, Basin and Range extensional tectonics at the latitude of Las Vegas, Nevada: Geological Society of America Bulletin, v. 100, p. 1738–1757.

Wernicke, B.P., Guth, P.L, and Axen, G.J., 1984, Tertiary extensional tectonics in the Sevier thrust belt of southern Nevada, *in* Lintz, J.P., ed., Western geological excursions: Mackay School of Mines, Reno, University of Nevada, Geological Society of America, Cordilleran Section, Field Trip Guidebook, p. 473–510.

Wernicke, B.P., Hodges, K.V., and Walker, J.D., 1986, Geological setting of the Tucki Mountain area, Death Valley National Monument, California, *in* Dunne, G.C., ed., Mesozoic and Cenozoic structural evolution of selected areas, east-central California (Geological Society of America Cordilleran Section meeting guidebook, field trips 2 and 14): Los Angeles, California State University, p. 67–80.

Winograd, I.J., and Pearson, F.J., Jr., 1976, Major carbon 14 anomaly in a regional carbonate aquifer—Possible evidence for megascale channeling, south-central Great Basin: Water Resources Research, v. 12, p. 1125–1143.

Winograd, I.J., and Thordarson, William, 1975, Hydrogeologic and hydrochemical framework, south-central Great Basin, Nevada-California, with special reference to the Nevada Test Site: U.S. Geological Survey Professional Paper 712–C, 126 p.

Workman, J.B., Menges, C.M., Page, W.R., Ekren, E.B., Rowley, P.D., and Dixon, G.L., 2002, Tectonic map of the Death Valley ground-water model area, Nevada and California: U.S. Geological Survey Miscellaneous Field Studies Map MF–2381–B, scale 1:350,000, 1 plate with pamphlet. Accessed September 1, 2004, at *http://pubs.usgs.gov/mf/2002/mf-2381/.*

Workman, J.B., Menges, C.M., Page, W.R., Taylor, E.M., Ekren, E.B., Rowley, P.D., Dixon, G.L., Thompson, R.A., and Wright, L.A., 2002, Geologic map of the Death Valley ground-water model area, Nevada and California: U.S. Geological Survey Miscellaneous Field Studies Map MF–2381–A, scale 1:250,000. Accessed September 1, 2004, at *http://pubs.usgs.gov/mf/2002/mf-2381/.*

Wright, L.A., 1989, Overview of the role of strike-slip and normal faulting in the Neogene history of the region northeast of Death Valley, California–Nevada, *in* Ellis, M.A., ed., Late Cenozoic evolution of the southern Great Basin: Nevada Bureau of Mines and Geology Open-File Report 89–1, Selected papers from a workshop at University of Nevada, Reno, November 10–13, 1987, p. 1–11.

Wright, L.A., Greene, R.C., Cemen, I., Johnson, F.C., and Prave, A.R., 1999, Tectonostratigraphic development of the Miocene-Pliocene Furnace Creek Basin and related features, Death Valley region, California, *in* Wright, L.A., and Troxel, B.W., eds., Cenozoic basins of the Death Valley region: Geological Society of America Special Paper 333, p. 87–114.

Wright, L.A., Thompson, R.A., Troxel, B.W., Pavlis, T.L., DeWitt, E., Otton, J.K., Ellis, M.A., Miller, M.G., and Serpa, L.F., 1991, Cenozoic magmatic and tectonic evolution of the east-central Death Valley region, California, *in* Walawender, M.J., and Hanan, B.B., eds., Geological excursions in southern California and Mexico: Geological Society of America, Geological Society of America Annual Meeting Guidebook 1991, p. 93–127.

Wright, L.A., and Troxel, B.W., 1993, Geologic map of the central and northern Funeral Mountains and adjacent areas, Death Valley region, southern California: U.S. Geological Survey Miscellaneous Investigations Series Map I–2305, scale 1:48,000.

Wright, L.A., Troxel, B.W., Williams, E.G., Roberts, M.T., and Diehl, P.E., 1974, Precambrian sedimentary environments of the Death Valley region, eastern California and Nevada, *in* Guidebook—Death Valley Region, California and Nevada: Geological Society of America 70th annual meeting of the Cordilleran section Field Trip Number 1, Shoshone Calif., The Death Valley Publishing Company, p. 27–35.

END POINT COORDINATES (METERS)

REQUESTER: PAUL DIXON PA

SUPPLIER: ROBERT SAUNDERS RDP

DRIFT	NORTHING	EASTING	ELEVATION
2-1W	236324 236151	171666 171133	1038 1038
NOT SHOWN	236142 236062	171104 170861	1038 1038
2-2W	236237 236052	171662 171091	1039 1039
3-1	236043 235911	171063 170657	1039 1039
2-3W	236139 235953	171620 171049	1040 1040
3-2	235944 235768	171021 170480	1040 1040
2-4W	236040 235854	171578 171007	1041 1041
3-3	235845 235660	170979 170408	1041 1041
2-1E	236137 235993	172140 171696	1042 1042
2-5W	235941 235756	171536 170965	1042 1042
3-4	235746 235561	170937 170366	1042 1042
3-5	235462 235648	170324 170895	1044 1044
2-6W	235657 235842	170923 171494	1044 1044
2-2E	235894 236082	171654 172231	1044 1044
2-3E	236013 235795	172281 171612	1045 1045
2-7W	235743 235558	171452 170881	1045 1045
3-6	235549 235363	170853 170282	1045 1045
3-7	235265 235450	170240 170811	1046 1046
2-8W	235459 235645	170839 171410	1046 1046
2-4E	235697 235937	171570 172309	1046 1046
2-5E	235836 235598	172261 171528	1047 1047
2-9W	235546 235360	171368 170797	1047 1047
3-8	235351 235166	170769 170198	1047 1047
3-9	235062 235253	170141 170728	1048 1048
2-10W	235262 235449	170757 171331	1048 1048
2-6E	235493 235734	171467 172209	1048 1048
2-7E	235632 235397	172157 171435	1049 1049
2-11W	235359 235172	171318 170742	1049 1049
3-10	234970 235155	170120 170690	1049 1049
3-11	234883 235068	170115 170685	1051 1051
2-12W	235085 235273	170737 171314	1051 1051
2-8E	235311 235530	171431 172105	1051 1051
2-9E	235428 235224	172053 171426	1052 1052
2-13W	235186 234999	171309 170733	1052 1052
3-12	234982 234797	170681 170111	1052 1052
3-13	234710 234895	170106 170676	1053 1053
2-14W	234912 235099	170728 171305	1053 1053
2-10E	235137 235326	171422 172001	1053 1053

B

DRIFT	NORTHING	EASTING	ELEVATION
2-11E	235223 235051	171949 171417	1054 1054
2-15W	235013 234825	171300 170724	1054 1054
3-14	234809 234623	170672 170101	1054 1054
3-15	234537 234722	170097 170667	1055 1055
2-16W	234739 234926	170719 171296	1055 1055
2-12E	234964 235121	171413 171897	1055 1055
2-13E	235024 234878	171859 171408	1056 1056
2-17W	234839 234652	171291 170715	1056 1056
3-16	234635 234450	170663 170092	1056 1056
3-17	234363 234549	170088 170658	1058 1058
2-18W	234565 234753	170710 171287	1058 1058
2-14E	234791 234932	171404 171837	1058 1058
2-15E	234838 234704	171810 171399	1059 1059
2-19W	234666 234479	171282 170705	1059 1059
3-18	234462 234277	170654 170083	1059 1059
3-19	234190 234375	170079 170649	1060 1060
2-20W	234392 234580	170701 171278	1060 1060
2-16E	234618 234749	171395 171800	1060 1060
2-17E	234658 234531	171781 171390	1061 1061
2-21W	234493 234306	171273 170696	1061 1061
3-20	234289 234103	170644 170074	1061 1061
3-21	234018 234202	170072 170640	1062 1062
2-22W	234219 234406	170692 171268	1062 1062
2-18E	234444 234566	171386 171761	1062 1062
2-19E	234475 234358	171742 171381	1063 1063
2-23W	234320 234132	171264 170687	1063 1063
3-22	234116 233935	170638 170080	1063 1063
3-23	233852 234036	170087 170654	1065 1065
1-1	234085 234233	170804 171259	1065 1065
1-2	234146 233967	171255 170703	1066 1066
3-24	233950 233769	170650 170094	1066 1066
3-25	233686 233863	170101 170645	1067 1067
1-3	233880 234060	170697 171250	1067 1067
1-4	233973 233793	171246 170693	1068 1068
3-26	233776 233604	170641 170109	1068 1068
3-27	233521 233690	170116 170636	1069 1069
1-5	233709 233886	170694 171241	1069 1069
1-6	233800 233637	171237 170734	1070 1070
2-28	233604 233439	170634 170126	1070 1070
3-29	233364 233529	170159 170667	1072 1072
1-7	233713 233578	171232 170818	1072 1072
3-30	233476 233298	170764 170217	1073 1073

DRIFT	NORTHING	EASTING	ELEVATION
1-8	233626 233522	171228 170905	1073 1073
5-1	233367 233129	171214 170482	1076 1076
5-2	233043 233280	170481 171209	1077 1077
5-3	233193 232957	171205 170479	1079 1079
5-4	232872 233107	170478 171200	1080 1080
5-5	233020 232786	171196 170476	1081 1081
5-6	232701 232933	170475 171191	1082 1082
5-7	232847 232615	171187 170473	1083 1083
5-8	232529 232760	170472 171182	1085 1085
5-9	232673 232444	171178 170470	1086 1086
5-10	232358 232587	170469 171173	1087 1087
5-11	232500 232273	171169 170470	1088 1088
5-12	232188 232413	170472 171164	1089 1089
5-13	232327 232104	171159 170473	1090 1090
5-14	232019 232240	170474 171155	1092 1092
5-15	232154 231934	171150 170476	1093 1093
5-16	231850 232067	170477 171146	1094 1094
5-17	231980 231765	171141 170479	1095 1095
5-18	231681 231894	170483 171137	1096 1096
5-19	231807 231598	171132 170488	1097 1097
5-20	231513 231720	170490 171128	1099 1099
5-21	231634 231428	171123 170490	1100 1100
5-22	231342 231547	170487 171119	1101 1101
5-23	231460 231257	171114 170488	1102 1102
5-24	231172 231374	170489 171110	1103 1103
5-25	231285 231089	171098 170496	1104 1104
5-26	231013 231188	170524 171063	1106 1106
5-27	231089 230944	171018 170573	1107 1107

CONTINGENCY

NOTES:

1. COORDINATES SHOWN ARE ROUNDED TO NEAREST METER. DESIGN TOLERANCE ± 10 METERS.
2. ELEVATIONS SHOWN ARE ROUNDED TO NEAREST METER. DESIGN TOLERANCE ± 3 METERS.
3. DRIFT SPACING SHOWN 81 METERS. TOLERANCE ± 2 METERS.
4. COORDINATE INFORMATION CORRESPONDS TO CENTERLINE OF DRIFT.

B

01/07/2003
EFFECTIVE DATE

THIS DRAWING IS PRELIMINARY AND NOT INTENDED FOR CONSTRUCTION, PROCUREMENT OR FABRICATION.

DESIGN INPUTS
SEE DOCUMENT INPUT REFERENCE SYSTEM (DIRS)

REV	DESCRIPTION	DATE	DRN	ORG	CHK	DLE	QER	PM RDP	PM PA
B	UPDATED SUBSURFACE LAYOUT PLAN, DRIFT LABEL CALLOUTS, TITLE BLOCK AND RELATED NOTES. REVISED DECAY HEAT GENERATION INFORMATION AND DOCUMENT IDENTIFIER NUMBER FROM DWG-MGR-MD-000003.	12/23/02	RC	ET	BS MR	BTS	LGA	JJ	RA
A	INITIAL ISSUE	05/20/02	RFC	ET	TMC	BTS	LGA	RJB/LJT	RWA

APPROVALS	INITIAL/DATE
DRAWN R CHESTNEY	RC 12/20/02
ORIGINATOR E THOMAS	ET 12/20/02
CHECKED M REINECK	BS for MR 12/20/02
DESIGN LEAD ENGINEER B STANLEY	BTS 12/20/02
QUALITY ENGINEERING REP L ABERNATHY	12/20/02
PROJECT MANAGER RDP L TRAUTNER	JJ 12/23/02
PROJECT MANAGER PA R ANDREWS	

U.S. DEPARTMENT OF ENERGY
Yucca Mountain Site Characterization Project
BECHTEL SAIC COMPANY, LLC — Civilian Radioactive Waste Management System MANAGEMENT & OPERATING CONTRACTOR

REPOSITORY DESIGN
REPOSITORY/PA IED
SUBSURFACE FACILITIES

SIZE: D | W.B.S.: 1.2.22 | DOCUMENT IDENTIFIER: 800-IED-EBS0-00402-000-00B | REV
SCALE: NONE | QA CLASSIFICATION: QA | CAD FILE NUMBER: 800IEDEBS000402.dgn
CAGE CODE:

RECORDS DESIGNATOR QA:QA

800-IED-EBS0-00402-00B

MOL.20030109.0146

20-DEC-2002 15:21

chestneyr   N:\ME\Dwg\800\800IEDEBS000402.dgn

Hydrologic Components for Model Development

By Carma A. San Juan, Wayne R. Belcher, Randell J. Laczniak, and Heather M. Putnam

Chapter C of

Death Valley Regional Ground-Water Flow System, Nevada and California—Hydrogeologic Framework and Transient Ground-Water Flow Model

Edited by Wayne R. Belcher

Prepared in cooperation with the
U.S. Department of Energy
Office of Environmental Management, National Nuclear Security Administration, Nevada Site Office,
under Interagency Agreement DE–AI52–01NV13944, and
Office of Repository Development,
under Interagency Agreement DE–AI08–02RW12167

Scientific Investigations Report 2004–5205

U.S. Department of the Interior
U.S. Geological Survey

Contents

Figures

Tables

CHAPTER C. Hydrologic Components for Model Development

By Carma A. San Juan, Wayne R. Belcher, Randell J. Laczniak, and Heather M. Putnam

Introduction

Hydrologic components of the Death Valley regional ground-water flow system (DVRFS) were evaluated to support development of a ground-water flow model. The components evaluated are those affecting the water budget: the distribution and volume of natural ground-water discharge, ground-water pumpage, ground-water recharge, and lateral inflow and outflow; the hydraulic conductivity values of the major hydrogeologic units (HGUs); and water levels (fig. C–1). This information is used in Chapter D to conceptualize ground-water flow through the Death Valley region and in Chapter F to develop discharge and hydraulic-head observations for model calibration.

Although previous investigators have attempted to quantify all or some of these major flow components in parts of the DVRFS region (Malmberg and Eakin, 1962; Walker and Eakin, 1963; Hunt and others, 1966; Malmberg, 1967; Glancy, 1968; Rush, 1968; Miller, 1977; Waddell, 1982; Rice, 1984; Harrill, 1986; Harrill and others, 1988; Dettinger, 1989), only a few have developed comprehensive estimates for the entire DVRFS region (IT Corporation, 1996a and b; D'Agnese and others, 1997). Attempts to combine results from past investigations often are complicated by uncertainties and differences in the definition of basin and study area boundaries (D'Agnese and others, 2002).

A series of studies was conducted to reassess previous estimates of the major flow components and hydraulic properties of the DVRFS region to improve the data for the conceptual model and for model calibration as part of the DVRFS investigation. These studies, the results of which are described in this chapter, focused on refining estimates of natural ground-water discharge by developing local estimates of evapotranspiration (ET), and compiling and making additional spring-flow measurements; compiling ground-water pumpage information to estimate the history of ground-water development; estimating ground-water recharge from numerical simulations of net infiltration; estimating boundary inflow and outflow by using regional hydraulic gradients and water budgets of areas adjacent to the DVRFS model domain; estimating hydraulic properties from available literature and aquifer-test data; and evaluating available water-level data to estimate representative pre- and post-pumping hydraulic head information. In general, existing and newly acquired data were evaluated using current technology and concepts, analyses were refined or new algorithms were implemented for making interpretations, and values appropriate for the regional extent and scale of the model were estimated.

Water Budget

A water budget is developed to evaluate the balance between the flow into and flow out of a ground-water flow system. The primary components of the water budget are natural discharge, recharge, and lateral flow into and out of an area across its boundary. The introduction of pumping as a discharge from the flow system initially decreases hydraulic heads and ultimately affects one or more flow components either by decreasing natural discharge or increasing recharge. The following sections describe these major flow components and provide estimates of each component as used in the development of the transient flow model of the DVRFS. Ground-water discharge estimates derived from estimates of ET computed from micrometeorological measurements and from spring-flow measurements are the primary mass-balance observations used to calibrate the transient flow model. Estimates of recharge and boundary flow, although quantified and discussed in this chapter, are based on model simulations or on less direct measurements. Together, these flow components also were used to develop a general water budget for pre-pumped and pumped conditions.

Ground-Water Discharge

Ground-water discharge from the DVRFS model domain occurs both naturally and nonnaturally. Natural ground water recharge occurs as ET and spring flow and, to a small extent, as lateral flow to adjacent basins. Nonnaturally, ground water discharges as artesian flow from wells (1913–45) or as pumpage from wells in agricultural areas such as Pahrump and Penoyer Valleys and the Amargosa Desert. Moreo and others (2003) estimated that by 1998 pumpage was equivalent to nearly 75 percent of the natural discharge estimated for the DVRFS model domain prior to ground-water development.

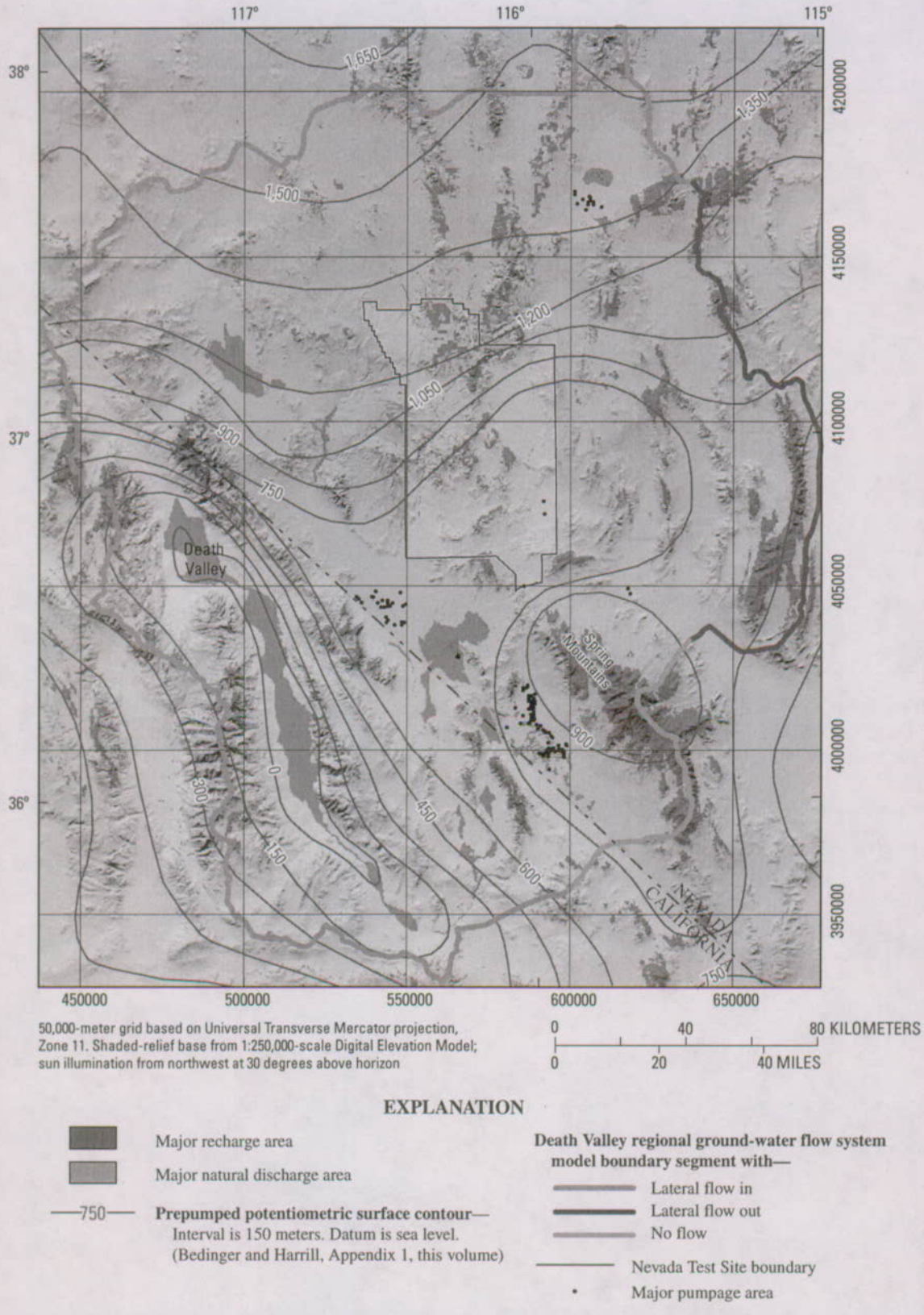

Figure C–1. Major areas of ground-water recharge, natural discharge, and pumpage, and model boundary segments of lateral flow in the Death Valley regional ground-water flow system region.

The following sections describe estimates of natural discharge and pumping as developed for simulating ground-water flow in the DVRFS model domain.

Natural Ground-Water Discharge

Areas of natural discharge cover less than 5 percent of the DVRFS model domain (fig. C–2). These areas include wet playas, wetlands with free-standing water or surface flow, narrow drainages lined with riparian vegetation, and broad areas of phreatophytic shrubs and grasses. The largest discharge areas by flow volume are Death Valley, Ash Meadows, and Sarcobatus Flat, respectively (fig. C–2). Each of these discharge areas represents a unique environment and together they include most of the different types of local habitat supported by ground-water discharge throughout the DVRFS region. Death Valley is dominated by a saltpan surrounded by alluvial fans and by numerous locally and regionally fed springs fringed with a variety of desert shrubs, trees, and grasses. Ash Meadows is a unique desert oasis that consists of broad wetlands fed by orifice-type springs. These large-volume springs are surrounded by extensive grass meadows interspersed with moderately dense to sparse stands of trees and shrubs. Sarcobatus Flat is a broad playa surrounded by moderately dense grasses and sparse shrubs that are supported by a few small springs and seeps and a moderately shallow water table.

The quantity of ground water discharging from most of the major discharge areas in the DVRFS model domain (fig. C–2) has been estimated in previous studies. These estimates were developed primarily from spring-flow measurements, ET estimates, or a combination of both. Usually, ground-water discharge was estimated only for an individual discharge area or at a specific location, and not for the entire flow system. Reports estimating ground-water discharge are Malmberg and Eakin (1962), Walker and Eakin (1963), Pistrang and Kunkel (1964), Hunt and others (1966), Malmberg (1967), Glancy (1968), Rush (1968), Van Denburgh and Rush (1974), Winograd and Thordarson (1975), Miller (1977), Harrill (1986), Czarnecki (1997), D'Agnese and others (1997), Laczniak and others (1999), Reiner and others (2002), and DeMeo and others (2003). Discrepancies in discharge estimates between more recent and previous reports typically reflect differences in the delineation of the area contributing to ET, the number of springs measured, ET rates estimated for vegetation types, or some combination thereof (Laczniak and others, 2001, p. 31; D'Agnese and others, 2002, p. 26).

Evapotranspiration

Recent investigations of natural ground-water discharge in the DVRFS region estimate discharge by calculating ET. The underlying assumption of this approach is that most of the ground water issuing from springs and seeps within the discharge area ultimately is evaporated or transpired locally in the DVRFS region and therefore is accounted for in estimates of ET. Most of the discharge data used to develop the discharge observations presented in Chapter F (this volume) are based on estimates of ET in recent reports by Laczniak and others (1999 and 2001), Reiner and others (2002), and DeMeo and others (2003). The report by Laczniak and others (2001) is the most comprehensive evaluation of ground-water discharge in that it provides estimates of ground-water discharge for 9 of the 15 major ET-dominated discharge areas in the DVRFS model domain (fig. C–2). Their estimate of discharge in Oasis Valley was revised in a subsequent study (Reiner and others, 2002). Laczniak and others (2001) made no attempt to revise estimates of natural discharge from Pahrump and Penoyer Valleys because ground water withdrawn for irrigation had locally altered the distribution of native vegetation and decreased local spring flow. D'Agnese and others (2002, p. 26) provide an estimate of natural discharge from Pahrump Valley but state that their estimate was based on an ET analysis that used a map delineating the native phreatophyte distribution in 1959–61 (Malmberg, 1967, pl. 3)—a time by which vegetation already had been significantly affected by local pumping. These same authors present an estimate of natural discharge from Penoyer Valley that was first documented in a reconnaissance report by Van Denburgh and Rush (1974, p. 23) and later reported by IT Corporation (1996a). A recent study by DeMeo and others (2003) was the primary source used to develop estimates of ground-water discharge from the floor of Death Valley.

The more recent investigations were similar in that continuous micrometeorological data were collected to estimate local ET rates, and remotely sensed multi-spectral data were used to distribute measured ET rates over the area evaluated. Micrometeorological data were collected continuously at 15 stations for 1 to 3 years each in Ash Meadows and Oasis Valley (Laczniak and others, 1999; Reiner and others, 2002) and at 6 sites in Death Valley over a 4-year period (DeMeo and others, 2003). Remotely sensed images, aerial photographs, and soils and wetland maps were integrated using geographic information system (GIS) techniques and were used in these studies to delineate ET units (areas of similar vegetation and moisture conditions) and distribute calculated ET rates over respective discharge areas. This process resulted in more consistent and generally improved estimates of ground-water discharge than in previous studies.

Most ET-based estimates of ground-water discharge assume that in addition to ground water, all precipitation falling on a discharge area, any surface water flowing into a discharge area, and all local infiltration to the shallow flow system ultimately are evaporated or transpired by the local vegetation. Accordingly, mean annual ground-water discharge (estimated from ET) is the difference between the mean annual ET and the sum of mean annual precipitation and any surface-water inflow. In more recent studies, mean annual ET is computed by multiplying the area of an ET unit by the mean annual ET rate calculated for a unit. Mean annual ET rates for individual ET units range from less than 0.06 meter (m) for bare and salt-encrusted soil (DeMeo and others, 2003) to 2.75 m for open water (Laczniak and others, 2001). Adjustments made for precipitation were typically small because mean annual precipitation ranges from less than 0.08 m in

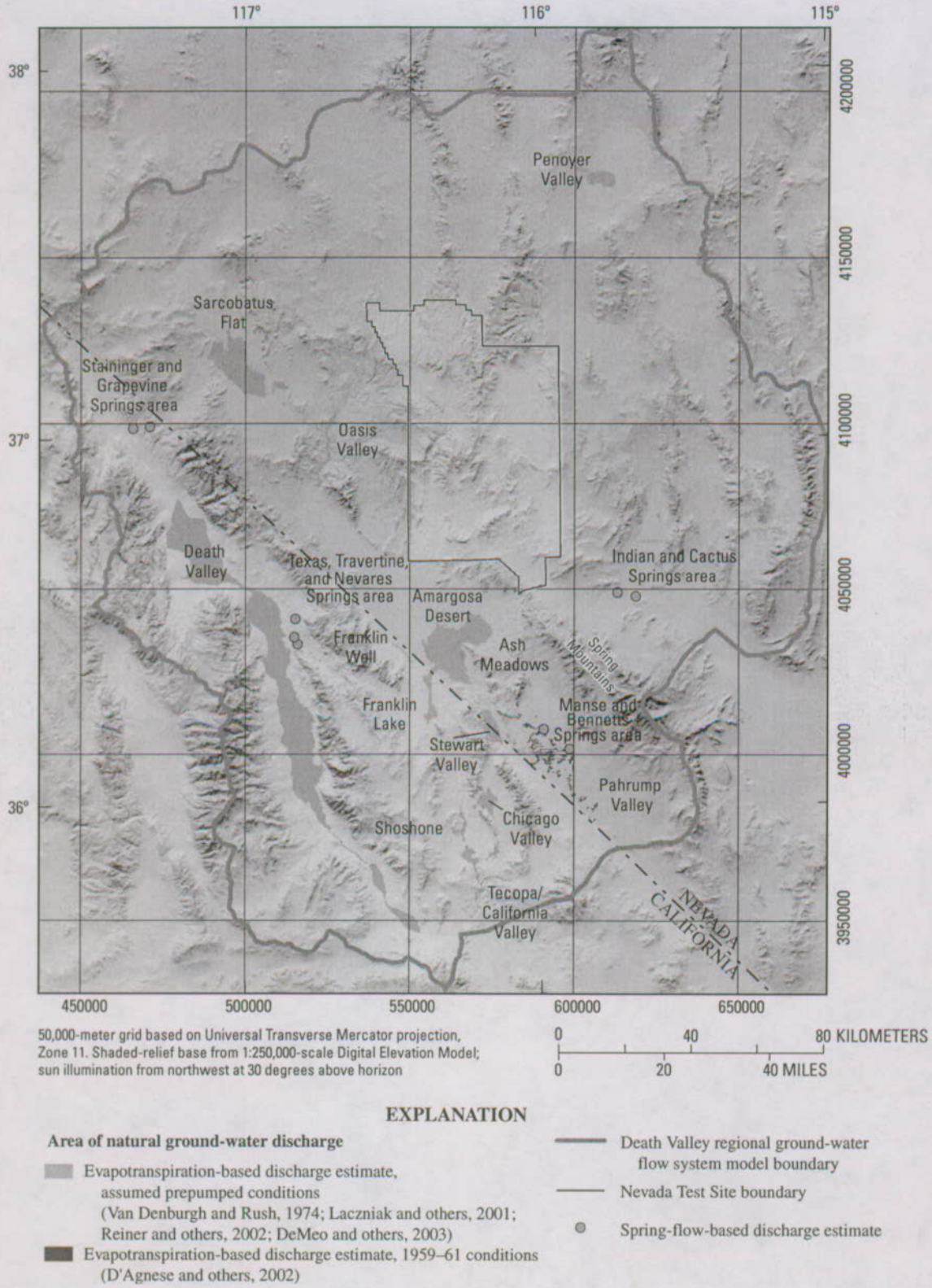

Figure C–2. Major areas of natural ground-water discharge in the Death Valley regional ground-water flow system model domain.

Death Valley (DeMeo and others, 2003) to about 0.15 m in Sarcobatus Flat and Oasis Valley (Laczniak and others, 2001). Runoff into major discharge areas from adjacent highlands was assumed to be minimal and was not calculated. Accordingly, ground-water discharge for most major ET-dominated discharge areas (fig. C–2) was calculated as the difference between mean annual ET and mean annual precipitation.

Accurate mapping of soil and vegetation in discharge areas was critical to improving estimates of the size of ET units. These more recent studies identified most of the vegetation, soil, and water-dominated ET units in major discharge areas using remotely sensed, spectral imagery acquired during 1989–96. Wetland maps produced by the U.S. Fish and Wildlife Service for the National Wetlands Inventory Project were used to delineate two soil-dominated ET units—bare and salt encrusted—in Death Valley (DeMeo and others, 2003). Other ET units included areas of open playa; sparse to dense vegetation; moist, bare soil; and open water (Laczniak and others, 2001; Reiner and others, 2002). Death Valley, the largest discharge area, has an estimated area of about 445.5 square kilometers (km^2) and is dominated by extensive flats of moist, bare, and salt-encrusted soil. Sarcobatus Flat has an estimated area of about 138.6 km^2 and is predominantly sparse to moderately dense shrubland. The fourth largest ET area, Ash Meadows, has an area of about 50.5 km^2 and ranges from broad, sparse grassland to dense, riparian wetland adjacent to spring pools. The estimated sizes of the other major ET-dominated major discharge areas are given in table C–1.

Micrometeorological data were collected continuously and averaged over 20-minute periods. These 20-minute averages were used to compute ET rates for the different ET units delineated throughout the DVRFS region. Microclimate stations were operated at 10 sites in Ash Meadows from 1993 to 1997 (Laczniak and others, 1999, table 6), at 5 sites in Oasis Valley from 1996 to 2000 (Reiner and others, 2002, table 3), and at 6 sites in Death Valley from 1997 to 2001 (DeMeo and others, 2003, table 3). Annual ET rates were computed from the micrometeorological data using the Bowen ratio solution of the energy-budget equation (Bowen, 1926). Average annual ET rates for ET-dominated discharge areas ranged from 0.20 meter per year (m/yr) in Stewart Valley to 0.79 m/yr in Pahrump Valley (table C–1).

Mean annual ground-water discharge for each major ET-dominated discharge area was calculated as the product of the adjusted-annual ET rate and the area of the ET unit (table C–1). Annual ET rates were adjusted by removing water contributed by local precipitation. Although a comparison of these and previous discharge estimates is complicated by differences in the procedures used to estimate ET rates and in the mapped extent of individual discharge

Table C–1. Estimates of mean annual ground-water discharge from major evapotranspiration-dominated discharge areas in Death Valley regional ground-water flow system model domain.

[Ground-water discharge rounded to nearest thousand. Rates rounded to nearest hundredth. Mean annual ground-water discharge may not equal product of precipitation-adjusted ET rate and area because of rounding. Dash (--) indicates that no value was reported in referenced source or that the information given was insufficient to compute a value. Abbreviations: ET, evapotranspiration; m/yr, meters per year; km^2, square kilometer; m^3, cubic meter; Mm^3, million cubic meters]

Discharge area (shown in fig. C–2)	Estimated mean annual ET rate (m/yr)	Area (km^2)	Annual precipitation rate (m/yr)	Estimated precipitation-adjusted annual ET rate (m/yr)	Estimated mean annual ground-water discharge (m^3)
Ash Meadows[1]	0.55	50.5	0.11	0.44	22,203,000
Chicago Valley[1]	0.34	2.48	0.11	0.23	530,000
Franklin Lake[1]	0.23	9.43	0.10	0.13	1,234,000
Franklin Well area[1]	0.46	1.20	0.11	0.35	432,000
Oasis Valley[2]	0.70	13.9	0.15	0.55	7,401,000
Pahrump Valley[3]	0.79	12.2	0.12	0.67	[3]8,082,000
Penoyer Valley[4]	--	76.9	--	0.06	4,650,000
Sarcobatus Flat[1]	0.27	138.6	0.15	0.12	16,035,000
Shoshone area[1]	0.55	5.62	0.09	0.46	2,590,000
Stewart Valley[1]	0.20	12.2	0.11	0.09	1,234,000
Tecopa/California Valley area[1]	0.64	14.2	0.09	0.55	7,894,000
Death Valley floor[5]	--	445.5	--	0.01	[6]43,172,000
Total					**115,457,000**

[1]Laczniak and others (2001, tables 5 and 10).

[2]Reiner and others (2002, table 5).

[3]D'Agnese and others (2002, table 3). Mean annual ground-water discharge during the period 1959–61.

[4]Van Denburgh and Rush (1974, table 8 and p. 23); D'Agnese and others (2002, p. 26).

[5]DeMeo and others (2003, table 4).

[6]Estimate varies from about 27.1–43. 2 Mm^3 as adjusted for different flood recurrence intervals (DeMeo and others, 2003, p. 24). Flood-adjusted ET estimate reported by DeMeo and others (2003, p. 24) is 40.7 Mm^3.

areas, Laczniak and others (2001, p. 29–30) state that their estimates, in general, are greater than those reported in the literature for the more northern discharge areas and less than those previously reported for the more southern discharge areas.

The mean annual ground-water discharge given for Death Valley (DeMeo and others, 2003, p. 24) is considered a partial estimate because evaporation, transpiration, and flow diversions associated with a series of regional springs along the northeastern margin of the valley are not included. The total mean annual ground-water discharge from Death Valley is equal to the sum of ET estimated for the valley floor and reported flow from valley-margin springs discussed in the following section. This method may account twice for underflow from these valley-margin springs into sediment beneath the valley floor. The error resulting from any double accounting of underflow is expected to be small because most of the water discharged from these springs is transpired, evaporated, or diverted for local water supply.

All discharge estimates given in table C–1, except those for Pahrump and Penoyer Valleys, are assumed to represent discharge for both prepumped and current conditions. This assumption is reasonable considering that pumping from these major discharge areas is negligible and climate has been relatively stable over the period. The total amount of ground water discharging annually from the DVRFS model domain (computed by summing all estimates in table C–1) is about 115.5 million cubic meters (Mm^3).

Limitations inherent in an ET-based approach for estimating ground-water discharge can be attributed to errors in delineating the extent of ET units and errors in calculating ET rates (Laczniak and others, 2001, p. 31). Other factors potentially affecting the accuracy of ET-based estimates of ground-water discharge include (1) the assumption that all spring flow ultimately is evaporated or transpired from within the discharge area, (2) the assumption that surface-water inflow is minimal, (3) the short period of record used to compute mean annual ET rates, (4) the limited number of local sites used to estimate mean annual ET rates, (5) uncertainties associated with estimating ET on the basis of relative differences in vegetation density, and (6) uncertainties in the amount of water contributed by precipitation and surface flow to the ET estimates (Laczniak and others, 2001, p. 31).

Springs

Most of the ground water discharged naturally from the DVRFS region flows from springs and seeps. Regional high-volume springs having flows greater than 1,500 cubic meters per day (m^3/d) discharge in Oasis Valley, Ash Meadows, Pahrump Valley, the Shoshone and Tecopa areas, and on the floor of Death Valley (fig. C–2). Typically, these regional springs discharge water with temperatures greater than 30 degrees Celsius (°C) (U.S. Geological Survey, National Water Information System, retrieved June 2003) directly from the rocks that make up the regional aquifer. Because most flow from springs and seeps in major ET-dominated discharge areas is evaporated and(or) transpired by the local riparian vegetation, ET estimates are assumed to be inclusive of spring and seep flow (table C–1; Laczniak and others, 2001; Reiner and others, 2002).

Spring discharge cannot always be quantified accurately using ET-based methods. For example, ET-based methods are not well suited for estimating discharge in areas where springs support limited vegetation or where local pumping has decreased spring flow. Estimates of ground-water discharge from areas of spring flow not estimated by an ET technique were derived solely on the basis of spring-flow measurements and are presented in table C–2. Areas of discharge not included in ET-based estimates are the Stainginger and Grapevine Springs areas near Scotty's Castle in Death Valley; Texas, Travertine, and Nevares Springs areas near Furnace Creek Ranch in Death Valley; Indian and Cactus Springs areas near Indian Springs, Clark County, Nev.; and the Manse and Bennetts Springs areas in Pahrump Valley (fig. C–2). All discharge estimates, except those for Pahrump Valley (Bennetts and Manse Springs), were based on flow measurements made or compiled by C.S. Savard (U.S. Geological Survey, written commun., 2001). Thus any nonreferenced discharge values in the following sections are attributed to Savard's unpublished work. The total annual discharge from spring flow summarized in table C–2 is about 16.8 Mm^3.

Stainginger and Grapevine Springs

Mean ground-water discharge from Stainginger Spring, the water supply for Scotty's Castle area in Death Valley, is estimated at 1,035 $m^3/d \pm 15$ percent (table C–2). This estimate was based on four historical flow measurements, three of which were reported by Miller (1977): 1,019 m^3/d in 1924, 981 m^3/d in 1958, 1,025 m^3/d in 1971, and the fourth, 1,090 m^3/d in 1967 by Rush (1968). Other reported values of discharge from this spring—2,271 m^3/d (Ball, 1907), 54 m^3/d (Waring, 1915), and 163 m^3/d (Waring, 1965)—were considered to be unreliable because they did not measure the entire spring flow.

The aggregate discharge from about 12 springs and seeps in the Grapevine Springs area is estimated at 2,450 $m^3/d \pm 20$ percent (table C–2). This estimate was originally made by Miller (1977) on the basis of discharge measurements made at a few accessible springs and a cursory quantification of ET. Previous reports by Ball (1907) and Mendenhall (1909) mention these springs but do not provide a discharge estimate. Rush (1968) reports discharge from a single unnamed spring at 109 m^3/d.

Texas, Travertine, and Nevares Springs

Discharge from Texas Spring from 1989 to 1996 is estimated at 1,220 $m^3/d \pm 15$ percent (table C–2). This estimate is based on measurements reported in LaCamera and Westenburg (1994), Hale and Westenburg (1995), Westenburg and LaCamera (1996), LaCamera and others (1996), and

Table C–2. Estimates of mean annual natural ground-water discharge from major spring areas not included in evapotranspiration-based discharge estimates (table C–1) in the Death Valley regional ground-water flow system model domain.

[--, no value reported; m^3/d, cubic meters per day; discharge rate rounded to nearest five; ground-water discharge rounded to nearest hundred]

Spring name/area	General location	Estimated mean discharge rate (m^3/d)	Estimated mean annual ground-water discharge (m^3)	Estimated percent accuracy
Staininger Spring[1]	Scotty's Castle, Death Valley, Calif.	1,035	378,000	15
Grapevine Springs[1]	Scotty's Castle, Death Valley, Calif.	2,450	894,900	20
Texas Spring[1]	Furnace Creek Ranch, Death Valley, Calif.	1,220	445,600	15
Travertine Spring[1]	Furnace Creek Ranch, Death Valley, Calif.	4,630	1,691,100	10
Nevares Spring[1]	Furnace Creek Ranch, Death Valley, Calif.	1,885	688,500	--
Indian and Cactus Springs[1]	Indian Springs, Clark County, Nev.	2,240	818,200	10
Bennetts and Manse Springs[2]	Pahrump, Nev.	32,400	11,834,100	25
Total		**45,860**	**16,750,400**	--

[1]Estimate based on flow measurements made or compiled by C.S. Savard (U.S. Geological Survey, written commun., 2001).

[2]Estimate of ground-water discharge based on flow measurements from Bennetts and Manse Springs made before 1913 when ground-water pumping began (Maxey and Jameson, 1948; Malmberg, 1967; and Harrill, 1986).

LaCamera and Locke (1997). Earlier reports give discharge rates from Texas Spring that range from 136 m^3/d in 1915 (Waring, 1915) to 685 m^3/d in 1926 (Pistrang and Kunkel, 1964). A tunnel constructed into the spring between 1926 and 1941 nearly doubled spring discharge. Reported discharge measurements taken after tunnel construction were 930 m^3/d in 1941 (Pistrang and Kunkel, 1964); 1,150 to 1,223 m^3/d from 1956 to 1963 (Pistrang and Kunkel, 1964); and 1,145 m^3/d in 1976 (Miller, 1977).

Mean discharge from the Travertine Spring area is estimated at 4,630 $m^3/d \pm 10$ percent. This estimate is based on measurements made from 1956 to 1972 (table C–2; Miller, 1977). Estimates developed by summing measurements made at 10 springs in the Travertine Springs area between 1955 and 1965 ranged from 4,111 to 4,747 m^3/d (Pistrang and Kunkel, 1964). The aggregate discharge estimate of 3,815 m^3/d given in Miller (1977) was based on measurements made at only three springs in 1977. Other periodic measurements made at individual springs are difficult to composite into an estimate of discharge for the entire area because of differences in measurement dates.

Natural discharge from the Nevares Spring area is estimated at 1,885 m^3/d (table C–2; Pistrang and Kunkel, 1964). This estimate includes discharge from nearby Cow (100 m^3/d) and Salt Springs (25 m^3/d). Early measurements of discharge from the main area of Nevares Spring averaged 1,470 m^3/d for the period 1956 to 1957, while discharge from other nearby springs in the Nevares Spring area totaled 290 m^3/d (Pistrang and Kunkel, 1964). Hunt and others (1966) report combined discharge from the five major springs in the area at 1,790 m^3/d in 1951 and 1,760 m^3/d in 1957. An aggregate discharge of about 1,420 m^3/d was reported by Miller (1977) for Nevares Spring and a nearby, unnamed spring.

Indian and Cactus Springs

Discharge from the Indian and Cactus Springs area is estimated at 2,240 $m^3/d \pm 10$ percent (table C–2). The first reported estimate of discharge at Indian Springs, 2,230 m^3/d (Carpenter, 1915), was made in 1912. Subsequent estimates of 2,180 m^3/d (Maxey and Jameson, 1948) and 2,365 m^3/d (Malmberg, 1965) varied by less than 10 percent. Rush (1970) reports an anomalously low discharge of 1,690 m^3/d. He attributes the decrease to be an effect of nearby pumping. Reported estimates of discharge from Cactus Spring are all less than 5 m^3/d (Carpenter, 1915; Maxey and Jameson, 1948).

Bennetts and Manse Springs

Natural discharge from Bennetts and Manse Springs in Pahrump Valley (fig. C–2) is estimated at 32,400 $m^3/d \pm 25$ percent (table C–2) for the period prior to ground-water pumping. This estimate is based on reported discharges before 1913 of 17,900 m^3/d from Bennetts Spring and 14,500 m^3/d from Manse Spring (Maxey and Jameson, 1948). The estimates of spring flow from Bennetts and Manse Springs are based on measurements made before 1913 and represent prepumped conditions (Maxey and Jameson, 1948; Malmberg, 1967; and Harrill, 1986). The relatively large inaccuracy given to the estimate accounts for uncertainties associated with the nature of the measurements.

Bennetts and Manse Springs were the largest springs in Pahrump Valley and discharged from the base of alluvial fans at the foot of the Spring Mountains. After 1945, large-scale agricultural development accompanied by the drilling and pumping of wells to irrigate cropland drastically decreased spring flows throughout the valley (Harrill, 1986). Bennetts Spring stopped flowing in 1959. Manse Spring virtually

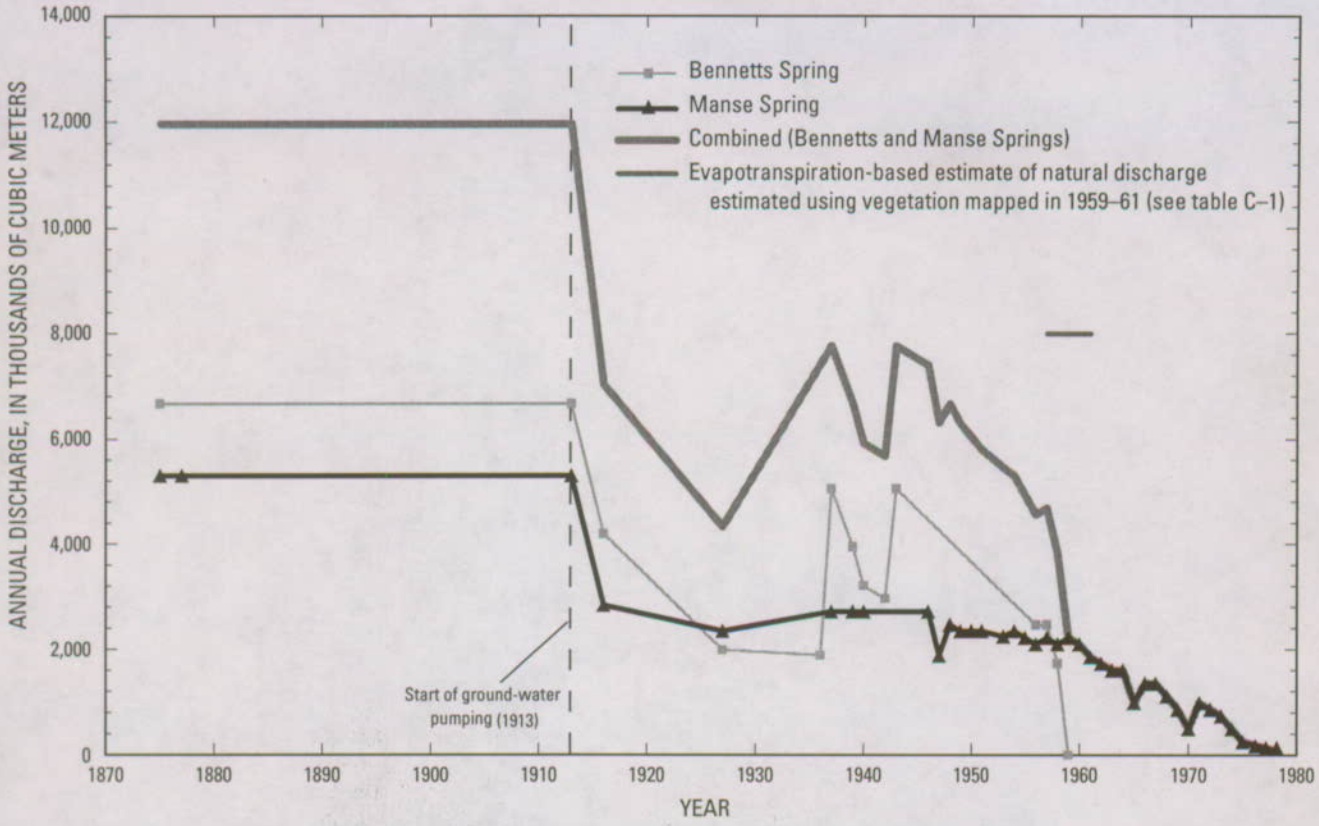

Figure C–3. Annual discharge from regional springs in Pahrump Valley, Bennetts and Manse Springs, 1875–1978.

stopped flowing in 1977 although small intermittent flows during the winter season have been reported. Estimated annual discharge from Bennetts and Manse Springs is shown in figure C–3 for 1875–1978.

The mean annual discharge in Pahrump Valley estimated from ET by D'Agnese and others (2002) also is shown in figure C–3. During 1959–61, mean annual discharge was estimated as about 8.1 Mm^3.

Pumpage

Substantial quantities of ground water have been pumped from the DVRFS region. Ground-water pumping started around 1913 in Pahrump Valley to support a small agricultural community and has continued throughout the region to support local agriculture, mining, industry, and rural and urban growth. The number of pumping wells in the DVRFS region increased substantially from only a few wells in 1913 to nearly 9,300 wells in 1998 (Moreo and others, 2003).

Pumpage from wells, and the physical description and location of pumping wells in the DVRFS region, are reported intermittently in publicly available reports and databases. These sources lack sufficient information, however, from which to develop the complete history of ground-water development for the DVRFS region. Moreo and others (2003) compiled available information and developed annual pumpage estimates to complete the annual pumpage history for the period 1913–98. Their database contains estimates of annual ground-water withdrawal at each known pumping well in the DVRFS region and was used to develop pumping stresses for model simulation of pumped conditions (see Chapter F, this volume).

About 8,600 of the approximately 9,300 wells investigated by Moreo and others (2003) are in the DVRFS model domain (fig. C–4). A few wells included in Moreo and others (2003) that had estimated open intervals that did not match the interpolated horizons in the hydrogeologic framework model (Chapter E, this volume) were removed from the dataset. The combined pumpage from these few wells removed from the data set accounted for less than 0.001 percent (about 8,000 m^3 of the total ground water pumped for the period 1913–98).

About 97 percent of the pumping wells are in the southern part of the model domain (fig. C–4 and table C–3). These wells are concentrated primarily in the southern part of Amargosa Desert and in Pahrump Valley. Penoyer Valley has the greatest concentration of pumping wells in the northern part of the model domain. About 95 percent of the pumpage estimated from 1913 to 1998 was withdrawn from these three hydrographic areas (fig. C–4 and table C–3) delineated by Cardinalli and others (1968) on the basis of topographic basins. Table C–3 presents estimates of total pumpage from the DVRFS model domain for the period 1913–98 and for

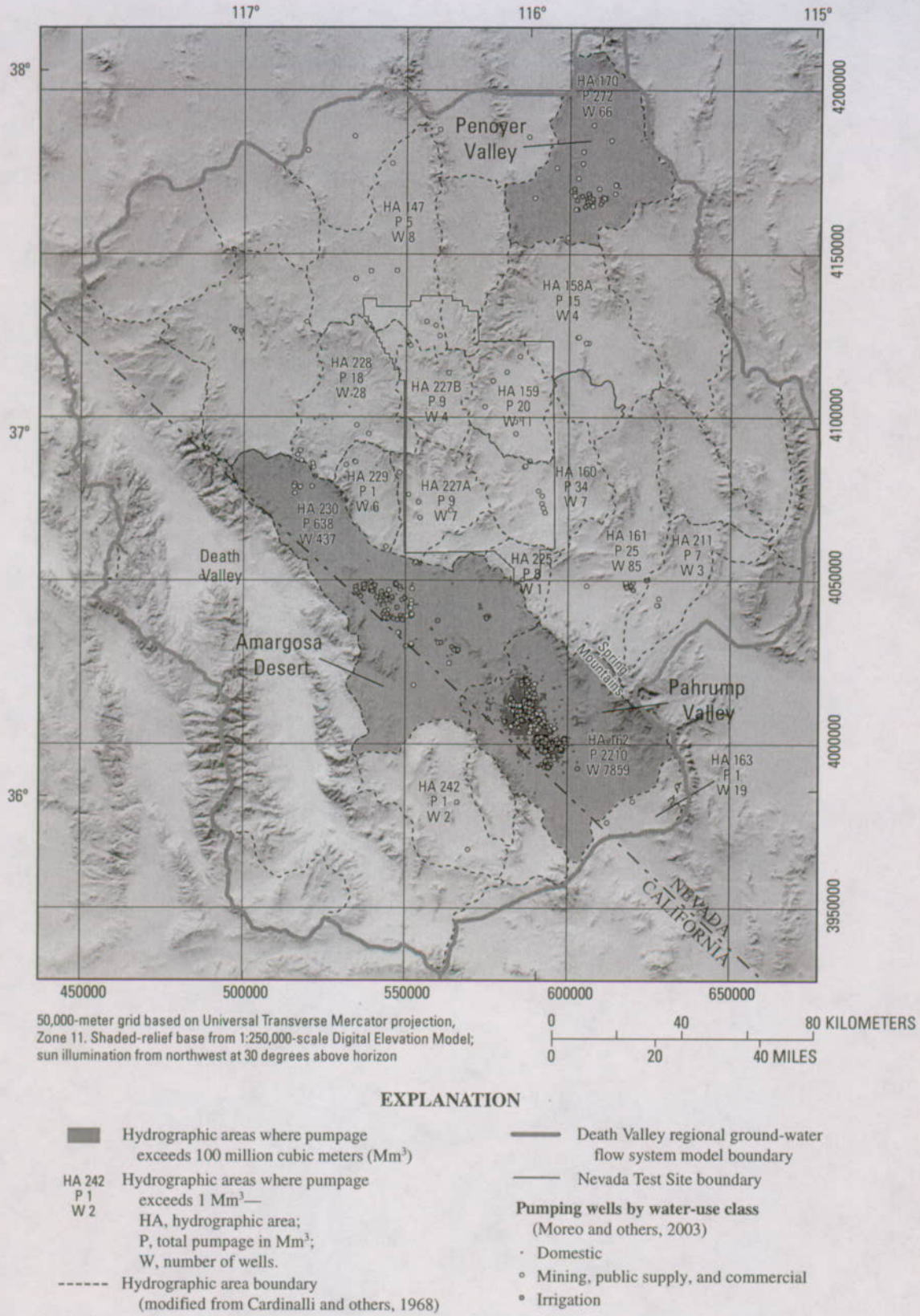

Figure C–4. Spatial distribution of pumping wells by water-use class and total pumpage for 1913–98 by hydrographic area.

Table C–3. Number of wells and estimated total pumpage for 1913–98 by hydrographic area for the Death Valley regional ground-water flow system model domain.

[Annual pumpage estimates computed from data in Moreo and others (2003) for 22 hydrographic areas having reported pumpage; m^3, cubic meters; pumpage values for 1913–98 are rounded to the nearest thousand and for 1998 to the nearest ten]

Hydrographic area		Number of wells 1913–98	Estimated pumpage	
Number	Name		1913–98 (m^3)	1998 (m^3)
144	Lida Valley	1	12,000	860
146	Sarcobatus Flat	15	850,000	25,160
147	Gold Flat	8	4,561,000	43,170
148	Cactus Flat	2	866,000	56,740
158A	Emigrant Valley	4	15,196,000	345,380
159	Yucca Flat	11	20,023,000	91,280
160	Frenchman Flat	7	34,272,000	534,100
161	Indian Springs Valley	85	25,422,000	789,680
162	Pahrump Valley	7,859	2,210,135,000	43,855,360
163	Mesquite Valley[1]	19	1,059,000	31,080
170	Penoyer Valley	66	272,390,000	15,669,790
173A	Railroad Valley[1]	2	197,000	4,930
211	Three Lakes Valley (southern part)	3	6,986,000	410,750
225	Mercury Valley	1	8,479,000	3,700
226	Rock Valley	1	38,000	860
227A	Fortymile Canyon (Jackass Flats)	7	8,510,000	184,650
227B	Fortymile Canyon (Buckboard Mesa)	4	8,674,000	117,180
228	Oasis Valley	28	17,880,000	309,600
229	Crater Flat	6	1,094,000	171,450
230	Amargosa Desert	437	637,619,000	30,729,610
242	Lower Amargosa Desert	2	1,132,000	33,300
243	Death Valley	1	497,000	40,700
	Total	**8,569**	**3,275,892,000**	**93,449,330**

[1]Only part of hydrographic area contained in Death Valley regional ground-water flow system model domain.

1998 by hydrographic area. Of the 38 hydrographic areas in the DVRFS model domain, 16 have no reported pumping during this period.

Moreo and others (2003) grouped pumping wells into three water-use categories: (1) irrigation; (2) mining, public supply, and commercial; and (3) domestic. Although nearly 93 percent of the wells are for domestic use, 90 percent of the water pumped was for irrigation. Pumpage determined for each water-use category was estimated using different methods. The results and techniques used to develop a pumpage history for the DVRFS region are summarized in the following paragraphs. Moreo and others (2003) provide more detail.

Well-construction information was used to estimate the open-interval depths of each pumping well. Approximately 85 percent of the irrigation wells, 97 percent of the mining, public supply, and commercial wells, and 98 percent of the domestic wells had reported completion intervals (Moreo and others, 2003). For wells for which construction information was absent, open intervals were estimated using construction data from nearby wells of the same water-use category. Moreo and others (2003) reported that most pumping wells are open to basin-fill deposits and were drilled to depths of less than about 150 m, with less than 1 percent having depths exceeding about 300 m.

Irrigation accounted for 90 percent of the ground water pumped from the DVRFS model domain during 1913–98. Irrigation gradually declined from about 100 percent (about 4,940 Mm^3) of the ground water used in 1913 to about 80 percent (about 74,710 of 93,450 Mm^3) in 1998 (fig. C–5). Moreo and others (2003) estimated annual irrigation by multiplying an irrigated acreage by a crop application rate. These investigators identified the extent and years that a field was irrigated from pumping inventories and remotely sensed data available since 1972; the crop type from pumping inventories and field visits; and the application rate of the representative crop from published sources. Application-rate estimates for alfalfa had the greatest effect on estimated pumpage. The high sensitivity of application rates, particularly that of alfalfa, is not unexpected considering that 75 percent of the ground water withdrawn from 1913–98 was used to irrigate alfalfa (Moreo

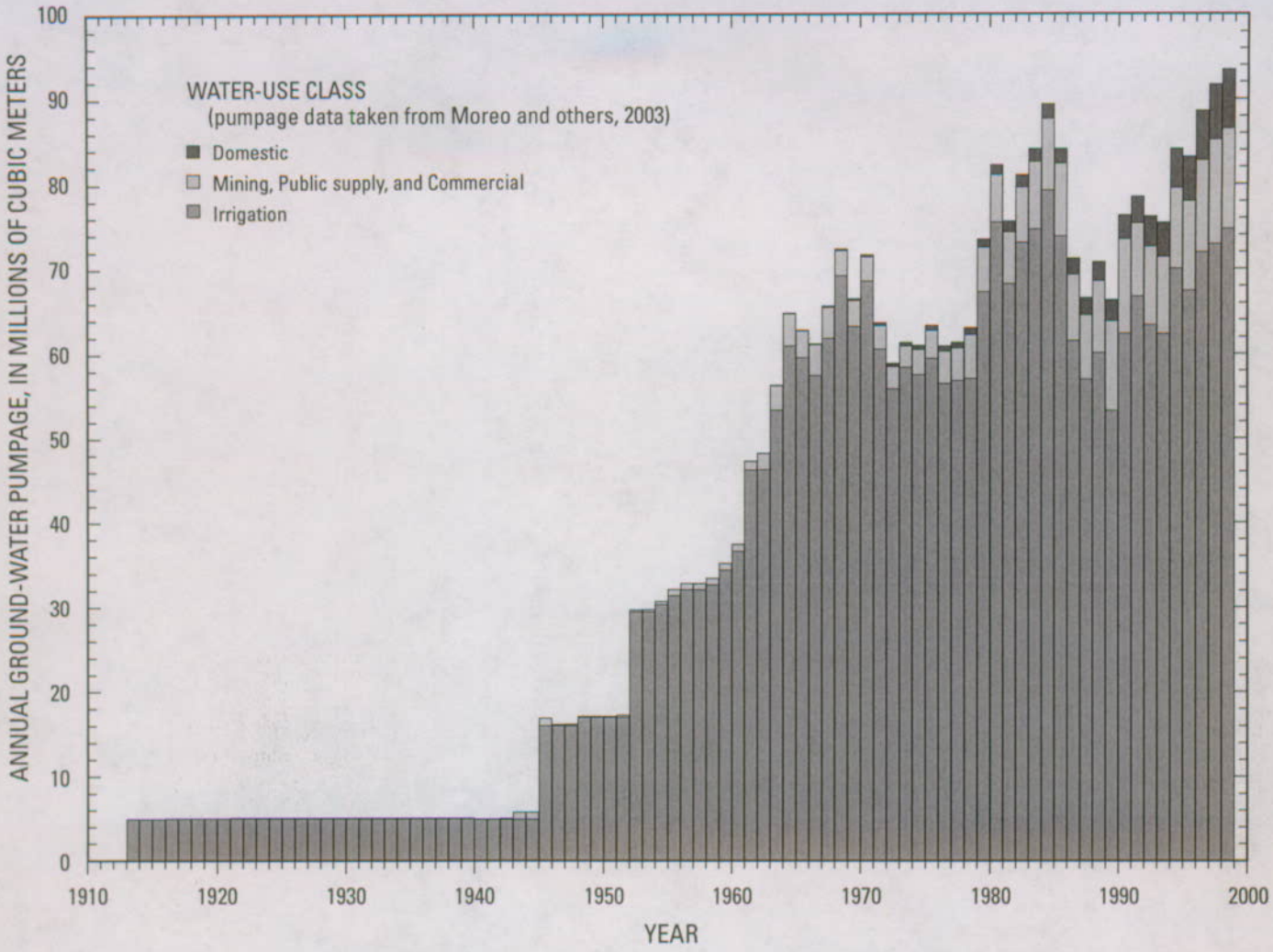

Figure C–5. Annual ground-water pumpage estimates developed by water-use class from Death Valley regional ground-water flow system model domain, 1913–98.

and others, 2003). The uncertainty in annual irrigation was expressed by Moreo and others (2003) as a range between a minimum and maximum estimate, with the most likely value closer to the minimum.

Mining, public supply, and commercial pumpage accounted for about 8 percent of all the ground water pumped from 1913–98. By 1998 pumpage in this category increased, accounting for nearly 13 percent of the annual total (fig. C–5). Pumpage for mining, public supply, and commercial use was estimated primarily from metered and inventoried data. Estimates for this water-use category were considered accurate within 5 percent (Moreo and others, 2003).

Pumpage for domestic use accounted for about 2 percent of the total amount of ground water pumped from 1913 to 1998. The percentage of water pumped for domestic use gradually increased over the years and by 1998 accounted for more than 7 percent of the annual total (fig. C–5). Moreo and others (2003) estimated domestic pumpage as the product of the average annual rate (per household) of domestic consumption and the number of domestic wells permitted for use. The number of domestic wells may have been slightly overestimated because the history of well abandonment is not known. The uncertainty in the domestic-use estimate was expressed as a range defined by a minimum and maximum value that reflects, primarily, the uncertainty in the per household consumption rate. The minimum estimate of domestic pumpage was based on an annual per household consumption of 616.5 m^3 and the maximum estimate on an annual per household consumption of 1,233 m^3 (Moreo and others, 2003).

Annual ground-water pumpage estimates from the DVRFS model domain increased from about 5 Mm^3 in 1913 to about 93.5 Mm^3 in 1998 (fig. C–5 and table C–3). The greatest number of wells and the largest withdrawals are in Pahrump Valley, Amargosa Desert, and Penoyer Valley (fig. C–4). During 1913–45, ground water was used primarily for irrigation and was supplied by about 30 flowing wells in Pahrump Valley (Moreo and others, 2003). After 1945, local water use relied on pumps and continued to increase as access to the region

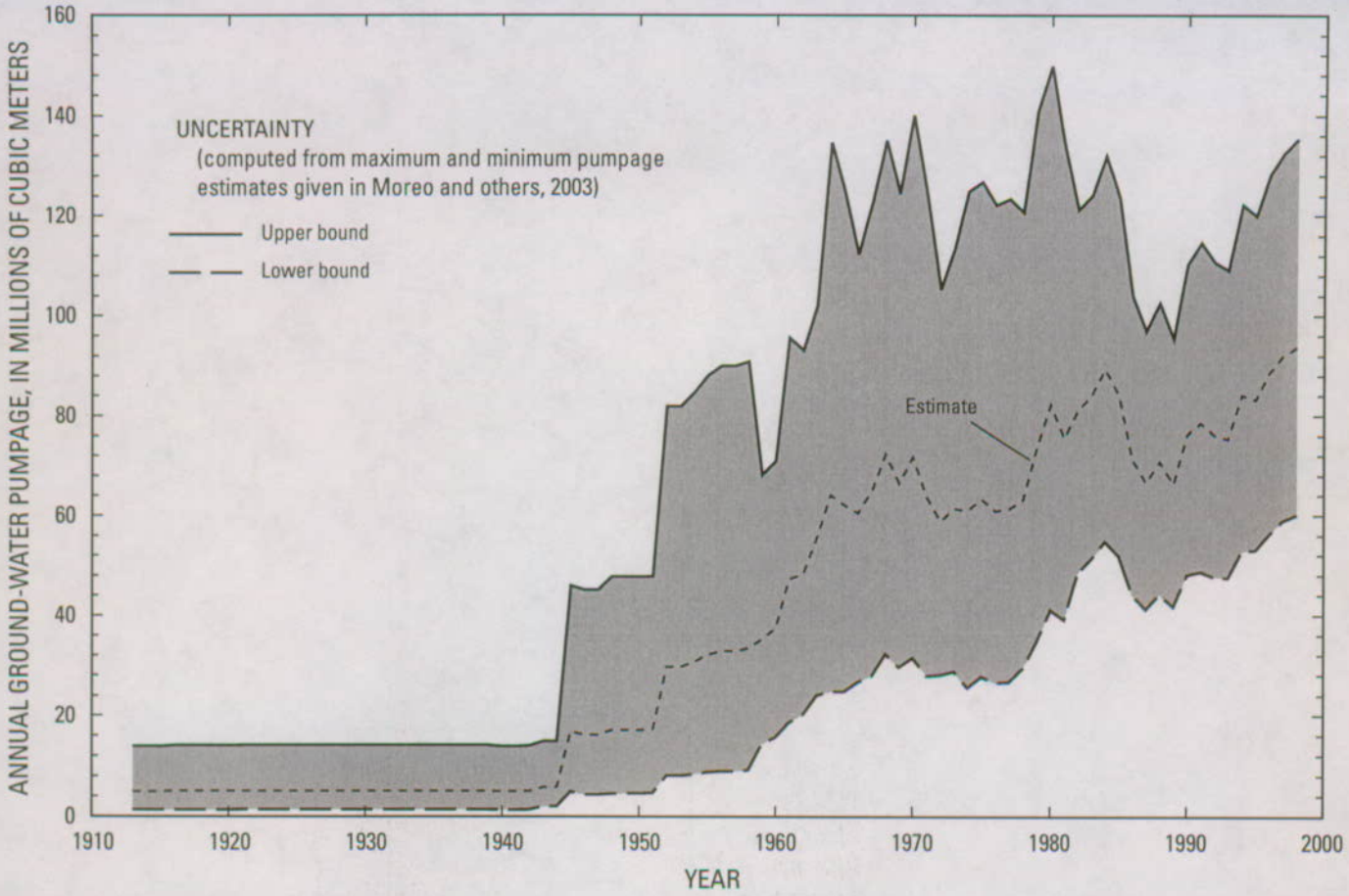

Figure C–6. Uncertainty in annual ground-water pumpage estimates developed for Death Valley regional ground-water flow system model domain, 1913–98.

improved (fig. C–5; Moreo and others, 2003). The percentage of ground water pumped for nonirrigation uses (domestic, mining, public supply, and commercial) began to increase from only a small percentage in 1960 to about 20 percent of the annual total in 1998. This trend is expected to continue as the population of Pahrump Valley and Amargosa Desert increases as a consequence of continued urbanization.

The total amount of ground water pumped from the DVRFS model domain during the period 1913–98 is estimated at 3,276 Mm^3 (table C–3). Moreo and others (2003) expressed uncertainty in their estimate of annual pumpage as a range defined by a minimum and maximum estimate (fig. C–6). Accordingly, the uncertainty in their estimate of total pumpage from the DVRFS model domain during the period 1913–98 ranges from 1,616 to 6,081 Mm^3. This large uncertainty is attributed to incomplete pumping records, misidentification of crop type, and errors associated with estimating annual domestic consumption, the irrigated area, and crop application rates (Moreo and others, 2003). The error associated with the uncertainty in the application rate, which differs spatially and temporally with variations in potential ET, length of growing season, irrigation systems, crop type, and management practices, exceeds that of all other uncertainties combined (Moreo and others, 2003).

Moreo and others (2003) did not adjust estimates of annual pumpage for water potentially returned to the flow system through subsequent infiltration of excess irrigation, lawn water, or septic tank wastewater. Although some return flow is likely to occur in the DVRFS model domain, the magnitude and timing of these returns have not been precisely quantified. Harrill (1986, p. 19) estimates return flows for Pahrump Valley as 70 percent of domestic pumpage, 50 percent of public-supply and commercial pumpage, and 25 percent of irrigation pumpage and states that the returns depend on the timing and method by which the water is returned to the flow system.

Stonestrom and others (2003) estimate return flows beneath three irrigated fields in the southern part of the Amargosa Desert. These estimates are made using the chloride mass-balance method and downward velocities inferred from peaks of chloride and nitrate concentrations noted in borehole depth profiles. Estimates of the rate at which irrigation water percolates downward through the unsaturated zone toward the water table ranged from 0.1 to 0.5 m/yr. On the basis of these rates and the depth to water beneath the fields, irrigation returns would take between 10 and 70 years to reach the water table. The water returned to the water table beneath individual irrigated fields was estimated to be 8 to 16 percent of the irrigation (Stonestrom and others, 2003, p. 19).

Many difficulties are associated with estimating return flows. These include uncertainties in pumpage, in the hydraulic properties of unsaturated zone sediment, and delineating the actual areas where water is or was returned to the environment. For example, ground water pumped for irrigation does not return to the flow system at the well (point of withdrawal) but rather to the water table beneath the field or fields irrigated by the well. The actual location of these fields, especially those of historical significance, can be highly uncertain. Despite these uncertainties, a method was developed to compute informal estimates of return flow. Return flows were computed as the product of the estimated annual pumpage and a user-defined return-flow percentage, and could be lagged in time by a user-defined value. All computed return flows were assumed to return to the water table at the location of the pumped well. Return flows were evaluated using the transient model in Chapter F of this volume.

Ground-Water Recharge

Ground-water recharge is defined as water that infiltrates downward through the unsaturated zone into the water table. Most of the ground-water recharge in the DVRFS region originates from precipitation that falls on mountainous areas throughout the DVRFS region (fig. C–7). The distribution and quantification of recharge for basins in the DVRFS region have been evaluated using empirical (Maxey and Eakin, 1950; Malmberg and Eakin, 1962; Walker and Eakin, 1963; Malmberg, 1967; Winograd and Thordarson, 1975; Miller, 1977; Harrill, 1986; IT Corporation, 1996a; D'Agnese and others, 1997), water-balance (Rice, 1984; West, 1988), chloride mass-balance (Dettinger, 1989; Lichty and McKinley, 1995; Russell and Minor, 2002), and distributed-parameter (Hevesi and others, 2002; Hevesi and others, 2003) methods. Each of these methods attempts to capture the complex array of factors that control recharge.

The distributed-parameter method described by Hevesi and others (2003) provided an estimate of the potential recharge based on net infiltration, and was used primarily to distribute recharge in the model domain. The potential recharge estimated by their method was adjusted across the model domain to better balance with discharge (Chapter F, this volume). Hevesi and others (2003) estimated potential recharge using a net-infiltration model, INFILv3. Net infiltration is considered a reasonable indicator of ground-water recharge because most of the net infiltration and surface runoff that originates as precipitation in the model domain eventually moves downward through the unsaturated zone to recharge the ground-water flow system (Hevesi and others, 2003). In general, the uncertainty of approximating potential recharge from net infiltration increases as the thickness and heterogeneity of the unsaturated zone increases. INFILv3 simulates surface-water flow, snowmelt, transpiration, and ground-water drainage in the root zone and has as a climate algorithm that simulates daily climate conditions in local watersheds. Topography, geology, soils, and vegetation data are input to represent local drainage-basin characteristics. Improved vegetation distributions were delineated from a western region vegetation map developed by the U.S Geological Survey Gap Analysis Program (WESTVEG GAP) and soil distributions from the U.S. Department of Agriculture (1994) State Soils Geographic Database (STATSGO).

On a daily basis, INFILv3 simulated major components of the mass-balance equation within the unsaturated zone to a depth of 6 m, the depth at which the seasonal effects of ET become insignificant. Net infiltration equaled the sum of snowmelt, precipitation, and infiltrating surface flow minus the sum of ET, runoff, and changes in root-zone storage. Each of these components was estimated on a cell-by-cell basis by using secondary governing equations (Hevesi and others, 2003). Runoff was generated in the model when and where available water exceeded the root-zone storage capacity or the saturated hydraulic conductivity of the soil or bedrock. A surface-water routing process was used to move runoff downstream through a simulated drainage basin and allow the surface water potentially to infiltrate through the root zone.

Net-infiltration simulations were calibrated by fitting the simulated daily discharge from modeled watersheds to streamflow records at 31 gaged sites in the DVRFS region (fig. C–7). Model fit was evaluated both qualitatively and quantitatively by comparing simulated to measured daily and annual hydrographs. Model calibration was complicated by sparse daily climate records and information regarding stream-channel characteristics and base-flow contributions, the absence of collocated climate stations and stream-gaging stations in a watershed, and the nonuniqueness of model results (Hevesi and others, 2003). To increase the confidence in the net-infiltration estimates, model results were constrained by prior estimates of recharge that were calculated using alternative methods.

The calibrated net-infiltration model (model 1 in Hevesi and others, 2003) was used to simulate daily net infiltration from 1950 through 1999 across the DVRFS model domain (fig. C–8). This period was selected for simulation primarily because of the availability of climate and streamflow records. An average annual net infiltration of 2.8 millimeters (mm) was estimated over the entire model domain by averaging simulated daily net infiltration over the 50-year simulation period. This estimate is less than 2 percent of the average annual precipitation computed for the same period (Hevesi and others, 2003). An annual potential recharge of about 125 Mm^3 was computed by multiplying the average annual infiltration by the area of the model domain. Results presented by Hevesi and others (2003) indicate a wide range in the simulated rate of net infiltration across the model domain. Local net-infiltration rates ranged from near zero to a maximum of about 1,262 millimeters per year (mm/yr) beneath a stream channel. The simulated average annual runoff over the 50-year simulation period was 2.2 mm, of which 0.2 mm eventually flowed into lowland playas where it was evaporated or infiltrated into the subsurface (Hevesi and others, 2003). About 14 percent of the total net infiltration simulated over the 50-year period was from overland flow, but locally the overland flow accounted for as much as 40 percent (Hevesi and others, 2003).

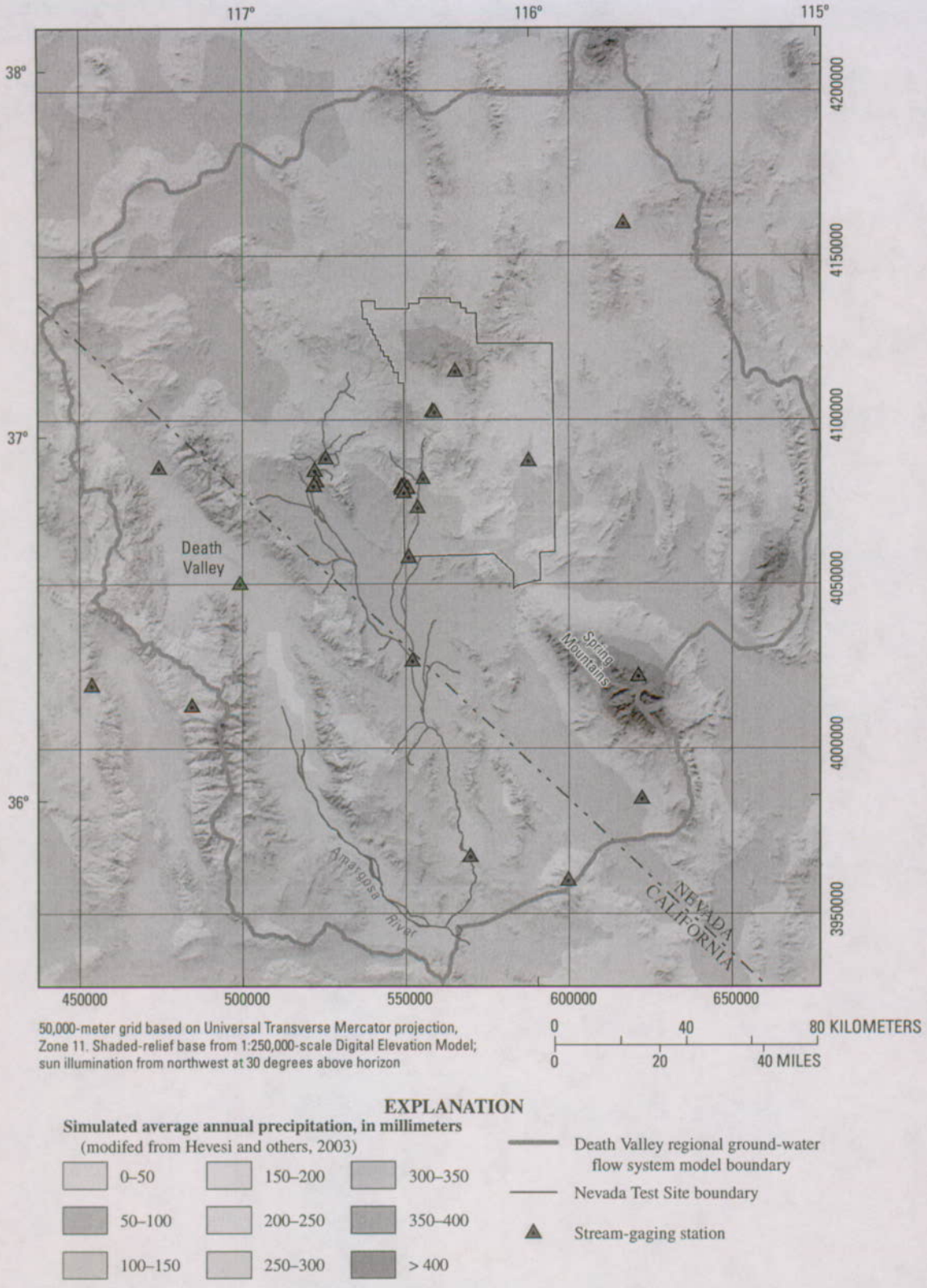

Figure C–7. Simulated average annual precipitation and stream-gaging stations used to calibrate the net-infiltration model in the Death Valley regional ground-water flow system model region.

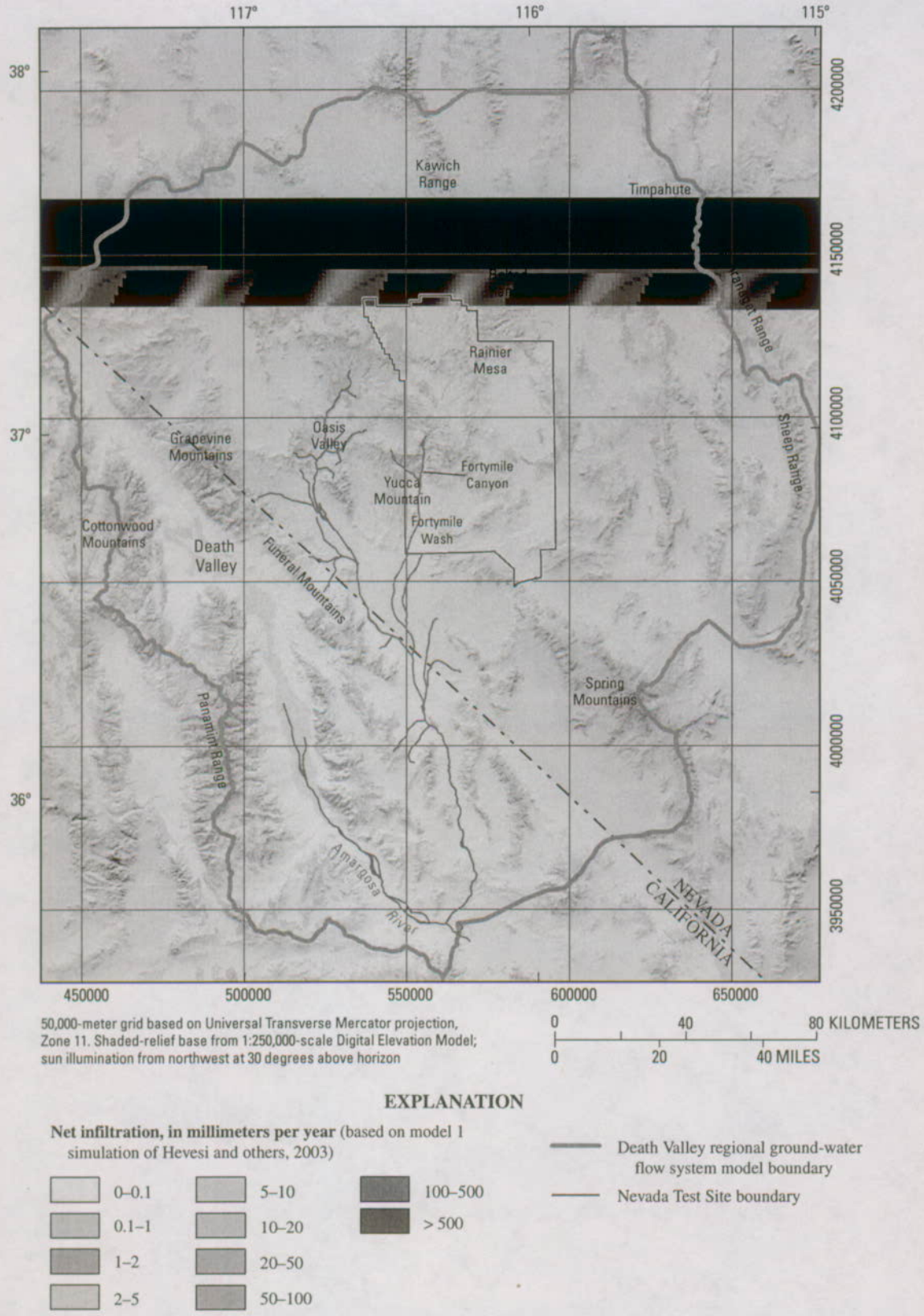

Figure C–8. Simulated net infiltration used to estimate recharge to the Death Valley regional ground-water flow system model region, 1950–99.

Simulated net-infiltration rates, averaged over the period 1950–99, were generally consistent with published (Hevesi and others, 2003, table 1) estimates of recharge in the DVRFS region. The reported annual estimate of recharge from 42 conterminous hydrographic areas including most of the DVRFS region was about 157 Mm^3 (Hevesi and others, 2003). The simulated annual net infiltration for this same area was 4 percent less at 151 Mm^3.

The uncertainty in model-generated net infiltration estimates was related to uncertainties associated with the representation of the near-surface environment and the unsaturated zone processes. Hevesi and others (2003) presented model uncertainty qualitatively because the results of their study could not support a rigorous quantification of uncertainty. Model uncertainty remained high for many model inputs such as bedrock permeability, soil thickness, root density as a function of depth, stream-channel properties, spatial distribution of climate by month (computed from daily records), and potential evapotranspiration coefficients. Although the general magnitude of the simulated net-infiltration volume was consistent with prior discharge and recharge estimates for the DVRFS region, substantial differences were observed in some local basins. Nonetheless, the spatial distribution of estimated net infiltration was considered a reasonable indication of the spatial distribution of the potential recharge across the model domain under current climate conditions (Hevesi and others, 2003).

On the basis of the net infiltration simulated by Hevesi and others (2003), the major areas of the model domain receiving recharge are along the eastern model boundary beneath the Timpahute, Pahranagat, and Sheep Ranges and the Spring Mountains; along the western part of the model boundary beneath the Panamint Range and Cottonwood Mountains; beneath the Kawich and Belted Ranges and Rainier Mesa, near the northern part of the NTS area; and beneath the Grapevine Mountains and the southern part of the Funeral Mountains, along the eastern margin of Death Valley (fig. C–8). In addition, small concentrated areas of recharge occur beneath major drainages, such as Fortymile Canyon and Fortymile Wash near Yucca Mountain and the Amargosa River near Oasis Valley, and beneath channels draining the Panamint Range and along well-developed drainages that incise major alluvial fans in Death Valley.

Lateral Flow

Areas of potential inflow and outflow, or lateral ground-water flow, along the DVRFS model boundary were defined for prepumped conditions (Appendix 2, this volume). Hydraulic gradients determined from a regional potentiometric map (plate 1 and Appendix 1, this volume) indicate that one boundary segment has no flow and that flow occurs across 11 of 12 lateral boundary segments of the model domain—7 boundary segments have inflow (Eureka and Saline are combined) and 3 have outflow (fig. C–9).

Lateral flow was estimated using the Darcy equation with hydraulic gradients defined by regional water levels, and estimates of hydraulic conductivity and the cross-sectional area of HGUs along the model boundary. Where possible, lateral-flow estimates were constrained by inflows and outflows estimated from available water-budget information for areas adjacent to the model domain. Where discrepancies between Darcy and water-budget flow estimates were great, alternative interpretations of the data, such as local adjustments to the composite hydraulic conductivity or reappraisals of the surrounding area water budgets, were used to further develop a reasonable estimate of lateral-boundary flow for the boundary segment.

Lateral-flow estimates for each boundary segment are given in table C–4. The table includes Darcy and water-budget estimates and the estimate considered most reasonable for prepumped conditions (Appendix 2, this volume). On the basis of these estimates of lateral flow, nearly 18.4 Mm^3 of ground water flows into the model domain annually, primarily along the western and northern parts of the model boundary, and 9.5 Mm^3 flows out, primarily along the eastern part of the model boundary (fig. C–9 and table C–4). The greatest inflow occurs from the area west of Death Valley, and the greatest outflow to the area east of the Sheep Range. The estimated annual net lateral flow is about 8.8 Mm^3 into the model domain.

Balance of Components

The water budget commonly is used to assess the significance of individual flow components in the ground-water system and to evaluate the balance between inflows and outflows. The volumetric flows estimated for the major water-budget components of the DVRFS from data previously presented in this chapter are summarized in table C–5. For prepumped conditions, annual recharge accounted for about 87 percent of the total inflow (143.4 Mm^3), and natural discharge (ET and spring flow) about 93 percent of the total outflow (133.8 Mm^3). The remainder (less than 10 percent) of the inflow and outflow is accounted for by lateral flows into and out of the model domain. The difference between estimated prepumped inflows and outflows is less than 7 percent of the estimated inflow. By 1998, pumpage was about 93.5 Mm^3, which equates to about 70 percent of the total outflow estimated for prepumped conditions. It should be noted that this pumpage estimate is not adjusted for any potential return flow and that table C–5 does not include return flow as a potential inflow to the 1998 water budget.

Water naturally discharging as spring flow and(or) ET and water stored in pore spaces of subsurface rock units are two likely sources for the ground water pumped from the DVRFS. A decrease in estimated spring discharge—from 16.8 Mm^3 for prepumped conditions to 5 Mm^3 in 1998 (table C–5)—indicates that ground-water pumping has affected natural discharge. The water budget given in table C–5 also indicates that ET in 1998 is likely to be less than that estimated for prepumped conditions and possibly

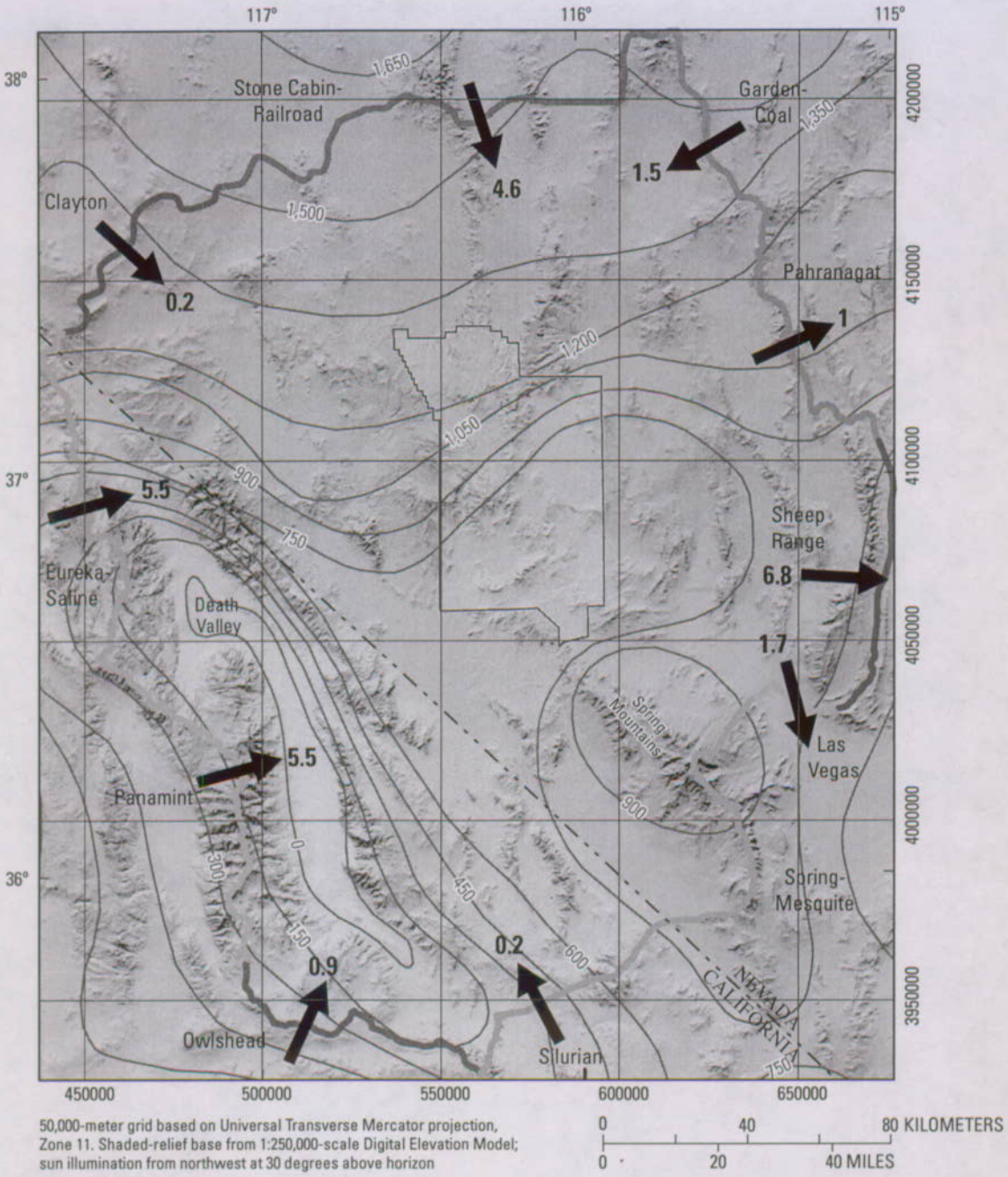

Figure C–9. Regional ground-water potentiometric surface and lateral flow across boundary segments of the Death Valley regional ground-water flow model domain.

Table C–4. Estimates of flow across lateral boundary segments of the Death Valley regional ground-water flow system model domain for prepumped conditions.

[+ values, flow into model domain; – values, flow out of model domain; --, no value was reported or estimate was unreliable; m^3/d, cubic meter per day; m^3, cubic meter]

Boundary segment (shown in fig. C–9)	Boundary flow estimate (m^3/d)			Estimate of annual boundary flow[1] (m^3)
	Darcy calculation	Water-budget calculation	Most reasonable estimate	
Silurian	–125	–11,400	500[2]	183,000
Spring-Mesquite	–782	--	0[3]	0
Las Vegas	–4,575	--	–4,575	–1,671,000
Sheep Range	–18,747	--	–18,747	–6,847,000
Pahranagat	–2,783	--	–2,783	–1,016,000
Garden-Coal	4,139	--	4,139	1,512,000
Stone Cabin-Railroad	12,476	--	12,476	4,557,000
Clayton	667	--	667	244,000
Eureka-Saline[4]	20,873	14,600–15,600	15,100	5,515,000
Panamint	14,050	14,000–16,000	15,000	5,479,000
Owlshead	2,382	--	2,382	870,000
Total	**27,576**		**24,193**	**8,826,000**

[1]Volume calculated using most reasonable estimate of boundary flow; from data analyses in Appendix 2 (this volume), rounded to the nearest 1,000 m^3.

[2]See Appendix 2 (this volume) for explanation of method used to determine most reasonable estimate.

[3]No significant flow estimated across boundary because segment closely coincides with natural no-flow boundary.

[4]Estimate is sum of flows across Saline and Eureka boundary segments.

represents a source of natural discharge reduced by local pumpage. Given the relatively short time period (less than a century), this decrease in discharge is probably not due to climatic influences. Accordingly, this interpretation would support a higher estimate of prepumped discharge than that presented in table C–5.

The other potential source of ground water pumped from the DVRFS model domain is water stored in the pores of subsurface rock. This water, when removed from the flow system, decreases the hydraulic head in the aquifer. Although the actual volume of stored ground water is uncertain, preliminary estimates, based on sparse available data on storage properties, indicate that storage accounts for the largest amount of the available water (Harrill, 1986, p. 18; Dettinger, 1989, p. 22). Measured declines in hydraulic head and only small decreases in spring discharge relative to the total amount of ground water being pumped from the DVRFS strongly indicate that the primary source of water pumped from the DVRFS model domain is stored ground water.

Hydraulic Properties

Belcher and others (2001) compiled published and unpublished hydraulic-property data to estimate hydraulic properties of the major HGUs defined for the DVRFS (see Chapter B, this volume). The hydraulic-property estimates included those for transmissivity, hydraulic conductivity, storage coefficient, and anisotropy ratios. With the exception of the lower clastic-rock confining unit (LCCU), however, only aquifer tests were used to estimate the hydraulic properties of an HGU. Belcher and others (2001) evaluated these data to characterize the hydraulic properties of the major HGUs. Hydraulic conductivity was the only property with a sufficient number of estimates to generate statistical distributions for specific HGUs. Belcher and others' (2001) compilation provided the data set from which hydraulic properties, primarily hydraulic conductivity, were estimated for the transient flow model. Storage coefficients are not discussed because field data are extremely limited (Harrill, 1986, p. 31; Belcher and others, 2001; Carroll and others, 2003). Consequently, values given in standard hydrogeology textbooks were considered adequate for purposes of this investigation.

Hydraulic Conductivity

Belcher and others (2001) estimated horizontal hydraulic conductivity (hereinafter referred to as hydraulic conductivity) by dividing transmissivity calculated from an aquifer test by the total thickness of the aquifer material being tested. Because an HGU is typically stratified and the individual aquifers or confining units have unknown thicknesses, Belcher and others (2001) used the length of the open interval of the well or borehole as the unit thickness. Belcher and others (2001) indicate that while this simplifying approach is not optimal, it is considered appropriate given the available data and nature of the units tested. This approach also was used in previous regional modeling studies in the DVRFS region (IT Corporation, 1996b).

Table C–5. Annual volumetric flow estimates of major water-budget components of the Death Valley regional ground-water flow system model domain for prepumped conditions and 1998 conditions.

[--, no estimate was made or available; Mm^3, millions of cubic meters; ET, evapotranspiration]

Water-budget component	Estimated annual volumetric flow (Mm^3)	
	Prepumped conditions	1998
Inflow		
Recharge (net infiltration)	125	125
Boundary inflow (table C–4)	18.4	--
Total	**143.4**	
Outflow		
Natural discharge: ET[1]	107.5	[3]<107.5
Spring flow[2] (table C–2)	16.8	5
Boundary outflow (table C–4)	9.5	--
Pumpage (table C–3)	0	93.5
Total	**133.8**	
Difference (inflow-outflow)	**9.6**	
Difference (percent)	**6.7**	

[1]Estimate for prepumped conditions not included in estimate given in table C–1 for Pahrump Valley.

[2]Bennetts and Manse Springs were reported dry after 1975.

[3]"Less than" symbol is not intended to quantify discharge, but only to indicate that the component likely is less than the prepumped natural discharge.

Pumping and companion observation wells commonly are constructed in water-producing zones of an HGU in the model domain. Data collected from these wells may represent the more transmissive zones of an HGU; therefore, transmissivities calculated from these data may be biased to larger values. This bias may be compounded further by the assumption that the thickness of a unit is limited to the length of the open interval of the well when calculating hydraulic conductivity. Thus, the means and variances presented by Belcher and others (2001) may be most representative of the hydraulic properties of the more productive zones in an HGU.

Variability inherent in the HGUs across the DVRFS region increases the uncertainty of the estimated hydraulic conductivity values. Lithologic factors, such as facies changes in sedimentary rock, changes in welding in volcanic rock, and degree of fracturing, can cause hydraulic conductivity values to vary substantially over relatively short distances. Variability also can result from sampling bias. Variability for estimates of the matrix permeability commonly depends upon the variable lithology and interval penetrated by the well within a particular unit. Sampling variability also can be a factor in fractured rocks if boreholes intersect rocks with different degrees of fracturing.

Probability Distributions

Data from Belcher and others (2001) were used to estimate probability distributions and to provide reasonable ranges of hydraulic conductivity for the major HGUs in the DVRFS region (Belcher and others, 2002). Fracturing appears to have the greatest influence on the permeability of bedrock HGUs—the greater the degree of fracturing, the greater the permeability. Alteration and welding in the Cenozoic volcanic rocks also greatly influence hydraulic conductivity. Alteration decreases hydraulic conductivity, and welding forms brittle rocks that fracture more easily, thereby increasing hydraulic conductivity. In Chapter B (this volume), these relations are used to establish hydraulic-conductivity zones. Table C–6 presents probability distributions of hydraulic conductivity for the major HGUs in the DVRFS region.

Depth Decay

Intuitively, hydraulic conductivity decreases with depth as the geostatic load increases, compressing favorably oriented fractures, faults, and sedimentary units. Analyses of covariance confirmed the assumption that depth was a significant factor in the variability of hydraulic conductivity in the DVRFS region, but variability in hydraulic-conductivity estimates because of other factors prevents a rigorous quantification of a depth decay function.

The relation between hydraulic conductivity and depth in the DVRFS region has been postulated by Bedinger and others (1989), IT Corporation (1996b), and D'Agnese and others (1997). Bedinger and others (1989) developed a series of curves defining the distribution of hydraulic conductivity for hydrogeologic units in the region. The hydraulic-conductivity values of each unit were affected by the variation of rock properties by depth and degree of faulting. Using these findings, D'Agnese and others (1997) indicate qualitatively that the hydraulic conductivity decreases rapidly for most rocks between depths of 300 to 1,000 m across the model domain. At depths greater than 1,000 m, matrix permeability probably dominates, except in regional fault zones. At depths greater than 5,000 m, the geostatic load probably keeps faults and fractures closed (D'Agnese and others, 1997). The study by the IT Corporation (1996b, p. 29) postulated a relation of exponentially decreasing hydraulic conductivity with depth in the alluvial aquifer (equivalent to the AA and ACU units in table C–6), in the volcanic aquifer (equivalent to part of the Cenozoic volcanic-rock HGUs), and in the lower carbonate-rock aquifer (LCA). Decreasing trends in hydraulic conductivity are evident in the data presented in this study (IT Corporation, 1996b, figs. 6–1, 6–2, and 6–3), despite a great deal of apparent scatter in the data.

On the basis of regression analysis, Belcher and others (2001) found the best relation was between $\log_{10}$-transformed hydraulic conductivity and depth. The logarithmic values of hydraulic conductivity were used for statistical calculations because this parameter tends to be log-normally distributed

Table C–6. Horizontal hydraulic-conductivity estimates of hydrogeologic units in the Death Valley regional ground-water flow system (modified from Belcher and others, 2001; 2002).

[Abbreviations: AA, alluvial aquifer; ACU, alluvial confining unit; BRU, Belted Range unit; CFBCU, Crater Flat–Bullfrog confining unit; CFPPA, Crater Flat–Prow Pass aquifer; CFTA, Crater Flat–Tram aquifer; CHVU, Calico Hills volcanic-rock unit; ICU, intrusive-rock confining unit; LCA, lower carbonate-rock aquifer; LCCU, lower clastic-rock confining unit; LFU, lava-flow unit; OAA, older alluvial aquifer; OACU, older alluvial confining unit; OVU, older volcanic-rock unit; PVA, Paintbrush volcanic-rock aquifer; SCU, sedimentary-rock confining unit; TMVA, Thirsty Canyon–Timber Mountain volcanic-rock aquifer; UCA, upper carbonate-rock aquifer; UCCU, upper clastic-rock confining unit; VSU, volcanic- and sedimentary-rock unit; XCU, crystalline-rock confining unit; YAA, younger alluvial aquifer; YACU, younger alluvial confining unit; YVU, younger volcanic-rock unit; NA, not applicable]

Hydrogeologic unit or subunit	Hydraulic conductivity (meters per day)				95-percent confidence interval	Number of measurements
	Geometric mean[1]	Arithmetic mean	Minimum	Maximum		
AA[2]	1.5	10.8	0.00006	130	0.005–430	52
ACU[3]	3	10.5	0.003	34	0.02–470	15
LFU	NA	NA	0.002	4	NA	2
YVU & VSU	0.06	1.5	0.00004	6	0.00005–80	15
TMVA	0.01	2	0.0002	20	0.00001–18	11
PVA	0.02	4	0.000007	17	0.0000003–1300	9
CHVU	0.2	0.55	0.008	2	0.007–5	14
BRU	0.3	1.03	0.01	4	0.006–17	6
CFTA	0.05	0.4	0.003	2	0.0004–5.3	11
CFBCU	0.4	6.8	0.0003	55	0.0006–240	34
CFPPA	0.3	13	0.001	180	0.000006–2.4	19
OVU	0.004	0.07	0.000001	1	0.00002–5	46
ICU	0.01	0.3	0.0006	1.4	0.00002–5	7
SCU	0.002	0.02	0.0002	0.3	0.00004–0.09	16
UCA & LCA	2.5	90	0.0001	820	0.0008–7700	53
fractured	19	150	0.01	820	0.03–11,000	32
unfractured	0.1	1.6	0.0001	14	0.0002–70	21
UCCU & LCCU[4]	0.00002	0.2	3×10^{-8}	5	1×10^{-10}–3	29
shale	0.01	0.07	0.0002	0.4	0.0001–1.4	9
quartzite	0.000001	0.24	3×10^{-8}	5	1×10^{-10}–0.006	19

[1]Values determined from log-transformed distribution.

[2]AA is the combined YAA and OAA.

[3]ACU is the combined YACU and OACU.

[4]One measurement could not be classified as shale or quartzite.

(Neuman, 1982). The Cunnane plotting position method was used to assess the normality of the logarithms of hydraulic-conductivity estimates for each major HGU (Helsel and Hirsch, 1992, p. 27–29). In most cases, the assumption of a normal distribution for log hydraulic conductivity was true.

For the major HGUs, 14 of the 15 relations between depth and log hydraulic conductivity had a correlation coefficient that ranged from virtually zero to 0.52. Depth and log hydraulic conductivity possibly are correlated for the Belted Range unit (r^2=0.78), although the regression was determined with only six data pairs.

Despite poor results from the regression analysis, a relation between depth and hydraulic conductivity might exist at the scale of this investigation. Hydraulic-conductivity estimates were available only to depths of less than 3,600 m, and the average depth investigated was only 700 m. A possible relation between depth and hydraulic conductivity could be investigated further through calibration of regional models.

Hydraulic Head

Hydraulic-head measurements at each measurement site were composited to develop hydraulic-head observations. Errors in well altitude and location, nonsimulated transient stress, and water-level measurement were estimated to quantify the uncertainty of the head observations.

Head Observations

Periodic depth-to-water measurements and continuous down-hole water pressure measurements made in wells throughout the DVRFS model domain were used to develop hydraulic-head observations. The observations for each well, which composite one or more water-level measurements, were used in calibrating the ground-water flow model. These data were acquired as part of activities associated with many historical and currently active water-level monitoring networks,

each of which was established to address a specific interest in a study area. Active monitoring networks include those funded or operated by Nye County, the States of Nevada and California, U.S. Geological Survey, National Park Service, U.S. Fish and Wildlife Service, and the U.S. Department of Energy Yucca Mountain Project and Underground Test Area Program. Much of these data and other water-level information available from local mining operations have been included in the U.S. Geological Survey's National Water Information System (NWIS). NWIS, specifically its ground-water component, the Ground-Water Site Inventory (GWSI), served as the primary source and repository for water levels and associated borehole information used to develop and calibrate the DVRFS ground-water flow model. Temporal and spatial gaps in water-level data were evaluated and, where possible, addressed by making additional measurements and by entering any previously omitted water-level information into the GWSI.

The GWSI, although comprehensive and complete in terms of water-level measurements and borehole and well information, has limited options for assigning ancillary information to individual water-level measurements. Thus, a project database was designed to retrieve site, construction, borehole, and water-level information directly from GWSI and store additional information about each water-level measurement.

Ancillary information about each water level was incorporated into the project database by assigning attributes. This information included one general-condition attribute and multiple detailed-condition attributes for each water-level measurement (table C–7). The general-condition attribute indicates the appropriateness of the measurement as a steady-state or transient head observation. The detailed-condition attribute provides additional information about the condition or state of the measurement or of the well at the time the measurement was made.

The general-condition attribute identifies measurements determined acceptable as head observations for calibration of the regional ground-water flow model. Measurements representative of regional ground-water conditions were identified as regional-scale measurements. All other general-condition attributes indicate that the measurement is unacceptable for developing head observations for calibration of the regional ground-water flow model. These regional measurements were attributed as either steady state or transient. A regional transient designation is assigned only to those water levels in which the measured response is considered to be the result of ground-water pumpage. Detailed-condition attributes provide information to support the general condition assigned to the measurement. These attributes include information about the condition and location of the well, observed trends in the water level, and reported and likely explanations for measured water-level changes.

Attributes assigned to each category were determined by analyzing hydrographs, reviewing reports pertaining to water levels measured nearby, and evaluating the well location relative to centers of pumping and underground nuclear tests. Reports include mainly those published as part of previously mentioned monitoring networks. Open-interval depth information for wells also was evaluated to assess whether measured fluctuations result from precipitation variations or evapotranspiration. Measurements from wells having insufficient information from which to determine or estimate an open interval were not used to develop head observations. This attributing procedure is illustrated by an annotated hydrograph of water levels from a well in Pahrump Valley (fig. C–10).

Nearly 40,000 water levels measured in about 2,100 wells were evaluated in the model domain. Of these, about 12,000 water levels in 700 wells were assigned attributes indicating that the water level represented regional, steady-state conditions. Head observations for calibration of prepumped conditions were computed at each of the 700 wells as the average of all measurements attributed as representing regional, steady-state conditions. The spatial distribution of the 700 steady-state head observations is shown in figure C–11. Head observations range from about 2,500 m above sea level in the Spring Mountains to nearly 100 m below sea level in Death Valley. In general, head decreased from north to south. Local areas of higher head are coincident with mountainous areas where regional aquifers receive recharge from precipitation.

Nearly 15,000 water levels measured in about 350 wells were attributed to indicate that the measurements represented regional, transient (pumped) conditions (fig. C–12). These measurements, along with those attributed as regional steady-state water-level measurements, were used to develop the set of transient-head observations used to calibrate the ground-water flow model. Water-level records for individual wells spanned periods from 1 to about 50 years. Water levels attributed as representing regional steady-state or transient conditions were averaged by year and by well to compute the almost 5,000 head observations used to calibrate the transient ground-water flow model.

The earliest reported water level usable for the DVRFS ground-water flow model was measured in 1907. Most wells having longer term water-level records are in Pahrump Valley (fig. C–12). Nearly 100 wells in the DVRFS model domain have a record of 20 years or longer. The greatest drawdown measured in the DVRFS model domain is 76 m, which was measured in a well in the Beatty area just north of Amargosa Desert (fig. C–12). Most wells have less than 15 m of measured drawdown; wells having the greatest drawdown (>15 m) typically are in areas of concentrated irrigation use, primarily the Amargosa Desert and Pahrump and Penoyer Valleys (fig. C–12).

Every well in which a water level was measured was attributed to indicate the depth of the interval contributing water to the well. Two depth attributes were assigned to each well—one representing the top of the uppermost open interval, and the other, the bottom of the lowermost open interval. Depth attribute values were determined from well-construction and borehole information stored in GWSI. For wells in which specific screen- or open-interval information was not known, top and bottom interval values were estimated from reported well depths, hole depths, casing information, and water levels.

Table C–7. Description of attributes assigned to water levels retrieved from Ground-Water Site Inventory (GWSI) for simulation of ground-water flow in the Death Valley regional ground-water flow system model domain.

General-condition attribute		
Attribute name	**Description**	**Considered appropriate for regional evaluation**
Duplicate	Measurement entered under another site identifier.	NO
Insufficient data	Measurement does not have sufficient supporting information to determine general condition.	NO
Localized	Measurement represents localized hydrologic conditions.	NO
None	Water level not measured because well was dry or obstructed.	NO
Nonstatic level	Measurement affected by sampling, testing, construction, or some other local activity.	NO
Steady state–LOCAL	Measurement represents prepumped, equilibrium conditions in a local-scale flow system.	NO
Steady state–REGIONAL	Measurement represents prepumped, equilibrium conditions in regional ground-water flow system.	YES
Superseded	Measurement replaced by another that more accurately represents ground-water conditions at the site.	NO
Suspect	Measurement is erroneous or affected by unnatural conditions.	NO
Transient–LOCAL	Measurement reflects transient conditions in or near borehole.	NO
Transient–REGIONAL	Measurement reflects changes caused by pumping from the regional ground-water flow system.	YES

Detailed-condition attribute	
Attribute name	**Description**
Erratic/Unstable	Measurement appears to be erratic and unstable.
Evapotranspiration response	Measurement appears to be responding to evapotranspiration.
Flowing	Measurement is above land surface. In some cases an accurate water level could not be determined due to flowing conditions.
Insufficient data	Measurement does not have sufficient information to determine detailed conditions.
Limited data	Measurement is one of a limited number, but general condition is assumed to represent regional conditions.
Missing	Measurement not assigned a value.
No date	Measurement not associated with a date.
Obstruction	Measurement not assigned a value because of an obstruction in borehole.
Nuclear test effect	Measurement appears to be responding to nearby nuclear test (1951–92).
Not adjusted for temperature	Measurement not adjusted for a reported temperature effect.
Precipitation response	Measurement appears to be responding to a recent precipitation event.
Pumping area	Site is located in an area that may have been affected by ground-water pumping.
Pumping steady state	Measurement appears to represent steady- or near steady-state conditions during sustained pumping.
Pumping/recovery	Measurement appears to be responding to pumping in the borehole or in a nearby borehole.
Reported perched water	Measurement is reported to represent local perched-water conditions.
Rising trend	Measurement appears to be part of a discernible, overall, rising trend. Possible causes include decrease in nearby pumping and a local precipitation event.
Seasonal pumping	Measurement appears to be responding to nearby seasonal pumpage.
Suspect	Measurement is suspect.
Suspected perched water	Measurement assumed to represent local perched-water conditions.
Testing area	Well located in area of past nuclear testing.
Undeveloped	Well not sufficiently developed.

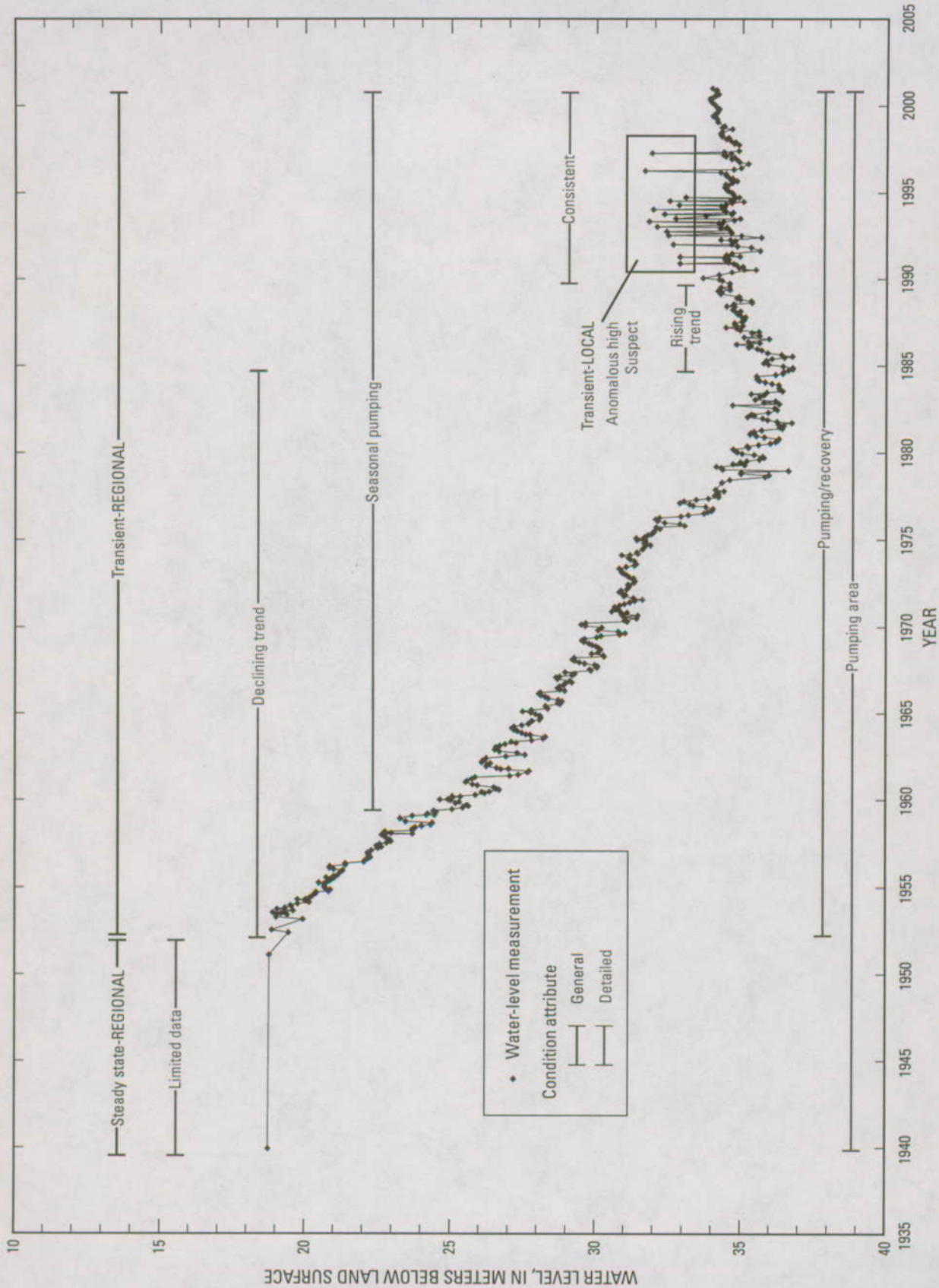

Figure C–10. Annotated hydrograph showing general- and detailed-condition attributes assigned to water-level measurements from a well in Pahrump Valley.

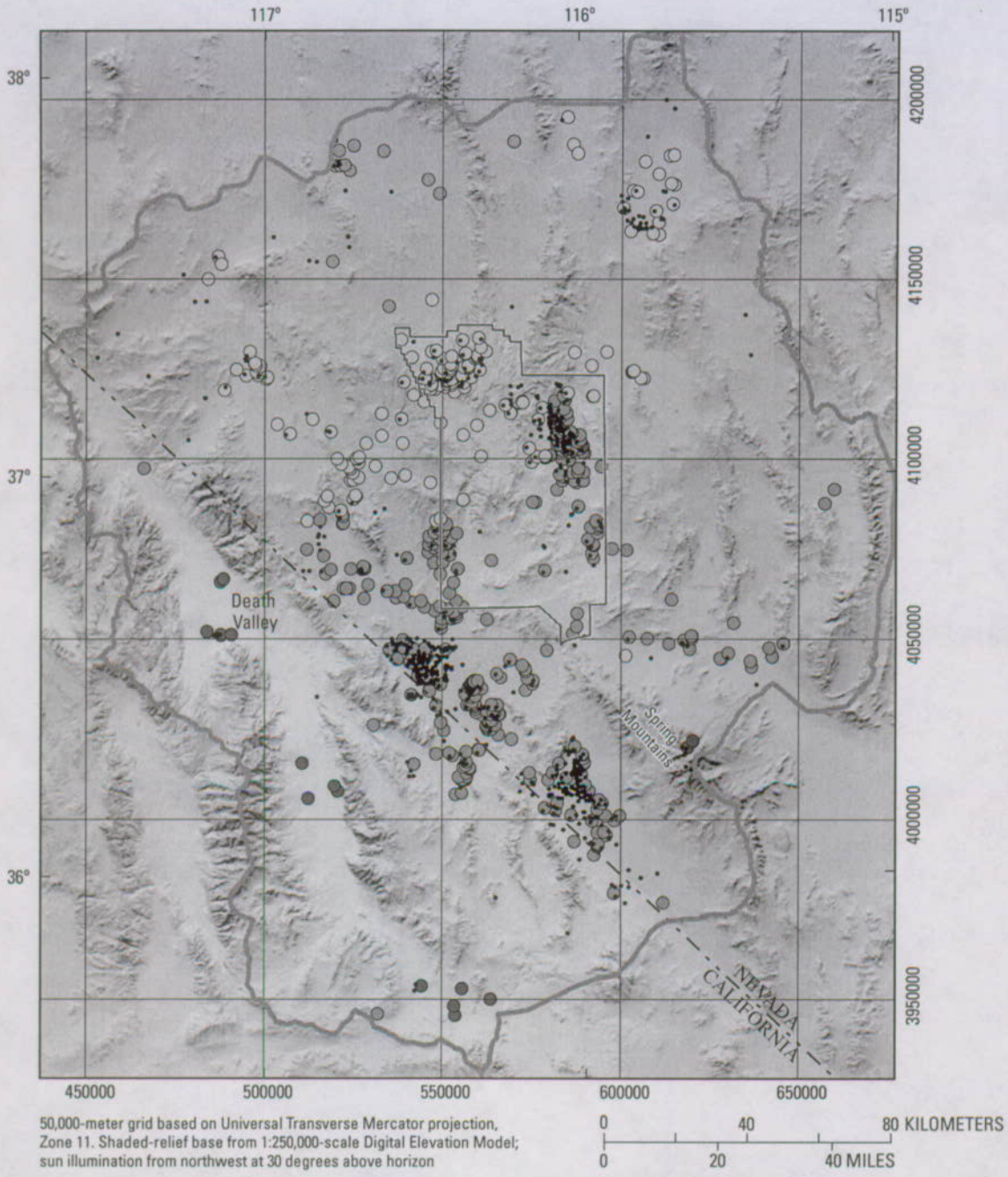

Figure C–11. Spatial distribution and altitude of head observations in wells representing regional, steady-state conditions used in calibration of the Death Valley regional ground-water flow system model.

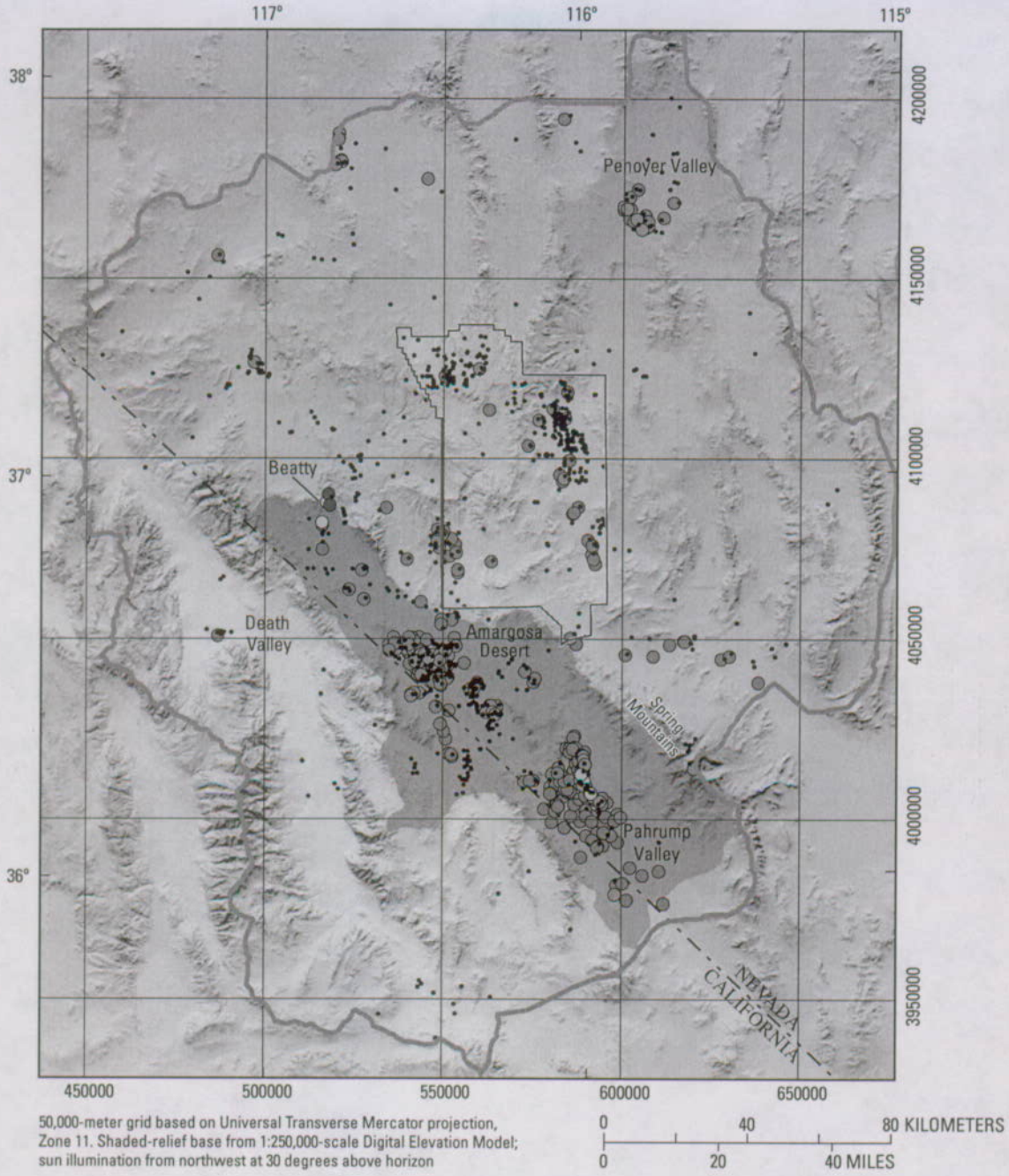

Figure C–12. Spatial distribution and maximum drawdown of head observations in wells representing regional, transient conditions used in calibration of the Death Valley regional ground-water flow system model.

As previously stated, measurements from wells for which information was insufficient to determine or estimate an open interval were not used to calibrate the transient ground-water flow model. Wells used to calibrate the transient flow model are summarized in table C–8. The table lists wells in depth ranges based on the depth of the bottom of the open interval. About 43 percent of the wells have open intervals at depths less than 100 m, and less than 10 percent at depths greater than 1,000 m. The spatial distribution of wells with shallow and deep openings is shown in figure C–13. Most wells having deeper openings are in or near the NTS. The typical depth of the open interval of wells in major agricultural areas of the DVRFS model domain (Amargosa Desert and Penoyer and Pahrump Valleys) is less than 100 m.

Head-Observation Uncertainty

Errors that contribute most to the uncertainty of head observations are associated with potential inaccuracies in the altitude and location given for a well and in the measurement of a water level, and fluctuations introduced by variations in climate or any other nonsimulated transient stress. These errors were estimated from available information and were used to quantify the uncertainty of a head observation.

Table C–8. Bottom depth of open interval for wells used to calibrate the Death Valley regional ground-water flow system model.

[≤, less than or equal to]

Bottom depth of open interval (meters)	Number of wells	Percentage of wells
≤100	369	42.5
≤500	642	74.
≤1,000	803	92.5
≤5,000	868	100.

Well-Altitude Error

Well-altitude error directly affects the calculation of the hydraulic head as referenced to a common datum. The error associated with the potential inaccuracy in well altitude was computed from the altitude accuracy code given in GWSI, expressed as a plus/minus (±) range related directly to the method by which the altitude was determined. This range varies from ±0.03 m for high-precision methods, such as spirit level and differential global positioning system (GPS) surveys, to ±25 m for estimates determined from topographic maps having large (50 m) contour intervals. The range defined by the altitude accuracy code is assumed to represent, with 95 percent confidence (two standard deviations), the true well-altitude uncertainty. Assuming that the head observation represents the mean value and that the error is normally distributed, the uncertainty of the head observation, with respect to the well-altitude error, can be expressed as a standard deviation by the following equation:

$$sd = AAC / 2 \quad (1)$$

where

sd is the standard deviation,

and

AAC is the value of the GWSI altitude accuracy code, in meters.

Accordingly, the standard deviation for well-altitude error could range from 0.015 to 12.5 m.

Well-Location Error

Well-location errors can cause a discrepancy between observed and simulated heads. The magnitude of this discrepancy depends directly on the hydraulic gradient at the well—the steeper the gradient, the greater the discrepancy. Well-location error was calculated as the product of the distance determined from the coordinate accuracy code values given in GWSI and the hydraulic gradient estimated for a given well location. Latitude and longitude coordinate accuracy codes given for wells in the DVRFS range from about 0.1 to 100 seconds. In the DVRFS region, a second represents about 33 m. Accordingly, the largest distance accuracy that could be computed for a well in the DVRFS model domain would be about ±3,300 m. The hydraulic gradient at a well was estimated from a regional potentiometric surface map developed by D'Agnese and others (1998). The largest gradient estimated from their map was nearly 15 percent and the smallest about 2 percent. The range defined by the value of the coordinate accuracy code is assumed to represent, with 95 percent confidence (or two standard deviations), the true error in the head observation as related to well-location uncertainty. Assuming that the head observation represents the mean value and that the error is normally distributed, the uncertainty of the head observation, with respect to the well-location error, can be expressed as a standard deviation calculated by the following equation:

$$sd = (CAC / 2) \times HG, \quad (2)$$

where

sd is the standard deviation;

CAC is the value of the GWSI coordinate accuracy code, in meters;

and

HG is hydraulic gradient, in percent slope divided by 100.

Accordingly, the standard deviation for well-location error could range from about 0.03 to 250 m.

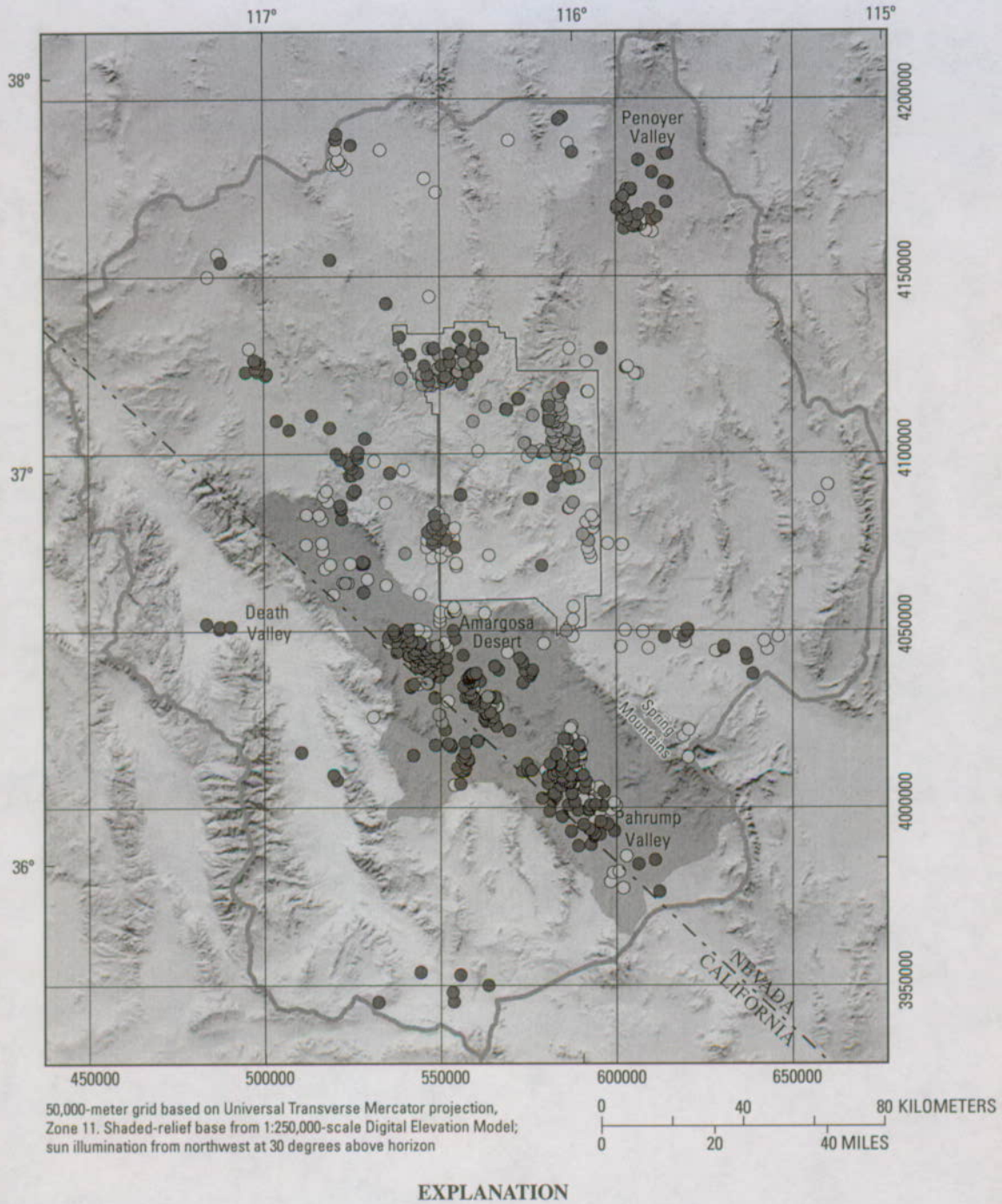

Figure C–13. Spatial distribution and bottom depth of opening in head-observation wells (steady-state and transient conditions) used in calibration of the Death Valley regional ground-water flow system model.

Nonsimulated Transient Error

Nonsimulated transient errors result from uncertainty in the magnitude of water-level response caused by stresses not simulated in the flow model, which are typically seasonal and long-term climate changes. Seasonal water-level fluctuations of nearly 5 m have been measured in shallow wells in the DVRFS model domain. These seasonal fluctuations decrease as the depth of the open interval increases. The quantification of uncertainty associated with seasonal fluctuations in the water level requires a sufficient number of measurements made over an entire year. For observations computed with less than 7 measurements per year, the seasonal fluctuation was set to 5 m for wells with open intervals less than 15 m below land surface and 1.5 m for open intervals greater than 15 m below land surface. For observations computed from seven or more measurements per year, the fluctuation is computed as the difference between the highest and lowest water-level measurement. It was assumed that if at least seven measurements were made per year, then these measurements spanned the entire year.

The long-term climatic response in the water-level record is much more difficult to discern and commonly is masked by pumping effects. On the basis of an analysis of available water-level data, long-term climatic response is relatively small throughout the DVRFS region (less than 1.5 m). The potential error associated with long-term climate response at a well was not calculated independently but instead was accounted for by adding 1 m to the seasonal fluctuation assigned to each well. The range defined by this sum is assumed to represent, with 95-percent confidence (or two standard deviations), the true error in the head observation as related to nonsimulated transient uncertainty. Assuming that the head observation represents the mean value and that the error is normally distributed, the uncertainty of the head observation, with respect to the nonsimulated transient error, can be expressed as a standard deviation calculated by the following equation:

$$sd = (SF + LTC) / 4, \quad (3)$$

where

sd is the standard deviation;

SF is seasonal fluctuation as defined by water-level measurements, in meters;

and

LTC is the long-term climate trend defined as 1 m.

Accordingly, the maximum standard deviation for nonsimulated transient error is 1.5 m for wells having less than 7 measurements and an open interval within 15 m of land surface, and 0.625 m for deeper wells.

Measurement Error

Measurement errors result from inaccuracies in the measurement of the depth to water. Measurement accuracy depends primarily on the device being used to make the measurement. Typically, the accuracies of measurement devices are less than a meter and are defined as a percentage of the depth of the measurement—the deeper the depth-to-water measurement, the greater the potential error. Errors associated with most devices used to measure water levels in the DVRFS region are described in a standard operating procedure report for water-level measurements at the NTS (U.S. Geological Survey, Las Vegas, Nev., written commun., 2001). The greatest error associated with any of these devices equates to about ±1 m per 1,000 m or 0.1 percent. Water-level depths measured in the region range from near land surface to about 750 m below land surface. A value computed as 0.1 percent of the water-level measurement was used to represent the potential error in measurement accuracy. The range defined by this value is assumed to represent, with 95-percent confidence (or two standard deviations), the true error in the head observation as related to measurement uncertainty. Assuming that the head observation represents the mean value and that the error is normally distributed, the uncertainty of the head observation, with respect to the measurement-accuracy error, can be expressed as a standard deviation calculated by the following equation:

$$sd = (DOOBS \times 0.001) / 2, \quad (4)$$

where

sd is the standard deviation,

and

$DOOBS$ is depth of the observation, in meters above or below land surface.

Accordingly, the standard deviation for the measurement-accuracy error could range from near 0 to 0.375 m.

Total Head-Observation Error

The potential error associated with each head observation is the composite of all errors contributed by the different sources. This uncertainty, expressed as a standard deviation, was computed as:

$$(sd_1^2 + sd_2^2 + sd_3^2 + sd_4^2)^{1/2}, \quad (5)$$

where

sd_1 is standard deviation of well-altitude error,

sd_2 is standard deviation of well-location error,

sd_3 is standard deviation of nonsimulated transient error,

and

sd_4 is standard deviation of measurement-accuracy error.

Accordingly, the standard deviations representing the uncertainty of head observations used to calibrate steady-state (prepumped) conditions generally range from less than 1 to about 40 m (fig. C–14*A*). About 95 percent of the head observations had an uncertainty of less than 10 m and nearly

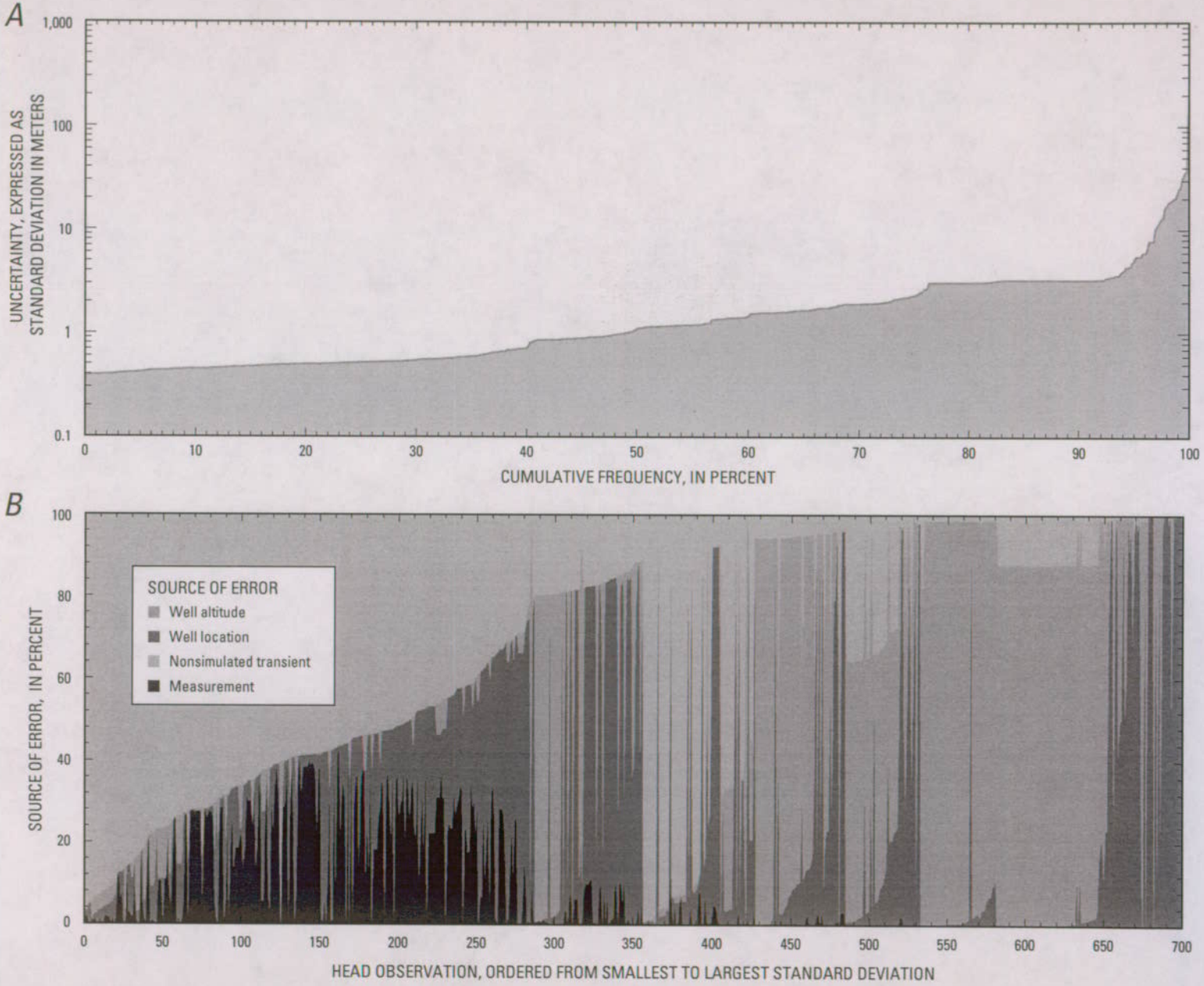

Figure C–14. Uncertainty of 700 head observations computed to represent prepumped, steady-state conditions in the Death Valley regional groundwater flow system model domain.

50 percent had an uncertainty of less than 1 m. The contribution of individual sources to head observation uncertainty varies; but in general, smaller uncertainties were dominated by nonsimulated transient and measurement errors and larger uncertainties by well-altitude and well-location errors (fig. C–14*B*).

Summary

Information from a series of investigations was compiled to conceptualize and quantify hydrologic components of the ground-water flow system in the Death Valley regional ground-water flow system (DVRFS) model domain and to provide hydraulic-property and head-observation data to be used in the calibration of the transient-flow model. These studies, completed as part of the overall DVRFS investigation, reevaluated natural ground-water discharge occurring through evapotranspiration (ET) and spring flow; the history of ground-water pumping from 1913 through 1998; ground-water recharge simulated as net infiltration; model boundary inflows and outflows based on regional hydraulic gradients and water budgets of surrounding areas; hydraulic conductivity and its relation to depth; and water levels and their appropriateness for regional simulation of prepumped and pumped conditions in the DVRFS model domain. Results appropriate for the regional extent and scale of the model were provided by acquiring additional data, by reevaluating existing data using current technology and concepts, and by refining interpretations using new analyses or algorithms.

Estimates of natural ground-water discharge were evaluated for Death Valley, Oasis Valley, and the other major discharge areas in the DVRFS model domain. Natural ground-water discharge was estimated from evaporation from open water and moist, bare soil and from transpiration by the phreatophytes growing in the discharge area. Discharge from the many regional springs in these discharge areas was accounted for because most spring flow eventually is evapotranspired. In Pahrump and Penoyer Valleys, where ground water is discharged both naturally and by pumping, natural discharge estimates were based on published sources and were assumed to vary with local pumping. In discharge areas not affected by pumping, rates of natural ground-water discharge were assumed to remain fairly constant, presuming no major changes in climate. Mean annual discharge from ET for the model domain is estimated at about 115.5 million cubic meters (Mm^3).

The ET investigations did not account for spring flow where springs supported narrow bands of riparian habitat along the valley margins or where local pumping had decreased spring flow. Previously published spring-discharge rates and some additional measurements of discharge from selected springs were compiled. Annual natural discharge from springs not accounted for in ET studies is estimated at about 16.8 Mm^3.

The composite annual discharge from Bennetts and Manse Springs, the largest springs in Pahrump Valley, is estimated at 12 Mm^3 prior to ground-water pumping. The local pumping of ground water for large-scale agricultural use in Pahrump Valley caused Bennetts Spring to stop flowing in 1959 and Manse Spring to stop flowing around 1977.

A history of ground-water use for the DVRFS region (1913–98) was developed by compiling available information and using various estimation methods to fill gaps where data were missing. In 1913, ground water used to support agriculture in Pahrump Valley was estimated at less than 5 Mm^3. Ground-water pumping remained relatively constant through 1944 and thereafter increased steadily in response to agricultural expansion. The estimated total volume of ground water pumped from the DVRFS model domain for the period 1913–98 is about 3,276 Mm^3 and in 1998 about 93.5 Mm^3. These estimates are not adjusted for water potentially returned to the ground-water flow system.

Recharge in the DVRFS region was estimated from net infiltration using a deterministic mass-balance method. The approach simulated daily climate changes and numerous near-surface processes controlling infiltration. The net-infiltration model, INFILv3, was calibrated to available surface-water flow measurements and constrained by prior estimates of recharge and discharge. The INFILv3 model simulated a mean annual potential recharge to the model domain of about 125 Mm^3 for the period 1950–99.

Lateral flow across the boundary of the DVRFS model domain was estimated. Flows from water-budget studies were compared to those computed by Darcy calculations by using hydraulic gradients obtained from a regional potentiometric-surface map (Appendix 1) and estimated hydraulic conductivities of the hydrogeologic units (HGUs) along the model boundary. The estimated mean annual ground-water flow into the model domain is about 18.4 Mm^3 and out of the model domain is about 9.5 Mm^3.

A water budget for the prepumping period (pre-1913) computed for the DVRFS model domain was balanced to within about 7 percent. For prepumped conditions, annual recharge accounted for about 87 percent of the total inflow, and natural discharge (ET and spring flow) about 93 percent of the total outflow. Although natural discharge by ET was assumed to represent prepumped conditions, actual discharge may have been reduced some by local pumpage. The remainder of the inflow and outflow is accounted for by lateral flows into and out of the model domain.

The water budget for pumped conditions for the DVRFS model domain is incomplete because accurate estimates for the major hydrologic components are not available. Pumpage in 1998 was about 70 percent of the total outflow estimated for prepumped conditions. A likely source of most of the water being pumped from the DVRFS region is ground water in storage. This water, when removed from the flow system, potentially decreases the hydraulic head within aquifers and decreases natural discharge through ET and from spring flow.

These decreases are partly reflected by declining water-level measurements in areas of pumping and by estimates showing declining spring discharge in Pahrump Valley.

Previously developed reasonable ranges of hydraulic properties, primarily horizontal hydraulic conductivity, were used for the major HGUs of the DVRFS region. Fracturing appears to have the greatest influence on the permeability of bedrock HGUs—the greater the degree of fracturing, the greater the permeability. In the Cenozoic volcanic rocks by alteration decreases hydraulic conductivity, and welding forming brittle rocks that fracture more easily, increases hydraulic conductivity. Storage coefficients from the literature were used because field data necessary to develop HGU-specific values were extremely limited.

The average depth represented by hydraulic-conductivity estimates for the model domain is 700 m with a maximum depth of 3,600 m. Using these limited data, hydraulic conductivity decreased with depth. A rigorous quantification of a depth-decay function was prevented by the variability in available hydraulic-conductivity data.

Nearly 40,000 water levels measured since 1907 in about 2,100 wells were evaluated as part of the DVRFS investigation. Almost 100 wells in the DVRFS model domain have a record of 20 years or longer. Most wells having 30 or more years of water-level record are in Pahrump Valley. About 43 percent of the wells have openings at depths less than 100 m, and less than 10 percent at depths greater than 1,000 m. Wells having deeper openings are generally in or near the NTS. The depth of the open interval for wells in major areas of ground-water pumping (Amargosa Desert and Penoyer and Pahrump Valleys) is typically less than 100 m.

Head observations representing steady-state, prepumped conditions were computed from about 12,000 water levels averaged at 700 wells in the DVRFS model domain. Head observations range from about 2,500 m above sea level in the Spring Mountains to nearly 100 m below sea level in Death Valley. Transient, pumped conditions were represented by head observations computed from nearly 15,000 water levels measured in about 350 wells. Water-level records for individual wells spanned periods from 1 to about 50 years. Most wells have less than 15 m of measured drawdown. Wells having measured drawdown greater than 15 m typically are in areas of concentrated irrigation use, primarily the Amargosa Desert and Pahrump and Penoyer Valleys. The largest drawdown is 76 m, which was measured in a well located in the Beatty area just north of the Amargosa Desert.

Each head observation was assigned an uncertainty based on potential errors related to uncertainties in the altitude and location given for a well, potential inaccuracies in the measurement of a water level, and fluctuations introduced by variations in climate or any other nonsimulated transient stress. The uncertainty of each head observation was represented by a standard deviation calculated by compositing the individual source errors. Standard deviations representing the uncertainty of the head observations range from less than 1 to about 200 m with only one observation having an uncertainty exceeding 40 m.

References Cited

Ball, S.H., 1907, A geologic reconnaissance in southwestern Nevada and eastern California: U.S. Geological Survey Bulletin 308, 218 p., 3 plates.

Bedinger, M.S., Langer, W.H., and Reed, J.E., 1989, Hydraulic properties of rocks in the Basin and Range province, *in* Bedinger, M.S., Sargent, K.A., Langer, W.H., Sherman, F.B., Reed, J.E., and Brady, B.T., Studies of geology and hydrology in the Basin and Range province, southwestern United States, for isolation of high-level radioactive waste—Basis of characterization and evaluation: U.S. Geological Survey Professional Paper 1370–A, p. 16–18.

Belcher, W.R., Elliott, P.E., and Geldon, A.L., 2001, Hydraulic-property estimates for use with a transient ground-water flow model of the Death Valley regional ground-water flow system, Nevada and California: U.S. Geological Survey Water-Resources Investigations Report 01–4120, 33 p.

Belcher, W.R., Sweetkind, D.S., and Elliott, P.E., 2002, Probability distributions of hydraulic conductivity for the hydrogeologic units of the Death Valley regional groundwater flow system, Nevada and California: U.S. Geological Survey Water-Resources Investigations Report 02–4212, 24 p.

Bowen, I.S., 1926, The ratio of heat losses by conduction and by evaporation from any water surface: Physical Review, v. 27, p. 779–787.

Cardinalli, J.L., Roach, L.M., Rush, F.E., and Vasey, B.J., 1968, State of Nevada hydrographic areas: Nevada Division of Water Resources map, 1:500,000 scale.

Carpenter, Everett, 1915, Groundwater in southeastern Nevada: U.S. Geological Survey Water-Supply Paper 365, 86 p., 5 plates.

Carroll, Rosemary W.H., Giroux, B., Pohll, G., Hershey, R.L., Russell, C.E., and Howcraft, W., 2003, Numerical simulation of groundwater withdrawal at the Nevada Test Site: Las Vegas, University and Community College System of Nevada, Desert Research Institute Publication 45163, 20 p.

Czarnecki, J.B., 1997, Geohydrology and evapotranspiration at Franklin Lake playa, Inyo County, California, *with a section on* Estimating evapotranspiration using the energy-budget eddy-correlation technique by D.I. Stannard: U.S. Geological Survey Water-Supply Paper 2377, 75 p.

D'Agnese, F.A., Faunt, C.C., and Turner, A.K., 1998, An estimated potentiometric surface of the Death Valley region, Nevada and California, developed using geographic information system and automated interpolation techniques: U.S. Geological Survey Water-Resources Investigations Report 97–4052, 15 p.

D'Agnese, F.A., Faunt, C.C., Turner, A.K., and Hill, M.C., 1997, Hydrogeologic evaluation and numerical simulation of the Death Valley regional ground-water flow system, Nevada and California: U.S. Geological Survey Water-Resources Investigations Report 96–4300, 124 p.

D'Agnese, F.A., O'Brien, G.M., Faunt, C.C., Belcher, W.R., and San Juan, C.A., 2002, A three-dimensional numerical model of predevelopment conditions in the Death Valley regional ground-water flow system, Nevada and California: U.S. Geological Survey Water-Resources Investigations Report 02–4102, 114 p. Accessed September 22, 2004, at *http://pubs.water.usgs.gov/wri024102/.*

DeMeo, G.A., Laczniak, R.J., Boyd, R.A., Smith, J.L., and Nylund, W.E., 2003, Estimated ground-water discharge by evapotranspiration from Death Valley, California, 1997–2001: U.S. Geological Survey Water-Resources Investigations Report 03–4254, 27 p.

Dettinger, M.D., 1989, Distribution of carbonate-rock aquifers in southern Nevada and the potential for their development, summary of findings, 1985–88—Program for the study and testing of carbonate-rock aquifers in eastern and southern Nevada, Summary Report No. 1: State of Nevada, Carson City, 37 p.

Glancy, P.A., 1968, Water-resources appraisal of Mesquite-Ivanpah Valley area, Nevada and California: Nevada Department of Conservation and Natural Resources, Water Resources—Reconnaissance Series Report 46, 57 p.

Hale, G.S., and Westenburg, C.L., 1995, Selected ground-water data for Yucca Mountain region, southern Nevada and eastern California, calendar year 1993: U.S. Geological Survey Open-File Report 95–0158, 67 p.

Harrill, J.R., 1986, Ground-water storage depletion in Pahrump Valley, Nevada-California, 1962–1975: U.S. Geological Survey Water-Supply Paper 2279, 53 p.

Harrill, J.R., Gates, J.S., and Thomas, J.M., 1988, Major ground-water flow systems in the Great Basin region of Nevada, Utah, and adjacent States: U.S. Geological Survey Hydrologic Investigations Atlas HA–694–C, scale 1:1,000,000.

Helsel, D.R., and Hirsch, R.M., 1992, Statistical methods in water resources: Amsterdam, Elsevier, 529 p.

Hevesi, Joseph A., Flint, Alan L., and Flint, Lorraine E., 2002, Preliminary estimates of spatially distributed net infiltration and recharge for the Death Valley region, Nevada-California: U.S. Geological Survey Water-Resources Investigations Report 02–4010, 36 p.

Hevesi, J.A., Flint, A.L., and Flint, L.E., 2003, Simulation of net infiltration and potential recharge using a distributed-parameter watershed model of the Death Valley Region, Nevada and California: U.S. Geological Survey Water-Resources Investigations Report 03–4090, 161 p.

Hunt, C.B., Robinson, T.W., Bowles, W.A., and Washburn, A.L., 1966, Hydrologic basin, Death Valley, California: U.S. Geological Survey Professional Paper 494–B, 138 p.

IT Corporation, 1996a, Underground test area subproject phase I, Data analysis task, volume II—Groundwater recharge and discharge data documentation package: Las Vegas, Nev., Report ITLV/10972–81 prepared for the U.S. Department of Energy, 8 volumes, various pagination.

IT Corporation, 1996b, Underground test area subproject phase I, Data analysis task, volume IV—Hydraulic parameter data documentation package: Las Vegas, Nev., Report ITLV/10972–81 prepared for the U.S. Department of Energy, 8 volumes, various pagination.

LaCamera, R.J., and Locke, G.L., 1997, Selected ground-water data for Yucca Mountain region, southern Nevada and eastern California, through December 1996: U.S. Geological Survey Open-File Report 97–821, 79 p.

LaCamera, R.J., and Westenburg, C.L., 1994, Selected ground-water data for Yucca Mountain region, southern Nevada and eastern California, through December 1992: U.S. Geological Survey Open-File Report 94–54, 161 p.

LaCamera, R.J., Westenburg, C.L., and Locke, G.L, 1996, Selected ground-water data for Yucca Mountain region, southern Nevada and eastern California, through December 1995: U.S. Geological Survey Open-File Report 96–553, 75 p.

Laczniak, R.J., DeMeo, G.A., Reiner, S.R., Smith, J.L., and Nylund, W.E., 1999, Estimates of ground-water discharge as determined from measurements of evapotranspiration, Ash Meadows area, Nye County, Nevada: U.S. Geological Survey Water-Resources Investigations Report 99–4079, 70 p.

Laczniak, R.J., Smith, J. LaRue, Elliott, P.E., DeMeo, G.A., Chatigny, M.A., and Roemer, G.J., 2001, Ground-water discharge determined from estimates of evapotranspiration, Death Valley regional glow system, Nevada and California: U.S. Geological Survey Water-Resources Investigations Report 01–4195, 51 p.

Lichty, R.W., and McKinley, P.W., 1995, Estimates of groundwater recharge rates for two small basins in central Nevada: U.S. Geological Survey Water-Resources Investigations Report 94–4104, 31 p.

Malmberg, G.T., 1965, Available water supply of the Las Vegas ground-water basin, Nevada: U.S. Geological Survey Water-Supply Paper 1780, 116 p.

Malmberg, G.T., 1967, Hydrology of the valley-fill and carbonate-rock reservoirs, Pahrump Valley, Nevada-California: U.S. Geological Survey Water-Supply Paper 1832, 47 p.

Malmberg, G.T., and Eakin, T.E., 1962, Ground-water appraisal of Sarcobatus Flat and Oasis Valley, Nye and Esmeralda Counties, Nevada: Nevada Department of Conservation and Natural Resources, Ground-Water Resources—Reconnaissance Series Report 10, 39 p.

Maxey, G.B., and Eakin, T.E., 1950, Ground water in White River Valley, White Pine, Nye, and Lincoln Counties, Nevada: Nevada State Engineer Water Resources Bulletin No. 8, 59 p.

Maxey, G.B., and Jameson, C.H., 1948, Geology and water resources of Las Vegas, Pahrump, and Indian Springs Valleys, Clark and Nye Counties, Nevada: Nevada State Engineer Water Resources Bulletin no. 5, 43 p.

Mendenhall, W.C., 1909, Some desert watering places in southeastern California and southern Nevada: U.S. Geological Survey Water-Supply Paper 224, 98 p.

Miller, G.A., 1977, Appraisal of the water resources of Death Valley, California-Nevada: U.S. Geological Survey Open-File Report 77–728, 68 p.

Moreo, M.T., Halford, K. J., La Camera, R.J., and Laczniak, R.J., 2003, Estimated ground-water withdrawals from the Death Valley regional flow system, Nevada and California, 1913–98: U.S. Geological Survey Water-Resources Investigations Report 03–4245, 28 p.

Neuman, S.P., 1982, Statistical characterization of aquifer heterogeneities—An overview, *in* Narasimhan, T.N., ed., Recent trends in hydrogeology: Boulder, Colo., Geological Society of America Special Paper 189, p. 81–102.

Pistrang, M.A., and Kunkel, F., 1964, A brief geologic and hydrologic reconnaissance of the Furnace Creek Wash area, Death Valley National Monument, California: U.S. Geological Survey Water-Supply Paper 1779–Y, 35 p.

Reiner, S.R., Laczniak, R.J., DeMeo, G.A., Smith, J.L., Elliott, P.E., Nylund, W.E., and Fridrich, C.J., 2002, Ground-water discharge determined from measurements of evapotranspiration, other available hydrologic components, and shallow water-level changes, Oasis Valley, Nye County, Nevada: U.S. Geological Survey Water-Resources Investigations Report 01–4239, 65 p.

Rice, W.A., 1984, Preliminary two-dimensional regional hydrologic model of the Nevada Test Site and vicinity: Albuquerque, N. Mex., Sandia National Laboratories Report SAND83–7466, 89 p.

Rush, F.E., 1968, Water-resources appraisal of Clayton Valley–Stonewall Flat area, Nevada and California: Nevada Department of Conservation and Natural Resources, Water Resources–Reconnaissance Series Report 45, 54 p.

Rush, F.E., 1970, Regional ground-water systems in the Nevada Test Site area, Nye, Lincoln, and Clark Counties, Nevada: Carson City, Nevada Department of Conservation and Natural Resources, Ground-Water Resources—Reconnaissance Series Report 54, 25 p.

Russell, C.E., and Minor, T., 2002, Reconnaissance estimates of recharge based on an elevation-dependent chloride mass balance approach: Las Vegas, University and Community College System of Nevada, Desert Research Institute Publication 45164, 57 p.

Stonestrom, D.A., Prudic, D.E., Laczniak, R.L., Akstin, K.C., Boyd, R.A., and Henkelman, K.K., 2003, Estimates of deep percolation beneath native vegetation, irrigated fields, and the Amargosa River channel, Amargosa Desert, Nye County, Nevada: U.S. Geological Survey Open-File Report 03–104, 83 p.

U.S. Department of Agriculture, 1994, State Soil Geographic (STATSGO) Data Base—Data use information: U.S. Department of Agriculture Miscellaneous Publication no. 1492.

Van Denburgh, A.S., and Rush, F.E., 1974, Water-resources appraisal of Railroad and Penoyer Valleys, east-central Nevada: Nevada Department of Conservation and Natural Resources, Water Resources—Reconnaissance Series Report 60, 61 p.

Waddell, R.K., 1982, Two-dimensional, steady-state model of ground-water flow, Nevada Test Site and vicinity, Nevada-California: U.S. Geological Survey Water-Resources Investigations Report 82–4085, 72 p.

Walker, G.E., and Eakin, T.E., 1963, Geology and ground water of Amargosa Desert, Nevada-California: Nevada Department of Conservation and Natural Resources, Ground-Water Resources—Reconnaissance Series Report 14, 45 p.

Waring, G.A., 1915, Springs of California: U.S. Geological Survey Water-Supply Paper 338, 410 p.

Waring, G.A., revised by Blankenship, R.R., and Bentall, Ray, 1965, Thermal springs of the United States and other countries of the world—A summary: U.S. Geological Survey Professional Paper 492, 383 p.

West, N.E., 1988, Intermountain deserts, shrub steppes, woodlands, *in* Barbour, M.G., and Billings, W.D., eds., North American terrestrial vegetation: Cambridge, Cambridge University Press, 434 p.

Westenburg, C.L., and LaCamera, R.J., 1996, Selected groundwater data for Yucca Mountain region, southern Nevada and eastern California, through December 1994: U.S. Geological Survey Open-File Report 96–205, 73 p.

Winograd, I.J., and Thordarson, William, 1975, Hydrologic and hydrochemical framework, south-central Great Basin, Nevada-California, with special reference to the Nevada Test Site: U.S. Geological Survey Professional Paper 712C, p. C1–C126.

Hydrology

By Claudia C. Faunt, Frank A. D'Agnese, and Grady M. O'Brien

Chapter D of

Death Valley Regional Ground-Water Flow System, Nevada and California—Hydrogeologic Framework and Transient Ground-Water Flow Model

Edited by Wayne R. Belcher

Prepared in cooperation with the
U.S. Department of Energy
Office of Environmental Management, National Nuclear Security Administration, Nevada Site Office,
under Interagency Agreement DE–AI52–01NV13944, and
Office of Repository Development,
under Interagency Agreement DE–AI08–02RW12167

Scientific Investigations Report 2004–5205

U.S. Department of the Interior
U.S. Geological Survey

Contents

Figures

Table

CHAPTER D. Hydrology

By Claudia C. Faunt, Frank A. D'Agnese, and Grady O'Brien

Introduction

The hydrology of the Death Valley regional ground-water flow system (DVRFS), as in all flow systems, is influenced by geology and climate and varies with time. In general, ground water moves through permeable zones under the influence of hydraulic gradients from areas of recharge to areas of discharge in the regional system (fig. D–1). The topography produces numerous local subsystems within the major flow system (Freeze and Cherry, 1979, p. 196). Water that enters the flow system in a recharge area may be discharged in the nearest topographic low, or it may be transmitted to a regional discharge area.

Ground-water flow in the DVRFS region is dominated by interbasin flow with several relatively shallow and local on flow systems that are superimposed on deeper intermediate and regional flow systems (fig. D–1). The regional ground-water flow patterns do not coincide with local topographic basins. Regional ground-water flow generally follows the regional topographic gradient as water moves toward the lowest point in the region at Death Valley, Calif. (fig. D–2). Bedinger and Harrill (plate 1 and Appendix 1, this volume) developed regional potentiometric-surface contours of the areas contributing ground-water flow to the DVRFS model domain to define the regional ground-water flow across the lateral boundary of the model. For conceptualization of the ground-water flow system and for the construction of a numerical flow model (D'Agnese and others, 1997), D'Agnese and others (1998) developed an approximation of the regional potentiometric surface. This surface depicted mounds, troughs, and depressions indicating areas of recharge and discharge that may be characteristic of a relatively shallow and local flow system (fig. D–2). Differences between the potentiometric surfaces of the deep regional system (plate 1 and Appendix 1, this volume) and those in the shallower local systems depicted on D'Agnese and others (1998) are emphasized by areas of generally downward flow (recharge areas) to, and generally upward flow (discharge areas) from, the regional system (fig. D–2).

Hydrochemistry

The chemically and thermally dynamic nature of ground water can be used to help define flow systems and evaluate the relative importance of ground-water sources and pathways using chemical, isotope, temperature, and hydraulic data for ground water. For example, leakage from the carbonate-rock aquifer into overlying aquifers can be distinguished by differences in water quality along with differences in water temperature and hydraulic potential. Discharge temperatures for many modern springs commonly are higher than mean annual air temperature, indicating that the water has thermally equilibrated along deep flow paths. Cooler temperatures or lower altitude recharge are usually associated with shallower and shorter ground-water flow paths. Chemical and thermal heterogeneities are common in the DVRFS region due to fracture flow through contrasting lithologies, and these data were used, where possible, to help delineate the flow system.

Ground water of the DVRFS region may be divided into hydrochemical categories that reflect equilibration with (1) tuffaceous rocks or tuffaceous basin-fill sediments (a sodium and potassium bicarbonate type); (2) primarily carbonate rocks or carbonate basin-fill sediments (a calcium and magnesium bicarbonate type); and (3) both kinds of rocks or sediments, or a mixing of different types of water (Schoff and Moore, 1964; Winograd and Thordarson, 1975). These categories define hydrochemical signatures for the water that can be used to identify sources and flow paths. In some areas water can reflect equilibration with playa deposits. Isotopic information from water or discharge deposits can provide substantial information on the hydrochemical signature of ground water. For example, higher levels of strontium appear to be fairly common in water samples from the regional carbonate-rock aquifer (the associated carbonate rocks are relatively low in strontium), which indicates that more flow occurs through the fractured basement rocks (clastic and intrusive rocks, which are relatively high in strontium) than had been thought previously (Peterman and Stuckless, 1992a, b).

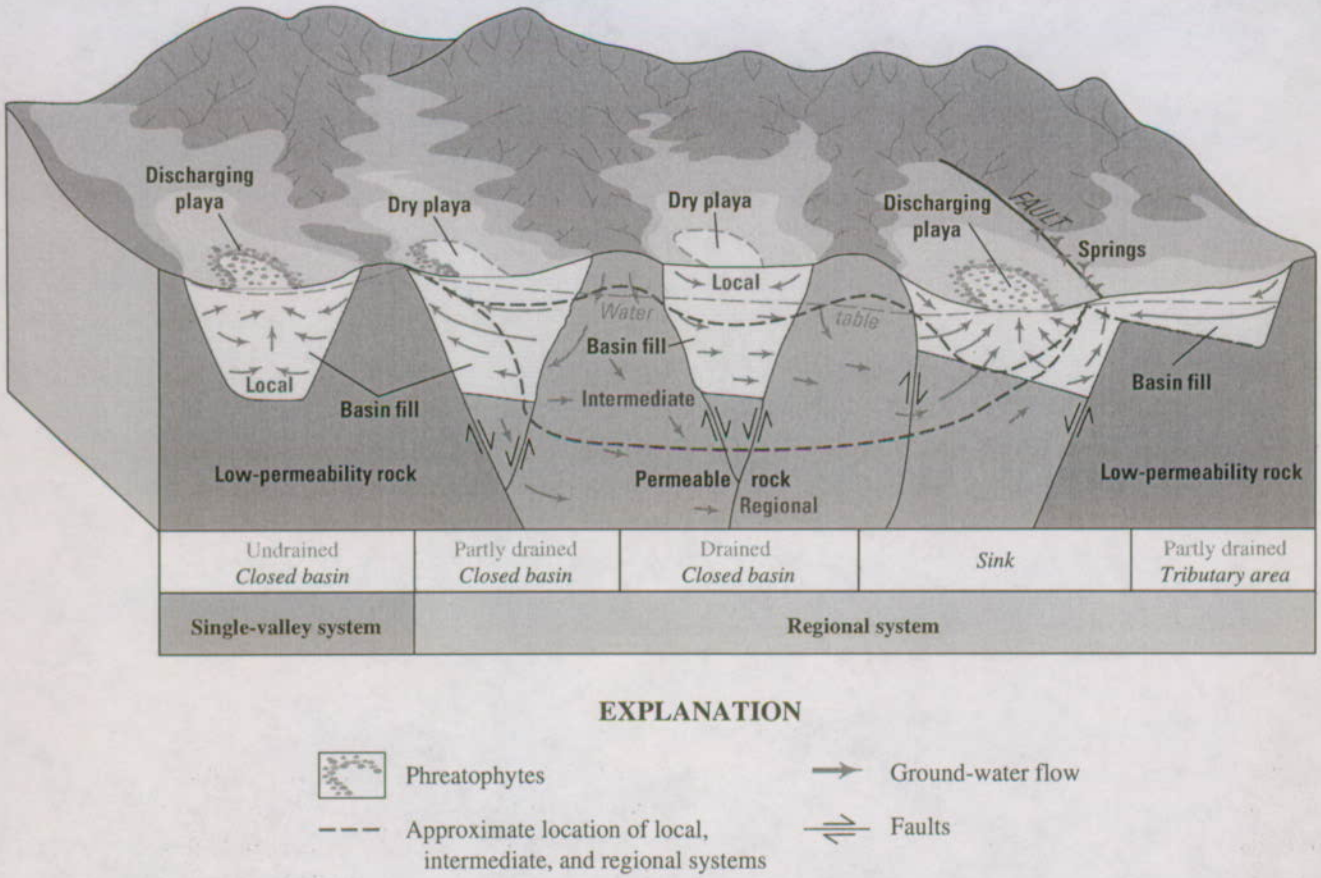

Figure D–1. Schematic block diagram of Death Valley and other basins illustrating the structural relations between mountain blocks, valleys, and ground-water flow (modified from Eakin and others, 1976).

Ground-Water Hydrology

Within the DVRFS region, ground-water flow is strongly influenced by the physical framework of the system, which is characterized by aquifers, confining units, and flow barriers. In order to simulate the regional flow system, the boundaries of the system must be identified and defined for the model.

Source and Movement of Ground Water

Current sources of ground-water flow in the DVRFS region are (1) recharge from precipitation in the mountains (usually winter storms) within the model domain, and (2) lateral flow into the model boundary, predominantly through the carbonate-rock aquifer. Most ground-water recharge results from infiltration of precipitation and runoff on the mountain ranges (Bedinger and others, 1989) (fig. D–3). Water may infiltrate from melting snowpack in the mountains primarily on volcanic or carbonate rocks or adjacent to the mountains from streams flowing over alluvium (fans and channels) (Harrill and Prudic, 1998). Lateral ground-water flow across the model boundary is governed in part by regional hydraulic gradients in the DVRFS region.

Current ground-water discharge in the DVRFS region is from (1) seeps and spring flow from the regional carbonate-rock aquifer and local systems; (2) evapotranspiration (ET); (3) pumpage for irrigation, mining, public supply, commercial, and domestic uses; and (4) subsurface flow out of the model boundary (fig. D–3 and plate 1). Most ground-water discharge today originates as spring or seep flow caused by variations in permeability created by geologic structures and varying lithologies (Winograd and Thordarson, 1975; Chapter B, this volume; fig. D–1). In particular, many of the regional (larger volume and higher temperature) springs occur along major faults (figs. D–1 and D–3). Most spring discharge is ultimately consumed by ET. Major discharge areas primarily occur in the lower part of intermontane valleys where the potentiometric surface is near or above land surface. Discharge also occurs as pumping for irrigation, mining, public supply, commercial, and domestic uses (Bedinger and others, 1989; Moreo and others, 2003; Chapter C, this volume) (fig. D–3). Lateral flow into the model domain, predominantly through the carbonate-rock aquifer, is small compared to the internal discharge (fig. D–3; Appendix 2, this volume).

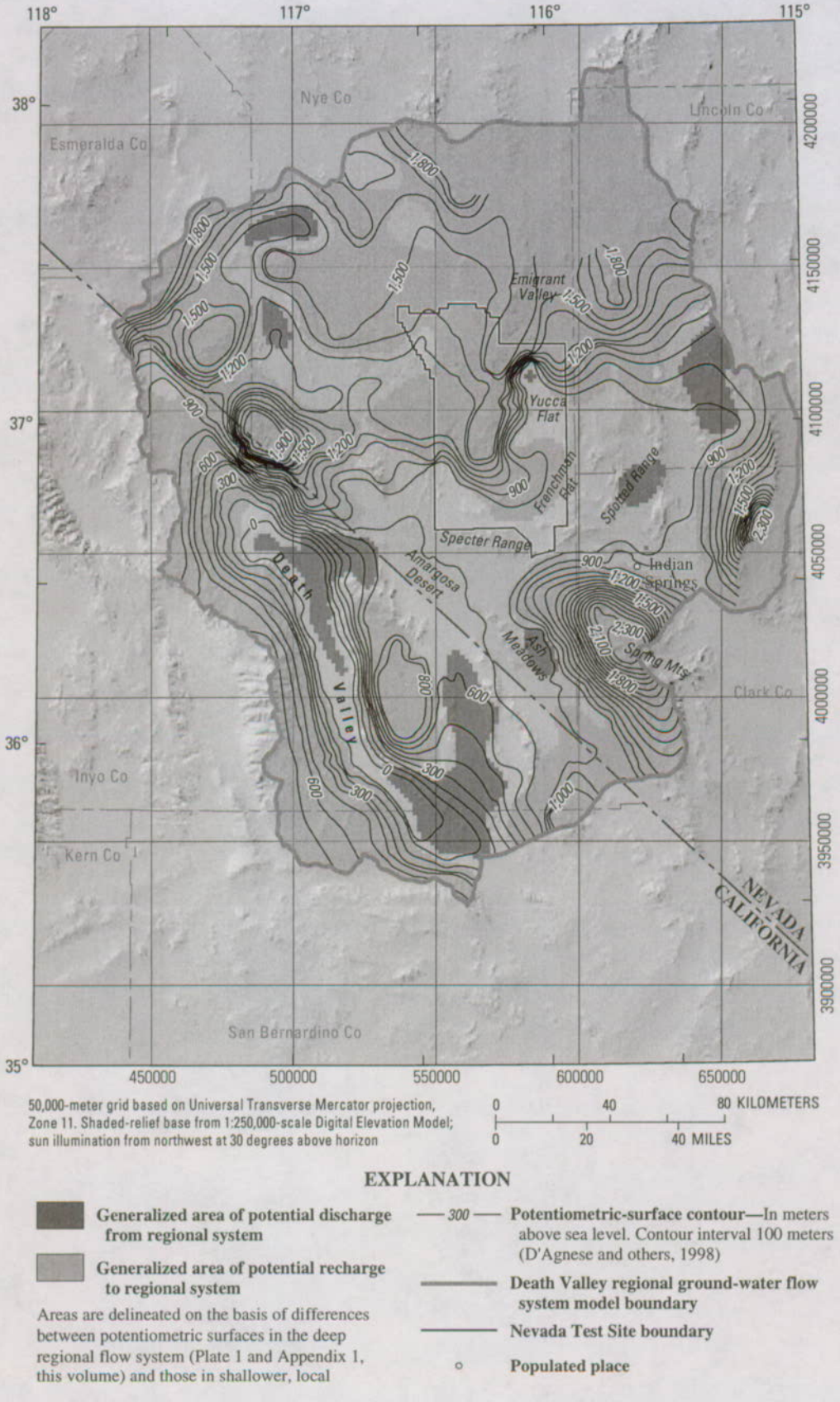

Figure D–2. Generalized areas of potential recharge and discharge based on potentiometric surfaces for the Death Valley regional ground-water flow system model.

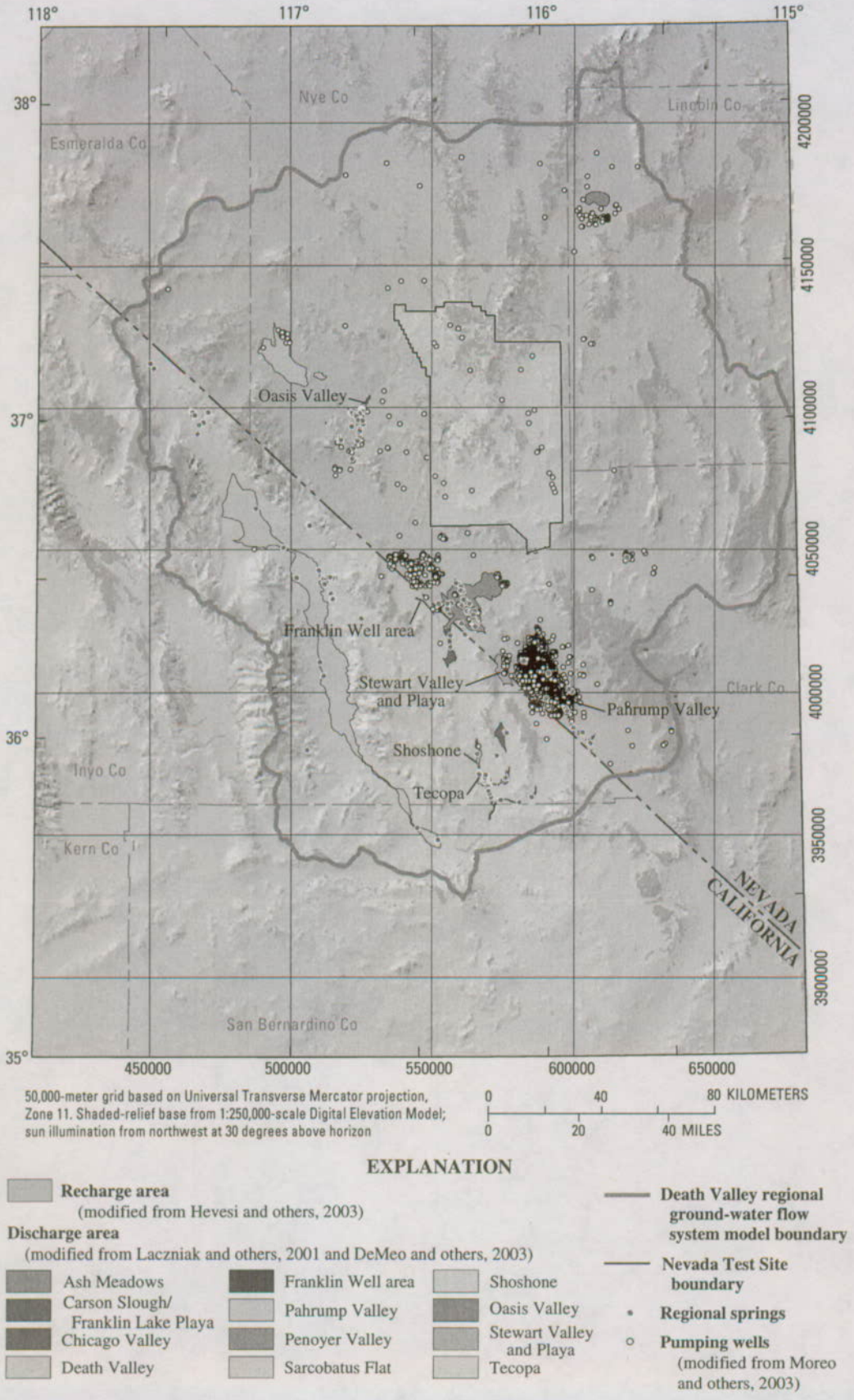

Figure D–3. Generalized areas of recharge and discharge, and location of regional springs and pumping wells in the Death Valley regional ground-water flow system region.

Regional Aquifers, Flow Barriers, and Confining Units

Hydraulic compartmentalization may occur throughout the DVRFS region owing to the complex hydrogeologic framework. Ground water flows through a diverse assemblage of rocks and sediments in the region, and geologic structures exert significant control on ground-water movement as well (Chapter B, this volume).

Hydrogeologic units (HGUs) that are important to the hydrology of the DVRFS region include Cenozoic basin-fill units, Cenozoic volcanic-rock units of the southwestern Nevada volcanic field, the carbonate-rock aquifer, and confining units present at the water table (fig. D–4). Three types of aquifers exist in the region: basin-fill, volcanic-rock, and carbonate-rock aquifers (Chapter B, this volume). Some ground-water basins are part of multibasin flow systems connected by surface-water streams or by flow through the basin-fill sediments or permeable bedrock, and others are topographically and hydraulically isolated by low-permeability bedrock (figs. D–1 and D–4).

Juxtaposition of thick, low-permeability clastic-rock strata and rocks forming aquifers by folding or faulting commonly forms barriers to ground-water flow (Chapter B, this volume). Although the clastic rocks are subjected to the same deformational history as the carbonate rocks, the clastic rocks are generally relatively impermeable because of their low susceptibility to solution and their lack of significant secondary permeability. Most of the clastic rocks, when deformed, will break into fragments that reconsolidate into impermeable rock (quartzites) or will yield ductilely (shale) and, in either case, will not result in significant openings through which water can flow. In general, crystalline rocks have low permeability; however, where fractured, crystalline rocks may have significant permeability (Winograd and Thordarson, 1975).

In the DVRFS region, the relative permeability of faulted rock may vary either directly as the result of the fault orientation with respect to the present-day stress field or indirectly as zones of fracturing adjacent to the fault. The present-day stress field in the DVRFS region tends to enhance flow along northeast-southwest-trending features while decreasing the permeability along features oriented northwest-southeast (Carr, 1984; Faunt, 1997). Despite their orientation to the stress field, faults with low-permeability gouge may be barriers to ground-water flow (Winograd and Thordarson, 1968).

Flow-System Model Boundaries

The DVRFS model domain is contained within the DVRFS and can be defined by a series of boundaries. For modeling purposes, a ground-water flow system is a set of three-dimensional (3D) pathways through the subsurface rocks and sediments by which ground water moves from recharge areas to discharge areas. Below the water table, the saturated volume of rock is bounded on all sides by a boundary surface (Franke and others, 1987). For the flow-system model, this boundary surface is represented by the upper, lower, and lateral extents of the model.

The upper boundary of the DVRFS model is the water table. Under natural (prepumping) conditions, water moves across this boundary as recharge or as discharge. When stressed (from climate change or pumping), the upper boundary may fluctuate with changes in recharge and discharge.

The lower boundary of the DVRFS model is the depth at which ground-water flow is dominantly horizontal or parallel to the boundary. Near the lower boundary, permeabilities are so low that flow near this boundary does not substantially affect regional flow. The depth of this boundary can vary and generally corresponds to the upper surface of low-permeability basement rocks.

The lateral boundary of the DVRFS model is a combination of no-flow boundaries resulting from physical barriers or hydraulic separation of flow regimes (ground-water divides and[or]) regional flow lines) and arbitrary lateral-flow (throughflow) boundaries where water is allowed to flow across the model boundary. When the system is at steady state, no-flow conditions exist where ground-water movement across the boundary is impeded by physical barriers, which results in flow paths parallel to the boundary, or where ground-water flow paths diverge, which results from ground-water divides. Under transient-state conditions, the location of flow paths and ground-water divides may shift if hydraulic-head changes occur. An estimated regional potentiometric-surface map was developed for the DVRFS region to delineate areas outside the model domain that contribute inflow to or receive outflow from the DVRFS across the model boundary (Appendixes 1 and 2, this volume; plate 1).

Flow-System Subregions

Ground-water flow in the DVRFS model domain is described simply in terms of the northern, central, and southern Death Valley subregions (fig. D–5) of D'Agnese and others (1997, p. 62–67). The subregions are further subdivided into ground-water sections, with the sections in the central Death Valley region grouped into ground-water basins (table D–1). These subregions, basins, and sections are used for descriptive purposes only, and the boundaries do not define independent flow systems. The subregions, basins, and sections are delineated primarily on (1) location of recharge areas; (2) regional hydraulic gradients; (3) distribution of aquifers, structures, and confining units that affect flow; (4) location of major discharge areas; and (5) hydrochemical composition of the ground water. Flow directions across the model boundary, as indicated in figure D–5, are based on the lateral flow estimates provided in Appendix 2.

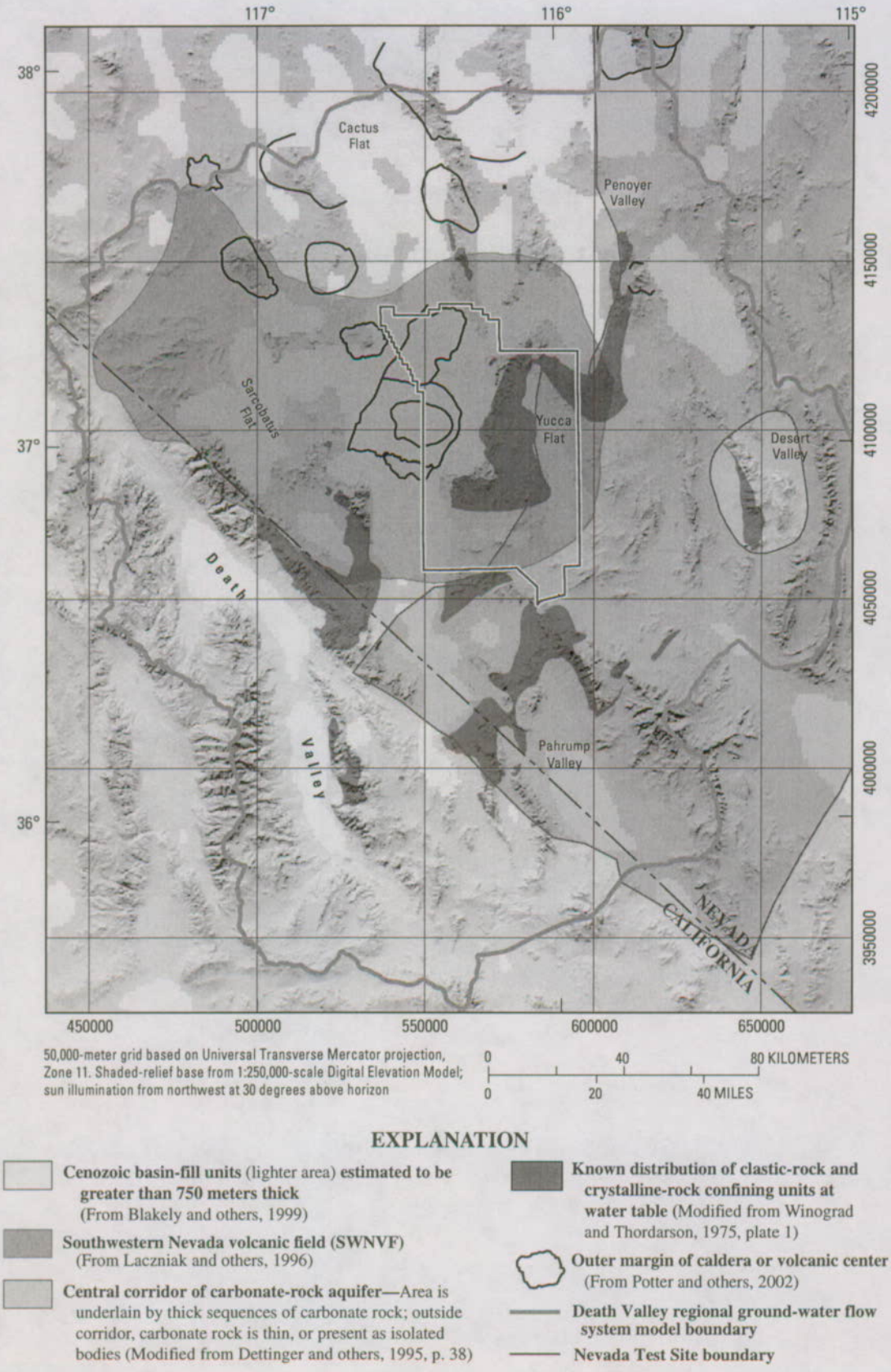

Figure D–4. Generalized distribution of deep Cenozoic basins, southwestern Nevada volcanic field, regional carbonate-rock aquifer, and confining units at the water table for the Death Valley regional ground-water flow system region.

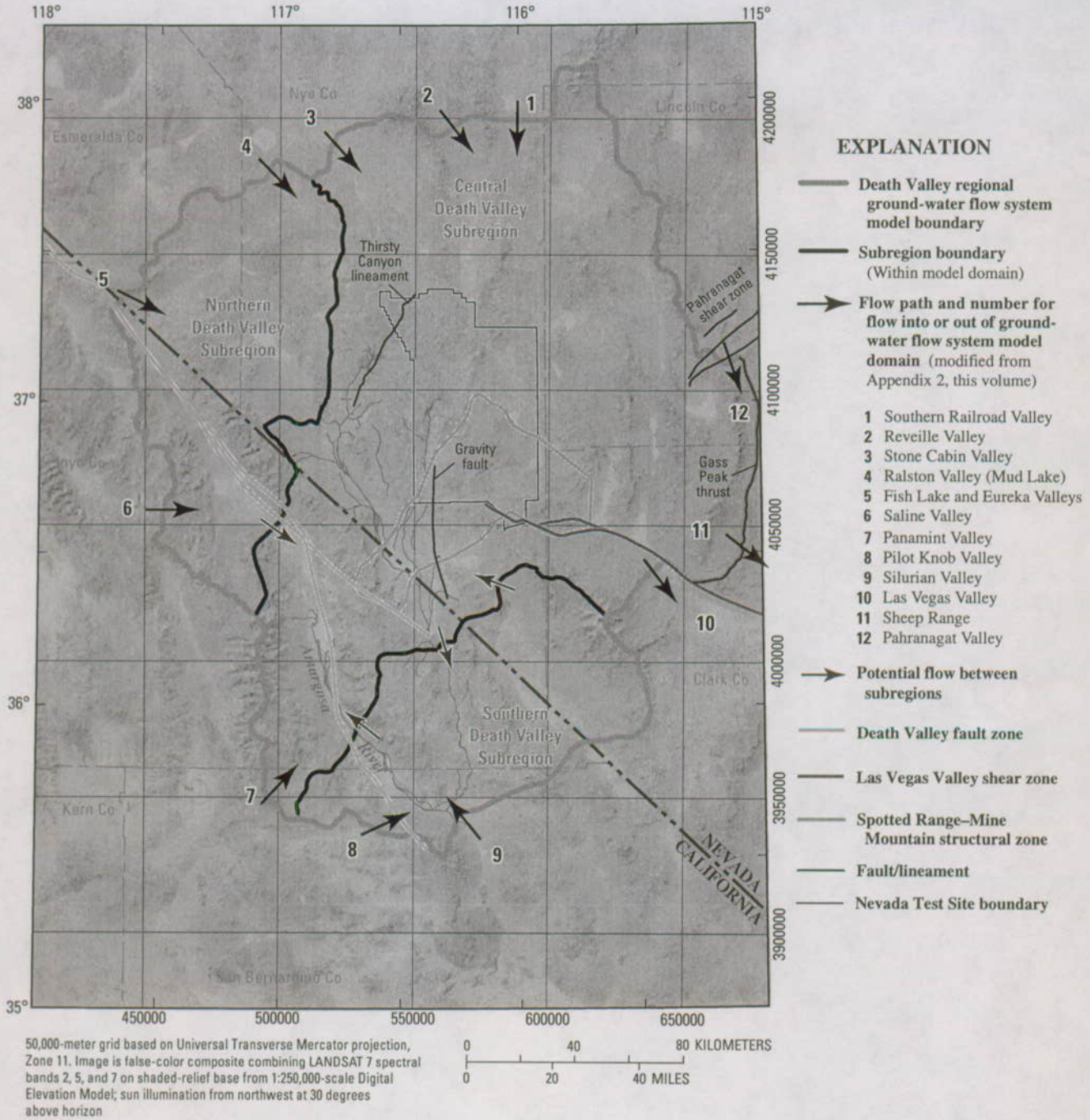

Figure D–5. Subregions and associated flow paths of the Death Valley regional ground-water flow system region.

Northern Death Valley Subregion

Ground water in the northern Death Valley subregion is derived from precipitation on the Montezuma and Panamint Ranges, Slate Ridge, and the Palmetto, Gold, and Stonewall Mountains (fig. D–6). Ground water also may be entering the subregion across the DVRFS model boundary from Eureka Valley and the southern part of Saline Valley and possibly across the northern part of the Panamint Range (Appendix 2, this volume). Much of the ground-water flow is controlled by northeast-southwest-trending structural zones (Carr, 1984; Chapter B, this volume). Deep regional flow is unlikely because the relatively low-permeability, shallow, intrusive-rock confining unit (ICU), the lower elastic-rock confining unit (LCCU), and the crystalline-rock confining unit (XCU) underlie most of the subregion. Extensive outcrops of the lower carbonate-rock aquifer (LCA) occur in the Grapevine and Cottonwood Mountains in the southern part of the subregion. The LCA has been interpreted to exist in the subsurface

Table D–1. Divisions of the Death Valley regional ground-water flow system.

Northern Death Valley Subregion
Lida-Stonewall section
Sarcobatus Flat section
Grapevine Canyon–Mesquite Flat section
Oriental Wash section
Central Death Valley Subregion
Pahute Mesa–Oasis Valley ground-water basin
Southern Railroad Valley section
Kawich Valley section
Oasis Valley section
Ash Meadows ground-water basin
Pahranagat section
Tikaboo Valley section
Indian Springs section
Emigrant Valley section
Yucca–Frenchman Flat section
Specter Range section
Alkali Flat–Furnace Creek ground-water basin
Fortymile Canyon section
Amargosa River section
Crater Flat section
Funeral Mountains section
Southern Death Valley Subregion
Pahrump Valley section
Shoshone–Tecopa section
California Valley section
Ibex Hills section

in the southern part of the subregion (Grose, 1983; Sweetkind and others, 2001), including the southern part of Sarcobatus Flat and in the vicinity of Grapevine Springs in the northern part of Death Valley. Pumpage in the northern Death Valley subregion has been negligible, and the change in the volume of ground-water storage relative to the total amount in storage is negligible (Moreo and others, 2003). The subregion can be divided into four sections: Lida-Stonewall, Sarcobatus Flat, Grapevine Canyon–Mesquite Flat, and Oriental Wash.

The Lida-Stonewall section (section A, fig. D–6) potentially receives recharge by throughflow from Ralston Valley and precipitation on areas along the northern boundary of the subregion. The dominant regional flow path is to the south. Field observation and analysis of satellite imagery reveal that the playas at Stonewall Flat and near Lida Junction have very little phreatophytic vegetation, indicating that the small amounts of ET in these areas are probably from local surface water that infiltrates intermittently. Discharge from the section occurs as throughflow to Sarcobatus Flat and Death Valley.

Ground water in the Sarcobatus Flat section (section B, fig. D–6) may originate on the western part of Pahute Mesa (D'Agnese and others, 1997) and flows southwest as throughflow from the central Death Valley subregion by way of Cactus and Gold Flats. Throughflow from the Lida-Stonewall section also may contribute flow to the section. Precipitation on the Grapevine Mountains may contribute recharge in the western part of Sarcobatus Flat, but is not sufficient to maintain the discharge at Sarcobatus Flat. Other potential sources of recharge for this area are Pahute Mesa and the Kawich Range to the east. Ground water may flow to the southeast along or parallel to buried structures (Grauch and others, 1999) discharging by ET at areas on or adjacent to the playas of Coyote Hole or Sarcobatus Flat. Recent studies indicate that discharge at Sarcobatus Flat is much greater than previously thought (Laczniak and others, 2001). As a result, throughflow from Ralston Valley and from the central Death Valley subregion may be much greater than described by D'Agnese and others (1997). In addition, uncertainty exists about the potential for ground-water flow through the Bullfrog Hills to Amargosa Desert.

Ground water in the Grapevine Canyon–Mesquite Flat section (section C, fig. D–6) originates as throughflow from the northeast past Sarcobatus Flat (D'Agnese and others, 1997). Additional ground water may enter the flow system from Saline Valley. A small amount of recharge may result from precipitation on the Grapevine Mountains. The Grapevine Canyon–Mesquite Flat section contains a major discharge area that includes Grapevine and Stainginger Springs. These high-discharge springs are aligned with northeast-oriented regional structural features (Carr, 1984) and their waters have chemical characteristics indicative of an origin from rocks in the eastern part of the DVRFS region (Steinkampf and Werrell, 2001). In addition, numerous seeps and low-discharge springs in and along the flanks of the Grapevine Mountains reflect structural controls of flow on local recharge and the chemistries of these sources (Steinkampf and Werrell, 2001). Ground water that does not discharge at these springs and seeps continues past this discharge area to flow through Death Valley to discharge at Mesquite Flat or farther down the valley. Potential inflow from Saline Valley may discharge at Mesquite Flat or continue through Death Valley.

Some ground water in the Oriental Wash section (section D, fig. D–6) is from locally derived recharge on the predominantly granitic mountains to the north. In addition, ground water may enter the system as throughflow from Eureka and Saline Valleys. Ground-water flow is apparently directed toward a small-volume and low-temperature spring area at Sand Spring in the northern part of Death Valley along the axis of Oriental Wash. This spring area appears to be associated with a northeast-southwest-trending structural zone (Carr, 1984), and the discharge occurs along the northern terminus of the Death Valley fault zone. Some ground water moving along this flow path may bypass Sand Spring and flow through Death Valley toward Mesquite Flat.

Central Death Valley Subregion

In the central Death Valley subregion, the dominant flow paths have been interpreted to be associated with major regional or intermediate discharge areas and have been grouped into three ground-water basins based on the major discharge areas (fig. D–7): Pahute Mesa–Oasis Valley basin, Ash Meadows basin, and Alkali Flat–Furnace Creek basin (Waddell, 1982; D'Agnese and others, 1997, 2002).

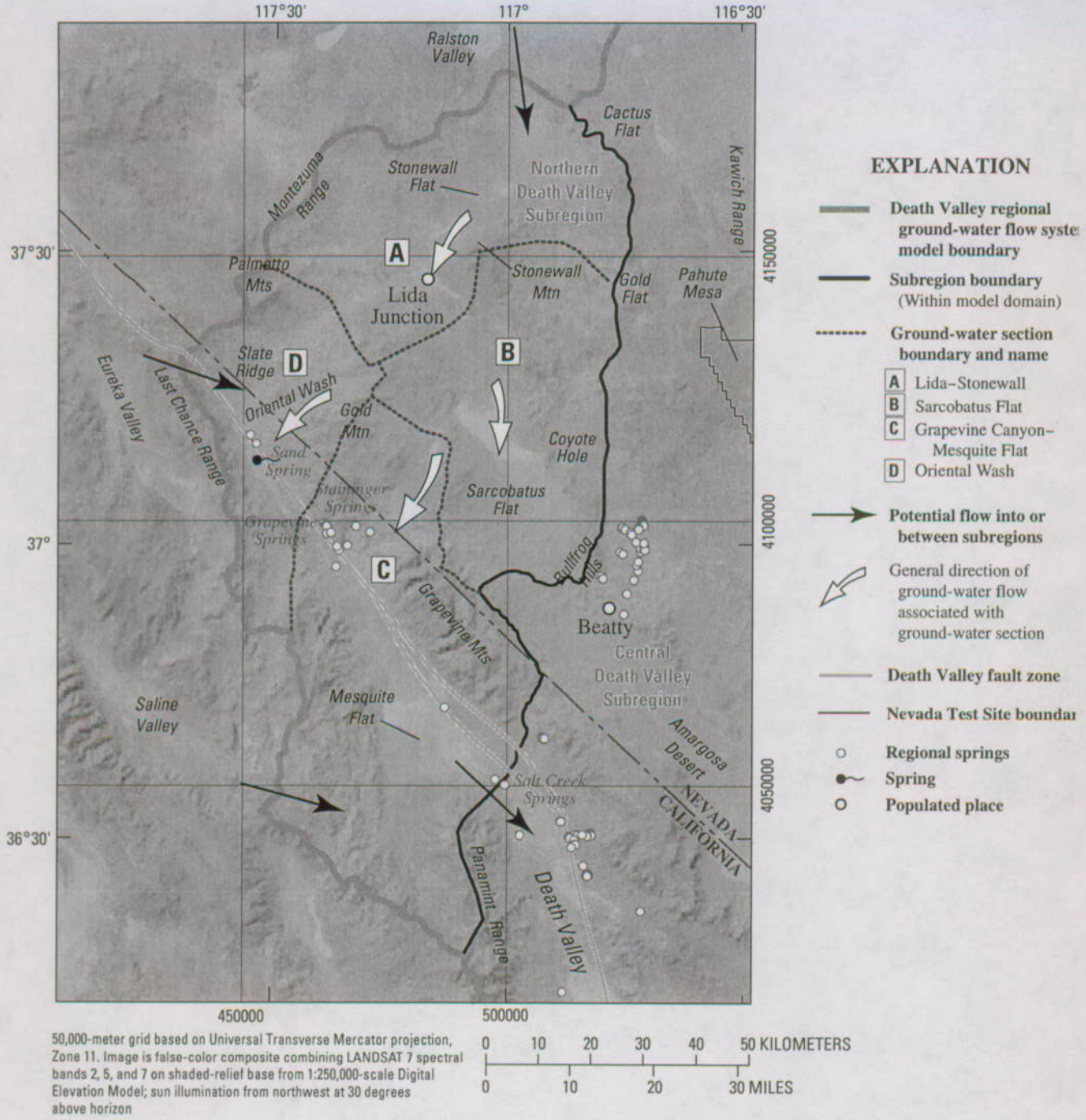

Figure D–6. Northern Death Valley subregion of the Death Valley regional ground-water flow system showing ground-water sections and flow directions.

Pahute Mesa–Oasis Valley Basin

The Pahute Mesa–Oasis Valley ground-water basin is the smallest and northernmost of the three basins and its extent is not well defined (fig. D–7). Ground water is derived primarily from recharge in Pahute Mesa and the Kawich, Cactus, and Belted Ranges (D'Agnese and others, 1997). Additional recharge from within the basin may occur at Black and Quartz Mountains. Throughflow into the Pahute Mesa–Oasis Valley basin may occur from the southern part of Railroad, Reveille, and Stone Cabin Valleys (Appendix 2, this volume).

At Oasis Valley, ground water is diverted upward by the confining units along faults to discharge by ET and spring flow at and along the flood plain of the Amargosa River and tributary drainages (fig. D–5) (White, 1979; Laczniak and others, 1996). Mass-balance calculations indicate that about one-half the water that flows to Oasis Valley discharges through ET

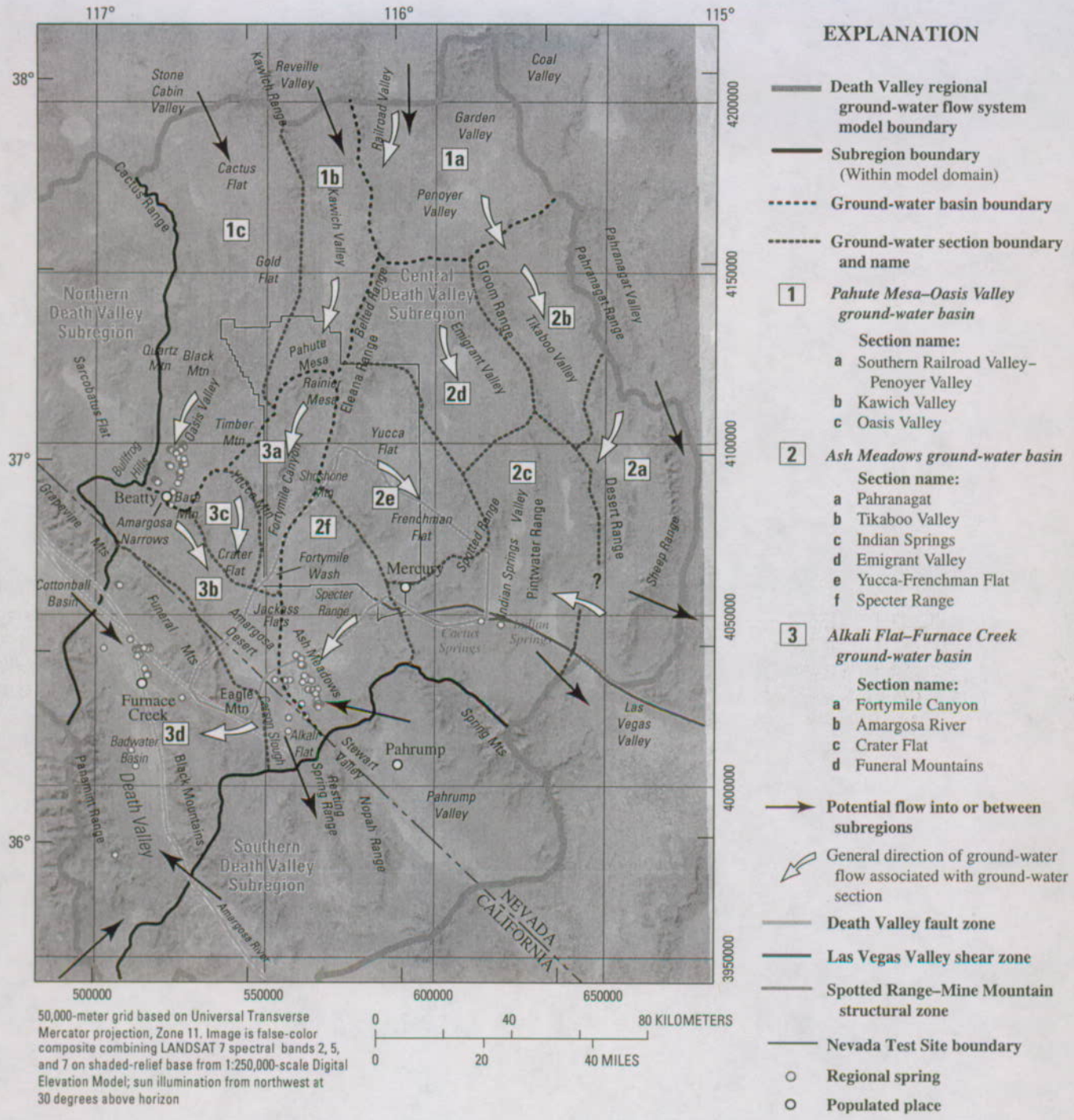

Figure D–7. Central Death Valley subregion of the Death Valley regional ground-water flow system showing ground-water basins, sections, and flow directions.

(White, 1979). Ground water that does not discharge within Oasis Valley flows through a veneer of alluvium or the low-permeability basement rocks at Amargosa Narrows south of Beatty, Nev. (fig. D–7), and into the Alkali Flat–Furnace Creek basin (Waddell, 1982; Laczniak and others, 1996).

Some ground water may not reach Oasis Valley and may flow around the northern part of Bare Mountain toward Crater Flat (fig. D–7). Likewise, some ground water in the northwestern part of the section (parts of Cactus and Gold Flats) may flow toward the eastern part of Sarcobatus Flat. Based on general flow patterns, the Pahute Mesa–Oasis Valley basin may be divided into three sections: southern Railroad Valley–Penoyer Valley, Kawich Valley, and Oasis Valley.

Ground water in the southern Railroad Valley–Penoyer Valley section originates either as recharge on the flanking mountains or as throughflow from the north (fig. D–7)

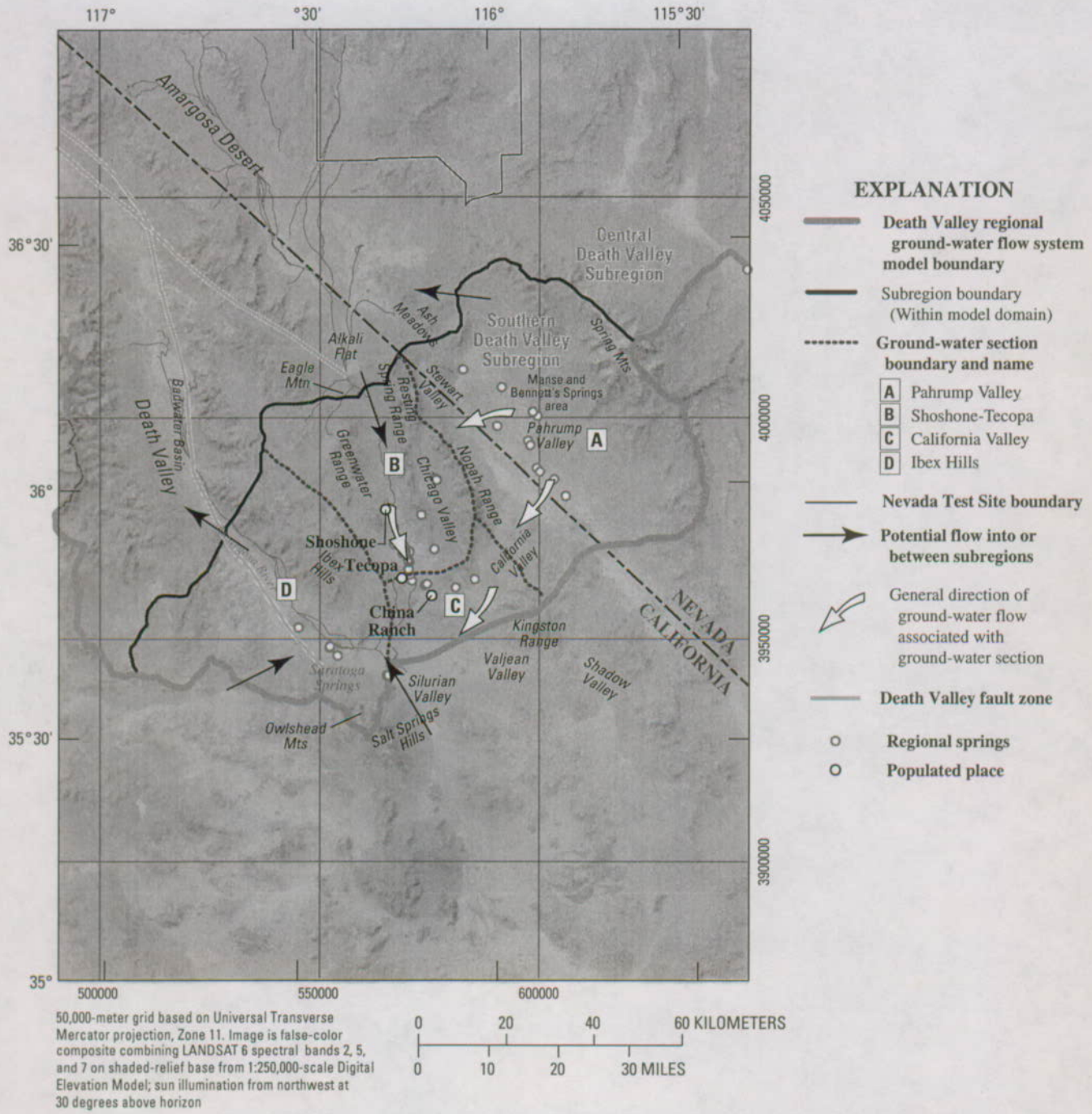

Figure D–8. Southern Death Valley subregion of the Death Valley regional ground-water flow system showing ground-water sections and flow directions.

(D'Agnese and others, 1997; Appendix 2, this volume). Ground water in the section flows dominantly south and southwest toward Kawich Valley and southeast toward Penoyer and Emigrant Valleys. The section has little internal discharge and most, if not all, of the water leaves the system as throughflow. Penoyer Valley traditionally has been characterized as part of the Colorado River ground-water flow system. Some studies indicate that it is possible that the valley is connected to the DVRFS (IT Corporation, 1996). A small discharge area occurs at the playa in the southern part of Penoyer Valley. Water that is not discharged there may continue to flow south into Emigrant and Tikaboo Valleys.

Ground water in the Kawich Valley section originates mainly as throughflow from the southern Railroad Valley section and as recharge on the Kawich Range and Pahute and Rainier Mesas (fig. D–7). On Pahute and Rainier Mesas, water percolates down and commonly encounters low-permeability volcanic rocks, forming perched and semiperched

water that can be elevated several hundred meters above the regional water table. From the recharge areas, ground water in the Kawich Valley section flows toward a trough in the potentiometric surface beneath the western part of Pahute Mesa (figs. D–2 and D–7) (Waddell and others, 1984). The Thirsty Canyon lineament (fig. D–5) may act as a limited-flow barrier, created by caldera-boundary faults juxtaposing low-permeability rocks on the west and more permeable rocks to the east, diverting westward-moving water to the south (Blankennagel and Weir, 1973, p. 24). The hydraulic gradient across the barrier indicates some eastward flow. The barrier concept is supported by distinct differences in the major anion chemistry of ground-water samples collected on either side of the feature (Laczniak and others, 1996). This section has little internal discharge. Ground water leaving the southern margins of Pahute Mesa flows southwestward in Oasis Valley toward the Amargosa River and south through Fortymile Canyon, ultimately discharging at Oasis Valley, Alkali Flat, and(or) Death Valley.

The Oasis Valley section contains the major discharge area for the basin. The section receives subsurface inflow from the Kawich Valley section, by way of Pahute Mesa, and Gold Flat to the north is the largest source of ground water to the Oasis Valley section (fig. D–7) (Laczniak and others, 1996; White, 1979). The location and nature of the boundary separating the Oasis Valley section from the Alkali Flat–Furnace Creek basin is not well understood, and it is uncertain how much of the water discharging at Oasis Valley actually passes through rocks beneath Pahute Mesa (Laczniak and others, 1996).

Water is withdrawn for irrigation, domestic, and public supply in upper Oasis Valley. Pumping occurred periodically since the 1950's on the Pahute Mesa–Oasis Valley basin part of the Nevada Test Site for water supplies and long- and short-term aquifer tests to help characterize the flow system. Most of this development has been small in scale and likely has had little long-term effect on the system. Similarly, the relatively small amount of pumpage in the area of Penoyer Valley for irrigation likely has had little long-term effect (Moreo and others, 2003).

Ash Meadows Basin

The Ash Meadows basin is the largest basin in the central Death Valley subregion (fig. D–7) (Waddell, 1982). Much of the ground water in this basin is derived from recharge on the Spring Mountains and the Sheep, Pahranagat, and Belted Ranges. Recharge also may occur within the basin on the Spotted, Pintwater, and Desert Ranges (Laczniak and others, 1996). The Ash Meadows basin is subdivided into six sections: Pahranagat, Tikaboo Valley, Indian Springs, Emigrant Valley, Yucca–Frenchman Flat, and Specter Range.

The Ash Meadows discharge area (fig. D–7) represents the terminus of the Ash Meadows basin. Water entering Ash Meadows encounters a northwest-southeast trending fault that juxtaposes fine-grained basin-fill sediments and the more permeable carbonate-rock aquifer (Dudley and Larson, 1976, p. 9–10). The discharge at Ash Meadows occurs at approximately 30 springs along a 16-kilometer (km) long spring line that generally coincides with the trace of the buried fault. All the major springs emerge from circular pools, are relatively warm, and discharged at nearly constant rates from 1953 until agricultural development began in the area in 1969 (Dettinger and others, 1995, p. 79). Most of the spring discharge at Ash Meadows may reinfiltrate and recharge the basin-fill aquifers, much of this discharging as ET from the alluvium along the Amargosa River, Carson Slough, and Alkali Flat (Czarnecki and Waddell, 1984; Czarnecki, 1997).

Ground water is pumped from wells scattered throughout the Ash Meadows basin. Wells near Ash Meadows tap the basin-fill aquifers adjacent to the carbonate-rock aquifer. Wells on the NTS within the basin are used to supply about 50 percent of the water demand at the NTS (Laczniak and others, 1996). Pumping from basin-fill aquifers around Devils Hole, a collapse feature in the carbonate rock supporting an endemic species of desert pupfish (*Cyprinidon diabolis*) (see fig. A–1), caused water-level declines observed in Devils Hole and the decrease or temporary cessation of flow from several major springs issuing from the carbonate aquifer. After pumping ceased, water levels and spring flow gradually recovered. The effect of pumping on individual springs differed, indicating that a variable degree of hydraulic connection exists between the basin-fill and carbonate-rock aquifers (Dettinger and others, 1995, p. 80).

Previous conceptual models of the Ash Meadows basin indicate significant amounts of flow from Pahranagat Valley to Ash Meadows. Evaluations of hydrochemical data, however, indicate that the volume of this inflow could be negligible (J.M. Thomas and William Sicke, Desert Research Institute, Reno, Nev., written commun., 2003). Analysis of calcite veins precipitated at Devils Hole (Winograd and others, 1992) also indicates that most, if not all, of the ground water in Ash Meadows originates from the Spring Mountains.

Ground water that bypasses the springs at Ash Meadows may continue as throughflow to Furnace Creek (fig. D–7) or may recharge the basin-fill sediments and join other ground water in the basin-fill sediments to flow southward toward Alkali Flat, where it either discharges or continues south to the southern Death Valley subregion. Three springs at the southern end of the Ash Meadows spring line (Big, Bole, and Last Chance) have elevated strontium values, which may indicate that they receive some flow from a different origin, such as the Pahrump Valley (Peterman and Stuckless, 1992a, p. 70; Peterman and Stuckless, 1992b, p. 712). High-resolution aeromagnetic surveys conducted over the Amargosa Desert and Pahrump indicate a possible hydraulic connection between Pahrump Valley and the Amargosa Desert through Stewart Valley (Blakely and Ponce, 2001).

Ground water recharged on the mountain areas of the Ash Meadows basin flows toward the Spotted Range–Mine Mountain structural zone (fig. D–7). It is generally accepted that ground water in Tikaboo and Emigrant Valleys

and Yucca and Frenchman Flats flows toward a trough in the potentiometric surface beneath Frenchman Flat and the Specter and Spotted Ranges (figs. D–2 and D–7) (Winograd and Thordarson, 1975; Faunt, 1997; D'Agnese and others, 1997). This trough may be a zone of relatively high permeability in the carbonate-rock aquifer associated with the Spotted Range–Mine Mountain structural zone (Carr, 1984; Faunt, 1997; D'Agnese and others, 1998). The Las Vegas Valley shear zone (LVVSZ) bounds the trough on the south and southeast. The flow paths along the trough are directed through the Specter Range area until they encounter the fault at Ash Meadows.

The basin-fill and volcanic-rock aquifers in Emigrant Valley and Yucca and Frenchman Flats (fig. D–7) provide recharge (fig. D–2) to the regional carbonate-rock aquifer by downward percolation (Winograd and Thordarson, 1975; Laczniak and others, 1996). The water chemistry at Indian Springs Valley indicates that these waters have had little opportunity for contact with volcanic rock or basin-fill sediments composed of volcanic rocks indicating that the ground water beneath Tikaboo and Emigrant Valleys and Yucca and Frenchman Flats is not moving southward toward Indian Springs Valley. The water in the carbonate-rock aquifer in these locations may be moving toward the Amargosa Desert, where the ground water is generally of mixed chemical character and has high levels of sodium (Schoff and Moore, 1964; Winograd and Thordarson, 1975). Ultimately most of the ground water discharges at Ash Meadows.

In the Pahranagat section, near the Sheep Range, the DVRFS boundary is uncertain and has been postulated in various locations (Harrill and others, 1988; Bedinger and others, 1989; Harrill and Prudic, 1998; D'Agnese and others, 1997, 2002; Appendix 2, this volume). For this study, the DVRFS model boundary was placed along the Gass Peak thrust (fig. D–5; Appendix 2, this volume), the easternmost feature postulated as a boundary. This places the boundary between the Colorado River ground-water flow system and the DVRFS model domain farther east than in most previous studies. Consequently, the deeper carbonate rocks may allow substantial amounts of water to flow to the Colorado River ground-water flow system to the east. If this occurs, then a ground-water divide should exist somewhere near the Desert Range, and flow into the Ash Meadows basin must occur through or north of the northern part of the Sheep Range (fig. D–7; Appendix 2, this volume). Regional-potential data (Appendix 1, this volume) also indicate that the flow-system boundary should be along a divide in the approximate location of the Desert Range (fig. D–7). If this divide exists, a significant amount of discharge from the Pahranagat section to the east into the Colorado River ground-water system occurs through the carbonate-rock aquifer in the Sheep Range. West of this divide, discharge occurs as throughflow into Indian Springs Valley.

Recharge to the Pahranagat section occurs partly as throughflow from Tikaboo Valley and in the Sheep Range (fig. D–7). Recharge also may occur at the higher mountains of the Spotted, Pintwater, and Desert Ranges (Laczniak and others, 1996). As previously mentioned, hydrochemical data indicate that little or no flow comes into the DVRFS model domain from the Pahranagat Range. Flow that does come into this section is thought to exit through short pathways to the southeast through the Sheep Range (Appendix 2, this volume).

Recharge to the Tikaboo Valley section occurs in the Pahranagat Range (fig. D–7). Although the eastern boundary of the Tikaboo Valley section is aligned along the Pahranagat Range parallel with the boundary of the Colorado River flow system, throughflow may occur along the flow-system boundary at the Pahranagat Range, especially in the south along the Pahranagat shear zone (Winograd and Thordarson, 1975) (fig. D–5). Little is known about water levels or flow directions in the basin-fill sediments. The water in the carbonate-rock aquifer in Tikaboo Valley is thought to be moving toward the Amargosa Desert (Workman and others, 2002). On the basis of recent interpretations of regional hydraulic gradients (Appendix 2, this volume), however, some, if not all, flow occurs out of the eastern boundary into the Colorado River flow system.

Regional ground water recharged on the Sheep Range and Spring Mountains flows into the Indian Springs section (fig. D–7) from the south and east and into the potentiometric trough (fig. D–2). Recharge also may occur on higher mountains of the Spotted, Pintwater, and Desert Ranges (Laczniak and others, 1996), most of which are underlain by carbonate rocks. Most of the water has had little opportunity for contact with volcanic rock or basin-fill sediments composed of volcanic rocks. As a result, hydrochemical data can be useful in delineating flow paths to and from this region.

Potentiometric data for both the basin-fill and carbonate-rock aquifers in the southern part of Indian Springs Valley indicate a prominent east-trending hydraulic barrier between the Nye County line and Indian Springs (fig. D–2) (Winograd and Thordarson, 1968), corresponding to the LVVSZ (fig. D–7). Because no clastic-rock confining units are known within the upper part of the saturated zone in this area, this flow barrier may be created by the LVVSZ (Winograd and Thordarson, 1975), causing discharge at Indian and Cactus Springs. In addition to Indian and Cactus Springs, discharge from the Indian Springs section occurs as throughflow to the Specter Range. Ground-water flow in the section converges in the carbonate-rock aquifer along the trough in the potentiometric surface (fig. D–2) and travels toward the Amargosa Desert, ultimately discharging at Ash Meadows.

Another flow barrier formed by the juxtaposition of the LCCU and the LCA (Winograd and Thordarson, 1968) is postulated approximately 8 km to the north of the LVVSZ. Potentiometric data in the area indicate that flow may be to the north in the basin-fill sediments and to the west between the two flow barriers in the carbonate-rock aquifer north of the barriers.

Recharge to the Emigrant Valley section occurs as throughflow from the north or precipitation to the Belted and Groom Ranges (fig. D–7). Flow is generally to the south in the basin-fill sediments to Yucca Flat but is disrupted at depth by low-permeability clastic-rock units. Basin-fill aquifers

in Emigrant Valley provide recharge to the carbonate-rock aquifer by percolation downward through basin-fill sediments. The western one-half of Emigrant Valley is bordered on the east, south, and southwest by clastic rocks. Geologic mapping indicates that this area of the valley is part of a highly faulted anticline, which, prior to extensional faulting, brought clastic rocks to the surface over a wide region (Winograd and Thordarson, 1968). Gravity surveys indicate that the bedrock beneath western Emigrant Valley is overlain by as much as 1,200 m of basin-fill sediments (Winograd and Thordarson, 1968).

The steep hydraulic gradients on both sides of Emigrant Valley (fig. D–2) are believed to reflect the movement of water through thick clastic-rock confining units (fig. D–4) toward points of lower hydraulic head in Yucca Flat and in the eastern part of Emigrant Valley (Winograd and Thordarson, 1968). The relatively flat hydraulic gradient in Emigrant Valley reflects the large permeability of the basin-fill aquifers. Both the steep and the flat hydraulic gradients probably are caused by a thick sequence of clastic-rock confining units separating the western part of Emigrant Valley from areas of lower ground-water potential to the east and west. The steep hydraulic gradients may be continuous or may represent discontinuous levels within blocks separated by low-permeability faults. Ground-water flow in the carbonate-rock aquifer in Emigrant Valley appears to be moving toward the trough in the potentiometric surface (fig. D–2).

Recharge to the Yucca–Frenchman Flat section is predominantly throughflow from Emigrant Valley to the north and northeast and possibly precipitation on Rainier Mesa and the adjacent Eleana and Belted Ranges (fig. D–7). Water-level contours (fig. D–2) show a southeastern flow component away from Rainier Mesa toward Yucca Flat. The carbonate-rock aquifer beneath the central and northern parts of Yucca Flat is isolated from the carbonate-rock aquifer in adjacent valleys to the north and east by the bordering clastic-rock confining units. Ground water moving between the basins into the carbonate-rock aquifer would have to pass through and would be controlled by the transmissivities of the clastic-rock confining units (Winograd and Thordarson, 1968, p. 43). Discharge from Yucca and Frenchman Flats occurs primarily as throughflow in the carbonate-rock aquifer toward a trough in the potentiometric surface (fig. D–2) near the Spotted Range–Mine Mountain structural zone (fig. D–7), continuing to the southwest toward the Amargosa Desert.

Recharge to the Specter Range section is mostly from throughflow in the carbonate-rock aquifer along the trough in the potentiometric surface (fig. D–2). The distribution of precipitation and the resulting infiltration indicates that ground water moves long distances through different HGUs before reaching Ash Meadows. Ground water flows through the Specter Range section along the trough in the potentiometric surface and utimately discharges at Ash Meadows.

Alkali Flat–Furnace Creek Basin

The Alkali Flat–Furnace Creek basin lies south and west of the Ash Meadows and Pahute Mesa–Oasis Valley basins and covers a large part of the western one-half of the NTS (fig. D–7). Ground water in this basin is derived from recharge on Pahute Mesa, Timber and Shoshone Mountains, and the Grapevine and Funeral Mountains. Additional recharge to this basin may occur as throughflow from Sarcobatus Flat, Oasis Valley, and Ash Meadows. Recharged ground water from throughflow and local recharge moves through volcanic-rock aquifers in the north and basin-fill and carbonate-rock aquifers in the south toward discharge areas in the southern and southwestern parts of the basin. Subsurface outflow follows the general course of the Amargosa River drainage through a veneer of alluvium near Eagle Mountain into the southern Death Valley subregion (Walker and Eakin, 1963). As with the other basins, the location of the boundary of the Alkali Flat–Furnace Creek basin is neither well established nor fully understood. The Alkali Flat–Furnace Creek basin is divided into four sections: the Fortymile Canyon, Amargosa River, Crater Flat, and Funeral Mountains sections.

The Alkali Flat–Furnace Creek basin supplies water to rural communities in the Amargosa Desert and to private recreational establishments and Federal facilities within Death Valley National Park, Calif. (Laczniak and others, 1996; see fig. A–1)). Domestic and smaller scale irrigation withdrawal started in the 1970's and continues to the present in the western Amargosa Desert. The withdrawal has caused local water-level declines. Withdrawal connected with mining operations south of Beatty has caused lower water levels in the northwestern arm of the Amargosa Desert (Moreo and others, 2003).

The main discharge area in the basin is the springs in the Furnace Creek area (fig. D–7) including Texas, Travertine, and Nevares springs (see fig. C–2). Hydrochemical data indicate that spring flow in the major springs at the Furnace Creek area likely derives from the carbonate-rock aquifer (Winograd and Thordarson, 1975, p. C95). Similar hydrochemistry between spring waters at Ash Meadows and the Furnace Creek area (Czarnecki and Wilson, 1991; Steinkampf and Werrell, 2001) indicate a hydraulic connection between these two discharge areas through the regional carbonate-rock aquifer by way of large-scale fractures or channels in the carbonate-rock aquifer (Winograd and Pearson, 1976).

Downgradient from the Furnace Creek springs, the remaining ground water and reinfiltrated spring flow moves toward the Death Valley saltpan and is transpired either by stands of mesquite on the lower part of the Furnace Creek fan or is evaporated from the saltpan in Badwater Basin (fig. D–7). The Death Valley saltpan is the largest playa in the region (fig. D–3), and despite the low rate of ET from the saltpan proper, the great area of this feature results in a significant amount of discharge (DeMeo and others, 2003). In addition, the saltpan is surrounded by alluvial fans and numerous springs fringed with vegetation. Ground water is shallow near

the distal end of most of the fans sloping from the mountains ringing Death Valley and in the areas between them. Marshes, phreatophytes, and small springs that occur at the base of the fans discharge local recharge from the surrounding mountains and throughflow from adjacent basins.

Recharge to the Fortymile Canyon and Fortymile Wash section is primarily from throughflow from the volcanic rocks of the eastern part of Pahute Mesa and the western part of Rainier Mesa (fig. D–7). Infiltration of surface runoff in the alluvium of the upper reaches of Fortymile Canyon and Fortymile Wash during periods of moderate to intense precipitation may be another source of locally important recharge (Czarnecki and Waddell, 1984; Laczniak and others, 1996; Savard, 1998; Hevesi and others, 2003). Hydraulic gradients based on sparse water-level data indicate that the principal flow direction in the section is southward from the eastern part of Pahute Mesa and western part of Rainier Mesa. Data from the northern part of this section are insufficient to assess whether flow continues south beneath Timber Mountain or is diverted around it toward Shoshone Mountain, Yucca Mountain, and Jackass Flats. The southern part of the Fortymile Canyon and Wash section includes Yucca Mountain. At and near Yucca Mountain, hydraulic gradients are dominantly upward in the volcanic-rock units from the carbonate-rock aquifer (Luckey and others, 1996). From Fortymile Wash, flow continues southward as throughflow into the Amargosa River section (Laczniak and others, 1996).

Recharge to the Amargosa River section is predominantly by throughflow in the basin-fill sediments from the Oasis Valley, Crater Flat, Fortymile Canyon and Wash, and Specter Range sections (fig. D–7). Recharge to the carbonate-rock aquifer also occurs by throughflow from the Specter Range and Fortymile Canyon and Wash sections. In the northwestern part of the Amargosa River section, intermediate ground-water movement is dominantly lateral and downward toward regional flow paths (Czarnecki and Waddell, 1984; Sinton, 1987; Kilroy, 1991). In the south-central parts of the basin, near the Nevada-California border, regional ground-water movement is mostly upward from the carbonate-rock aquifer into the intermediate system and toward discharge areas along the Amargosa River, Carson Slough, and Alkali Flat (Czarnecki and Waddell, 1984; Czarnecki, 1997). Hydrochemical data suggest that water in the carbonate-rock aquifer to the north and northeast and in volcanic-rock aquifers to the north and northwest flows toward the Amargosa Desert, where ground water generally is of mixed chemical character and has a large amount of sodium (Schoff and Moore, 1964).

Hydraulic and hydrochemical data indicate that water in the regional flow system in the southern part of Amargosa Desert (fig. D–7) either may flow southwest toward Death Valley through fractures in the southeastern end of the Funeral Mountains or flow southward and toward the surface at Alkali Flat (or Franklin Lake playa), deflected by the low-permeability quartzites of the Resting Spring Range (fig. D–7) (Czarnecki and Waddell, 1984; Czarnecki and Wilson, 1991). The carbonate rocks beneath the Funeral Mountains also might provide preferential conduits or drains for flow from the basin-fill sediments beneath the Amargosa Desert toward Death Valley (Czarnecki and Waddell, 1984; Luckey and others, 1996, p. 14).

Recharge to the Funeral Mountains section is thought to be predominantly from throughflow in the carbonate-rock aquifer in the southern part of the Funeral Mountains (fig. D–7). Additional ground water enters Death Valley as throughflow from Panamint Valley and the Owlshead Mountains in the southern Death Valley subregion. Local precipitation in the Panamint Range and in the Black and Funeral Mountains, and to a lesser extent in the Greenwater Range, supports mountain-front recharge as surface water seeps into the ground when it reaches alluvial fans ringing the floor of Death Valley. In addition, a small amount of throughflow originating in the northern and southern Death Valley subregions may occur in the relatively fine-grained basin-fill sediments in Death Valley. The Funeral Mountains section contains the major discharge area at the Furnace Creek area for the Alkali Flat–Furnace Creek basin.

Southern Death Valley Subregion

Ground water in the southern Death Valley subregion primarily is derived from recharge at the Spring Mountains and to a lesser extent from recharge at the Nopah, Kingston, and Greenwater Ranges (fig. D–8). Ground water also may be entering the system as throughflow in the basin-fill sediments of the Silurian Valley and valleys adjacent to the Owlshead Mountains (Appendix 2, this volume). Additional minor ground-water inflow may occur across the boundary from the Alkali Flat–Furnace Creek basin south of Alkali Flat (fig. D–8). The largest discharge area in the subregion is in Pahrump Valley, which contains a broad playa with several springs. The subregion contains four sections: Pahrump Valley, Shoshone-Tecopa, California Valley, and Ibex Hills, each with a significant discharge area. The Valjean section of D'Agnese and others (1997) is thought to have very little flow into the DVRFS model domain and is not used in this study (Appendix 2, this volume). The interconnection between the four sections is much more apparent than sections in the northern and central subregions.

Before extensive development, the playa area in Pahrump Valley contained some phreatophytic vegetation and was surrounded by sparse shrubland vegetation rising into alluvial fans. Ground-water withdrawals accompanying large-scale agricultural development in the Pahrump Valley section has caused cessation of flow of some major springs in the area during withdrawal, with the gradual recovery of spring flow after some withdrawal stopped. Historically, Manse and Bennetts Springs discharged along the base of the broad alluvial fans at the foot of the Spring Mountains. Ground-water withdrawal in the valley caused these springs to cease flowing in the 1970's. In the late 1990's, Manse Spring began to flow again, perhaps due to changes in the amount of agriculture and

agricultural practices in the valley. Withdrawal in the valley does continue for domestic uses and small-scale agriculture uses (Moreo and others, 2003).

Ground water in the Pahrump Valley section that does not discharge at Pahrump Valley flows either west toward Stewart Valley and the northern end of Chicago Valley, or southwest toward California Valley (fig. D–8). Direct ground-water flow to Death Valley from Pahrump Valley is unlikely because of low-permeability quartzites of the Resting Spring Range (Winograd and Thordarson, 1975; Grose, 1983, Sweetkind and others, 2001) that may bifurcate ground-water flow. Some of the ground water flowing toward the south and west is consumed by ET from playas in Stewart and Chicago Valleys.

In the Shoshone-Tecopa section, recharge predominantly is throughflow from adjacent sections with some contribution from local recharge in the Nopah Range (fig. D–8). Ground-water throughflow from Pahrump Valley mixes with ground water flowing south from Alkali Flat. Discharge occurs from ET and springs along the flood plain of the Amargosa River between the towns of Shoshone and Tecopa, Calif. Discharge in the Shoshone-Tecopa section may be from (1) basalt flows to the west damming shallow ground water, (2) normal faults beneath the Amargosa River south of Eagle Mountain forcing ground-water upward (Steinkampf and Werrell, 2001, p. 20), and(or) (3) a shallow (less than 10 km deep) intrusive body influencing the flow of ground water (Steinkampf and Werrell, 2001, p. 20). Ground water that does not discharge in the Shoshone-Tecopa area may continue flowing to the southwest into the Ibex Hills section through faulted and fractured crystalline rocks. Ground water continues flowing south in the alluvium along the Amargosa River channel into the California Valley section.

In addition to this throughflow from Pahrump Valley, recharge to the California Valley section is from precipitation on the Kingston Range and ground water that flows south from the Shoshone-Tecopa section (fig. D–8). South of Tecopa, Calif., a structural uplift brings ground water to the surface and feeds a perennial reach of the Amargosa River. Ground water leaves the California Valley section as surface-water flow or throughflow in the alluvium along the Amargosa River.

In addition to throughflow from the Shoshone-Tecopa section, flow into the Ibex Hills section also occurs along the Amargosa River channel as surface water or ground water in the associated alluvium (fig. D–8). Some additional ground water may enter the section as throughflow from Valjean, Shadow, and Silurian Valleys (which drain an extensive area south of the Kingston Range) and adjacent to the Owlshead Mountains. Discharge occurs primarily as ET and spring flow in the Saratoga Springs area. This area is supported by ground-water discharge from the regional carbonate-rock aquifer and includes adjacent areas of shallow ground water along the flood plain of the Amargosa River. A small amount of ground-water flow may continue north past Saratoga Springs to the central Death Valley subregion and discharge at Badwater Basin.

Surface-Water Hydrology

In the DVRFS region, perennial streamflow is sparse. Most surface water in the region is either runoff or spring flow discharge. Precipitation falling on the slopes of the mountains (such as the Panamint Range or the Black and Funeral Mountains), forms small, intermittent streams that quickly disappear and infiltrate as ground-water recharge. In addition, several streams originate from snowmelt in the high altitudes of the Spring and Magruder Mountains. Both of these types of streams have highly variable base flows and in dry years have almost imperceptible discharges. Springs maintain perennial flow for short distances in some of the drainages.

Surface-water flows in the DVRFS region have been categorized on the basis of hydrologic units (fig. D–9) that are the basic units used by State and local agencies for water-resources planning (Seaber, 1987). Hydrologic units are delineated primarily on the basis of topography and geologic structures and generally correspond to major surface drainages.

Drainage Areas

The Death Valley watershed contains two primary drainage basins—the Amargosa River basin in the south and the Salt Creek basin in the north. The Amargosa River Basin drainage area composes approximately two-thirds of the 22,100-km^2 Death Valley watershed and has the largest drainage basin discharging into Death Valley (Grasso, 1996). The Amargosa River is the only large perennial stream in the DVRFS region, originating in the mountains of southwestern Nevada and flowing south and west, terminating in the sinks and playas of Death Valley (fig. D–9). Despite the large drainage area, most of the Amargosa River and its tributaries are ephemeral.

Salt Creek drains the northwest part of Death Valley, an area of about 5,700 km^2 (fig. D–9). Although Salt Creek drains only one-third as much area as does the Amargosa River, it discharges more surface water to the Death Valley saltpan than does the Amargosa River (Hunt, 1975). Ground water discharging as seeps and spring flow from Mesquite Flat feeds Salt Creek (Hunt, 1975). Though Mesquite Flat is without perennial surface water, an extensive growth of phreatophytes is supported by shallow ground water.

Springs

There are four principal kinds of springs in the DVRFS model domain: those discharging along (1) high-angle faults, (2) low-angle faults, (3) low-permeability structural barriers, and (4) lithologic gradations into less-permeable material (Hunt and others, 1966). The largest and most significant springs for this study are those discharging along the high-angle faults, for example, Travertine, Texas, and Nevares

Hydrologic unit and code

117	Fish Lake Valley
141	Ralston Valley
142	Alkali Spring Valley
143	Clayton Valley
144	Lida Valley
145	Stonewall Flat
146	Sarcobatus Flat
147	Gold Flat
148	Cactus Flat
149	Stone Cabin Valley
156	Hot Creek Valley
157	Kawich Valley
158	Emigrant Valley
	A Groom Lake Valley
	B Papoose Lake Valley
159	Yucca Flat
160	Frenchman Flat
161	Indian Springs Valley
162	Pahrump Valley
163	Mesquite Valley
164A	Northern Ivanpah Valley
168	Three Lakes Valley (Northern part)
169	Tikaboo Valley
	A Northern part
	B Southern part
170	Penoyer Valley
171	Coal Valley
172	Garden Valley
173A	Southern Railroad Valley
173B	Northern Railroad Valley
209	Pahranagat Valley
210	Coyote Spring Valley
211	Three Lakes Valley (Southern part)
212	Northern Las Vegas Valley
216	Garnet Valley
225	Mercury Valley
226	Rock Valley
227	Fortymile Canyon
	A Jackass Flats
	B Buckboard Mesa
228	Oasis Valley
229	Crater Flat
230	Amargosa Desert
231	Grapevine Canyon
232	Oriental Wash
240	Chicago Valley
241	California Valley
242	Lower Amargosa Valley
243	Death Valley
244	Valjean Valley
253	Racetrack Valley
258	Lost Lake-Owl Lake Valley

Figure D–9. Hydrologic units for the Death Valley regional ground-water flow system.

Springs along the Furnace Creek fault zone (Hunt and others, 1966), and the springs at Ash Meadows (fig. D–10) (Laczniak and others, 1999). In the mountains, springs discharge at low-angle faults no more than a few gallons per minute (Hunt, 1975). Most of the springs in the Panamint Range are of this type. The third type of spring occurs where ground water is ponded behind a low-permeability structural barrier, such as the spring area at Mesquite Flat. The fourth type of spring is found at the edge of the Death Valley floor where ground water is ponded in the gravel and sand of the fans as they grade into silt under the valley floor. Larger volume and higher temperature springs that occur along major faults are generally considered to be regional springs.

Paleohydrology

Ground-water flow systems respond to and change with climate. The modern ground-water flow system may not be in equilibrium with the modern climate and most likely contains relics of past climates. Forester and others (1999) indicate that during the last glacial cycle [peaking 12,000 years ago (12 ka)], moisture fluxes were greater than current fluxes, and water tables were higher throughout the region (Quade and others, 1995). There is strong evidence that, during Quaternary time, there has been a steady decline in the regional potentiometric surface (Winograd and Szabo, 1988). Stands of mesquite in Death Valley, which are dependent on ground water of fairly good quality, have been dying and are not being replaced, which may indicate that the water supply is continuing to diminish. Whether this decline is because of a decrease in the supply of water or an increase in salinity, or both, is uncertain (Hunt, 1975).

Fossil, isotopic, and petrographic data provide evidence of past changes in precipitation, temperature, and evaporation, which are the manifestations of large-scale climate changes. In this study, climate change is of interest because of the effect of past climates on water levels. For example, plant macrofossils in the DVRFS region indicate that the mean annual precipitation in the past 40 to 10 ka was variable but was typically as much as twice the modern mean annual precipitation (Forester and others, 1999). These plant macrofossil data, together with aquatic fossils, indicate lower mean annual temperature than today (Forester and others, 1999). The increased precipitation and cooler temperatures resulted in a greater than modern level of effective moisture. Greater than modern levels of effective moisture resulted in regional aquifer recharge that was much higher during past pluvial periods (40 to 10 ka; Forester and others, 1999) than today (Benson and Kleiforth, 1989).

Evidence for a higher regional water table at some time in the past has been suggested on the basis of many lines of evidence. J.B. Paces (U.S. Geological Survey, written commun., 2004) points out that records of climate change that may indicate higher water levels can be categorized into three groups: (1) surface features (paleolimnology, paleobotany, and sedimentology); (2) saturated-zone features (paleohydrographs and paleorecharge); and (3) unsaturated-zone features (pore water and secondary hydrogenic minerals). The data indicate that the water table may have been 10 to 30 meters (m) higher in the past; some researchers postulate the water table may have been as much as 120 m higher.

Extensive paleodischarge deposits and paludal sediments were identified by Swadley and Carr (1987). The location and description of these deposits were refined on the basis of secondary mineral occurrences (Levy, 1991) and strontium isotopic variations from calcite collected from boreholes (Marshall and others, 1993) by Forester and others (1999) and Paces and Whelan (2001). Synchronous paleodischarge at numerous paleodischarge sites distributed over a broad area with heterogeneous hydrogeological conditions indicates the likelihood of a widespread rise in the regional water table (Forester and others, 1999) (**fig. D–10**). Under these wetter climate conditions, discharge from all sources probably greatly exceeded that which occurred during historical time.

Wetlands from the past pluvial periods of 40 to10 ka, such as those represented by the deposits at Cactus, Cow Creek, and Tule Springs, were supported by discharge from both the ground-water and surface-water systems. Increased recharge in the Spring Mountains and Sheep Range probably resulted in spring discharge from the alluvial fans at the foot of the mountain ranges.

Deposits in the northern part of Amargosa Desert and the southern part of Crater Flat (fig. D–10) probably also represent an area of focused ground-water discharge during the late Pleistocene (40–12 ka) (Forester and others, 1999). Deposits north of Death Valley Junction, Calif., adjacent to the southern end of the Funeral Mountains (fig. D–10), show an interplay of surface flow and spring discharge as do the deposits in the Amargosa Desert. Interpretations of paleodischarge deposits are not available for Ash Meadows. Quade and others (1995) have identified and studied late Pleistocene wetland deposits in the Coyote Springs and Pahrump Valleys. Extensive spring-discharge and wetland deposits are known from the Pahrump Valley, and according to Quade and others (1995), deposits from about 21 ka and older probably do exist there.

Pluvial lakes occupied many basins in the central and eastern Great Basin during the late Pleistocene (Forester and others, 1999). Within the region, shallow (less than 1.3 m deep) lakes existed in Gold Flat and Emigrant and Kawich Valleys. Fortymile Wash and the Amargosa River were probably perennial streams that helped supply Lake Manly. To produce and maintain this lake would have required either (1) a sizable increase in the volume of precipitation over the saltpan and runoff from the watershed, (2) a substantial decrease in temperature to reduce annual lake evaporation, or (3) a combination of these climatic changes (Grasso, 1996).

Hydrologic models that are based on assumed increased recharge during Pleistocene time (Czarnecki, 1985; D'Agnese and others, 1999) seem to confirm these observations. D'Agnese and others (1999) have reported on a conceptual model of the paleohydrology, based on their climate

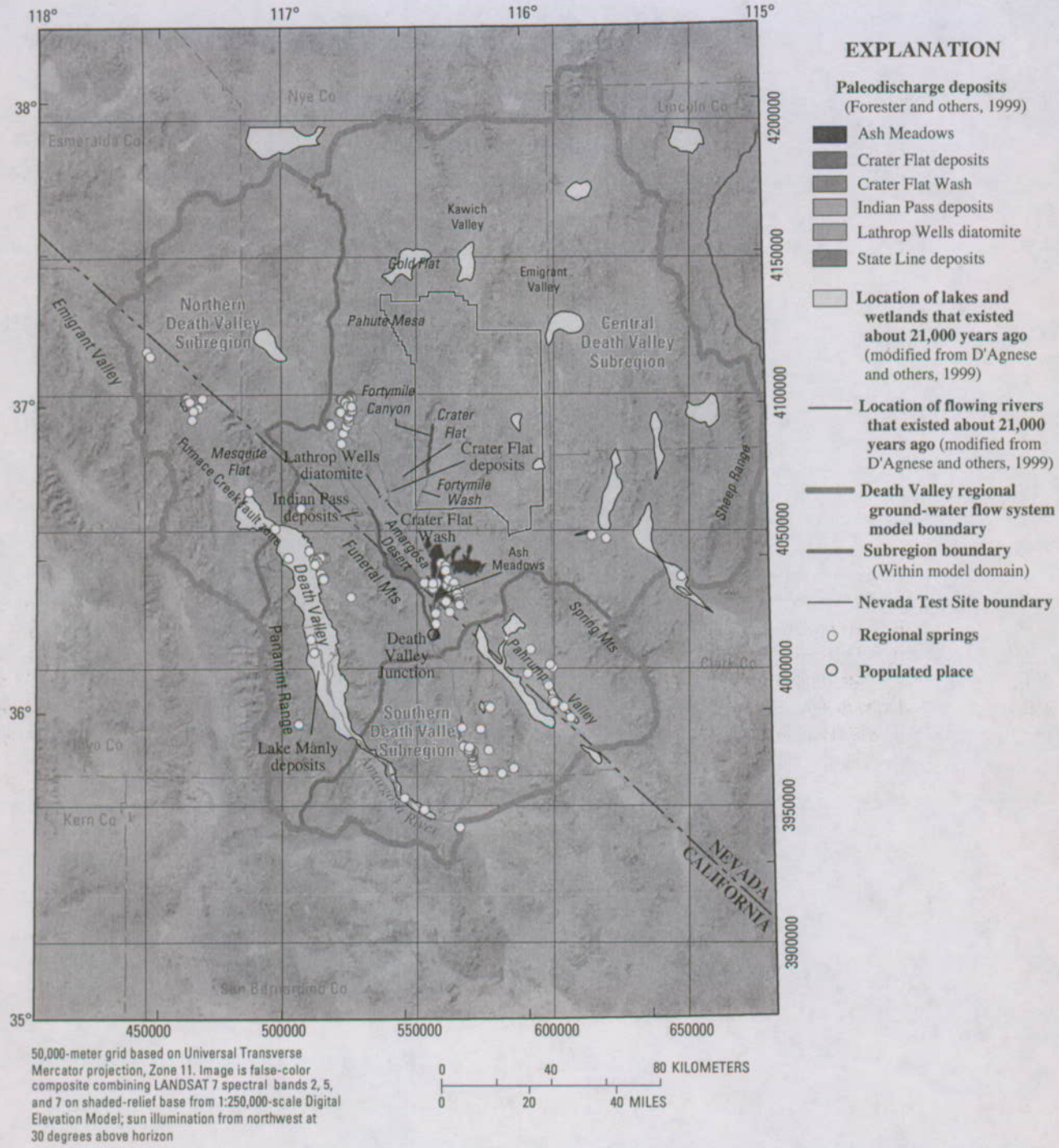

Figure D–10. Location of paleodischarge areas and regional springs in the Death Valley regional ground-water flow system region.

simulation of the Yucca Mountain Project/Hydrologic Resource Management Program (YMP/HRMP) regional ground-water flow model (D'Agnese and others, 1997). In this simulation, the region was assumed to be much cooler and wetter than present, and the lakes and greater discharges described above were supported. It must be remembered, however, that these models have many limitations, not the least of which is the representation of the system as steady state.

Summary

Ground water in the Death Valley region occurs in several interconnected, extremely complex ground-water flow systems. The water moves along relatively shallow and localized flow paths that are superimposed on deeper, regional flow paths. Regional ground-water flow is predominantly through conduits in the carbonate rocks. This flow field is

influenced by complex geologic structures created by regional faulting and fracturing that can create conduits or barriers to flow.

Infiltration of precipitation and runoff on high mountain ranges is the largest source of ground-water recharge. Springs and evapotranspiration are the dominant natural ground-water discharge processes. Discharge related to human activities is associated with ground-water pumping for agricultural, commercial, and domestic uses and is not negligible.

The water table is the upper boundary of the flow system and both no-flow and flow boundaries exist at the lateral extent of the defined flow system. The lower boundary surface of the Death Valley regional ground-water flow system model (DVRFS) domain is the depth at which ground-water flow is dominantly horizontal or parallel to the lower surface and generally corresponds with the upper surface of low-permeability basement rock. Ground-water inflow to the DVRFS model domain occurs in the vicinities of Garden, Coal, Stone Cabin, the southern part of Railroad, Eureka, and Saline Valleys, and the Panamint Range, with possibly small amounts in the Owlshead Mountains. Ground-water outflow occurs at the Sheep Range and parts of the Pahranagat Range, and the western part of Las Vegas Valley and, to a small degree, Silurian Valley.

The region is subdivided into the northern, central, and southern subregions. Ground water flows between these subregions, each which of has distinctive characteristics.

In the northern Death Valley subregion, water levels indicate that much of the ground-water flow is shallow, as the area is underlain by low-permeability bedrock. Ground-water flow is controlled by northeast-southwest-trending structural zones through the mountain ranges east of Death Valley. Ground water entering the subregion as throughflow from the northern boundary or recharge from precipitation flows south to Sarcobatus Flat and Death Valley. Some of this flow discharges at Grapevine and Stainginger Springs. These springs result from the intersection of high- and low-permeability structures.

The central Death Valley subregion includes the major discharge areas of Oasis Valley, Ash Meadows, and Alkali Flat–Furnace Creek. These major discharge areas result from flow paths that are complicated by ground water possibly entering the subregion in the vicinities of Stone Cabin, Garden, Coal, and the southern part of Railroad Valleys. Ground-water flow is generally from Pahute Mesa toward Oasis Valley or from the north toward the potentiometric trough north-northeast of Ash Meadows. The major flow paths in the subregion appear to coincide with high-permeability zones created by regional fault or fracture zones. Some of the ground water that originates as recharge in mountain areas or as inflow to the subregion discharges at Ash Meadows. Some continues south and discharges in the Alkali Flat–Furnace Creek basin.

Ground-water movement in the central Death Valley subregion is dominantly lateral and downward toward regional flow paths in the northwestern parts of the Amargosa Desert. Near Yucca Mountain and in areas immediately to the south, vertical gradients are dominantly upward from the carbonate-rock aquifer into the intermediate system and flow is toward discharge areas to the south and southwest. Ground water in the southern Amargosa Desert may either flow through fractures in the southeastern end of the Funeral Mountains and discharge in the Furnace Creek area or flow southward and discharge at Alkali Flat.

The southern Death Valley subregion is dominated by flow derived primarily from precipitation and subsequent infiltration on the Spring Mountains. Water moves toward the major discharge areas in Pahrump Valley. Springs on the distal edges of alluvial fans in Pahrump Valley have diminished flow, which might result from local ground-water use. Ground water that is not intercepted in Pahrump Valley flows southwest toward discharge areas in Chicago and California Valleys and, ultimately, Saratoga Springs.

In the DVRFS model domain, the entire ground-water system is not in equilibrium. The system has been modified by generally local pumping in (1) Pahrump Valley, (2) Amargosa Desert, (3) Penoyer Valley, and, to a lesser extent, (4) the Nevada Test Site. Although there are virtually no perennial streams in the region, there is evidence for surface-water features, such as perennial streams, lakes, and marshes as well as higher ground-water levels, resulting from wetter climates in the past. Residual effects from past climate change during the Pleistocene, although identifiable in some areas, are thought to be negligible.

References Cited

Bedinger, M.S., Langer, W.H., and Reed, J.E., 1989, Ground-water hydrology, *in* Bedinger, M.S., Sargent, K.A., and Langer, W.H., eds., Studies of geology and hydrology in the Basin and Range Province, southwestern United States, for isolation of high-level radioactive waste—Characterization of the Death Valley region, Nevada and California: U.S. Geological Survey Professional Paper 1370–F, p. 28–35.

Benson, L.V., and Kleiforth, H., 1989, Stable isotopes in precipitation and ground water in the Yucca Mountain region, southern Nevada—Paleoclimatic implications, *in* Peterson, D.H., ed., Aspects of climate variability in the Pacific and the western Americas: American Geophysical Union Monograph 55, p. 41–59.

Blakely, R.J., Jachens, R.C., Calzia, J.P., and Langenheim, V.E., 1999, Cenozoic basins of the Death Valley extended terrane as reflected in regional gravity anomalies, *in* Wright, L.A., and Troxel, B.W., eds., Cenozoic basins of the Death Valley Region: Geological Society of America Special Paper 333, p. 1–16.

Blakely, R.J., and Ponce, D.A., 2001, Map showing depth to pre-Cenozoic basement in the Death Valley ground-water model area, Nevada and California: U.S. Geological Survey Miscellaneous Field Studies Map, MF–2381–E, 1 sheet, 1:250,000-scale sheet, 6 pages of explanatory text.

Blankennagel, R.K., and Weir, J.E., Jr., 1973, Geohydrology of the eastern part of Pahute Mesa, Nevada Test Site, Nye County, Nevada: U.S. Geological Survey Professional Paper 712–B, 35 p.

Carr, W.J., 1984, Regional structural setting of Yucca Mountain, southwestern Nevada, and late Cenozoic rates of tectonic activity in part of the southwestern Great Basin, Nevada and California: U.S. Geological Survey Open-File Report 84–854, 114 p.

Czarnecki, J.B., 1997, Geohydrology and evapotranspiration at Franklin Lake Playa, Inyo County, California: U.S. Geological Survey Water-Supply Paper 2377, 75 p.

Czarnecki, J.B., 1985, Simulated effects of increased recharge on the ground-water flow system of Yucca Mountain and vicinity, Nevada-California: U.S. Geological Survey Water-Resources Investigations Report 84–4344, 33 p.

Czarnecki, J.B., and Waddell, R.K., 1984, Finite-element simulation of ground-water flow in the vicinity of Yucca Mountain, Nevada-California: U.S. Geological Survey Water-Resources Investigations Report 84–4349, 38 p.

Czarnecki, J.B., and Wilson, W.E., 1991, Conceptual models of the regional ground-water flow and planned studies at Yucca Mountain, Nevada: Hydrological Science and Technology, v. 7, no. 1–4, p. 15–25.

D'Agnese, F.A., Faunt, C.C., and Turner, A.K., 1998, An estimated potentiometric surface of the Death Valley region, Nevada and California, using geographic information systems and automated techniques: U.S. Geological Survey Water-Resources Investigations Report 97–4052, 15 p., 1 plate.

D'Agnese, F.A., Faunt, C.C, Turner, A.K., and Hill, M.C., 1997, Hydrogeologic evaluation and numerical simulation of the Death Valley regional ground-water flow system, Nevada, and California: U.S. Geological Survey Water-Resources Investigations Report 96–4300, 124 p.

D'Agnese, F.A., O'Brien, G.M., Faunt, C.C., Belcher, W.R., and San Juan, C.A., 2002, A three-dimensional numerical model of predevelopment conditions in the Death Valley regional ground-water flow system, Nevada and California: U.S. Geological Survey Water-Resources Investigations Report 02–4102, 114 p. Accessed September 22, 2004, at *http://pubs.water.usgs.gov/wri024102/.*

D'Agnese, F.A., O'Brien, G.M., Faunt, C.C., and San Juan, C.A., 1999, Simulated effects of climate change on the Death Valley regional ground-water flow system, Nevada and California: U.S. Geological Survey Water-Resources Investigations Report 98–4041, 40 p.

DeMeo, G.A., Laczniak, R.J., Boyd, R.A., Smith, J.L., and Nylund, W.E., 2003, Estimated ground-water discharge by evapotranspiration from Death Valley, California, 1997–2001: U.S. Geological Survey Water-Resources Investigations Report 03–4254, 27 p.

Dettinger, M.D., Harrill, J.R., and Schmidt, D.L., 1995, Distribution of carbonate-rock aquifers and the potential for their development, southern Nevada and adjacent parts of California, Arizona, and Utah: U.S. Geological Survey Water-Resources Investigations Report 91–4146, 100 p.

Dudley, W.W., Jr., and Larson, J.D., 1976, Effect of irrigation pumping on desert pupfish habitats in Ash Meadows, Nye County, Nevada: U.S. Geological Survey Professional Paper 927, 52 p.

Eakin, T.E., Price, Don, and Harrill, J.R., 1976, Summary appraisals of the Nation's ground-water resources—Great Basin region: U.S. Geological Survey Professional Paper 813–G, 37 p.

Faunt, C.C., 1997, Effect of faulting on ground-water movement in the Death Valley region, Nevada and California: U.S. Geological Survey Water-Resources Investigations Report 95–4132, 42 p.

Forester, R.M., Bradbury, J.P., Carter, C., Elvidge-Tuma, A.B., Hemphill, M.L., Lundstrom, S.C., Mahan, S.A., Marshall, B.D., Neymark, L.A., Paces, J.B., Sharpe, S.E., Whelan, J.F., and Wigand, P.E., 1999, The climatic and hydrologic history of southern Nevada during the late Quaternary: U.S. Geological Survey Open-File Report 98–0635, 63 p.

Franke, O.L., Reilly, T.E., and Bennett, G.D., 1987, Definition of boundary and initial conditions in the analysis of saturated ground-water flow systems—An introduction: U.S. Geological Survey Techniques of Water-Resources Investigations, book 3, chap. B5, 15 p.

Freeze, R.A., and Cherry, J.A., 1979, Ground water: Englewood Cliffs, N.J., Prentice-Hall, Inc., 604 p.

Grauch, V.J.S., Sawyer, D.A., Fridrich, C.J., and Hudson, M.R., 1999, Geophysical framework of the southwestern Nevada volcanic field and hydrogeologic implications: U.S. Geological Survey Professional Paper 1608, 39 p.

Grasso, D.N., 1996, Hydrology of modern and late Holocene lakes, Death Valley, California: U.S. Geological Survey Water-Resources Investigations Report 95–4237, 53 p.

Grose, T.L., 1983, Thirty-two geologic cross sections, Clark, Esmeralda, Lincoln, Mineral and Nye Counties, Nevada and adjacent areas in California: Nevada Bureau of Mines and Geology Open-File Report 83–13.

Harrill, J.R., Gates, J.S., and Thomas, J.M., 1988, Major ground-water flow systems in the Great Basin region of Nevada, Utah, and adjacent States: U. S. Geological Survey Hydrologic Investigations Atlas HA–694–C, 2 sheets.

Harrill, J.R., and Prudic, D.E., 1998, Aquifer systems in the Great Basin region of Nevada, Utah, and adjacent States—A summary report: U.S. Geological Survey Professional Paper 1409–A, 66 p.

Hevesi, J.A., Flint, A.L., and Flint, L.E., 2003, Simulation of net infiltration and potential recharge using a distributed parameter watershed model of the Death Valley region, Nevada and California: U.S. Geological Survey Water-Resources Investigations Report 03–4090, 161 p.

Hunt, C.B., 1975, Death Valley geology, ecology, and archaeology: Los Angeles, University of California Press, 234 p.

Hunt, C.B., Robinson, T.W., Bowles, W.A., Washburn, A.L., 1966, Hydrologic basin, Death Valley, California: U.S. Geological Survey Professional Paper 494–B, 138 p.

IT Corporation, 1996, Underground test area subproject phase I, Data analysis task, volume VI—Groundwater flow model data documentation package: Las Vegas, Nev., Report ITLV/10972–81 prepared for the U.S. Department of Energy, 8 volumes, various pagination.

Kilroy, K.C., 1991, Ground-water conditions in Amargosa Desert, Nevada-California, 1952–87: U.S. Geological Survey Water-Resources Investigations Report 89–4101, 91 p.

Laczniak, R.J., Cole, J.C., Sawyer, D.A., and Trudeau, D.A., 1996, Summary of hydrogeologic controls on ground-water flow at the Nevada Test Site, Nye County, Nevada: U.S. Geological Survey Water-Resources Investigations Report 96–4109, 59 p.

Laczniak, R.J., DeMeo, G.A., Reiner, S.R., Smith, J.L., and Nylund, W.E., 1999, Estimates of ground-water discharge as determined from measurements of evapotranspiration, Ash Meadows area, Nye County, Nevada: U.S. Geological Survey Water-Resources Investigations Report 99–4079, 70 p. Accessed September 1, 2004 at: *http:// water.usgs.gov/pubs/wri/wri994079/*

Laczniak, R.J., Smith, J.L., Elliott, P.E., DeMeo, G.A., Chatigny, M.A., and Roemer, G.J., 2001, Ground-water discharge determined from estimates of evapotranspiration, Death Valley regional flow system, Nevada and California: U.S. Geological Survey Water-Resources Investigations Report 01–4195, 51 p.

Luckey, R.R., Tucci, Patrick, Faunt, C.C., Ervin, E.M., Steinkampf, W.C., D'Agnese, F.A., and Patterson, G.L., 1996, Status of understanding of the saturated-zone ground-water flow system at Yucca Mountain, Nevada as of 1995: U.S. Geological Survey Water-Resources Investigations Report 96–4077, 71 p.

Levy, S.S., 1991, Mineralogic alteration history and paleohydrology at Yucca Mountain, Nevada, *in* High Level Radioactive Waste Management, Proceedings of the Second Annual International Conference, Las Vegas, Nevada, April 28–May 3, 1991: La Grange Park, Ill., American Nuclear Society, p. 477–485.

Marshall, B.D., Peterman, Z.E. and Stuckless, J.S., 1993, Strontium isotopic evidence for a higher water table at Yucca Mountain, *in* Proceedings of the High Level Radioactive Waste Management Fourth Annual International Conference, Las Vegas, Nevada, April 26–30, 1993: La Grange Park, Ill., American Nuclear Society, p. 1948–1952.

Moreo, M.T., Halford, K. J., La Camera, R.J, and Laczniak, R.J., 2003, Estimated ground-water withdrawals from the Death Valley regional flow system, Nevada and California, 1913–98: U.S. Geological Survey Water-Resources Investigations Report 03–4245, 28 p.

Paces, J.B., and Whelan, J.F., 2001, Water-table fluctuations in the Amargosa Desert, Nye County, Nevada, *in* High-Level Radioactive Waste Management, Proceedings of the Ninth International Conference, Las Vegas, Nev., April 29–May 3, 2001: LaGrange Park, Ill., American Nuclear Society, published on CD–ROM.

Peterman, Z.E., and Stuckless, J.S., 1992a, Applications of strontium and other radiogenic tracer isotopes to paleohydrologic studies—Paleohydrogeological methods and their applications: Proceedings of a Nuclear Energy Agency Workshop, Paris, France, November 9–10, 1992, p. 59–84.

Peterman, Z.E., and Stuckless, J.S., 1992b, Strontium isotope characterization of flow systems in southern Nevada, USA: Mineralogical Magazine, v. 58A, p. 711–712.

Potter, C.J., Sweetkind, D.S., Dickerson, R.P., and Kilgore, M.L., 2002, Hydrostructural maps of the Death Valley regional flow system, Nevada and California: U.S. Geological Survey Miscellaneous Field Studies MF–2372, 2 sheets, 1:250,000 scale, 14 p.

Quade, Jay, Mifflin, M.D., Pratt, W.L., McCoy, William, and Burckle, Lloyd, 1995, Fossil spring deposits in the southern Great Basin and their implications for changes in water-table levels near Yucca Mountain, Nevada, during Quaternary time: Geological Society of America Bulletin, v. 107, p. 213–230.

Savard, C.S., 1998, Estimated ground-water recharge from streamflow in Fortymile Wash near Yucca Mountain, Nevada: U.S. Geological Survey Water-Resources Investigations Report 97–4273, 30 p.

Schoff, S.L., and Moore, J.E., 1964, Chemistry and movement of ground water, Nevada Test Site: U.S. Geological Survey Trace Elements Report 838, 75 p.

Seaber, P.R., Kapinos, F.P., and Knapp, G.L, 1987, Hydrologic unit maps: U.S. Geological Survey Water-Supply Paper 2294, 63 p., 1 pl.

Sinton, P.O., 1987, Three-dimensional, steady-state, finite-difference model of the ground-water flow system in the Death Valley ground-water basin, Nevada-California: Golden, Colorado School of Mines, Master's thesis, 145 p.

Steinkampf, W.C., and Werrell, W.E., 2001, Ground-water flow to Death Valley, as inferred from the chemistry and geohydrology of selected springs in Death Valley National Park, California and Nevada: U.S. Geological Survey Water-Resources Investigations Report 98–4114, 37 p.

Swadley, W.C., and Carr, W.J., 1987, Geologic map of the Quaternary and Tertiary deposits of the Big Dune quadrangle, Nevada-California: U.S. Geological Survey Miscellaneous Investigations Series Map I–1767, scale 1:48,000, 1 sheet.

Sweetkind, D.S., Dickerson, R.P., Blakely, R.J., and Denning, P.D., 2001, Interpretive geologic cross sections for the Death Valley regional flow system and surrounding areas, Nevada and California: U.S. Geological Survey Miscellaneous Field Studies Map MF–2370, 3 plates, 32 pages of explanatory text. Accessed September 1, 2004 at: *http://greenwood.cr.usgs.gov/pub/mf-maps/mf-2370/*

Waddell, R.K., 1982, Two-dimensional, steady-state model of ground-water flow, Nevada Test site and vicinity, Nevada-California: U.S. Geological Survey Water-Resources Investigations Report 84–4267, 72 p.

Waddell, R.K., Robison, J.H., and Blakennagel, R.K., 1984, Hydrology of Yucca Mountain and vicinity, Nevada-California—Investigative results through mid-1983: U.S. Geological Survey Water-Resources Investigations Report 84–4267, 72 p.

Walker, G.E., and Eakin, T.E., 1963, Geology and ground water of Amargosa Desert, Nevada-California: Carson City, Nevada Department of Conservation and Natural Resources, Ground-Water Resources-Reconnaissance Series Report 14, 45 p.

White, A. F., 1979, Geochemistry of ground water associated with tuffaceous rocks, Oasis Valley, Nevada: U.S. Geological Survey Professional Paper 712E, p. E1–E25.

Winograd, I.J., Copeland, T.B., Landwehr, J.M., Riggs, A.C., Ludwig, K.R., Simmons, K.R., Szabo, B.J., Kolesar, P.T., and Revesz, K.M., 1992, Continuous 500,000-year climatic record from vein calcite in Devils Hole, Nevada: Science, v. 258, p. 255–260.

Winograd, I.J., and Pearson, F.J., Jr., 1976, Major carbon-14 anomaly in a regional carbonate aquifer—Possible evidence for megascale channeling, south-central Great Basin: Water Resources Research, v. 12, p. 1125–1143.

Winograd, I.J., and Szabo, B.J., 1988, Water-table decline in the south-central Great Basin during the Quaternary period—Implications for toxic waste disposal, *in* Carr, M.D., and Yount, J.C., eds., Geologic and hydrologic investigations of a potential nuclear waste disposal site at Yucca Mountain, southern Nevada: U.S. Geological Survey Bulletin 1790, p. 147–152.

Winograd, I.J., and Thordarson, William, 1968, Structural control of ground-water movement in miogeosynclinal rocks of south-central Nevada, *in* Eckel, E.B., ed., Nevada Test Site: Geological Society of America Memoir 110, p. 35–48.

Winograd, I.J., and Thordarson, William, 1975, Hydrologic and hydrochemical framework, south-central Great Basin, Nevada-California, with special reference to the Nevada Test Site: U.S. Geological Survey Professional Paper 712C, p. C1–C126.

Workman, J.B., Menges, C.M., Page, W.R., Taylor, E.M., Ekren, E.B., Rowley, P.D., Dixon, G.L., Thompson, R.A., and Wright, L.A., 2002, Geologic map of the Death Valley ground-water model area, Nevada and California: U.S. Geological Survey Miscellaneous Field Studies Map MF–2381–A. Accessed September 1, 2004 at: *http://greenwood.cr.usgs.gov/pub/mf-maps/mf-2381/*

Three-Dimensional Hydrogeologic Framework Model

By Claudia C. Faunt, Donald S. Sweetkind, and Wayne R. Belcher

Chapter E of

Death Valley Regional Ground-Water Flow System, Nevada and California—Hydrogeologic Framework and Transient Ground-Water Flow Model

Edited by Wayne R. Belcher

Prepared in cooperation with the
U.S. Department of Energy
Office of Environmental Management, National Nuclear Security Administration, Nevada Site Office,
under Interagency Agreement DE–AI52–01NV13944, and
Office of Repository Development,
under Interagency Agreement DE–AI08–02RW12167

Scientific Investigations Report 2004–5205

U.S. Department of the Interior
U.S. Geological Survey

Contents

Figures

Tables

CHAPTER E. Three-Dimensional Hydrogeologic Framework Model

By Claudia C. Faunt, Donald S. Sweetkind, and Wayne R. Belcher

Introduction

The complex stratigraphic and structural framework of the Death Valley region, described in Chapter B of this volume, controls ground-water flow in the Death Valley regional ground-water flow system (DVRFS). A three-dimensional (3D) hydrogeologic framework model (HFM), described herein, was constructed to represent the hydrogeologic units (HGUs) and major structures in the DVRFS region for the development of the transient numerical ground-water flow model (Chapter F, this volume).

Construction of the Hydrogeologic Framework Model

The HFM consists of 196 rows, 162 columns, and 28 units (including the base). The north-south-oriented HFM grid has a horizontal resolution of 1,500 m (fig. E–1). Resolution in the vertical dimension ranges from 0 to the maximum thickness of each HGU. Software constraints require that the HFM grid be constructed for a bounding rectangle, but the gridded surfaces are truncated at the model boundary for input to the ground-water flow model. The depth of the HFM extends to 4,000 m below sea level to encompass nearly all of the aquifer units in the region (Chapter B, this volume). Some small areas in Tikaboo Valley and the northern Pahranagat Range in the northeastern part of the DVRFS model domain (fig. A–1, this volume), however, may have relatively thin stratigraphic sections of potential aquifer material that extend deeper than this. Those thin sections are assumed to have little, if any, effect on regional ground-water flow.

Conceptual Model of the Hydrogeologic Framework

The HFM was constructed to represent the complexity of the hydrogeology of the DVRFS region (Chapter B, this volume). The unconsolidated sediments and consolidated rocks were subdivided into 27 HGUs on the basis of lateral extent, physical characteristics, and structural features to construct the HFM (table E–1).

Modeling Approach

The HFM is constructed by combining and extracting information from a variety of data sets, such as elevation models, geologic maps, borehole lithologic logs, cross sections, and digital geologic models. Because the HFM is a regional model, data sources (such as maps and cross sections) contain geological details typically shown on regional 1:250,000- to 1:100,000-scale maps. Some data sources, such as lithologic logs, were simplified to represent a regional scale.

A number of different software packages were selected for various parts of the HFM construction process. Each software package was chosen for its proficiency in a particular task and(or) suitability for project needs, but other software packages could have been used.

Spatial data, such as digital elevation, outcrop, and borehole information, were manipulated using Environmental Science Research Institute (ESRI) ARC/INFO® geographic information system (GIS) software. Cross-sectional hydrogeologic data were manipulated using Intergraph Corporation Modular GIS Environment® (MGE). Gridded surfaces were constructed using Petrosys Pty. Ltd. Petrosys® and Golden Software SURFER® gridding software. The HFM itself was constructed using Landmark Graphics Stratigraphic Geocellular Modeler® (SGM® or Stratamodel®). SGM is designed to accurately represent stratigraphic and structural relations of sedimentary basins, including deposition (and onlap), erosion, and unconformities, as well as truncation of units and faulting. Arrays representing HGU geometries were developed from the HFM and visualized and processed using ARC/INFO®.

The geometries (horizons and thicknesses) of the HGUs were exported from the HFM and incorporated into the flow model MODFLOW-2000 (Harbaugh and others, 2000; Hill and others, 2000) by using the Hydrogeologic-Unit Flow (HUF) package (Anderman and Hill, 2000). The HUF package resamples the HGUs into the flow-model grid, calculating which HGUs are in each flow-model layer.

Data Inputs

The construction of the HFM involves the use of data from several sources to define the top surface and extent of each regional HGU. These surfaces are termed "horizons."

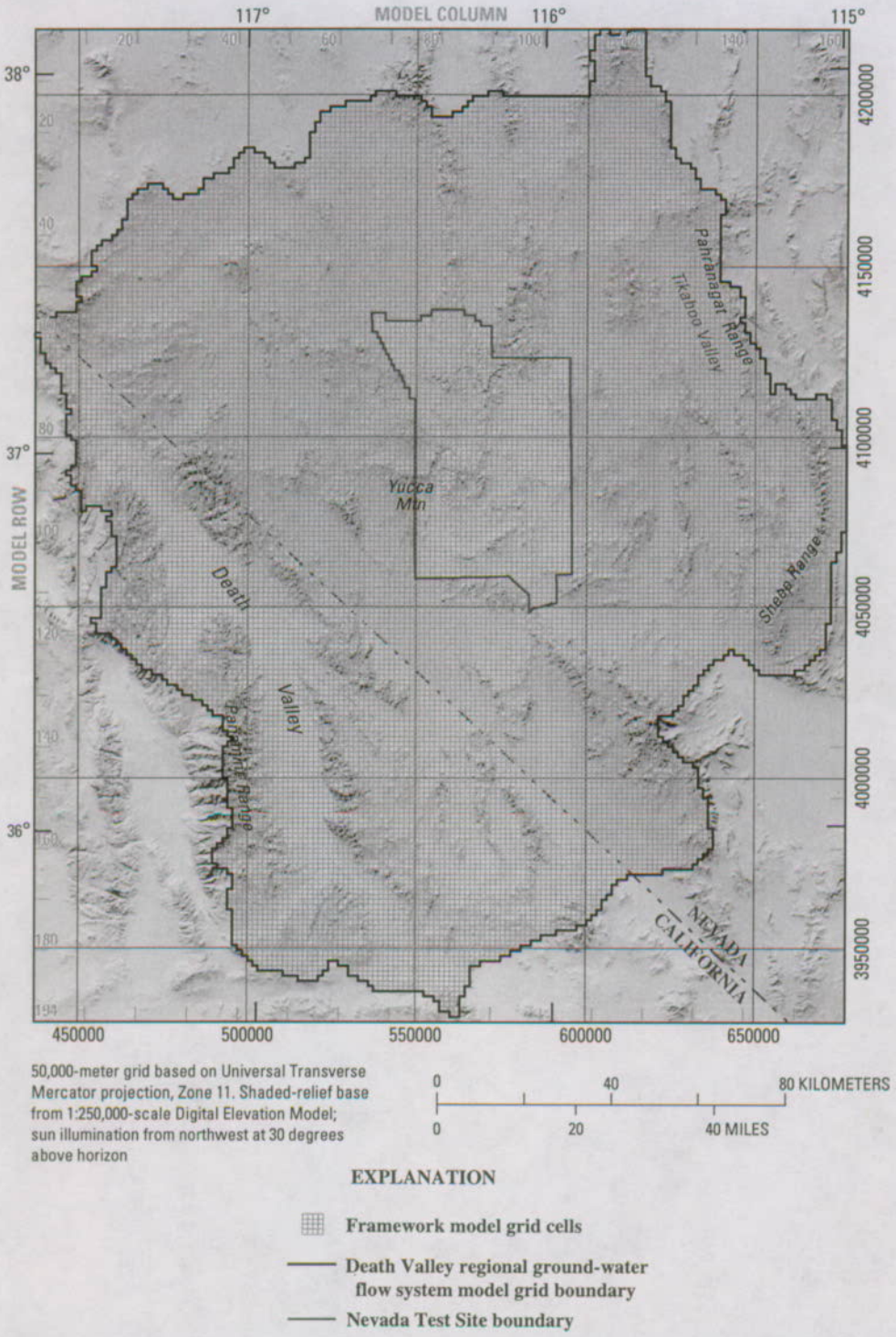

Figure E–1. Model grid for the Death Valley regional ground-water flow system hydrogeologic framework model.

Input data are the result of a comprehensive geologic interpretation (Chapter B, this volume) using digital elevation models, geologic and structural geologic maps, lithologic data from boreholes, cross sections, gridded data from previously constructed geologic framework models, and hydrologically important faults and structures (table E–2 and fig. E–2).

Topographic Data

Digital elevation data from the 1:250,000-scale and 7.5-minute National Elevation Data (NED) digital elevation models (DEMs) (U.S. Geological Survey, 2004) were merged into a single DEM for the DVRFS in Universal Transverse Mercator (UTM) projection Zone 11, North American Datum

Table E–1. Hydrogeologic units for the Death Valley regional ground-water flow system hydrogeologic framework model.

[Stacking order, the order that gridded surfaces were entered into the model during construction, with 1 being first and 27 being last; NTS, Nevada Test Site; SWNVF, southwestern Nevada volcanic field]

Hydrogeologic unit abbreviation	Hydrogeologic unit name	Description	Stacking order
YAA	Younger alluvial aquifer	Pliocene to Holocene coarse-grained basin-fill deposits	27
YACU	Younger alluvial confining unit	Pliocene to Holocene playa and fine-grained basin-fill deposits	26
OAA	Older alluvial aquifer	Pliocene to Holocene coarse-grained basin-fill deposits	25
OACU	Older alluvial confining unit	Pliocene to Holocene playa and fine-grained basin-fill deposits	24
LA	Limestone aquifer	Cenozoic limestone, undivided	23
LFU	Lava-flow unit	Cenozoic basalt cones and flows and surface outcrops of rhyolite-lava flows	22
YVU	Younger volcanic-rock unit	Cenozoic volcanic rocks that overlie the Thirsty Canyon Group	21
Upper VSU	Volcanic- and sedimentary-rock unit	Cenozoic volcanic and sedimentary rocks, undivided, that overlie volcanic rocks of SWNVF	20
TMVA	Thirsty Canyon–Timber Mountain volcanic-rock aquifer	Miocene Thirsty Canyon and Timber Mountain Groups, plus Stonewall Mountain tuff, undivided	19
PVA	Paintbrush volcanic-rock aquifer	Miocene Paintbrush Group	18
CHVU	Calico Hills volcanic-rock unit	Miocene Calico Hills Formation	17
WVU	Wahmonie volcanic-rock unit	Miocene Wahmonie and Salyer Formations	16
CFPPA	Crater Flat–Prow Pass aquifer	Miocene Crater Flat Group, Prow Pass Tuff	15
CFBCU	Crater Flat–Bullfrog confining unit	Miocene Crater Flat Group, Bullfrog Tuff	14
CFTA	Crater Flat–Tram aquifer	Miocene Crater Flat Group, Tram Tuff	13
BRU	Belted Range unit	Miocene Belted Range Group	12
OVU	Older volcanic-rock unit	Oligocene to Miocene; near the NTS consists of all volcanic rocks older than the Belted Range Group. Elsewhere, consists of all tuffs that originated outside of the SWNVF	11
Lower VSU	Volcanic- and sedimentary-rock unit	Cenozoic volcanic and sedimentary rocks, undivided; where named Cenozoic volcanic rocks exist, lower VSU underlies them	10
SCU	Sedimentary-rock confining unit	Paleozoic and Mesozoic sedimentary and volcanic rocks	9
UCA	Upper carbonate-rock aquifer	Paleozoic carbonate rocks (UCA only used where UCCU exists, otherwise UCA is lumped with LCA)	8
UCCU	Upper clastic-rock confining unit	Upper Devonian to Mississippian Eleana Formation and Chainman Shale	7
LCA_T1	Lower carbonate-rock aquifer (thrusted)	Cambrian through Devonian predominantly carbonate rocks – thrusted	6
LCCU_T1	Lower clastic-rock confining unit (thrusted)	Late Proterozoic through Lower Cambrian primarily siliciclastic rocks (including the Pahrump Group and Noonday dolomite) – thrusted	5
LCA	Lower carbonate-rock aquifer	Cambrian through Devonian predominantly carbonate rocks	4
LCCU	Lower clastic-rock confining unit	Late Proterozoic through Lower Cambrian primarily siliciclastic rocks (including the Pahrump Group and Noonday dolomite)	3
XCU	Crystalline-rock confining unit	Middle Proterozoic metamorphic and igneous rocks	2
ICU	Intrusive-rock confining unit	All intrusive rocks, regardless of age	1

1927 (NAD27) with a grid spacing of approximately 90 m. To ensure that topographic data were consistent with other data, the land-surface altitudes from the DEMs were replaced by reported land-surface altitudes at borehole locations.

Geologic Maps

Data from three geologic maps were used as input to the HFM. The primary source of data was the 1:250,000-scale geologic compilation of the DVRFS region (Workman, Menges, Page, Taylor, and others, 2002). Because the DVRFS HFM will be used for site-scale models at Yucca Mountain and the Nevada Test Site (NTS), additional stratigraphic detail was required in that area for specific Cenozoic volcanic-rock units. The locations of outcrops of the Calico Hills Formation, intrusive rocks at the Wahmonie volcanic center, and the Prow Pass, Bullfrog, and Tram Tuffs of the Crater Flat Group were extracted from the 1:120,000-scale map of the NTS (Slate and others, 2000). In the vicinity of Yucca Mountain, data from the 1:50,000-scale map of Potter, Dickerson, and others (2002) were used to define the locations of the Tram, Bullfrog, and Prow Pass Tuffs of the Crater Flat Group.

Table E–2. Data sources for hydrogeologic units in the hydrogeologic framework model for the Death Valley regional ground-water flow system.

[YMP, Yucca Mountain Project; GFM, geologic framework model; SCCC, Silent Canyon caldera complex; PMOV, Pahute Mesa–Oasis Valley]

Hydro-geologic unit abbreviation	Hydrogeologic unit name	Map[1]	Bore-hole[2]	Cross sections[3]	Unit extent map[4]	Hydro-structural map[5]	YMP GFM[6]	SCCC GFM[7]	PMOV GFM[8]
YAA	Younger alluvial aquifer	X							
YACU	Younger alluvial confining unit	X							
OAA	Older alluvial aquifer	X							
OACU	Older alluvial confining unit	X							
LA	Limestone aquifer		X						
LFU	Lava-flow unit	X	X	X		1, 2			
YVU	Younger volcanic-rock units	X		X		1, 2			X
Upper VSU	Volcanic- and sedimentary-rock unit	X	X	X		1, 2, 3			
TMVA	Thirsty Canyon–Timber Mountain volcanic aquifer	X	X	X	X	1, 2, 3, 4			X
PVA	Paintbrush volcanic-rock aquifer	X	X	X	X	1, 2, 3, 4	X	X	X
CHVU	Calico Hills volcanic-rock unit	X	X	X	X	1, 2, 4	X	X	X
WVU	Wahmonie volcanic-rock unit	X	X	X	X	1, 2, 4			
CFPPA	Crater Flat–Prow Pass aquifer	X	X	X		1, 2, 3, 4	X	X	X
CFBCU	Crater Flat–Bullfrog confining unit	X	X	X		1, 2, 3, 4	X	X	X
CFTA	Crater Flat–Tram aquifer	X	X	X		1, 2, 3, 4	X		
BRU	Belted Range unit	X	X	X		1, 2, 4		X	X
OVU	Older volcanic-rock unit	X	X	X		1, 2, 4		X	X
Lower VSU	Volcanic- and sedimentary-rock unit	X	X	X		1, 2, 3			
SCU	Sedimentary-rock confining unit	X	X	X		1, 2			
LCA_T1	Lower carbonate-rock aquifer - thrust	X	X	X	X	Thrust extent			
LCCU_T1	Lower clastic-rock confining unit - thrust	X		X	X	Thrust extent			
UCA	Upper carbonate-rock aquifer	X	X	X		1, 2, 3, 4, 5, 6, 7			
UCCU	Upper clastic-rock confining unit	X	X	X		1, 2, 3, 4, 5, 6, 7			
LCA	Lower carbonate-rock aquifer	X	X	X		1, 2, 3, 4, 5, 6, 7			
LCCU	Lower clastic-rock confining unit	X	X	X		1, 2, 3, 4, 5, 6, 7			
XCU	Crystalline-rock confining unit	X	X	X		1, 2, 3, 4, 5, 6, 7			
ICU	Intrusive-rock confining unit	X	X	X		1, 2, 3, 4, 5, 6, 7			X

[1]Workman, Menges, Page, Taylor, and others, 2002.

[2]U.S. Geological Survey National Water Information System (NWIS).

[3]Sweetkind and others, 2001; Potter, Dickerson, and others, 2002; R.W. Spengler, U.S. Geological Survey, written commun., 2001.

[4]Workman, Menges, Page, Ekren and others, 2002; Potter, Sweetkind, and others, 2002; Sweetkind and others, 2001.

[5]1 (normal), 2 (strike slip), 3 (detachment), 4 (caldera boundary), 5 (thrust), 6 (inferred thrust), 7 (transverse); Potter, Sweetkind, and others, 2002.

[6]Bechtel SAIC Company, 2002.

[7]McKee and others, 2001.

[8]Bechtel Nevada, 2002.

A surface hydrogeology map was constructed by merging the mapped lithostratigraphic units from the sources into HGUs using the computer-based GIS methods described in Faunt and others (1997). The geometry of HGU outcrops was defined by integrating the hydrogeologic map and the array of DEM and topographic information. Topographic data with x,y,z coordinate locations within each outcrop area were assigned to the appropriate HGU and exported as a series of files. Table E–3 shows the correlation of lithostratigraphic units used in the sources with the HGUs used in the HFM. Figure E–3 shows a simplified version of the resulting surface hydrogeology map in which the 27 HGUs are grouped into the 10 HGUs displayed in the figure.

Borehole Lithologic Data

Lithologic log data from 1,533 boreholes in the DVRFS region were compiled and manipulated as input for the HFM (fig. E–4), resulting in approximately 7,000 lithologic contacts between HGUs. Borehole lithologic data came from the

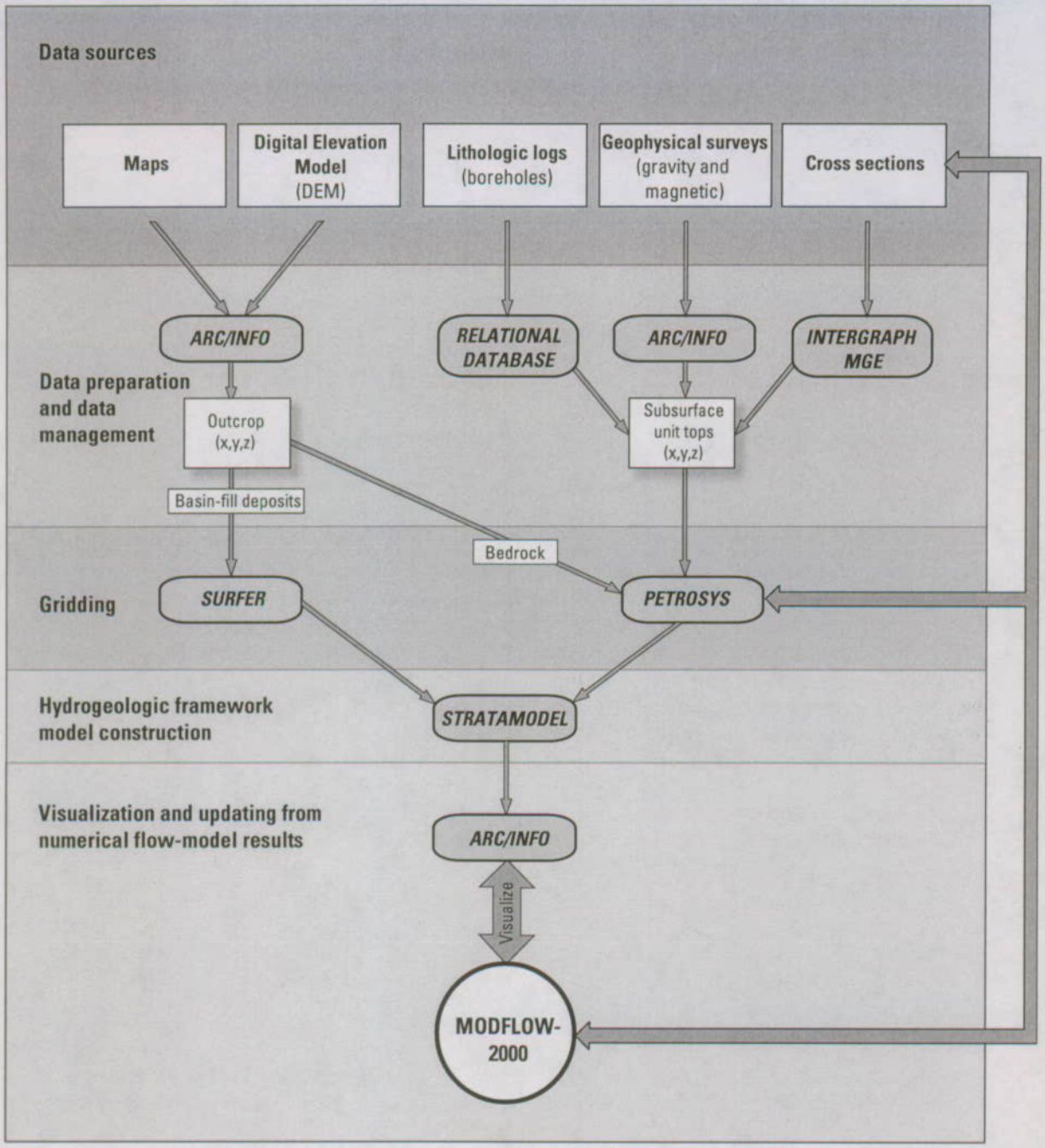

Figure E–2. Process of integration of data into Death Valley regional ground-water flow system hydrogeologic framework model.

following sources: (1) the USGS National Water Information System (NWIS), (2) well drillers' reports obtained through the Nevada Division of Water Resources, (3) previously compiled data from 235 boreholes from the SWNVF (Warren and others, 1998); (4) unpublished data collected by the USGS for the YMP as part of site characterization, (5) borehole data from the Nye County Early Warning Drilling Program (EWDP) (Nye County, 2004), (6) borehole data compiled for the DOE/NV-UGTA model (IT Corporation, 1996a), and (7) borehole reports by Federal and State agencies.

The lithostratigraphic units in the borehole records were correlated with HGUs and the locations defining the HGU horizons were extracted. The x,y,z coordinates are defined by the location and depth from the land surface (the altitude of the top of the HGU horizon was calculated by subtracting the depth from the land-surface altitude). If the land-surface altitude was not reported in the borehole records, DEMs were used to interpolate the land-surface altitude at the borehole. Boreholes outside the model domain were retained for control along the model boundary.

Table E–3. Correlation of hydrogeologic units with lithostratigraphic units from geologic map and cross sections.

Hydro-geologic unit abbreviation	Hydrogeologic unit name	Regional cross sections (Sweetkind and others, 2001)	Geologic map (Workman, Menges, Page, Taylor, and others, 2002)	Nye County cross sections (R.W. Spengler, U.S. Geological Survey, written commun., 2001)
YAA	Younger alluvial aquifer	Qu	Qc, Qay, Qayo, Qau, Qe, QTau, QTls	Qal, Qa
YACU	Younger alluvial confining unit	Qu	Qp, Qayf, QTd, Qayfe	Not depicted
OAA	Older alluvial aquifer	QTu	Qao, QTa, Qlc	QTa, QTu, Tal, Trx
OACU	Older alluvial confining unit	QTu	QTsf	Not depicted
LA	Limestone aquifer	Not depicted	Not depicted	not depicted
LFU	Lava-flow unit	QTb	Qa, Qb, QTb, Tb, Tr, Tar, Tas, Tgy, Tvg	Tby, Tvy
YVU	Younger volcanic-rock unit	Not depicted	Tt4, Tv	Not depicted
Upper and lower VSU	Volcanic- and sedimentary-rock unit	Tvu (Tgv, Tvu, Tvuy), Tsu (Tsu, Tso, Ts3, Ts4)	Ta4, Tls, Ts, Ts1, Ts3, Ts4, Tso	Tge, Tget, Tab
TMVA	Timber Mountain volcanic-rock aquifer	Tt, Tm	Tmt, Tst	Tmr, Tma
PVA	Paintbrush volcanic-rock aquifer	Tp, Tvx	Tpt	Tpc, Tpcbt, Tpt, Tptbt
CHVU	Calico Hills volcanic-rock unit	Ta	Not depicted	Tac
WVU	Wahmonie volcanic-rock unit	Tw	Tw	Tw
CFPPA	Crater Flat–Prow Pass aquifer	Not depicted	Tct (Tcp)	Tcp, Tcpbt
CFBCU	Crater Flat–Bullfrog confining unit	Not depicted	Tct (Tcb)	Tcb, Tcbbt, Tcbss
CFTA	Crater Flat–Tram aquifer	Not depicted	Tct (Tct)	Tct, Tcts
BRU	Belted Range unit	Tb	Tbt	
OVU	Older volcanic-rock unit	Tov, Tvuo	Ta2, Ta3, Tkv, Tlt, Tqv, Tt2, Tt3, Tuv	Trl, Trlbt, Trls, Trr
SCU	Sedimentary-rock confining unit	Pkt, ₸cm, Ja	₸c, ₸m, Ja, Klw, Mzsv, PIPkc, Pkt, Pov, Pr, Pzu	Not depicted
UCA	Upper carbonate-rock aquifer	PIPu where Me or Mc is present	PIPMb, PIPt	Not depicted
UCCU	Upper clastic-rock confining unit	Me, Mc	IPMsc, MDe	Not depicted
LCA and LCA_T1	Lower carbonate-rock aquifer and thrusts	Cnbc, Ou, Sdu, Mu	€b, €c, €e, €ms, €n, €nb, €nbc, €u, D€d, D€m, D€u, Dlb, Ds, Dsf, DShv, DSlm, DSsl, DSu, MDu, Mu, Mm, Oep, Oepn, Oeu, Oe, Oee, Oes, Opa, PSu, Sr	Dn, Du, Su, Ou, Cn, Cb, Cc
LCCU and LCCU_T1	Lower clastic-rock confining unit and thrusts	LCCU, ZYp, Zu, Zj, CZw, Pzx, Zs	€cam, €h, €po, €z, €Zcaa, €Zw, €Zws, Zd, Zj, Zs	Cz, CZw
XCU	Crystalline-rock confining unit	ZYXm, ZYm, Xmi	Tws, Xmi, ZYp	ZYm, Xm
ICU	Intrusive-rock confining unit	Ti, TKi	J₸qm, Tai, TKd, TKi, ₸g, Tgo	Not depicted

Geologic and Hydrogeologic Cross Sections

Cross sections from five sources were used as input to the HFM (fig. E–4): (1) DVRFS region (Sweetkind and others, 2001), (2) southern Nevada and eastern California (Grose, 1983; Grose and Smith, 1989), (3) DOE/NV-UGTA model (IT Corporation, 1996a), (4) Yucca Mountain area (Potter, Dickerson, and others, 2002), and (5) the southern part of Yucca Mountain and the northern part of Amargosa Desert (R.W. Spengler, U.S. Geological Survey, written commun., 2001).

Many of the cross sections in Grose (1983), Grose and Smith (1989), and IT Corporation (1996a) are inconsistent with or superseded by cross sections developed using new data and structural interpretations. Of the 32 1:250,000-scale cross sections in Grose (1983) and Grose and Smith (1989),

EXPLANATION

Hydrogeologic units (some combined; modified from Workman, Menges, Page, Taylor, and others, 2002)

The 27 hydrogeologic units used in the hydrogeologic framework model are simplified by grouping into 10 hydrogeologic units in this figure.

- Younger alluvial aquifer/Older alluvial aquifer (YAA/OAA)
- Younger alluvial confining unit/Older alluvial confining unit (YACU/OACU)
- Cenozoic volcanics (11 combined units)
- Volcanic- and sedimentary-rock units (VSU)
- Sedimentary-rock confining unit (SCU)
- Upper clastic-rock confining unit (UCCU)
- Upper/lower carbonate-rock aquifer (UCA/LCA)
- Lower clastic-rock confining unit (LCCU)
- Crystalline-rock confining unit (XCU)
- Intrusive-rock confining unit (ICU)
- **Nevada Test Site**
- **Death Valley regional ground-water flow system model boundary**

Figure E–3. Outcrop of hydrogeologic units at the land surface for the Death Valley regional ground-water flow system region.

Figure E–4. Locations of boreholes and cross sections used to construct the hydrogeologic framework model.

6 were used as data input to the HFM (NCT1, NCT9, NCT10, NT7, NT8, and CT1). These cross sections portray the geology north of the NTS and the southern part of Death Valley and the Mojave Desert (see fig. A–1, this volume).

Of the 52 cross sections from the DOE/NV-UGTA model (IT Corporation, 1996a), 22 were used as data input to the HFM. These cross sections portray the hydrogeology of specific areas of the NTS at scales ranging from 1:12,000 to 1:100,000. These cross sections provide greater detail with regard to Cenozoic unit thickness and the location of faults in the Cenozoic stratigraphic sequence.

As a part of this study, 28 regional geologic cross sections of the DVRFS region were developed (Sweetkind and others, 2001); all were used as input to the HFM (fig. E–4). These cross sections, constructed at 1:250,000 scale, form a network across the central part of the model domain (fig. E–4). The cross sections were constructed on the basis of interpretive maps of geology (Workman, Menges, Page, Taylor, and others, 2002), tectonics (Workman, Menges, Page, Ekren, and others, 2002), aeromagnetics (Ponce and Blakely, 2001), isostatic gravity (Ponce and others, 2001), and the depth-to-basement (Blakely and Ponce, 2001).

To provide additional detail for the geologic formations that constitute the Crater Flat Group (Prow Pass, Bullfrog, and Tram Tuffs) in the vicinity of Yucca Mountain and Crater Flat, data on four cross sections that were developed from 1:50,000-scale mapping at Yucca Mountain (Potter, Dickerson, and others, 2002) were used as input for the HFM. These cross sections are similar to those constructed by Sweetkind and others (2001) but provide greater stratigraphic detail, especially within the Cenozoic volcanic-rock stratigraphy.

Three unpublished cross sections of southern Yucca Mountain and the northern Amargosa Desert that were developed by the USGS for the Yucca Mountain Project (YMP) (R.W. Spengler, written commun., 2001) were used as input data for the HFM. These cross sections incorporate detailed stratigraphic data for the Cenozoic rocks south and southeast of Yucca Mountain from the Nye County EWDP boreholes that were not available during construction of the other cross sections used in this study.

The lithostratigraphic units on the cross sections were correlated with the HGUs (table E–3) and used to extract horizontal (x,y) and altitude (z) coordinates for the HGU horizon along a given trace. The MGE software allowed the x,y,z coordinates of the HGU horizon on the cross sections to be extracted by merging and scaling the digital file of each cross section to fit its surface trace digitized from a map. Each cross section was queried to determine the altitudes of points spaced every 250 m horizontally along an HGU horizon and a series of files that contained x,y,z coordinates for each HGU horizon was exported.

Existing Geologic Framework Models

Several 3D geologic framework models have been constructed for various studies of areas in the region, primarily for the YMP and the Underground Test Area (UGTA) program. Data from three existing framework models were used in the HFM (fig. E–5): (1) Yucca Mountain Project geologic framework model (YMP-GFM) (Bechtel SAIC Company, 2002), (2) Pahute Mesa–Oasis Valley (PMOV) model (Bechtel Nevada, 2002), and (3) Silent Canyon caldera complex (SCCC) model (McKee and others, 2001). Data from these models provided greater detail of the geometry of Cenozoic volcanic-rock HGUs in areas critical to ground-water flow and provided more consistency between the regional HFM these local-scale models. Because of the scale of these models, they contain more detailed HGUs grouped into many of the regional HGUs. The gridded horizons from the group of local HGUs were merged into a single gridded horizon representing the regional HGU by comparing the individual local HGU grids with each other and selecting the highest altitude that occurs in each grid cell.

The YMP-GFM (Bechtel SAIC Company, 2002) is an interpretation of the geology at the proposed underground geologic repository for high-level radioactive waste at Yucca Mountain. The model represents an area of 168 km^2. The boundary of the YMP-GFM (fig. E–5) was chosen to provide a geologic framework over the area of interest for ground-water flow and radionuclide transport through the unsaturated zone.

The PMOV hydrostratigraphic model was constructed to portray subsurface geologic units at Pahute Mesa, a nuclear testing area at the NTS, and Oasis Valley, a ground-water discharge area downgradient from Pahute Mesa (fig. E–5). The model area covers more than 2,700 km^2 and is geologically complex (Bechtel Nevada, 2002). To build the PMOV model, a hydrostratigraphic interpretation was formulated using a structural model of the PMOV that subdivides the area into a series of structural blocks that may not be detectable from surface mapping (Warren and others, 2000). The model depicts the thickness, extent, and geometric relations of more than 40 HGUs, as well as all the major structural features that control them, including calderas and faults. Data from the PMOV were not used to modify the units for the UCA, UCCU, LCA, LCCU, and XCU (table E–4).

Examination of the regional ICU horizon revealed great differences between the cross-section data (Sweetkind and others, 2001) and the intrusive rock horizons from the PMOV model. The ICU surfaces of the PMOV model were strictly interpreted from gravity data (Bechtel Nevada, 2002), whereas the cross sections (Sweetkind and others, 2001) tended to be more conceptual. Because of this, ICU cross-section data from within the limits of the PMOV model were deleted to avoid conflicting data sets.

A 3D caldera model of the Silent Canyon caldera complex (SCCC) in the central part of Pahute Mesa based on gravity inversion, drill-hole data, and geologic mapping was constructed using a more traditional interpretation of the caldera structure as an alternative to the PMOV model (McKee and others, 2001). The traditional interpretation, which assumes a circular collapse feature to explain the caldera shape, is analogous to the structure and shape of other calderas worldwide (Lipman, 1984; Lipman 1997) and is consistent with gravity-model interpretations from Pahute Mesa (Hildenbrand and others, 1999). For the SCCC model, 47 Cenozoic stratigraphic

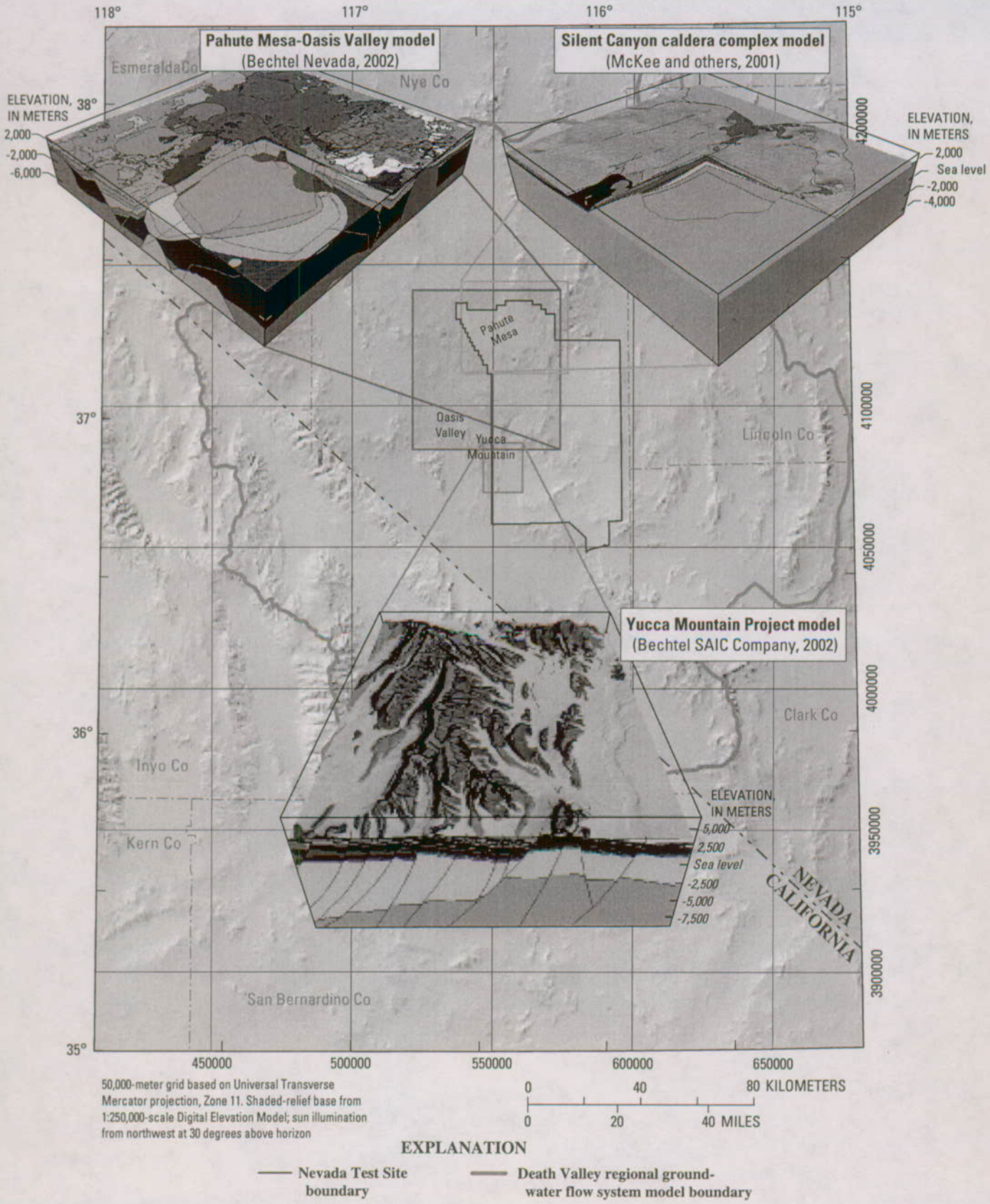

Figure E–5. Location and isometric views of local-scale geologic framework models used to construct the regional hydrogeologic framework model.

Table E–4. Correlation of units in the geologic framework models for Yucca Mountain, Pahute Mesa–Oasis Valley, Silent Canyon caldera complex, and the Death Valley regional ground-water flow system.

[DVRFS, Death Valley regional ground-water flow system; YMP-GFM, Yucca Mountain Project geologic framework model; PMOV, Pahute Mesa–Oasis Valley; SCCC, Silent Canyon caldera complex]

DVRFS hydrogeologic unit	YMP-GFM units (Bechtel SAIC Company, 2002)	PMOV hydrostratigraphic model units (Bechtel Nevada, 2002)	SCCC units (McKee and others, 2001)
Younger volcanic-rock unit (YVU)		YVCM	
Thirsty Canyon–Timber Mountain volcanic-rock aquifer (TMVA)		WWA, FCCU, TMA, THCM, THLFA, TMCM, FCA, FCCM, DVA, DVCM, TCVA	
Paintbrush volcanic-rock aquifer (PVA)	Tpbt2, Tpbt3, Tpbt4, Tpbt1, TpcLD, Tpcp, Tpcpv1, Tpcpv2, Tpcpv3, Tptf, Tptpll, Tptpln, Tptpmn, Tptpul, Tptpv1, Tptpv2, Tptpv3, Tptrl, Tptrn, Tptrv1, Tptrv2, Tptrv3, Pah, PostTivaNorth, RHH, Tiva_Rainier	PCM, PVTA, BA, UPCU, TCA, PLFA, LPCU, TSA	ba, lp, tca, tsa
Calico Hills volcanic-rock unit (CHVU)	Tac, Tacbt	CHCU, CHZCM, CHVCM, CHVTA	ch
Crater Flat–Prow Pass aquifer (CFPPA)	Tcplv, Tcplc, Tcpmd, Tcpuc, Tcpuv, Tcpbt	IA, CFCM, CFCU, KA	cf, ia
Crater Flat–Bullfrog confining unit (CFBCU)	Tcblv, Tcblc, Tcbmd, Tcbuc, Tcbuv, Tcbbt	BCU	bf
Crater Flat–Tram aquifer (CFTA)	Tctlv, Tctlc, Tctmd, Tctuc, Tctuv, Tctbt	Not used	
Belted Range unit (BRU)	Not used	BRA	br
Older volcanic-rock unit (OVU)	Not used	PBRCM	pbr
Intrusive-rock confining unit (ICU)	Not used	MGCU, SCICU, CHICU, CCICU, RMICU, ATICU, BMICU, SCVCU	

units shown on the geologic map of Wahl and others (1997), or encountered in drill holes on Pahute Mesa and classified by Warren and others (1998), were defined as aquifers, confining units, and composite units according to their hydrologic properties (table E–4).

Although the PMOV and the SCCC models used the same data, differences in modeled horizons reflect the different approaches in modeling geologic structures. The SCCC model better reflects the traditional interpretation of a caldera system, as opposed to the structural block model used in the PMOV model. As a result, the SCCC model horizons were used for the HGUs common to both models (BRU, CFBCU, CHVU, OVU, and PVA) within the boundary of the SCCC model.

Structures

Regionally important faults that influence ground-water flow were used in the construction of the DVRFS HFM (fig. E–6). Maps showing the surface expression of faults and other structures and cross sections showing faults were used to incorporate offsets in HGUs during the gridding process. For the purposes of the HFM, the structures were classified as: normal, strike-slip, detachment, caldera boundary, thrust, inferred thrust, or transverse zone (Potter, Sweetkind, and others, 2002). On the basis of these classifications, structures were incorporated into the HGUs that they affected (table E–2). Faults and other structures in the model area can dip at almost any angle, but most are high-angle faults (greater than 60 degrees). These high-angle faults are simplified in the HFM as vertical features.

Thrust faults can create a stratigraphic repetition of HGUs, which were incorporated in the HFM where they are thought to be hydrologically important. Because horizons must be represented as grids in the HFM, they cannot have multiple altitudes at a single location. Therefore, the repeated stratigraphy in thrusted areas was modeled by constructing a separate gridded surface of the overlying hanging wall part of the thrusted unit. In map view, the spatial extent of the perimeter of the thrust sheet was defined by combining the surface trace of the fault from Workman, Menges, Page, Ekren, and others (2002) and Potter, Sweetkind, and others (2002) (see fig. B–31, this volume) with the interpreted downdip extent of the thrust sheets from the cross sections (Sweetkind and others, 2001). For the purposes of the HFM, the trailing edge of the thrust was defined as the point at which the HGU is no longer stratigraphically repeated. Within this thrust boundary, the horizons were treated as defining unique additional HGU horizons for the LCA and LCCU (fig. E–7). The interpreted subsurface extents of nine thrust plates (see fig. B–31, this volume) were defined. The thrust plates were selected for their size, offset, and potential hydrologic importance in juxtaposing the regional aquifer and confining units. Although a number of other thrusts are known within the model boundaries (see Snow and Wernicke, 2000, and references cited therein), these were not treated explicitly in the HFM.

Figure E–6. Traces of structures represented in the hydrogeologic framework model.

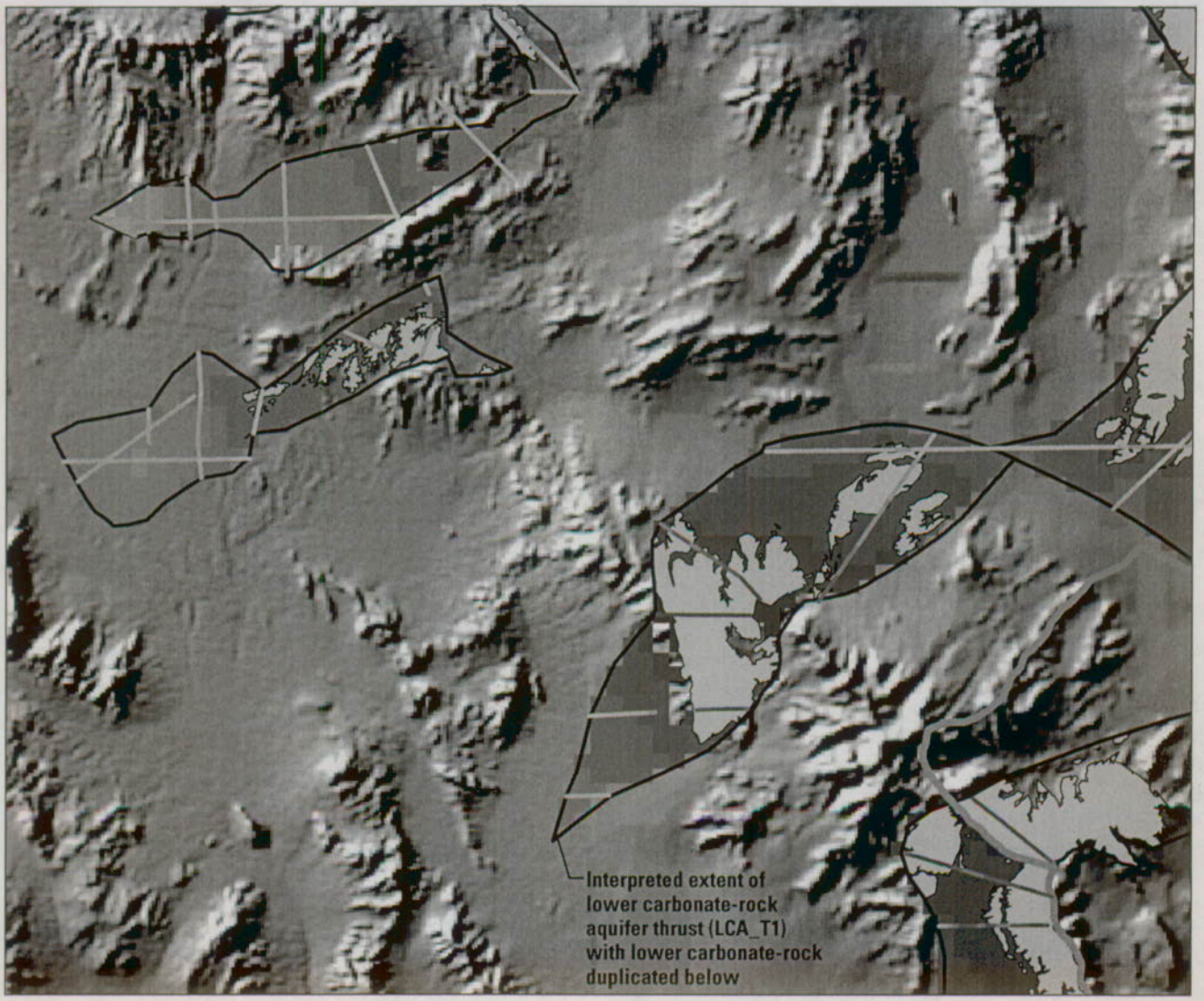

EXPLANATION

Extent of LCA_T1 on geologic map (modified from Workman, Menges, Page, Ekren, Taylor, and others, 2002; Sweetkind and others, 2001). Altitude data from digital elevation model (DEM).

Lower altitude — Higher altitude

Cross-section data, coded by depth (Sweetkind and others, 2001)

Lower altitude — Higher altitude

Altitude of gridded surface shown in purple

Thrust plate extent (Chapter B, this volume)

Death Valley regional ground-water flow system model boundary

Figure E–7. Example of the lower carbonate-rock aquifer thrust (LCA_T1), showing data sources and interpreted extents.

Gridding of Hydrogeologic Unit Horizons

The gridded surfaces defining the HGU horizons were interpolated and extrapolated from the available data and information. For all of the HGUs except for the YAA, YACU, OAA, and OACU, a hybrid gridding algorithm (Petrosys Pty. Ltd., 2003) was used to calculate the grid from the top surface of each HGU defined by the text files containing spatial coordinates from surface exposures, borehole lithologic logs, cross sections, and geologic models and by taking into account structural discontinuities from faulting (table E–2). The hybrid gridding algorithm is a combination of minimum curvature and first-order least-squares algorithms (Petrosys Pty. Ltd., 2003). It uses the first-order least squares algorithm within one grid cell of a fault and the minimum curvature algorithm to calculate all other grid cells. The minimum curvature algorithm involves several iterations to converge on an optimal grid definition by fitting a minimum curvature spline through the data points on either side of the point being calculated, thus preserving the rate of change of slope. The first-order least-squares algorithm fits a plane through the data points on either side of the model cell being calculated. The hybrid gridding process generates a coarse grid that is progressively refined with further iterations. During each iteration, the goodness-of-fit between the grid and the data was calculated to determine if more iterations were necessary. The effect of this iterative process caused a trendlike solution in areas of sparse data, though the grid accurately represented existing data points. Because the algorithms can extrapolate or interpolate grid cells that may be higher than land surface, each grid was limited by the topographic surface.

A clipping distance was applied to each gridded surface to limit the extent of extrapolation. These clipping distances varied for each interpreted gridded surface with assumed extents of the units and data density. The gridded surfaces were manually edited to clip areas where the gridding algorithms were judged to have over-extrapolated the HGU extents. As an example, figure E–8 presents an oblique view of the gridded surface of the LCA.

The accuracy of individual gridded surfaces depends on the available defining data and the complexity of the geologic unit being modeled. For example, because of their relatively simple geometry, planar bedded tuffs can be represented accurately with only a few data points, whereas faulted and folded rocks with more complex geometries are much more difficult to represent even with a large number of data points. Some gridded HGU surfaces were relatively well defined by numerous well-distributed data. Other gridded surfaces, such as those HGUs that crop out less, were less defined. In general, the lower an HGU is stratigraphically, the less defined it is, and the more structurally complex (Sweetkind and others, 2001).

In areas with more data, the computer-generated gridded surfaces generally are thought to be acceptable. In areas with sparse data, computer-generated gridding is more suspect. In these suspect areas, the gridded surfaces of all of the pre-Cenozoic HGUs were examined and compared with the altitude of the top of the pre-Cenozoic surface based on the gravity inversion model (Blakely and Ponce, 2001) and revised as necessary. All gridded surfaces were edited manually to ensure that they followed structural trends and honored faults, surface data, and subsurface data.

Gridded surfaces for the basin-fill units (YAA, YACU, OAA, and OACU) were defined on the basis of geologic map data and stratigraphic depositional rules. Owing to lack of lithologic information, these units are not defined in boreholes. The nearest-neighbor algorithm (Golden Software, Inc., 1997) was used to populate the grid. Each grid cell that had at least one basin-fill data point was attributed with the altitude of the point nearest the grid cell center. Because these basin-fill HGUs have an identifiable stratigraphic succession, a set of rules based on surficial stratigraphy in the area (table E–5) was developed to define the stratigraphic order and maximum thickness of each basin-fill HGU (E.M. Taylor, U.S. Geological Survey, written commun., 2002). In this scheme, the top of each basin-fill HGU is defined by outcrop, by stratigraphic order, and(or) defined thickness. Because the thickness of the actual basin-fill HGUs is unknown, the VSU was defined to fill in the remaining depth of the basin. Where the LA exists, the YACU was allowed to extend to a greater thickness.

Building the Model

The HFM was constructed in SGM by importing gridded surfaces to define the horizons of the HGUs that were stacked in stratigraphic sequence to form a 3D digital solid. The geometries of the ICU and the thrust plate units affected the stratigraphic order in which the HGUs were imported into the HFM. Because SGM is not designed to handle time-stratigraphic emplacement of intrusions (unit 6 in fig. E–9*A*), these features were inserted into the HFM out of their correct time sequence (unit 1 in fig. E–9*B*). Therefore, the youngest intrusion represented the lowest ("oldest") deposition surface. In the thrust fault areas, the overlying thrust horizons unit 5b in fig. E–9*B* were emplaced as a second step for the same HGU (unit 5a in fig. E–9*B*). Although neither of these accommodations for the geometries of the intrusions and the thrusted units affected the resulting model, it did affect the order in which they were put into the model. Table E–1 presents the order in which the HGUs were inserted (stacking order) to produce the HFM. Visualizations of the HFM as a fence diagram (fig. E–10) and a block diagram (fig. E–11) show the internal and external shape of the HGUs.

Evaluation of the Hydrogeologic Framework Model

The HFM was evaluated for accuracy by visual inspection and by mathematical manipulations of the gridded surfaces for extent and thickness of the HGUs. The HFM was compared to the known extent of HGUs, input cross sections, and other 3D framework models.

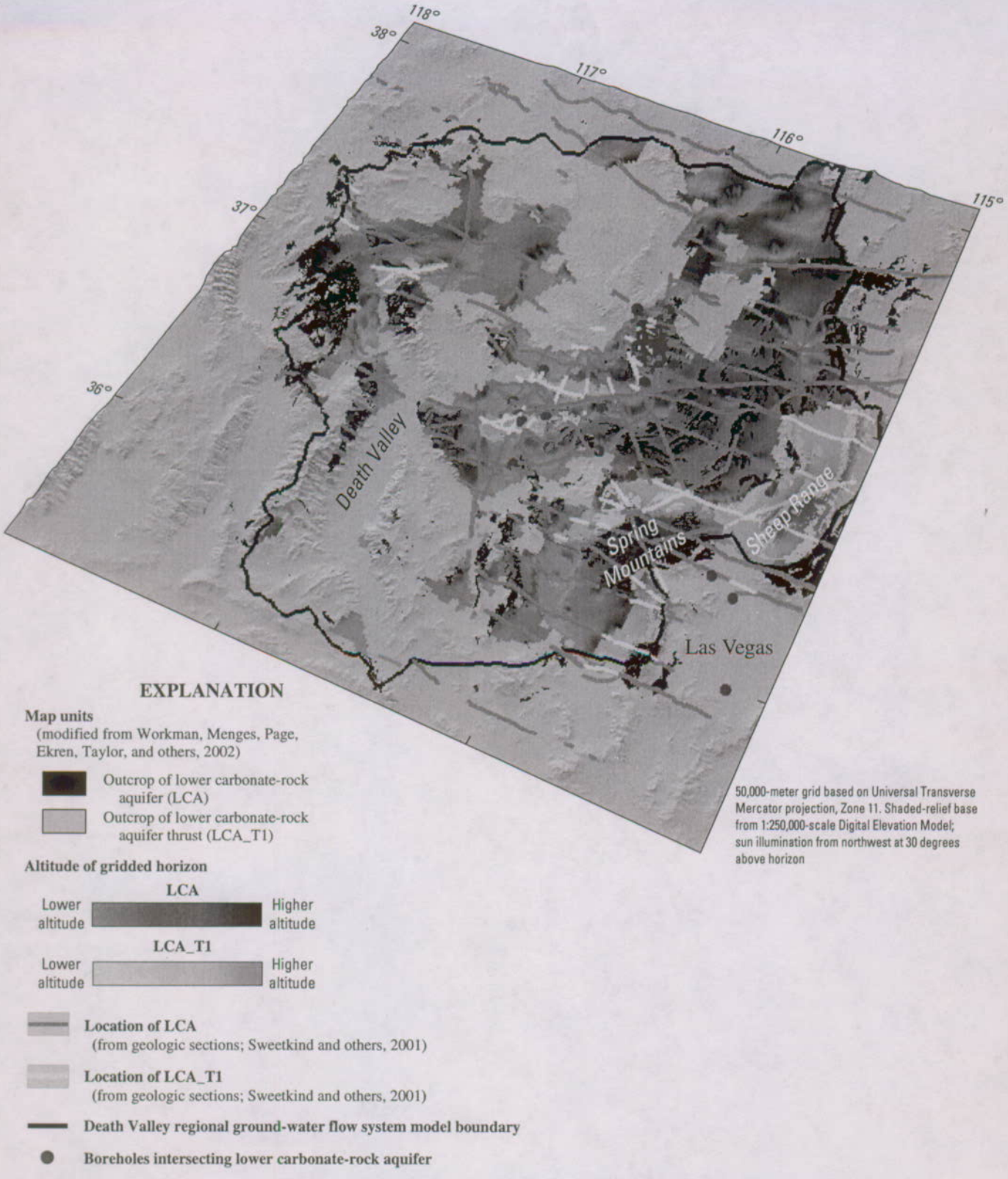

Figure E–8. Oblique view of gridded surface of the regional carbonate-rock aquifer with associated data sources.

Table E–5. Basin-fill hydrogeologic unit stratigraphic succession.

[Abbreviations: LA, limestone aquifer; OAA, older alluvial aquifer; OACU, older alluvial confining unit; VSU, volcanic- and sedimentary-rock units; YAA, younger alluvial aquifer; YACU, younger alluvial confining unit; >, greater than]

Surface hydrogeologic unit	Maximum thickness (meters)	Underlying hydrogeologic unit(s)
YAA	25	OAA, LA, VSU, or bedrock
YACU	25 (>25 where LA exists)	LA, VSU, or bedrock
OAA	45	LA, VSU, or bedrock
OACU	100	VSU or bedrock
LA	10	VSU or bedrock

Comparison of Gridded Surfaces with Known Extents of Hydrogeologic Units

Gridded surfaces of the HGU horizons were compared to the input data used to construct the surfaces to assess the accuracy of the gridding processes. Grids of unit thickness were constructed to examine areas of potential anomalous thickness. Comparing the gridded surfaces and thickness with the input data provided a suitable method of evaluating the representation of the HGUs in the HFM. Where necessary, a gridded surface was recalculated using different gridding algorithm settings (such as search radius and distance weighting) or manually edited to produce a more accurate match to known geologic conditions.

Comparison of Model Sections to Input Cross Sections

Visually comparing the vertical slices of the model along traces of the cross sections of Sweetkind and others (2001) (fig. E–5) with the input cross sections provided an acceptable method of evaluating the model representation (fig. E–12). On the basis of gross morphology, no discrepancies deemed geologically or hydrologically significant were recognized. The model sections retain the basic geometric characteristics from the input cross sections but typically did not include minor features. Discrepancies occurred mainly where HGUs are thin and undulating.

Comparison with Other 3D Framework Models

Comparing the surfaces from the input 3D models (YMP-GFM, PMOV, and SCCC) to the gridded surfaces from the HFM provided an acceptable method of evaluating the HFM representation. On the basis of gross morphology, reasonably good agreement between the input surfaces from other 3D models and the HFM surfaces was found and no discrepancies deemed geologically or hydrologically significant were identified. Although they were not directly input, the YMP/HRMP HFM (D'Agnese and others, 1997) and the DOE/NV-UGTA geologic model (IT Corporation, 1996a) were compared to the HFM. On the basis of gross morphology, reasonably good agreement between the HFM and these two previous HFMs was found.

Major differences between this HFM and previous HFMs are:

1. In the Emigrant Valley area (fig. A–1, this volume), the LCA most likely eroded prior to volcanic rock deposition (IT Corporation, 1996a, fig. G1–1). Potentiometric data show a steep hydraulic gradient between Emigrant Valley and Yucca Flat (fig. C–2, this volume). Calibration of both the DOE/NV-UGTA (IT Corporation, 1996b) and previous USGS flow models (D'Agnese and others, 1997; D'Agnese and others, 2002) was difficult with a carbonate-rock corridor present in this area. As a result, an alternative interpretation was used in this regional HFM that provides a partial barrier to southward flow by involving structurally higher LCCU instead of the thick carbonate-rock corridor.

2. In Penoyer Valley (fig. A–1, this volume), the DOE/NV-UGTA model has basin-fill sediments in overlying volcanic rocks which in turn overlie LCA (IT Corporation, 1996a). This configuration does not provide enough low-permeability rocks to support ground-water levels near the ground surface and produce the steep hydraulic gradient between Penoyer and Desert Valleys (fig. C–2, this volume). In order to simulate the steep hydraulic gradient, the DOE/NV-UGTA geologic model (IT Corporation, 1996a) was updated at Penoyer Valley with an underlying LCCU. This interpretation was included in this regional HFM.

3. Geologic information was incorporated in the regional HFM at Yucca Mountain by using the more recent YMP-GFM (Bechtel SAIC Company, 2002), mainly to help define the location of the volcanic-rock HGUs in greater detail than the previous models.

4. New information from the Nye County EWDP boreholes was incorporated along with new interpretations based on these data (R.W. Spengler, U.S. Geological Survey, written commun., 2002). A more abrupt termination of the volcanic rocks in the basin fill and more detailed definition of the basin fill south and east of Yucca Mountain are indicated.

5. The definition of the basement rocks (LCA and LCCU) at the Striped Hills southeast of Yucca Mountain (fig. A–1, this volume) in the regional HFM is based on the more recent interpretation of Potter, Dickerson, and others (2002). This interpretation portrays the LCCU as part of a series of imbricated thrusts, which may form a significant barrier to ground-water flow in the area.

6. The PMOV model further defines the geologic units in this area (Bechtel Nevada, 2002). The classic interpretation of a caldera system (McKee and others, 2001) is used in the regional HFM as opposed to the structural block model

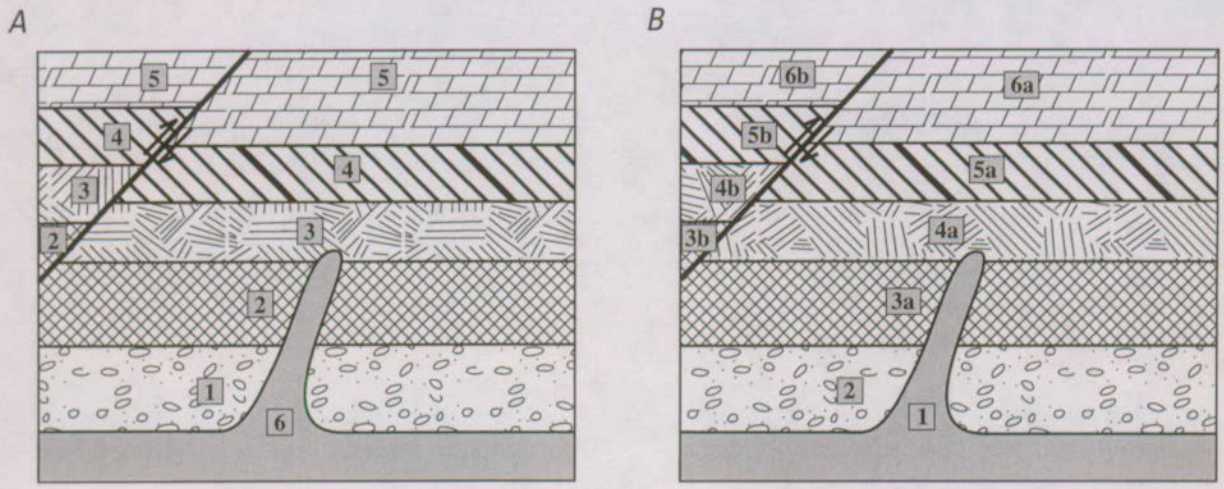

Figure E–9. Diagrams showing (*A*) time-stratigraphic and (*B*) model-construction order of geologic events.

(Warren and others, 2000) used by the DOE/NV-UGTA geologic model (IT Corporation, 1996a) and the PMOV model (Bechtel Nevada, 2002).

7. Recent drilling near Rainier Mesa (fig. A–1, this volume) has revealed the presence of the UCCU (Warren and others, 1998). Vertical hydraulic gradients in the boreholes in this area are an indication that the UCA is separated from the LCA. This regional HFM attempts to replicate this local stratigraphy.

8. The basin-fill HGUs have not been segregated much in previous models. The regional HFM splits the basin fill into seven units: YAA, YACU, OAA, OACU, LA, upper VSU, and lower VSU. This allows ground-water flow in the local and intermediate flow systems, where most of the ground-water development has occurred, to be defined in greater detail.

Revisions During Flow-Model Calibration

The flow modeling process also provided a mechanism to evaluate the HFM. These analyses were used in conjunction with independent hydrogeologic data to modify and improve the existing conceptual model, observation data sets, and weighting of the observations of the flow model (Chapter F, this volume). Modifications to the HFM were made only when supporting independent hydrogeologic criteria were identified, not simply to improve flow-model calibration.

Description of the Hydrogeologic Framework Model

The following describes the manner in which the HGUs were simulated in the HFM. This description includes the extent and thickness of the hydrogeologic units and key areas within the HFM.

Representation of Hydrogeologic Units in the Model

The HGUs as they are depicted in the HFM are described below. The extent and thickness of each HGU are those from the HFM and may differ somewhat from those described in Chapter B (this volume). The distribution of the data sources is shown in the "*A*" figures and the thickness of the HGU as simulated in the HFM is shown in the "*B*" figures.

Younger and Older Alluvial Aquifers (YAA and OAA)

The distribution of the younger alluvial aquifers (YAA) (fig. E–13*A*) and, to a lesser extent, the older alluvial aquifers (OAA) (fig. E–14*A*) is less in the HFM than shown in the surface exposures. The coarse grid resolution and stacking of HGUs from older to younger favors the older HGU in a grid cell when more than one unit is present. As a result, the YAA is often represented as a much smaller area where it does not cover an entire cell. The maximum thicknesses of the YAA and OAA in the HFM are 25 m and 45 m, respectively (figs. E–13*B* and E–14*B*).

Younger and Older Alluvial Confining Units (YACU and OACU)

The younger and older alluvial confining units (YACU and OACU, respectively) tend to be confining units and are restricted to the topographically lowest areas of structural basins in the DVRFS region. In particular, Death Valley, Pahrump Valley, and the Amargosa Desert have extensive deposits of YACU (fig. E–15*A*). Like the basin-fill aquifers, the distribution

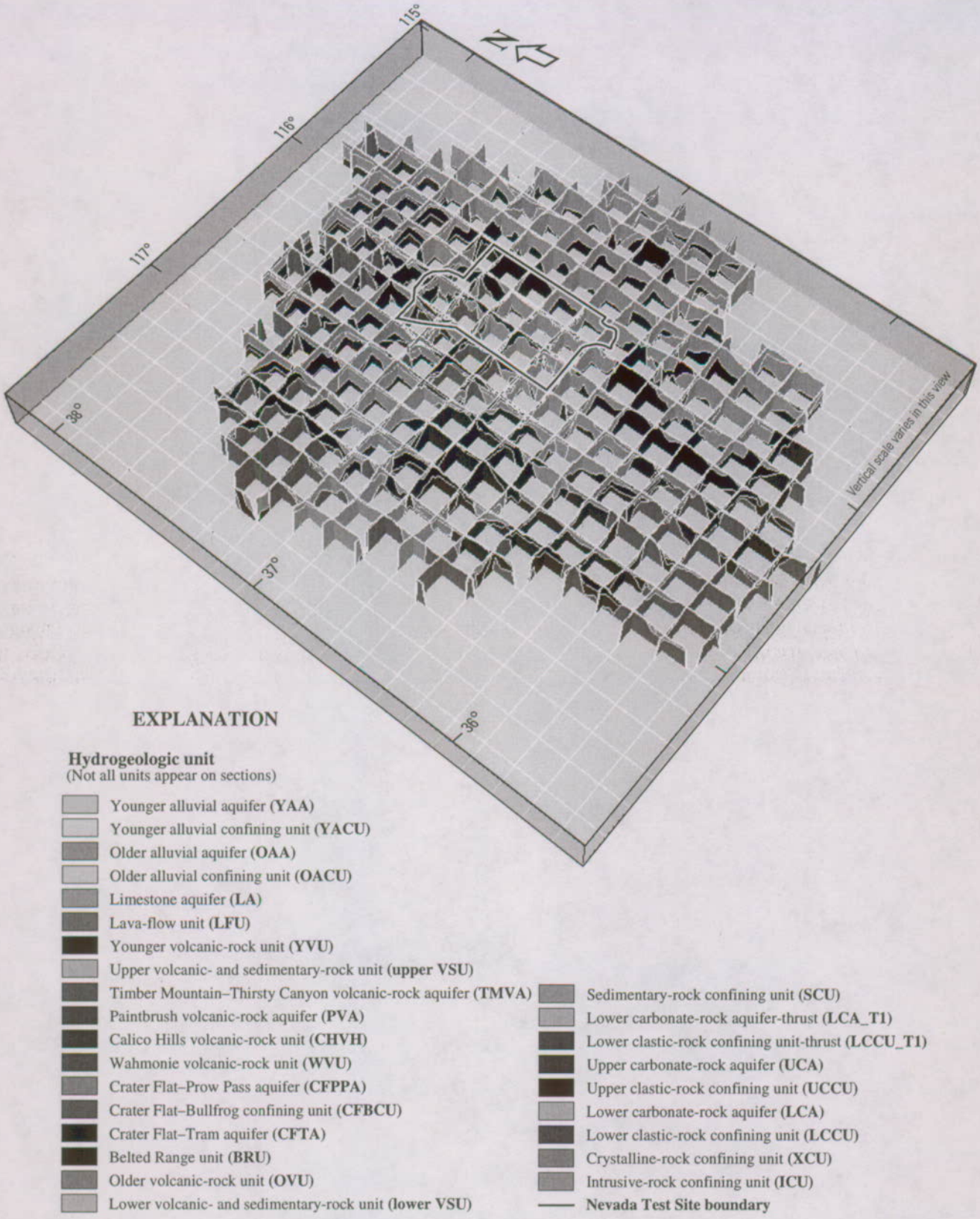

Figure E–10. Oblique view of three-dimensional hydrogeologic framework model in which a fence diagram shows the distribution of the hydrogeologic units.

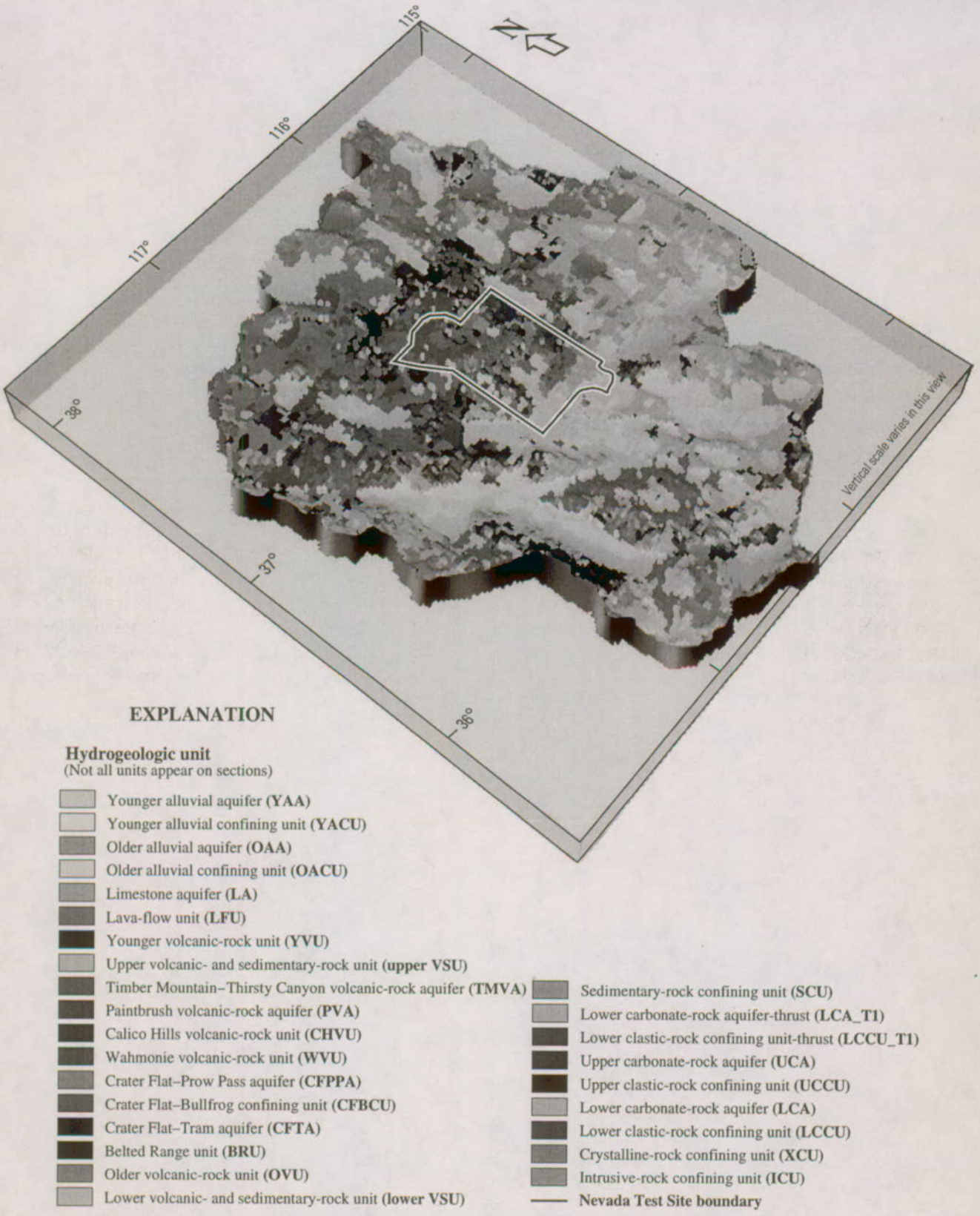

Figure E–11. Oblique view of three-dimensional hydrogeologic framework model in which a solid block shows the distribution of the hydrogeologic units.

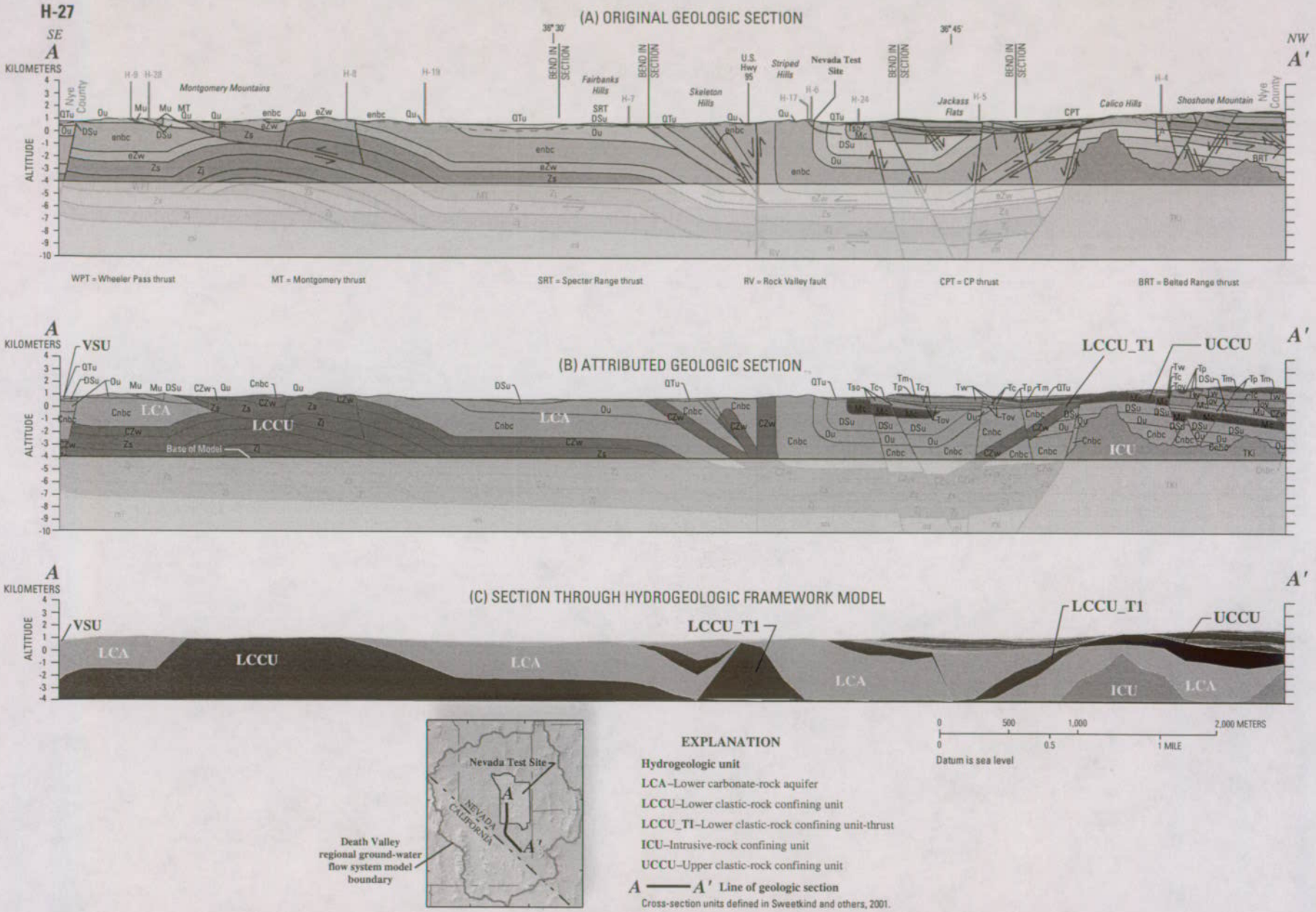

Figure E–12. Examples of (*A*) original input geologic section, (*B*) attributed geologic section, and (*C*) section through hydrogeologic framework model.

of the YACU (fig. E–15*A*) and, to a lesser extent, the OACU (fig. E–16*A*) is less in the HFM than shown in the surface exposure maps because an older HGU in a grid cell is favored when more than one unit is present. As a result, the younger HGUs are often represented as much smaller areas where they do not cover an entire cell. The YACU is defined with a maximum thickness of 25 m (table E–5 and fig. E–15*B*), except in the Amargosa Desert where the limestone aquifer (LA) exists and the YACU is defined to have thicknesses greater than 25 m. In this area, the maximum thickness of the YACU is about 160 m. Generally, the unit thickens along the axes of the deeper structural basins. The OACU is assumed to have a maximum thickness of 100 m (table E–5 and fig. E–16*B*) and only occurs in the northern part of Death Valley and in the area of Shoshone, Calif., and Tecopa, Calif.

Limestone Aquifer (LA)

The limestone aquifer (LA) is limited in areal extent to the Amargosa Desert and is known primarily through drilling records (fig. E–17*A*). The LA is assumed to have a maximum thickness of 10 m (fig. E–17*B* and table E–5), but may be thicker locally. Below the LA is either bedrock or the upper VSU. The LA was modeled as a relatively continuous unit in the Amargosa Desert but actually may be more discontinuous owing to its original lacustrine depositional environment and resulting overrepresentation in the HFM.

Lava-Flow Unit (LFU)

The individual lava flows that make up the lava-flow unit (LFU) are not laterally extensive (fig. E–18*A*) and reach a maximum thickness of about 900 m in the Greenwater Range (fig. E–18*B*). Most of the LFU is above the water table and has a limited influence on ground-water flow in the region. Where they are below the water table, fractures in the LFU can create locally productive aquifers.

Younger Volcanic-Rock Unit (YVU)

Most of the volcanic rocks making up the younger volcanic-rock unit (YVU) are localized within the SWNVF. The YVU is not laterally extensive and is most expansive northeast of Timber Mountain and at Black Mountain (fig. E–19*A*). The thickness of the YVU approaches 300 m (fig. E–19*B*). Most of the unit occurs above the water table and is thought to have limited influence on ground-water flow in the DVRFS model domain. Like the basin-fill aquifers and confining units, the extent of the YVU is less in the HFM than is indicated by the unit outcrop (fig. E–19*A*) because an older HGU in a grid cell is favored when more than one unit is present.

Volcanic- and Sedimentary-Rock Units (VSU)

The volcanic- and sedimentary-rock units (VSU) have been divided into upper and lower parts. In general, these two divisions are lithologically similar but are of different ages. The upper VSU and lower VSU encase the Cenozoic volcanic-rock units of the SWNVF.

The upper VSU is defined to lie above the Cenozoic volcanic rocks (fig. E–20*A*). Below it is either bedrock or lower VSU. Because the units are lithologically similar, in areas where the lower VSU lies directly beneath the upper VSU the contact between the units is arbitrary. The upper VSU has a maximum thickness of about 2,700 m and reaches thicknesses greater than 1,000 m at the northern and southern parts of Death Valley and Cactus Flat (fig. E–20*B*).

The lower VSU lies below the basin-fill HGUs or the upper VSU, and the Cenozoic volcanic rock HGUs (fig. E–21*A*). Below the basin-fill units and upper VSU, the top of the lower VSU is arbitrary. Where the lower VSU is present below the volcanic-rock unit HGUs, it is defined as being 50 m below the top surface of the stratigraphically lowest volcanic-rock HGU defined in the area and fills the space below the volcanic rocks and above the Paleozoic bedrock. In most of the SWNVF and the northern part of the model domain, the lower VSU represents the deeply buried older volcanic-rock units. As a result of this arbitrary definition, this HGU is as thick as about 5,500 m in many areas of the model domain (fig. E–21*B*).

Thirsty Canyon–Timber Mountain Volcanic-Rock Aquifer (TMVA)

The Thirsty Canyon–Timber Mountain volcanic-rock aquifer (TMVA) is extensive and covers most of the SWNVF, reaching into the northern end of the Amargosa Desert (fig. E–22*A*). Thicknesses exceeding 500 m occur at Pahute Mesa and in the vicinity of Timber Mountain (fig. E–22*B*). The TMVA reaches a maximum thickness of about 2,600 m within its source caldera at Timber Mountain.

Paintbrush Volcanic-Rock Aquifer (PVA)

Like the basin-fill units, the distribution of the Paintbrush volcanic-rock aquifer (PVA) in the HFM (fig. E–23*A*) is less than is shown by the borehole data in western Yucca Flat because the older units dominate where the PVA does not cover an entire cell. Thick accumulations of intracaldera PVA are present to the north of Yucca Mountain, where it reaches thicknesses of nearly 2,400 m (fig. E–23*B*); however, the PVA at Yucca Mountain and eastern and central Pahute Mesa is generally above the water table. Conversely, the PVA is below the water table in western Pahute Mesa, east and south of Yucca Mountain, and in Crater Flat.

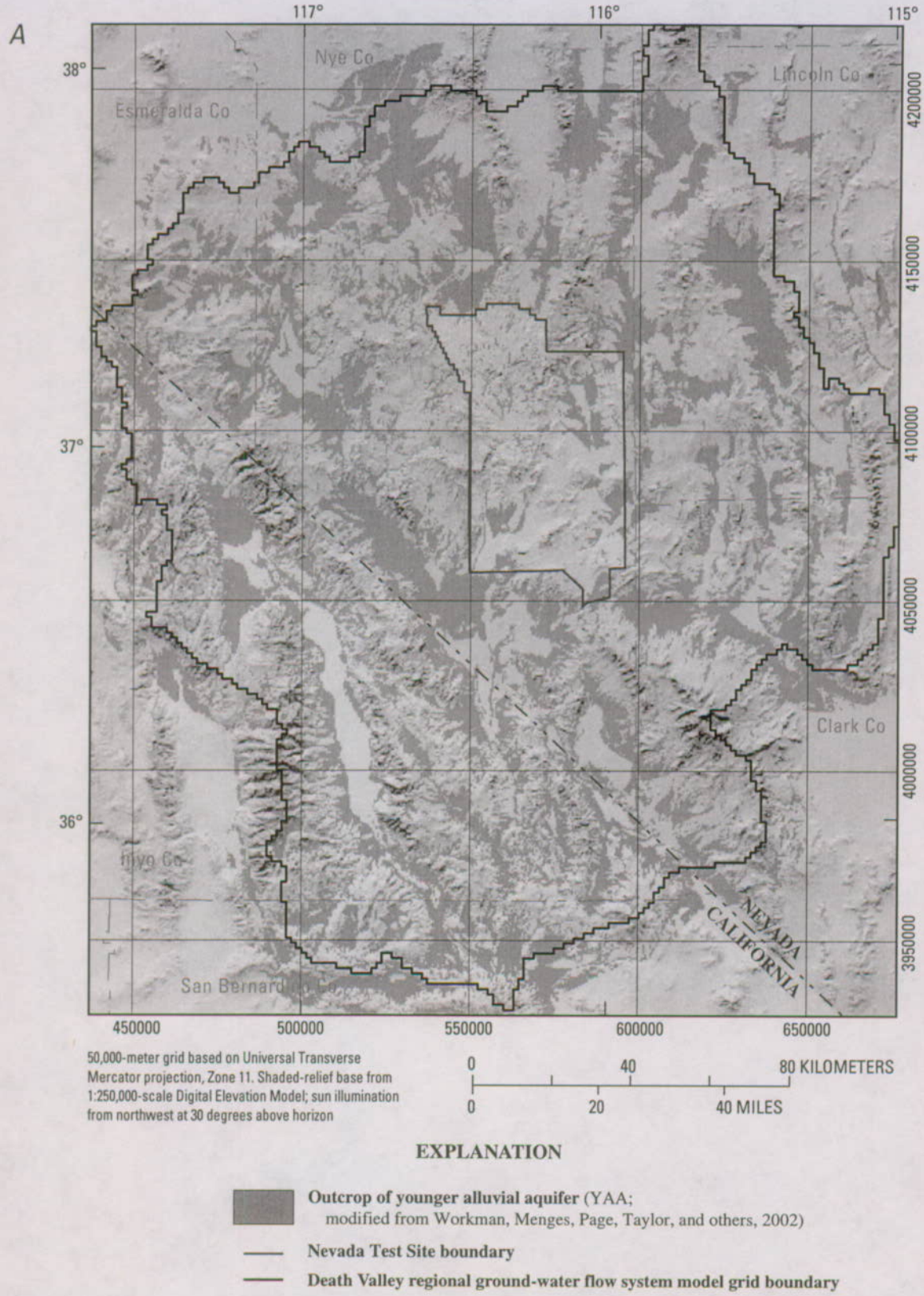

Figure E–13. (*A*) Data sources and (*B*) thickness of younger alluvial aquifer.

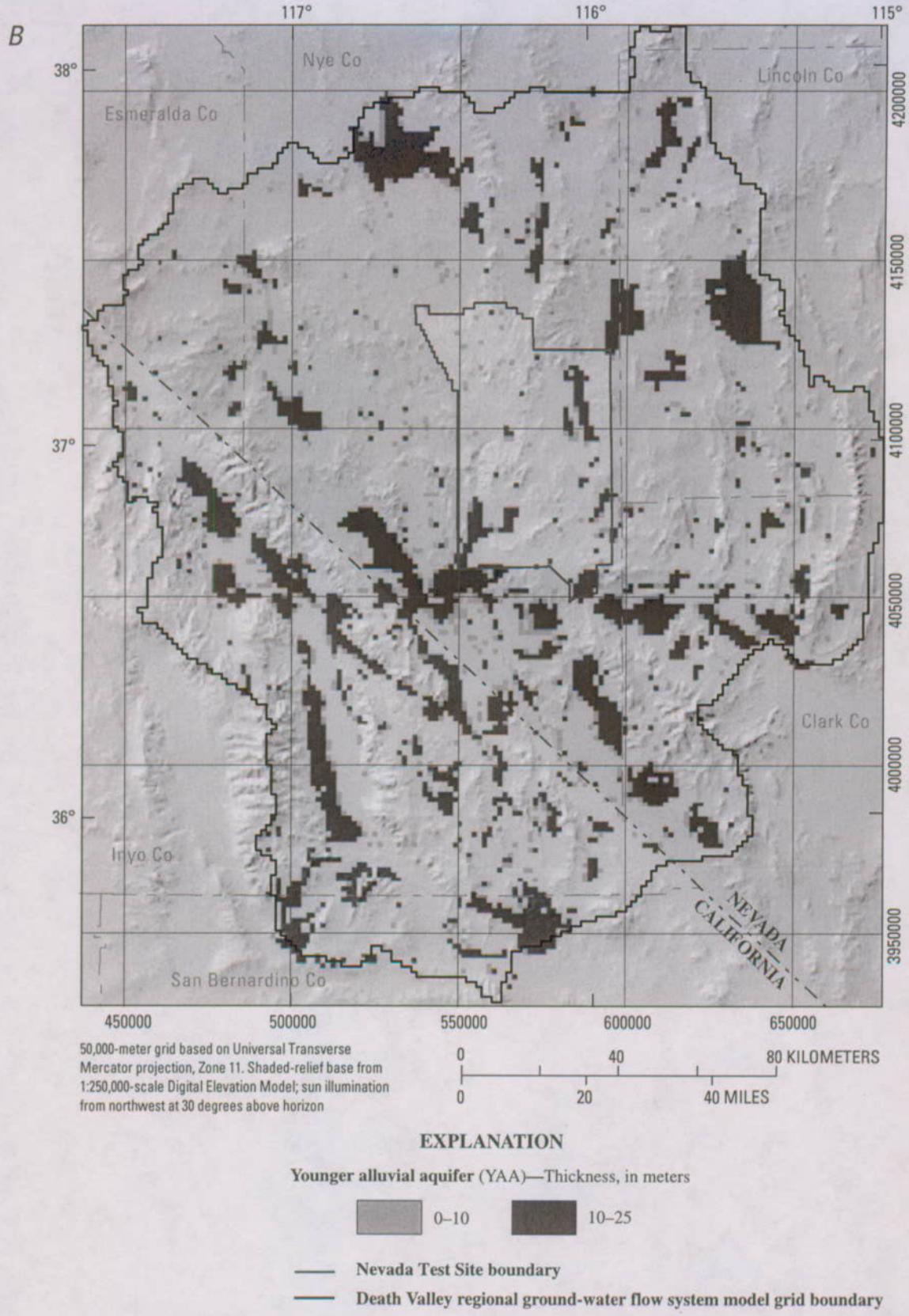

Figure E–13. (*A*) Data sources and (*B*) thickness of younger alluvial aquifer.—Continued

Figure E–14. (*A*) Data sources and (*B*) thickness of older alluvial aquifer.

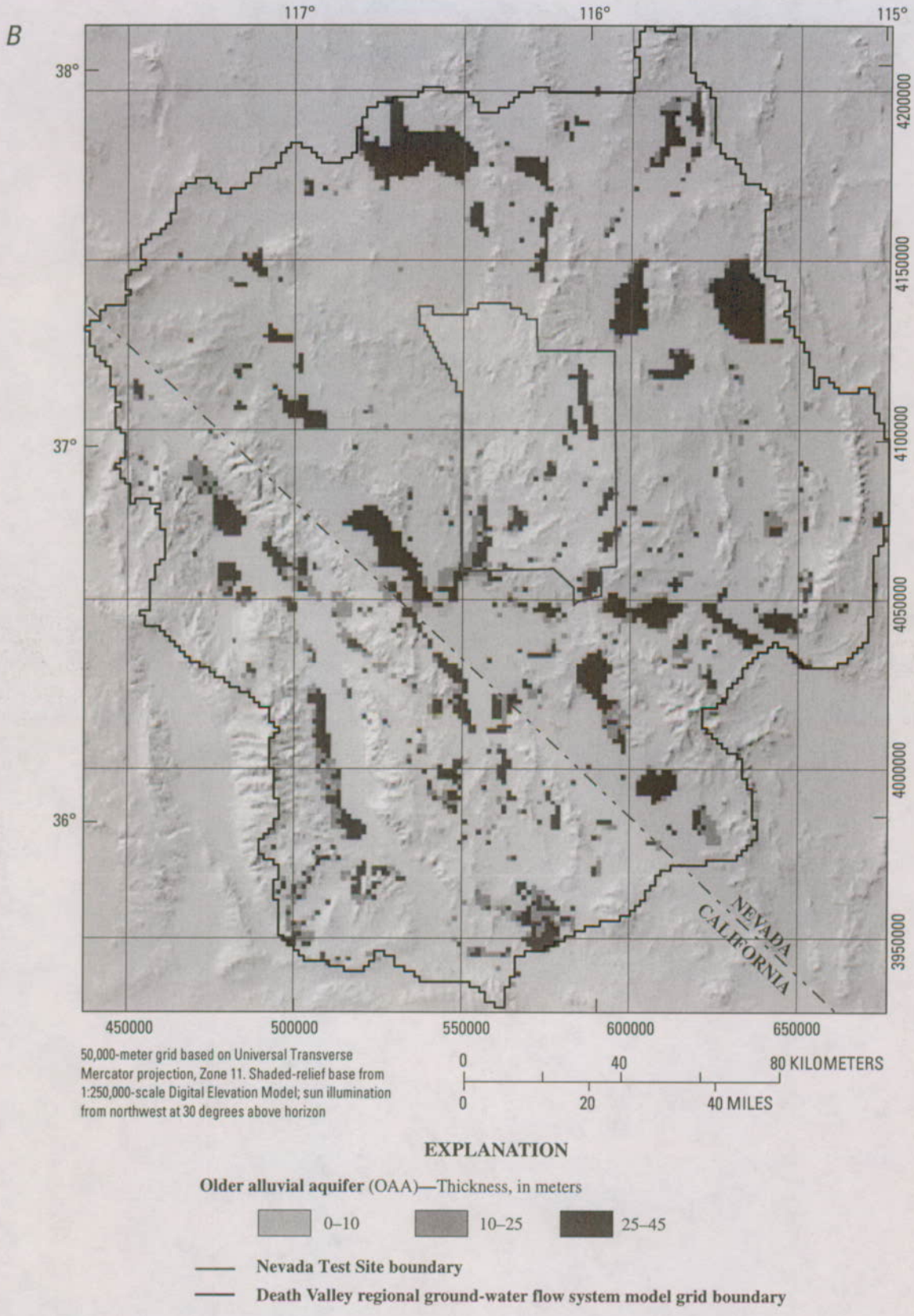

Figure E–14. (*A*) Data sources and (*B*) thickness of older alluvial aquifer.—Continued

Figure E–15. (*A*) Data sources and (*B*) thickness of younger alluvial confining unit.

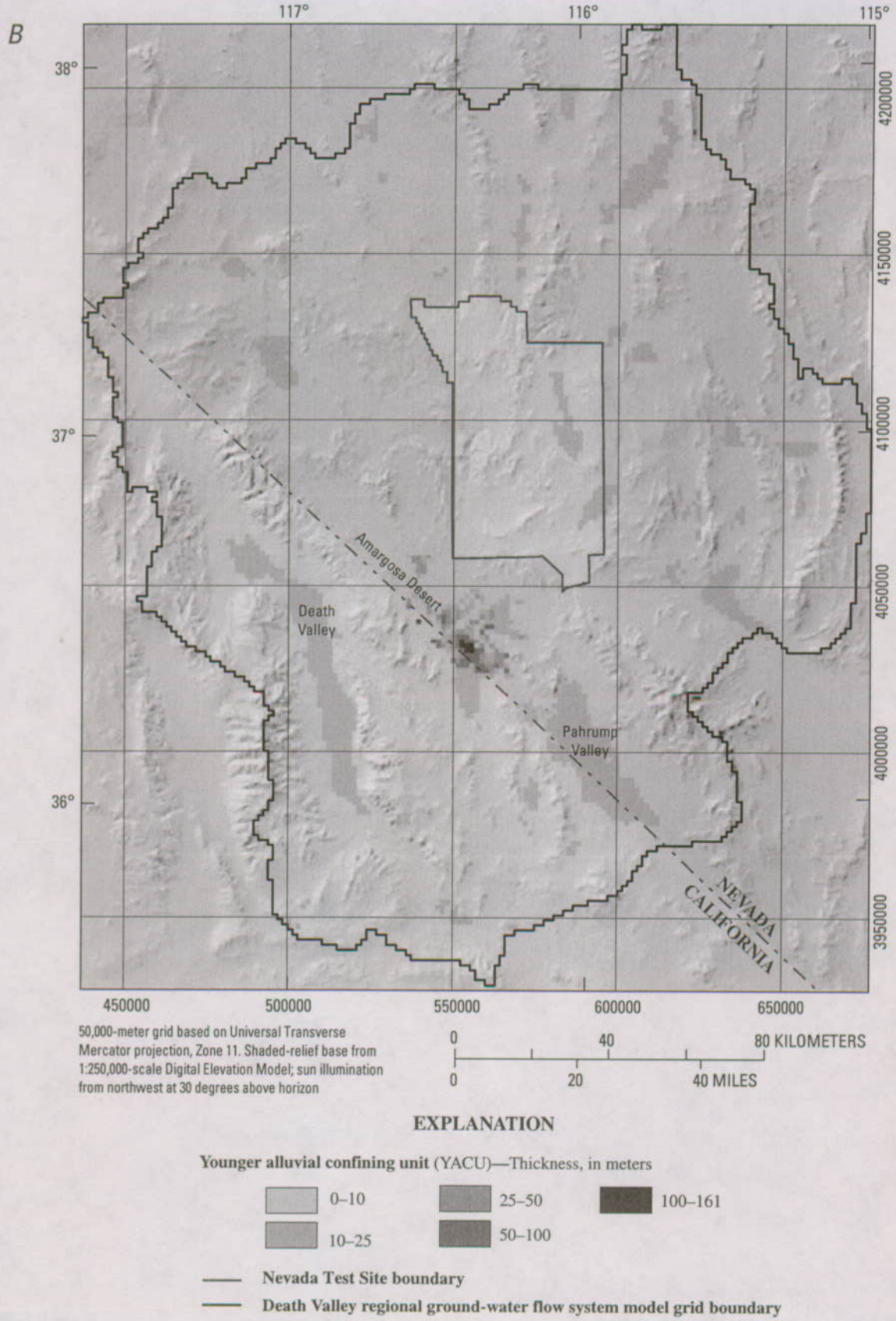

Figure E–15. (*A*) Data sources and (*B*) thickness of younger alluvial confining unit.—Continued

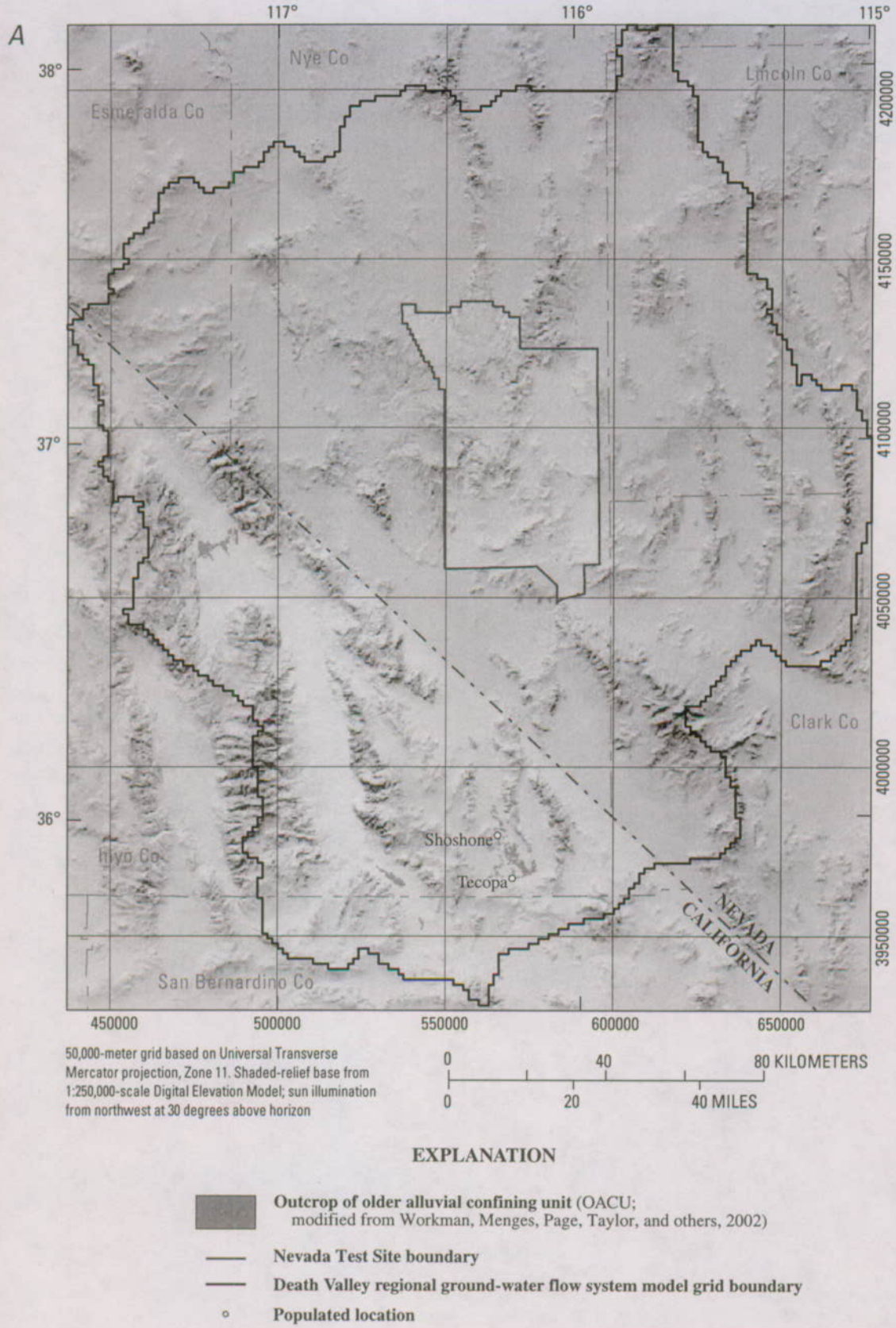

Figure E–16. (*A*) Data sources and (*B*) thickness of older alluvial confining unit.

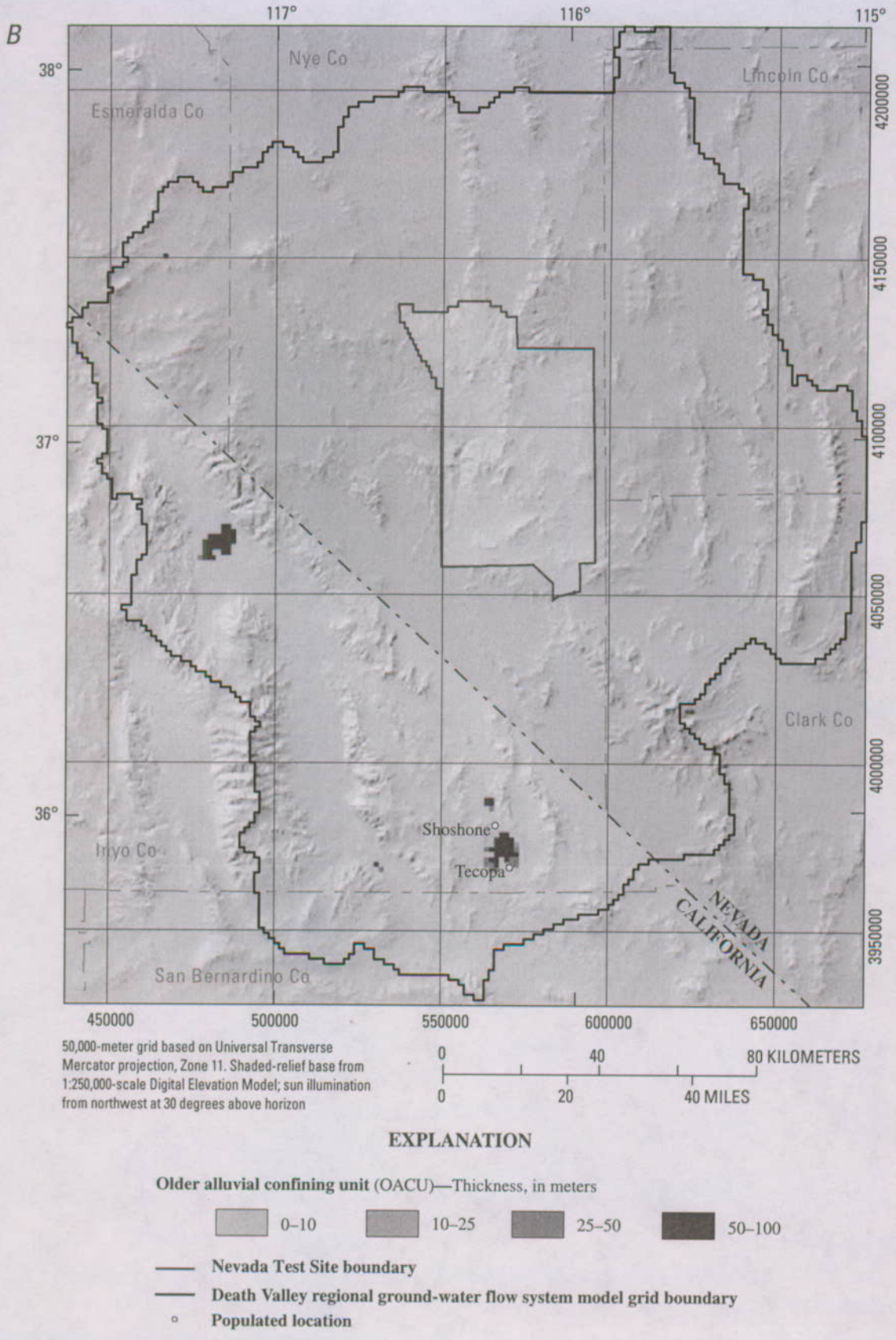

Figure E–16. (*A*) Data sources and (*B*) thickness of older alluvial confining unit.—Continued

Figure E–17. (*A*) Data sources and (*B*) thickness of limestone aquifer.

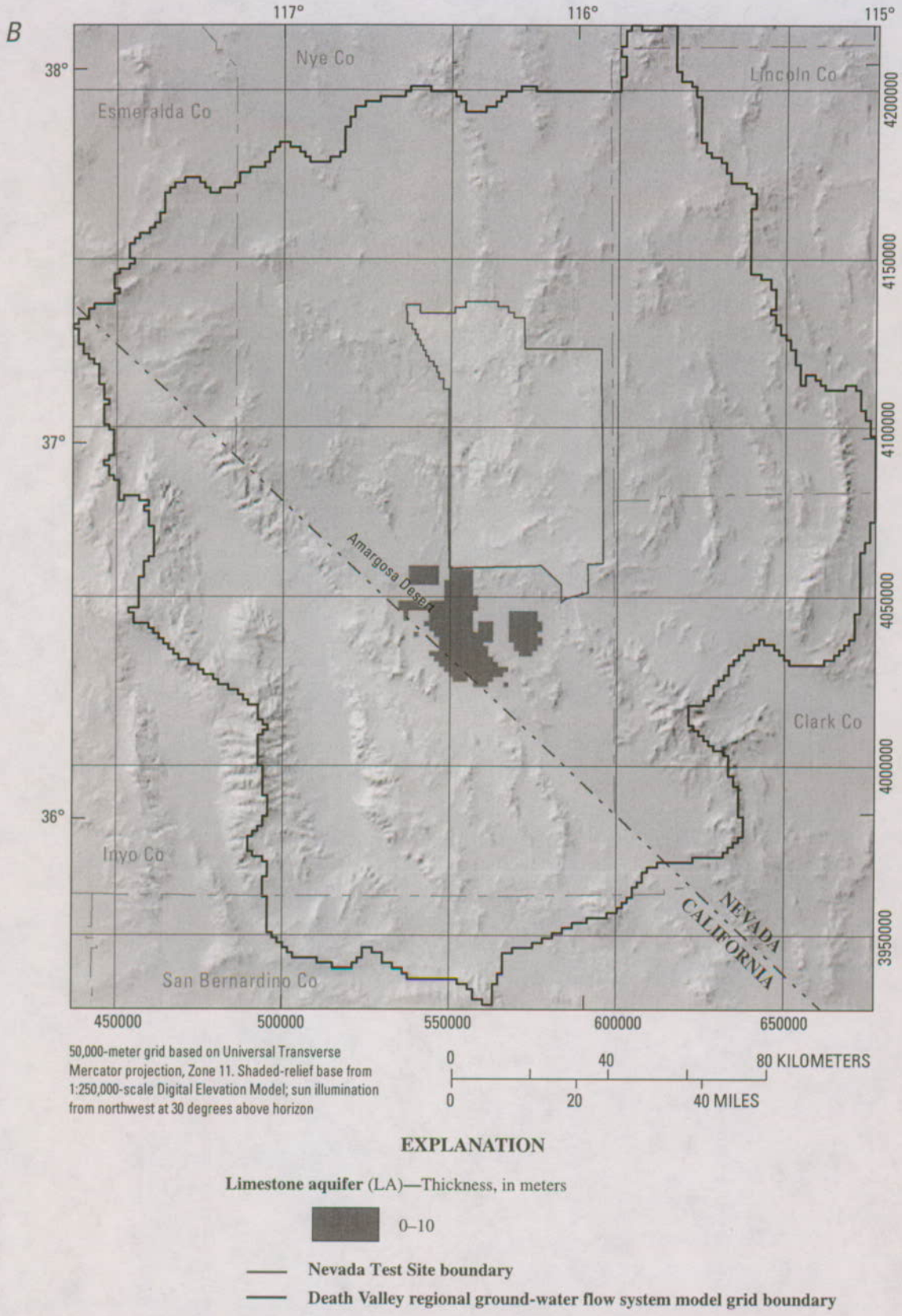

Figure E–17. (*A*) Data sources and (*B*) thickness of limestone aquifer.—Continued

Figure E–18. (*A*) Data sources and (*B*) thickness of lava-flow unit.

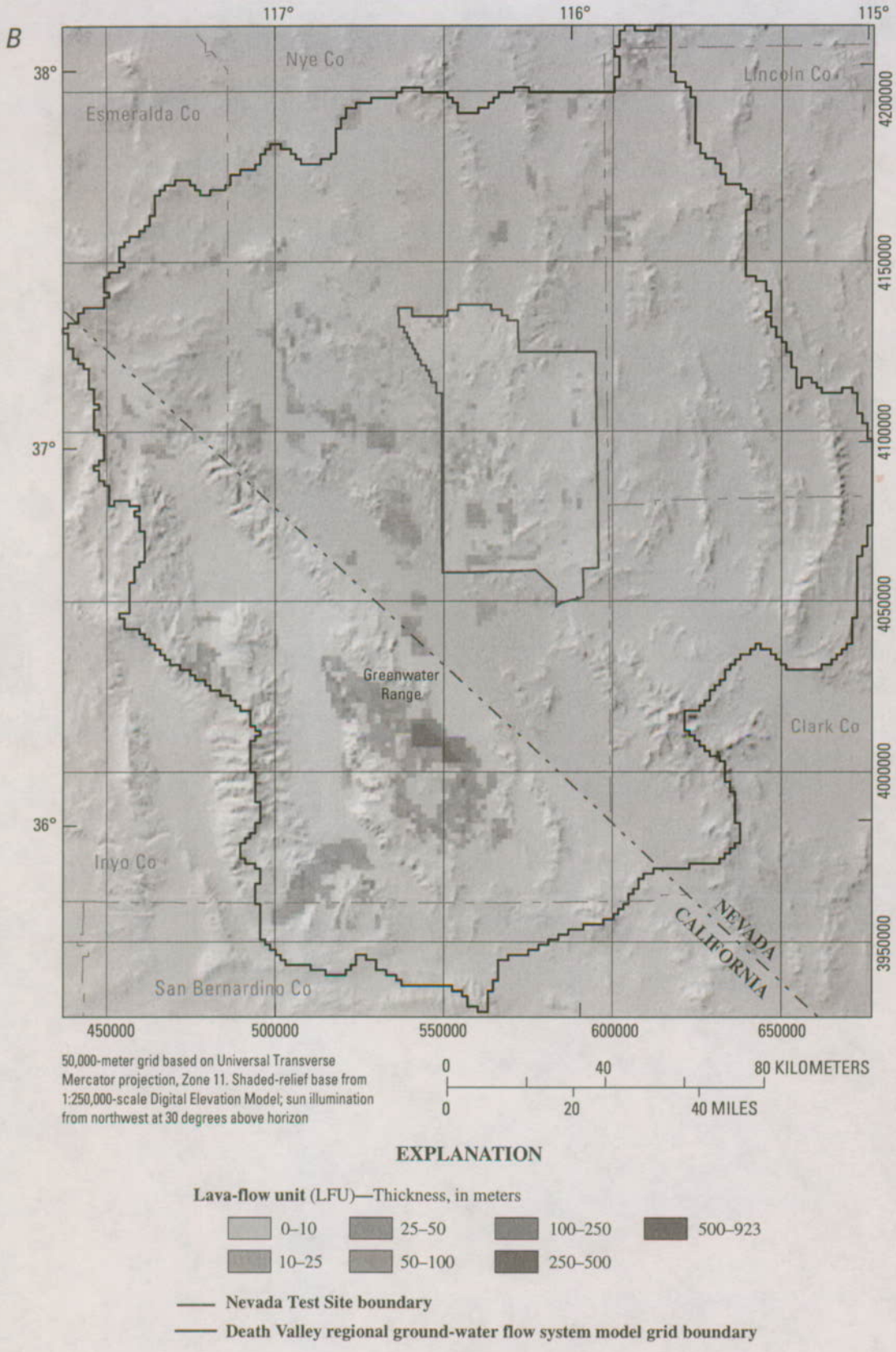

Figure E–18. (*A*) Data sources and (*B*) thickness of lava-flow unit.—Continued

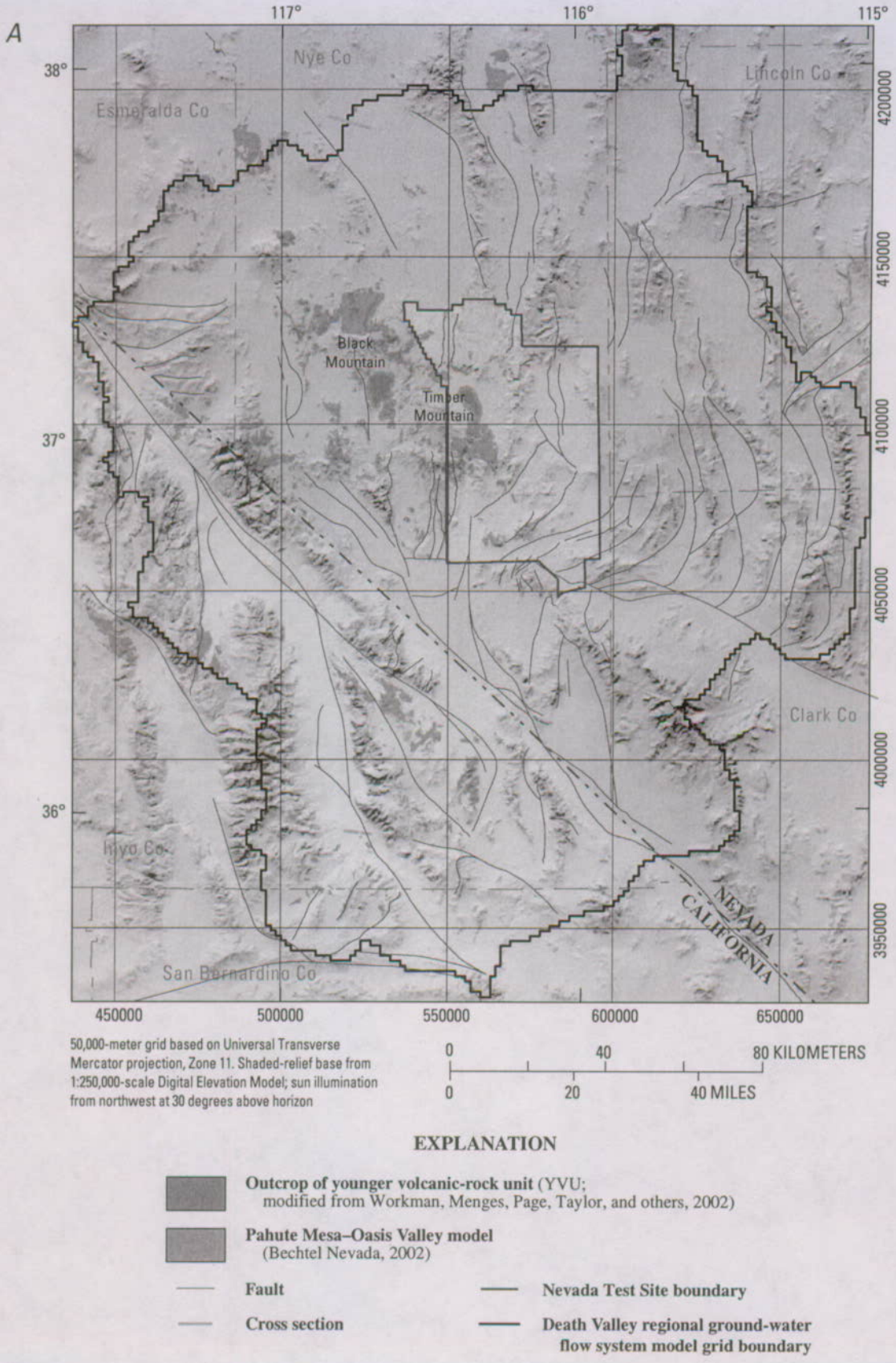

Figure E–19. (*A*) Data sources and (*B*) thickness of younger volcanic-rock unit.

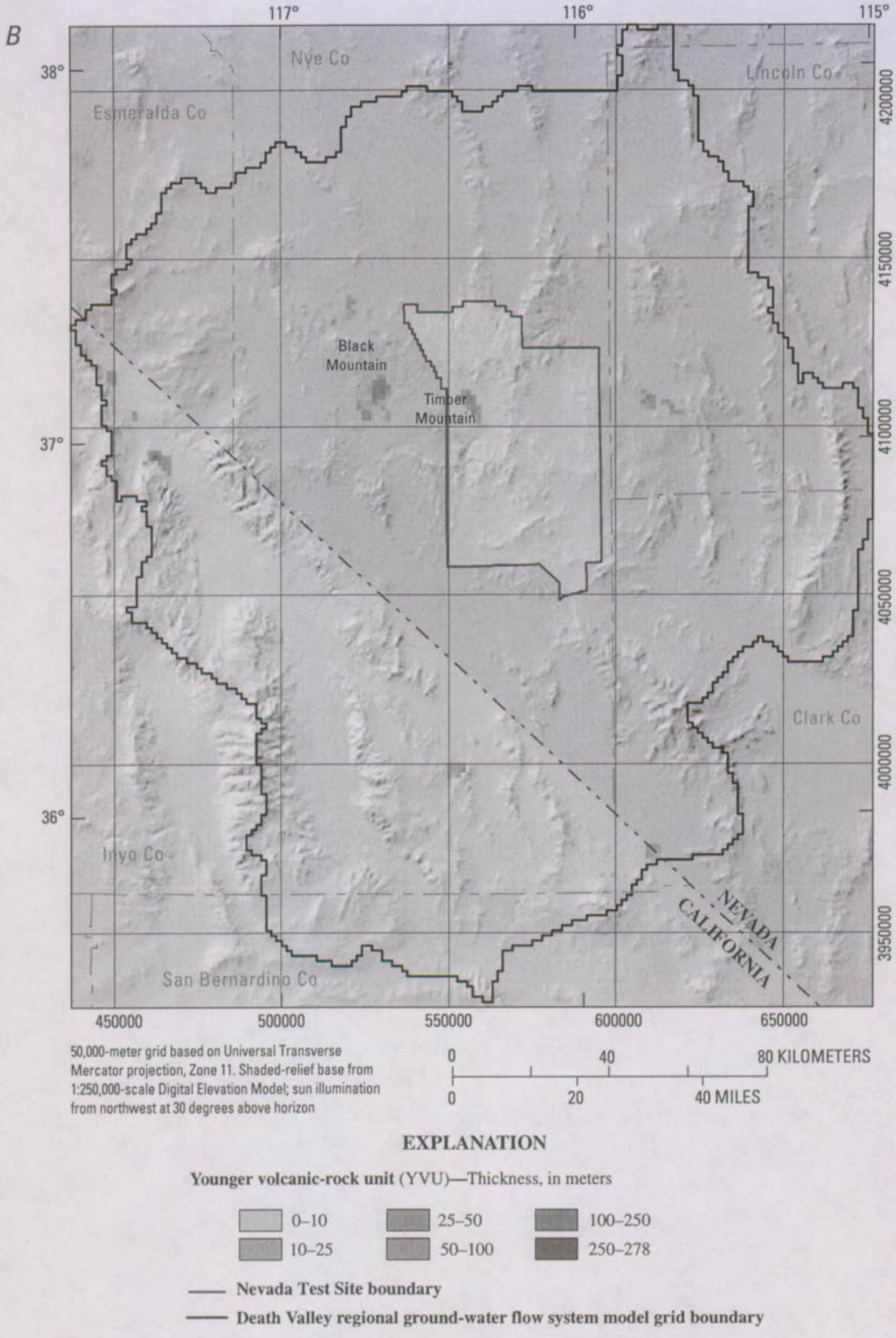

Figure E–19. (*A*) Data sources and (*B*) thickness of younger volcanic-rock unit.—Continued

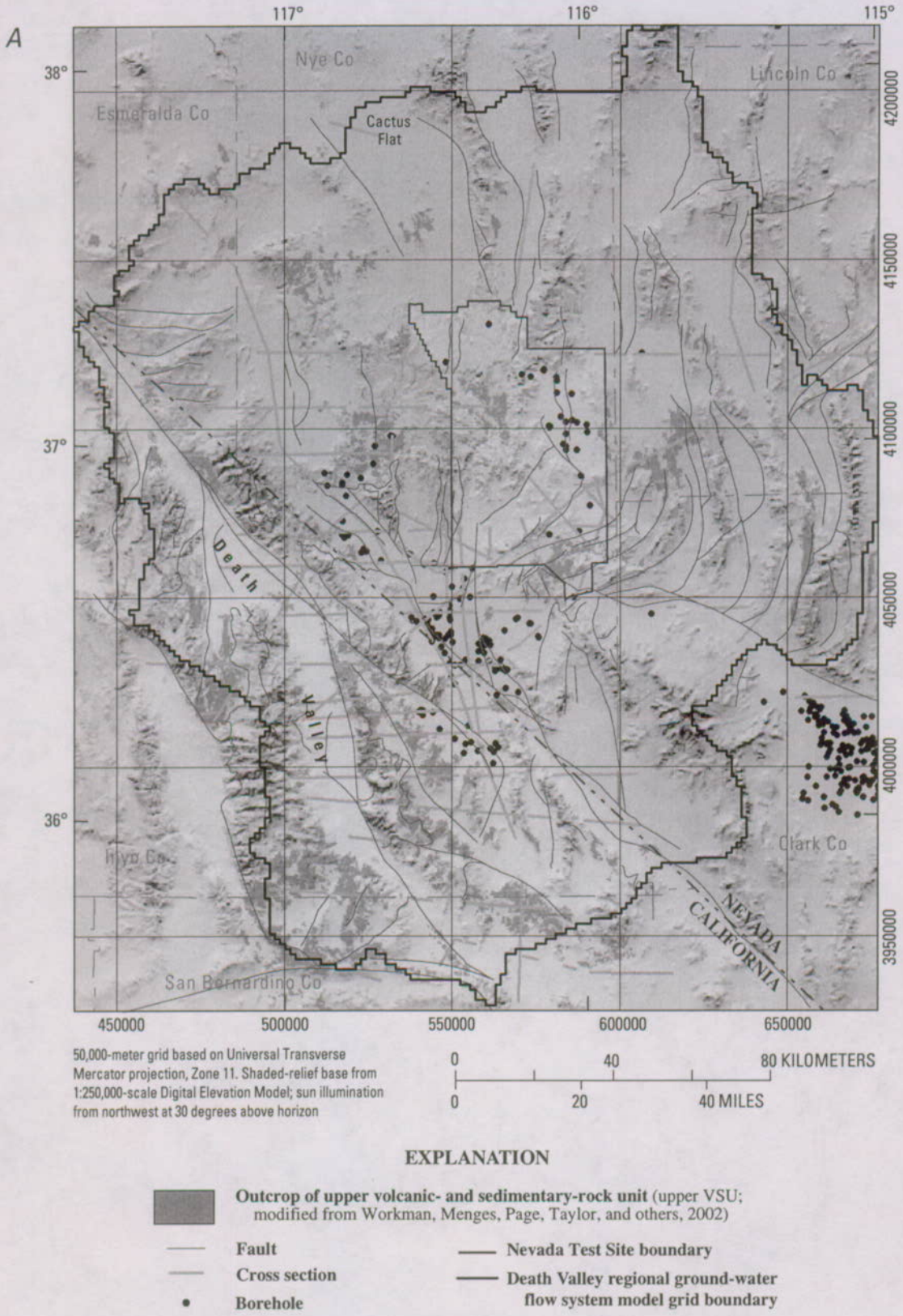

Figure E–20. (*A*) Data sources and (*B*) thickness of upper volcanic- and sedimentary-rock unit.

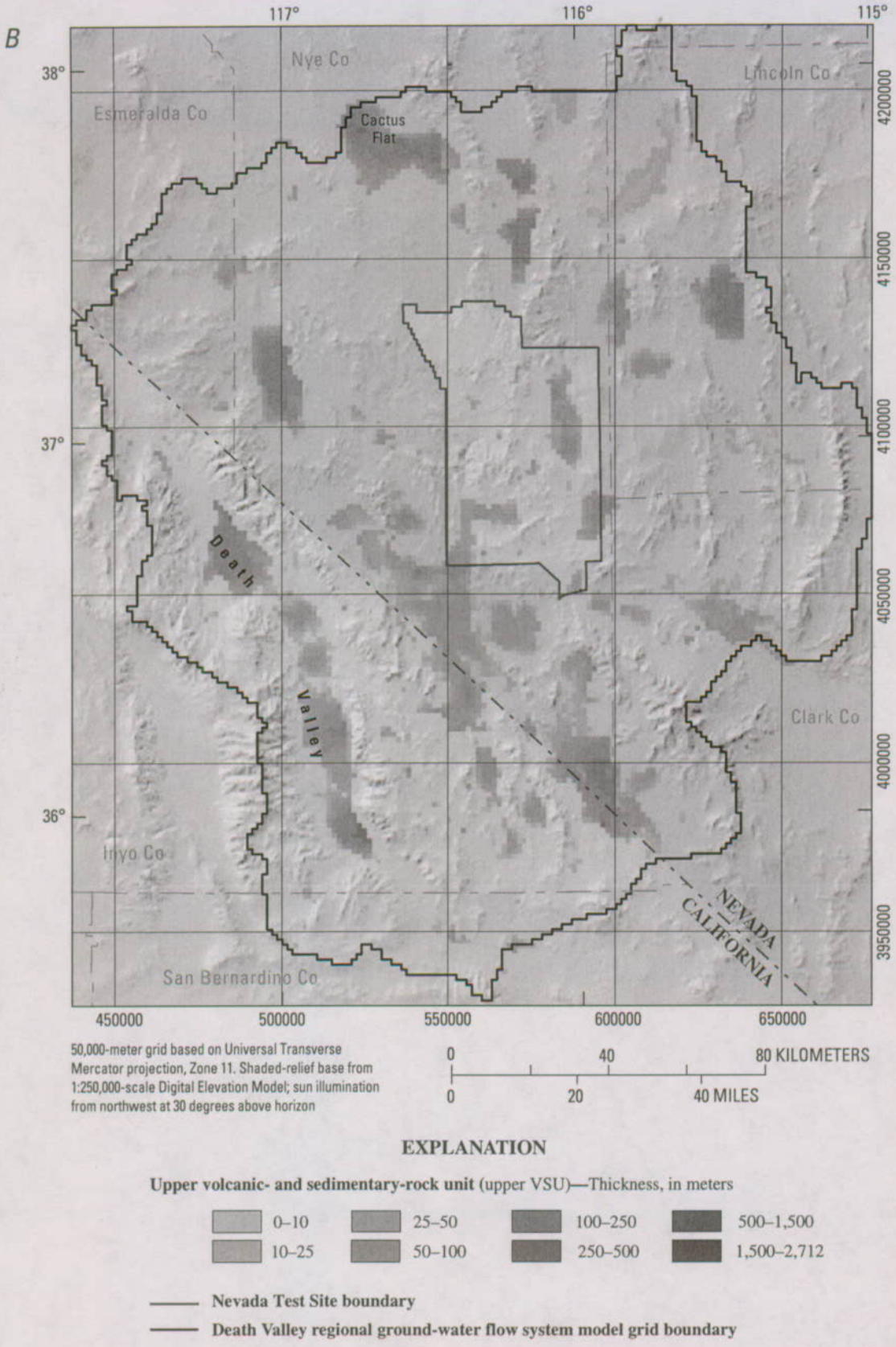

Figure E–20. (*A*) Data sources and (*B*) thickness of upper volcanic- and sedimentary-rock unit.—Continued

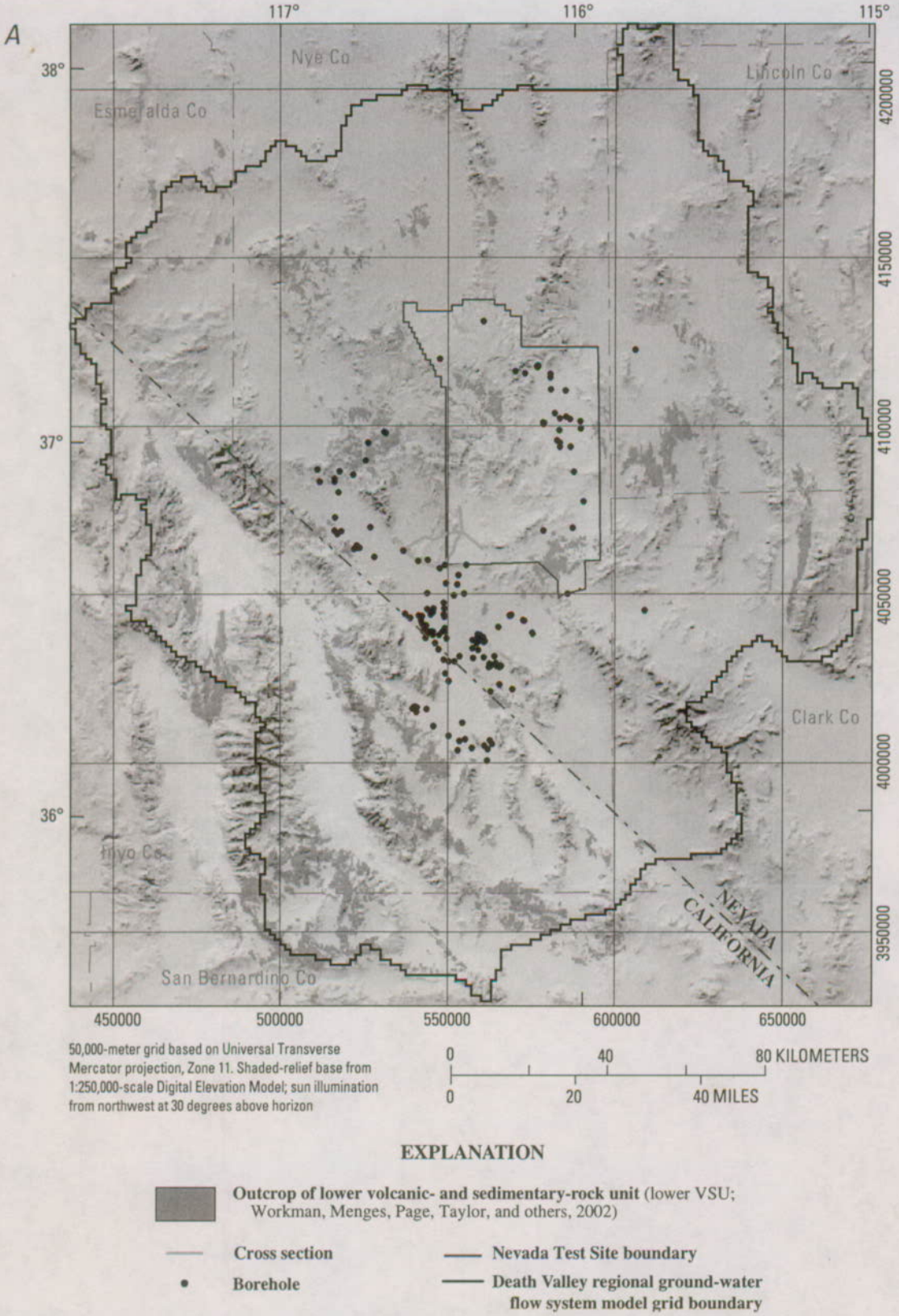

Figure E–21. (*A*) Data sources and (*B*) thickness of lower volcanic- and sedimentary-rock unit.

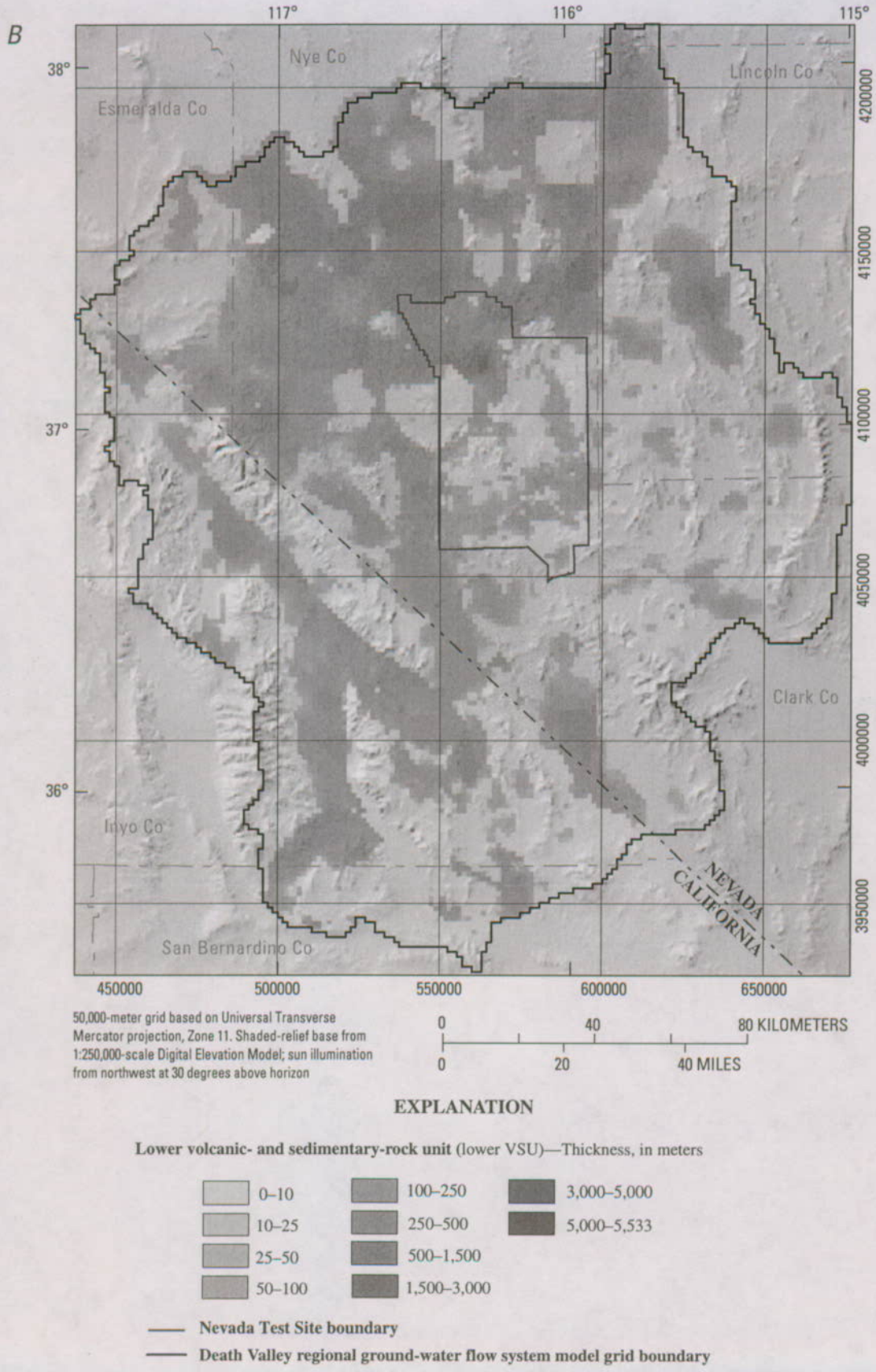

Figure E–21. (*A*) Data sources and (*B*) thickness of lower volcanic- and sedimentary-rock unit. —Continued

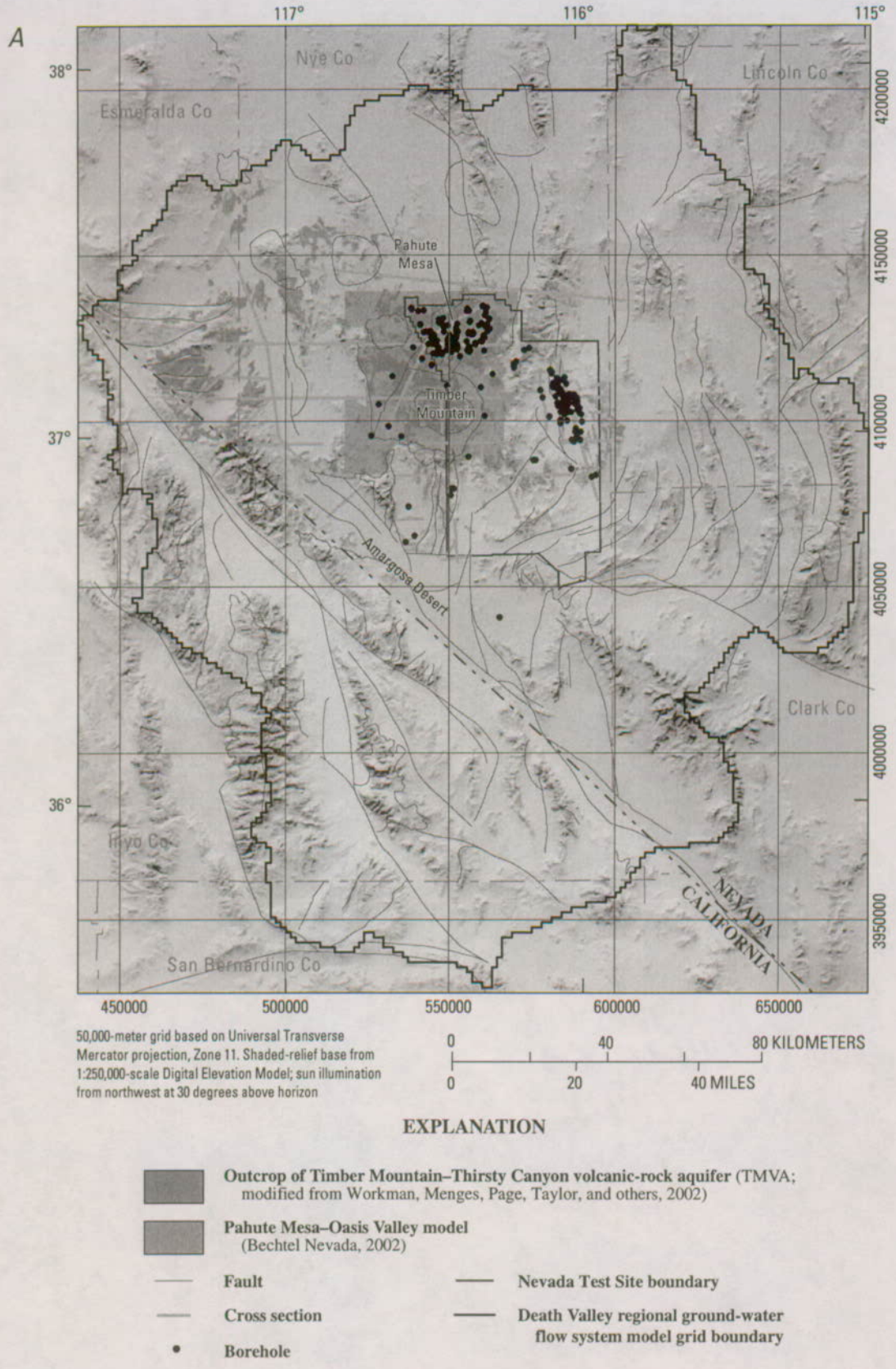

Figure E–22. (*A*) Data sources and (*B*) thickness of Thirsty Canyon–Timber Mountain volcanic-rock aquifer.

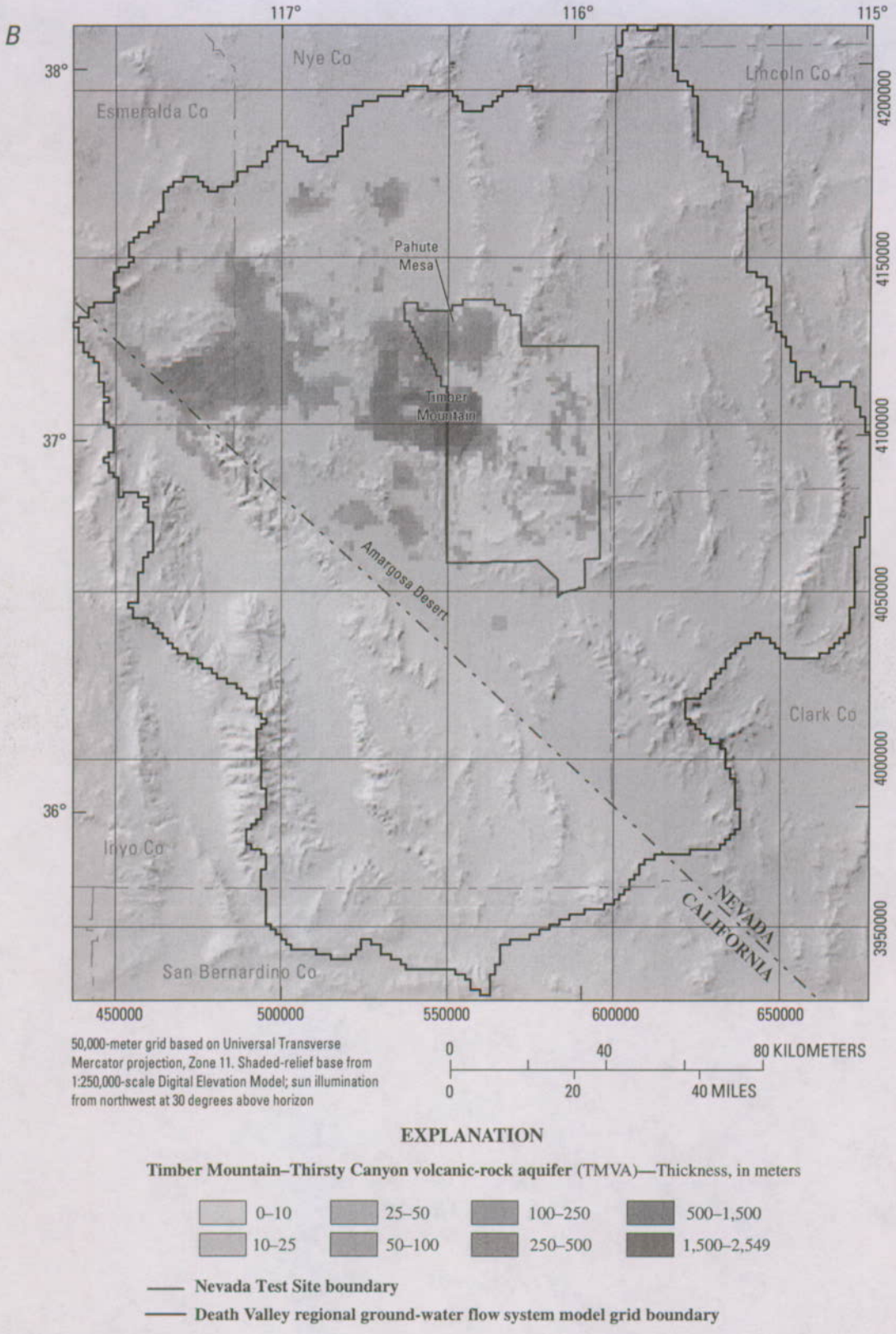

Figure E–22. (*A*) Data sources and (*B*) thickness of Thirsty Canyon–Timber Mountain volcanic-rock aquifer.—Continued

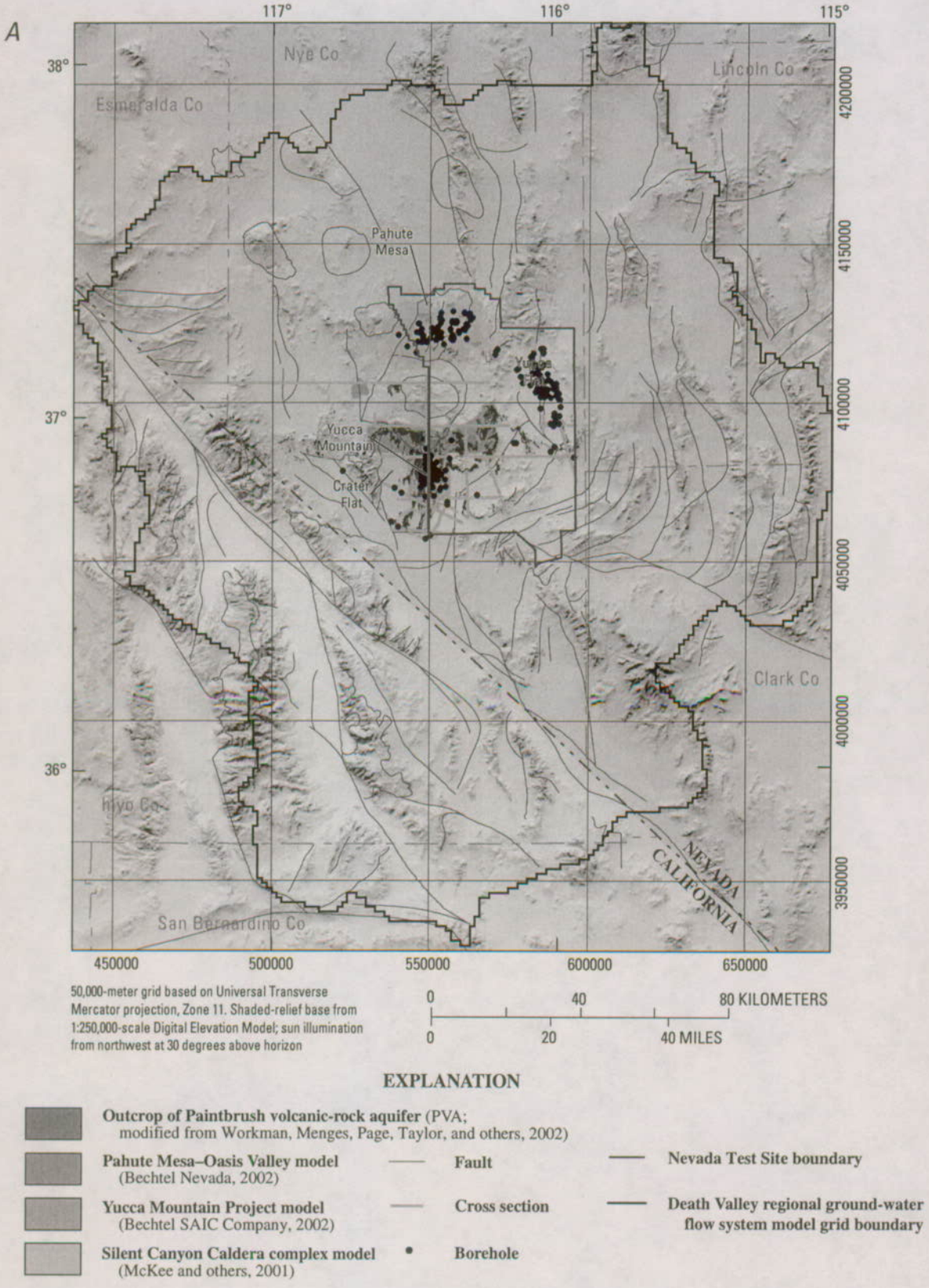

Figure E–23. (*A*) Data sources and (*B*) thickness of Paintbrush volcanic-rock aquifer.

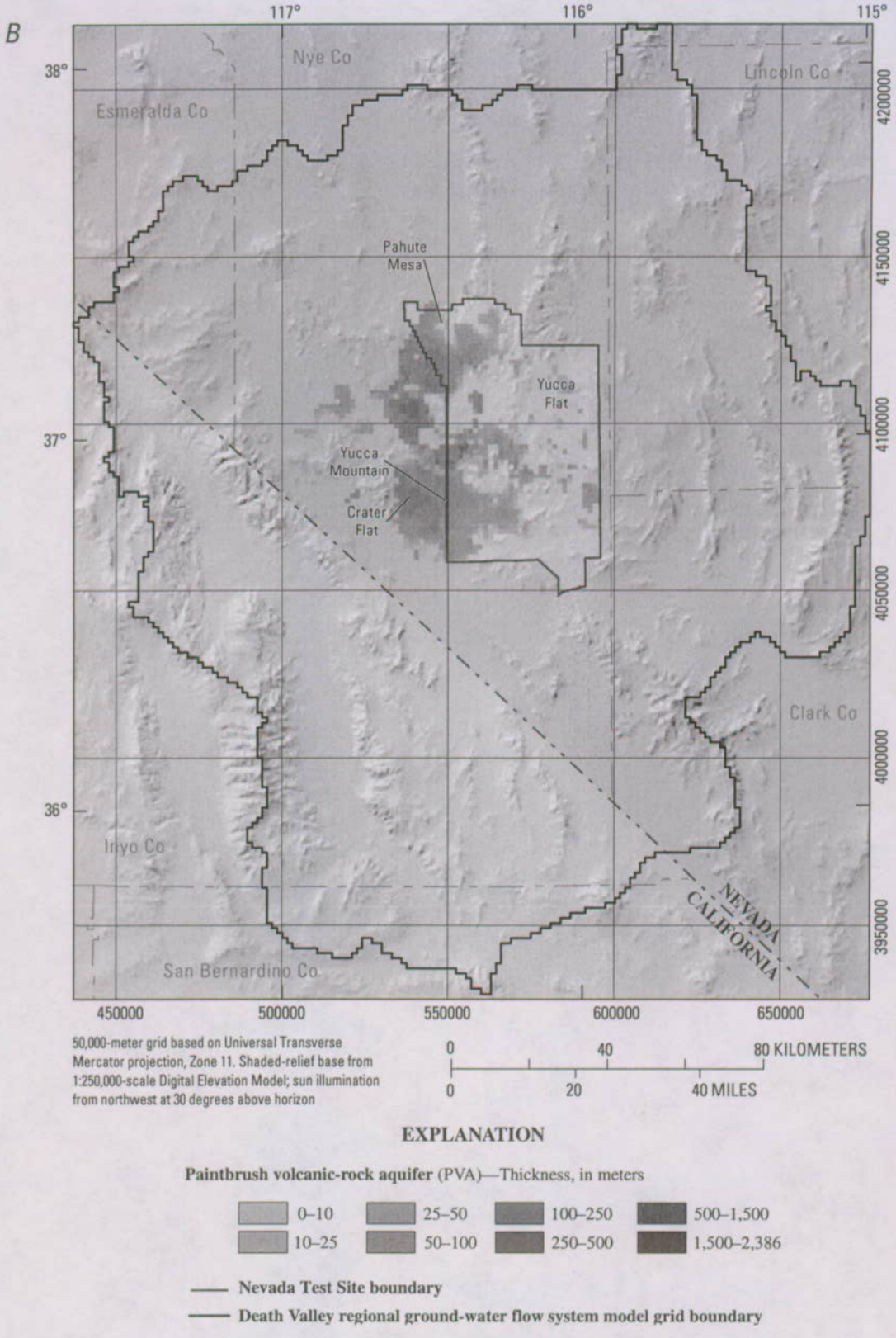

Figure E–23. (*A*) Data sources and (*B*) thickness of Paintbrush volcanic-rock aquifer.—Continued

Calico Hills Volcanic-Rock Unit (CHVU)

The Calico Hills volcanic-rock unit (CHVU) is exposed at the surface in the Calico Hills, Fortymile Canyon, and Paintbrush Canyon (fig. E–24*A*), where thicknesses exceed 500 m (fig. E–24*B*). Thicknesses of the unit reach about 1,500 m in the caldera moat just west of Timber Mountain.

Wahmonie Volcanic-Rock Unit (WVU)

Regionally, the Wahmonie volcanic-rock unit (WVU) extends east to Yucca Flat, north to Rainier Mesa, and southwest to Little Skull Mountain, Busted Butte, and southern Yucca Mountain (fig. E–25*A*). In general, the unit lies south and east of the CHVU. The WVU reaches a maximum thickness of about 1,100 m southeast of the Calico Hills (fig. E–25*B*).

Crater Flat–Prow Pass Aquifer (CFPPA)

The Crater Flat–Prow Pass aquifer (CFPPA) thins westward into Crater Flat but extends southward to its southernmost exposures at the southern end of Yucca Mountain (fig. E–26*A*), where it has a thickness approaching 340 m in the HFM (fig. E–26*B*). The aquifer is thickest beneath Pahute Mesa, where it reaches almost 1,400 m.

Crater Flat–Bullfrog Confining Unit (CFBCU)

The Crater Flat–Bullfrog confining unit (CFBCU) is widely distributed south, southwest, southeast, and north of the Timber Mountain caldera complex (TMCC) (fig. E–27*A*) (Carr and others, 1986). The CFBCU has a maximum simulated thickness of about 1,000 m (fig. E–27*B*). Although the CFBCU is present directly south of Little Skull Mountain, it is not represented there in the HFM because of the relatively coarse discretization of the HFM.

Crater Flat–Tram Aquifer (CFTA)

The Crater Flat–Tram aquifer (CFTA) is present in the area of Yucca Mountain (fig. E–28*A*). Although the CFTA is present along the south side of Little Skull Mountain and along the flank of Shoshone Mountain (Carr and others, 1986), it is not represented there in the HFM because of the relatively coarse discretization of the HFM. The CFTA reaches its greatest modeled thickness of more than 1,600 m to the north of Yucca Mountain (fig. E–28*B*).

Belted Range Unit (BRU)

The Belted Range unit (BRU) is present beneath and extends outward from Pahute Mesa (fig. E–29*A*). The BRU thickens toward the eastern margin of the SCCC, where it reaches a maximum thickness of about 1,700 m (fig. E–29*B*). The BRU is not present in the southern parts of the SWNVF or beneath Yucca Mountain.

Older Volcanic-Rock Unit (OVU)

The older volcanic-rock unit (OVU) is present in much of the northern half of the model domain (fig. E–30*A*). In the HFM, the OVU has a maximum thickness of more than 2,800 m near Timber Mountain (fig. E–30*B*) and elsewhere, the OVU has extensive areas of thicknesses exceeding 500 m.

Sedimentary-Rock Confining Unit (SCU)

The sedimentary-rock confining unit (SCU) outcrops in the Spring Mountains and to the east outside the DVRFS model domain, in the lower plate of the Keystone thrust fault (fig. E–31*A*). The SCU also is present in the northern part of the model domain. The SCU has a maximum thickness of about 2,400 m in the HFM (fig. E–31*B*).

Upper Carbonate-Rock Aquifer (UCA)

The upper carbonate-rock aquifer (UCA) is present primarily in the area of Yucca Flat, the northern part of Jackass Flats, and the Eleana Range where these carbonate rocks are preserved in a syncline at Syncline Ridge and several isolated remnants above the UCCU (fig. E–32*A*). The UCA has a maximum thickness of about 1,200 m in the HFM (fig. E–32*B*).

Upper Clastic-Rock Confining Unit (UCCU)

The upper clastic-rock confining unit (UCCU) is present primarily in the area of Yucca Flat, the northern part of Jackass Flats, and the Eleana Range (fig. E–33*A*). The thickest parts of the UCCU are in the Eleana Range and western part of Yucca Flat, where it is about 3,100 m thick (fig. E–33*B*).

Lower Carbonate-Rock Aquifer (LCA) and Thrusts (LCA_T1)

The lower carbonate-rock aquifer (LCA) covers an extensive part of the DVRFS model domain, especially in the eastern and southern parts (fig. E–34*A*). The LCA is missing in the northwestern and central part of the model domain because of volcanic activity and associated igneous intrusions and thick accumulations of volcanic rocks (Chapter B, this volume). The area between the southern Funeral Mountains and the Spring Mountains contains separately defined thrust-fault areas where the thrusted LCA_T1 is repeated in the stratigraphic sequence above the LCA (fig. E–35*A*).

The LCA is particularly thick and continuous beneath the Pintwater and Spotted Ranges area (fig. E–34*B*) where it is in a regional syncline. One of the thickest parts of the LCA is in

the structural trough west of the Spring Mountains. Because the base of the HFM is higher than the base of the LCA in some areas, the maximum thickness of the LCA in the HFM is only 6,500 m. The maximum thickness of the LCA_T1 is about 5,500 m (fig. E–35*B*).

Lower Clastic-Rock Confining Unit (LCCU) and Thrusts (LCCU_T1)

The lower clastic-confining unit (LCCU) is exposed through a broad area including the Spring Mountains, the NTS, and some of the mountains surrounding Death Valley (fig. E–36*A*). The area between the southern Funeral Mountains and the Spring Mountains contains separately defined thrust-fault areas where the thrusted LCCU_T1 is repeated in the stratigraphic sequence above the LCCU (fig. E–37*A*). The LCCU reaches a maximum thickness of about 6,300 m (fig. E–36*B*) where it outcrops in the mountains and extends to the base of the model. The LCCU_T1 reaches a maximum thickness of about 4,400 m (fig. E–37*B*).

Crystalline-Rock Confining Unit (XCU)

The crystalline-rock confining unit (XCU) consists of cratonic rocks that likely lie beneath the entire model domain, except directly beneath the calderas. The extent of the XCU outcrops in the HFM is shown in figure E–38*A*. In many areas the HFM truncates this unit at the base of the model 4,000 m below sea level. The XCU reaches a maximum thickness of about 6,500 m in the model (fig. E–38*B*).

Intrusive-Rock Confining Unit (ICU)

In most of the DVRFS region, the ICU occurs as small stocks, such as the Climax Stock in Yucca Flat and the Gold Meadows Stock on Rainier Mesa (Houser and others, 1961) (fig. E–39*A*). In the mountain ranges on the west and east sides of Death Valley, intrusive bodies are greater in size, more irregular in shape, and more common than elsewhere in the DVRFS region (Grose and Smith, 1989). Thicknesses vary but are about 6,700 m in parts of the HFM (fig. E–39*B*). The HFM truncates this unit at the base of the model 4,000 m below sea level. The intrusive bodies in the HFM are treated as vertical-sided blocks intruding through one or all other HGUs.

Representation of Key Areas in the Model

Key areas in the HFM that represent significant hydrogeologic features in the DVRFS model domain were compared to features in those areas of the hydrogeologic framework. Geometric relations of the HGUs in the HFM were visualized by producing a series of subparallel sections through four key areas of the HFM (fig. E–40): (1) the Sheep Range and adjacent areas, (2) the Eleana Range and Calico Hills, (3) the SWNVF, and (4) the Funeral Mountains and Amargosa Desert. Visual inspection of sections from the HFM is complicated by several confusing factors that need to be considered, such as graphic artifacts from grid spacing, the abrupt truncation of HGUs, and representation of faults as steep offsets in onlapping relations in the HFM.

Sheep Range and Adjacent Areas

The Sheep Range is hydrologically important because it is a center of recharge and is near the boundary between the DVRFS and the Colorado River ground-water flow system. Sections from the HFM in the vicinity of the Sheep Range show two structural highs of LCCU (fig. E–41) that represent the north-trending Pintwater anticline to the west (Longwell and others, 1965) and the LCCU_T1 in the upper plate of the Gass Peak thrust to the east. North of the LVVSZ, Cenozoic extensional faults have overprinted the Mesozoic thrust belt (Guth, 1981, 1990; Wernicke and others, 1984). The HFM portrays the effect of these faults as variable thicknesses of LCCU_T1 in the upper plate of the Gass Peak thrust.

Eleana Range and Calico Hills

In the vicinity of the Eleana Range and Calico Hills thrusted LCCU is present in the upper plate of the Belted Range thrust and is almost completely buried beneath volcanic-rock HGUs, as portrayed in the HFM (fig. E–42). The Belted Range thrust is intruded by the Gold Meadows Stock (ICU) beneath Rainier Mesa and by a pluton beneath the Calico Hills, both represented in the HFM. Few faults appear to interrupt the continuity of the thrust system in the subsurface, although the thrusts are disrupted by the TMCC and the Claim Canyon caldera, as portrayed in the HFM. Below the Belted Range thrust is a series of footwall imbricate thrusts that carry UCCU in their upper plate (Cole and Cashman, 1999) and generally serve as the westward truncation of the LCA. Although not visible at the scale of figure E–42, this imbricate thrust is represented in the HFM by the UCCU in the lower plate of the Belted Range thrust.

Southwestern Nevada Volcanic Field

Sections from the HFM in the vicinity of the SWNVF (fig. E–43) portray the thickness and extent of the various volcanic-rock HGUs in the SCCC and the TMCC. Within the calderas of the SWNVF, the HFM portrays the Paleozoic and older bedrock (LCA, LCCU, and XCU) as missing or present only at very deep levels.

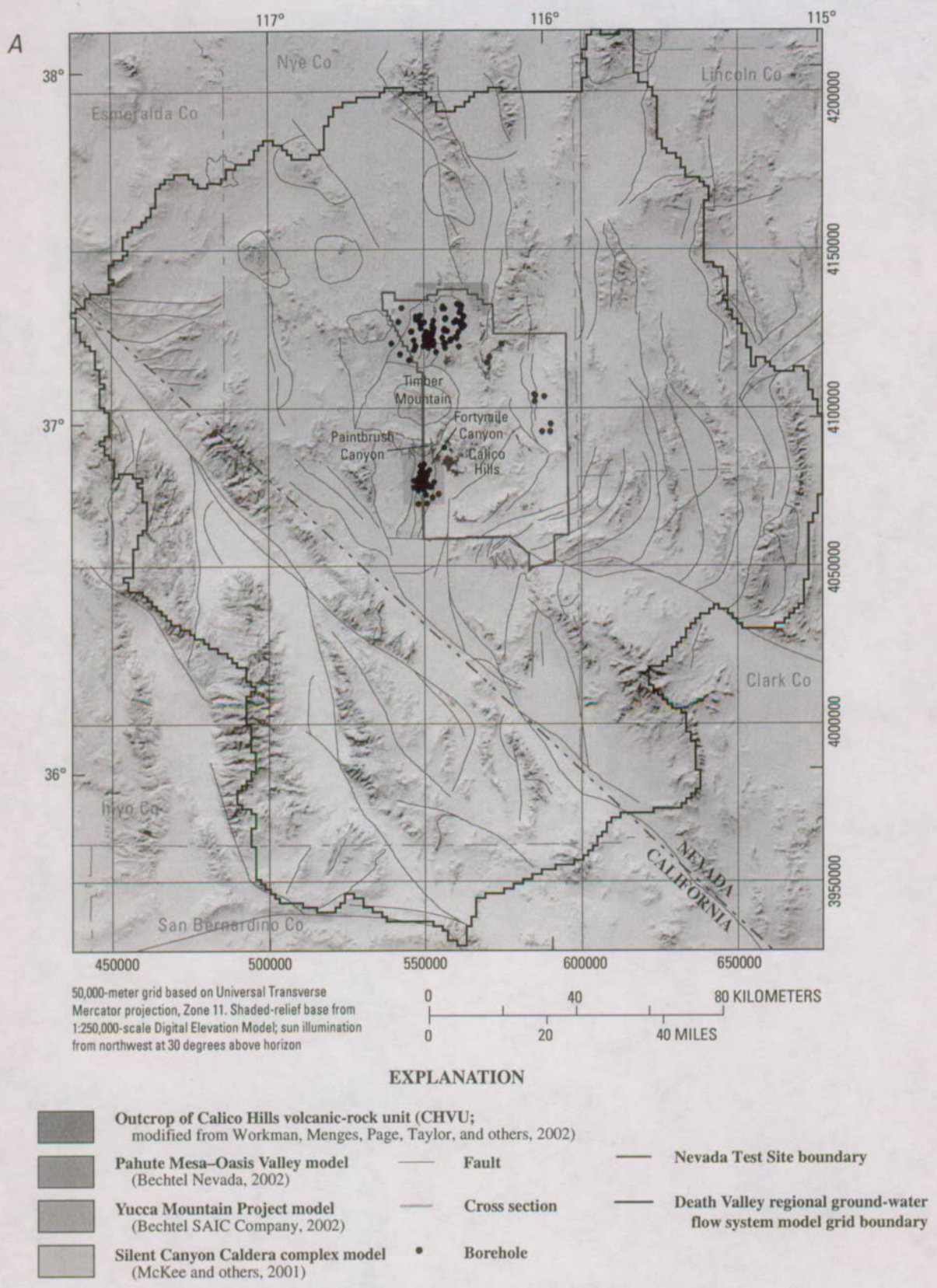

Figure E–24. (*A*) Data sources and (*B*) thickness of Calico Hills volcanic-rock unit.

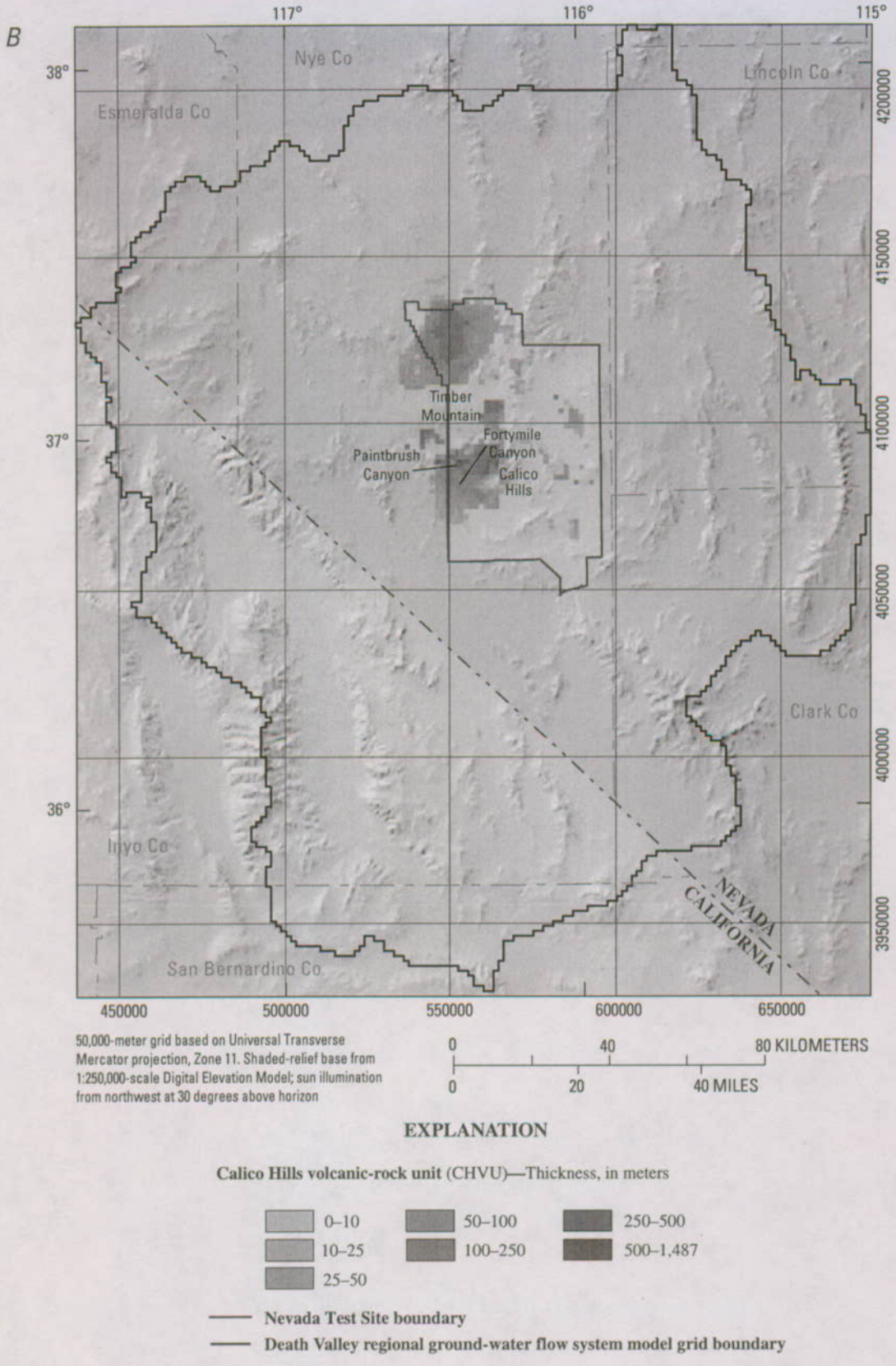

Figure E–24. (*A*) Data sources and (*B*) thickness of Calico Hills volcanic-rock unit.—Continued

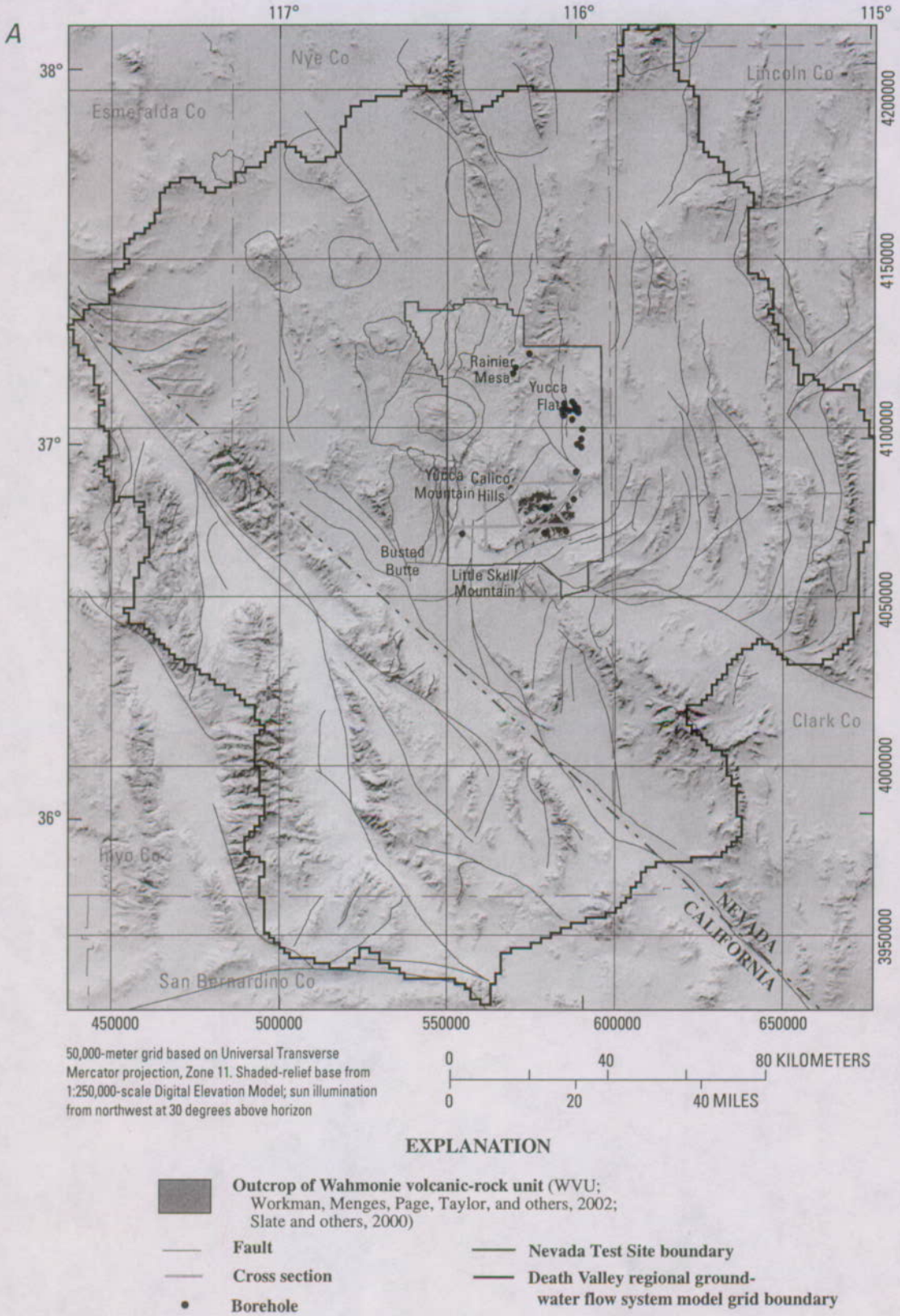

Figure E–25. (*A*) Data sources and (*B*) thickness of Wahmonie volcanic-rock unit.

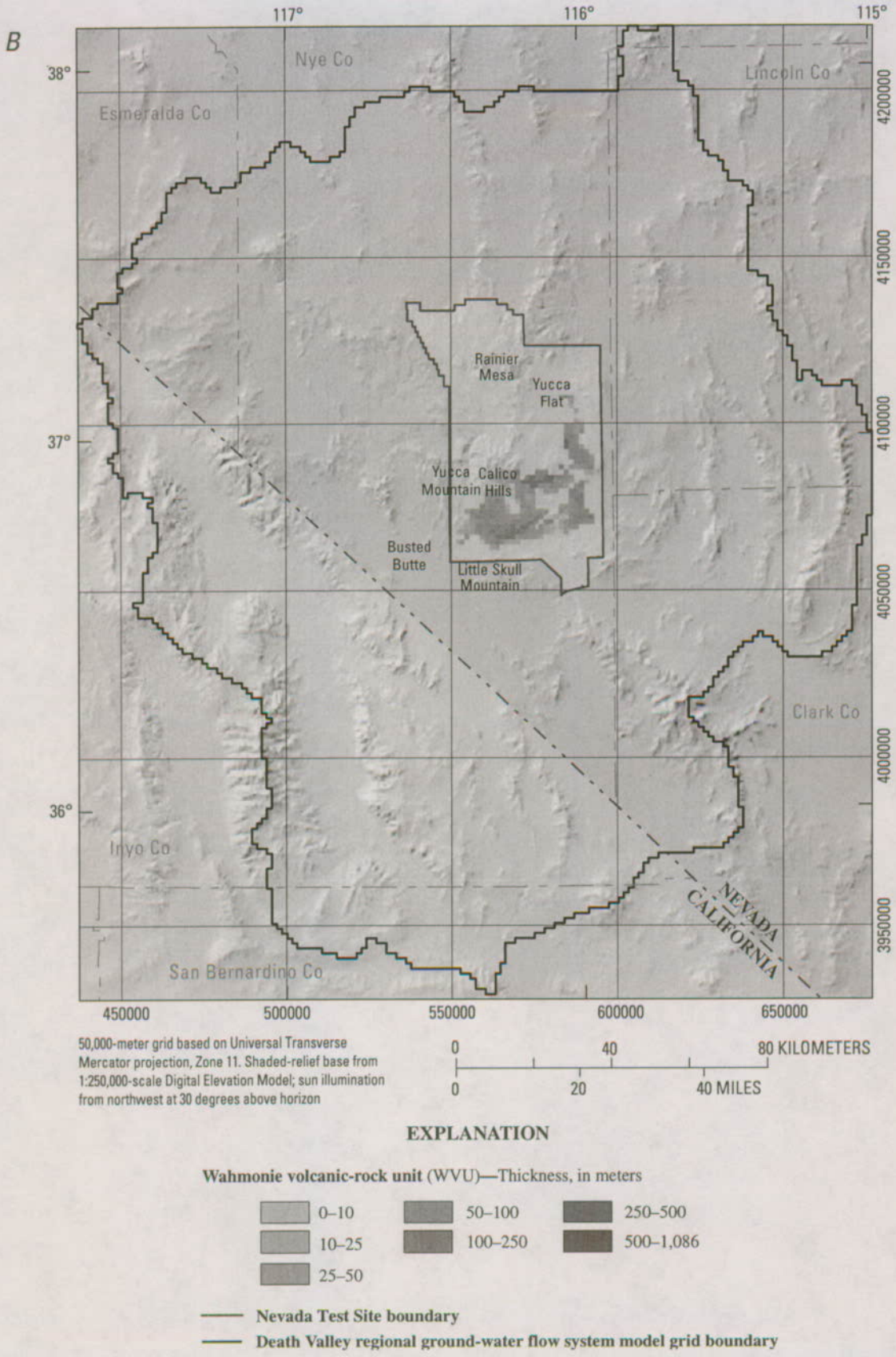

Figure E–25. (*A*) Data sources and (*B*) thickness of Wahmonie volcanic-rock unit.—Continued

Figure E–26. (*A*) Data sources and (*B*) thickness of Crater Flat–Prow Pass aquifer.

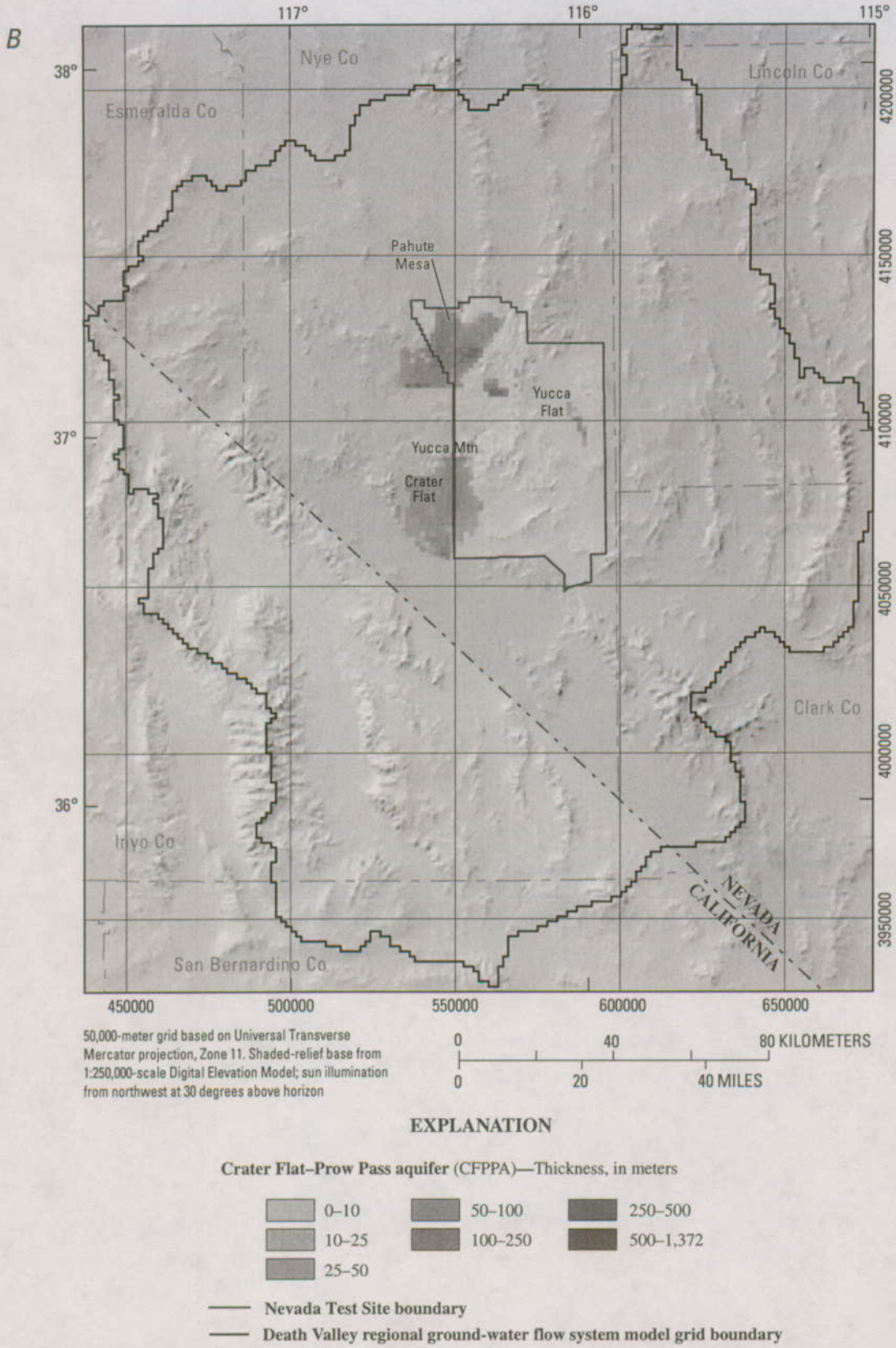

Figure E–26. (*A*) Data sources and (*B*) thickness of Crater Flat–Prow Pass aquifer.—Continued

Figure E–27. (*A*) Data sources and (*B*) thickness of Crater Flat–Bullfrog confining unit.

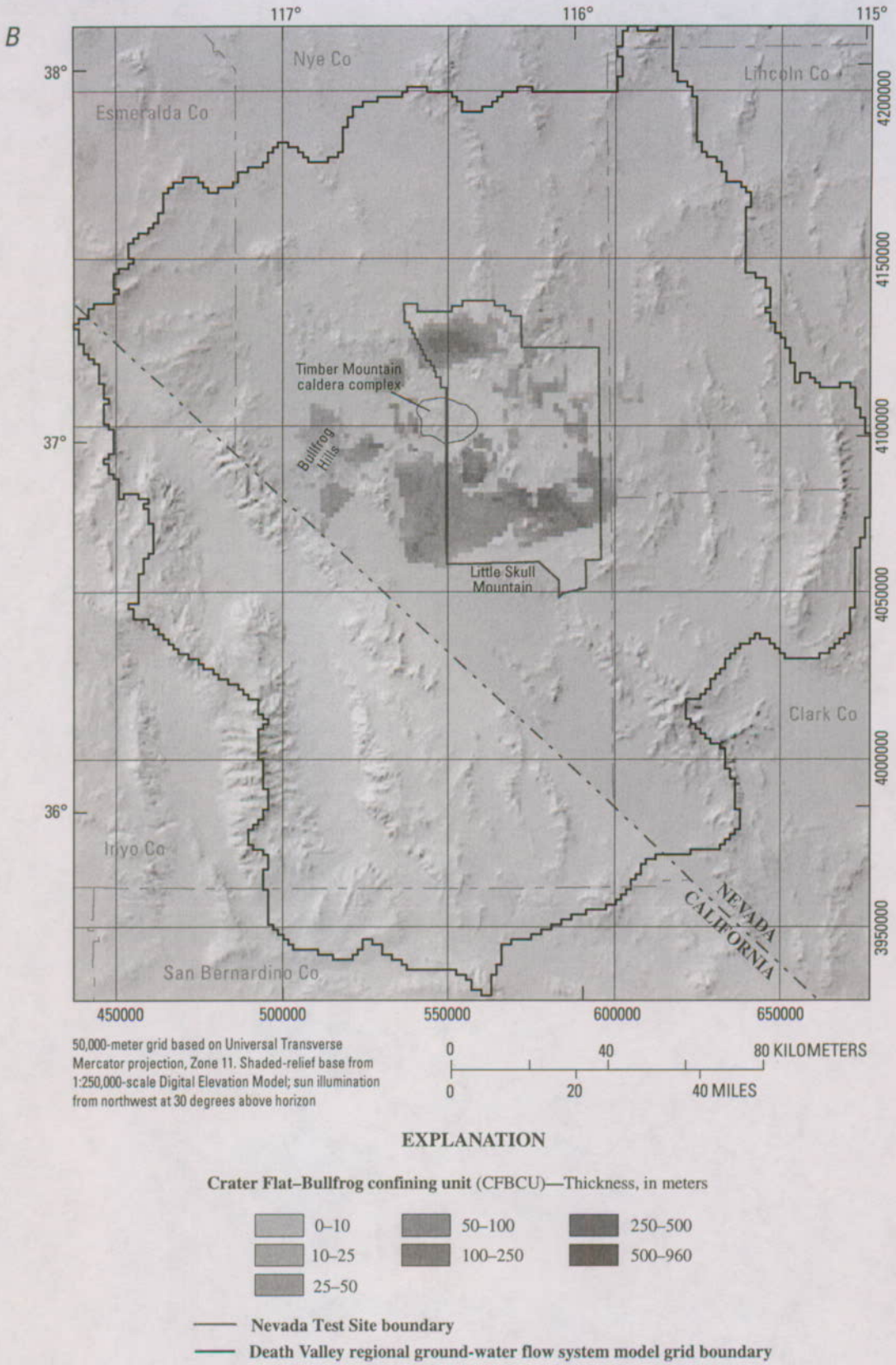

Figure E–27. (*A*) Data sources and (*B*) thickness of Crater Flat–Bullfrog confining unit.—Continued

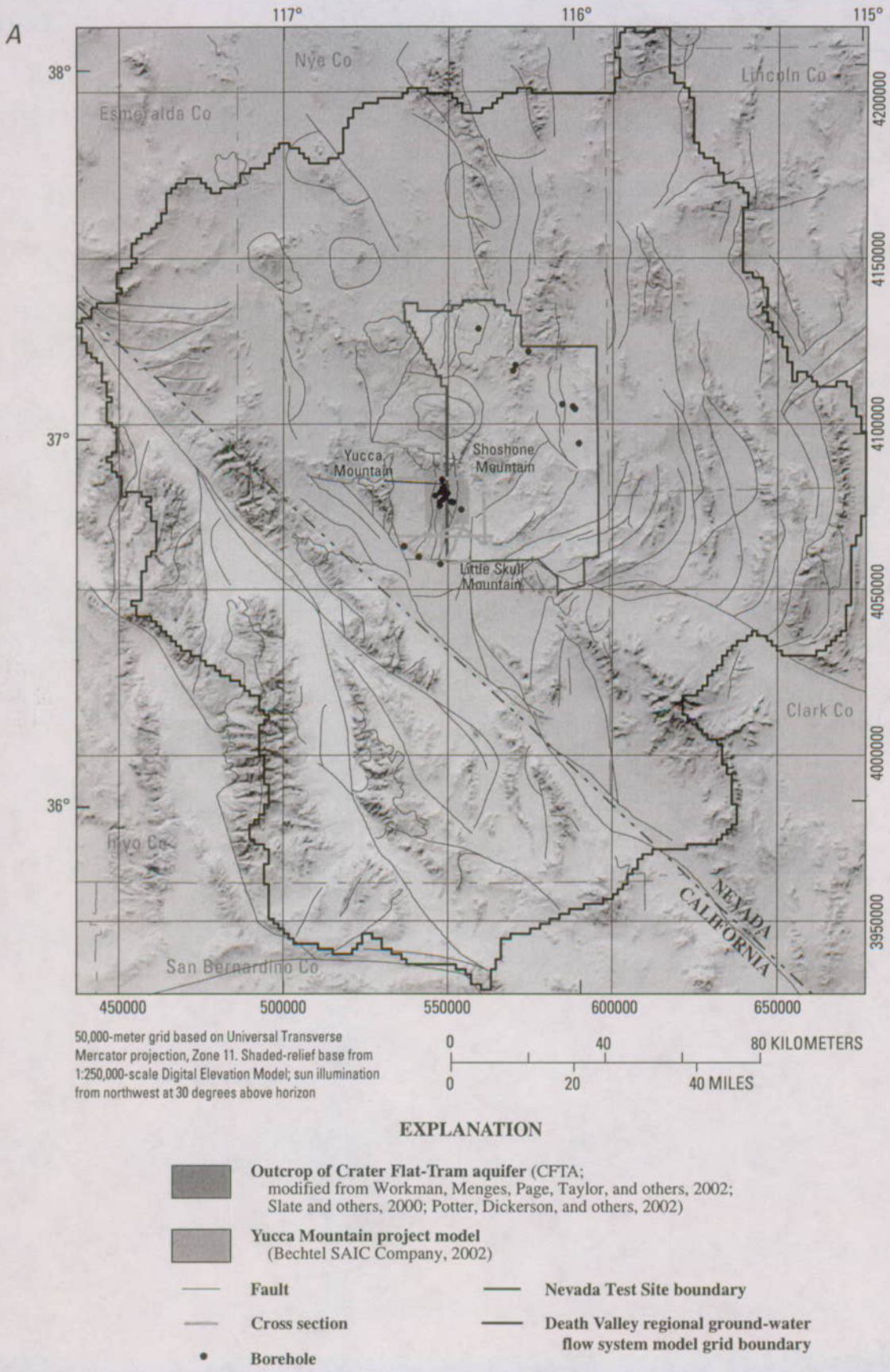

Figure E–28. (*A*) Data sources and (*B*) thickness of Crater Flat–Tram aquifer.

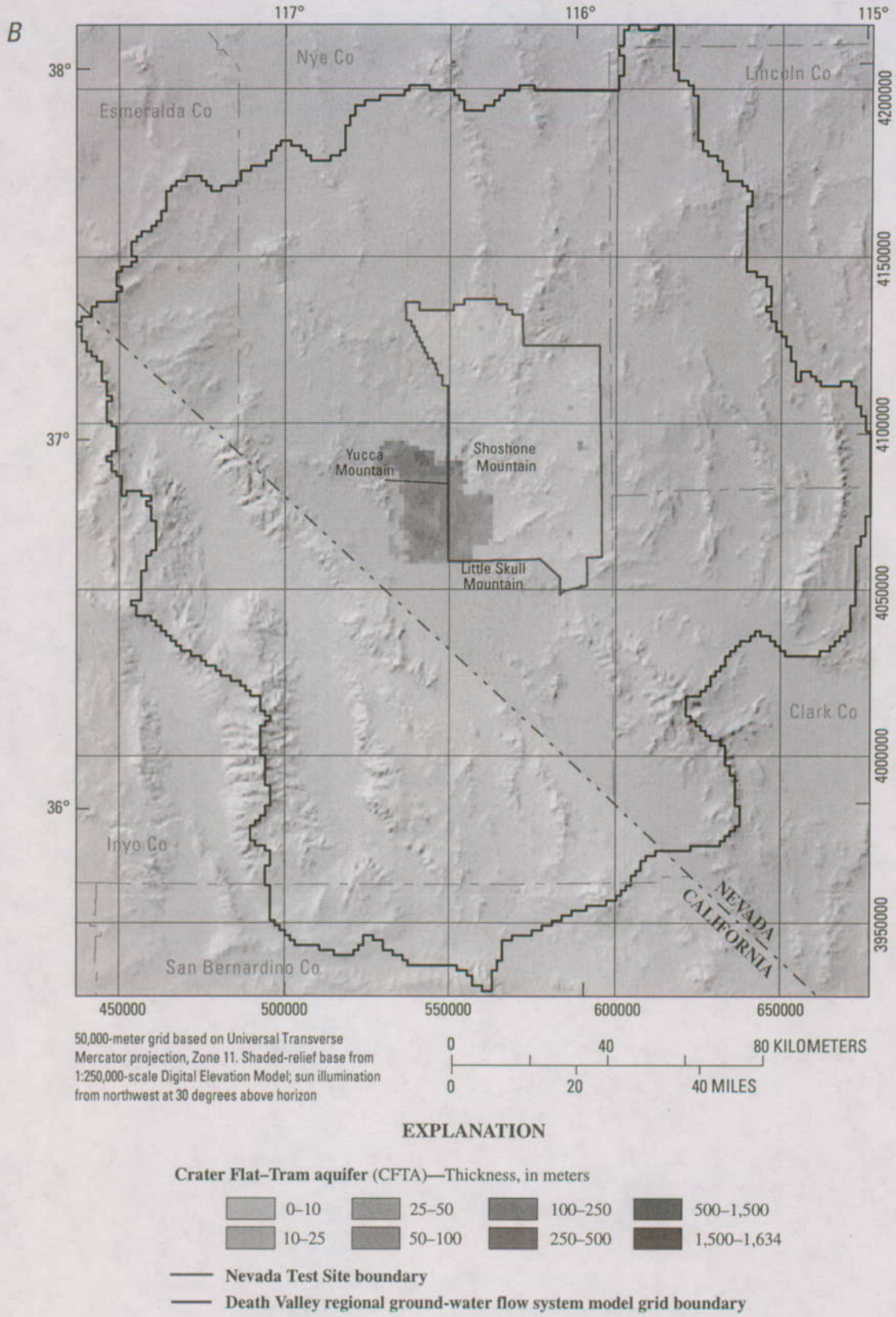

Figure E–28. (*A*) Data sources and (*B*) thickness of Crater Flat–Tram aquifer.—Continued

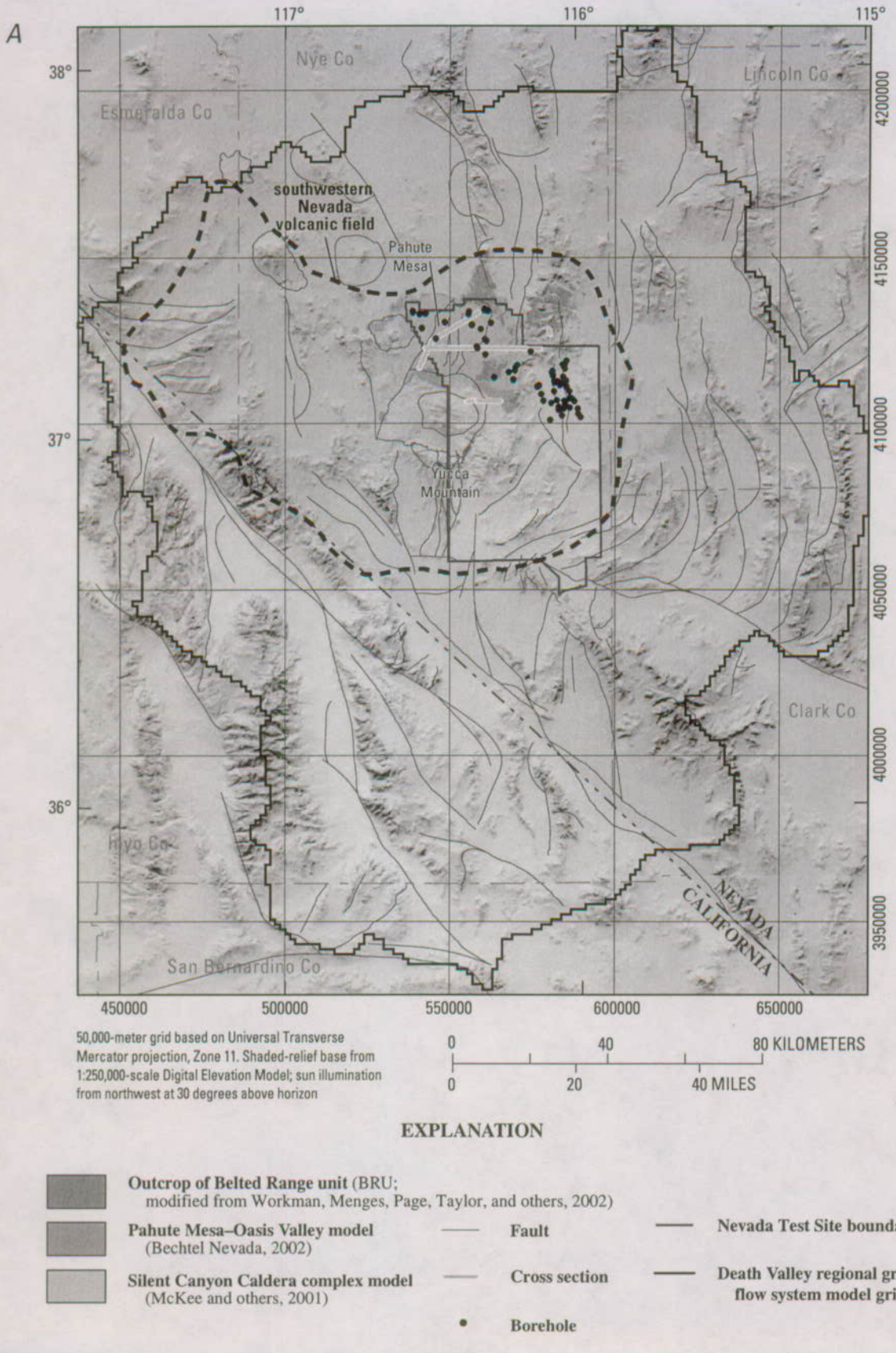

Figure E–29. (*A*) Data sources and (*B*) thickness of Belted Range unit.

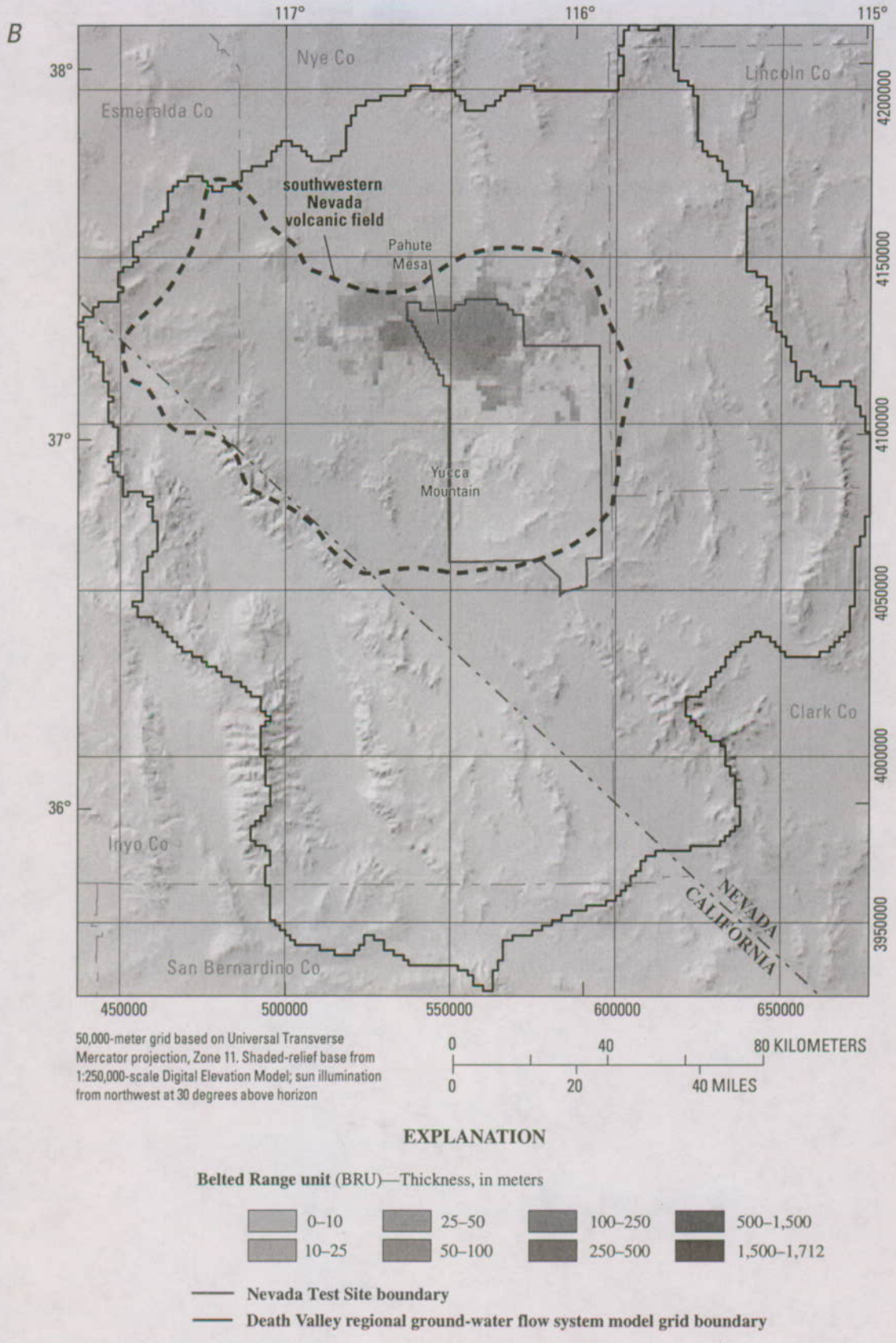

Figure E–29. (*A*) Data sources and (*B*) thickness of Belted Range unit.—Continued

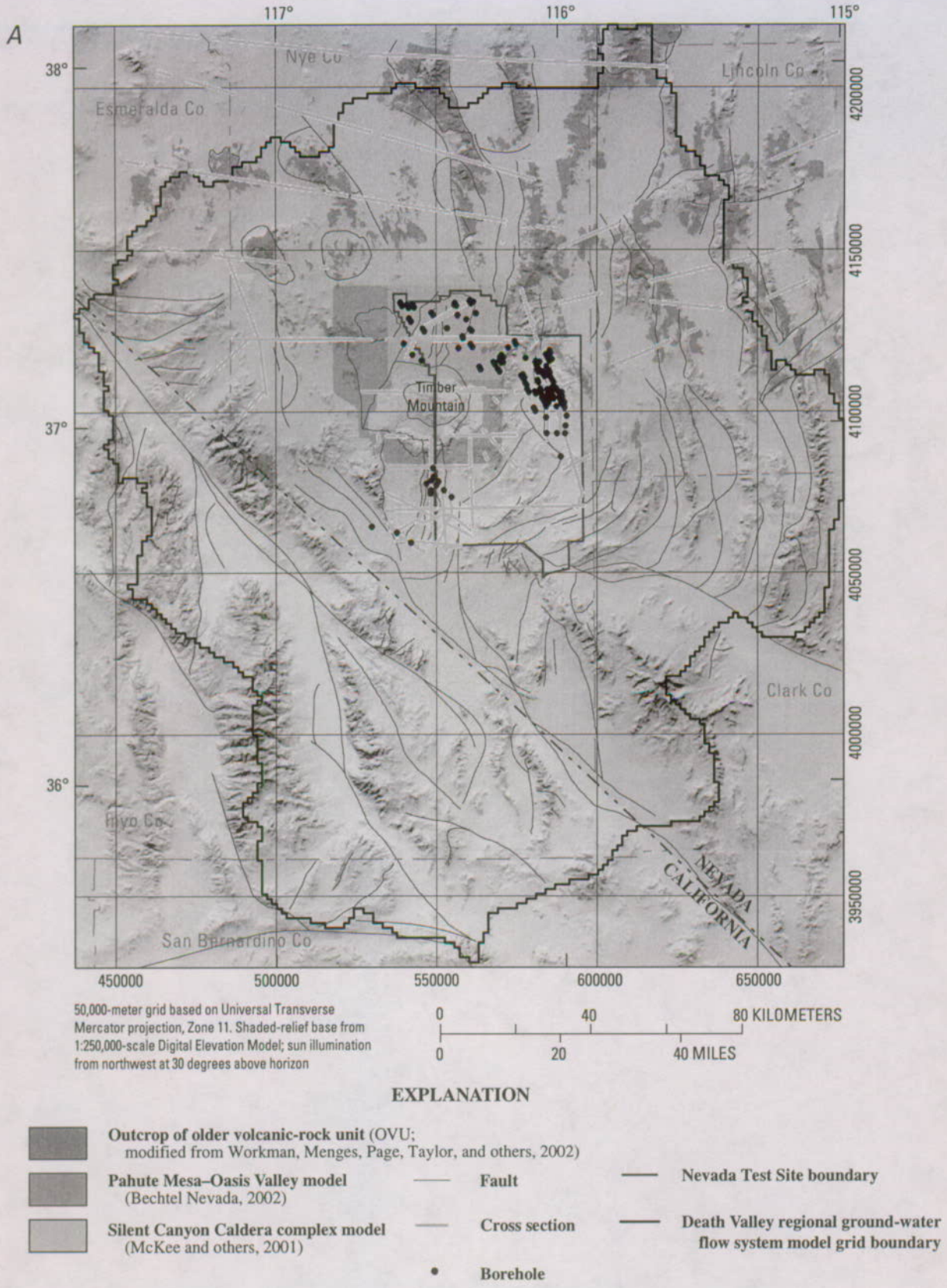

Figure E–30. (*A*) Data sources and (*B*) thickness of older volcanic-rock unit.

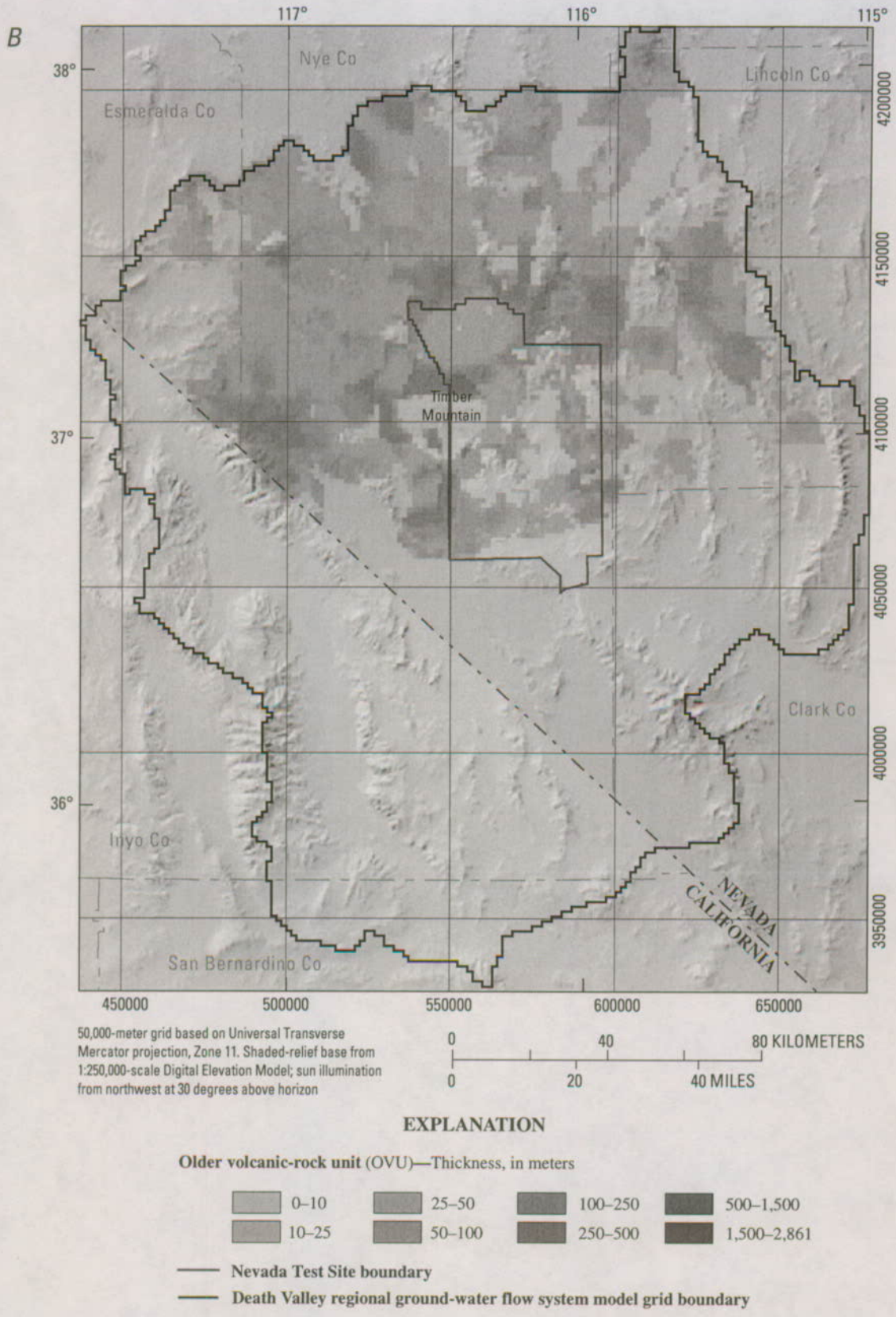

Figure E–30. (*A*) Data sources and (*B*) thickness of older volcanic-rock unit.—Continued

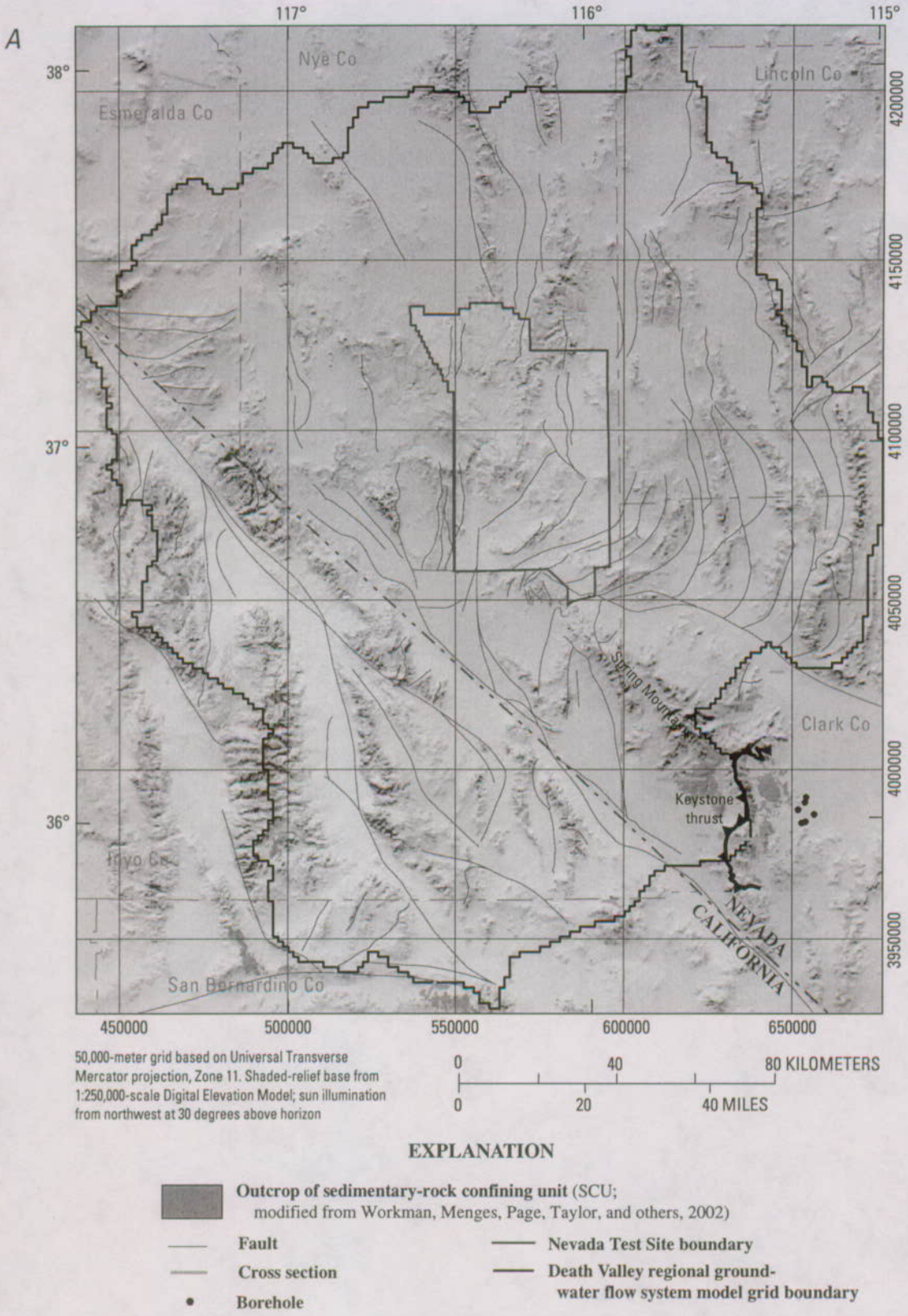

Figure E–31. (*A*) Data sources and (*B*) thickness of sedimentary-rock confining unit.

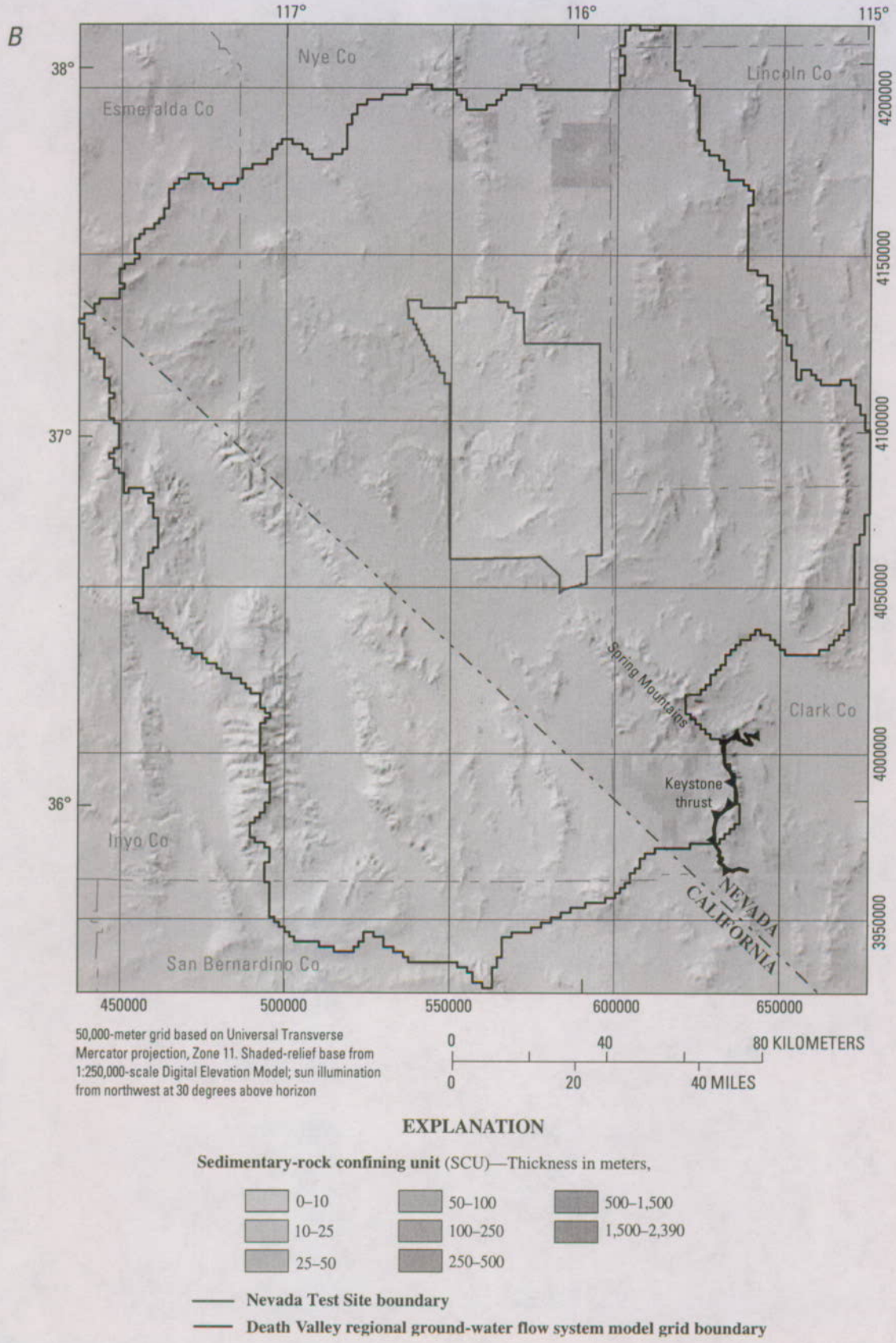

Figure E–31. (*A*) Data sources and (*B*) thickness of sedimentary-rock confining unit.—Continued

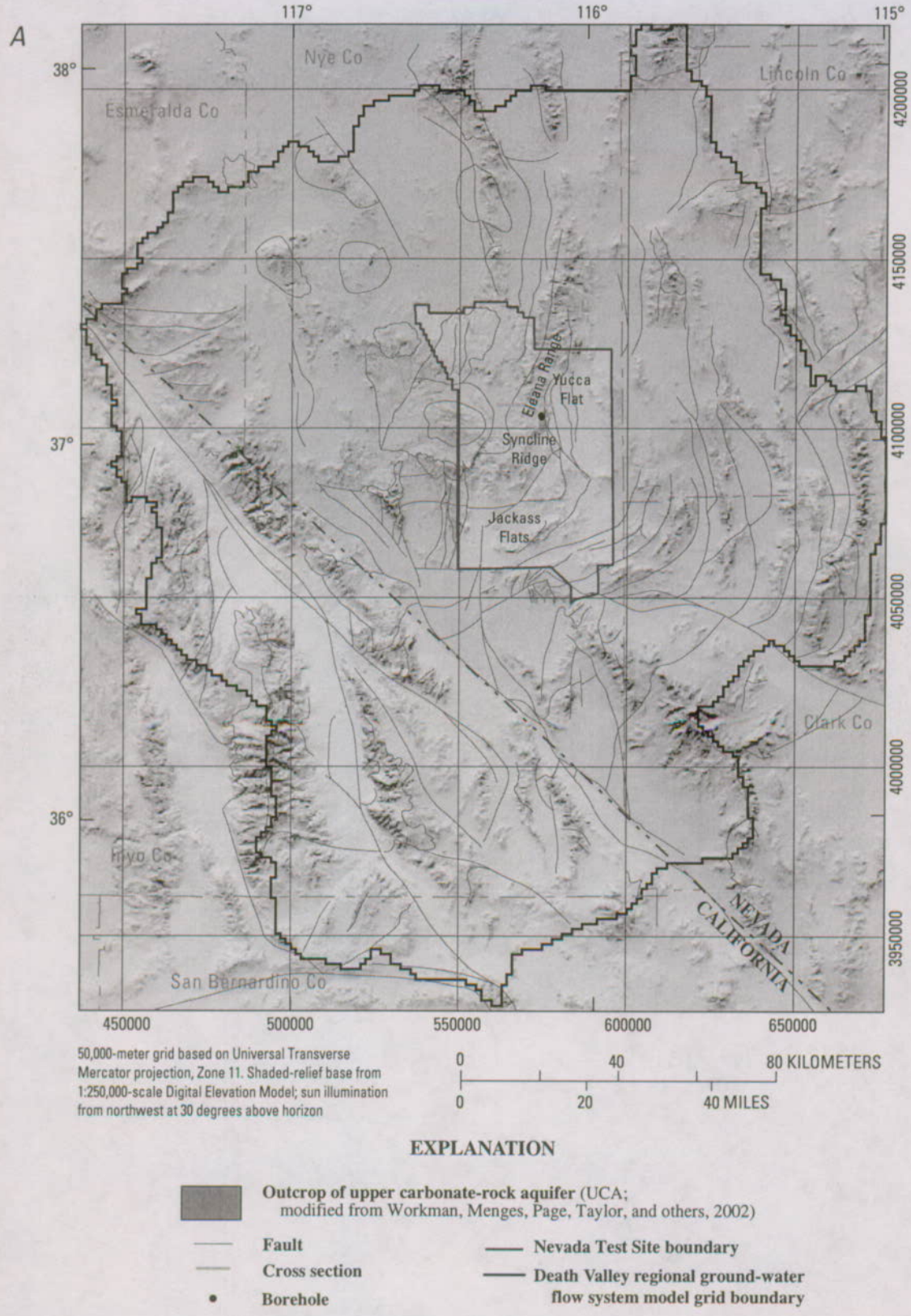

Figure E–32. (*A*) Data sources and (*B*) thickness of upper carbonate-rock aquifer.

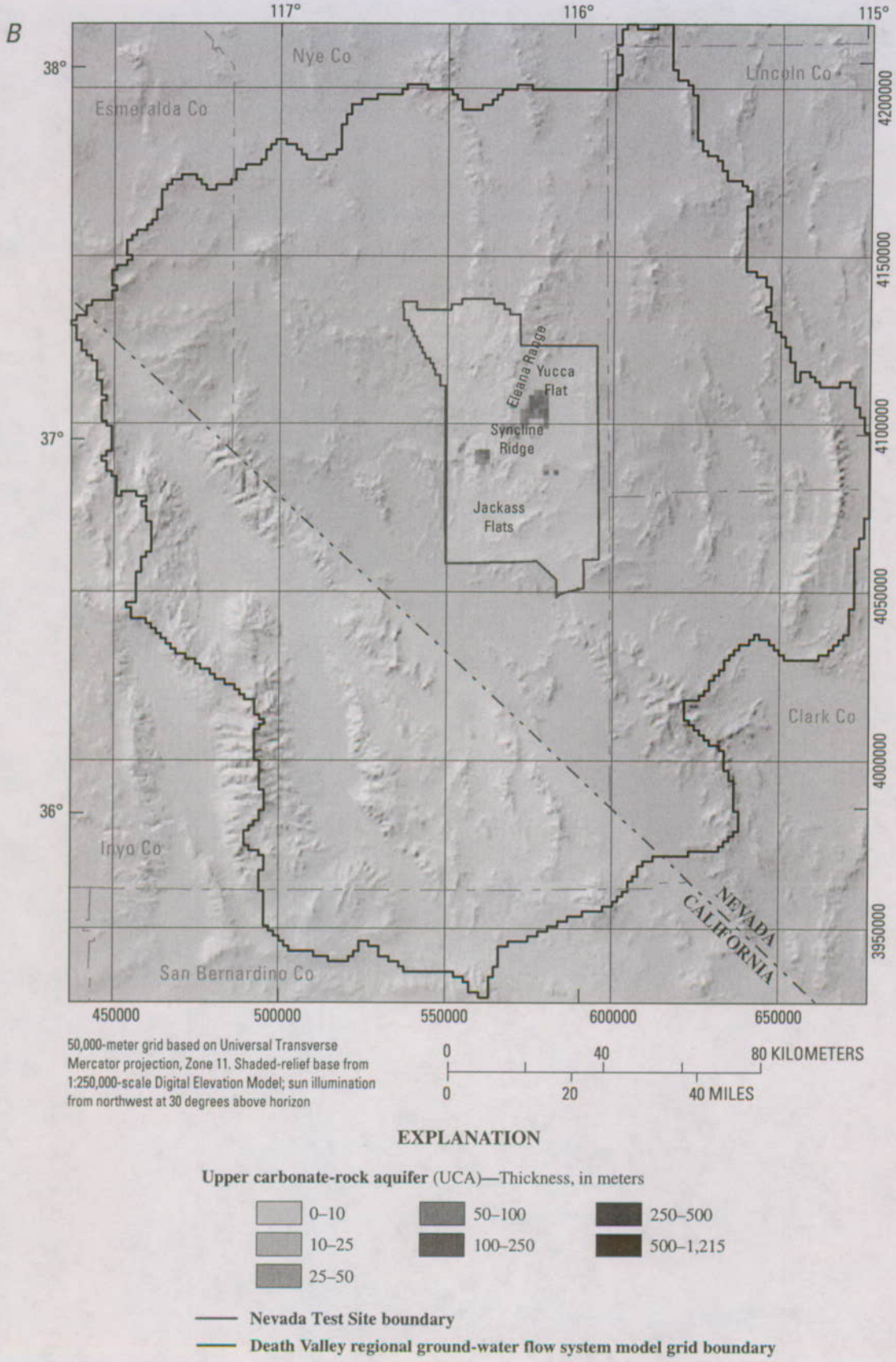

Figure E–32. (*A*) Data sources and (*B*) thickness of upper carbonate-rock aquifer.—Continued

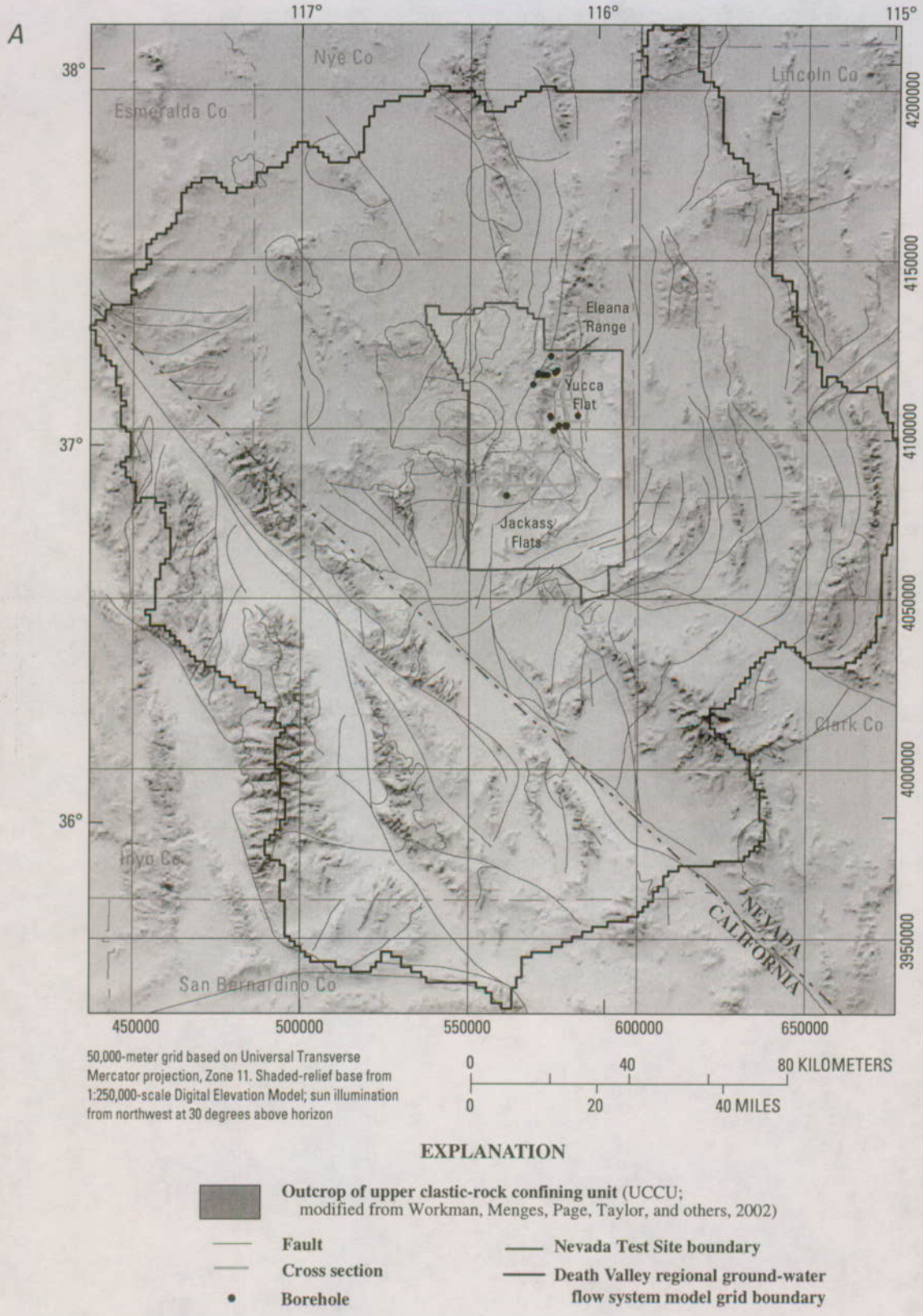

Figure E–33. (*A*) Data sources and (*B*) thickness of upper clastic-rock confining unit.

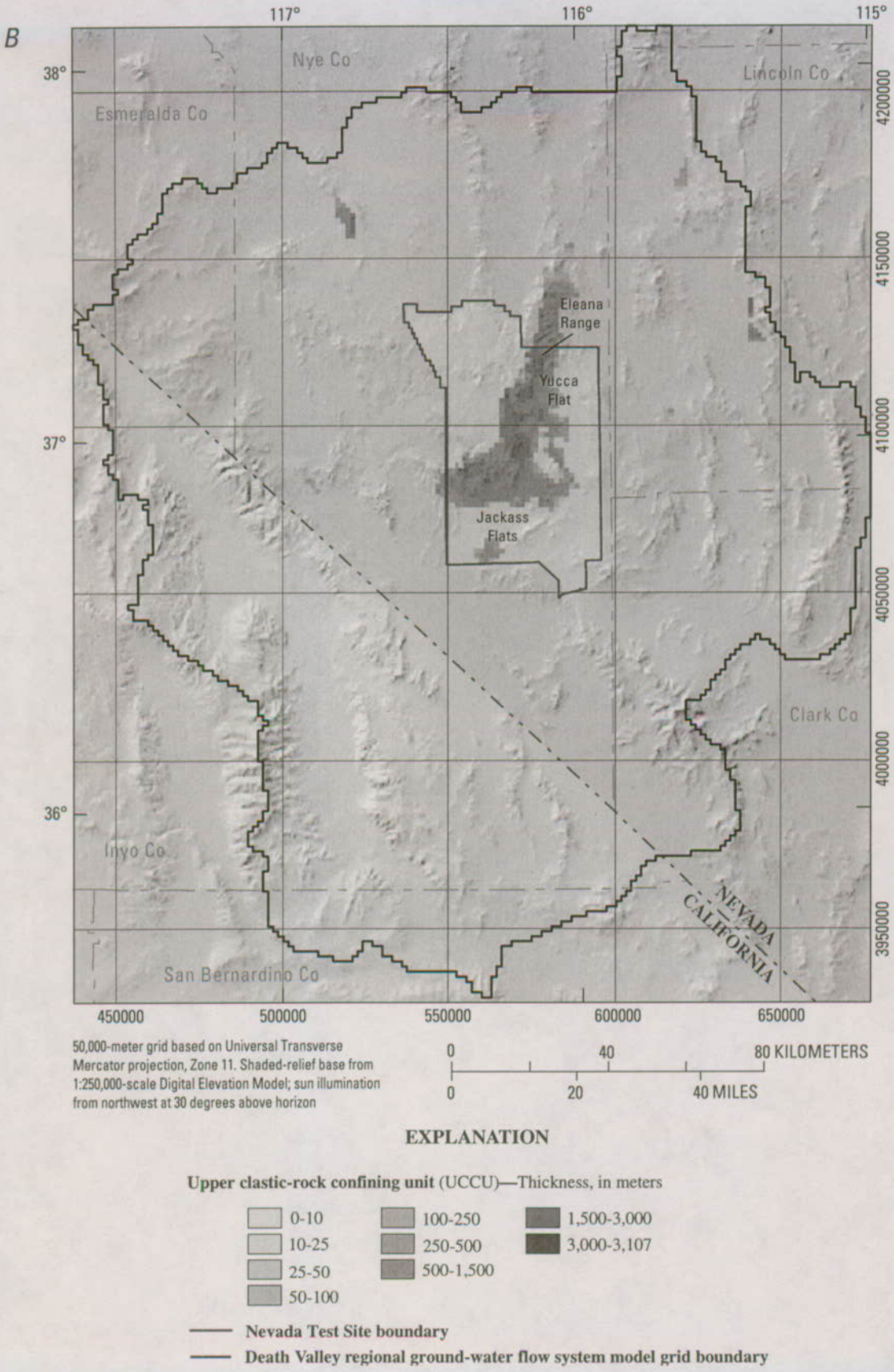

Figure E–33. (*A*) Data sources and (*B*) thickness of upper clastic-rock confining unit.—Continued

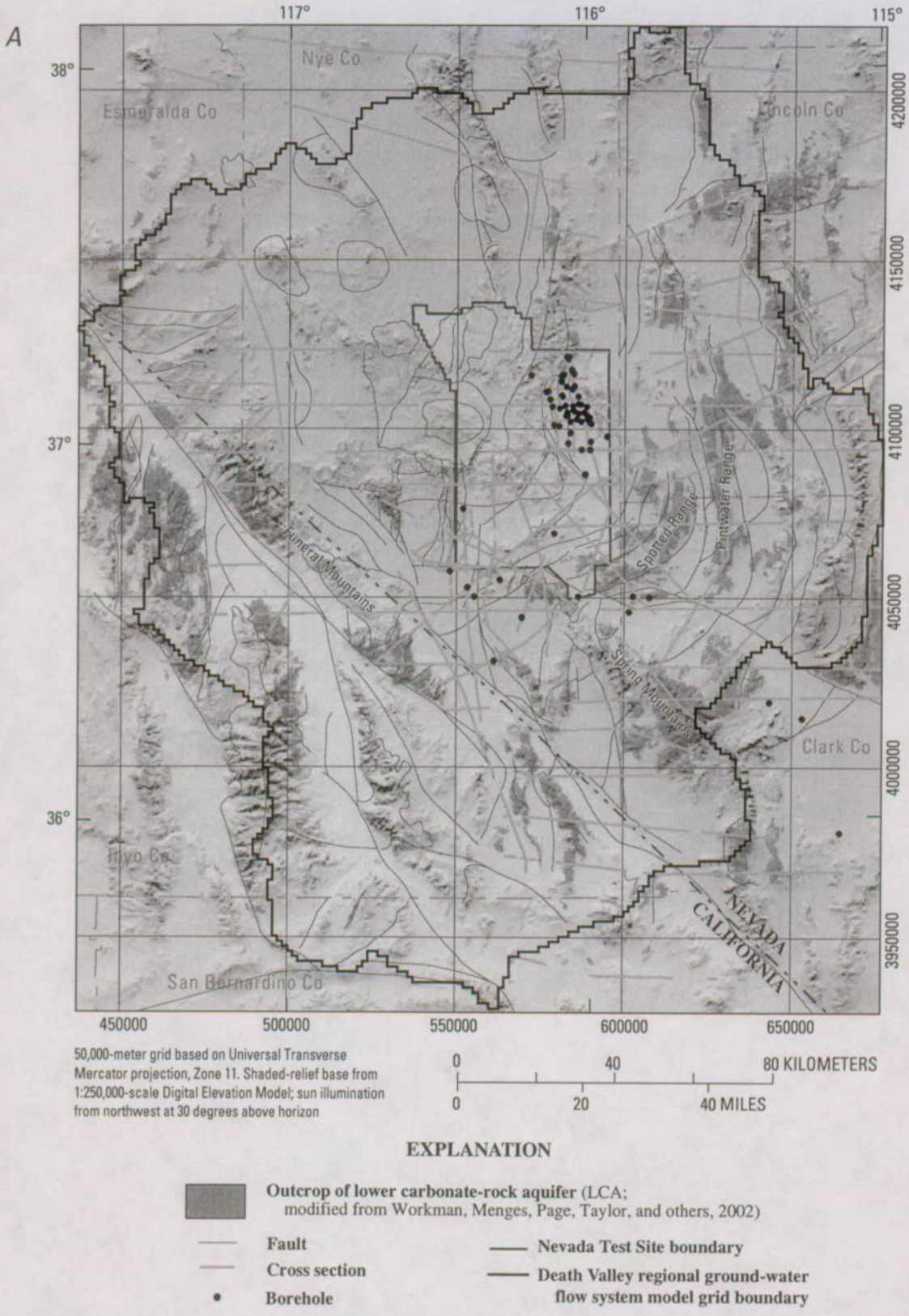

Figure E–34. (*A*) Data sources and (*B*) thickness of lower carbonate-rock aquifer.

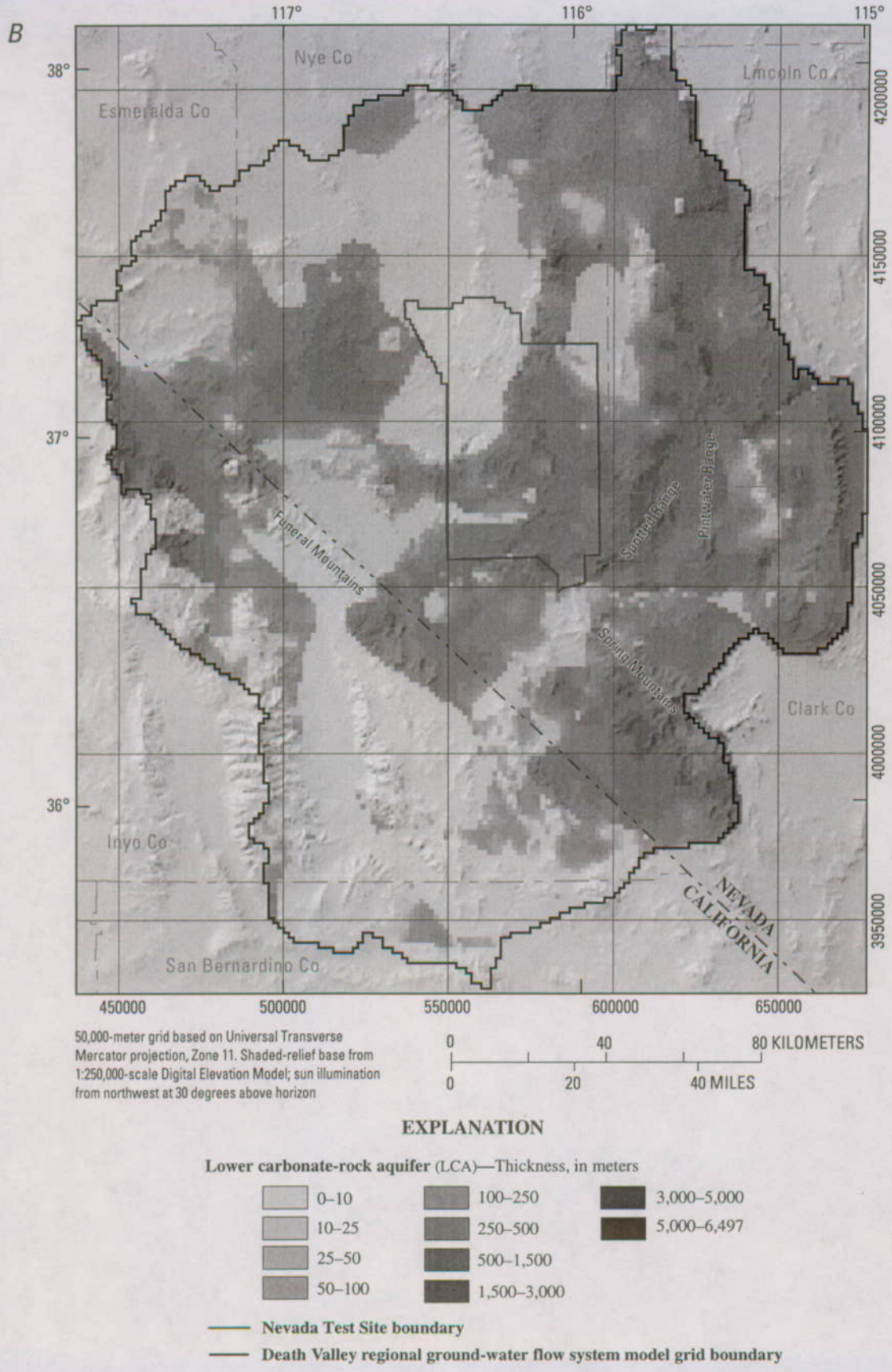

Figure E–34. (*A*) Data sources and (*B*) thickness of lower carbonate-rock aquifer.—Continued

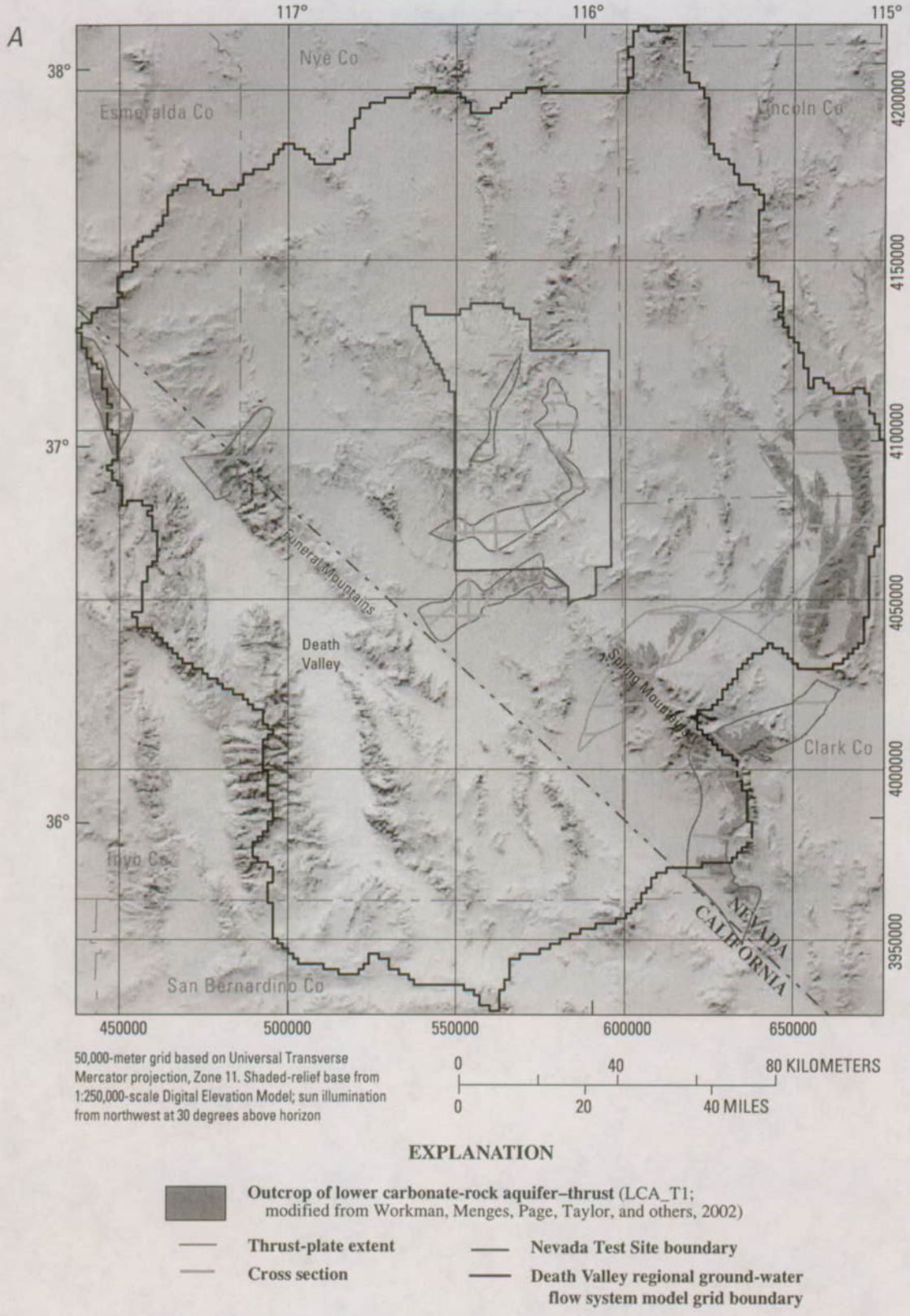

Figure E–35. (*A*) Data sources and (*B*) thickness of thrusted lower carbonate-rock aquifer.

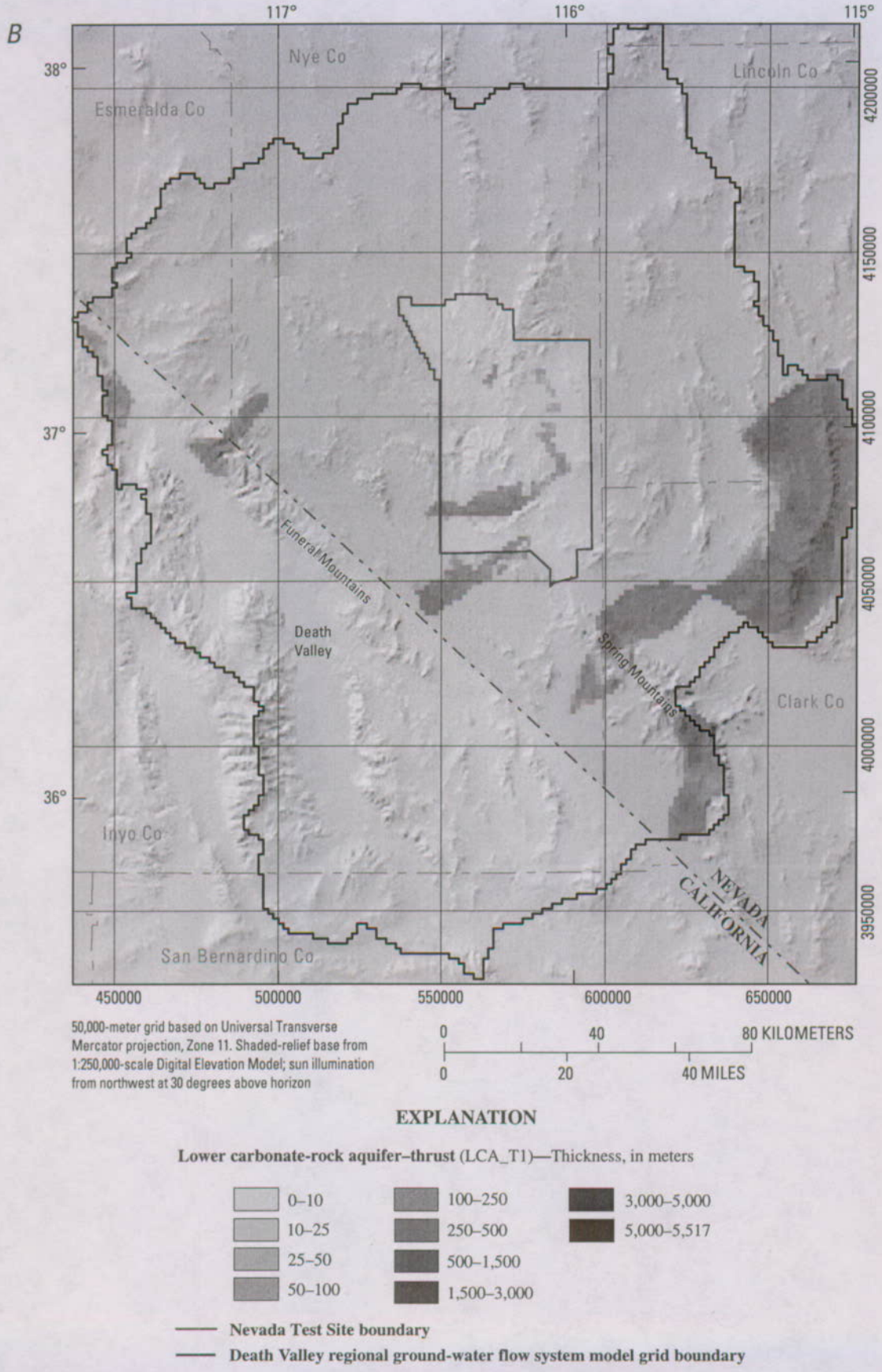

Figure E–35. (*A*) Data sources and (*B*) thickness of thrusted lower carbonate-rock aquifer.—Continued

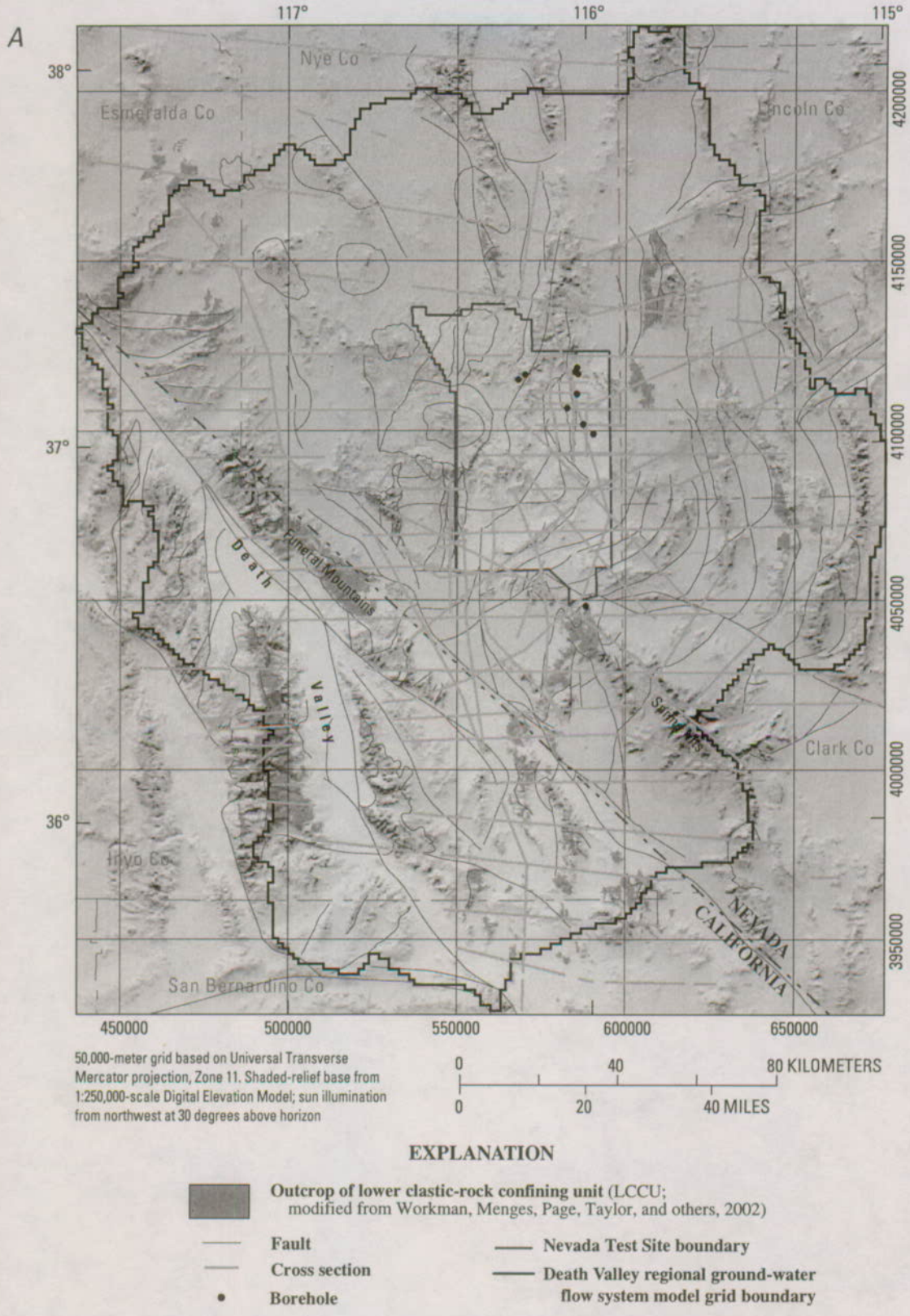

Figure E–36. (*A*) Data sources and (*B*) thickness of lower clastic-rock confining unit.

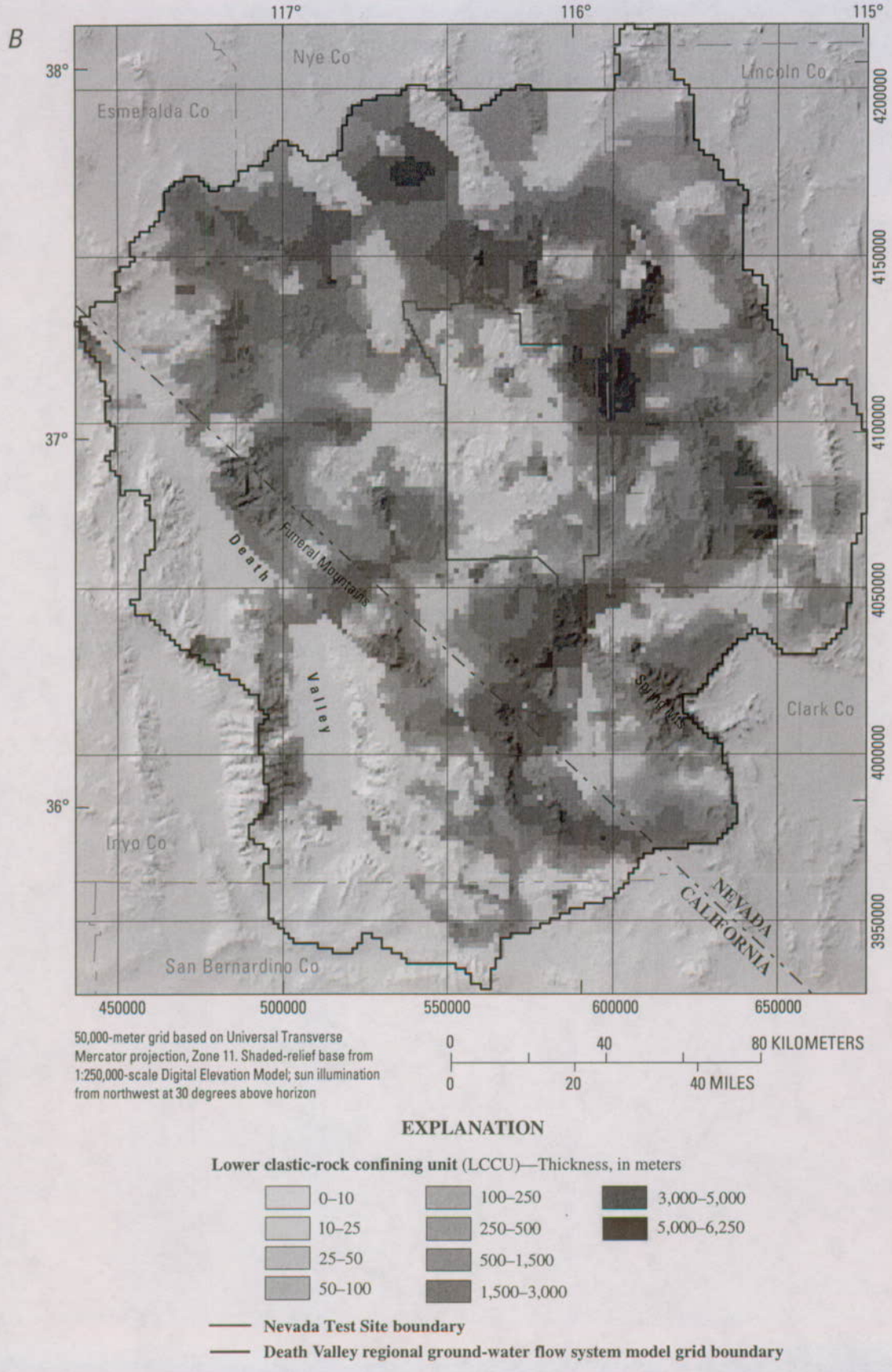

Figure E–36. (*A*) Data sources and (*B*) thickness of lower clastic-rock confining unit.—Continued

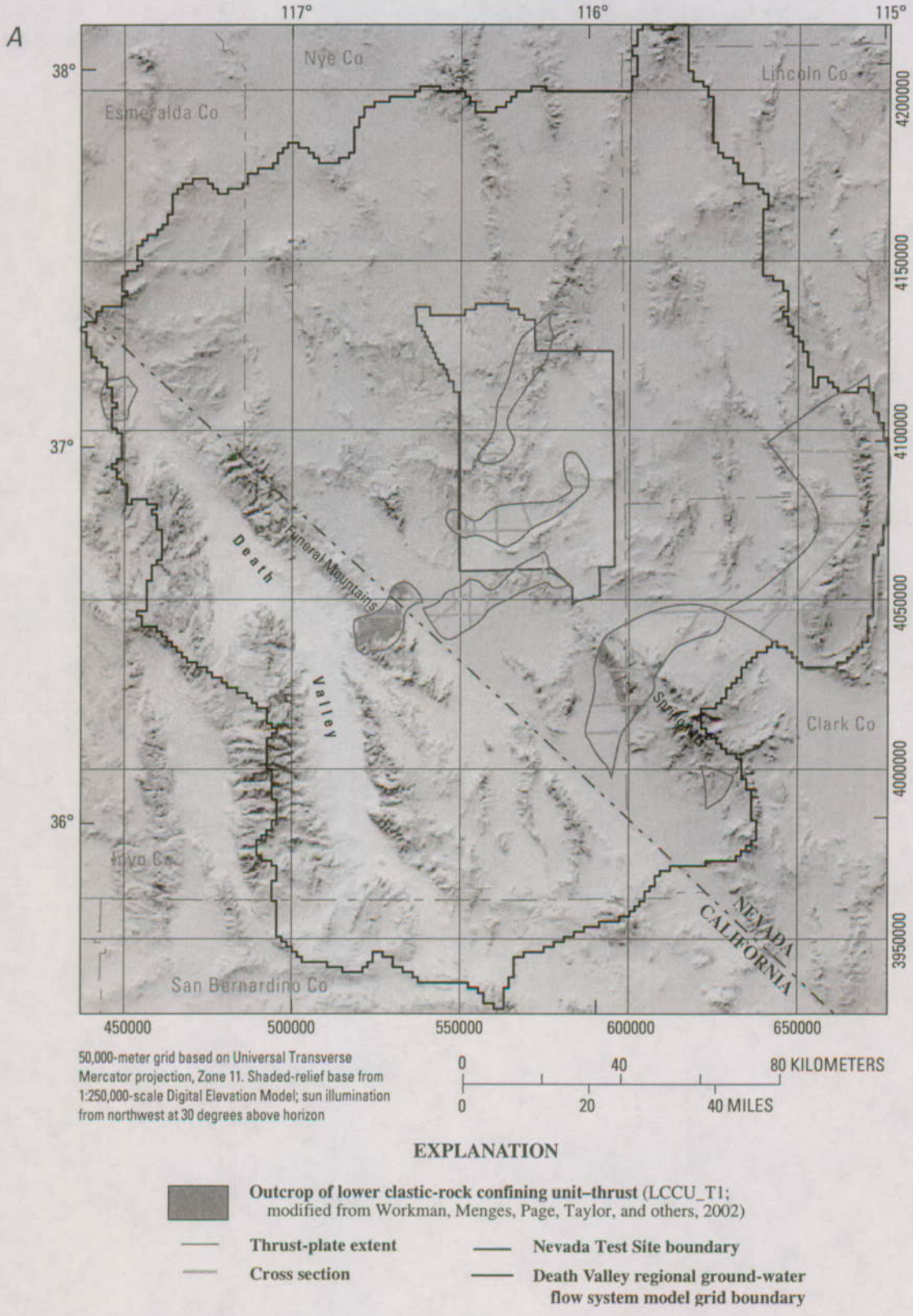

Figure E–37. (*A*) Data sources and (*B*) thickness of thrusted lower clastic-rock confining unit.

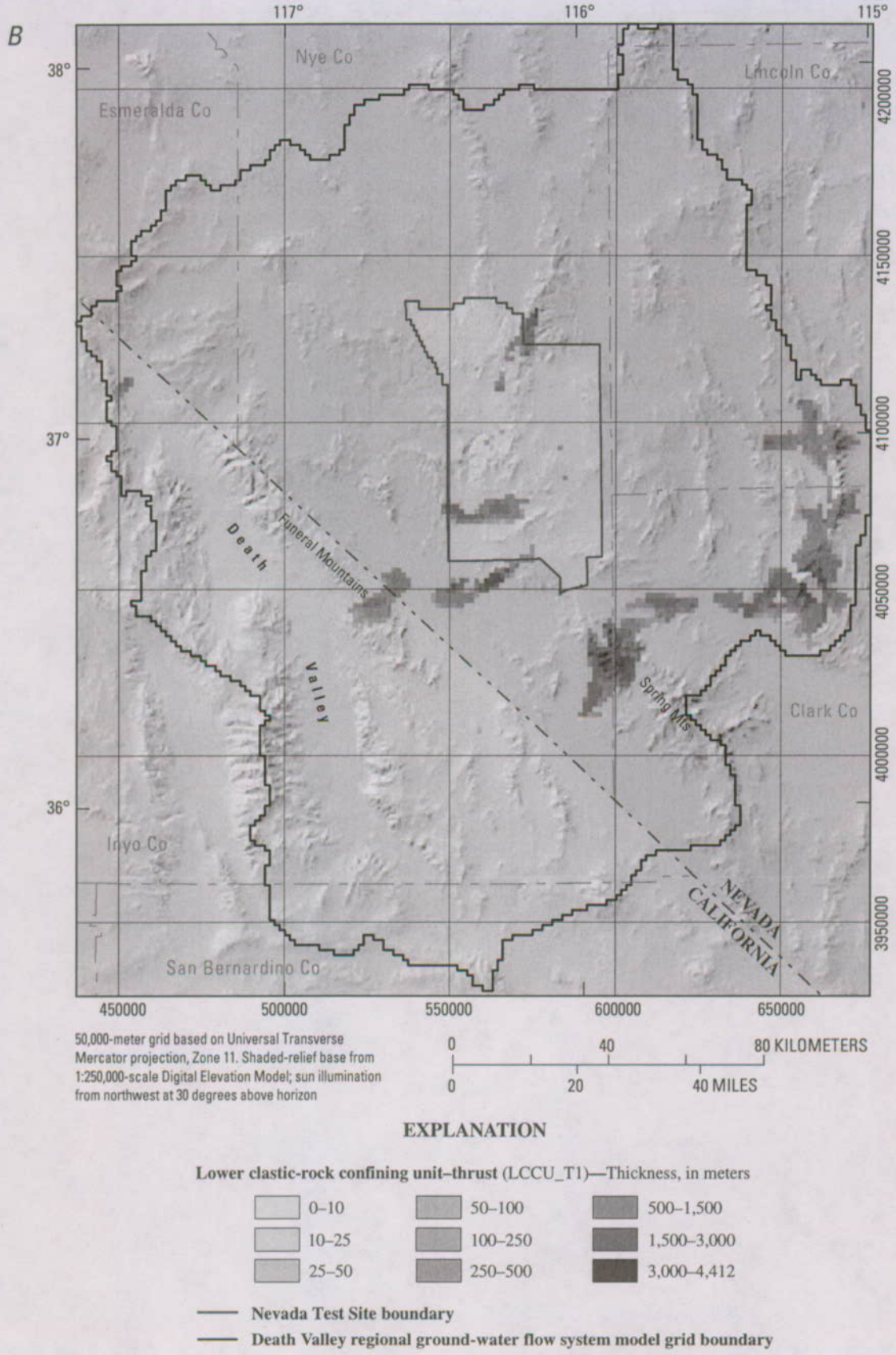

Figure E–37. (*A*) Data sources and (*B*) thickness of thrusted lower clastic-rock confining unit.—Continued

Figure E–38. (*A*) Data sources and (*B*) thickness of crystalline-rock confining unit.

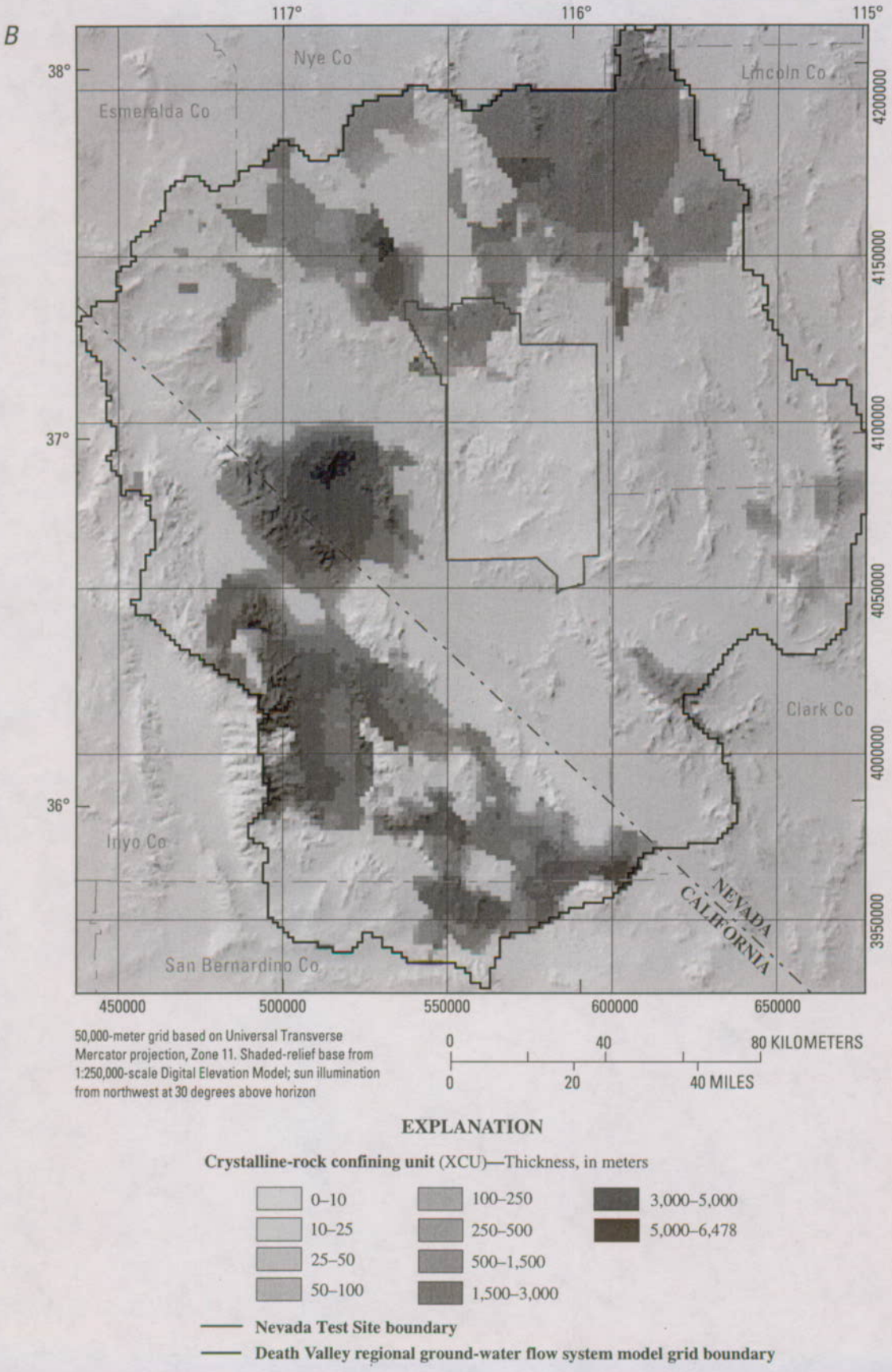

Figure E–38. (*A*) Data sources and (*B*) thickness of crystalline-rock confining unit.—Continued

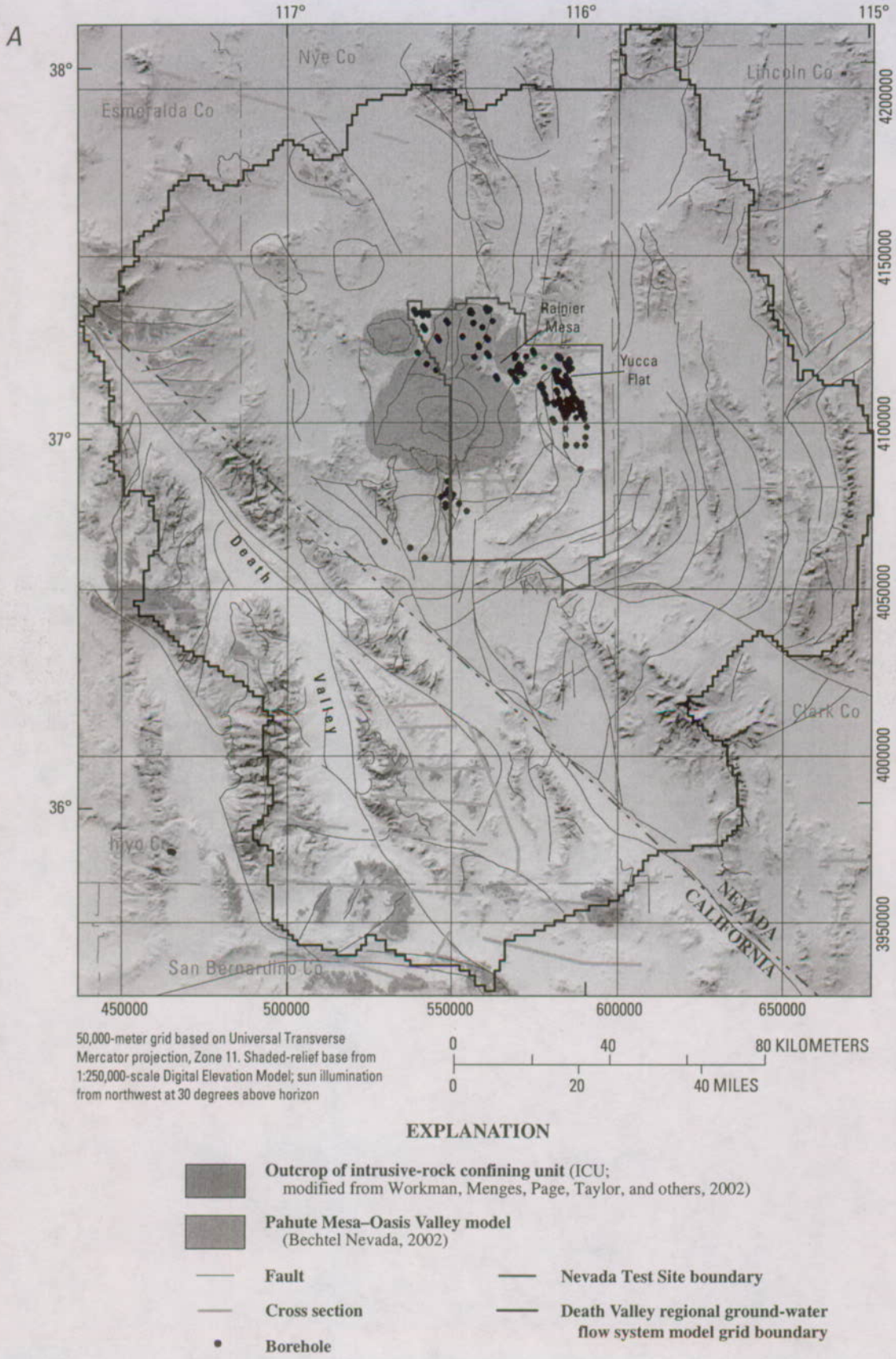

Figure E–39. (*A*) Data sources and (*B*) thickness of intrusive-rock confining unit.

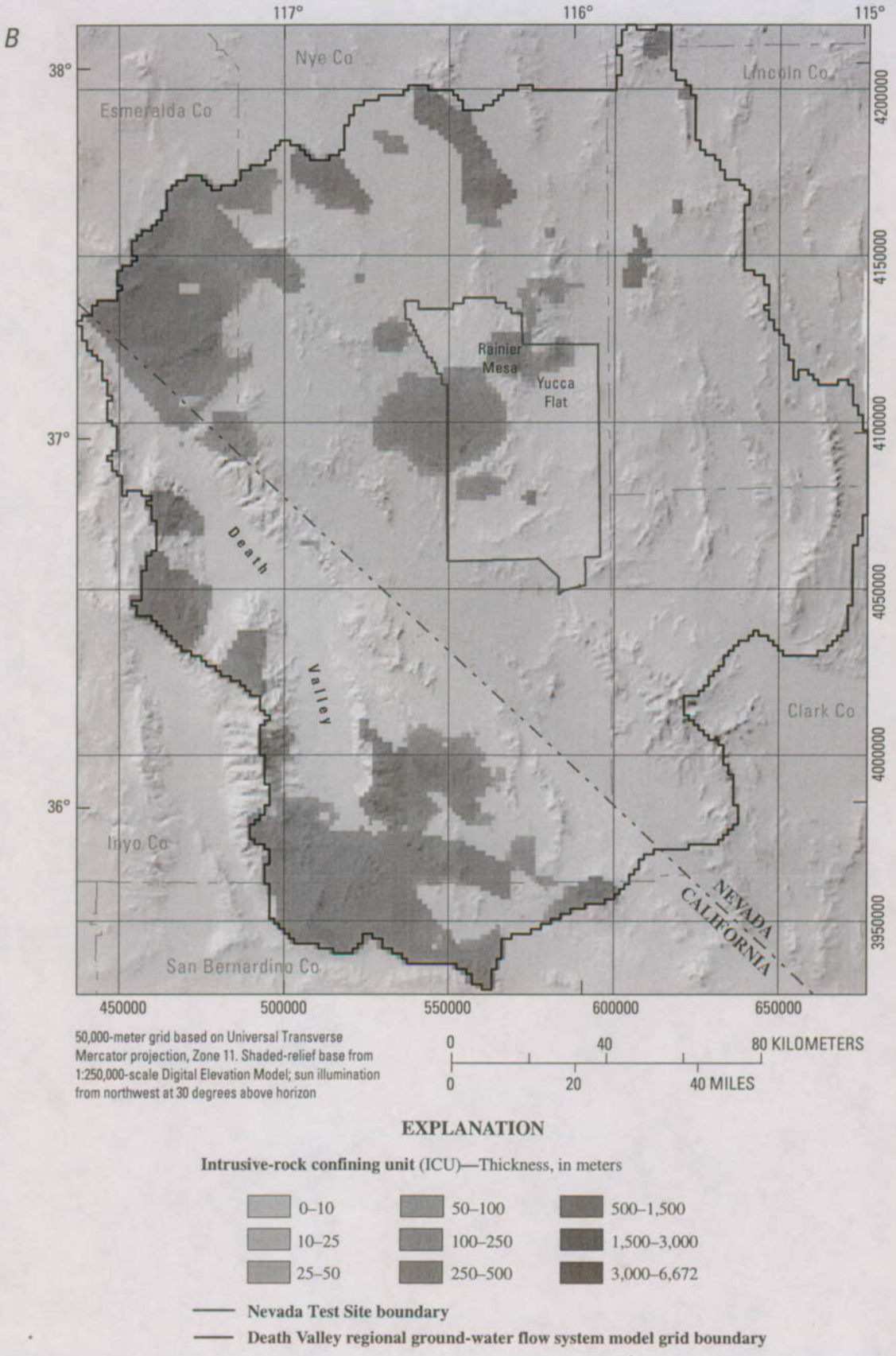

Figure E–39. (*A*) Data sources and (*B*) thickness of intrusive-rock confining unit.—Continued

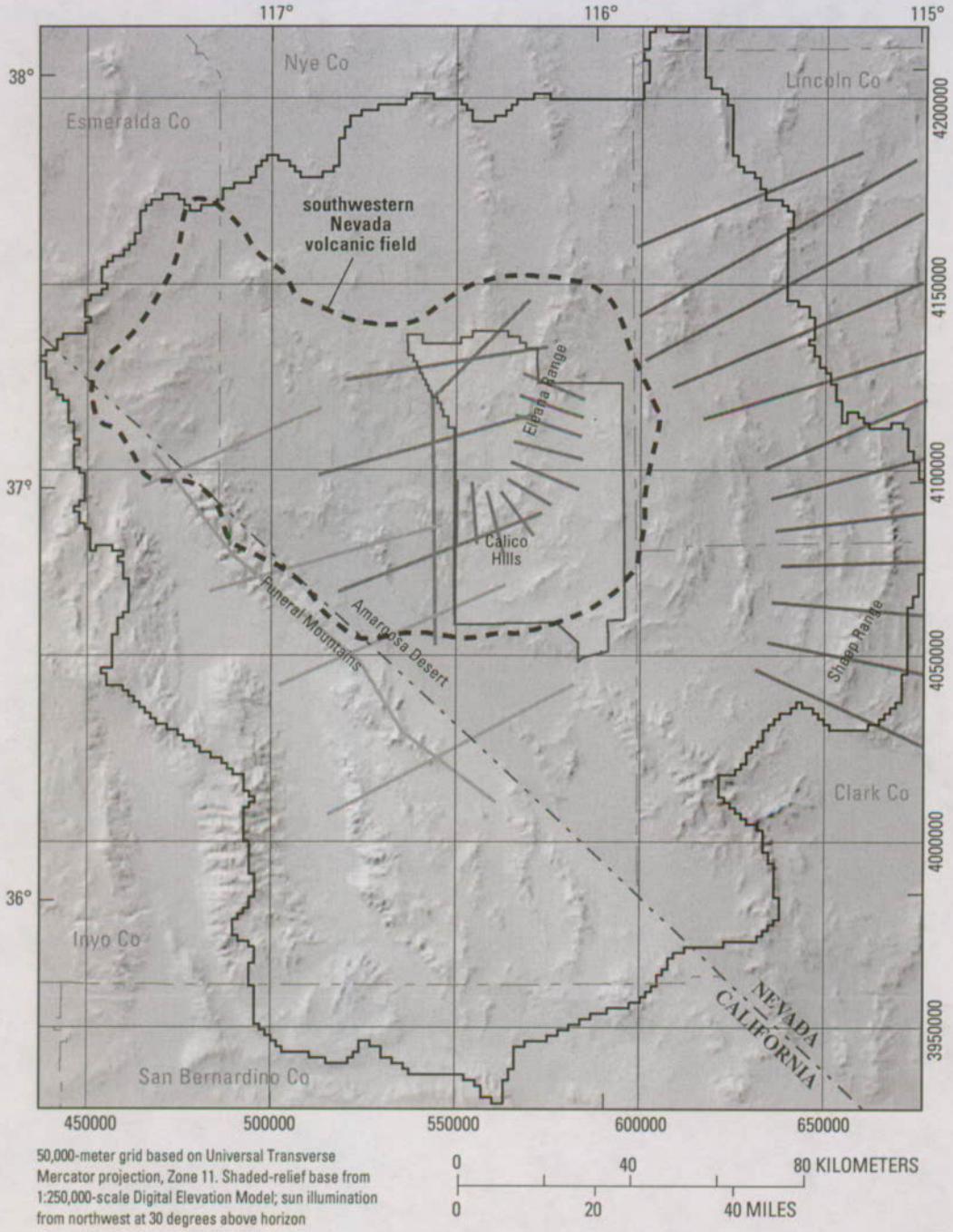

EXPLANATION

Sections—

- Sheep Range and Pahranagat Range
- Eleana Range and Calico Hills
- Southwestern Nevada volcanic field
- Funeral Mountains and Amargosa Desert

Nevada Test Site boundary

Death Valley regional ground-water flow system model grid boundary

Figure E–40. Locations of sections from the hydrogeologic framework model in key areas.

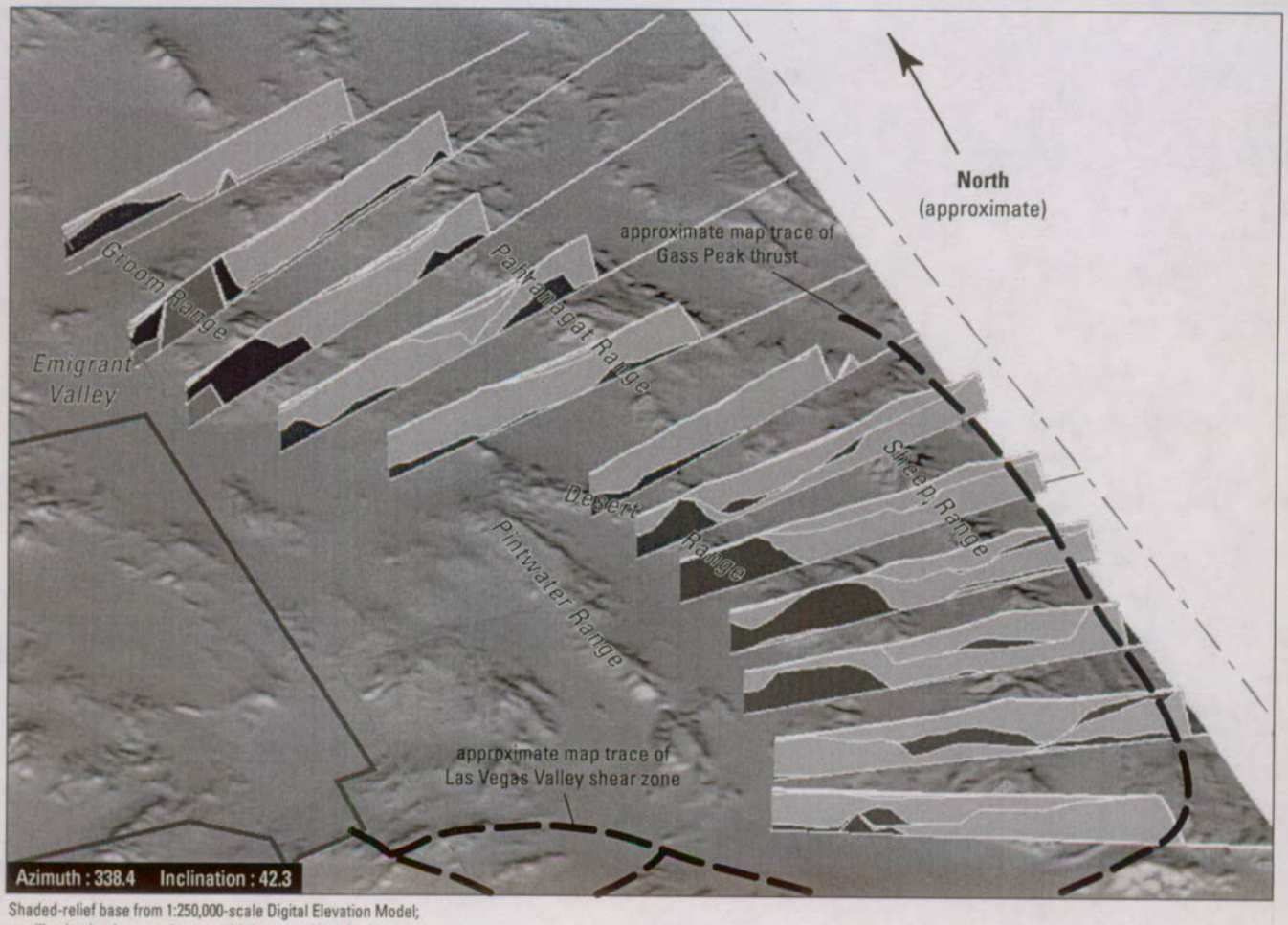

Shaded-relief base from 1:250,000-scale Digital Elevation Model;
sun illumination from northwest at 30 degrees above horizon

EXPLANATION

Hydrogeologic unit
(Not all units appear on sections)

- Younger alluvial aquifer (**YAA**)
- Younger alluvial confining unit (**YACU**)
- Older alluvial aquifer (**OAA**)
- Older alluvial confining unit (**OACU**)
- Limestone aquifer (**LA**)
- Lava-flow unit (**LFU**)
- Younger volcanic-rock unit (**YVU**)
- Upper volcanic- and sedimentary-rock unit (**upper VSU**)
- Timber Mountain–Thirsty Canyon volcanic-rock aquifer (**TMVA**)
- Paintbrush volcanic-rock aquifer (**PVA**)
- Calico Hills volcanic-rock unit (**CHVU**)
- Wahmonie volcanic-rock unit (**WVU**)
- Crater Flat–Prow Pass aquifer (**CFPPA**)
- Crater Flat–Bullfrog confining unit (**CFBCU**)
- Crater Flat–Tram aquifer (**CFTA**)
- Belted Range unit (**BRU**)
- Older volcanic-rock unit (**OVU**)
- Lower volcanic- and sedimentary-rock unit (**lower VSU**)
- Sedimentary-rock confining unit (**SCU**)
- Lower carbonate-rock aquifer-thrust (**LCA_T1**)
- Lower clastic-rock confining unit-thrust (**LCCU_T1**)
- Upper carbonate-rock aquifer (**UCA**)
- Upper clastic-rock confining unit (**UCCU**)
- Lower carbonate-rock aquifer (**LCA**)
- Lower clastic-rock confining unit (**LCCU**)
- Crystalline-rock confining unit (**XCU**)
- Intrusive-rock confining unit (**ICU**)

Base of each cross section corresponds to the base of the regional hydrogeologic framework model (4,000 meters below sea level)

Azimuth—Specifies horizontal angle that north end of model has been rotated from north

Inclination—Specifies vertical angle that the model has been rotated from horizontal

County line

Nevada Test Site boundary

Figure E–41. Sections from the hydrogeologic framework model across the Sheep Range and adjacent areas.

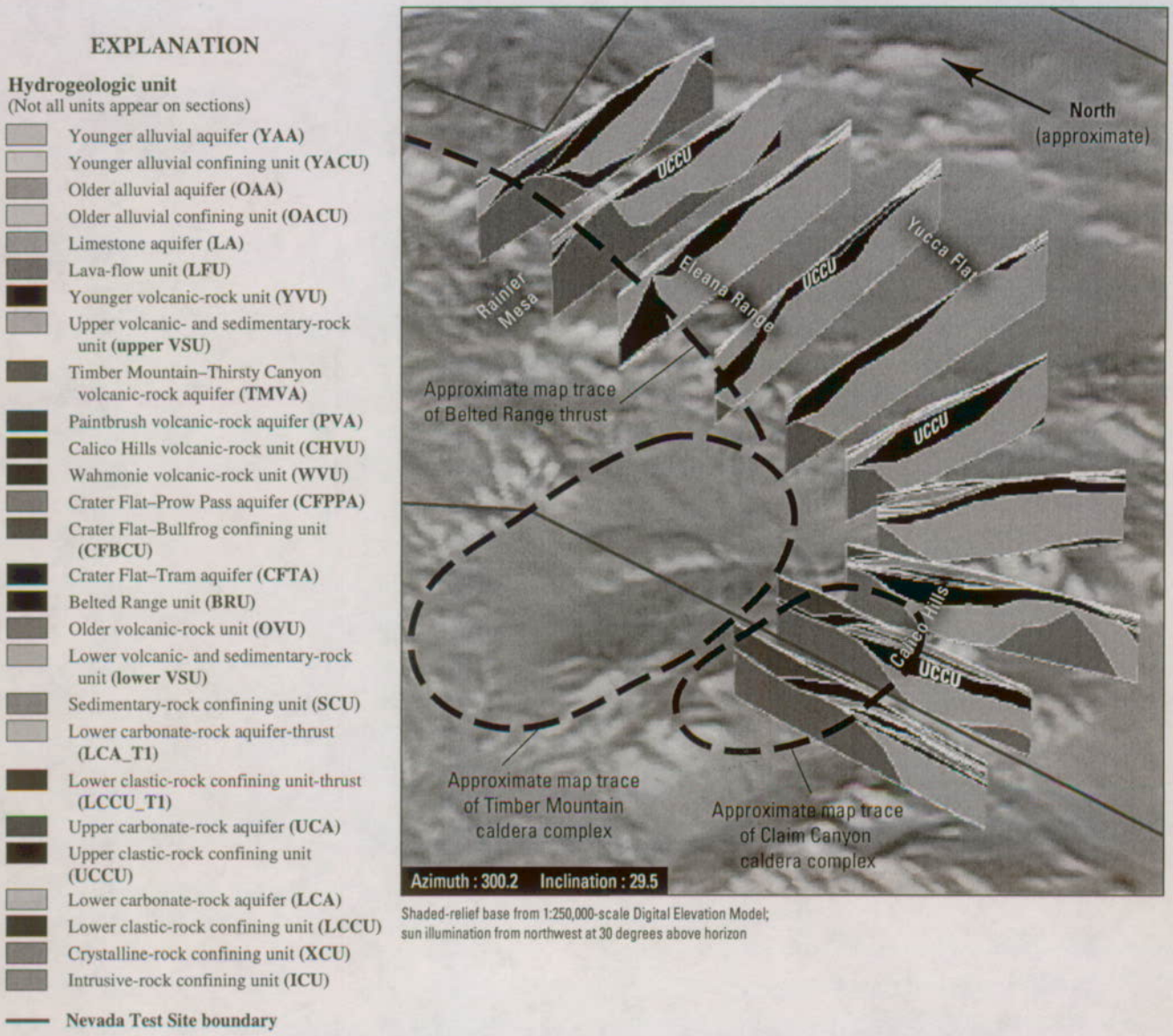

Shaded-relief base from 1:250,000-scale Digital Elevation Model; sun illumination from northwest at 30 degrees above horizon

Figure E–42. Sections from the hydrogeologic framework model across the Eleana Range and Calico Hills.

Funeral Mountains and Amargosa Desert

The Boundary Canyon detachment in the central Funeral Mountains is a gently dipping fault that juxtaposes LCCU and XCU in the lower plate, and the unmetamorphosed rocks of the upper plate (Wright and Troxel, 1993; Hamilton, 1988). Sections from the HFM in the vicinity of the Funeral Mountains (fig. E–44) portray the archlike Boundary Canyon detachment in the Grapevine and Funeral Mountains. In the vicinity of the Grapevine Mountains, the upper plate of the detachment fault as portrayed in the HFM contains LCCU and LCA, which are onlapped by volcanic rocks in the vicinity of Sarcobatus Flat and Grapevine Canyon (northernmost section in fig. E–44). In the vicinity of Furnace Creek, the HFM is dominated by LCCU above the Boundary Canyon detachment fault and both LCCU and XCU exist beneath this fault. The southeastern end of the Funeral Mountains is dominated by LCA, with LCCU being carried in the upper plates of the thrusts.

The southernmost section from the HFM (fig. E–44) extends from the vicinity of Badwater Basin in Death Valley through Furnace Creek Wash, the southern Funeral Mountains, and the Amargosa Desert. The eastern end of the section includes the vicinity of Devils Hole and Amargosa Flat. This section portrays the juxtaposition of the basin fill and the LCA in the Amargosa Desert. The Furnace Creek fault zone

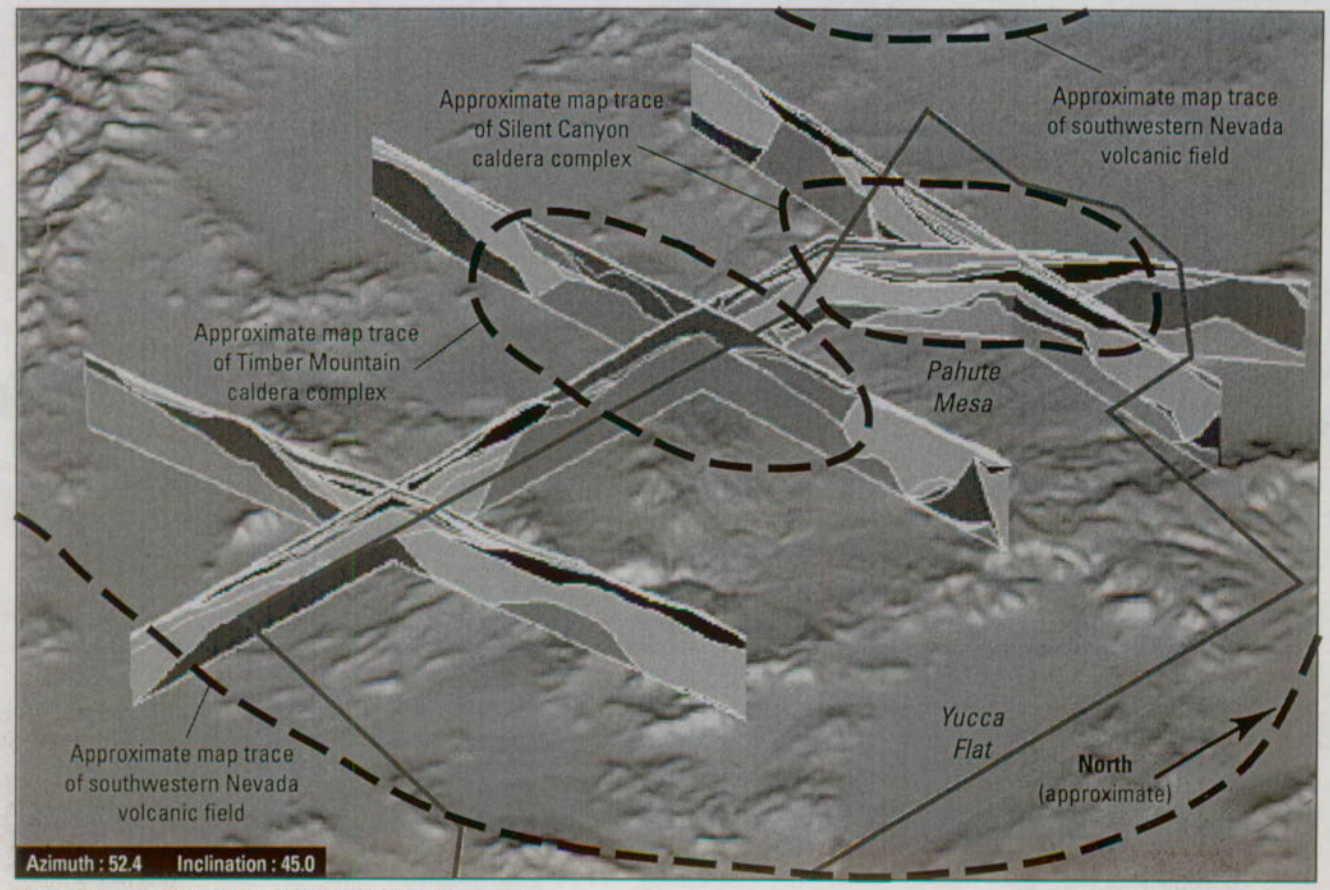

Shaded-relief base from 1:250,000-scale Digital Elevation Model; sun illumination from northwest at 30 degrees above horizon

EXPLANATION

Hydrogeologic unit
(Not all units appear on sections)

- Younger alluvial aquifer (**YAA**)
- Younger alluvial confining unit (**YACU**)
- Older alluvial aquifer (**OAA**)
- Older alluvial confining unit (**OACU**)
- Limestone aquifer (**LA**)
- Lava-flow unit (**LFU**)
- Younger volcanic-rock unit (**YVU**)
- Upper volcanic- and sedimentary-rock unit (**upper VSU**)
- Timber Mountain–Thirsty Canyon volcanic-rock aquifer (**TMVA**)
- Paintbrush volcanic-rock aquifer (**PVA**)
- Calico Hills volcanic-rock unit (**CHVU**
- Wahmonie volcanic-rock unit (**WVU**)
- Crater Flat–Prow Pass aquifer (**CFPPA**)
- Crater Flat–Bullfrog confining unit (**CFBCU**)
- Crater Flat–Tram aquifer (**CFTA**)
- Belted Range unit (**BRU**)
- Older volcanic-rock unit (**OVU**)
- Lower volcanic- and sedimentary-rock unit (**lower VSU**)
- Sedimentary-rock confining unit (**SCU**)
- Lower carbonate-rock aquifer-thrust (**LCA_T1**)
- Lower clastic-rock confining unit-thrust (**LCCU_T1**)
- Upper carbonate-rock aquifer (**UCA**)
- Upper clastic-rock confining unit (**UCCU**)
- Lower carbonate-rock aquifer (**LCA**)
- Lower clastic-rock confining unit (**LCCU**)
- Crystalline-rock confining unit (**XCU**)
- Intrusive-rock confining unit (**ICU**)

Base of each cross section corresponds to the base of the regional hydrogeologic framework model (4,000 meters below sea level)

Azimuth—Specifies horizontal angle that north end of model has been rotated from north

Inclination—Specifies vertical angle that the model has been rotated from horizontal

County line

Nevada Test Site boundary

Figure E–43. Sections from the hydrogeologic framework model across the southwestern Nevada volcanic field.

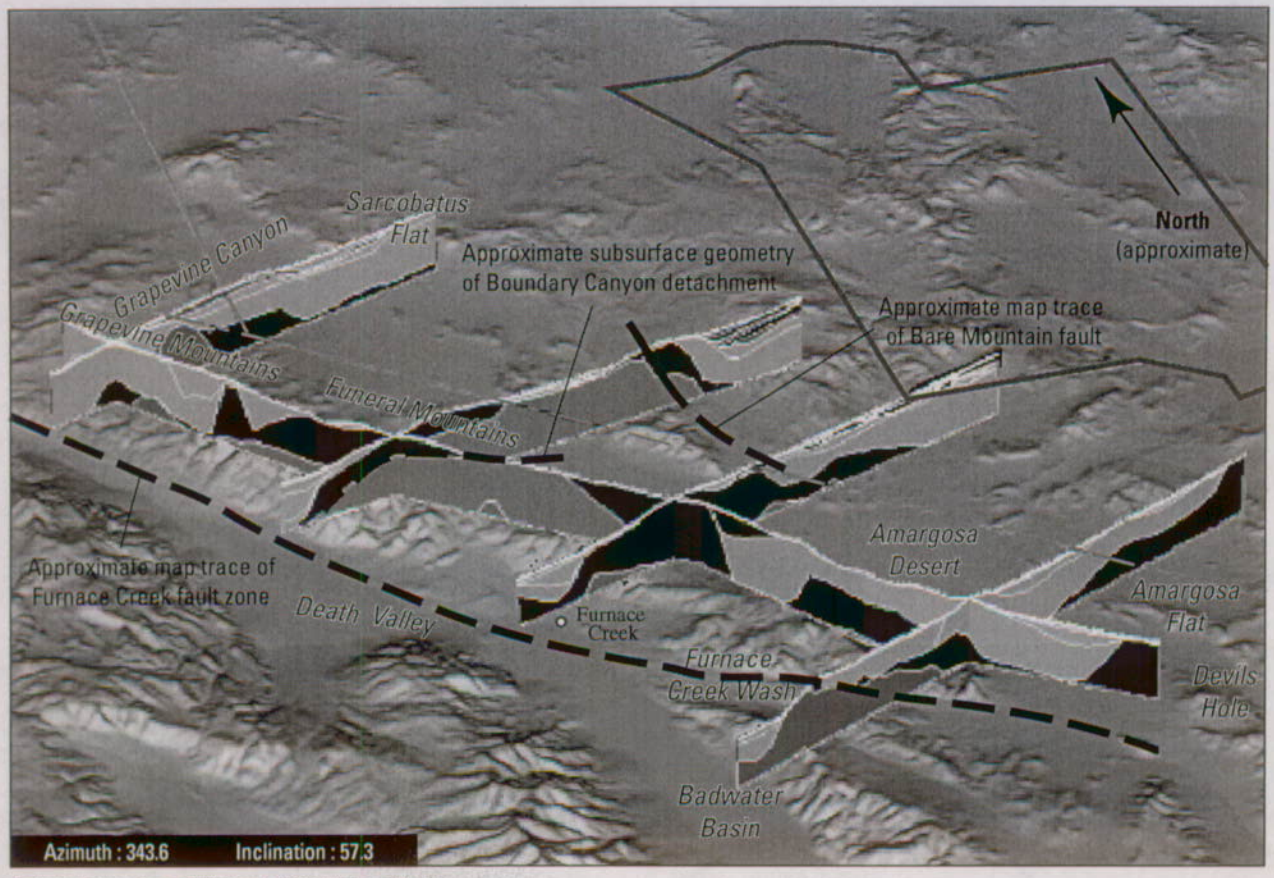

Shaded-relief base from 1:250,000-scale Digital Elevation Model; sun illumination from northwest at 30 degrees above horizon

EXPLANATION

Hydrogeologic unit
(Not all units appear on sections)

- Younger alluvial aquifer (**YAA**)
- Younger alluvial confining unit (**YACU**)
- Older alluvial aquifer (**OAA**)
- Older alluvial confining unit (**OACU**)
- Limestone aquifer (**LA**)
- Lava-flow unit (**LFU**)
- Younger volcanic-rock unit (**YVU**)
- Upper volcanic- and sedimentary-rock unit (**upper VSU**)
- Timber Mountain–Thirsty Canyon volcanic-rock aquifer (**TMVA**)
- Paintbrush volcanic-rock aquifer (**PVA**)
- Calico Hills volcanic-rock unit (**CHVU**)
- Wahmonie volcanic-rock unit (**WVU**)
- Crater Flat–Prow Pass aquifer (**CFPPA**)
- Crater Flat–Bullfrog confining unit (**CFBCU**)
- Crater Flat–Tram aquifer (**CFTA**)
- Belted Range unit (**BRU**)
- Older volcanic-rock unit (**OVU**)
- Lower volcanic- and sedimentary-rock unit (**lower VSU**)
- Sedimentary-rock confining unit (**SCU**)
- Lower carbonate-rock aquifer-thrust (**LCA_T1**)
- Lower clastic-rock confining unit-thrust (**LCCU_T1**)
- Upper carbonate-rock aquifer (**UCA**)
- Upper clastic-rock confining unit (**UCCU**)
- Lower carbonate-rock aquifer (**LCA**)
- Lower clastic-rock confining unit (**LCCU**)
- Crystalline-rock confining unit (**XCU**)
- Intrusive-rock confining unit (**ICU**)

Base of each cross section corresponds to the base of the regional hydrogeologic framework model (4,000 meters below sea level)

Azimuth—Specifies horizontal angle that north end of model has been rotated from north

Inclination—Specifies vertical angle that the model has been rotated from horizontal

- **County line**
- **Nevada Test Site boundary**
- **Populated location**

Figure E–44. Sections from the hydrogeologic framework model across the Funeral Mountains and Amargosa Desert.

abruptly terminates the LCA on the southwestern side of the Funeral Mountains. To the southwest, the Cenozoic sedimentary and volcanic rocks of the Furnace Creek Basin are portrayed by the lower VSU, deposited on LCCU/XCU/ICU, with the LCA having been tectonically removed through extreme extension (Chapter B, this volume).

Sections from the HFM in the vicinity of the western part of the Amargosa Desert (fig. E–44) portray a structurally high LCCU/XCU underlying a relatively thin (1,000 m or less) veneer of Cenozoic volcanic rocks and basin-fill deposits. Depth to pre-Cenozoic rocks increases east of the southern projection of the Bare Mountain fault, where basin fill reaches thicknesses of as much as 2,000 m on the basis of models of gravity data (Blakely and Ponce, 2001). The HFM portrays relatively continuous LCA deep beneath the Amargosa Desert. The basin-fill sedimentary rocks and unconsolidated deposits of the Amargosa Desert are largely portrayed by the lower VSU.

Summary

A three-dimensional (3D) digital hydrologic framework model (HFM) was constructed to develop an interpretation of the regional hydrogeology of the Death Valley regional ground-water flow system (DVRFS). The HFM integrates existing and new geologic information developed in the DVRFS region and describes the geometry and extent of the hydrogeologic units (HGUs) that control ground-water flow. It is an important information source for the DVRFS numerical ground-water flow model. The primary data sources used to develop the HFM are: digital elevation models, geologic maps, borehole lithologic logs, geologic and hydrogeologic cross sections, local 3D hydrogeologic framework models, and hydrostructural information. Approximately 70 regional geologic cross sections, reflecting a consistent interpretation of regional structural style, and approximately 7,000 lithologic contacts between HGUs from borehole information provided the subsurface control for the HFM. The geologic data from geologic maps, cross sections, and borehole lithologic logs were correlated into 27 HGUs. Gridded surfaces from other 3D hydrogeologic framework models constructed for the Nevada Test Site (NTS) and Yucca Mountain also were used.

The HFM defines regional-scale hydrogeology and structures to a depth of 4,000 m below sea level. The model has 1,500-m horizontal resolution and variable vertical thickness for the HGUs. The faults thought to be hydrologically significant were used for offsetting HGUs in the 3D model.

Evaluations of the HFM show that it generally portrays the regional hydrogeology. During flow-model calibration, in some locations the HFM did not allow accurate simulations. In such locations, the HFM was examined and the uncertainty in the existing interpretations considered; where alternative interpretations were appropriate and deemed necessary, the HFM was modified.

References Cited

Anderman, E.R., and Hill, M.C., 2000, MODFLOW-2000, the U.S. Geological Survey modular ground-water model; documentation of the Hydrogeologic-Unit Flow (HUF) Package: U.S. Geological Survey Open-File Report 00–0342, 89 p.

Bechtel Nevada, 2002, A hydrostratigraphic model and alternatives for the groundwater flow and contaminant transport model of Corrective Action Units 101 and 102: Central and Western Pahute Mesa, Nye County, Nevada: U.S. Department of Energy report DOE/NV/11718–706, various pagination.

Bechtel SAIC Company, 2002, Geologic framework model (GFM2000): Las Vegas, Nevada, U. S. Department of Energy report MDL–NBS–GS–000002, REV 01, Accession No. MOL.20020530.0078.

Blakely, R.J., and Ponce, D.A., 2001, Map showing depth to pre-Cenozoic basement in the Death Valley ground-water model area, Nevada and California: U.S. Geological Survey Miscellaneous Field Studies Map, MF–2381–E, 1 sheet, 5 p., scale 1:250,000.

Carr, W.J., Byers, F.M., Jr., and Orkild, P.P., 1986, Stratigraphic and volcano-tectonic relations of Crater Flat Tuff and some older volcanic units, Nye County, Nevada: U.S. Geological Survey Professional Paper 1323, 28 p.

Cole, J.C., and Cashman, P.H., 1999, Structural relationships of pre-Tertiary rocks in the Nevada Test Site region, southern Nevada: U.S. Geological Survey Professional Paper 1607, 39 p.

D'Agnese, F.A., Faunt, C.C, Turner, A.K., and Hill, M.C., 1997, Hydrogeologic evaluation and numerical simulation of the Death Valley regional ground-water flow system, Nevada, and California: U.S. Geological Survey Water-Resources Investigations Report 96–4300, 124 p.

D'Agnese, F.A., O'Brien, G.M., Faunt, C.C., Belcher, W.R., and San Juan, C., 2002, A three-dimensional numerical model of predevelopment conditions in the Death Valley regional ground-water flow system, Nevada and California: U.S. Geological Survey Water-Resources Investigations Report 02–4102, 114 p. Accessed September 22, 2004, at *http://pubs.water.usgs.gov/wri024102/.*

Faunt, C.C., D'Agnese, F.A., and Turner, A.K., 1997, A hydrogeologic map of the Death Valley region, Nevada and California, developed using GIS techniques: U.S. Geological Survey Water-Resources Investigations Report 95–4016, 18 p., 1 plate.

Golden Software, Inc., 1997, SURFER version 6 for Windows User's guide: Golden, Colo., Golden Software, various pagination.

Grose, T.L.T., 1983, Thirty-two geologic cross sections, Clark, Esmeralda, Lincoln, Mineral, and Nye Counties, Nevada, and adjacent areas in California: Nevada Bureau of Mines and Geology Open-File Report 83–13, University of Nevada-Reno, 90 p., 48 plates.

Grose, T.L., and Smith, G.I., 1989, Geology, *in* Bedinger, M.S., Sargent, K.A., and Langer, W.H., eds., Studies of geology and hydrology in the Basin and Range Province, Southwestern United States, for isolation of high-level radioactive waste: U.S. Geological Survey Professional Paper 1370–F, p. 5–19.

Guth, P.L., 1981, Tertiary extension north of the Las Vegas Valley shear zone, Sheep and Desert Ranges, Clark County, Nevada: Geological Society of America Bulletin, v. 92, p. 763–771.

Guth, P.L., 1990, Superposed Mesozoic and Cenozoic deformation, Indian Springs quadrangle, southern Nevada, *in* Wernicke, B.P., ed., Basin and Range extensional tectonics near the latitude of Las Vegas, Nevada: Geological Society of America Memoir 176, p. 237–249.

Hamilton, W.B., 1988, Detachment faulting in the Death Valley region, California and Nevada, *in* Carr, M.D., and Yount, J.C., eds., Geologic and hydrologic investigations of a potential nuclear waste disposal site at Yucca Mountain, southern Nevada: U.S. Geological Survey Bulletin 1790, p. 51–85.

Harbaugh, J.W., Banta, E.R., Hill, M.C., and McDonald, M.G., 2000, MODFLOW-2000, The U.S. Geological Survey's modular ground-water flow model—User guide to modularization concepts and the ground-water flow process: U.S. Geological Survey Open-File Report 00–92, 121 p.

Hill, M.C., Banta, E.R., Harbaugh, A.W., and Anderman, E.R., 2000, MODFLOW-2000, The U.S. Geological Survey's modular ground-water flow model—User guide to the observation, sensitivity, and parameter-estimation procedures and three post-processing programs: U.S. Geological Survey Open-File Report 00–184, 209 p., accessed on September 1, 2004, at *http://water.usgs.gov/nrp/gwsoftware/MODFLOW-2000/MODFLOW-2000.html*

Houser, F.N., Davis, R.E., and Emerick, W.L., 1961, Geologic reconnaissance of granitic intrusive masses at Gold Meadows, Tem Piute, and Trappman's Camp, Lincoln and Nye Counties, Nevada, and comparison with the Climax Stock at the Nevada Test Site: U.S. Geological Survey Open-File Report TEI–793, 20 p.

Hildenbrand, T.G., Langenheim, V.E., Mankinen, E.A., and McKee, E.H., 1999, Inversion of gravity data to define the pre-Tertiary surface and regional structures possibly influencing ground-water flow in the Pahute Mesa-Oasis Valley region, Nye County, Nevada: U.S. Geological Survey Open-File Report 99–49, 27 p.

IT Corporation, 1996a, Underground test area subproject, Phase I, Data analysis task, volume I—Geologic model data documentation package: Las Vegas, Nev., Report ITLV/10972–181 prepared for the U.S. Department of Energy, 8 vols., various pagination.

IT Corporation, 1996b, Underground test area subproject phase I, Data analysis task, volume VI—Groundwater flow model data documentation package: Las Vegas, Nev., Report ITLV/10972–81 prepared for the U.S. Department of Energy, 8 vols., various pagination.

Lipman, P.W., 1984, The roots of ash-flow calderas in western North America—Windows into the tops of granitic batholiths: Journal of Geophysical Research, v. 89, p. 8801–8841.

Lipman, P.W., 1997, Subsidence of ash-flow calderas—Relation to caldera size and magma chamber geometry: Bulletin Volcanologique, v. 59, p. 198–218.

Longwell, C.R., Pampeyan, E.H., Bowyer, Ben, and Roberts, R.J., 1965, Geology and mineral deposits of Clark County, Nevada: Nevada Bureau of Mines and Geology Bulletin 62, 218 p., 16 plates.

McKee, E.H., Phelps, G.A., and Mankinen, E.A., 2001, The Silent Canyon caldera—A three–dimensional model as part of a Pahute Mesa, Oasis Valley, Nevada, hydrogeologic model: U.S. Geological Survey Open-File Report 01–297. Accessed August 2, 2004, at *http://geopubs.wr.usgs.gov/open-file/of01-297/of01-297.pdf*

Nye County, 2004, Early warning drilling program: Nye County geologic data available on the Web. Accessed August 5, 2004, at *http://nyecounty.com/ewdpmain.htm*

Petrosys Pty. Ltd., 2003, Petrosys reference guide 12.3: Kent Town, Australia, Petrosys Pty, Ltd., various pagination.

Ponce, D.A., Blakely, R.J., Morin, R.L., and Mankinen, E.A., 2001, Isostatic map of the Death Valley ground-water model area, Nevada and California: U.S. Geological Survey Miscellaneous Field Studies Map MF–2381–C, 1:250,000 scale, 1 plate, with pamphlet. Accessed August 2, 2004, at *http://greenwood.cr.usgs.gov/pub/mf-maps/mf-2381/.*

Ponce, D.A., and Blakely, R.J., 2001, Aeromagnetic map of the Death Valley ground-water model area, Nevada and California, Miscellaneous Field Studies Map, MF–2381–D, 1 sheet, 1:250,000 scale, 5 pages of explanatory text.

Potter, C.J., Dickerson, R.P., Sweetkind, D.S., Drake III, R.M., Taylor, E.M., Fridrich, C.J., San Juan, C.A., and Day, W.C., 2002, Geological map of the Yucca Mountain region, Nye County, Nevada: U.S. Geological Survey Geologic Investigations Series I–2755, 1 sheet, 1:50,000 scale, 44 pages of explanatory text.

Potter, C.J., Sweetkind, D.S., Dickerson, R.P., and Kilgore, M.L., 2002, Hydrostructural maps of the Death Valley regional flow system, Nevada and California: U.S. Geological Survey Miscellaneous Field Studies Map MF–2372, 2 sheets, 1:250,000 scale, 14 pages of explanatory text.

Slate, J.L., Berry, M.E., Rowley, P.D., Fridrich, C.J., Morgan, K.S., Workman, J.B., Young, O.D., Dixon, G.L., Williams, V.S., McKee, E.H., Ponce, D.A., Hildenbrand, T.G., Swadley, WC, Lundstrom, S.C., Ekren, E.B., Warren, R.G., Cole, J.C., Fleck, R.J., Lanphere, M.A., Sawyer, D.A., Minor, S.A., Grunwald, D.J., Laczniak, R.J., Menges, C.M., Yount, J.C., and Jayko, A.S., 2000, Digital geologic map of the Nevada Test Site and vicinity, Nye, Lincoln, and Clark Counties, Nevada, and Inyo County, California: U.S. Geological Survey Open-File Report 99–554A, 53 p, scale 1:120,000.

Snow, J.K., and Wernicke, B.P., 2000, Cenozoic tectonism in the central Basin and Range—Magnitude, rate and distribution of upper crustal strain: American Journal of Science, v. 300, p. 659–719.

Sweetkind, D.S., Dickerson, R.P., Blakely, R.J., and Denning, P.D., 2001, Interpretive geologic cross sections for the Death Valley regional flow system and surrounding areas, Nevada and California: U.S. Geological Survey Miscellaneous Field Studies Map MF–2370, 3 plates, 32 pages of explanatory text. Accessed August 2, 2004, at *http://greenwood.cr.usgs.gov/pub/mf-maps/mf-2370/.*

U.S. Geological Survey, 2004, Geographic Data Download: U.S. Geological Survey data available on the Web. Accessed August 5, 2004, at *http://edc.usgs.gov/geodata*

Wahl, R.R., Sawyer, D.A., Minor, S.A., Carr, M.D., Cole, J.C., Swadley, WC, Laczniak, R.J., Warren, R.G., Green, K.S., and Engle, C.M., 1997, Digital geologic map of the Nevada Test Site area, Nevada: U.S. Geological Survey Open-File Report 97–140, scale 1:120,000.

Warren, R.G., Sawyer, D.A., Byers, F.M., Jr., and Cole, G.L., 1998, A petrographic/geochemical database and structural framework for the southwestern Nevada volcanic field: National Geophysical Data Center data available on the Web. Accessed August 5, 2004, at *http://queeg.ngdc.noaa.gov/seg/geochem/swnvf/.*

Warren, R.G., Cole, G.L., and Walther, Douglas, 2000, A structural block model for the three-dimensional geology of the Southwestern Nevada Volcanic Field: Los Alamos National Laboratory Report LA–UR—00–5866, unpaginated.

Wernicke, B.P., Guth, P.L, and Axen, G.J., 1984, Tertiary extensional tectonics in the Sevier thrust belt of southern Nevada, *in* Lintz, J.P., ed., Western geological excursions: Reno, Nev., Mackay School of Mines, University of Nevada, Geological Society of America, Cordilleran Section, Field Trip Guidebook, p. 473–510.

Workman, J.B., Menges, C.M., Page, W.R., Ekren, E.B., Rowley, P.D., and Dixon, G.L., 2002, Tectonic map of the Death Valley ground-water model area, Nevada and California: U.S. Geological Survey Miscellaneous Field Studies Map MF–2381–B, scale 1:350,000, 1 plate with pamphlet.

Workman, J.B., Menges, C.M., Page, W.R., Taylor, E.M., Ekren, E.B., Rowley, P.D., Dixon, G.L., Thompson, R.A., and Wright, L.A., 2002, Geologic map of the Death Valley ground-water model area, Nevada and California: U.S. Geological Survey Miscellaneous Field Studies Map MF–2381–A. Accessed August 2, 2004, at *http://greenwood.cr.usgs.gov/pub/mf-maps/mf-2381/.*

Wright, L.A., and Troxel, B.W., 1993, Geologic map of the central and northern Funeral Mountains and adjacent areas, Death Valley region, southern California: U.S. Geological Survey Miscellaneous Investigations Series Map I–2305, scale 1:48,000.

Transient Numerical Model

By Claudia C. Faunt, Joan B. Blainey, Mary C. Hill, Frank A. D'Agnese, and Grady M. O'Brien

Chapter F of

Death Valley Regional Ground-Water Flow System, Nevada and California—Hydrogeologic Framework and Transient Ground-Water Flow Model

Edited by Wayne R. Belcher

Prepared in cooperation with the
U.S. Department of Energy
Office of Environmental Management, National Nuclear Security Administration, Nevada Site Office,
under Interagency Agreement DE–AI52–01NV13944, and
Office of Repository Development,
under Interagency Agreement DE–AI08–02RW12167

Scientific Investigations Report 2004–5205

U.S. Department of the Interior
U.S. Geological Survey

Contents

Figures

Tables

CHAPTER F. Transient Numerical Model

By Claudia C. Faunt, Joan B. Blainey, Mary C. Hill, Frank A. D'Agnese, and Grady M. O'Brien

Introduction

The construction, calibration, and evaluation of the transient numerical flow model of the Death Valley regional ground-water flow system (DVRFS) are described in this chapter. Parameter-estimation techniques were used to calibrate the model to prepumping steady-state conditions before 1913 and to transient-flow conditions from 1913 to 1998 after pumping of ground water began.

Previous studies by Prudic and others (1995) and Waddell (1982) showed that it is difficult to use computer models to effectively describe ground-water flow in an area as geographically large, and geologically and hydrologically complex, as the Death Valley region. Prudic and others (1995) reiterated that the validity of the assumptions and hydrologic values used in simulating ground-water flow in such an area can be argued.

Inevitably, simplifications and assumptions must be made to adapt the complex conceptual model for numerical simulation. The simplifications and assumptions made in the development of the DVRFS model include the following:

1. Regional ground-water flow is assumed to be through a porous medium. Although the water flows through fractures, faults, and solution openings in the rocks, these features are small enough and densely distributed enough, relative to the large scale of the model, that the rocks can be represented as a porous medium.

2. Horizontal hydraulic conductivity is assumed to be isotropic within a model cell. Heterogeneity is simulated by varying horizontal hydraulic conductivity of model cells or groups of cells. A vertical anisotropy factor is used to scale vertical hydraulic conductivity based on specified values of horizontal hydraulic conductivity. Major faults likely to be subvertical and barriers to horizontal flow are represented explicitly and contribute horizontal anisotropy to the model.

3. Prepumping conditions are assumed to have been at equilibrium and to have represented average annual conditions so that system recharge equaled system discharge. During 1913–98, ground-water pumpage is assumed to be the only transient stress on the system to cause the observed decline in water levels in wells and is the only transient change simulated. This assumption is made because:

(a) Any long-term decline in hydraulic heads caused by decreased recharge since the wet period during the late Wisconsin glacial period (20 thousand years ago [ka] to 10 ka) can be neglected. Declines in water levels since the Wisconsin glacial period have been suggested by Prudic and others (1995) and Grasso (1996) and likely would be limited to slowly declining heads and seepage from low-permeability rocks and areas isolated from the rest of the system by low-permeability rocks. Simulating heads still affected by elevated water levels in Winconsin glacial period and neglecting the seepage could cause some model bias, but it is expected to be small. Also, the changes caused by this effect during the transient simulated period would be small (Prudic and others, 1995), so it is unlikely that drawdowns are affected.

(b) Decadal and seasonal fluctuations can be treated as noise in the observations. Thus, decadal and seasonal variations are accounted for through an analysis of observation errors, as discussed in the "Observations Used in Model Calibration" section of this chapter and in Chapter C (this volume).

Model Construction

The three-dimensional (3D) hydrogeologic data sets for the DVRFS described previously in this report (see Chapters B, C, and E) were discretized to develop the input arrays required for the model. Because the data sets were developed at grid cell resolutions ranging from 100 to 1,500 meters (m), their discretization to a common, larger grid cell resolution inevitably results in further simplification of the flow-system conceptual model and hydrogeologic framework model. This resampling and simplification of the 3D hydrogeologic data sets was apparent in (1) definition of the model grid, (2) assignment of boundary conditions, and (3) definition of model parameters.

A geographic information system (GIS) was used to ensure accurate spatial control of physical features and the finite-difference model grid. GIS also was used during calibration to manipulate and compare model input-data sets with model output.

Numerical Model Selection

The numerical modeling code used to simulate the DVRFS is the U.S. Geological Survey 3D ground-water flow model program MODFLOW-2000 with related packages (Harbaugh and others, 2000; Hill and others, 2000; Anderman and Hill, 2000, 2003; Hsieh and Freckleton, 1993). MODFLOW-2000 is a block-centered finite-difference code in which a 3D ground-water flow system is divided into a sequence of layers of porous material organized in a horizontal grid or array. MODFLOW-2000 (1) has the capabilities to represent the 3D complexities of the ground-water flow system; (2) contains methods for sensitivity analysis, calibration (including parameter estimation), and uncertainty evaluation; (3) includes a variety of hydrologic capabilities such as the simulation of wells and recharge; (4) can be applied to steady-state and transient flow conditions; and (5) is well documented, freely available, well tested, and widely accepted.

Grid Definition

The north-south-oriented grid for the flow model consists of 194 rows, 160 columns, and 16 layers, for a total of 496,640 cells with a constant grid-cell spacing of 1,500 m (fig. F–1). Because of the difference in grid definition between the mesh-centered hydrogeologic framework model (HFM) and the block-centered flow model, the HFM is one cell wider than the flow model. Finite-difference methods require that the model grid be constructed for the bounding rectangle of the DVRFS model domain, but only the cells within the model boundary are active and used to represent the flow system.

The model uses 16 layers to simulate the flow in the DVRFS. Most of these layers range in thickness from 50 to more than 300 m (table F–1 and fig. F–2). The thickness of model layer 16 varies and can extend as deep as 4,000 m below sea level; it is thickest in the Spring Mountains and isolated areas in the northeastern part of the model domain. With the exception of model layer 1, which has some thicker parts locally, model layer thickness generally increases with depth. This allows greater resolution at the top of the flow model where more hydrologic and geologic data are available.

The upper model layers are used to simulate relatively shallow flow primarily through basin-fill sediments and volcanic rocks and adjacent mountain ranges. The lower layers predominantly simulate deep flow through the regional carbonate-rock aquifer beneath the basin fill and mountain ranges. Model layer 1 is thick where low-permeability rocks, ground-water mounding, and(or) steep hydraulic gradients are present. It is thickest in the Spring Mountains and parts of the Grapevine Mountains.

The top of model layer 1 is set to the simulated potentiometric surface of layer 1. The bottom of layer 1 was set to always be below this simulated potentiometric surface. In a few isolated areas, the heads in layer 1 are simulated above land surface. These areas are in mountain ranges with low-permeability rocks and discharge areas. In the area around Mud Lake, heads also are simulated above land surface. This is not a realistic condition and most likely is a result of inaccurate portrayal of heads at the nearby constant-head boundaries.

In general, the model layers do not coincide with the hydrogeologic units (HGUs). The geometries of the HGUs in this system are complex because of considerable folding, faulting, and other processes, and it is not possible for model layers to conform to these irregular shapes (fig. F–2).

Temporal Discretization

For the DVRFS model, time is divided into steady-state or transient stress periods. The transient simulation begins with a prepumping steady-state period before 1913 in which no pumping is simulated. The subsequent 86-year period (1913–98) was divided into annual transient stress periods for which pumpage was defined. Within a single simulation, the same number of time steps, ranging from two to eight, was used in each stress period. The greater number of time steps did not improve model accuracy, and in the final calibrated model, two time steps per transient stress period are used.

Lateral Model Boundary Conditions

For previous simulations, the entire model boundary was represented as no flow and the only source of water in the model domain was recharge (D'Agnese and others, 1997, 2002). When using the recharge estimated from the net infiltration approximated by Hevesi and others (2003) (Chapter C, fig. C–8, this volume), ground-water levels and ground-water discharges could not be supported by the recharge, particularly in the north. Water-budget and Darcy-calculation estimates of flow from adjacent basins (Appendix 2, this volume) were used to help quantify flow into and out of the model domain. The type and location of the boundaries as well as the estimated flow are summarized in table F–2.

In order to simulate inflow or outflow across the model boundary, constant heads were specified in the cells along the boundary that are at or below the regional potentiometric surface. The hydraulic heads imposed at the constant-head cells were interpolated from the regional potentiometric surface (Appendix 1, this volume). As a result, the constant heads occur in different model layers along different parts of the boundary. The subsegment number and name are used as the observation name (table F–2). Observations are flows through subsegments defined as constant-head boundaries.

Hydraulic Properties

HGUs are the basis for assigning horizontal hydraulic conductivity, vertical anisotropy, depth decay of hydraulic conductivity, and storage characteristics to the cells of the model grid using the Hydrogeologic-Unit Flow (HUF) pack-

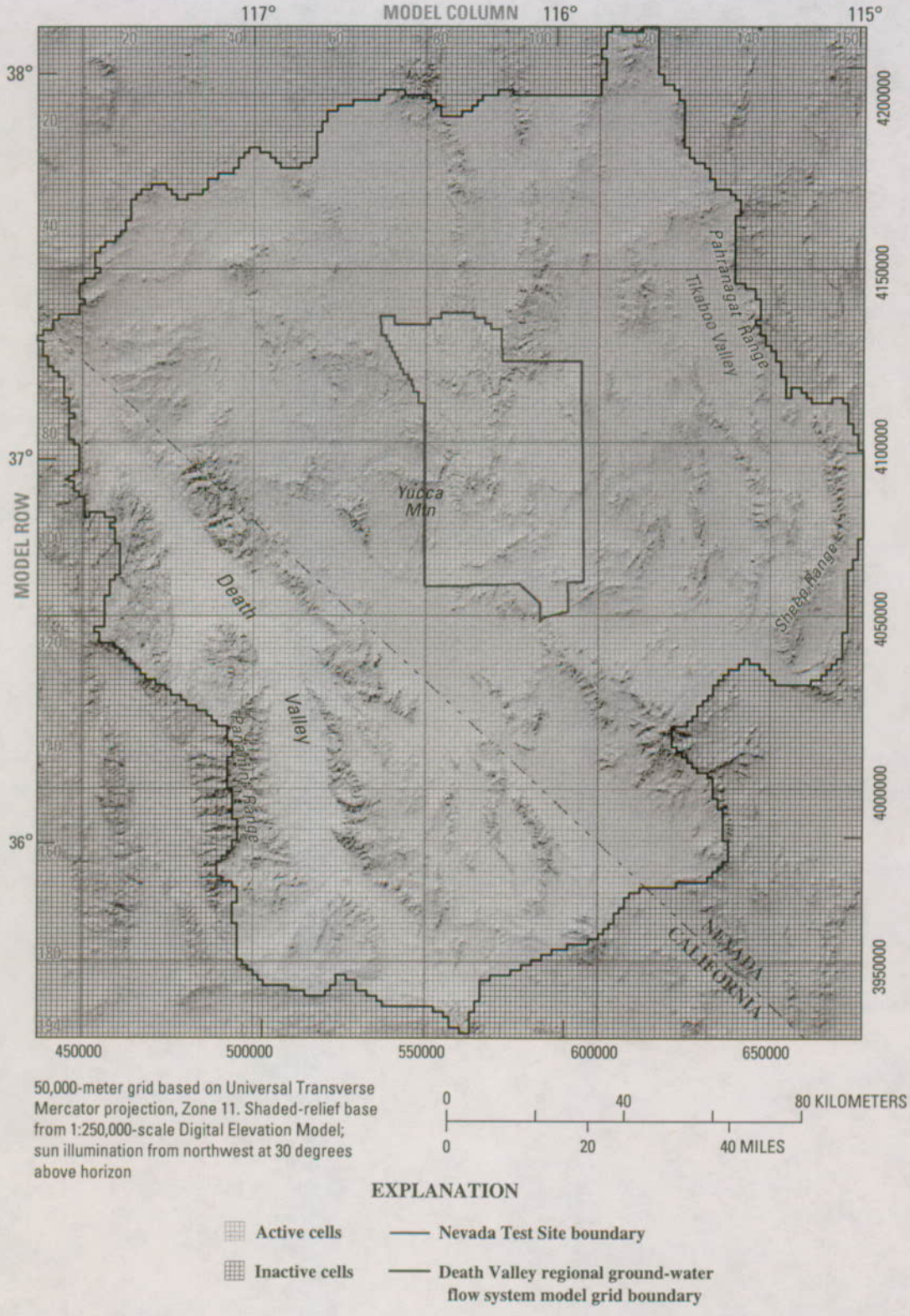

Figure F–1. Map showing location of model grid for the Death Valley regional ground-water flow system.

age (Anderman and Hill, 2000, 2003) for MODFLOW-2000. Model input arrays also were used to account for variations in the hydraulic properties within HGUs by zonation.

Hydrogeologic Units

The HUF package (Anderman and Hill, 2000, 2003) facilitates the discretization of the complicated geometry of the HGUs within the flow model. The HGUs are defined and assigned to model cells in the HUF package. Some model cells are filled by a single HGU; other model cells contain multiple HGUs. The HUF package vertically averages hydraulic properties for each cell based on the volume of the HGU occurring in the model cell.

Twenty-five HGUs (and two thrusted units) were defined for the DVRFS (Chapter B, this volume). These HGUs were combined into four major rock types representing the initial HGU parameters for the flow model: confining units (K1), carbonate-rock aquifers (K2), volcanic-rock units (K3), and basin-fill units (K4) (fig. F–3 and table F–3). These major rock types are shown in a fence diagram of the model domain in figure F–3.

Only 5 of the 27 HGUs defined in the flow model are spatially significant: the lower carbonate-rock aquifer (LCA), lower volcanic- and sedimentary-rock unit (lower VSU), lower clastic-rock confining unit (LCCU), crystalline-rock confining unit (XCU), and intrusive-rock confining unit (ICU). The LCCU, XCU, and ICU are generally of low permeability and form confining units. The LCA forms the regional aquifer and transports most of the flow from the north and east toward Death Valley. Locally, the basin-fill units are important for ground-water development in Pahrump and Penoyer Valleys and Amargosa Desert. The volcanic-rock units of the southwestern Nevada volcanic field (SWNVF) are important for ground-water flow and transport at the Nevada Test Site (NTS) and at Yucca Mountain (fig. F–3).

Table F–1. Thickness and depth to top of each layer of the flow model of the Death Valley regional flow system.

Model layer	Layer thickness (meters)	Minimum depth to top of layer (meters)
1	1 to 850	--
2	50	50
3	50	100
4	100	150
5	100	250
6	100	350
7	100	450
8	100	550
9	100	650
10	100	750
11	150	850
12	200	1,000
13	250	1,200
14	250	1,450
15	300	1,700
16	1,800 to 5,000	2,000

Depth Decay of Hydraulic Conductivity

To test the hypothesis that hydraulic conductivity decreases exponentially with depth (IT Corporation, 1996, p. 29), exponential decay was implemented in the HUF package of MODFLOW-2000 (Anderman and Hill, 2003), which allowed HGUs to be relatively impermeable at depth and relatively permeable near the land surface. The decay of hydraulic conductivity with depth is calculated as:

$$K_{Depth} = K_{Surface} 10^{-\lambda d} \quad (1)$$

where

K_{Depth} is the hydraulic conductivity at depth d [L/T],

$K_{Surface}$ is the hydraulic conductivity projected to the land surface [L/T],

λ is the depth-decay coefficient [L^{-1}],

and

d is the depth below land surface [L].

A value of $\lambda=1\times10^{-5}$ produces a hydraulic conductivity of 93 percent of the original value over 3,000 meters of depth; a value of $\lambda=1\times10^{-4}$ produces a hydraulic conductivity of 50 percent of the original value, and a value of $\lambda=1\times10^{-3}$ produces a hydraulic conductivity of 0.1 percent of the original value.

Vertical Anisotropy

Vertical anisotropy (the ratio of horizontal to vertical hydraulic conductivity) is defined for each HGU parameter by using the HUF package. Because of their layered nature, basin-fill sediments are likely to have significant vertical anisotropy. The assumed presence of solution features in carbonate rocks would indicate that these rocks have relatively small vertical anisotropy. The vertical anisotropy of other rocks and sediments would be expected to fall somewhere between these two extremes.

Storage Properties

In the HUF package, model layers can be defined as either confined or convertible between confined and unconfined (Anderman and Hill, 2003). Confined model layers are assigned a thickness that does not change during the simulation regardless of the simulated value of hydraulic head. In these layers, the storage coefficient generally equals the product of the specific storage and the model-layer thickness, where specific storage is defined for each HGU. If a cell contains more than one HGU, the specific-storage value for a cell equals a thickness-weighted average of the specific-storage values of the HGUs. All model layers were simulated as confined, and the storage consequences of water-table changes over time were simulated using a storage coefficient in the top model layer that was equivalent to a specific yield

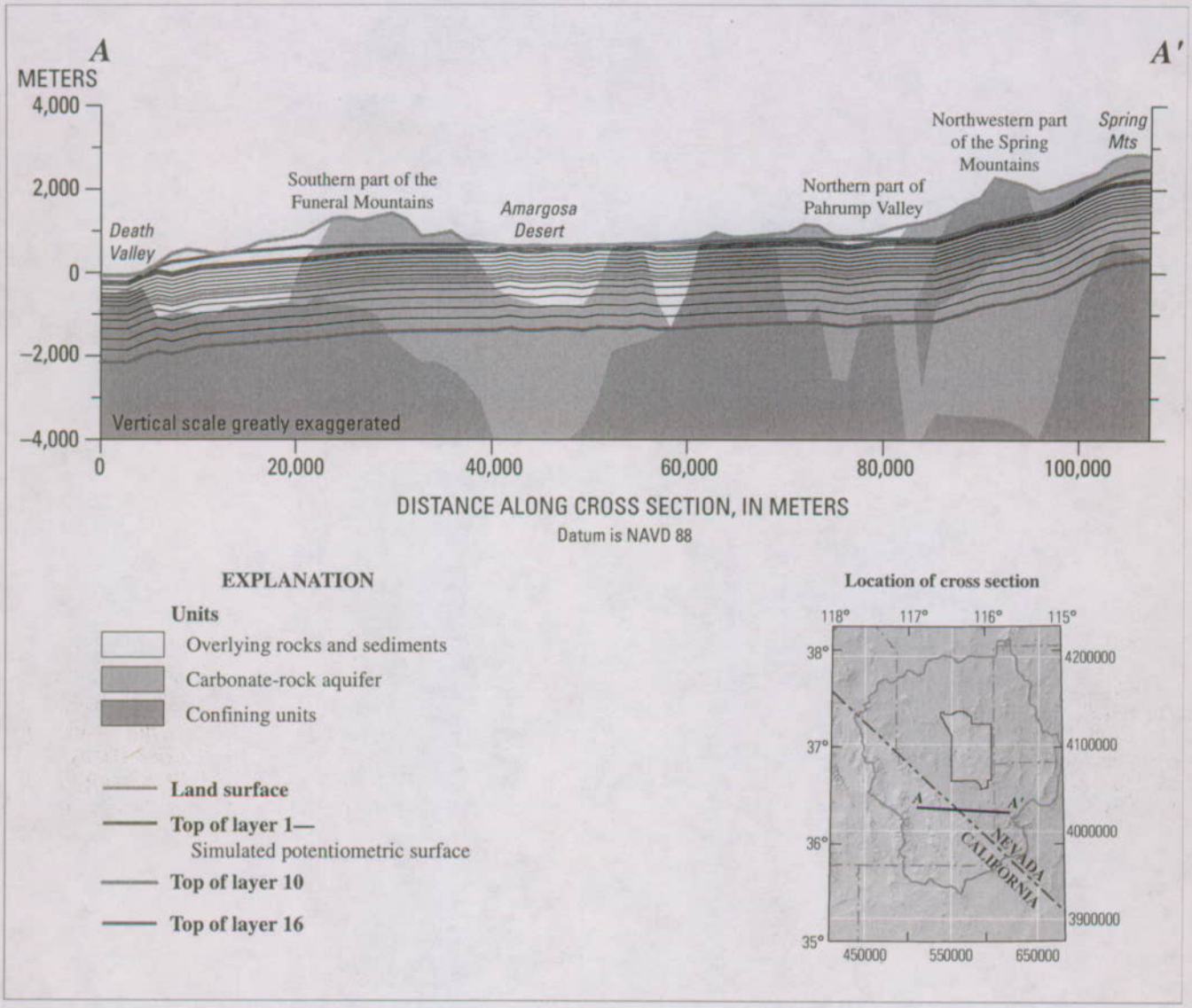

Figure F–2. Example cross section across the model domain of subsurface configuration of model layers.

(Anderman and Hill, 2003). The top model layer, layer 1, was defined as the simulated potentiometric surface in the unconfined part of the system.

Hydrogeologic Structures

A fault can be a barrier to flow for two reasons: (1) juxtaposition of low-permeability materials and relatively high-permeability materials, and (2) low-permeability material (fault gouge) in the fault zone itself, which forms a barrier to flow across the fault. Juxtaposition is represented in the flow model by the geometry of the HFM (described in Chapter E, this volume), and faults that contain fault gouge are simulated using the Horizontal-Flow Barrier (HFB) package (Hsieh and Freckleton, 1993). These flow barriers were located along cell boundaries to approximate the location of selected mapped faults (fig. F–4 and Chapter B, this volume). The model input required for the HFB package is the hydraulic characteristic of the barrier; that is, the hydraulic conductivity of the barrier divided by the width of the barrier. It is assumed that the width is 1 m. The hydraulic conductivity is determined using estimated parameters. Faults in the model domain simulated as potential flow barriers are shown in figure F–5.

Ground-Water Recharge

The recharge rates were calculated using a net-infiltration model (Hevesi and others, 2003; Chapter C, this volume) with a 278.5-m grid (fig. C–8 in Chapter C) resampled to the 1,500-m DVRFS model grid using a nearest neighbor approach (fig. F–6). Recharge represented average annual conditions for the entire simulation. Initial recharge rates ranged from 0 to 0.000468 m/d (Chapter C, this volume).

Table F–2. Flow through boundary segments of the Death Valley regional ground-water flow system model domain.

[--, standard deviation was considerably larger than the estimated flow and it was not quantified; m^3/d, cubic meters per day]

	Segment number and name (see fig. A2–3, this volume)	Conceptual boundary type	Comments	Observation name (subsegment number is last two digits) (see fig. A2–3, this volume)	Model boundary type[1]	Estimated boundary flow into (+) or out of (–) model domain (m^3/d)	Standard deviation)[2] (m^3/d)
1	Silurian	Flow in	Low-permeability rocks with hydraulic gradient nearly parallel to segment.	C_SILU0100	Constant head	500	500
2	Spring-Mesquite	No flow	Ground-water divide or hydraulic gradient parallel to segment; model boundary closely coincides with and is nearly parallel to the flow system boundary.	C_SPRM0200	No flow	0	--
3	Las Vegas	Flow out	Hydraulic gradient parallel to central part of segment, outflow from ends of segment is derived from recharge to the Spring Mountains and Sheep Range.	C_LASV0301	No flow	–942	--
				C_LASV0302	No flow	0	--
				C_LASV0303	Constant head	–3,633	3,500
4	Sheep Range	Flow out	Outflow from most of the boundary is derived from inflow from Pahranagat Valley and recharge to the Sheep Range; inflow on northern part of segment is derived from the Pahranagat Valley.	C_SHPR0401	Constant head	–4,410	4,000
				C_SHPR0402	Constant head	–15,305	15,000
				C_SHPR0403	Constant head	–4,959	4,500
				C_SHPR0404	Constant head	5,927	5,500
5	Pahranagat	Flow in and out	Southern part of segment has inflow adjacent to the Sheep Range. Most of the segment has outflow derived largely from Garden-Coal segment. Model boundary nearly parallel to flow-system boundary defined by a ground-water divide.	C_PAHR0501	Constant head	1,827	1,500
				C_PAHR0502	Constant head	–2,346	2,000
				C_PAHR0503	No flow	–102	--
				C_PAHR0504	No flow	359	--
				C_PAHR0505	Constant head	–2,521	2,500
6	Garden-Coal	Flow in	Inflow mainly results in outflow to Pahranagat segment.	C_GRDN0601	No flow	999	--
				C_GRDN0602	No flow	806	--
				C_GRDN0603	Constant head	2,334	2,000
7	Stone Cabin–Railroad	Flow in	Hydraulic gradients poorly defined. Inflow likely on the basis of water budget and Darcy calculation.	C_STNC0700	Constant head	12,476	12,000
8	Clayton	Flow in	Hydraulic gradient parallel to northern part of segment.	C_CLAY0800	Constant head	667	500
9	Eureka	Flow in	Hydraulic gradient parallel to segment.	C_EURS0900	Constant head	15,100	7,550
10	Saline	Flow in	Hydraulic gradient parallel to northern part of segment.				
11	Panamint	Flow in	Low-permeability rocks; steep hydraulic gradient.	C_PANA1100	Constant head	15,000	7,500
12	Owlshead	Flow in	Low-permeability rocks, but hydraulic gradient across boundary.	C_OWLS1201	No flow	304	
				C_OWLS1202	No flow	337	
				C_OWLS1203	Constant head	1,682	1,500
				C_OWLS1204	No flow	59	

[1]A no-flow boundary segment is defined if the absolute value of the flow is less than 1,000 m^3/d, except for the Silurian segment, where the local water budget strongly supports the small estimated value, and for the Clayton segment, where flow is likely.

[2]For flow estimates based on water-budget analyses (Appendix 2), the standard deviation was set to one-half of the estimated value. Otherwise, the standard deviation was set to the estimated flow value rounded down to the nearest 500.

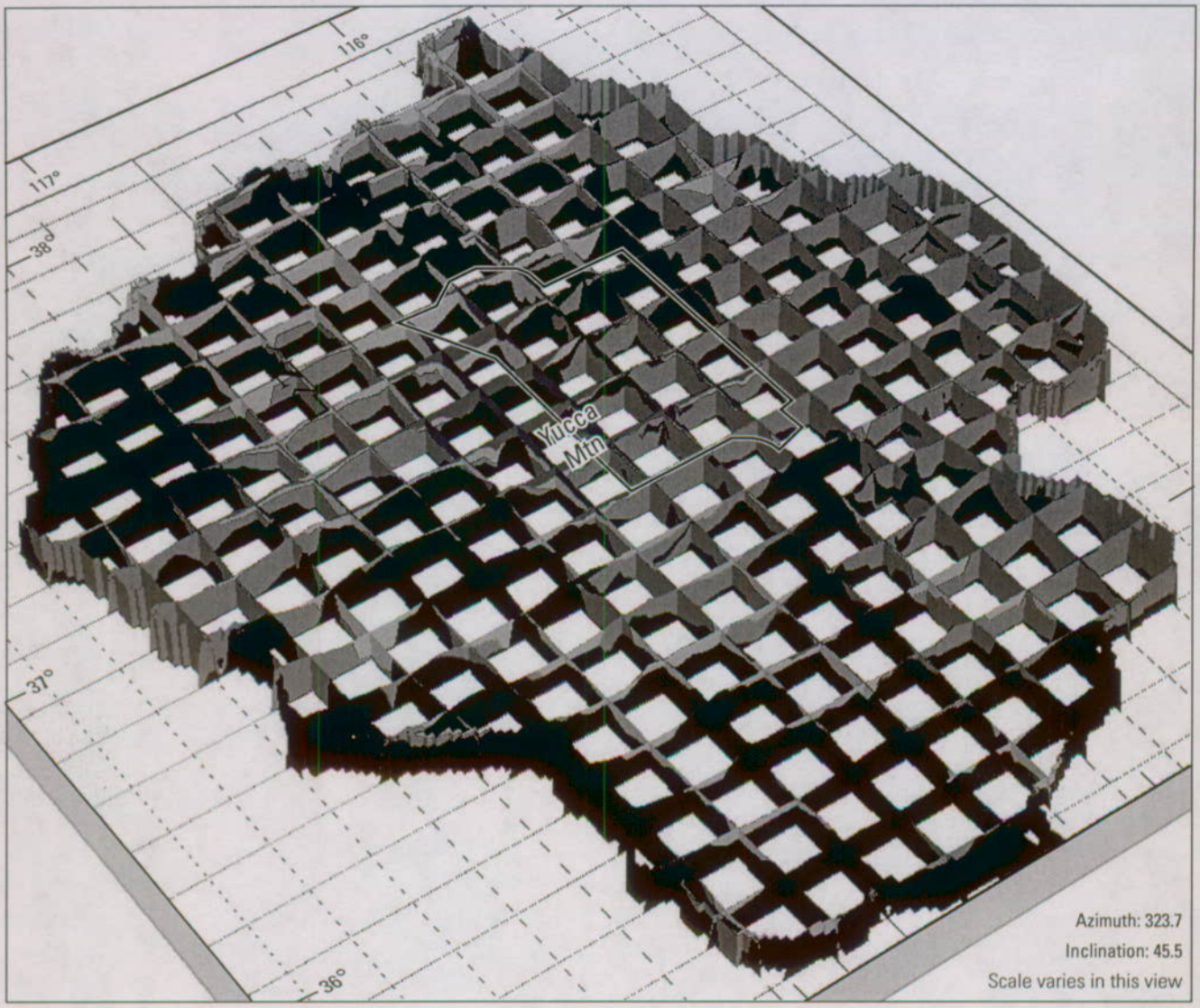

Figure F–3. Oblique view of three-dimensional hydrogeologic framework model showing the distribution of the four major rock units using a series of north-south and east-west-oriented cross-sectional slices.

Natural Ground-Water Discharge

Ground-water discharge by way of both evapotranspiration (ET) and spring flow is simulated using the Drain (DRN) package (Harbaugh and others, 2000) for MODFLOW-2000 (fig. F–7, table F–4). Discharge observations were developed from discharge data described in Chapter C (this volume), using average annual values for all data available for each observation. For cells covered only partly by an ET area, the fractional area was specified in the Drain package. Unless there was a spring in the cell, only cells with ET areas greater than 4 percent of the cell area were included as drain cells in the model.

The Drain package simulates ground-water discharge through a head-dependent boundary. Ground water is simulated as discharging from a finite-difference cell in which a drain is defined when the simulated head in the cell rises above a specified drain altitude. The simulated discharge is

Table F–3. Major rock types of hydrogeologic units of the Death Valley regional ground-water flow system model.

Major rock type (parameter)	Hydrogeologic unit	
	Abbreviation	Name
Basin-fill units (K4)	YAA	Younger alluvial aquifer
	YACU	Younger alluvial confining unit
	OAA	Older alluvial aquifer
	OACU	Older alluvial confining unit
	LA	Limestone aquifer
	Upper VSU	Upper volcanic- and sedimentary-rock unit
	Lower VSU[1]	Lower volcanic- and sedimentary-rock unit
Volcanic-rock units (K3)	LFU	Lava-flow unit
	YVU	Younger volcanic-rock unit
	TMVA	Thirsty Canyon–Timber Mountain volcanic-rock aquifer
	PVA	Paintbrush volcanic-rock aquifer
	CHVU	Calico Hills volcanic-rock unit
	WVU	Wahmonie volcanic-rock unit
	CFPPA	Crater Flat–Prow Pass aquifer
	CFBCU	Crater Flat–Bullfrog confining unit
	CFTA	Crater Flat–Tram aquifer
	BRU	Belted Range unit
	OVU	Older volcanic-rock unit
	Lower VSU[1]	Lower volcanic- and sedimentary-rock unit
Carbonate-rock aquifer (K2)	UCA	Upper carbonate-rock aquifer
	LCA, LCA_T1	Lower carbonate-rock aquifer and thrust
Confining units (K1)	SCU	Sedimentary-rock confining unit
	UCCU	Upper clastic-rock confining unit
	LCCU, LCCU_T1	Lower clastic-rock confining unit and thrust
	XCU	Crystalline-rock confining unit
	ICU	Intrusive-rock confining unit

[1]Lower VSU contains volcanic rocks and basin-fill deposits and is listed in both categories.

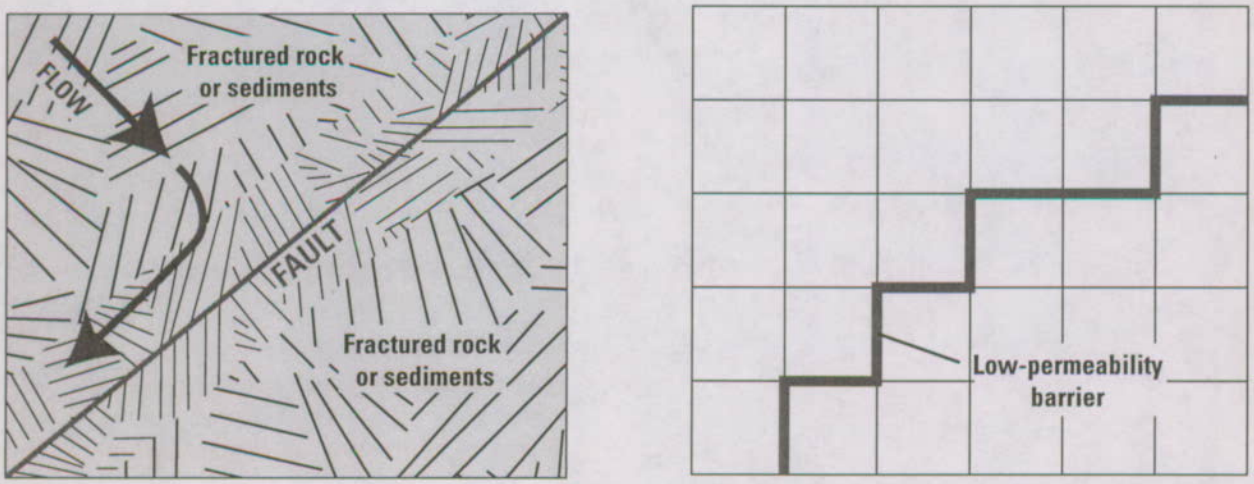

Figure F–4. Schematic diagrams showing representation of hydrologic flow barrier (fault) in horizontal flow barrier (HFB) package of MODFLOW-2000.

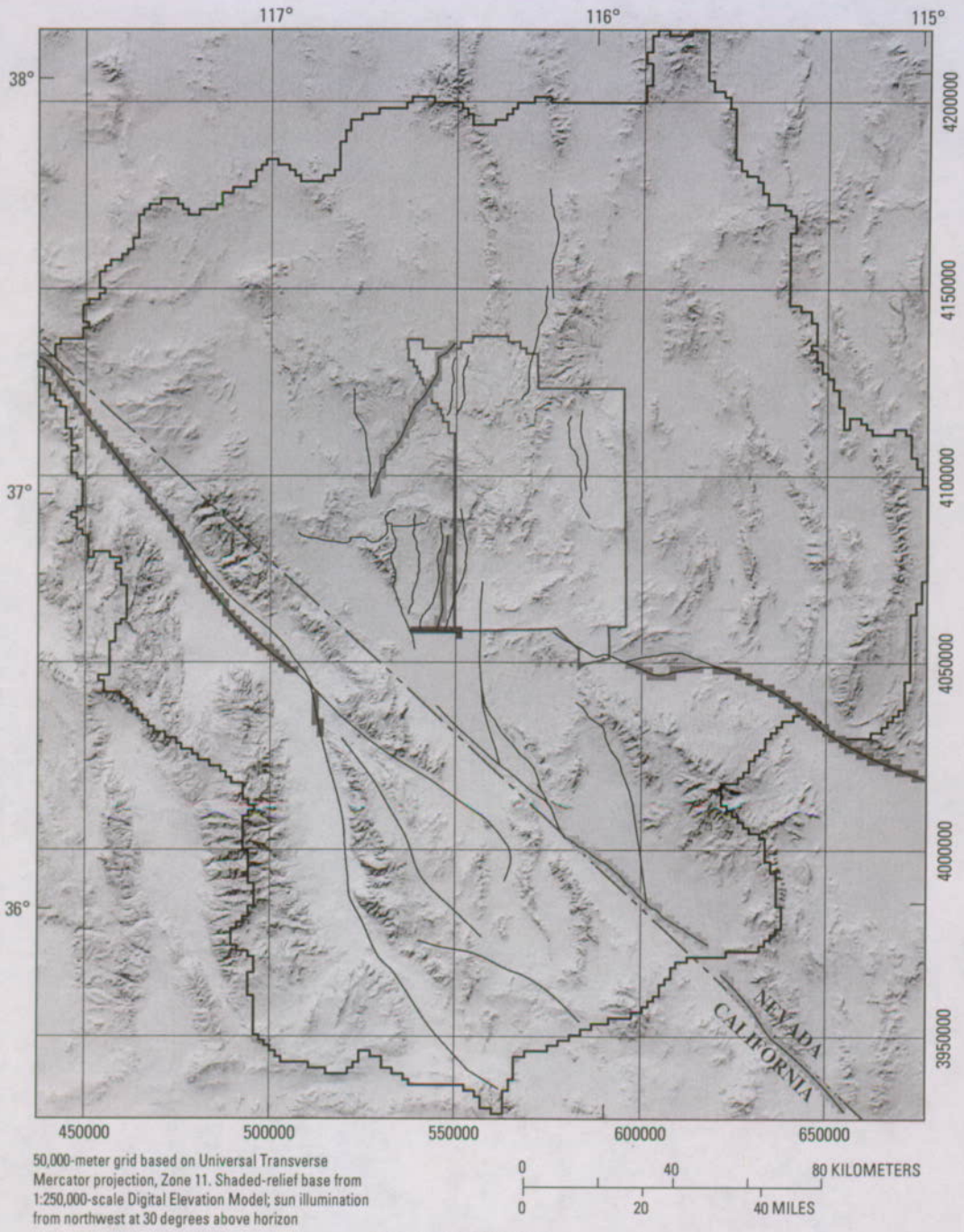

Figure F–5. Hydrogeologic features interpreted as potential flow barriers and parameters used for horizontal flow barriers.

Figure F–6. Recharge simulated in the Death Valley regional ground-water flow system model.

EXPLANATION

OBS-SARCO-NE **Model cell groups representing drains with observation name**—Observation descriptions provided in table F–4

Death Valley regional ground-water flow system model grid boundary

Nevada Test Site boundary

Figure F–7. Model cell groups representing drains used to simulate natural ground-water discharge.

Table F–4. Observed and simulated discharges for the cell groups representing drains for 1997 (stress period 86), Death Valley ground-water flow model.

[NA, not applicable]

Evapotranspiration (ET) zone	Observation name	Parameter name (conductance)	Observed discharge (cubic meters per day) (tables C–1 and C–2)	Simulated discharge (cubic meters per day)	Fractional difference	Coefficient of variation (D'Agnese and others, 2002)
Northern Death Valley Subregion						
Sarcobatus Flat ET			[7]44,662	39,340	0.12	NA
Northeastern	OBS-SARCO-NE	UP_PLY_DRN	[7]30,958	31,000	0.00	[6]0.46
Southwestern	OBS-SARCO-SW	UP_PLY_DRN	[7]12,174	7,290	0.40	[6]0.53
Twin Playas	OBS-SARCO-CH	UPPER_DRN	[7]1,530	1,050	0.31	[6]0.55
Grapevine Canyon Springs			3,485	3,247	0.07	NA
Grapevine Springs area	OBS-GRAPE-SP	DEEP_DRN	[3]2,450	2,400	0.02	0.20
Stainginger Springs area	OBS-GRAPE-SC	DEEP_DRN	[3]1,035	847	0.18	0.50
Part of Death Valley floor ET			29,002	44,900	–0.55	NA
Mesquite Flat	OBS-DV-MESQU	UP_DV_DRN	[4]29,002	44,900	–0.55	0.28
Central Death Valley Subregion—Pahute Mesa–Oasis Valley ground-water basin						
Penoyer Valley ET			12,833	4,890	0.62	NA
Penoyer Valley	OBS-PENOYERV	UPPER_DRN	[5]12,833	4,890	0.62	0.50
Oasis Valley ET			20,311	23,630	–0.16	NA
Upper	OBS-OV-COFFR	UPPER_DRN	[2]4,390	2,700	0.38	[6]0.19
Upper middle	OBS-OV-SPRDL	UPPER_DRN	[2]8,898	15,600	–0.75	[6]0.10
Lower middle	OBS-OV-OASIS	UPPER_DRN	[2]3,629	3,910	–0.08	[6]0.10
Lower	OBS-OV-BEATY	UPPER_DRN	[2]3,394	1,420	0.58	[6]0.13
Indian Springs	Not simulated	UPPER_DRN	[2]74	NA	NA	0.19
Crystal Springs	Not simulated	UPPER_DRN	[2]113	NA	NA	0.32
Upland Springs	Not simulated	UPPER_DRN	[2]45	NA	NA	0.23
Central Death Valley Subregion—Ash Meadows ground-water basin						
Indian Springs area			2,240	0	1.00	NA
Indian and Cactus Springs	OBS-INDIANSP	UPPER_DRN	2,240	0	1.00	0.10
Ash Meadows ET			60,372	61,098	–0.01	NA
Northern	OBS-AM-NORTH[1]	UP_PLY_DRN/ DEEP_DRN	[7]18,337	11,800	0.36	[6]0.14
Central	OBS-AM-CENTR[1]	UP_PLY_DRN/ DEEP_DRN	[7]23,193	24,300	–0.05	[6]0.15
Southern	OBS-AM-SOUTH[1]	UP_PLY_DRN/ DEEP_DRN	[7]9,484	18,700	–0.97	[6]0.23
Amargosa Flat	OBS-AM-AMFLT	UPPER_DRN	[7]5,660	2,340	0.59	[6]0.32
Carson Slough drainage	OBS-AM-CARSL	UP_PLY_DRN	[7]468	318	0.32	0.50
Upper drainage	OBS-AM-UPDRN	UP_PLY_DRN	[7]3,230	3,640	–0.13	0.15
Franklin Well area ET			1,150	520	0.55	NA
Franklin Well	OBS-FRANKWEL	UP_PLY_DRN	[7]1,150	520	0.55	0.50
Franklin Lake ET			3,519	7,240	–1.06	NA
Northern-central	OBS-FRNKLK-N	UP_PLY_DRN	[7]2,350	4,460	–0.90	[6]0.26
Southwest	OBS-FRNKLK-S	UP_PLY_DRN	[7]741	1,410	–0.90	[6]0.49
Southeast	OBS-FRNKLK-E	UP_PLY_DRN	[7]428	1,370	–2.20	[6]0.71
Central Death Valley Subregion—Alkali Flat–Furnace Creek ground-water basin						
Part of Death Valley floor ET			80,048	125,700	–0.57	NA
Mormon Point	OBS-DV-MORMN	UP_DV_DRN	[4]13,356	18,800	–0.41	0.28
Badwater Basin	OBS-DV-BADWT	UP_DV_DRN	[4]20,098	24,400	–0.21	0.28
Middle Basin	OBS-DV-MIDDL	UP_DV_DRN	[4]6,625	23,700	–2.58	0.28
Furnace Creek Ranch	OBS-DV-FRNFN	UP_DV_DRN	[4]11,522	9,020	0.22	0.28
Cottonball Basin	OBS-DV-COTTN	UP_DV_DRN	[4]10,224	33,400	–2.27	0.28
West side vegetation	OBS-DV-WESTF	UP_PLY_DRN	[4]18,223	16,400	0.10	0.28
Death Valley area springs			7,737	7,230	0.07	NA
Nevares Spring	OBS-DV-NEVAR[1]	DEEP_DRN	1,884	2,370	–0.26	0.15
Texas Spring	OBS-DV-TEXAS[1]	DEEP_DRN	1,220	1,450	–0.19	0.15
Travertine Spring	OBS-DV-TRVRT[1]	DEEP_DRN	4,633	3,410	0.26	0.10

Table F–4. Observed and simulated discharges for the cell groups representing drains for 1997 (stress period 86), Death Valley groundwater flow model.—Continued

[NA, not applicable]

Evapotranspiration (ET) zone	Observation name	Parameter name (conductance)	Observed discharge (cubic meters per day) (tables C–1 and C–2)	Simulated discharge (cubic meters per day)	Fractional difference	Coefficient of variation (D'Agnese and others, 2002)
Southern Death Valley Subregion						
Stewart Valley area ET			3,379	3,842	–0.61	NA
Upper Stewart Valley	OBS-STEWRT-V	UP_PLY_DRN	[7]2,383	672	0.33	[6]0.56
Lower Pahrump drainage	OBS-STEWRT-P	UP_PLY_DR	[7]996	3,170	–0.33	[6]0.16
Pahrump Valley area ET and springs						
Manse Spring (ET and spring flow) – steady state	OBS-PAH-MANS	UP_PAH_DRN	14,500	2,910	0.80	0.5
Manse fan (ET, spring dry) – 1960	OB-PAH-MANS	UP_PAH_DRN	5,375	2,480	0.54	0.5
Manse fan (ET, spring dry) – 1998	O-PAH-MANS	UP_PAH_DRN	821	1,370	–0.67	0.5
Bennetts Spring (ET and spring flow) – steady state	OBS-PAH-BENT	UP_PAH_DRN	17,900	19,600	–0.09	0.5
Pahrump fan (ET, spring dry) 1960	OB-PAH-BENT	UP_PAH_DRN	16,753	16,800	0.00	0.5
Pahrump fan (ET, spring dry) 1998	O-PAH-BENT	UP_PAH_DRN	2,557	7,650	–1.99	0.5
Tecopa Valley area ET			21,063	3,807	0.82	NA
Upper	OBS-TC-TECOP	UP_PLY_DRN	[7]12,097	1,470	0.88	[6]0.12
Middle	OBS-TC-AMCAN	UPPER_DRN	[7]3,360	853	0.75	[6]0.13
Lower	OBS-TC-SPERY	UPPER_DRN	[7]1,328	655	0.51	0.5
China Ranch	OBS-TC-CHNRC	UPPER_DRN	[7]1,766	263	0.85	0.5
Resting Springs	OBS-TC-RESTS	UPPER_DRN/ DEEP_DRN	[7]2,512	566	0.77	[6]0.16
Shoshone Valley area ET			7,015	3,650	0.48	NA
Upper	OBS-SHOSH-N	UPPER_DRN	[7]2,235	1,300	0.42	[6]0.16
Lower	OBS-SHOSH-S[2]	UP_PLY_DRN/ DEEP_DRN	[7]4,780	2,350	0.51	[6]0.15
Chicago Valley area ET			1,462	5,420	–2.71	NA
Chicago Valley	OBS-CHICAGOV	UP_PLY_DRN	[7]1,462	5,420	–2.71	[6]0.36
California Valley area ET			326	NA	NA	NA
California Ranch	Not simulated	NA	[7]326	NA	NA	0.22
Part of Death Valley floor ET			11,547	12,860	–0.11	NA
Saratoga Springs	OBS-DV-SARAT	UPPER_DRN	[4]8,311	7,060	0.15	0.28
Confidence Mill site	OBS-DV-CONFI	UPPER_DRN	[4]3,236	5,800	–0.79	0.28

[1]Observations for which 50 percent or more of the flow comes from springs.

[2]Reiner and others, 2002.

[3]Miller, 1977.

[4]DeMeo and others, 2003.

[5]Van Denburg and Rush, 1974.

[6]R.K. Waddell, Geotrans, Inc., written commun., 2003.

[7]Laczniak and others, 2001.

calculated as the drain conductance multiplied by the difference in altitude between the simulated head and the drain. The drain conductances are defined using the hydraulic properties of materials through which water flows to the surface ("Parameter name" column in table F–4): (1) DEEP_DRN, warm-water discharge indicates rapid flow from depth and the drain cell is located at the shallowest occurrence of the LCA; (2) UPPER_DRN, flow is through surficial materials that are coarser than playa materials (YAA and OAA); (3) UP_PLY_DRN, flow is through surficial fine-grained playa materials (YACU and OACU); (4) UP_DV_DRN, flow is from springs in Death Valley with substantial salt concentrations; and (5) UP_PAH_DRN, all discharge areas in Pahrump Valley where estimates of discharge over time are available.

The drain conductances were estimated as part of model calibration. The drain altitudes were set equal to 10 m below the lowest land-surface altitudes for each group of cells (fig. F–7). This value is assumed to represent a reasonable altitude below which ET would not occur and to account for springs being located in land-surface depressions that are lower than would be evident in the top surface of the HFM. This altitude would approximate the extinction depth for ET as well. Drains representing springs are set to these altitudes but are connected to the topmost occurrence of the lower carbonate-rock aquifer at that cell location. This occurs in model layers 1 through 10.

Many discharge areas represent individual springs that are significantly smaller in area than the simulated 1,500-m grid cell. At this scale, it is not possible to represent variations in hydraulic gradient, fault and fracture geometry, and abrupt changes in lithology that influence ground-water discharge rates at a regional scale. In some cases, however, individual springs, such as Travertine, Texas, and Nevares Springs, were simulated. Discharge areas with flow rates less than 1,000 cubic meters per day (m^3/d) were difficult to simulate, but the discharge contributions are relatively minor given the overall volumetric budget and model scale. Because of these simplifications in representing discharge areas in the model, errors in simulation can result.

Pumpage

Substantial volumes of ground-water discharge from the regional flow system through pumped wells are shown by model layer in figure F–8. Pumping from wells is simulated using the Multi-Node Well (MNW) package for MODFLOW-2000 (Halford and Hanson, 2002). In the DVRFS region wells typically are completed with screens that span multiple aquifers and thus multiple layers in the model. The MNW package uses the hydraulic conductivity and thickness to determine how much of the well pumpage is derived from each model layer. This allows pumpage to be redistributed as the estimates of the hydraulic-conductivity distribution change during model calibration.

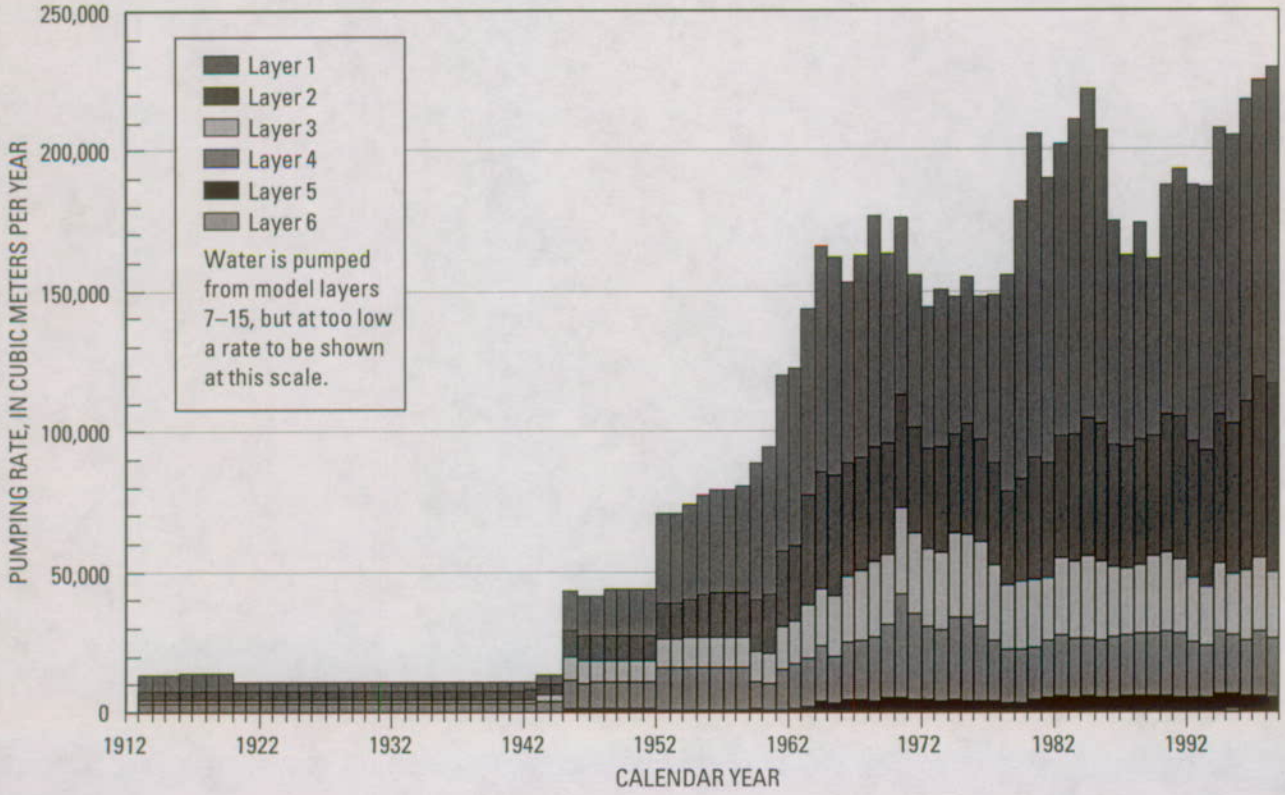

Figure F–8. Pumping by model layers, 1913–98.

Some return flow of pumpage through subsequent infiltration of excess irrigation, lawn water, or septic tank wastewater is likely to occur. The magnitude and timing of these returns have not been precisely quantified, but a method was developed to compute informal estimates of return flow (Chapter C, this volume). For each withdrawal point, return flow was estimated to be 20 percent of the estimated annual pumpage (Moreo and others, 2003), lagged by 7 years. The total pumpage for the wells in each cell is applied at the cell center (fig. F–9), resulting in 8,569 wells simulated by pumping in 432 cells (table F–5).

Observations Used In Model Calibration

Poorly quantified or unquantified characteristics of the system can be constrained on the basis of observations (composite field measurements used in calibrating the model). Observations used to calibrate the DVRFS model are those of hydraulic heads (water levels), changes in head over time due to pumpage, and discharge by ET and spring flow (table F–6). Estimated boundary flows (simulated as constant-head boundaries) are treated like observations but are less accurate than other observation types and are given less weight in the simulation.

Weighting values (or weights) are the inverse of the estimated variance of an observation. This weighting will result in parameter estimates with the smallest possible variance if (1) the estimated variances and the model are accurate, (2) the model is effectively linear, and (3) the number of observations is effectively large (Bard, 1974). In addition to variances, MODFLOW-2000 permits the designation of standard deviations or coefficients of variation (CVs), from which variances are calculated (Hill and others, 2000, p. 39–40, 53, 57, 65). These indicators of measurement precision are determined on the basis of an analysis of likely measurement error (Chapter C, this volume).

For the prepumped, steady-state stress period, all observations are considered representative of steady-state conditions. For the pumped, transient stress periods, some hydraulic-head and discharge observations are not influenced by pumping and thus are also considered representative of long-term steady-state conditions. Hydraulic-head observations influenced by pumping are treated as head-change observations. Natural discharge from ET and springs was considered to be constant and not influenced by pumping, with the exception of some springs in Pahrump Valley. It is assumed that constant-head observations used to simulate flow into and out of the model boundary are not influenced by pumping.

Heads, Head Changes, and Associated Errors

Water levels measured in boreholes and wells located within the model domain were used to develop hydraulic-head and head-change observations for calibration of the regional flow model. Only those water levels considered representative of regional ground-water conditions were used to calculate head observations (Chapter C, this volume). Prepumped, steady-state head observations were developed at 700 wells. Head observations at these wells were computed as the average of all water-level measurements throughout the entire record. For pumped, transient stress periods, hydraulic-head observations were computed as average annual water levels from nearly 15,000 water-level measurements considered representative of either steady-state or transient conditions (Chapter C, this volume). Head observations for wells having water-level measurements over multiple years were determined to be either affected or not affected by pumping. Head observations affected by pumping are treated in model calibration as a head change, which is calculated as the difference between the observation of interest and a reference observation (Hill and others, 2000, p. 33–34). The reference observation is the measurement prior to any pumping effect or the first measurement affected by pumping.

The areal distributions of the hydraulic-head and head-change observations are shown in figure F–10*A*. The number of observations representing steady-state and transient conditions over time is shown in figure F–10*B*, and the distribution of observations by the deepest open layer is shown in figure C–13 (this volume).

The open intervals of the wells were considered in determining the model layers associated with head and head-change observations (Chapter C, this volume). Most wells for which observations are available and that are open to multiple layers are on or near Pahute Mesa. Most head and head-change observations (82 percent) are from wells completed in the shallow part of the flow system (no deeper than model layer 5) and none are deeper than model layer 14. For wells open to more than one model layer, simulated heads are a weighted average calculated by MODFLOW-2000 using user-defined weights (Hill and others, 2000, p. 34–36).

The DVRFS model domain is dominated by observations in just a few areas: Pahrump Valley, Amargosa Desert, a few other small population centers, and the Nevada Test Site (fig. F–10*A*). Elsewhere, observations are sparse and the paucity of data is most pronounced in the distribution of hydraulic heads. Clustered data can be problematic if they dominate the regression analysis and result in a poor model fit in these areas.

In addition to the four sources of error discussed in Chapter C, two sources of error are associated with the modeling process: uncertainties in model discretization and pumpage estimates. Model-discretization errors result from inaccuracies in the geometric representation of HGUs and major structural features in the model (Hill and Tiedeman, 2003). The magnitude of these errors is assumed to be a function of nodal width, hydraulic gradient, and well-opening depth. The dependence on nodal width occurs because larger widths result in a less accurate representation of the geometry of HGUs and of major structural features relative to well location. The dependence on hydraulic gradient occurs because inaccurate geometric representations tend to shift the location of local hydraulic gradients. The depth dependence results from a decrease in

Figure F–9. Total withdrawal from pumpage by model cell, 1913–98.

Table F–5. Number of model cells representing wells and total pumpage by subregion from 1913 through 1998.

[Pumpage total in Chapter C (this volume) is slightly less because of rounding]

Division (see Chapter D, this volume)	Number of wells 1913–98	Number of cells in model	Pumpage 1913–98 (cubic meters)
Northern Death Valley subregion	16	11	1,110,751
Lida-Stonewall section	0	0	0
Sarcobatus Flats section	14	9	601,569
Grapevine Canyon–Mesquite Flat section	1	1	497,093
Oriental Wash section	1	1	12,088
Central Death Valley subregion	675	201	1,062,495,492
Pahute Mesa–Oasis Valley ground-water basin	109	63	299,170,575
Southern Railroad Valley/Penoyer Valley section	67	35	272,463,839
Kawich Valley section	6	5	4,208,641
Oasis Valley section	36	23	22,498,095
Ash Meadows ground-water basin	194	56	164,885,953
Tikaboo Valley section	0	0	0
Emigrant Valley section	4	2	15,196,498
Yucca–Frenchman Flat section	19	14	54,320,450
Pahranagat section	0	0	0
Indian Springs section	87	15	32,383,220
Specter Range section	84	25	62,985,785
Alkali Flat–Furnace Creek ground-water basin	372	82	598,438,964
Fortymile Canyon section	7	5	14,041,836
Amargosa River section	357	69	583,275,400
Crater Flat section	7	7	1,107,050
Funeral Mountains section	1	1	14,678
Southern Death Valley subregion	7,878	220	2,212,287,835
Pahrump Valley	7,876	218	2,211,155,498
Shoshone-Tecopa	2	2	1,132,336
California Valley section	0	0	0
Ibex Hills section	0	0	0
Total	**8,569**	**432**	**3,275,894,077**

the knowledge of HGUs and structures with depth. Assuming these generalizations are correct, the potential for model discretization error increases with the size of the grid, the steepness of the hydraulic gradient, and the depth of the open intervals in observation wells and model layers.

Model-discretization error could be quantified in a number of ways. Here, this error is assumed to be normally distributed about the head observation with the 95-percent confidence interval being directly proportional to the nodal width and hydraulic gradient. Hydraulic gradients were calculated from the regional potentiometric surface map (D'Agnese and others, 1998), assuming that model-simulated hydraulic gradients will be similar to those represented by the map. The product of nodal width and hydraulic gradient approximates the head difference across a finite-difference cell and therefore is assumed to represent the error contributed by potential inaccuracies in the geometry of HGUs and the location of major structural features.

A scalar that is a function of the well-opening depth is used to incorporate the potential error attributed to a decrease in geologic certainty with depth. This depth scalar is calculated as 2 plus the quotient of the depth of the top of the open interval and the approximate thickness of the aquifer material in the model (3,000 m). The depth scalar ranges from about 2 at the top of the flow system to 3 at the bottom of the flow system.

The 95-percent confidence interval is defined as four standard deviations, so the range defined by the model-discretization error is divided by four to obtain the standard deviation. The standard deviation for model-discretization error was computed as:

$$sd_5 = \{NW \times HG \times [(TOUPOPEN / MT) + 2]\} / 4 \qquad (2)$$

where

sd_5 is the standard deviation of model-discretization error;

NW is nodal width, in meters, and is equal to 1,500 meters;

HG is hydraulic gradient;

$TOUPOPEN$ is top of upper well opening, in meters below land surface;

and

MT is the approximate thickness of aquifer material in the model and is equal to 3,000 meters for this calculation.

Table F–6. Observations used in prepumped, steady-state stress period and pumped, transient stress periods of the model.

[≤, less than or equal to; >, greater than]

Type of observation	Number of observations	
	Steady state	Transient (includes steady-state observations)
Head	**700**	**2,227**
Observations with few measurements	156	195
Observations with many measurements	544	2,032
Head change	**0**	**2,672**
Observed value ≤1.0 m	0	1,069
Observed value >1.0 m	0	1,603
Discharge from evapotranspiration or springs	**45**	**49**
Constant-head boundary flow	**15**	**15**

The resulting standard deviations seem reasonable for model-discretization error. Given that the maximum hydraulic gradient in this system is 0.15 and the maximum top well opening depth is 750 m, the maximum standard deviation that could be computed using equation 1 is 125 m. Standard deviations computed for head observations were much smaller, seldom exceeding 50 m.

Using the standard deviations of a head observation based on the five potential errors, the standard deviation, sd_h, of each observation was computed by the equation:

$$sd_h = (sd_1^2 + sd_2^2 + sd_3^2 + sd_4^2 + sd_5^2)^{1/2} \quad (3)$$

where

sd_1 is standard deviation of well-altitude error;

sd_2 is standard deviation of well-location error;

sd_3 is standard deviation of nonsimulated transient error;

sd_4 is standard deviation of measurement-accuracy error;

and

sd_5 is standard deviation of model-discretization error.

Computed standard deviations of head observations used to calibrate prepumped, steady-state flow conditions ranged from less than 1 m to about 215 m, as shown on the vertical axis of the cumulative frequency diagram in figure F–11*A*. About 95 percent of the head observations had a standard deviation of less than 50 m and about 50 percent had a standard deviation of less than 10 m (fig. F–11*A*). The magnitudes of these standard deviations are larger than those discussed in Chapter C because of the addition of model-discretization error (fig. F–11*B*). Figure F–11*B* shows the percentage contribution of the five types of errors (including model-discretization error) for the 700 head observations.

Differences between simulated and observed head changes are expected to be dominated by errors in the estimates of pumpage; thus, this is the only error considered in calculating the weighting of head-change observations. Withdrawal-estimate error does not affect head observations assumed to represent prepumped, steady-state flow conditions.

Pumpage-estimate error results from uncertainties in the pumping rate, the location of the pumped well, and the depth of pumped-well openings. Pumping rates were estimated by a variety of methods and data, including irrigated acreage, flow-meter measurements, water-use reports, and power-consumption graphs (Chapter C, this volume). Errors typical of these estimation techniques are discussed in Chapter C of this report.

The relation between pumping and head change is approximately linear, whereas that between pumped-well location and head change is less predictable. The linear relation between pumping and head change indicates that the error related to uncertainties in the pumping rate can be represented by a coefficient of variation (CV), which results in standard deviations that increase linearly with pumping rate. The result of a linear increase is that the weights are small for large pumping rates and large for small pumping rates. The strict use of a CV in this model was problematic because larger head-change observations were given unrealistically large standard deviations and small weights, and vice versa. To remedy this problem, a function was developed that maintained the basic premise of larger standard deviations for larger head changes but tempered the difference in the standard deviation between large and small head-change observations. The function used to calculate the standard deviation of a head-change observation is

$$sd_{hc} = 4 + [0.8 \times \log(hc_{obs}/40)] \quad \text{for } hc_{obs} > 1.0 \quad (4)$$

$$sd_{hc} = 1, \quad \text{for } hc_{obs} \le 1.0$$

where

sd_{hc} is the standard deviation used to weight observed head change;

log denotes the natural log of the value in parentheses;

and

hc_{obs} is the head-change observation.

Standard deviations for head-change observations less than 1 were arbitrarily assigned a value of 1 to avoid very small errors that could cause numerical instability problems during calibration.

Ground-Water Discharge Observations and Errors

Discharge observations were developed primarily from discharge estimates that were derived from ET estimates and spring-flow measurements (Chapter C, this volume). Uncertainty in the discharge from each area was expressed as a CV. A higher CV implies less certainty in the estimate of ground-water discharge. Monte Carlo analyses were used to calculate CVs for the DVRFS (Laczniak and others, 2001, appendix). R.K. Waddell (GeoTrans, Inc., written commun., 2003) did a similar analysis for Pahrump Valley and updated the calculation by Laczniak and others. Both sets of CV calculations for discharge were compiled for the DVRFS model developed by D'Agnese and others (2002), and the compilation also was used in this study (table F–4). Where values were not available or new values were available, appropriate CVs were estimated or updated (table F–4).

Boundary Flow Observations and Errors

The boundary flow observations were obtained from the analysis in Appendix 2 (this volume) that estimates potential flow through 12 segments of the boundary of the DVRFS model domain. These values have a great deal of uncertainty associated with them but were used as observations during calibration. Standard deviations, and thus observation weights, were determined on the basis of the method used to determine the flow at the boundary (Appendix 2). For flow estimates based on water-budget analyses (Appendix 2), the standard deviation was set to one-half of the estimated value. Otherwise, the standard deviation was set to the estimated flow value rounded down to the nearest 500 m^3/d.

Model Calibration

Model calibration is the process of changing model input values in an attempt to match simulated and actual conditions. Models typically are calibrated either by trial and error or by using formal parameter-estimation methods. Calibration of parameter values of the DVRFS model primarily relied on the parameter-estimation techniques available in MODFLOW-2000 and was achieved using a two-step process. First, the model was calibrated to prepumped (steady-state) flow conditions. Once calibrated, this model formed the initial conditions for the transient-flow model. The model was calibrated again to simulate transient-flow conditions for 1913–98.

Approach

Sensitivity analysis was used to evaluate the information provided by the observations for the estimation of all defined parameters, and nonlinear regression was used to estimate parameter values that produced the best fit to observed hydraulic heads and discharges (Hill, 1998). For the DVRFS model, 100 parameters are used and more than 90 were estimated at some point during the modeling process. The maximum number of parameters estimated by nonlinear regression peaked at around 30.

Uncertain aspects of the hydrogeology were evaluated by constructing models with different hydraulic-property distributions and different methods to simulate ET, spring flow, recharge, and the boundary conditions. These models were evaluated through the sensitivity analysis and nonlinear regression methods. These evaluation tools are discussed briefly in the following sections, as well as how estimated parameter values considered unreasonable were used to detect model error. The linear confidence intervals used to evaluate the estimated parameter values also are discussed.

Sensitivity Analysis

Sensitivity analysis is used to assess the effects of different conceptual models (different model designs and parameter values) on the simulated heads and discharges, and to develop useful nonlinear regressions (Hill, 1998; Hill and Tiedeman, 2003). Changes in the conceptual model were assessed by evaluating the effect of the changes on model fit. These methods define parameter sensitivity as the partial derivative of the change in a simulated observation caused by a change in the parameter value. These sensitivities, when scaled properly, can be used to compare the importance of different observations to the estimation of a single parameter or the importance of different parameters to the simulation of an observed value (Hill, 1998, p. 15).

The sensitivity analysis focused on identifying parameter values that could be estimated by regression and identifying key observations that supported each parameter. As part of this analysis, three types of statistics were evaluated: (1) dimensionless scaled sensitivity, (2) composite scaled sensitivity, and (3) parameter correlation coefficient.

Dimensionless Scaled Sensitivity

Dimensionless scaled sensitivity (*DSS*) is used to evaluate the importance of an observation to the estimation of a single parameter. The *DSS* of each observation is calculated for each parameter as

$$DSS = w^{1/2}(\partial y' / \partial b)b \qquad (5)$$

where

w is the weight for observation y and is the inverse of the standard deviation of the observation;

y' is the simulated value of the observation y;

and

b is the parameter value.

Figure F–10. (*A*) Map showing spatial distribution of hydraulic-head observations used in calibration of the Death Valley regional ground-water flow model; (*B*) graph showing the number of hydraulic-head observations representing both steady-state and transient conditions over time.

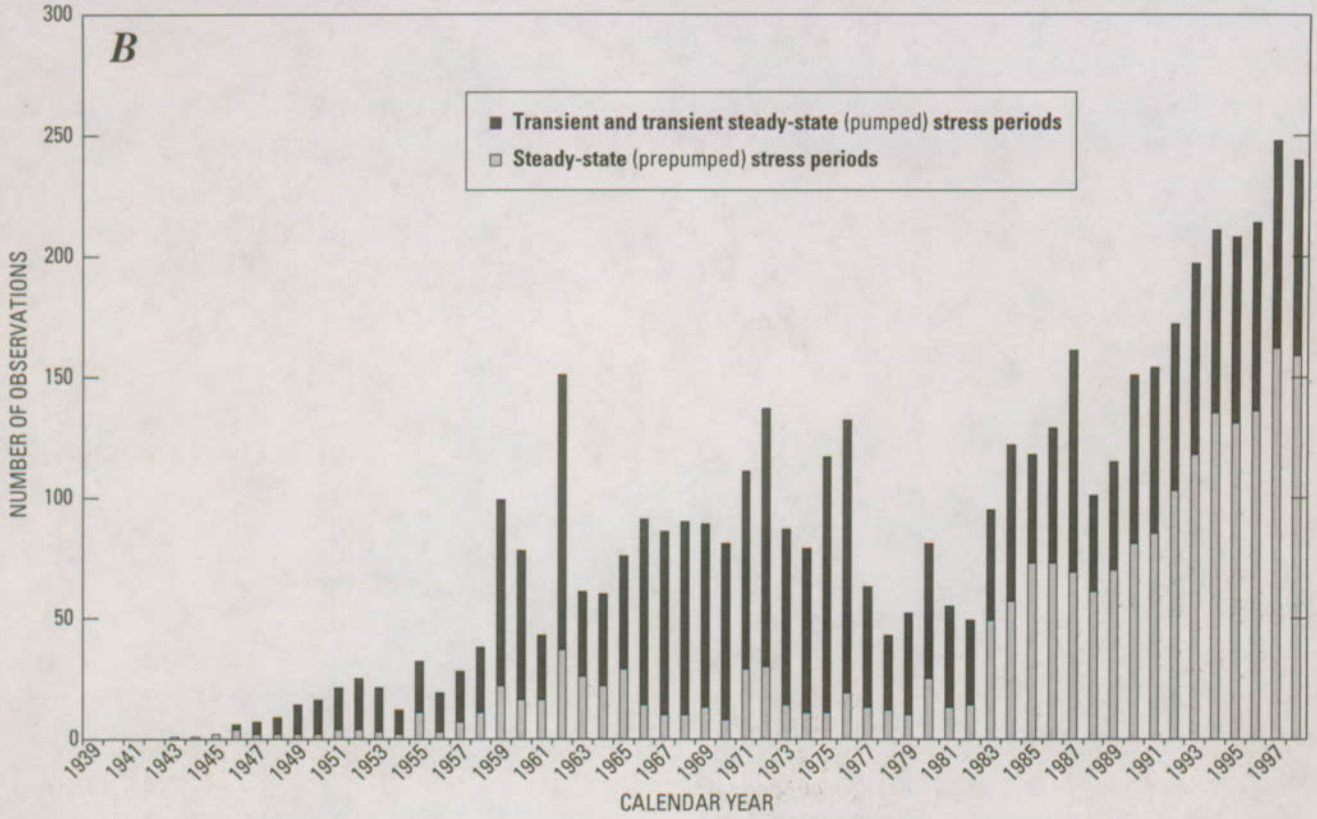

Figure F–10. (*A*) Map showing spatial distribution of hydraulic-head observations used in calibration of the Death Valley regional ground-water flow model; (*B*) graph showing the number of hydraulic-head observations representing both steady-state and transient conditions over time.—Continued

A parameter having a large *DSS* value for one observation and small values for all other observations is governed by that one observation. In this situation, any error in the one important observation will translate directly to the parameter and, therefore, the model. Parameters governed by only one observation are not estimated.

Composite Scaled Sensitivity

Composite scaled sensitivity (*CSS*) is used to evaluate the overall sensitivity of a parameter and is calculated as

$$CSS = \{[\sum_{i=1,n}(DSS)^2]/n\}^{1/2} \quad (6)$$

where n is the number of observations.

CSS typically is a good measure of the information observations contribute to the estimation of parameters. One exception is for parameters with values that change as the model is calibrated; for example, hydraulic heads at constant-head boundaries that were modified during calibration. *CSS* values are not presented for those types of parameters.

The relative size of *CSS* values can be used to assess whether additional parameters can be estimated. A relatively large *CSS* value indicates that observations contain enough information to represent that aspect of the system in more detail, using additional parameters. A relatively small *CSS* value (about two orders of magnitude less than the largest *CSS* value) indicates that the observations provide insufficient information with which to estimate the parameter. Parameters with small *CSS* values generally were assigned a fixed value, and(or) lumped with a parameter with a similar value.

Parameter Correlation Coefficient

Parameter correlation coefficients (*PCC*) are used to evaluate whether parameter values can be estimated uniquely and are calculated for each parameter pair (b_1, b_2). *PCC* can be expressed as

$$PCC = \text{Cov}\ (b_1, b_2)/[\text{var}\ (b_1)^{1/2}\text{var}(b_2)^{1/2}] \quad (7)$$

where Cov (b_1, b_2) is the covariance for the parameter pair b_1 and b_2 and var (b_1) and var (b_2) are the variances for parameters b_1 and b_2.

A correlation coefficient having an absolute value close to 1.00 indicates that the two parameters involved likely cannot be estimated uniquely. Generally, absolute values greater than 0.95 are cause for concern, but values as small as 0.85 are reported in MODFLOW-2000 output because less correlated parameters can affect the uncertainty of parameter estimates. If parameter correlation was high, the value of the

correlated parameter with the smallest *CSS* was adjusted, unless the high correlation was between a depth-decay parameter and the associated hydraulic conductivity. In this case, the hydraulic-conductivity parameter was estimated.

Nonlinear Regression

Nonlinear regression is used to find parameter values that produce simulations that best fit the observations. The fit between model simulation and observations is quantified using an objective function, $S(b)$, that minimizes the sum of squared weighted residuals. The objective function is calculated as:

$$S(\underline{b}) = (\underline{y}-\underline{y}')^T \underline{W} (\underline{y}-\underline{y}') \quad (8a)$$

where

$\underline{b}$ is an $np \times 1$ vector containing parameter values;

np is the number of parameters estimated by regression;

$\underline{y}$ and $\underline{y}'$ are $n \times 1$ vectors with elements equal to observed and simulated (using $\underline{b}$) values, respectively;

$y-y'$ is a vector of residuals, defined as the observed minus simulated values;

n is the number of measured and simulated hydraulic heads and flows;

$\underline{W}$ is an $n \times n$ weight matrix;

and

T superscripted indicates the transpose of the vector.

The weight matrix diagonal elements are calculated as

$$w_{ii} = 1/(s_1^2 + s_2^2 + \ldots s_n^2) \quad (8b)$$

where

w_{ii} is a diagonal element of the weight matrix $\underline{W}$,

s_1^2 is the estimated variance of error type 1,

s_2^2 is the estimated variance of error type 2,

and

s_n^2 is the estimated variance of error type n.

Although every potential error was not considered, it is expected that those that were considered were sufficient to obtain reasonable weighting of the observations. Parameter estimates obtained by nonlinear regression generally are not greatly affected by changes in weights within ranges supportable by an analysis of likely errors (Hill and Tiedeman, 2003). When errors are expected to produce a biased observation, the errors are accounted for through averaging or adjusting the observations. When errors are expected to be characterized as random, they are accounted for through observation weights.

MODFLOW-2000 calculates observation weights from user-defined variances, standard deviations, or CVs (Hill and others, 2000, p. 18–19). CVs equal the standard deviation divided by the observed value. For the DVRFS model, standard deviations are measures of hydraulic-head observation errors and CVs are specified as measures of ground-water discharge and head-change observation errors. Defining weights that reflect expected random observation error is necessary to accurately evaluate uncertainty (Hill and Tiedeman, 2003).

Model fit is evaluated using both unweighted and weighted residuals (the difference between observed and simulated values). Unweighted residuals have the same dimensions as the observations and can be misleading because observations are measured with different accuracy, and two unweighted residuals that are of equal value may not indicate an equally satisfactory model fit.

Weighted residuals reflect model fit relative to the expected observation error but are more difficult to interpret because they are dimensionless quantities that express model fit in terms of normalized values with respect to standard deviations of the observation errors. A weighted residual of 2.0, for example, indicates that the unweighted residual is twice the standard deviation of the observation error. For a hydraulic-head observation with a standard deviation of 10 m, a weighted residual of 2.0 corresponds to an unweighted residual of 20 m. Weighted residuals with larger absolute values indicate a less desirable model fit than do weighted residuals with smaller values.

Overall model fit can be measured using the standard error of the regression. The standard error of the regression is a dimensionless number, and smaller values generally are better. Generally, the better a model fits the observations, the more accurately the model represents the system. The standard error of regression is calculated as

$$\text{Standard error} = S(\underline{b})/(n-np) \quad (9)$$

Uncertainty Evaluation

Linear confidence intervals for the estimated parameter values are calculated using sensitivities calculated for the optimal parameter values. Linear confidence intervals are relevant only if weighted residuals are normally distributed and the model is effectively linear. A linear, 95-percent confidence interval on a parameter estimate that excludes reasonable values indicates model error or misinterpreted data on the parameter. Parameters with larger *CSS* values tend to have smaller confidence intervals.

Confidence intervals were used to assess whether all estimated parameters were warranted. For example, if the confidence intervals overlapped for two parameters representing the hydraulic conductivity of rock types of similar hydraulic properties, the rocks could be represented by a single hydraulic-conductivity parameter without adversely affecting model fit. Also, if the regression using fewer hydraulic-conductivity parameters yields a similar model fit to the

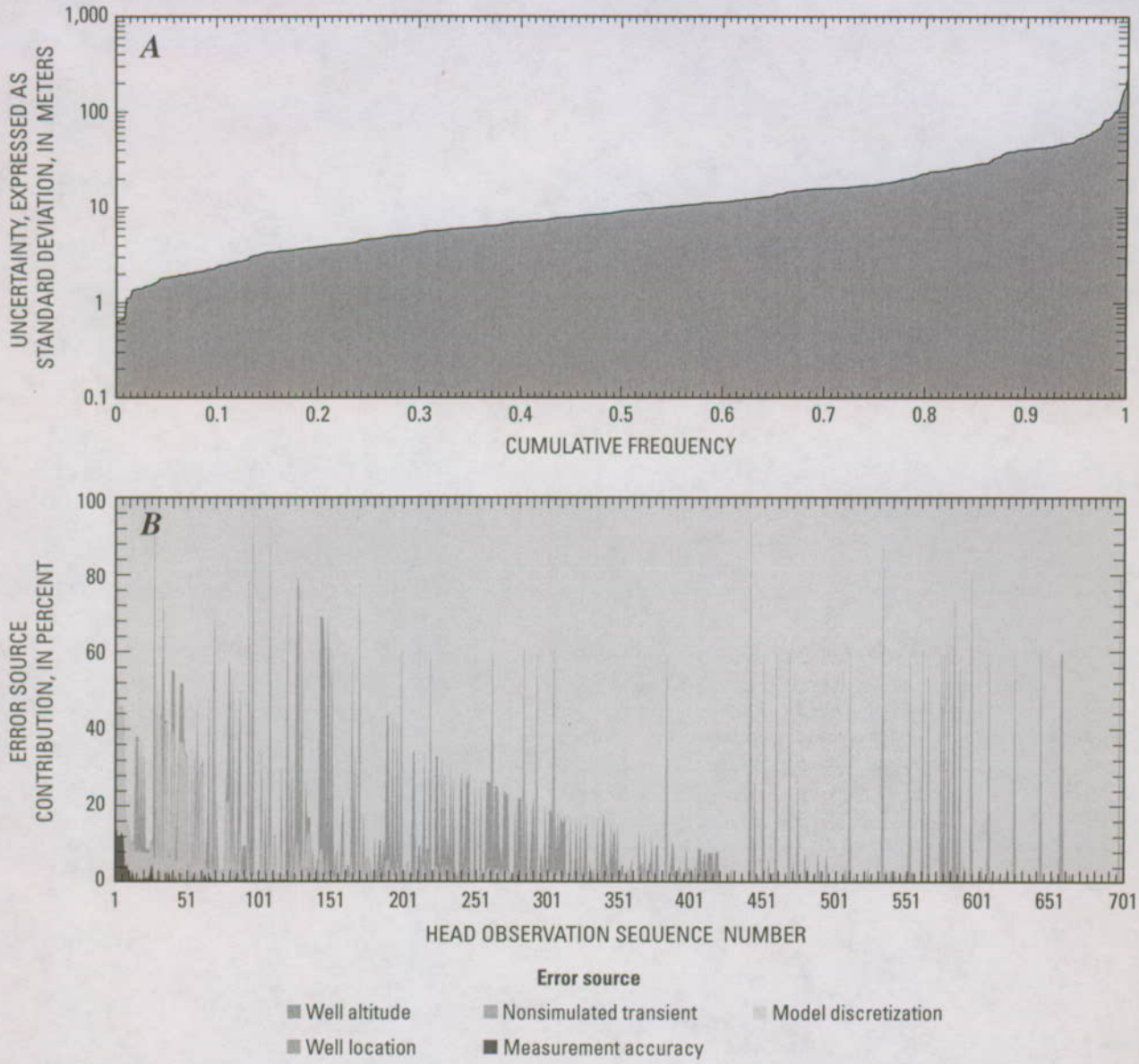

Figure F–11. Graphs showing calculated uncertainty of head observations used to calibrate Death Valley regional ground-water flow system model: (*A*) Cumulative frequency; (*B*) percent contribution.

observations, the available observations are insufficient to distinguish between the models. Thus, the model with more hydraulic-conductivity parameters represents a level of complexity that is not supported by the available data.

Unreasonable Parameter Estimates as Indicators of Model Error

An advantage to using regression to estimate parameter values is that the regression does not limit the estimates to reasonable values. Unreasonable estimated parameter values can indicate model error (Anderman and others, 1996; Poeter and Hill, 1997; Hill and others, 1998; and Hill, 1998, p. 13, 44). If a model represents a physical system adequately, and the observations used in the regression provide substantial information about the parameters being estimated, it is reasonable to assume that parameter values would be realistic. Model error would be indicated by unreasonable estimates of parameters for which the data provide substantial information. These unreasonable parameter estimates would indicate that further calibration is necessary.

Conceptual Model Variations

During calibration, a number of conceptual models were evaluated using the regression methods of MODFLOW-2000. A best fit to hydraulic-head, ground-water discharge, and boundary-flow observations was calculated for each conceptual model. Evidence of model error or data problems was investigated after each model run. These analyses were

used in conjunction with hydrogeologic data to modify and improve the existing conceptual model, observation data sets, and weighting.

Horizontal Hydraulic Conductivity

Horizontal hydraulic-conductivity parameters were assigned using the zonation capability of the HUF package (Anderman and Hill, 2000). Zones are used to define areas with similar properties within individual HGUs. The only variations of horizontal hydraulic conductivity simulated within zones were those related to depth decay.

Hydrogeologic evidence was used to initially define areas of similar horizontal hydraulic conductivity within the HGUs (Chapter B, this volume). Most zones were defined to represent geologic materials that likely have fairly uniform hydraulic properties. In some situations, however, single zones represent materials with differing hydraulic properties, and the properties of the dominant material were specified. Parameters defining the horizontal hydraulic conductivity were associated with each zone. During calibration, however, it became apparent that in some areas sufficient detail was not available from the geologic-property zonations or that the zonations did not match the hydraulic conditions in an HGU or part of an HGU. In these cases, additional zones were added.

Zonation was used to subdivide the units following hierarchical approach, where the model showed sensitivity to a particular parameter. The first division was based on the four major rock types (K1–K4) (tables F–3 and F–7) and each was assigned a homogeneous and isotropic hydraulic-conductivity (K) parameter. The second division was based on major groupings of the hydrogeologic units listed (table F–7). The third division was based on the individual HGUs and identification of rocks that likely have similar hydraulic properties. The fourth and fifth divisions were based on identification of rocks that likely have similar hydraulic properties using hydrogeologic considerations and model fit to observations. The final set of 56 horizontal hydraulic-conductivity parameters was used to calibrate the model. During calibration, in order to reduce the number of parameters, relatively insensitive hydraulic-conductivity parameters were combined with parameters of similar hydraulic conductivity. As a result, in some cases the hierarchy is not maintained, and rocks from different HGUs and different orders of parameters were grouped and the naming convention modified. Calibrated horizontal hydraulic-conductivity parameters are listed in tables by the four major rock types in following sections; accompanying maps show the extent of each HGU and its associated parameters and the value of the hydraulic-conductivity parameter projected to the land surface.

Confining Units

The geometry and location of the low-permeability units likely is more important than the specific value of horizontal hydraulic conductivity. Because the flow through these units is generally small, small changes in flow rate do not appreciably affect the discharge rates or water levels. In some cases, however, the hydraulic conductivity of these rocks is important to the magnitude and direction of ground-water flow and water levels. This is particularly true on the constant-head boundaries.

Zone arrays and parameters were used to refine the distribution of hydraulic-conductivity parameters for the confining units (clastic and crystalline rocks) (table F–8). The hydraulic-conductivity parameters for the crystalline-rock and clastic-rock confining units are defined by spatial zones and have varying degrees of effect on the flow model. *CSS* values for the ICU and XCU hydraulic-conductivity parameters were generally low. Where the hydraulic-conductivity parameters for the crystalline-rock and clastic-rock confining units were estimated to have similar properties, the zones were combined into one parameter.

The ICU was split into those areas inside and outside the major caldera centers (table F–8 and fig. F–12). This was done because the source for the intrusive rocks in the calderas likely is similar to, or the same as, the source of the volcanic rocks associated with the caldera.

It was necessary to simulate several zones in the XCU to accurately represent hydraulic gradients through the constant-head boundaries, heads, and discharges. The zonation for the XCU was initially based on the zonation described for the clastic units (Chapter B, this volume). Because these crystalline rocks are highly susceptible to deformation, zones based on structure (Chapter B, this volume) also were added. In the final calibration, and on the basis of the hydrologic information supplied to the simulation, only three zones were resolvable in the XCU (table F–8 and fig. F–13).

The LCCU (and LCCU_T1) was subdivided into several hydraulic-conductivity parameter zones on the basis of lithology and structure (Chapter B, this volume) (table F–8 and fig. F–14). The main facies transition within the LCCU is from an eastern region dominated by thick intervals of coarse clastics interbedded with shale (zones K1LCCU_XCU, K11C_XILCU, and K122fgLCCU; fig. F–14) to a more shale-dominated region with significant amounts of carbonate rocks (zone K122esLCCU; fig. F–14). The far northwestern part of the model domain contains a significant thickness of carbonate rocks (Sweetkind and White, 2001) with high permeability due to fractures. This area and the area along the Panamint Range in the western part of the model domain were combined into their own zone (zone K122esLCCU; fig. F–14). Because these zones alone were not enough to simulate some of the steep hydraulic gradients in the region, additional zones based on regional differences in deformational style (Chapter B, this volume) were added. Although the LCCU parameters generally have low hydraulic conductivity, higher hydraulic-conductivity values in zone K12223LCCU were required to simulate flow from Pahrump Valley to the Shoshone-Tecopa basin and then into the southern part of Death Valley (zone K12223LCCU, fig. F–14) because of a significant thickness of carbonate rocks in the LCCU in this area (Chapter B, this volume). The LCCU_T1 was simulated as a separate zone.

Table F–7. Hierarchy of horizontal hydraulic-conductivity parameters and major characteristics guiding parameter definition.

First-order parameters (major rock types)	Second-order parameters (major groupings of hydrogeologic units)	Third-order parameters (hydrogeologic units and(or) zones with similar characteristics)	Fourth- and fifth-order parameters (hydrogeologic units and(or) zones with similar characteristics)	Parameters used in final calibration
K1 Confining units – crystalline and clastic rocks	K11 Crystalline rocks	K111 Intrusive-rock confining unit (ICU)	Zoned inside or outside calderas	K11C_XILCU K11_ICU
		K112 Crystalline-rock confining unit (XCU)	Zoned inside or outside calderas	K11DV_XCU K1LCCU_XCU K11C_XILCU
	K12 Clastic rocks	K121 Sedimentary-rock confining unit (SCU)		
		K122 Clastic-rock confining units	K1221 Upper clastic-rock confining unit (UCCU)	K1221UCCU
			K1222 Lower clastic-rock confining units (LCCU, LCCU_T1) zoned based on facies and deformation	K12223LCCU K122fgLCCU K122esLCCU K11C_XILCU
K2 Carbonate rocks	K21 Western facies of lower carbonate-rock aquifer (LCA)	K211 Low deformation		K232_LCA
		K212 Deformed (oroflexes)		K232_LCA
	K22 Eastern facies of lower carbonate-rock aquifer (LCA) – low permeability	K221 Regional anticline		K221_LCA K242G_LCA
		K222 Disrupted by extension or calderas		K221_LCA
	K23 Poorly known areas of the lower carbonate-rock aquifer (LCA)	K231 Near extension		K232_LCA
		K232 Near moderate extension		K232_LCA
		K233 Near oroflex		K232_LCA
	K24 Eastern facies of lower carbonate-rock aquifer (LCA), thrusted lower carbonate-rock aquifer (LCA_T1), and upper carbonate-rock aquifer (UCA) – permeable	K241 Low deformation	K2411 Stable blocks	K241SM_LCA K2SHPLCA
			K2412 Semi-stable blocks	K2412_LCA K2412fLCA K2_DV_LCA K242G_LCA
			K2413 Thrusted lower carbonate-rock aquifer (LCA_T1)	K241LCA_T1
		K242 Moderate deformation	K2421 Rotated range blocks	K241SMWLCA K2421_LCA
			K2422 Basin-Range blocks	K242G_LCA K242YN_LCA K2YMLCA K242A_LCA K2422b_LCA K244_LCA
			K2423 Regional fold	K243_UCA

Table F–7. Hierarchy of horizontal hydraulic-conductivity parameters and major characteristics guiding parameter definition. —Continued

First-order parameters (major rock types)	Second-order parameters (major groupings of hydrogeologic units)	Third-order parameters (hydrogeologic units and(or) zones with similar characteristics)	Fourth- and fifth-order parameters (hydrogeologic units and(or) zones with similar characteristics)	Parameters used in final calibration
			K2424 Oroflexed stable block	K2SHPLCA
		K243 High deformation	K2431 Shear zone	K2SHPLCA K243_LCA
			K2432 Detachment	K243PP_LCA K243GV_LCA
			K2433 Multiply-deformed areas	K2421_LCA K243_LCA
			K2434 Upper carbonate-rock aquifer (UCA)	K243_UCA
K3 Volcanic rocks	K31 Younger volcanic rocks, tuffs and lava flows (LFU, YVU)	K311 Younger volcanic-rock unit (YVU)		K32BR4CH13
		K312 Lava-flow unit (LFU)	Zoned based on facies change	K42UP_VSU K3LFU_am
	K32 Southwestern Nevada volcanic field rocks	K321 Thirsty Canyon–Timber Mountain volcanic-rock aquifer (TMVA)	Zoned based on brittleness and alteration	K3C_TM K3211TMVA
		K32 Paintbrush volcanic-rock aquifer (PVA)	Zoned based on inside or outside caldera	K3C_PVA K3PVA
		K323 Calico Hills volcanic-rock confining unit (CHVU)	Zoned based on brittleness and alteration	K32CH24LF K32BR4CH13
		K324 Wahmonie volcanic-rock unit (WVU)		K32BR4CH13
		K325 Crater Flat Group volcanic rocks	K3251 Crater Flat–Prow Pass aquifer (CFPPA)	K321521_PP
			K3252 Crater Flat–Bullfrog confining unit (zoned based on brittleness and alteration) (CFBCU)	K3215BCU1 K3215BCU34
			K3253 Crater Flat–Tram aquifer (CFTA)	K3215TR
		K326 Belted Range unit (BRU)	Zoned based on brittleness and alteration	K3BRU123
	K33 Older volcanic unit (OVU)	Zoned based on inside/outside SWNVF		K33_OVU K33_OVUsw
K4 Basin fill	K41 Alluvial aquifers (YAA, OAA, LA)			K4_VF_AQ
	K42 Alluvial confining units (YACU, OACU, upper VSU, lower VSU)	K421 Younger and older alluvial confining units (YACU, OACU)		K4_VF_OAA K4_VF_CU
		K422 Volcanic- and sedimentary-rock unit (upper and lower VSU)	Zones based on facies changes	K4UP_VSUC K4UP_VSUP K42UP_VSU K42222_VSU K422LNEVSU K422LNWVSU K4222S_VSU K422DV_VSU K422GW_VSU K4222P_VSU K422GV_VSU

Table F–8. Calibrated horizontal hydraulic-conductivity parameters for confining units.

[Abbreviations: ICU, intrusive-rock confining unit; XCU, crystalline-rock confining unit; LCCU, lower clastic-rock confining unit; LCCU_T1, thrusted lower clastic-rock confining unit; UCCU, upper clastic-rock confining unit; NA, not available]

Parameter name	Description	Minimum – maximum hydraulic conductivity (meters per day) from Belcher and others (2001)	Composite scaled sensitivity	Hydraulic conductivity at land surface (meters per day)	Coefficient of variation[1]	Average depth (meters)	Hydraulic conductivity at average depth (meters per day)
K11_ICU	Extra-caldera ICU.	6×10^{-4} – 1.4	0.616	2.463×10^{-3}	0.0014	3,372	0.002461
K11DV_XCU	XCU rocks in the Death Valley area. Complex geologic structures and lack of subsurface data result in highly interpretive geometry, extent, and property distribution for rocks in this zone.	NA	0.831	1.086×10^{-1}	0.0017	2,625	0.002564
K11C_XILCU	Intracaldera ICU.	3×10^{-8} – 5	0.389	1.940×10^{-3}	0.0047	[2]4,092	0.001938
	Intracaldera parts of XCU rocks. In general, these rocks form a barrier to flow.	3×10^{-8} – 5					
	Deformed LCCU including Stirling Quartzite around calderas.	3×10^{-8} – 5					
K1LCCU_XCU	(1) LCCU in southern part of DVRFS model domain, including the Saratoga Springs area.	3×10^{-8} – 5	0.384	4.082×10^{-3}	0.0047	4,643	0.000005
	(2) XCU that generally form a barrier to flow. Where exposed, the rocks are often core complexes of detachment faults.						
K12223LCCU	(1) Thick section of LCCU (Stirling Quartzite) interpreted as extending beneath Pahrump Valley and to the west toward Shoshone and Tecopa basins. The rocks in this area are affected by extensional faulting that may increase the permeability of the more competent parts of this unit.	3×10^{-8} – 5	0.648	1.568×10^{-3}	0.0007	2,528	0.001567
	(2) Deformed part of LCCU (Stirling Quartzite); north central swath of model domain northern part of Death Valley.						
	(3) LCCU_T1.						
K122fgLCCU	(1) Spring Mountains and Sheep Range with deformed LCCU and LCCU_T1 (Stirling Quartzite).	3×10^{-8} – 5	0.100	6.000×10^{-5}	0.0002	3,561	0.000060
	(2) Yucca Mountain and the Amargosa Desert characterized by undeformed LCCU (Stirling Quartzite).						
	(3) Northeastern part of DVRFS model domain (no Stirling Quartzite).						
K122esLCCU	(1) Deformed LCCU in the Panamint Range-Death Valley area.	3×10^{-8} – 5	0.284	1.846×10^{-1}	0.12	3,561	0.1844
	(2) Deformed part of LCCU (Stirling Quartzite) in extreme northwestern part of DVRFS model domain (finer grained).						
K1221UCCU	Thick localized section of clastic rocks (UCCU) in Eleana Range separating the regional carbonate-rock aquifer into upper and lower parts.	0.0002 – 0.4	0.346	3.878×10^{-2}	0.0358	1,019	0.001147

[1]Values were log transformed.

[2]Average depth from most spatially expansive unit, XCU.

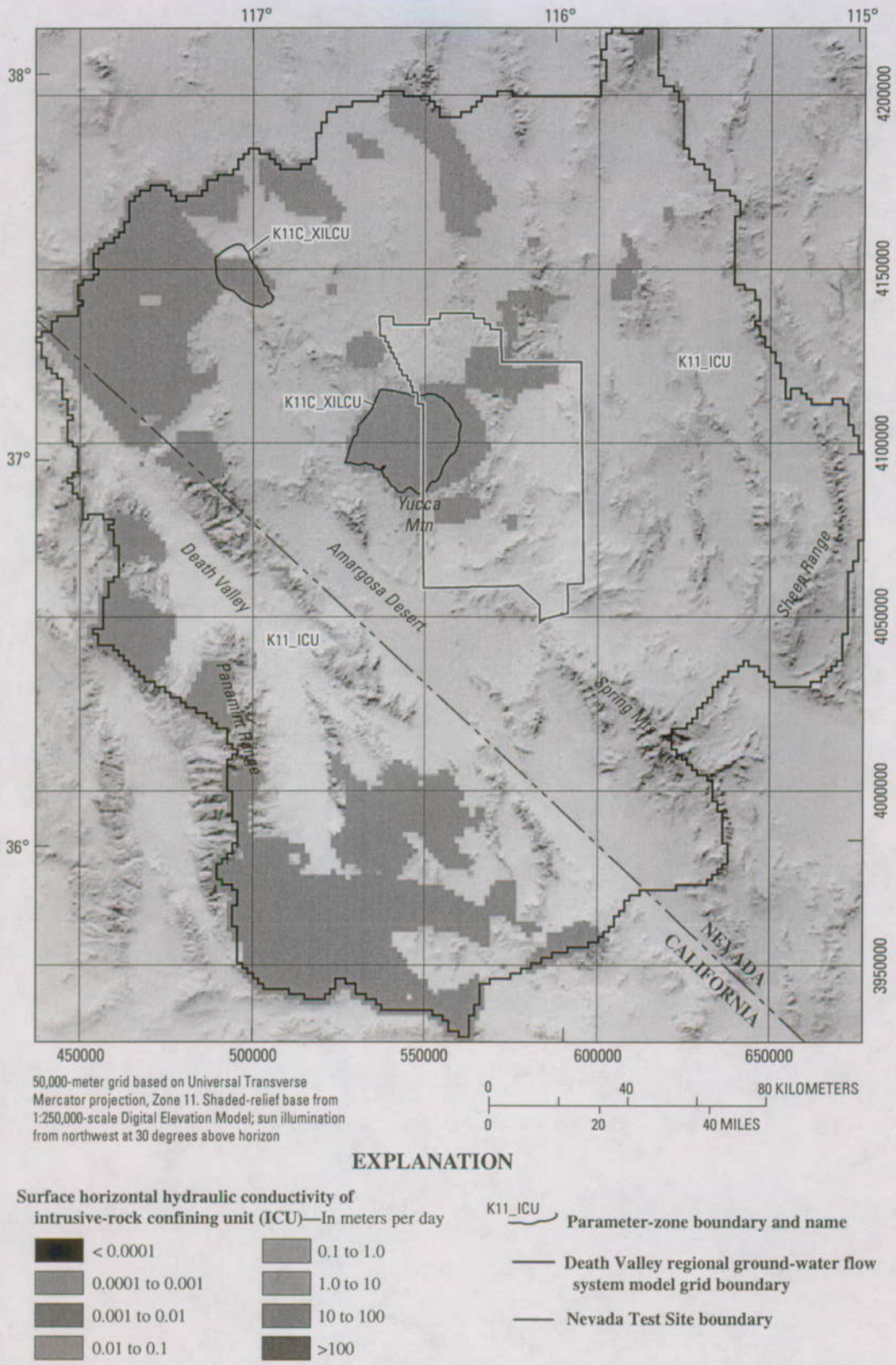

Figure F–12. Hydraulic-conductivity zone parameters, unit thickness, and extent for intrusive-rock confining unit.

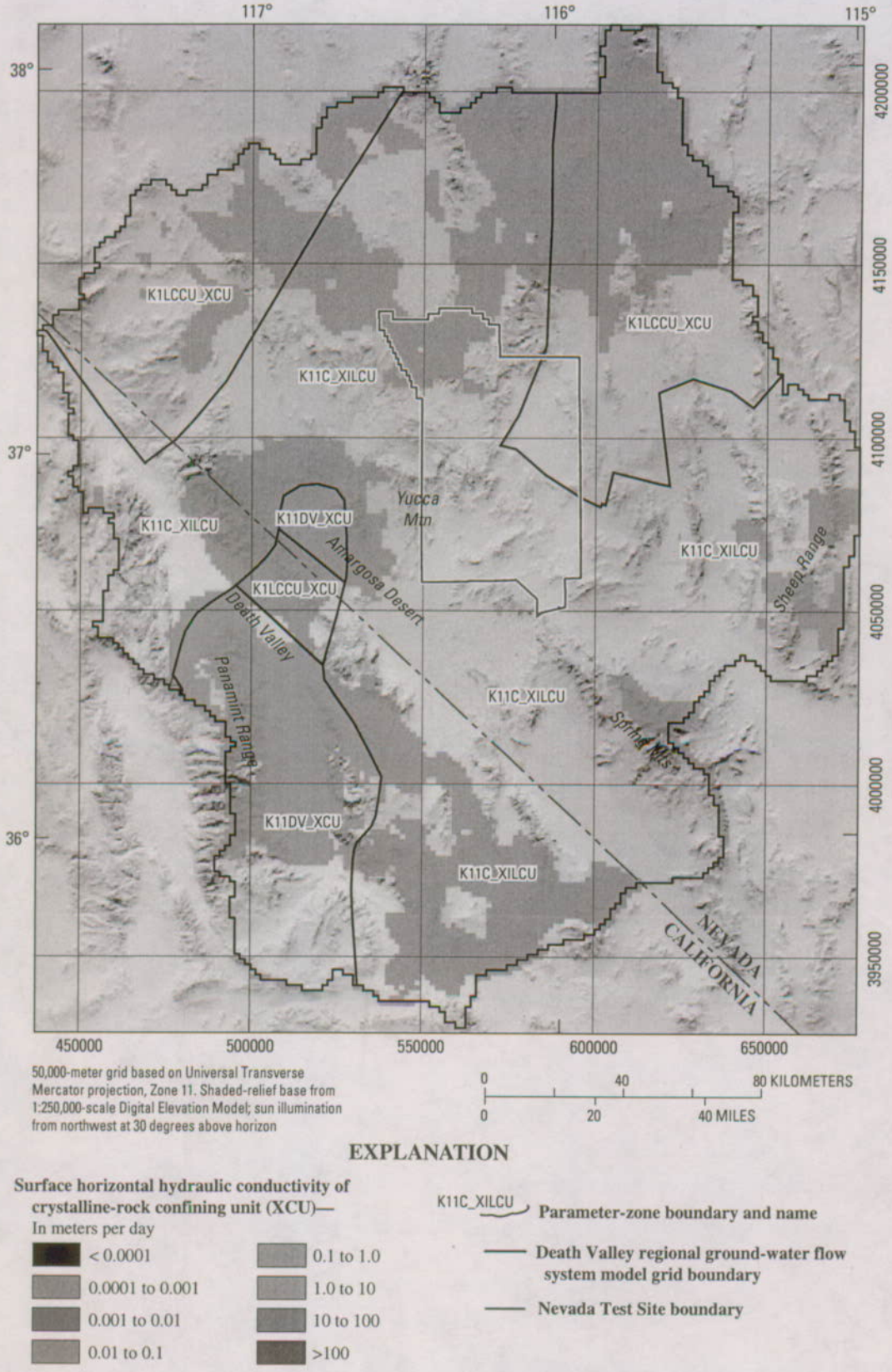

Figure F–13. Hydraulic-conductivity zone parameters, unit thickness, and extent for crystalline-rock confining unit.

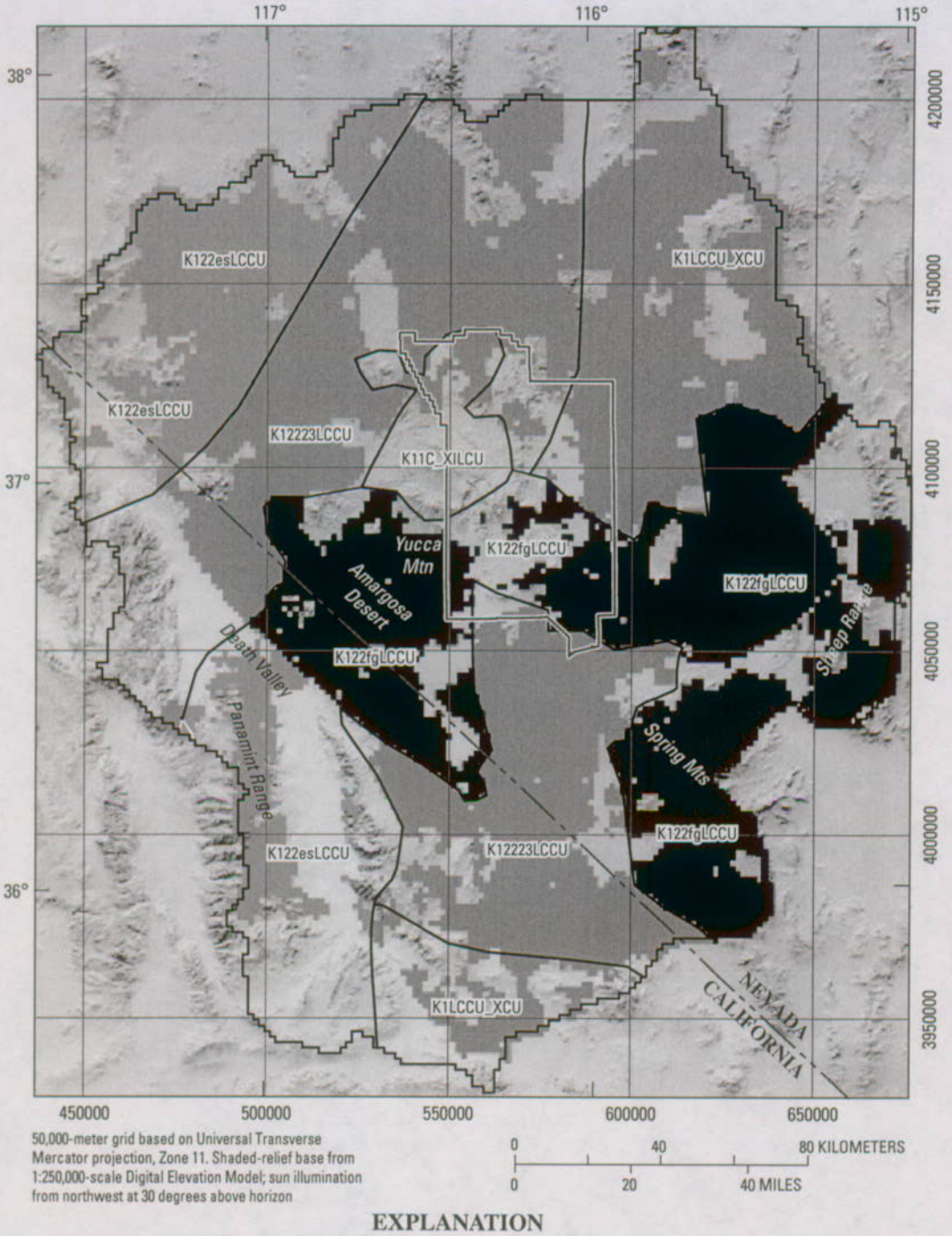

Figure F–14. Hydraulic-conductivity zone parameters, unit thickness, and extent for lower clastic-rock confining unit.

During calibration, the properties of the LCCU_T1 were found to be similar to the K122fgLCCU parameter, and the unit was combined with this parameter. Parts of the LCCU_T1 that may also have relatively higher hydraulic-conductivity values were combined into the K12223LCCU zone (fig. F–15).

An important feature in the flow model is the steep hydraulic gradient west of Yucca Flat that wraps around to Yucca Mountain and that is formed by the low permeability of the UCCU (fig. F–15). Because of this, the UCCU was separated as an individual parameter (K1221UCCU). Because of its geologic origin, the SCU commonly is of higher permeability and was also separated as a different parameter (K4UP_VSUP) (fig. F–16).

For some of the confining units, the hydraulic conductivity at the land surface is the same as or of higher magnitude than that of the aquifers. Depth-decay parameters, however, cause hydraulic conductivities to decrease rapidly with depth. Thus, where most of the flow occurs, these units have a much lower relative hydraulic-conductivity value. Calibrated hydraulic-conductivity values at the land surface and at an average depth are presented in table F–8. The assignment of relatively high hydraulic conductivities for the confining units at land surface also is reasonable because of the effects of weathering on the rocks (Bedinger and others, 1989).

Carbonate-Rock Aquifers

The HGUs constituting the carbonate rocks were initially grouped into one hydraulic-conductivity parameter (K2), and the resulting *CSS* value was more than four times greater than the parameters defining the other major rock types. Because of this sensitivity, this hydraulic-conductivity parameter was then subdivided into a series of hierarchical hydraulic-conductivity parameters (table F–9) based on geologic zonations (Chapter B, this volume). Initially, the LCA was split into eastern and western facies and poorly defined areas. The eastern facies was then split into permeable and low-permeability zones on the basis of the degree of rock deformation (Chapter B). The permeable eastern zones also include the LCA_T1 and the UCA. Recharge zone multipliers and flow out of the constant-head boundary at the Sheep Range were sensitive to the LCA_T1 parameter. The LCA was further subdivided into spatial zones defined on the basis of structural-physiographic subsections described in more detail in Chapter B.

Delineating the zones in the LCA described in Chapter B (this volume) helped improve model fit and the simulation of regional potentiometric features, but more zones were required to simulate discharge or heads in some areas (fig. F–17). Additional zones were added to the LCA in areas immediately north and east of the Las Vegas Valley shear zone (LVVSZ), where oroflexural bending occurs and may cause preferential flow directions along this structural fabric. Because of the sensitivity of the LCA_T1 parameter (K241LCA_T1), the LCA_T1 and UCA were broken out as separate parameters (fig. F–18).

Because of depth decay, either the hydraulic-conductivity values at depth are greater in the confining units than the LCA, or both values are so small that flow through the units is insignificant. In some areas, however, such as north of Yucca Mountain and along the Eleana Range, this reversal in relative permeability may indicate an unrealistic interpretation in the HFM and(or) perched water levels.

Volcanic-Rock Units

The hydrologic characteristics of the volcanic rocks are more difficult to define than those of the other units because of their great variability in aquifer test results and complex stratigraphy. In a general way, however, some hydrologic properties do correlate with stratigraphy. Because the HFM is based on stratigraphy, the HGU classifications were used first to subdivide the volcanic-rock units (K3) into three second-order parameters (table F–7), which then were subdivided further on the basis of caldera locations, welding, and(or) alteration (table F–10):

1. Older volcanic-rock unit (OVU) (fig. F–19)

2. SWNVF rocks (BRU, CFTA, CFBCU, CFPPA, WVU, CHVU, PVA, TMVA) (figs. F–20—F–27)

3. Younger volcanic rocks, tuffs, and lava flows (YVU, LFU) (figs. F–24 and F–28).

The OVU (fig. F–19) was subdivided into two general groups: (1) volcanic rocks associated with, and perhaps originating from, the SWNVF (K33_OVUsw) and (2) volcanic rocks that originated outside the SWNVF (K33_OVU) (Chapter B, this volume). The OVU within the SWNVF (K33_OVUsw) acts as a confining unit because of its generally nonwelded to partially welded nature, and widespread zeolitic alteration (Chapter B, this volume) (fig. F–19 and table F–10). The OVU outside the SWNVF (K33_OVU) can form local aquifers (Chapter B, this volume). The K33_OVU zone does not appear to have regionally connected fractures and serves as a regional confining unit (fig. F–19, table F–10).

Within the SWNVF units, the PVA and TMVA were assumed to have similar properties and were initially combined. Likewise, the CHVU and the WVU were combined on the basis of their similar geologic characteristics. During calibration, estimates of the hydraulic-conductivity parameters for the volcanic-rock units did not follow the zonation of brittle and altered rock described in Chapter B (this volume) and likely indicates the uncertainty of this zonation. Although the zones based on these properties were used to subdivide the HGUs, the calibrated hydraulic-conductivity value commonly did not agree with the expected value based on the hydraulic properties used for the zonation.

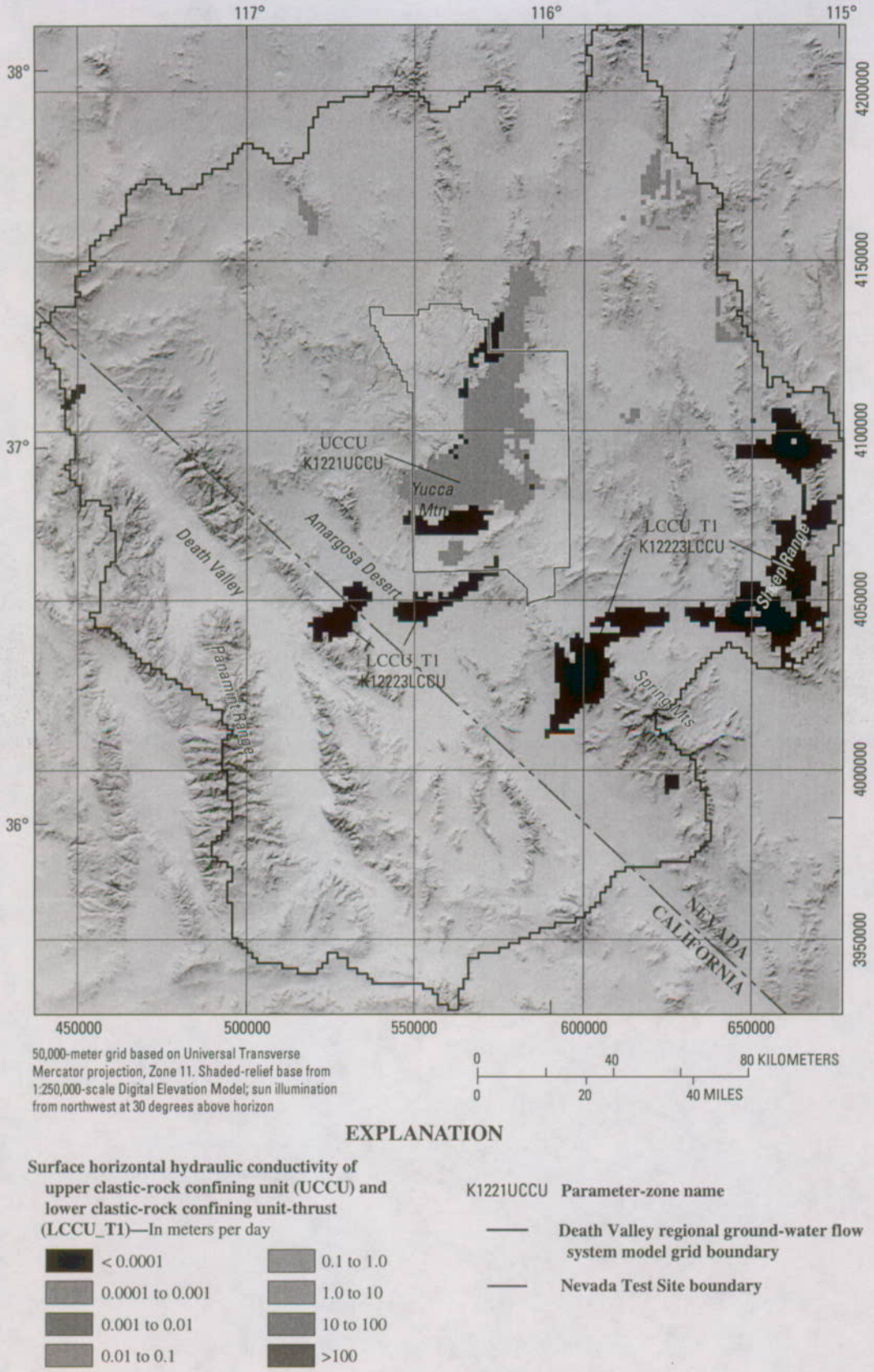

Figure F–15. Hydraulic-conductivity zone parameters, unit thickness, and extent for upper clastic-rock confining unit and thrusted lower clastic-rock confining unit.

Figure F–16. Hydraulic-conductivity zone parameters, unit thickness, and extent for sedimentary-rock confining unit.

Table F–9. Calibrated horizontal hydraulic-conductivity parameters for carbonate-rock aquifers.

[LCA, lower carbonate-rock aquifer; LCA_T1, thrusted lower carbonate-rock aquifer; NA, not applicable; UCA, upper carbonate-rock aquifer]

Parameter name	Description	Composite scaled sensitivity	Hydraulic conductivity at land surface[1] (meters per day)	Coefficient of variation[2]	Average depth, in meters	Hydraulic conductivity at average depth (meters per day)
K232_LCA	(1) Poorly defined areas with moderate extension (K23); character of LCA is highly uncertain. (2) Western facies (K21), low deformation; carbonate rocks are interbedded with shales.	0.096	1.000×10^{-3}	0.0041	1,956	6.37×10^{-4}
K221_LCA	Eastern (K22) low-permeability facies along regional anticline; the LCA may not exist in this area and is poorly defined.	0.171	6.089×10^{0}	0.5	1,396	4.41
K241SM_LCA	Eastern permeable facies with low deformation along stable block of the Spring Mountains.	0.735	1.510×10^{-3}	0.00029	2,670	1.26×10^{-3}
K241LCA_T1	Upper plate of thrusted LCA.	0.252	9.865×10^{-1}	0.5	1,056	0.0257
K241SMWLCA	Eastern permeable facies with moderate deformation along highly extended rotated range blocks.	0.361	3.7749×10^{-1}	0.31	1,353	0.275
K2_DV_LCA	Eastern low-permeability facies disrupted by extension along Death Valley.	0.049	3.000×10^{0}	0.5	981	2.81
K2412_LCA	Eastern permeable facies with low deformation along semi-stable blocks.	0.472	8.059×10^{-2}	0.038	2,041	5.04×10^{-1}
K2412fLCA	Eastern permeable facies with low deformation along semi-stable blocks of the Funeral Range.	0.825	1.206×10^{1}	0.5	2,042	1.04×10^{-2}
K242G_LCA	(1) Eastern permeable facies with low deformation along semi-stable blocks (K241) of the Grapevine Mountains. (2) Eastern permeable facies with moderate deformation (K242) of basin-range blocks. (3) Eastern low permeability facies along regional anticline (K221) on eastern part of Pahute Mesa; LCA may not exist in this area and is poorly defined.	2.883	6.463×10^{-2}	0.014	2,741	0.0344
K242YN_LCA	LCA along northern part of Yucca Mountain.	0.134	1.170×10^{-4}	0.00089	2,741	6.225×10^{-5}
K242A_LCA	Eastern permeable facies with moderate deformation (K242) around Yucca Flat.	0.195	3.393×10^{0}	0.5	2,180	2.05
K2SHPLCA	(1) Eastern permeable facies with low deformation along stable block of the Sheep Range. (2) Eastern permeable facies with moderate deformation of oroflexed stable block (strike-slip faults). (3) Eastern permeable facies with high deformation in regional shear zones (Pahranagat shear zone).	0.097	6.511×10^{-2}	0.19	3,152	0.0315
K2YMLCA	Eastern permeable facies with moderate deformation around Yucca Mountain.	0.442	4.2262×10^{-1}	0.41	2,766	0.225

Table F–9. Calibrated horizontal hydraulic-conductivity parameters for carbonate-rock aquifers.—Continued

[LCA, lower carbonate-rock aquifer; LCA_T1, thrusted lower carbonate-rock aquifer; NA, not applicable; UCA, upper carbonate-rock aquifer]

Parameter name	Description	Composite scaled sensitivity	Hydraulic conductivity at land surface[1] (meters per day)	Coefficient of variation[2]	Average depth, in meters	Hydraulic conductivity at average depth (meters per day)
K2421_LCA	(1) Eastern permeable facies with moderate deformation along highly extended rotated range blocks. (2) Eastern permeable facies with high deformation in multiply-deformed areas (oroflexes, extension, shear and regional folding).	0.930	1.573×10^{-2}	0.005	2,681	8.48×10^{-3}
K2422b_LCA	Eastern permeable facies with moderate deformation of basin-range blocks.	0.272	6.454×10^{-2}	0.033	2,314	0.0291
K243_LCA	(1) Eastern permeable facies with high deformation in regional shear zones (Mine Mountain shear zone). (2) Eastern permeable facies with high deformation in multiply deformed areas (oroflexes, extension, shear and regional folding).	2.438	2.189×10^{0}	0.5	2,398	1.78
K243_UCA	(1) UCA. (2) Eastern permeable facies with moderate deformation of regional fold along Spotted Range syncline.	0.0159	1.000×10^{-4}	NA	341	3.08×10^{-5}
K243PP_LCA	Eastern permeable facies with high deformation in upper plate of brittle detachments.	0.162	1.000×10^{0}	0.5	836	0.946
K243GV_LCA	(1) Eastern permeable facies with high deformation in upper plate of brittle detachments along Grapevine Mountains and Bare Mountain. (2) Poorly known areas near oroflex; character of LCA is highly uncertain.	0.086	2.398×10^{-3}	0.0036	1,367	2.19×10^{-3}
K244_LCA	Eastern permeable facies with moderate deformation centered around Ash Meadows.	0.014	2.000×10^{2}	NA	2,201	200.0

[1]Minimum and maximum hydraulic conductivity in meters per day for the UCA and LCA are 0.0001 to 820 (Belcher and others, 2001).

[2]Values were log transformed.

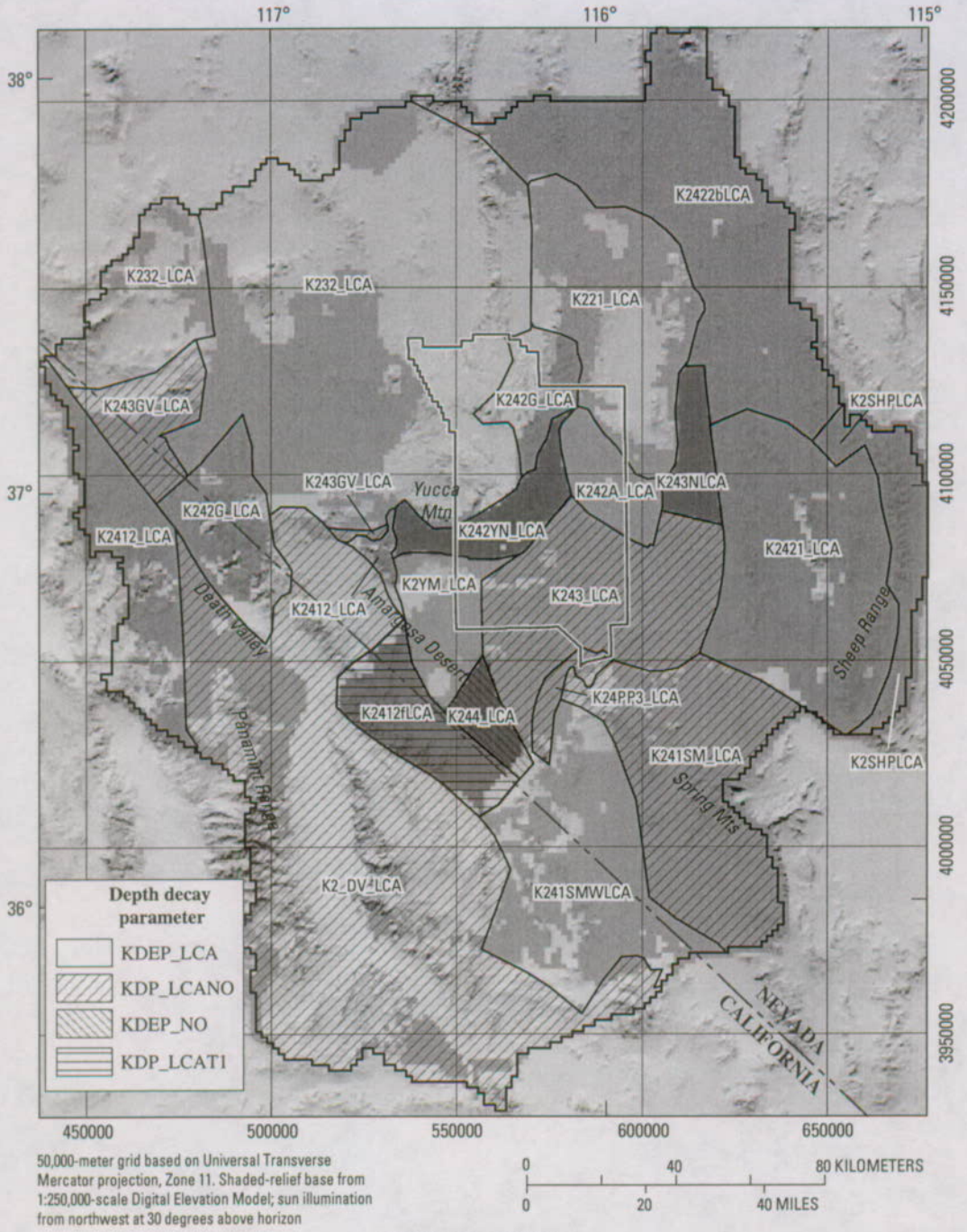

Figure F–17. Hydraulic-conductivity zone parameters, depth-decay parameters, unit thickness, and extent for lower carbonate-rock aquifer. Depth-decay parameter values presented in table F–12 and figure F–35.

Figure F–18. Hydraulic-conductivity zone parameters, unit thickness, and extent for upper carbonate-rock aquifer and thrusted lower carbonate-rock aquifer unit.

Table F–10. Calibrated horizontal hydraulic-conductivity parameters for the volcanic-rock units.

[BRU, Belted Range unit; CFBCU, Crater Flat–Bullfrog confining unit; CFPPA, Crater Flat–Prow Pass aquifer; CFTA, Crater Flat–Tram aquifer; CHVU, Calico Hills volcanic-rock unit; LFU, lava-flow unit; OVU, older volcanic-rock unit; PVA, Paintbrush volcanic-rock aquifer; SWNVF, southwestern Nevada volcanic field; TMVA, Thirsty Canyon–Timber Mountain volcanic-rock aquifer]

Parameter name	Description	Minimum – maximum hydraulic conductivity, in meters per day, from Belcher and others, 2001	Composite scaled sensitivity	Hydraulic conductivity at land surface (meters per day)	Coefficient of variation[1]	Average depth (meters)	Hydraulic conductivity at average depth (meters per day)
K311 YVU (lumped with part of CHVU; K32BR4CH13)							
K312 LFU (part lumped with VSU (upper); K42UP_VSU)							
K3LFU_am	LFU in Amargosa Desert area	0.002–4	0.0904	5.094×10^{-2}	0.23	38	0.0410
K3C_TM	TMVA - brittle (either altered or not)	[3]2×10^{-4}–20	1.029	8.440	0.5	144	3.71
K3211TMVA	TMVA - not brittle (either altered or not)	[3]2×10^{-4}–20	0.280	5.662×10^{-1}	0.44	588	0.197
K3C_PVA	Intracaldera PVA	[2]7×10^{-7}–17	0.08808	0.3162	NA	248	0.0767
K3PVA	Extra-caldera PVA	[2]7×10^{-7}–17	0.2820	2.885×10^{2}	[11]0.29	248	70.00
K32CH24LF	(1) CHVU – altered, brittle (2) CHVU – not altered, not brittle (3) LFU – all areas except Amargosa Desert	[4]0.002–4	0.1776	1.328×10^{-1}	0.42	[12]38	0.107
K32BR4CH13	(1) BRU – not brittle, not altered (2) WVU (3) CHVU – not altered, brittle (4) CHVU – altered, not brittle	[5]0.008–4	0.2840	1.604×10^{-1}	0.11	[13]175	0.05917
K321521_PP	CFPPA	[6]0.001–180	0.5710	1.661×10^{2}	0.5	693	3.183
K3215BCU1	CFBCU – not altered, brittle	[6]0.001–180	0.04711	1.000×10^{-2}	0.26	561	0.000406
K3215BCU34	CFBCU – not brittle (either altered or not)	[7]0.0003–55	0.3780	1.241	0.49	562	0.05012
K3215TR	CFTA	[8]0.003–2	0.1347	5.597×10^{-2}	0.49	721	0.000914
K3BRU123	(1) BRU – not altered, brittle (2) BRU – altered, brittle (3) BRU – altered, not brittle	[9]0.01–4	0.1597	1.894	0.5	561	0.07693
K33_OVU	OVU outside SWNVF	[10]1×10^{-6}–1	0.01341	9.900×10^{-3}	0.021	142	0.004388
K33_OVUsw	OVU inside SWNVF	[10]1×10^{-6}–1	0.1867	4.8638×10^{-2}	0.061	509	0.002658

[1]Values were log transformed.

[2]Range listed is for the PVA.

[3]Range listed is for the TMVA.

[4]Range listed is for the LFU, which includes the range of the CHVU.

[5]Minimum value listed is for CHVU and the maximum value listed is for the BRU.

[6]Range listed is for the CFPPA.

[7]Range listed is for the CFBCU.

[8]Range listed is for the CFTA.

[9]Range listed is for the BRU.

[10]Range listed is for the OVU.

[11]Parameter was not log transformed.

[12]Average depth is for the LFU, the most spatially extensive unit.

[13]Average depth is for the BRU, the most spatially extensive unit.

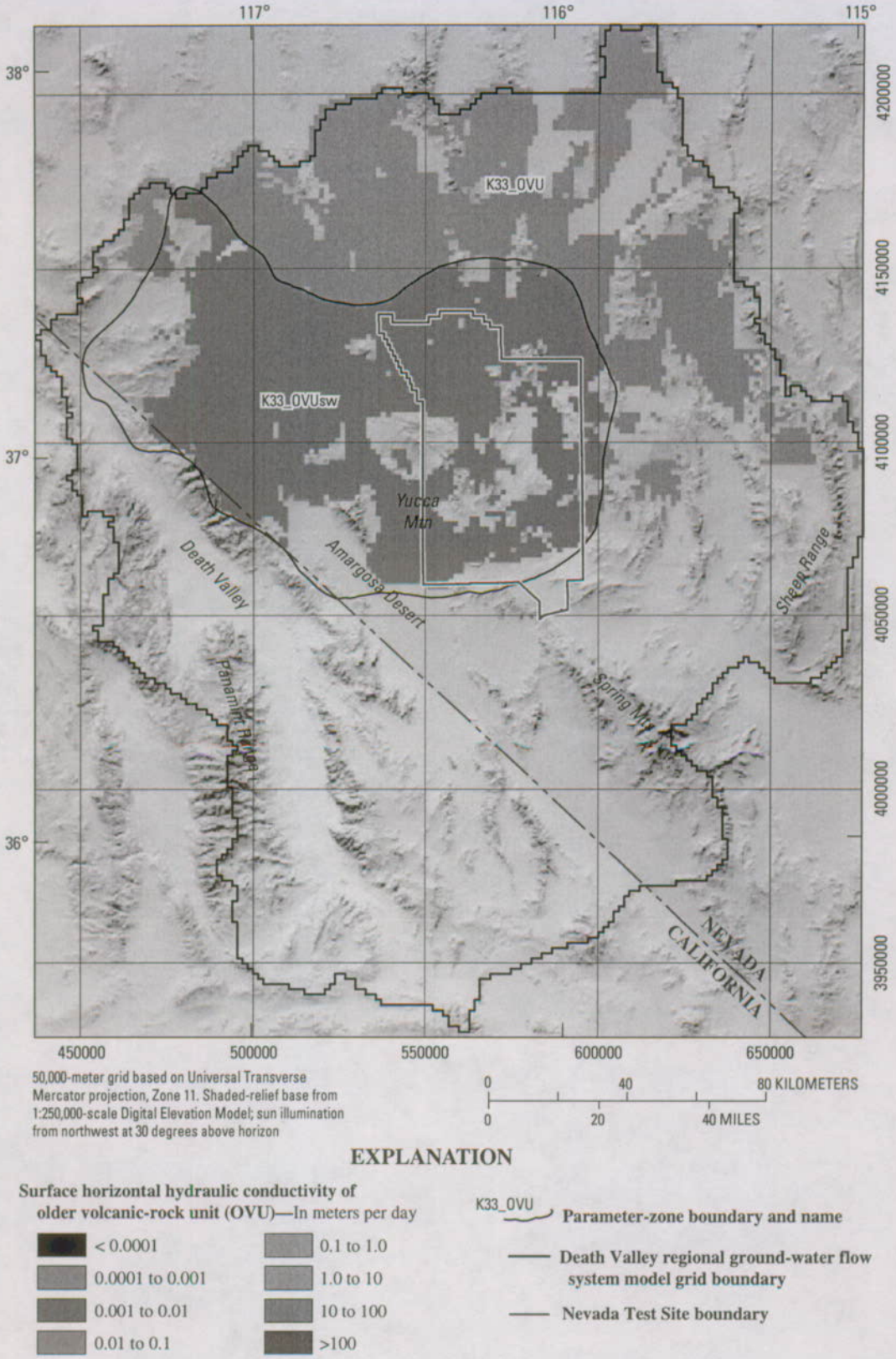

Figure F–19. Hydraulic-conductivity zone parameters, unit thickness, and extent for older volcanic-rock unit.

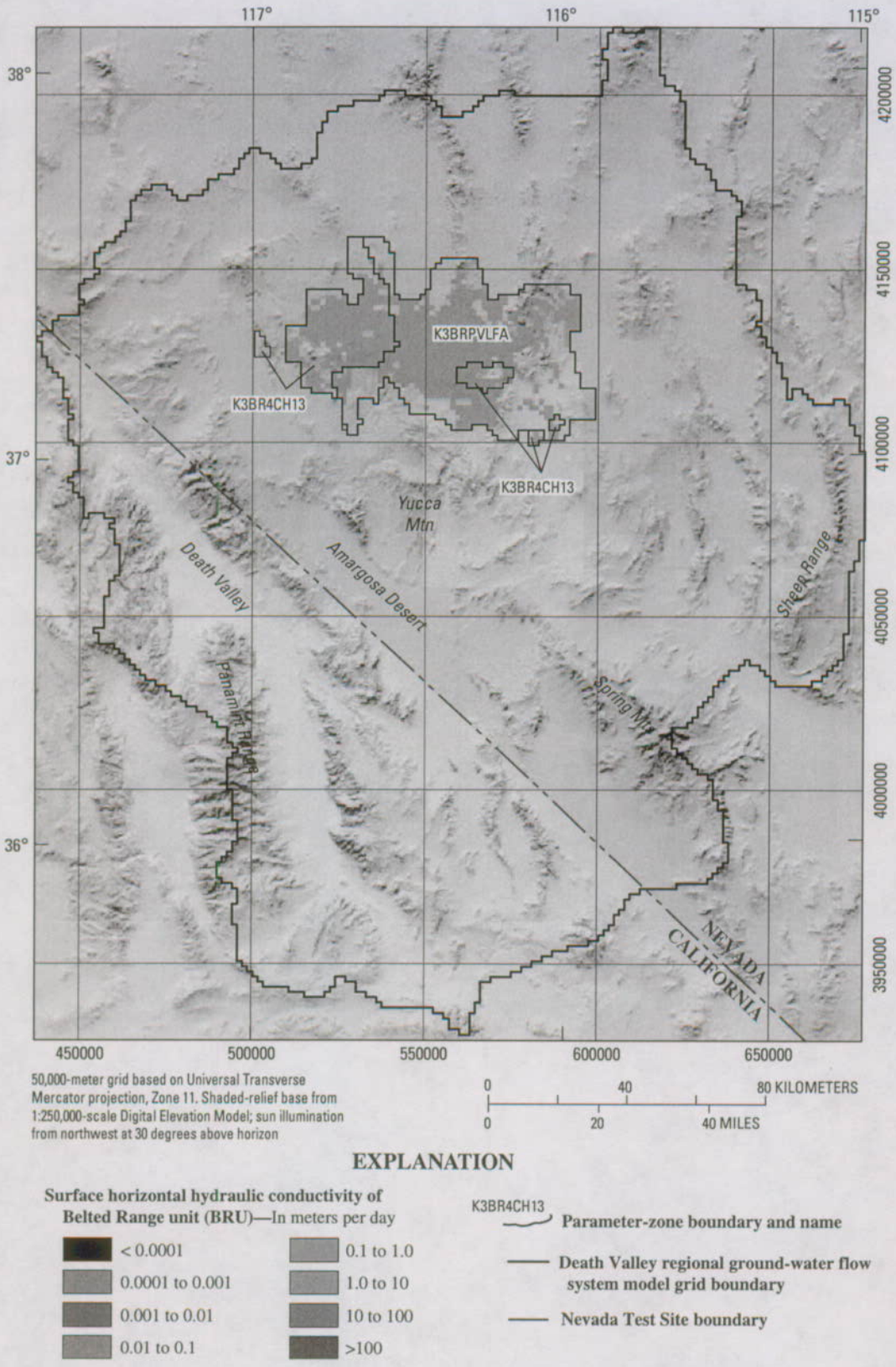

Figure F–20. Hydraulic-conductivity zone parameters, unit thickness, and extent for belted Range unit.

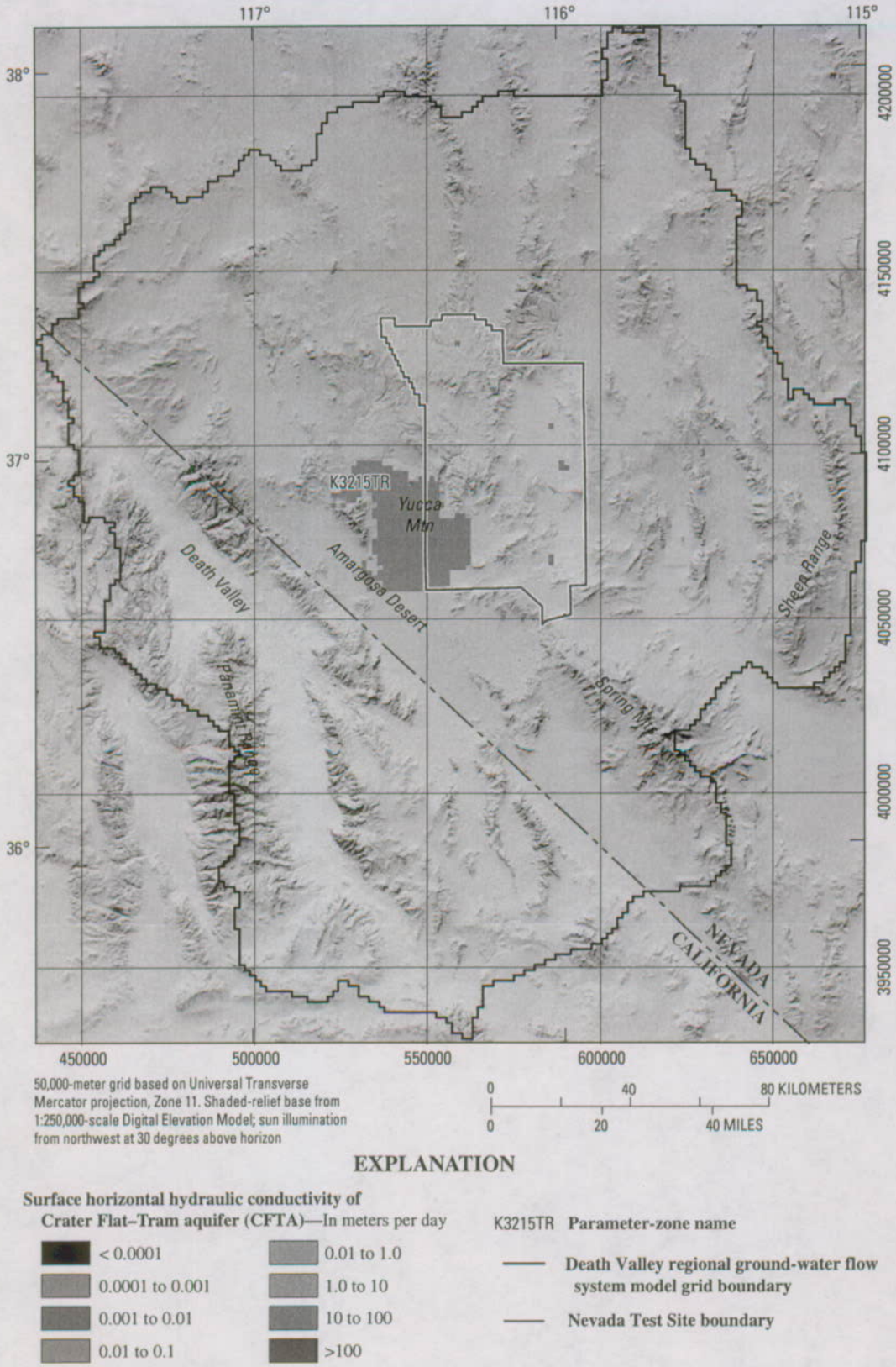

Figure F–21. Hydraulic-conductivity zone parameters, unit thickness, and extent for Crater Flat–Tram aquifer unit.

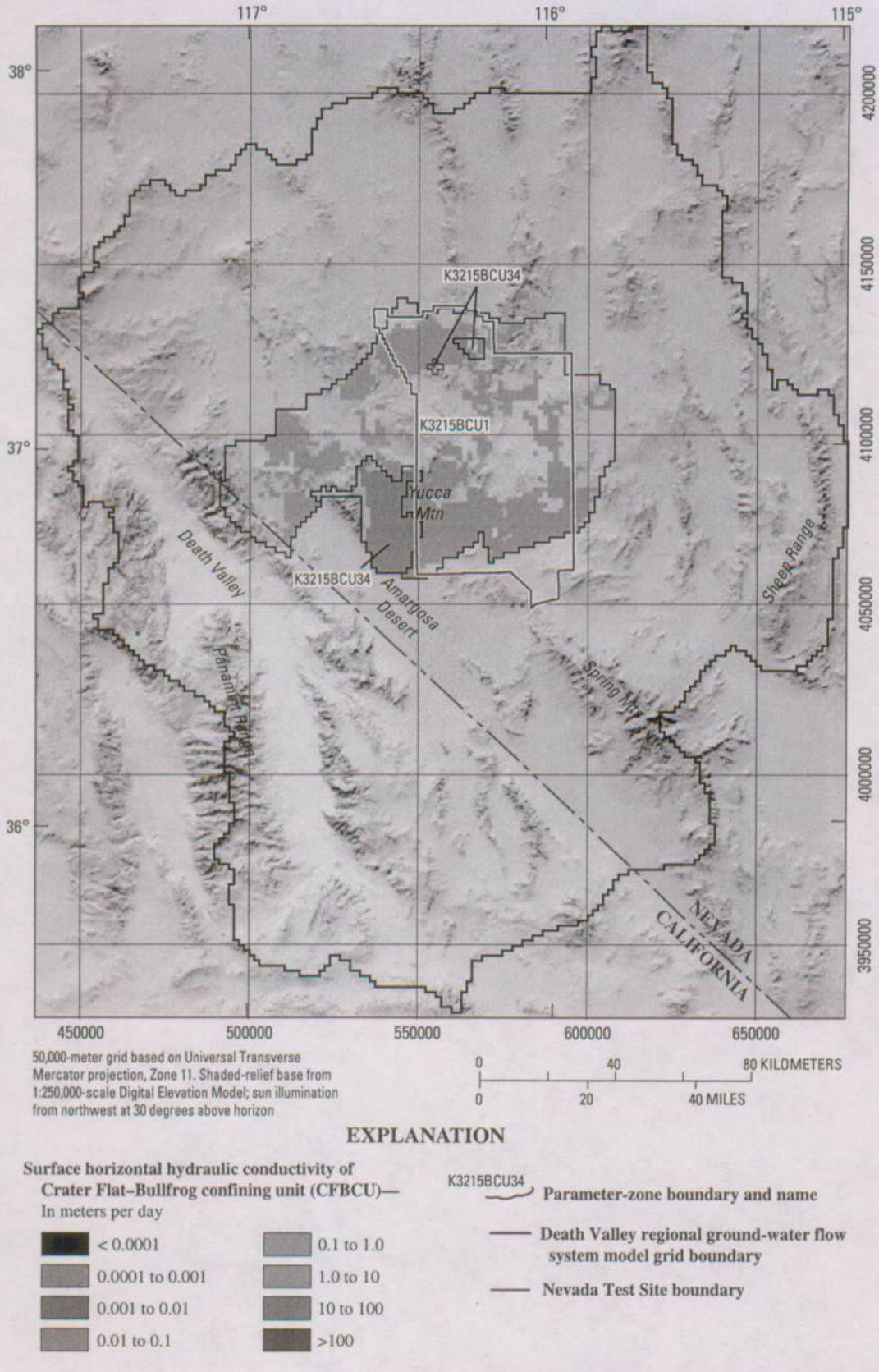

Figure F–22. Hydraulic-conductivity zone parameters, unit thickness, and extent for Crater Flat–Bullfrog confining unit.

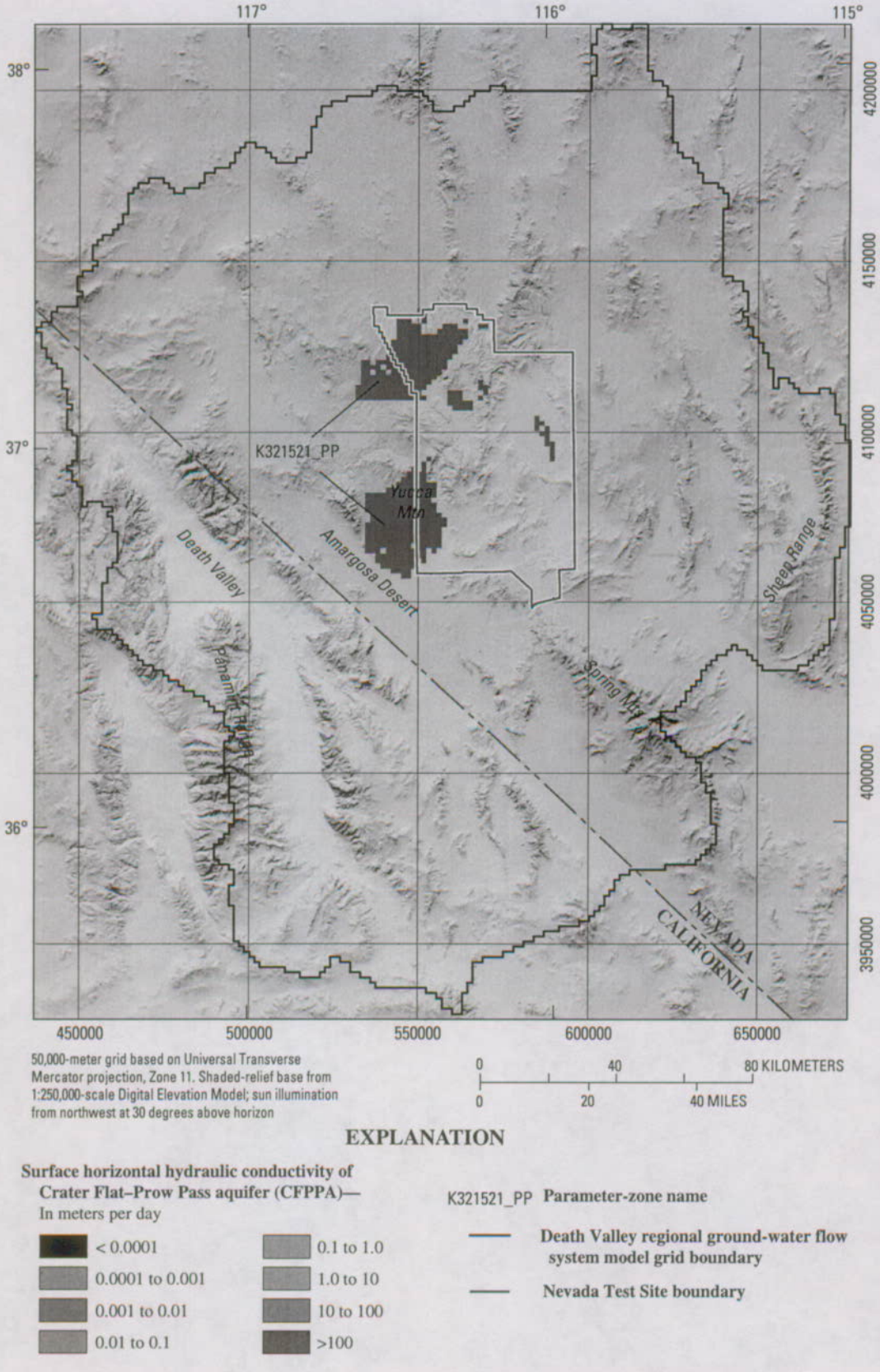

Figure F–23. Hydraulic-conductivity zone parameters, unit thickness, and extent for Crater Flat–Prow Pass aquifer unit.

Figure F–24. Hydraulic-conductivity zone parameters, unit thickness, and extent for Wahmonie volcanic-rock and younger volcanic-rock unit.

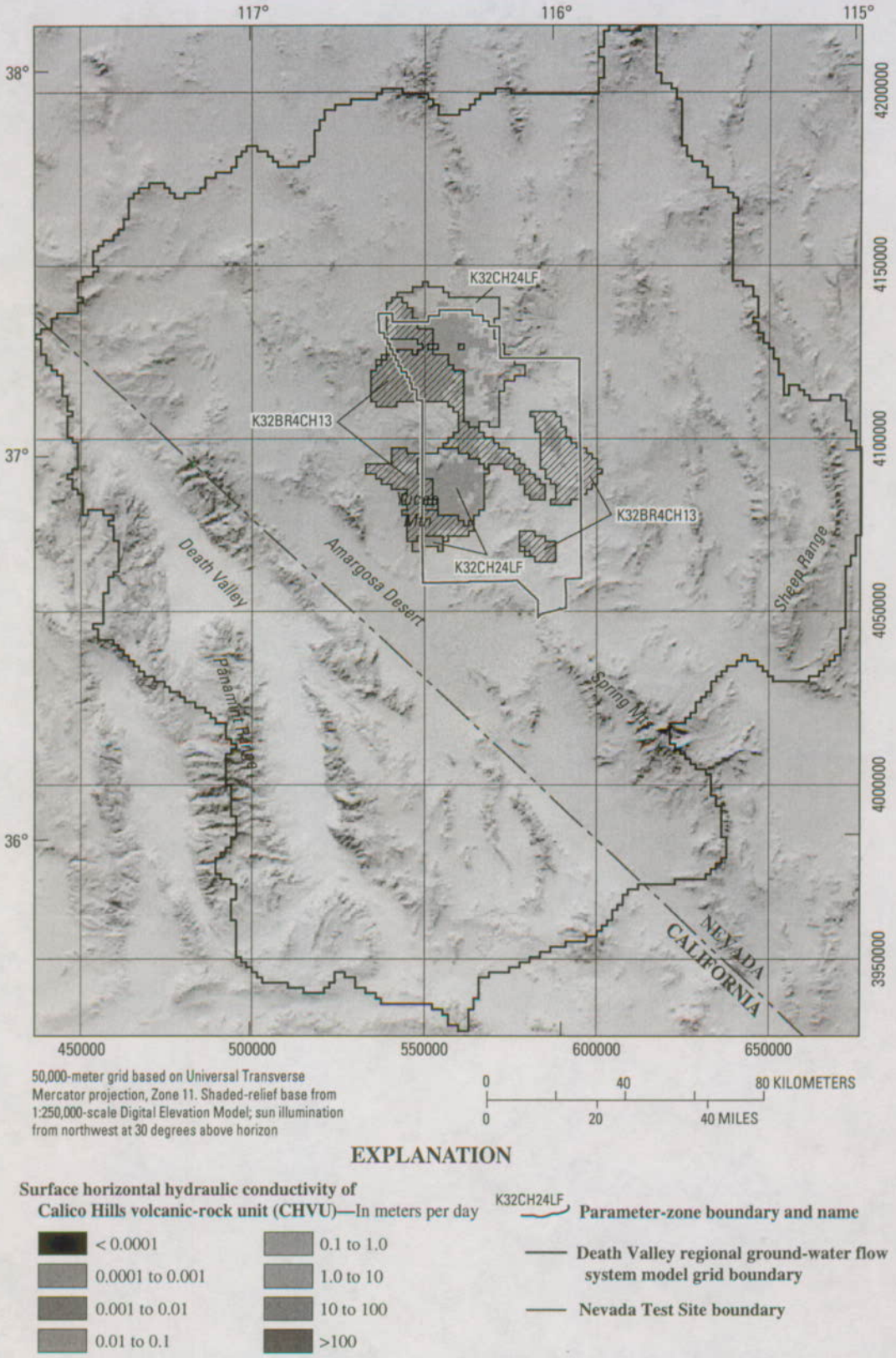

Figure F–25. Hydraulic-conductivity zone parameters, unit thickness, and extent for Calico Hills volcanic-rock unit.

Figure F–26. Hydraulic-conductivity zone parameters, unit thickness, and extent for Paintbrush volcanic-rock aquifer.

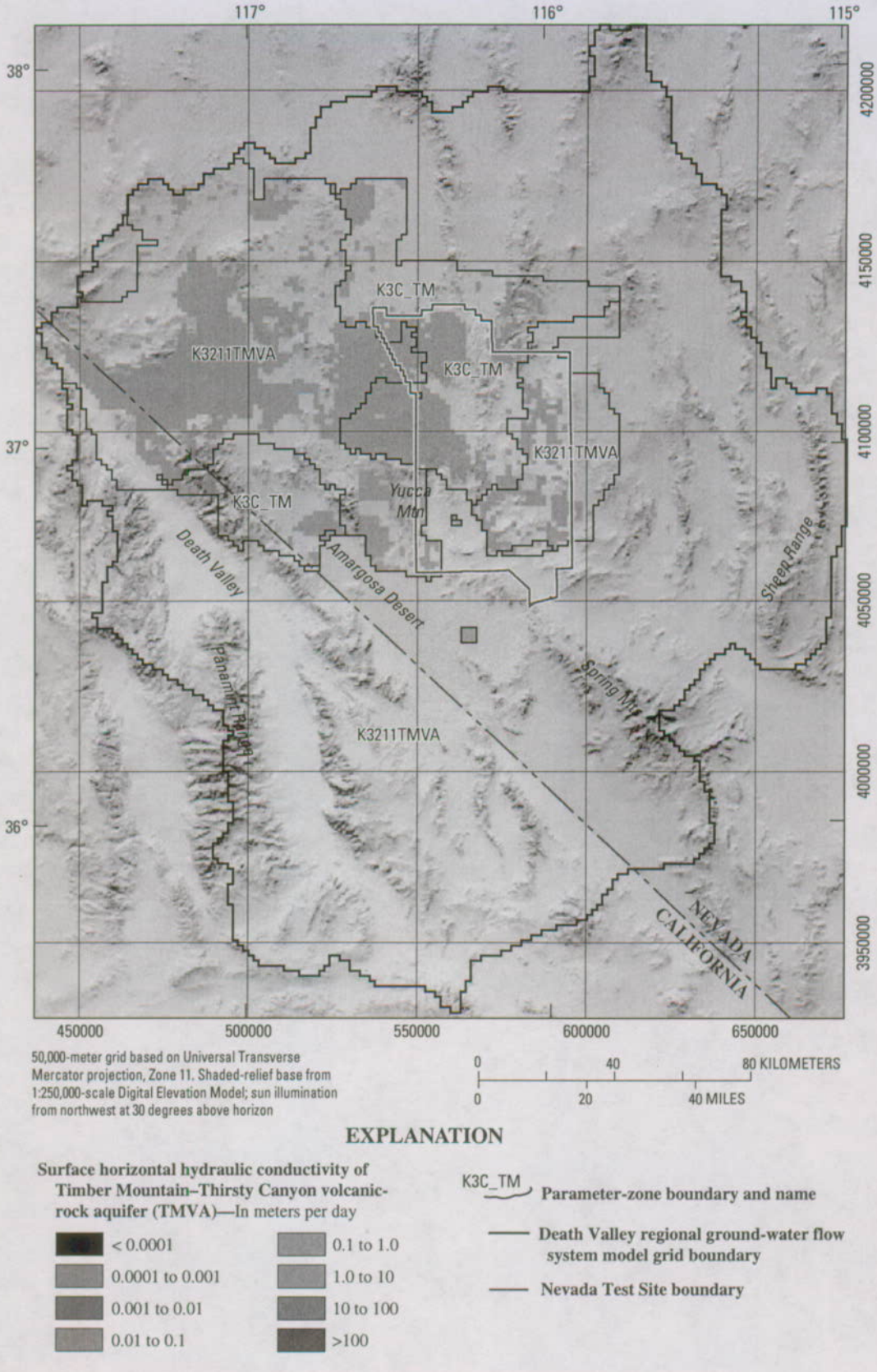

Figure F–27. Hydraulic-conductivity zone parameters, unit thickness, and extent for Thirsty Canyon–Timber Mountain volcanic-rock aquifer.

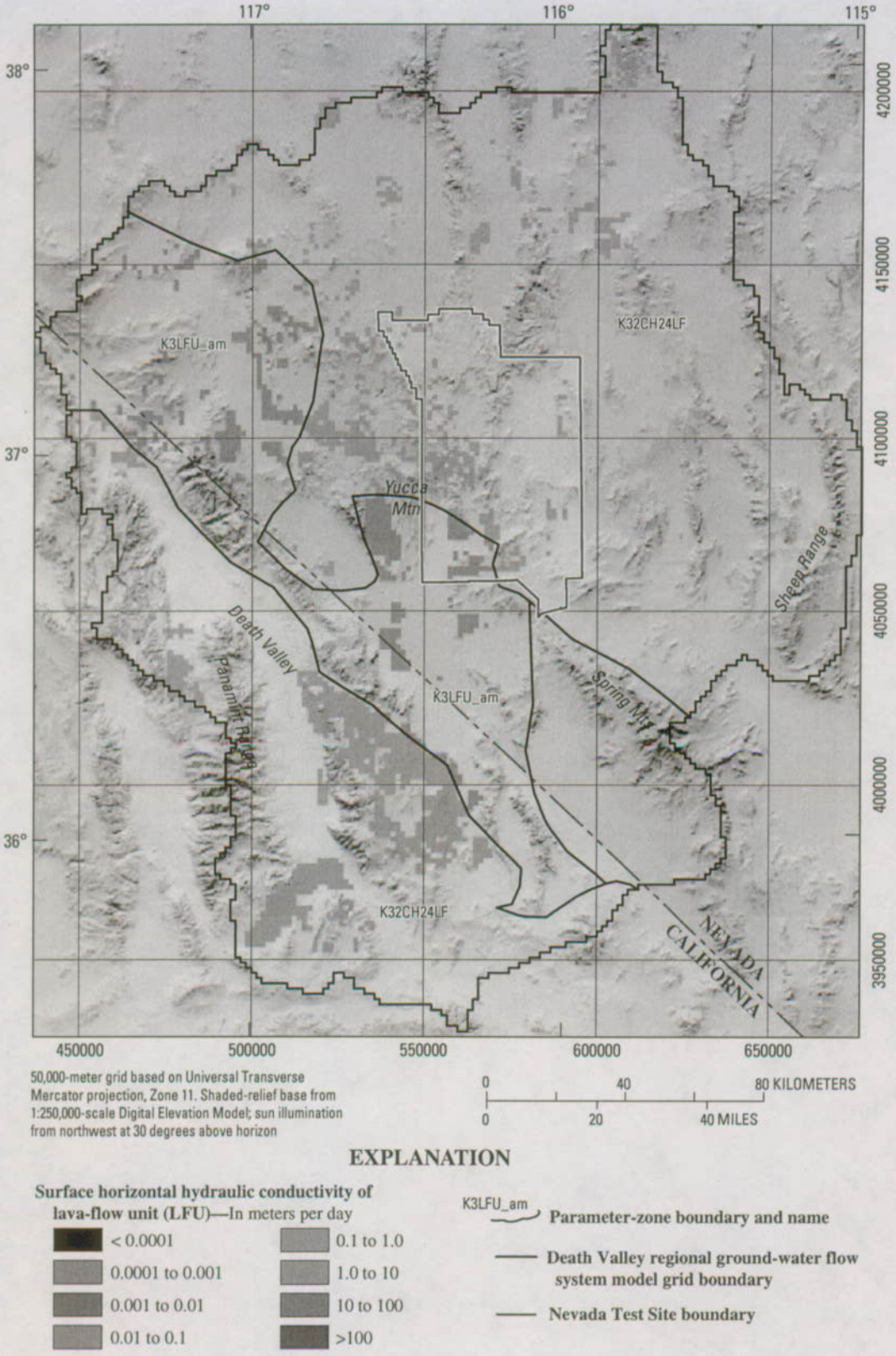

Figure F–28. Hydraulic-conductivity zone parameters, unit thickness, and extent for lava-flow unit.

Some volcanic HGUs, such as the WVU, did not have enough hydraulic information to subdivide into zones and thus were left intact and commonly combined with other HGUs. In one case, that of the PVA, the property zonations did not appear to support the hydraulic data at all. The PVA was divided on the basis of its relative location inside or outside caldera centers (fig. F–26), which likely coincides with fracture density.

Basin-Fill Units

The HGUs constituting the basin-fill units were initially grouped into one hydraulic-conductivity parameter (K4). These units were initially split into two hydraulic-conductivity parameters representing aquifers (YAA, LA, and OAA) and confining units (YACU, OACU, and upper and lower VSU (table F–11)). The upper and lower VSUs were assigned into a parameter defining units that tend to be confining units even though they can be both confining units and aquifers.

Because the upper and lower VSUs can represent both aquifers and confining units, they were split on the basis of depositional characteristics of the basins. Hydraulic-conductivity zone parameters for these basin-fill units were defined on the basis of facies (figs. F–29 and F–30). The lower VSU was initially subdivided by facies (Chapter B, this volume). During calibration, this unit was further subdivided, especially in Pahrump Valley (fig. F–29). The basin-fill deposits in Pahrump Valley likely are more carbonate-rich and possibly of different character. The playa deposits in Pahrump Valley contain large amounts of fine-grained clays typical of a dry playa. The lower VSU also was important for matching heads and discharges near Sarcobatus Flat (fig. F–29) and flow in from the constant-head boundary (Clayton and the western part of Stone Cabin–Railroad boundary segments) (fig. A2–3 in Appendix 2). As a result, the lower VSU section representing the SWNVF sediments was split into an SWNVF area and a northeast and northwest component (fig. F–29 and table F–11).

The upper VSU was zoned on the basis of the location of the YACU and OACU because these relatively low permeability, fine-grained deposits were assumed to persist through time. This resulted in parameter zones (K4UP_VSUC, K4UP_VSUP, and K42UP_VSU) with similar depositional environments (fig. F–30 and table F–11).

The upper part of the basin-fill deposits is composed of a sequence of older and younger deposits defined by grain size. The older basin-fill are composed of the OACU (fig. F–31) and the OAA (fig. F–32), whereas the younger basin-fill units are composed of the YACU (fig. F–33) and the YAA (fig. F–34). The coarse-grained deposits are represented by the YAA and OAA (and fine-grained deposits represented by the YACU and OACU. Localized limestone aquifers in the basin-fill deposits were represented by the LA, which was combined into the hydraulic-conductivity parameter representing basin-fill aquifers (K4_VF_AQ). During calibration, these units were lumped and split as necessary.

Parameter zones also were used to assess the importance of the lower and upper VSU units in controlling ground-water discharge (figs. F–29—F–30 and table F–11). The YACU and finer grained parts of the VSUs limit the flow of ground water to discharge areas and pumping centers, especially near Ash Meadows and in Pahrump Valley.

CSS values of many of the basin-fill units are much larger in the transient calibration than in the steady-state calibration. Additional parameters were created in the basin-fill units and the lower and upper VSU to discern confining units and aquifers (figs. F–29—F–34 and table F–11). Specific storage parameters and hydraulic conductivities were adjusted by examining the simulated and observed changes in both discharge and hydraulic-head observations over time.

Depth Decay of Hydraulic Conductivity

Depth decay of hydraulic conductivity was simulated using the HUF package (Anderman and Hill, 2003) (table F–12 and fig. F–35). Because of the uncertainty in depth decay of hydraulic conductivity and the great effect this can have on model calibration, the initial parameter values were inserted on the basis of previous estimates of hydraulic-conductivity decay with depth (IT Corporation, 1996, figs. 6–1—6–3). In general, depth decay was important in all of the volcanic-rock units, all of the basin-fill units, and of somewhat lesser importance in the carbonate-rock aquifer, as indicated by IT Corporation (1996). Depth decay applied to zones within the LCCU, SCU, XCU, and ICU confining units was helpful for improving the model. Initially, depth decay of hydraulic conductivity was assigned to all areas of the carbonate-rock aquifer. In some areas, depth decay reduced model fit and made calibrations less than optimal. In these areas, the rate of decrease in hydraulic conductivity with depth was reduced. Although this change is subjective, it improved model fit.

Depth decay produces some values of hydraulic-conductivity that are outside expected values. This may indicate that values of the depth-decay parameters are in error or that the decay of hydraulic conductivity with depth is not an exponential function (eq. 1). In addition, hydraulic-conductivity values become extremely small at depth for many of the units (table F–12). In reality, the hydraulic conductivity may not decrease below a certain threshold value. The flow system can be simulated adequately without this parameter. Because depth-decay of hydraulic conductivity is more important in simulating the contaminant migration than ground-water flow, transport simulations could be helpful to quantify this value.

Table F–11. Calibrated horizontal hydraulic-conductivity parameters for the basin-fill units.

[Abbreviations: LA, limestone aquifer; OAA, older alluvial aquifer; OACU, older alluvial confining unit; SCU, sedimentary-rock confining unit; VSU, volcanic- and sedimentary-rock units; YAA, younger alluvial aquifer; YACU, younger alluvial confining unit; YVU, younger volcanic-rock unit]

Parameter name	Description	Minimum – maximum hydraulic conductivity (meters per day) from Belcher and others (2001)	Composite scaled sensitivity	Hydraulic conductivity at land surface (meters per day)	Coefficient of variation[1]	Average depth (meters)	Hydraulic conductivity at average depth (meters per day)
K4_VF_AQ	(1) Basin-fill aquifers (coarser grained) (LA, YAA) (2) SCU	[1]6×10^{-5}–130	0.342	5.972×10^{-1}	0.5	10	0.4467
K4_VF_OAA	OAA	[1]6×10^{-5}–130	0.0349	5.920×10^{-2}	0.5	39	0.000197
K4_VF_CU	Basin-fill confining units (finer grained) (YACU, OACU)	[2]0.003–34	0.547	1.580	0.5	43	0.4655
K4UP_VSUC	Upper VSU (below YACU or OACU); finer grained	[4]0.00004–6	0.578	9.397×10^{-1}	0.13	164	0.18256
K4UP_VSUP	Upper VSU (below YACU) in Pahrump Valley; finer grained	[4]0.00004–6	0.253	2.077×10^{1}	0.5	160	4.169
K42UP_VSU	(1) Upper VSU ; coarser grained (anywhere not below YACU or OACU) (2) YVU	[4]0.00004–6	0.572	7.057	0.5	159	1.438
K42222_VSU	Lower VSU; mixture of fluvial and lacustrine sediments (LCCU-derived, nonvolcanic, and finer grained sediments); small area of Amargosa Desert added during calibration	[4]0.00004–6	0.130	5.000×10^{-3}	0.01	401	0.004476
K422LNEVSU	Lower VSU; SWNVF sediments – northeast	[4]0.00004–6	0.311	1.847×10^{-1}	0.0001	721	0.15135
K422LNWVSU	Lower VSU; SWNVF sediments – northwest	[4]0.00004–6	0.770	1.917×10^{-1}	0.04	1,144	0.1397
K4222S_VSU	Lower VSU; SWNVF sediments	[4]0.00004–6	0.927	1.264×10^{-1}	0.06	1,296	0.088357
K422DV_VSU	Lower VSU; coarse syntectonic sediments (nonvolcanic) in Death Valley	[4]0.00004–6	0.399	8.804×10^{-3}	0.02	608	0.007442
K422GW_VSU	Lower VSU; Greenwater volcanic sediments	[4]0.00004–6	1.078	1.524×10^{-2}	0.003	572	0.013008
K4222P_VSU	Lower VSU; fluvial and lacustrine sediments with few volcanic units in Pahrump Valley	[4]0.00004–6	0.0866	5.812×10^{-1}	0.5	601	0.49227
K422GV_VSU	Lower VSU; mixture of sediments with diverse lithologies in the Amargosa Desert area	[4]0.00004–6	0.325	4.630×10^{-2}	0.02	689	0.038276

[1]Values were log transformed.

[2]Range listed is for the alluvial aquifer (AA), which is the combined YAA and OAA and includes the range of the SCU.

[3]Range listed is for the alluvial confining unit (ACU), which is the combined YACU and OACU.

[4]Range listed is for the combined YVU/VSU.

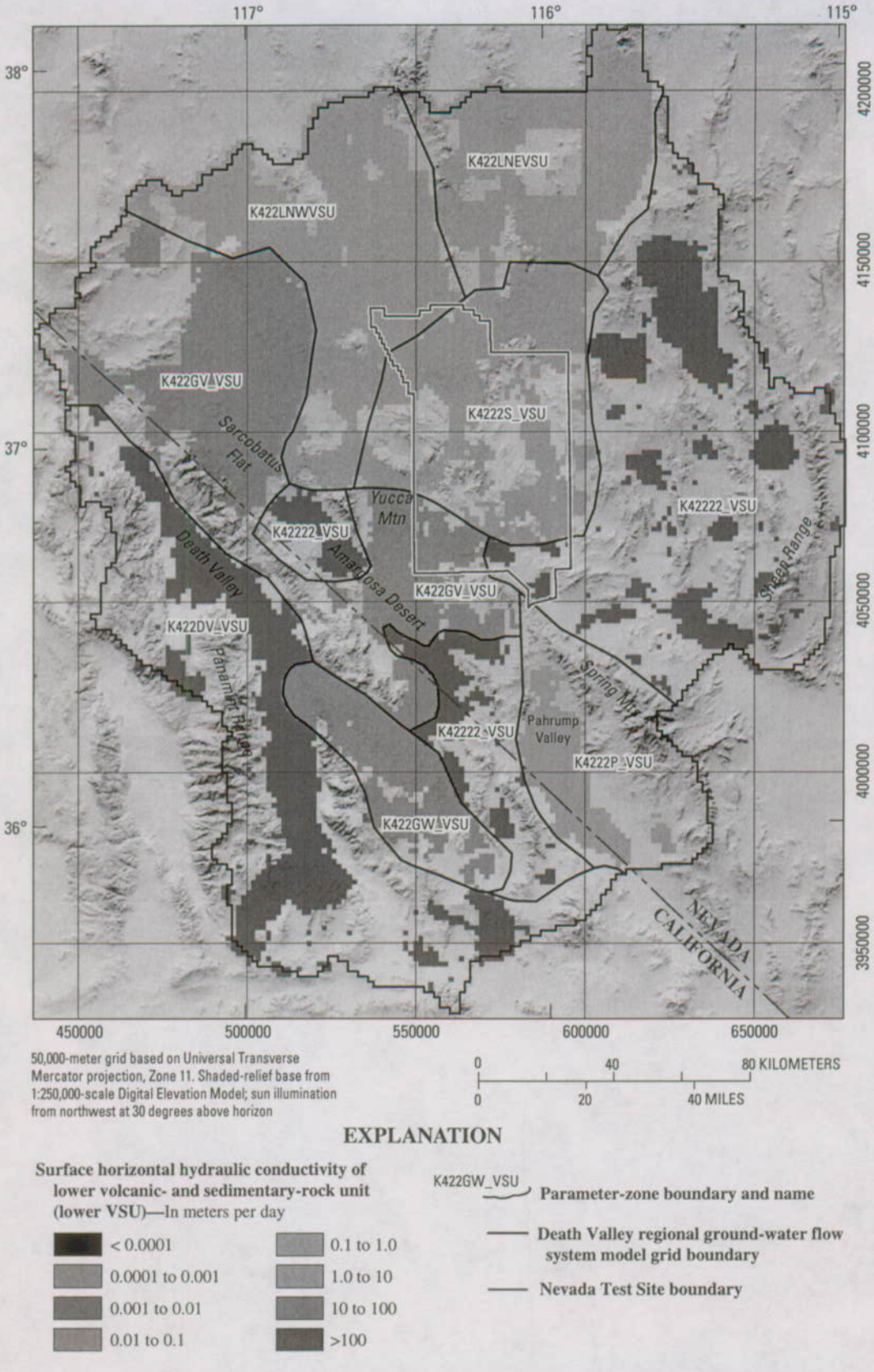

Figure F–29. Hydraulic-conductivity zone parameters, unit thickness, and extent for lower volcanic- and sedimentary-rock unit.

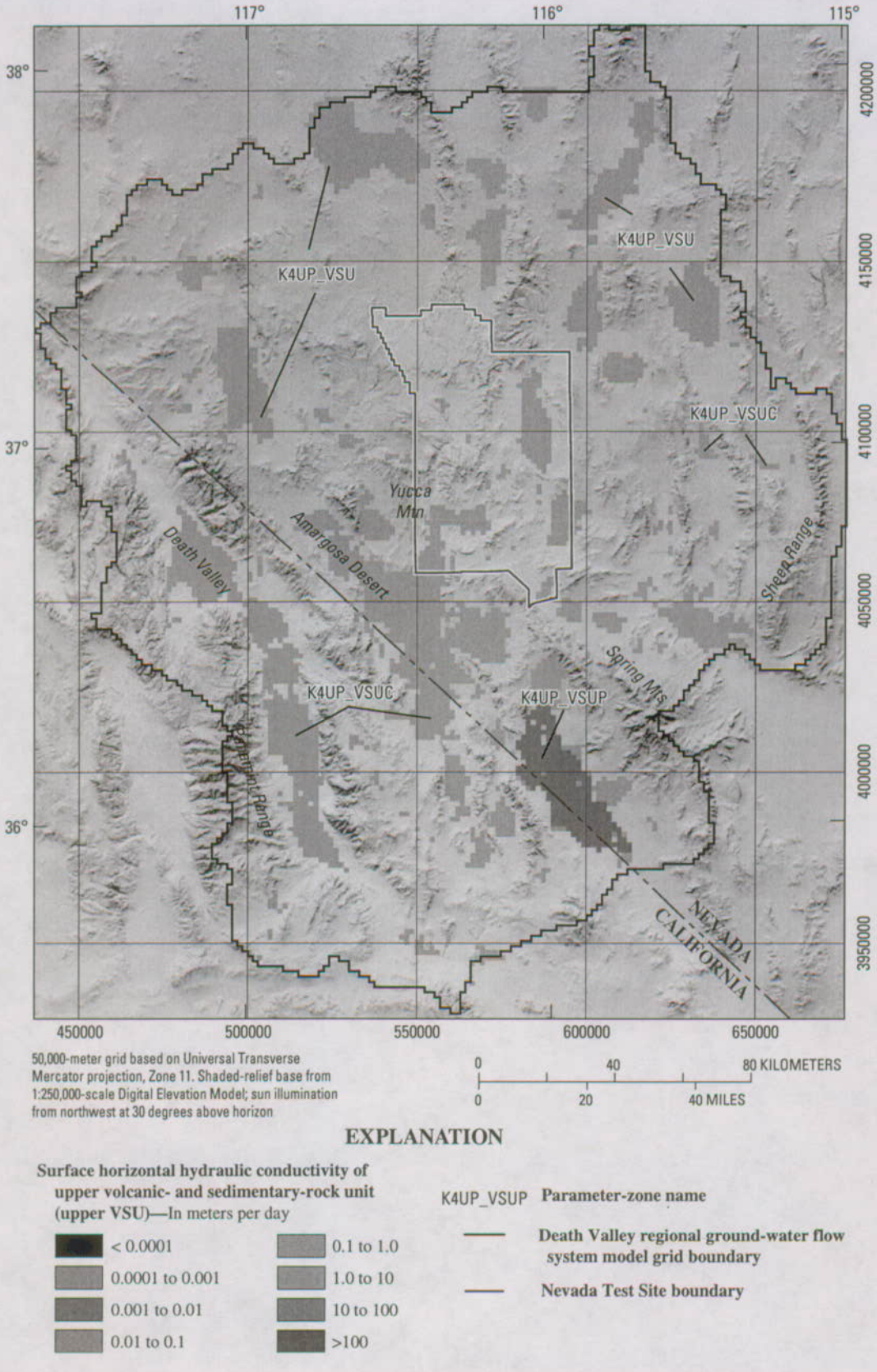

Figure F–30. Hydraulic-conductivity zone parameters, unit thickness, and extent for upper volcanic- and sedimentary-rock unit.

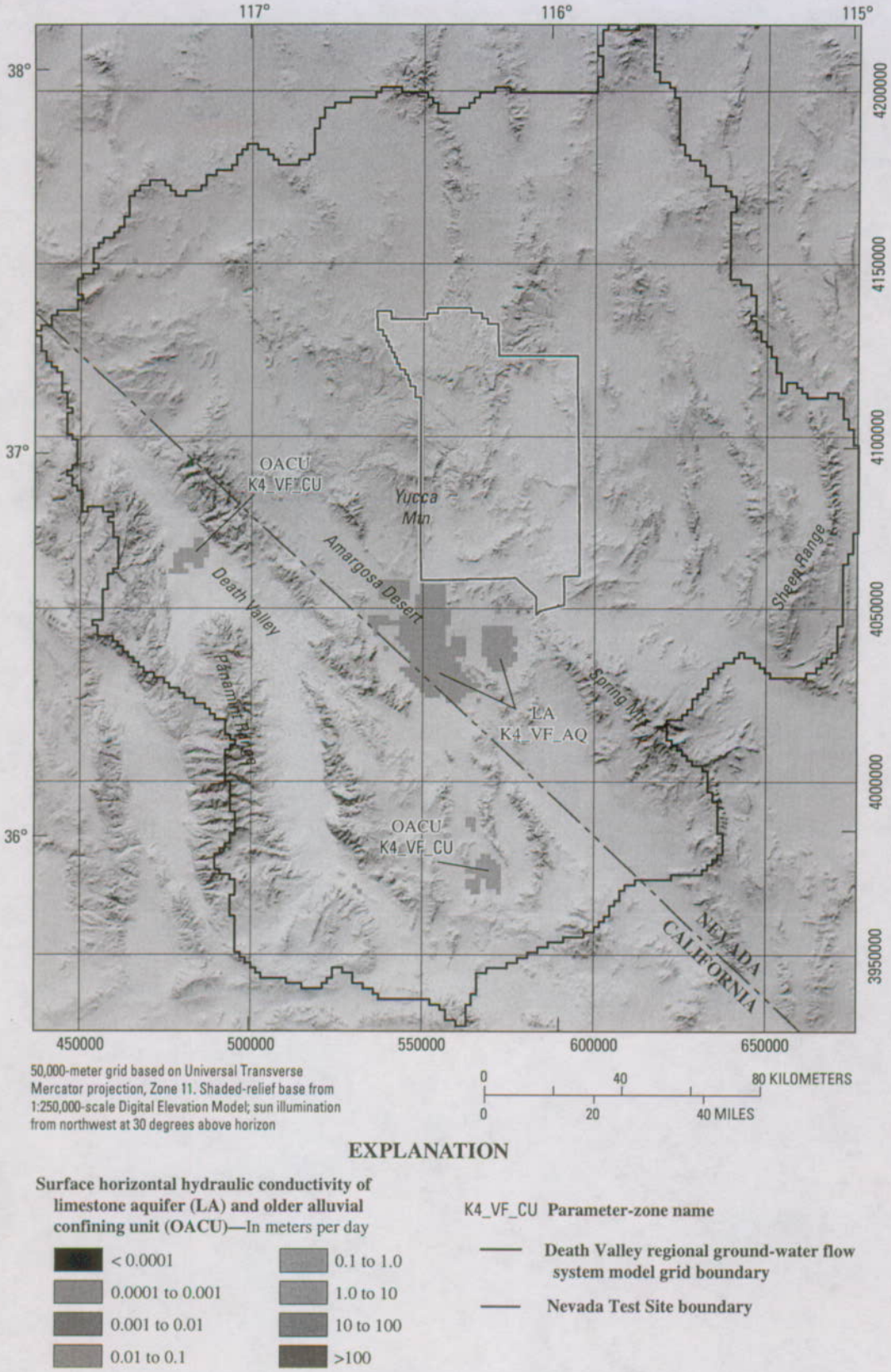

Figure F–31. Hydraulic-conductivity zone parameters, unit thickness, and extent for limestone aquifer and older alluvial confining units.

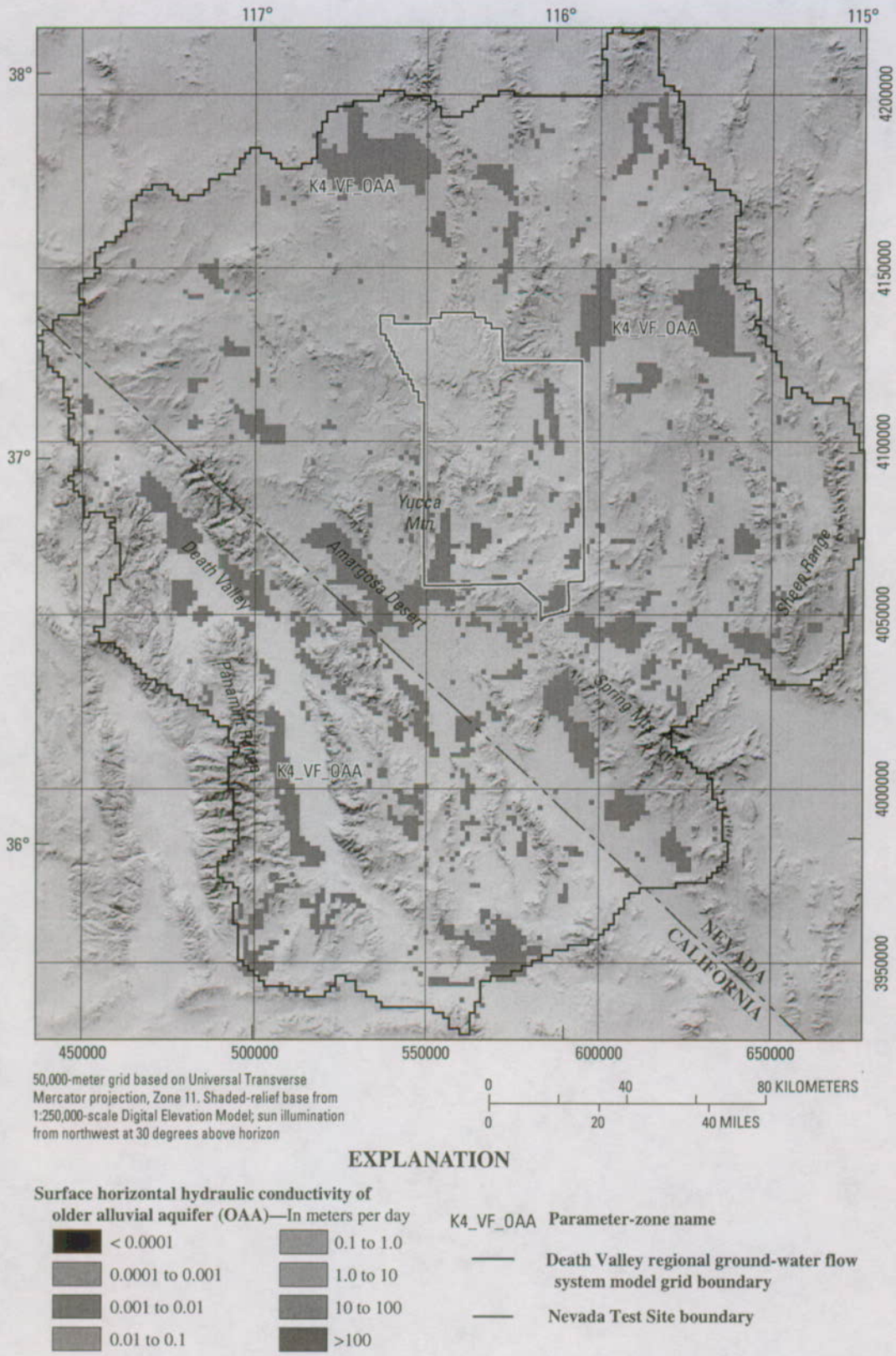

Figure F–32. Hydraulic-conductivity zone parameters, unit thickness, and extent for older alluvial aquifer.

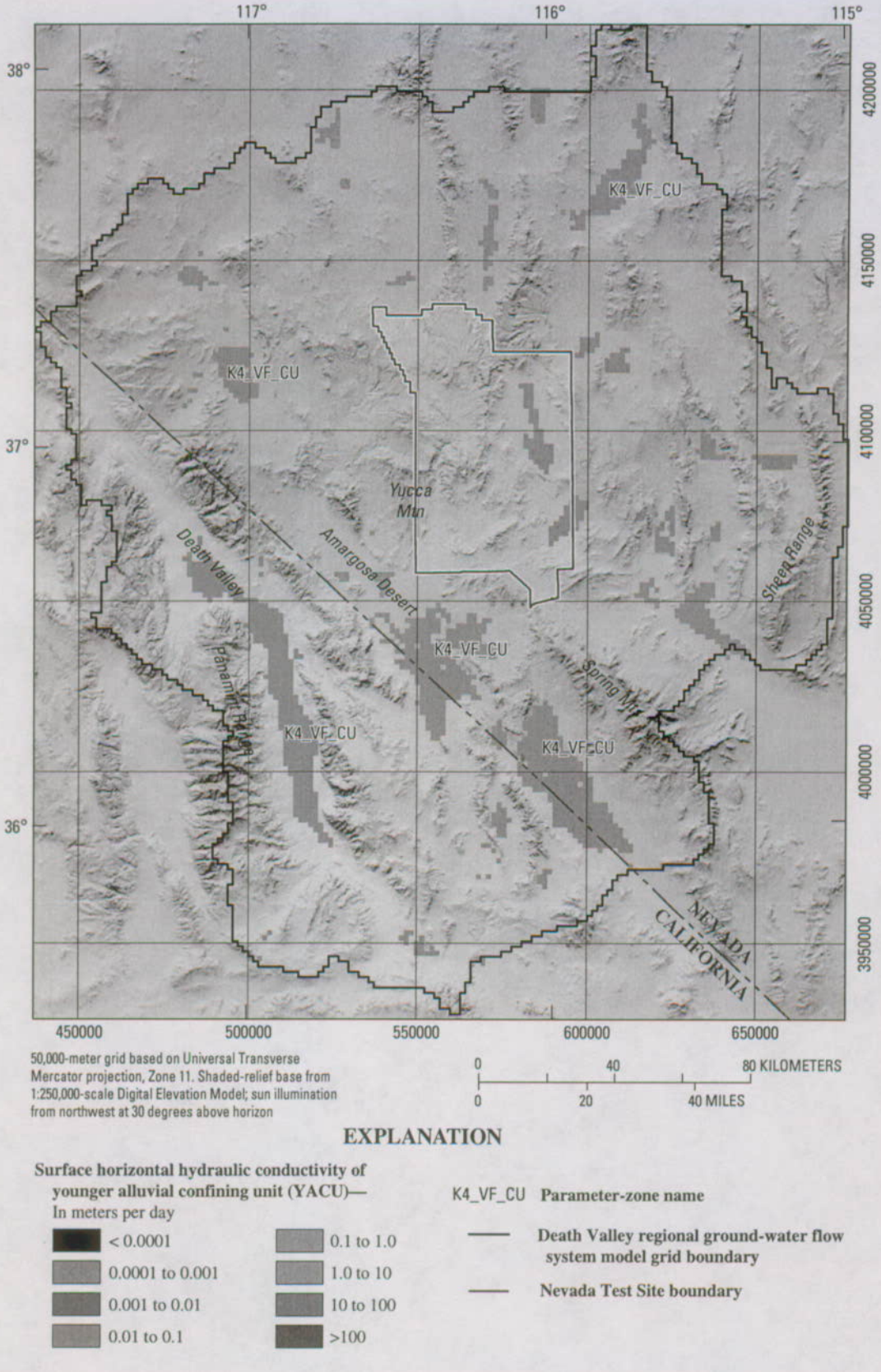

Figure F–33. Hydraulic-conductivity zone parameters, unit thickness, and extent for younger alluvial confining unit.

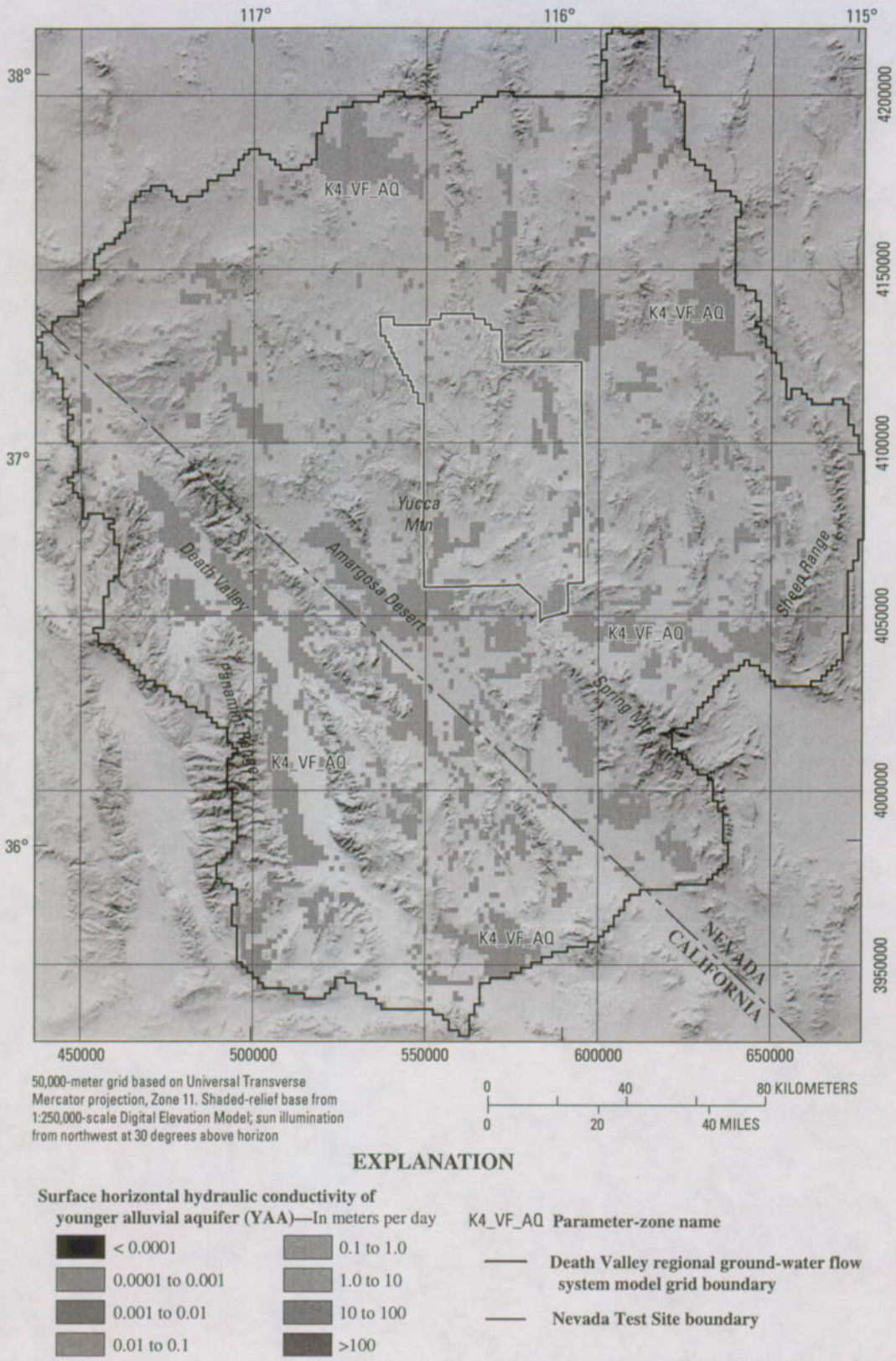

Figure F–34. Hydraulic-conductivity zone parameters, unit thickness, and extent for younger alluvial aquifer unit.

Table F–12. Calibrated depth-decay parameters.

[Abbreviations: LCA, lower carbonate-rock aquifer; LCCU, lower clastic-rock confining unit; NA, not applicable; TSDVS, Tertiary sediments, Death Valley section; UCA, upper carbonate-rock aquifer; UCCU, upper clastic-rock confining unit; VSU, volcanic- and sedimentary-rock unit; YAA, younger alluvial aquifer; YACU, younger alluvial confining unit]

Parameter name	Description	Initial depth-decay parameter value (IT Corp., 1996b)	Depth-decay parameter value (percentage of surface hydraulic conductivity at 1,000 meters)	Composite scaled sensitivity	Coefficient of variation[1]
KDEP_LCA	LCA (except as noted in KDP_LCANO, KDP_LCAT1 and KDEP_NO)	[2]0.00102	0.00010 (79.4%)	1.7	NA
KDP_LCANO	LCA (K243GV_LCA, K24ISM_LCA, K243PP_LCA, and K2_DV_LCA)	[2]0.00102	0.00002894 (93.6%)	0.4	NA
KDP_LCAT1	(1) LCA_T1 (2) LCA (K2421FLCA)	[2]0.00102	0.0015 (3.2%)	3.1	NA
KDP_VOL	Volcanic rocks	[3]0.00256	0.00248 (0.33%)	7.3	NA
KDEP_UCCU	UCCU and UCA	[4]0.0015	0.0015 (3.2%)	1.0	NA
KDEP_VFVL	Basin fill (YAA, YACU, OAA, OACU, and LA)	[5]0.00563	0.0123 (<0.005%)	0.2	0.5
KDEP_VSUU	Upper VSU	[6]0.004	0.0043457 (0.005%)	1.0	0.002
KDEP_VSUL	Lower VSU	[6]0.004	0.00012 (75.9%)	0.6	NA
KDEP_NO	(1) LCCU_T1 (2) LCCU (except as noted in KDEP_XL) (3) LCA (K2rr_LCA) (4) LFU (5) SCU (6) XCU (K11CXILCU) (7) ICU	[7]0.0012	0.0000001 (99.98%)	7.9×10^{-4}	NA
KDEP_XL	(1) XCU (2) LCCU (K1LCCU_XCU)	[8]0.0015	0.00061972 (24%)	1.7	NA

[1]Values were not log transformed.

[2]Mean exponential depth-decay coefficient for carbonate-rock aquifers.

[3]Mean exponential depth-decay coefficient for volcanic-rock aquifers.

[4]Exponential depth-decay coefficient for the UCCU.

[5]Mean exponential depth-decay coefficient for alluvial (basin-fill) aquifers.

[6]Exponential depth-decay coefficient for TSDVS.

[7]Exponential depth-decay coefficient for LCCU.

[8]Exponential depth-decay coefficient for intrusive rocks.

Vertical Anisotropy

Vertical anisotropy parameters were initially defined for the four major rock types and generally had small *CSS* values during steady-state simulations (table F–13). Pumping stresses the upper part of the system and tends to force water to flow more vertically than under a natural hydraulic gradient. This resulted in greater sensitivity to vertical anisotropy parameters during transient simulations. The basin-fill units, in which much of the pumpage occurs, were most sensitive (table F–13). These units also are most likely to have stratification that would tend to decrease the vertical conductivity relative to the horizontal (anisotropy ratios greater than 1).

Storage Properties

During calibration, conceptual models simulating the top of the DVRFS model as confined or unconfined model layers were evaluated. Confined conditions were simulated with the capability of the HUF package (Anderman and Hill, 2003). The unconfined simulations were numerically unstable and ultimately were abandoned. For most confined simulations (including the final calibration), the top of the model was defined using simulated hydraulic heads from the previous model run. Because the cones of depression caused by pumpage in this system are fairly modest, simulated results should be very close to results obtained with unconfined simulations.

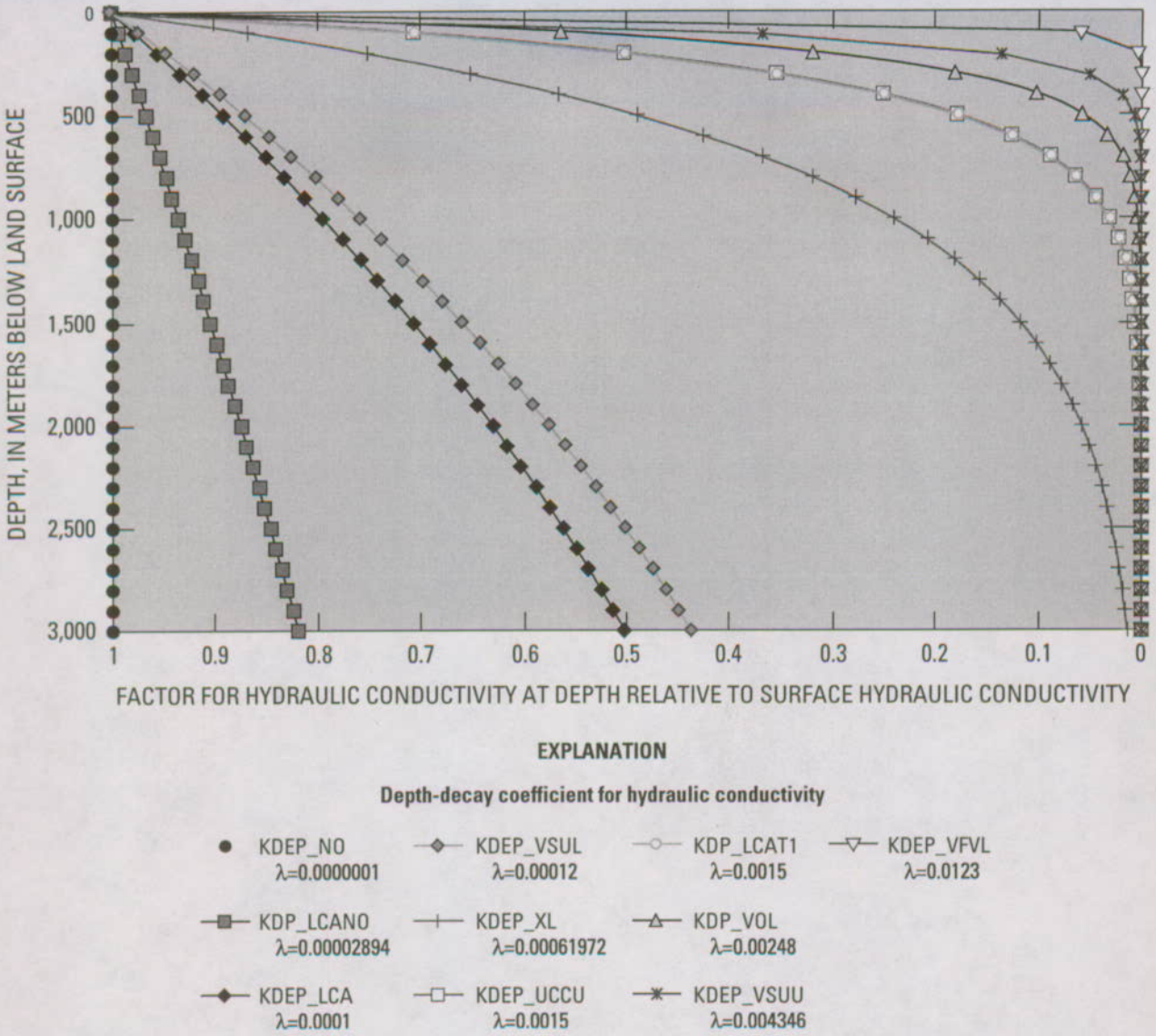

Figure F–35. Hydraulic conductivity values decreasing with depth relative to the surface hydraulic conductivity. The value of each depth-decay parameter is listed for each parameter.

Specific-storage values were determined from literature for the various HGUs in the model domain (table F–14). Specific-storage (Ss) values were used for model layers 2 through 16, and a specific yield (Sy) value was used for layer 1. Storativity values estimated from aquifer tests (Anderson and Woessner, 1992; Belcher and others, 2001) and other modeling studies in the region (Thomas and others, 1996; Schaeffer and Harrill, 1995) are similar to the values used in the DVRFS model (table F–14).

Specifying unique storage property values for each HGU was not necessary. Only those units strongly affected by pumping (predominantly the basin-fill units) were categorized by more than one storage property value. Parameter estimation methods did not provide reasonable storage property values; those values were always unreasonably high. As a result, values of specific storage and specific yield consistent with the literature (Thomas and others, 1989; Anderson and Woessner, 1992; Schaeffer and Harrill, 1995; Belcher and others, 2001) were specified (set by the user) and the hydraulic conductivities in the basin-fill units, which were most affected by pumping, were re-estimated. Model fit was much better with relatively high values of specific yield. Hence, these values were specified near the upper end of the reasonable range. Errors in simulated heads and discharges associated with errors in storage property values likely are small and were not quantified.

Hydrogeologic Structures

Many of the HFB parameters (fig. F–5) had little effect on the simulation of heads and discharges and were removed as barriers from the flow model. In the final calibration, only nine barriers had a significant effect on heads and discharges

Table F–13. Calibrated vertical anisotropy parameters.

[Abbreviations: ICU, intrusive-rock confining unit; LCA, lower carbonate-rock aquifer; LCA_T1, thrusted lower carbonate-rock aquifer; LCCU, lower clastic-rock confining unit; LCCU_T1, thrusted lower clastic-rock confining unit; NA, not applicable; OAA, older alluvial aquifer; OACU, older alluvial confining unit; UCCU, upper clastic-rock confining unit; XCU, crystalline-rock confining unit; YAA, younger alluvial aquifer; YACU, younger alluvial confining unit]

Parameter name	Description	Vertical anisotropy value[1]	Composite scaled sensitivity	Coefficient of variation[2]
K1_VANI	Confining units (XCU, ICU, UCCU, LCCU, and LCCU_T1)	1.267	0.132	0.5
K2CARBVANI	UCA, LCA, and LCA_T1	1.00	0.125	0.5
K3_VOLVANI	Volcanic-rock units	1.00	0.273	0.47
K4_VFVANIA	Basin-fill aquifers (YAA, OAA, coarser grained parts of upper VSU)	5,000.0	0.119	NA
K4_VFVANIC	Basin-fill confining units (YACU, OACU, finer grained parts of upper VSU)	5,000.0	0.215	NA
K4_VFVANVL	Lower VSU	2.184	0.233	0.5

[1]Ratio of horizontal to vertical (values less than 1 indicate higher vertical than horizontal hydraulic conductivity).

[2]Values were log transformed.

Table F–14. Calibrated storage property values.

[Specific-yield values were used for layer 1, specific-storage values were used for layers 2–16. Values in parentheses for comparison with storage-property values. Abbreviations: ICU, intrusive-rock confining unit; LCCU, lower clastic-rock confining unit; LCCU_T1, thrusted lower clastic-rock confining unit; OAA, older alluvial aquifer; OACU, older alluvial confining unit; UCCU, upper clastic-rock confining unit; XCU, crystalline-rock confining unit; YAA, younger alluvial aquifer; YACU, younger alluvial confining unit]

Parameter name	Description	Range of storage properties (specific storage m^{-1})	Composite scaled sensitivity	Storage parameter value
STOR_12	Confining units (XCU, ICU, UCCU, LCCU, LCCU_T1); Carbonate-rock aquifers (LCA, LCA_T1, UCA)	[1]1.5×10^{-8} – [2]6.3×10^{-2}	16,127.0	7.0×10^{-8}
STOR_34	Volcanic-rock units; Lower VSU; Basin-fill aquifers (YAA, OAA, LA, upper VSU)	[3]9.7×10^{-7} – [4]2×10^{-2}	5,598.5	1.0×10^{-5}
STOR_4VUP	Upper VSU - fine grained, Pahrump Valley	[3]4.7×10^{-7} – [2]4×10^{-2}	424.9	7.5×10^{-5}
STOR_4C	Basin-fill confining units (YACU, OACU)	[3]4.7×10^{-7} – [2]4×10^{-2}	50.6	5.0×10^{-5}
SY_OTHER	Specific yield for layer 1 in basin-fill units outside the Pahrump Valley (except for upper and lower VSU)	[1,2,3,4]0.001 – 0.47	9.5	1.9×10^{-1}
SY_PAH	Specific yield for layer 1 in basin-fill units in the Pahrump Valley	[1,2,3,4]0.001 – 0.47	13.1	2.0×10^{-1}
SY_PUMP	Specific yield for layer 1 in VSU (upper and lower) outside the Pahrump Valley	[1,2,3,4]0.001 – 0.47	8.7	1.9×10^{-1}

[1]Schaeffer and Harrill, 1995.

[2]Belcher and others, 2001.

[3]Thomas and others, 1996.

[4]Anderson and Woessner, 1992.

in that they supported the hydraulic gradients (table F–15 and fig. F–5). In particular, the B_LVVSZ_IS parameter (representing part of the LVVSZ) and the B_SOLTARIO parameter (representing the Solitario Canyon fault) have been well documented as to their potential effect on heads in the model domain and had a significant effect on the simulated heads. In most cases, the other potential barriers were found to be unimportant or were adequately represented by the juxtaposition of HGUs in the HFM (Chapter E, this volume).

Recharge

Recharge in the DVRFS model was initially defined using one parameter to vary the net infiltration (Hevesi and others, 2003) throughout the entire model domain by a constant factor (fig. F–6). The *CSS* value for this parameter during initial model runs was high and generally within the top three most sensitive parameters, indicating that adequate observations existed to describe recharge with additional parameters. Early model runs tended to overestimate net recharge, as was

Table F–15. Calibrated hydraulic characteristic parameters for hydrogeologic structures defined as horizontal-flow barriers.

[Abbreviations: NA, not applicable]

Parameter name	Description	Hydraulic characteristic parameter value (meters per day per meter)	Composite scaled sensitivity	Coefficient of variation[1]
B_HWY95	Highway 95 fault	2.95×10^{-4}	0.046	0.09
B_DVFC_FCR	Death Valley fault zone–Furnace Creek fault zone	1.00×10^{-7}	0.008	0.03
B_LVVSZ_1	Las Vegas Valley shear zone	9.00×10^{-4}	0.005	NA
B_LVVSZ_I2	Las Vegas Valley shear zone	4.19×10^{-8}	0.135	NA
B_PAHRUMP	Pahrump Valley part of Pahrump-Stewart Valley fault zone	5.52×10^{-7}	0.267	0.5
B_LVVSZ_IS	Unnamed splay of the Las Vegas Valley shear zone near Indian Springs	1.1×10^{-8}	0.046	NA
B_DV_N	Northern Death Valley-Furnace Creek fault	2.40×10^{-7}	0.247	NA
B_SOLTARIO	Solitario Canyon fault	4.45×10^{-5}	0.214	NA
B_TC_LINE	Thirsty Canyon lineament	1.00×10^{-7}	0.008	NA

[1]Values were log transformed.

evident from comparing the infiltration rates to the ET and spring-flow discharge observations. A recharge zone multiplication array adjusted the net infiltration model (Hevesi and others, 2003) to fit the discharge observations.

The net-infiltration distribution accounted only for surficial characteristics of the system and not the hydraulic conductivity of the rocks at the water table (Hevesi and others, 2003). Thus, in some areas large recharge rates into rocks with low hydraulic conductivity produced unrealistic simulated hydraulic heads. In reality, the recharge likely was redistributed in the process of percolation. To account for this dynamic, the distribution of recharge was modified by essentially moving high recharge rates from areas where the rocks at the water table were relatively low in permeability to downgradient areas where the rocks at the water table were relatively permeable. This was done by combining net-infiltration rates and the relative permeability of the rocks in the upper five model layers to produce the zones of recharge distribution (fig. F–36). The resulting recharge parameters were multipliers for net infiltration (table F–16).

The parameter zones were created by classifying the top five model layers as either consisting of predominantly (more than 50 percent) relatively higher permeability aquifer material (basin-fill, volcanic-rock, and carbonate-rock aquifers) or relatively lower permeability rocks not identified as aquifers. Cells with aquifer material represent areas where greater permeability would allow rapid infiltration. Because cells with aquifer materials receive most of the infiltration, these cells were further defined by rock type. The logarithm of the infiltration rate was classified into five zones representing areas with no infiltration to those with high infiltration rates. These two classifications (permeabiltiy based on rock type and infiltration rates) were combined into the parameters described in table F–16. Some of the parameters were insensitive, so they were combined with parameters having similar recharge multiplier values.

Separate parameters defined for recharge on the high-altitude, carbonate-rock aquifer material contributed the largest volumes of water to the ground-water system (parameters RCH_2 and RCH_8). High recharge rates on the Spring Mountains were necessary to properly simulate discharge in Pahrump Valley, Shoshone and Tecopa basins, Amargosa Desert, and Indian Springs (figs. F–6 and F–36). Parameter RCH_2 was used for recharge on the carbonate-rock aquifer, generally in the Spring Mountains and southern part of the Sheep Range (simulated mean recharge of about 70 millimeters per year [mm/yr]). Parameter RCH_8 was used in the eastern and central western (simulated mean recharge of about 38 mm/yr) part of the model domain. In the final calibration, recharge on the Spring Mountains was 76 percent of the value of net infiltration, whereas recharge on the northeastern and central western parts of the model domain was about 100 percent of the estimate of net infiltration (table F–16). The magnitude of the reduction of net infiltration seems reasonable considering that the composition of the carbonate-rock aquifer material is quite variable between these two areas of the model domain, and the extremely high estimate of net infiltration in the Spring Mountains could not be supported by rocks in the area.

During calibration, a ninth recharge zone was added (RCH_9) where infiltration rates exceeded the hydraulic-conductivity value of the underlying rocks and water ponded more than 20 m above land surface. The recharge rate was assumed to be negligible in these areas, and the recharge parameters (multipliers) in adjacent zones were increased.

In general, the estimated recharge was distributed similarly to the net-infiltration rate of Hevesi and others (2003). For the entire model domain, 92 percent of the net infiltration estimated by Hevesi and others (2003) or 303,415 cubic meters per day was simulated as recharge.

Figure F–36. Recharge zone multiplication array representing infiltration rates and relative permeability in upper five model layers.

Table F–16. Calibrated recharge parameters used as multipliers for infiltration rates defined for the recharge zones.

[NA, not applicable]

Recharge zone number	Relative permeability	Relative infiltration rate	Description	Recharge parameter name	Recharge parameter value[1]	Composite-scaled sensitivity	Coefficient of variation[2]
1	NA	None	No infiltration	NA	NA	NA	NA
2	High	High	High infiltration and high permeability (generally carbonate rocks in the Spring Mountains and southern part of the Sheep Range)	RCH_2	0.76	3.22	0.10
3	Low	High to moderate	High to moderate infiltration and low permeability (generally volcanic and(or) clastic rocks)	RCH_35	1.12	3.46	0.13
5	Low	Low	Low infiltration and low permeability (generally volcanic and(or) clastic rocks)	RCH_35	1.12	3.46	0.13
4	High	Moderate to low	Moderate to low infiltration and high permeability on various rock types	RCH_467	1.00	0.115	0.5
6	High	Moderate to low	Moderate to low infiltration and high permeability with basin-fill aquifers present in the upper five layers	RCH_467	1.00	0.115	0.5
7	High	Moderate to low	Moderate to low infiltration and high permeability with volcanic rocks present in the upper five layers	RCH_467	1.00	0.115	0.5
8	High	Moderate to low	Moderate to low infiltration and high permeability with carbonate rocks present in the upper five layers (eastern and central western part of the model domain)	RCH_8	1.00	0.0648	0.5
9	NA	NA	Cells where recharge exceeded hydraulic conductivity	RCH_9	0.000001	0.28×10^{-8}	NA

[1]The net-infiltration array values (fig. C–8) are multiplied by this value to calculate the simulated recharge (fig. F–6).

[2]Values were log transformed.

Ground-Water Discharge

The discharges through ET and spring flow were treated as observations in the flow model, and the conductances of the drain cells were estimated. Initially, the drain cells were divided into five types with the following parameter names (table F–17): (1) DEEP_DRN, warm-water discharge indicates rapid flow from depth and the drain cell is located at the shallowest occurrence of the LCA; (2) UPPER_DRN, flow is through surficial materials that are coarser than playa materials (YAA and OAA); (3) UP_PLY_DRN, flow is through surficial fine-grained playa materials (YACU and OACU); (4) UP_DV_DRN, springs in Death Valley that have substantial salt concentrations; and (5) UP_PAH_DRN, all discharge areas in Pahrump Valley where estimates of discharge over time are available. During calibration, drain conductance parameters were added for the northern part of Death Valley (UP_DVN_DRN) and the Furnace Creek area (FRNCR_DRN).

Hydraulic-Head and Discharge Observations

During calibration, 4,899 observations of hydraulic head and 49 of ground-water discharge and their corresponding weights were evaluated to assess whether the weighting scheme appropriately contributed to model fit. During calibration, weights on five hydraulic-head observations were decreased because of high sensitivity values. Weights on head-change observations in these same locations with particularly large weights also were decreased.

During calibration, the effect of data clustering was examined. The possibility that clustering contributed to the poor fit in areas where observations were limited was tested by grossly increasing the weights on some of the sparsely distributed observations during selected model runs. Because increased weights never significantly improved model fit at these data-sparse locations, calibration difficulties were attributed to some aspect of the model framework or hydrologic conceptualization. The problem then was investigated by examining the hydrologic conceptualization, indicating that

Table F–17. Calibrated drain conductance parameters.

[m/d/m, meter per day per meter; NA, not applicable]

Parameter	Description	Composite scaled sensitivity	Parameter value[1] (m/d/m)	Coefficient of variation[2]
DEEP_DRN	Deep, warm-water springs	1.86	45.6	0.50
UPPER_DRN	Springs in coarse-grained basin-fill deposits	0.70	107.8	0.50
UP_PLY_DRN	Springs in playa deposits	1.78	83.9	0.50
UP_DV_DRN	Death Valley springs with high salt concentrations	0.00855	10,000.0	NA
UP_PAH_DRN	Springs in Pahrump Valley	1.66	195.3	0.50
UP_DVN_DRN	Springs in the northern part of Death Valley	0.145	52.8	0.50
FRNCR_DRN	Spring in the Furnace Creek area	0.00149	10,000.0	NA

[1]The parameter value equals the conductance at most cells.

[2]Values were not log transformed.

data clustering is not a significant problem because most of the data clusters are in areas of high hydraulic conductivity, where the sensitivity of hydraulic heads to most parameters is relatively small.

Ground-water discharge observations did not vary throughout the steady-state or transient stress periods, except for Manse and Bennetts Springs in Pahrump Valley. For these springs, one steady-state and two transient discharge observations from 1960 and 1998 were used. All other ground-water discharge observations only appear once in the objective function (eq. 8a). The 49 ground-water discharge observations were combined into 45 discharge observation locations by combining the three observations for Manse and Bennetts Springs into one observation location for each spring.

Modifications also were made to ground-water-discharge observation CVs during the calibration process (but not the observations themselves) because the determination of CVs may not have considered adequately all sources of observation error. Model error, discharge-estimation methods, and magnitude of discharge rate were considered during the calibration process and, where necessary, CVs were modified to reflect (1) the cumulative error, (2) the relative observation importance, and (3) the confidence in the observation.

Final Calibration of Model

As described above, numerous conceptual models were evaluated to test the validity of interpretations of the flow system. For each conceptual model, a new set of parameters was estimated and the resulting simulated hydraulic heads, drawdowns, and ground-water discharges were compared to the observations. Only those conceptual model changes contributing to a significant improvement in model fit were retained. Figures F–37 and F–38 present the estimated parameter values for the final calibration. Figure F–37 shows the values for the hydraulic-conductivity parameters for the confining units, the carbonate-rock units, the volcanic units, and the basin-fill units. Figure F–38 shows the values for the conductances for the drain parameters, the net-infiltration multiplication factor for the recharge parameters, the values for specific storage and specific yields for the storage property parameters, the values for the vertical anisotropy parameters, and the hydraulic characteristics for the HFB parameters.

Model Evaluation

The calibrated DVRFS model was evaluated to assess the likely accuracy of simulated results. An advantage of using nonlinear regression to calibrate the model is that a substantial methodology exists for model evaluation that facilitates a better understanding of model strengths and weaknesses. A protocol exists to evaluate the likely accuracy of simulated hydraulic heads and ground-water discharges, estimated and specified parameter values and associated sensitivities and confidence intervals, and other measures of parameter and prediction uncertainty. As part of the model evaluation, the regional water budget, the model fit, values of parameter estimates and their associated sensitivities, and boundary flows were evaluated. A qualitative analysis also was performed by comparing the hydrologic conceptual model (Chapter D, this volume) to the overall simulation in several hydrologically significant areas.

Regional Water Budget

The simulated water budgets for the DVRFS for the steady-state prepumping stress period and transient stress period 86 are presented in table F–18 and figure F–39. Stress period 86 (representing year 1997) was used to evaluate the model because there were many observations, and all components except storage were quantified. Many of the observations were quantified with significant accuracy, and some were used as observations in model calibration. The greatest uncertainty is in the representation of recharge.

Figure F–37. Parameter values defining hydraulic conductivity for confining units and carbonate rocks, volcanic rocks, and basin-fill units.

Simulated discharges decrease slightly from 361,523 m^3/d for the prepumping steady-state stress period to 344,870 m^3/d in 1998 (figs. F–39 and F–40). This change can be attributed mostly to pumpage in Pahrump Valley (fig. F–9 and table F–4). In 1997 (transient stress period 86), the sum of observed ground-water discharge is 313,203 m^3/d; and the sum of all simulated ground-water discharge is 344,870 m^3/d. As of 1998, most of the pumpage came from aquifer storage and is only just beginning to affect the regional discharge from ET and spring flow (fig. F–39).

Flow paths were simulated to evaluate flow directions in the model. For the most part, the model simulates the conceptual model described in Chapter D (this volume). The major exception was that discharge at the Furnace Creek Wash springs (fig. A–1 in Chapter A, this volume) appears to originate from beneath the north-northwestern part of the Amargosa Desert and areas within the SWNVF rather than from the Spring Mountains through Ash Meadows.

Evaluation of Model Fit to Observations

Model fit is initially evaluated using summary statistics (table F–19) and then through more detailed evaluations, including (1) consideration of results from the prepumping steady-state stress period and the final transient stress period,

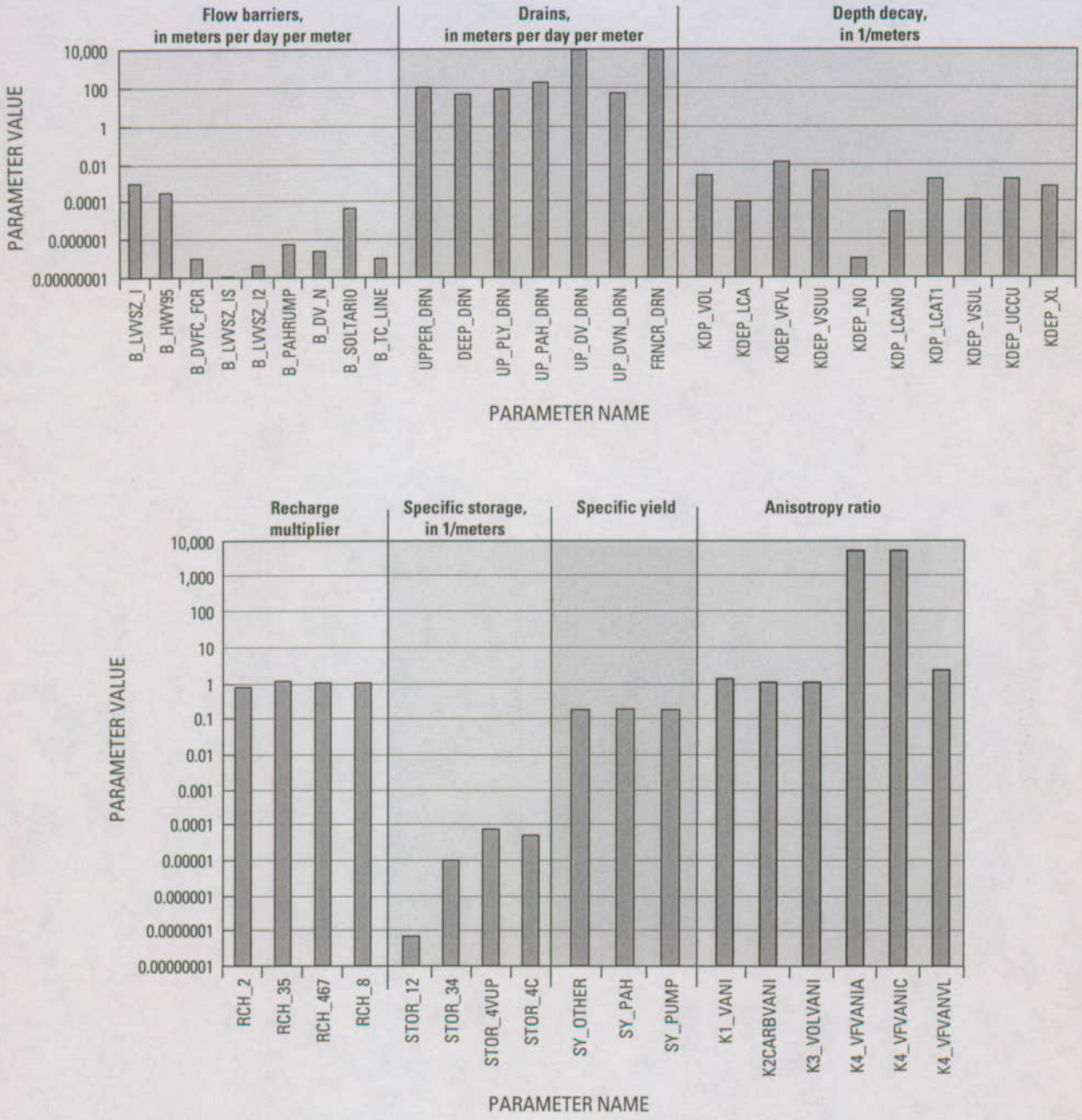

Figure F–38. Parameter values defining flow barriers, drains, and depth decay, recharge, storage, specific yield, and ratio of horizontal to vertical anisotropy.

(2) inspection of hydrographs calculated during transient stress periods, (3) assessment of spatial and temporal distribution of weighted and unweighted residuals, and (4) several graphical analyses. The sum of squared weighted residuals (SOSWR) are shown for completeness but indicate little about model fit. However, the square root of SOSWR divided by the number of observations (Nobs) provides a measure of model fit relative to the weighting that can be compared for different types of observations. A value of 1.0 indicates a match that is, overall, consistent with the observation error evaluation used to determine the weighting. The largest value, 5.4, is for constant-head boundary flow observations, indicating that the boundary flows are more poorly fit relative to the expected fit than are other types of observations. The second largest value, 3.6, was calculated for discharge observations. The CVs for discharges range from 10 to 71 percent (table F–4). Thus, on average, the difference between observed and simulated discharge can range from 36 to 360 percent of the observed discharge. Although the match to discharges is generally good and considered acceptable (fig. F–41), head-change data fit the observations best, relative to the standard deviations used to weight them.

Table F–18. Simulated and observed water budget for the steady-state prepumping stress period and transient stress period 86 (year 1997).

[ET, evapotranspiration; --, not available for combined observations; NA, not applicable]

Water-budget component	Steady-state prepumping stress period				Transient stress period 86, year 1997			
	Observed[1] (cubic meters per day)	Simulated[1] (cubic meters per day)	Fractional difference[2]	Coefficient of variation	Observed[1] (cubic meters per day)	Simulated[1] (cubic meters per day)	Fractional difference[2]	Coefficient of variation
Northern Death Valley Subregion								
FLOW IN								
Constant-head segment:								
Clayton	667	7,150	–9.72	0.75	667	7,240	–9.85	0.75
Eureka–Saline	15,100	15,700	–0.04	0.5	15,100	15,906	–0.05	0.5
Stone Cabin–Railroad	12,476	81,500	–5.53	0.96	12,476	85,305	–5.84	0.96
Panamint	15,000	25,400	–0.69	0.5	15,000	25,985	–0.73	0.5
FLOW OUT								
Discharge:[6]								
Sarcobatus Flat ET	–44,662	–27,458	0.39	--	–44,662	–39,340	0.12	--
Grapevine Canyon Springs	–3,485	–3,245	0.07	--	–3,485	–3,247	0.07	--
Central Death Valley Subregion								
FLOW IN								
Constant-head segment:								
Garden–Coal	[6]2,334	12,700	–4.44	0.86	[6]2,334	12,678	–4.43	0.86
FLOW OUT								
Constant-head segment:								
Las Vegas	[6]–3,633	–1,400	0.61	0.96	[6]–3,633	–1,396	0.62	0.96
Sheep Range	–18,747	–47,390	–1.53	--	–18,747	–47,324	–1.52	--
Pahranagat	[6]–3,040	–38,210	–11.57	--	[6]–3,040	–38,548	–11.68	--
Discharge:[6]								
Penoyer Valley ET	–12,833	–8,040	0.37	0.5	–12,833	–4,890	0.62	0.5
Oasis Valley ET	–20,311	–23,810	–0.17	--	–20,311	–23,630	–0.16	--
Indian Springs area	–2,240	–798	0.64	0.10	–2,240	0	1.00	0.10
Ash Meadows ET	–60,372	–64,106	0.06	--	–60,372	–61,098	–0.01	--
Franklin Well area ET	–1,150	–638	0.45	0.5	–1,150	–520	0.55	0.5
Franklin Lake ET	–3,519	–7,690	–1.19	--	–3,519	–7,240	1.06	--
Death Valley area springs and ET	–128,334	–186,020	–0.45	--	–128,334	–190,690	–0.49	--
Southern Death Valley Subregion								
FLOW IN								
Constant-head segment:								
Silurian	[6]500	–1,550	4.10	1.00	[6]500	3,710	4.12	1.00
Owlshead	[6]1,682	3,670	–1.18	0.89	[6]1,680	–1,560	–1.21	0.89
FLOW OUT								
Discharge:[6]								
Stewart Valley area ET	–3,379	–4,195	–0.24	--	–3,379	–3,842	0.14	--
Pahrump Valley area ET and springs	–32,400	–22,510	0.31	--	–3,378	–9,020	–1.67	--
Tecopa Basin area ET	–21,063	–3,806	0.82	--	–21,063	–3,807	0.82	--
Shoshone Valley area ET	–7,015	–3,620	0.48	--	–7,015	–3,650	0.48	--
Chicago Valley area ET	–1,462	–5,440	–2.72	0.36	–1,462	–5,420	–2.71	0.36

Table F–18. Simulated and observed water budget for the steady-state prepumping stress period and transient stress period 86 (year 1997).—Continued

[ET, evapotranspiration; --, not available for combined observations; NA, not applicable]

Water-budget component	Steady-state prepumping stress period				Transient stress period 86, year 1997			
	Observed[1] (cubic meters per day)	Simulated[1] (cubic meters per day)	Fractional difference[2]	Coefficient of variation	Observed[1] (cubic meters per day)	Simulated[1] (cubic meters per day)	Fractional difference[2]	Coefficient of variation
Southern Death Valley Subregion—Continued								
Total IN, constant heads	[6]47,759	144,570 (339,601)	--	--	[6]47,759	[7]149,264 (341,275)	--	--
Pumpage[3]	0	0	0	--	--	46,150	--	--
Storage	0	0	0	--	--	221,266	--	--
Recharge	[4]<342,000	303,415	NA	--	--	303,415	--	--
TOTAL IN:	<397,513	[7]447,985 (643,017)	--	--		[7]723,615 (720,095)		
Total OUT, constant heads	[6]–25,420	[7]–87,000 (281,913)	--	--	[6]–25,420	[7]–87,000 (–282,306)	--	--
Total, discharge:	–342,225	–361,523	–0.06	--	–313,203	–344,870	–0.07	--
Pumpage	0	0	0	--	NA	–275,978	NA	--
Storage	0	0	0	--	NA	–9,147	NA	--
TOTAL OUT:	--	–448,523 (–342,250)	--	--	NA	–912,301 (–912,302)	NA	--
FLOW IN – FLOW OUT:	--	[6,7]–538 (–420)	--	--	NA	[5,7]–192,206 (–194)	--	--

[1]Negative values indicate flow out of the model domain.

[2]Calculated as (observed–simulated)/observed.

[3]Simulated inflows are mostly from irrigation return flows and injection. A minor part of this is from well-bore inflow between pumping nodes connecting model layers in the Multi-Node Well package (Halford and Hanson, 2002).

[4]Total net infiltration from Hevesi and others (2003). Not used as an observation.

[5]The global budget error from the model in parenthesis. Steady-state is –0.07 percent, transient is –0.02 percent.

[6]Observed constant-head flow is less than that reported in table D–4 (this volume) because of no-flow boundaries applied in the model to subsegments where flow is less than 1,000 cubic meters per day.

[7]Value in parenthesis is cumulative numbers and takes into account flow in and out of given constant head segments. Individual constant head fluxes are composite numbers.

[8]Portions of Death Valley discharge are in northern and southern Death Valley subregion.

The standard error of regression (eq. 9) provides an overall measure of model fit. For the steady-state and transient simulations the standard error of the regression equals 2.7 (table F–19), which indicates that overall model fit is 2.7 times worse than would be consistent with the observation error statistics used to determine observation weights.

Ground-Water Discharge and Boundary Flow

Matching natural ground-water discharge from ET and springs was generally more difficult than matching hydraulic heads and hydraulic-head changes (table F–4) but provided important information for calibration. The overall fit of simulated ground-water discharge and boundary flow to observations is unbiased; simulated values plotted against observations are randomly scattered about the 1 to 1 line (fig. F–42*A*). Flow associated with the Stone Cabin–Railroad boundary segment (fig. A2–3 in Appendix 2, this volume) is an outlier where simulated flow into the model is higher than the observed flow. Most water entering the model along this northern boundary segment discharges at Sarcobatus Flat, where simulated discharge rates are less than the observed value. Fractional differences show how close the match was; the CV reflects expected observation error. If the model fits the observations in a manner that on average is as expected, the fractional differences would, on average, be similar to the CVs (table F–4). For the constant-head boundary flows, one weighted residual is greater than, and one weighted residual is less than, three times the standard error. Eighty-seven percent of the constant head boundary flows are within three times the standard error of regression.

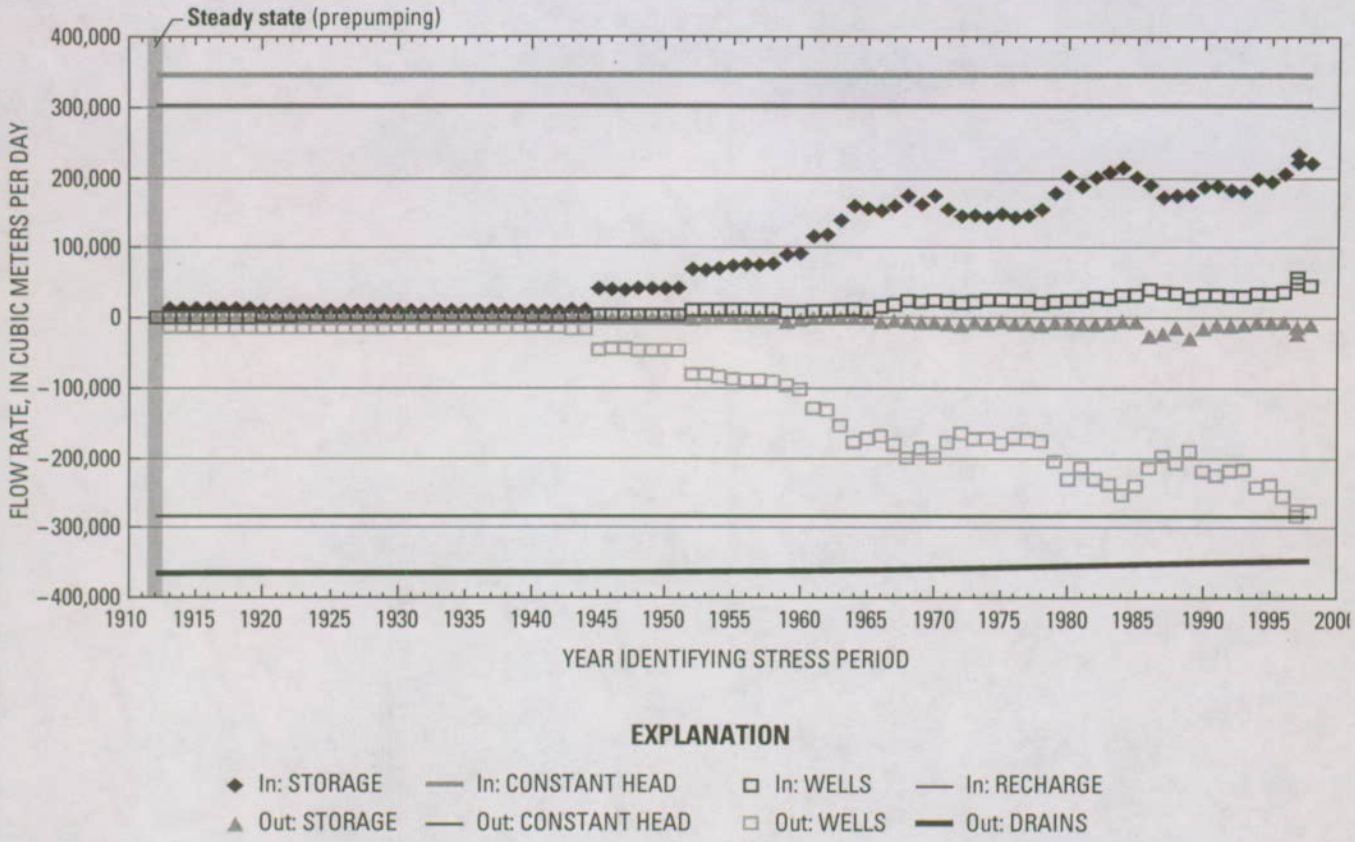

Figure F–39. Total simulated and observed ground-water discharge from evapotranspiration and spring flow for steady state and transient stress periods of the transient model.

Noting that ground-water discharges have been assigned a negative sign indicating flow out of the model, the weighted residuals for ground-water discharges appear to vary randomly about a value of zero with a slight overall bias toward being positive, indicating that simulated discharges in these areas are greater than observed discharges (fig. F–43). The greatest positive unweighted ground-water discharge residuals (simulated greater than observed) by volume (absolute value greater than 10,000 cubic meters/day) are at Death Valley (Cottonball Basin, middle, and Mesquite Flat) (OBS-DV-COTTN, OBS-DV-MIDDL, and OBS-DV-MESQU). The greatest negative unweighted ground-water discharge residuals (simulated less than observed) are at Sarcobatus-northeastern (OBS-SARCO-NE), early observations at Manse Spring in Pahrump (OBS-PAH-MANS) and upper Tecopa Valley (OBS-TC-TECOP). The two major discharge areas that contribute the largest error to the model are Death Valley and the Shoshone/Tecopa area. Two of the weighted residuals for ground-water discharges are greater than 8.2 and one is less than –8.2, indicating that 94 percent of the flow-weighted residuals are within three times the standard error of the regression. For the constant-head boundary flows, one weighted residual is greater than, and one weighted residual is less than three times the standard error. Eighty-seven percent of the constant head boundary flows are within three times the regression standard error.

The graph of weighted residuals for ground-water discharge (fig. F–43) indicates how well the model reproduces the observed discharges. An absolute value of 1.0 or less indicates that the residual was less than the standard deviation of the observation error. Weighted residuals that exceed 3.0 are considered to be large. For 35 of the 49 discharge observations, simulated ground-water discharge values are less than three times the standard error (fig. F–44). Simulated discharge from the regional ground-water discharge areas is shown in figure F–45. For these major discharge areas, simulated discharges are within one standard deviation, except at the Shoshone/Tecopa area and Death Valley.

Hydraulic Heads

Comparison of prepumping, steady-state simulated hydraulic heads (figs. F–46 and F–47) with the potentiometric surface of D'Agnese and others (1998) and the potentiometric surface of Appendix 1 (this volume) indicates that the DVRFS model results adequately depict major features of the hydraulic-head distribution. Local mounds of perched water (D'Agnese and others, 1998) are not represented in this simulation. In general, areas of nearly flat and steep hydraulic gradients are appropriately located and important hydraulic gradients are represented:

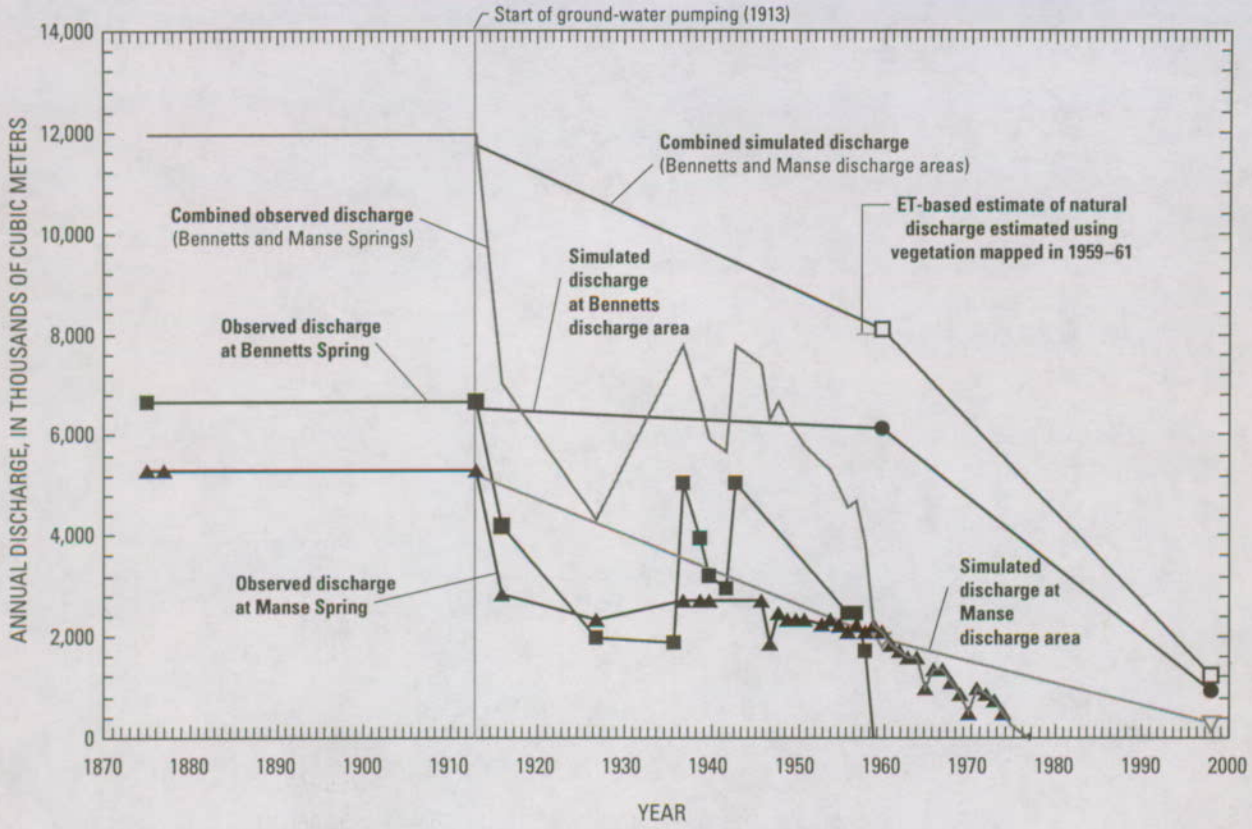

Figure F–40. Simulated and observed annual discharge from regional springs in Pahrump Valley.

Table F–19. Summary statistics for measure of model fit.

[SOSWR, sum of squared weighted residuals; Nobs, number of observations]

Type of observation	Number of observations	Average positive weighted residual	Average negative weighted residual	SOSWR	[SOSWR/Nobs]$^{1/2}$
Hydraulic head	2,227	2.1	–1.8	22,702	3.2
Hydraulic-head changes—transient[1]	2,672	1.6	–1.4	13,361	2.2
Discharge	49	2.9	–2.3	637	3.6
Constant-head boundary flow	15	3.7	–3.3	438	5.4
Total	**4,963**	**1.8**	**–1.6**	**37,146**	**2.7**
Other statistics					
Number of defined parameters	100				
Number of estimated parameters	Variable				
Standard error of the regression	2.7				

[1]Steady-state head observations are included with transient head observations if they are (1) classified as steady-state conditions and (2) located where there were no head observations during the initial steady-state stress period.

(1) The potentiometric-surface trough on Pahute Mesa, although subdued in the simulation, is represented;

(2) The generally west-to-east hydraulic gradient in the volcanic rocks at Yucca Mountain is simulated;

(3) The upward vertical hydraulic gradients from the carbonate-rock aquifer at Yucca Mountain are represented in the simulation (pl. 2, hydrograph [HG] 26); and

(4) The downward vertical hydraulic gradients in recharge areas of the Spring Mountains (pl. 2) and parts of Pahute Mesa (pl. 2, HG 18. 20, and 28) and upward vertical hydraulic gradients in discharge areas in Pahrump Valley (pl. 2, HGs 11, 12, and 14) and Ash Meadows (pl. 2, HG 1) are represented.

Simulated values plotted against observations generally fall on the 1 to 1 line, indicating a good model fit (fig. F–42*B*). The fit of simulated to observed hydraulic heads is generally

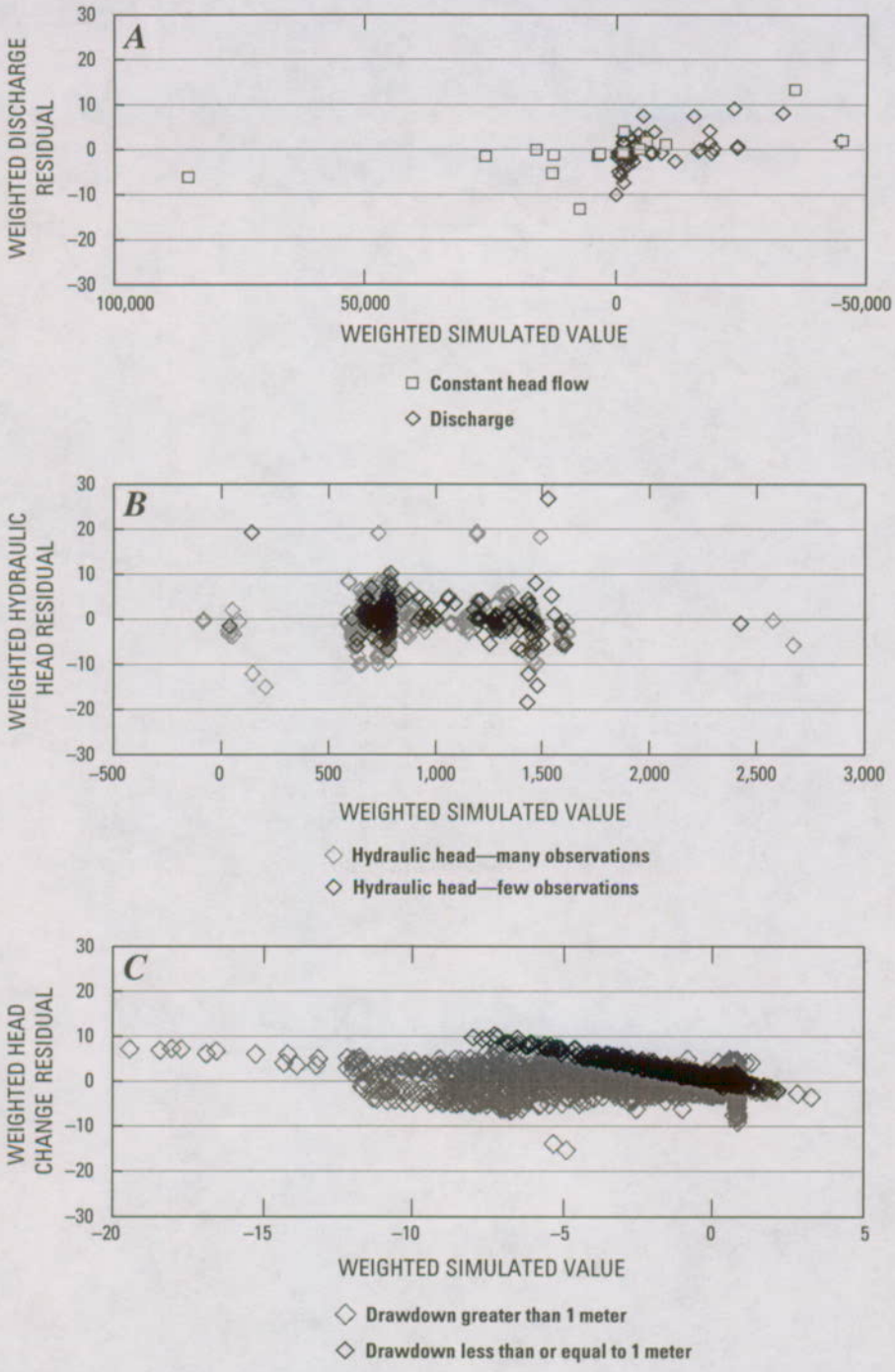

Figure F–41. Weighted residuals and simulated equivalent for (*A*) hydraulic head, (*B*) head change, and (*C*) constant-head flow and discharge.

good (unweighted residuals with absolute values less than 10 m) in most areas of nearly flat hydraulic gradients and moderate (residuals with absolute values of 10 to 20 m) in the remainder of the nearly flat hydraulic gradient areas (primarily in Pahrump Valley) (fig. F–46). The fit of simulated to observed heads is poorer (residuals with absolute values of greater than 20 m) in areas of steep hydraulic gradient. Poorest fit to observed hydraulic heads is in the vicinity of the steep hydraulic gradient along the Eleana Range and western part of Yucca Flat, and in the southern part of the Owlshead Mountains (fig. F–46). The fits also are poor in the southern part of the Bullfrog Hills and the north-northwestern part of the model domain. Most of these larger residuals can be attributed to (1) insufficient representation of the hydrogeology in the HFM, (2) misinterpretation of water levels, (3) model error associated with grid cell size, or (4) a combination of the first three factors.

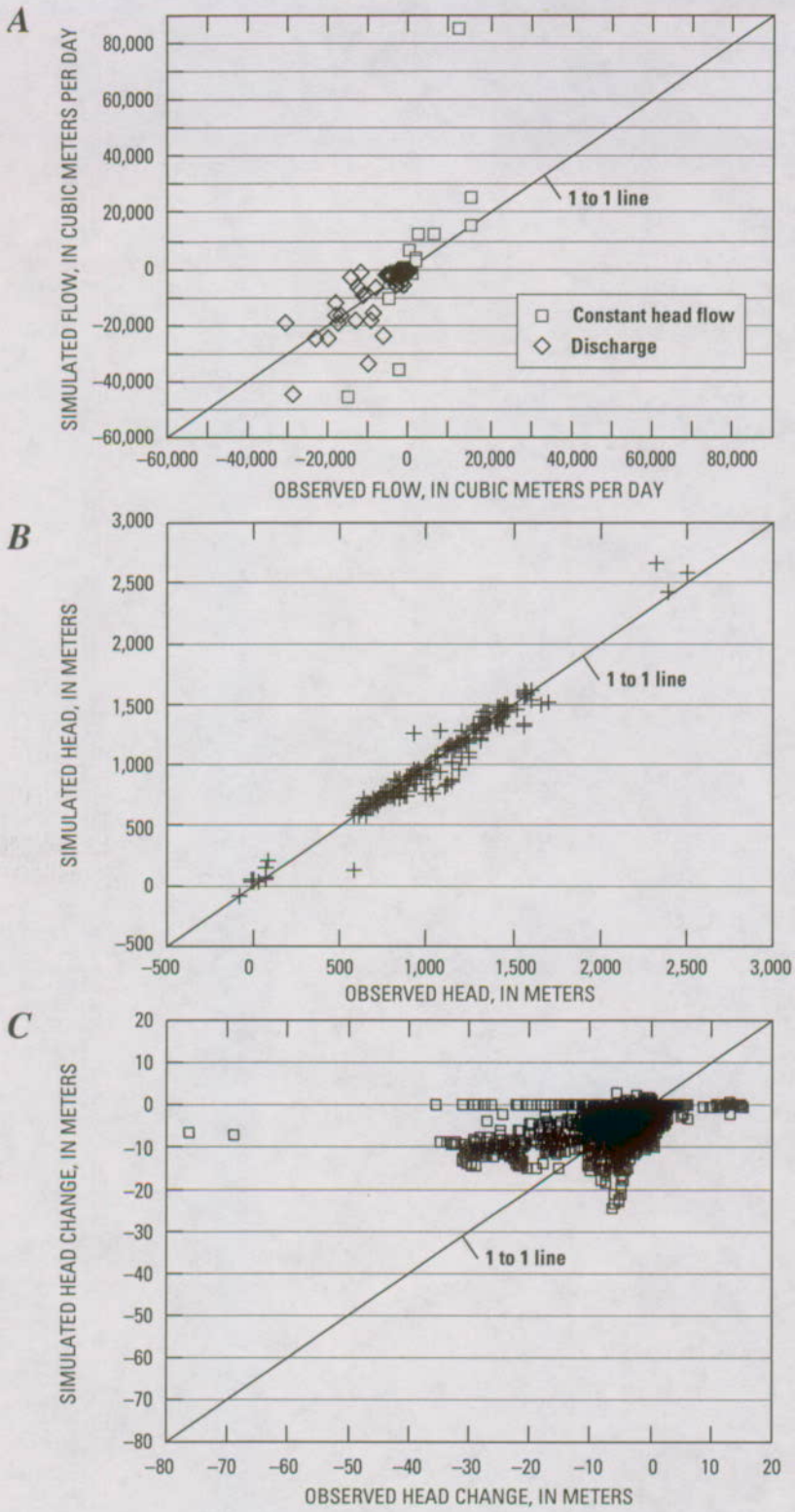

Figure F–42. Weighted observed value compared to weighted simulated values for (*A*) hydraulic head, (*B*) head change, and (*C*) constant-head flow and discharge.

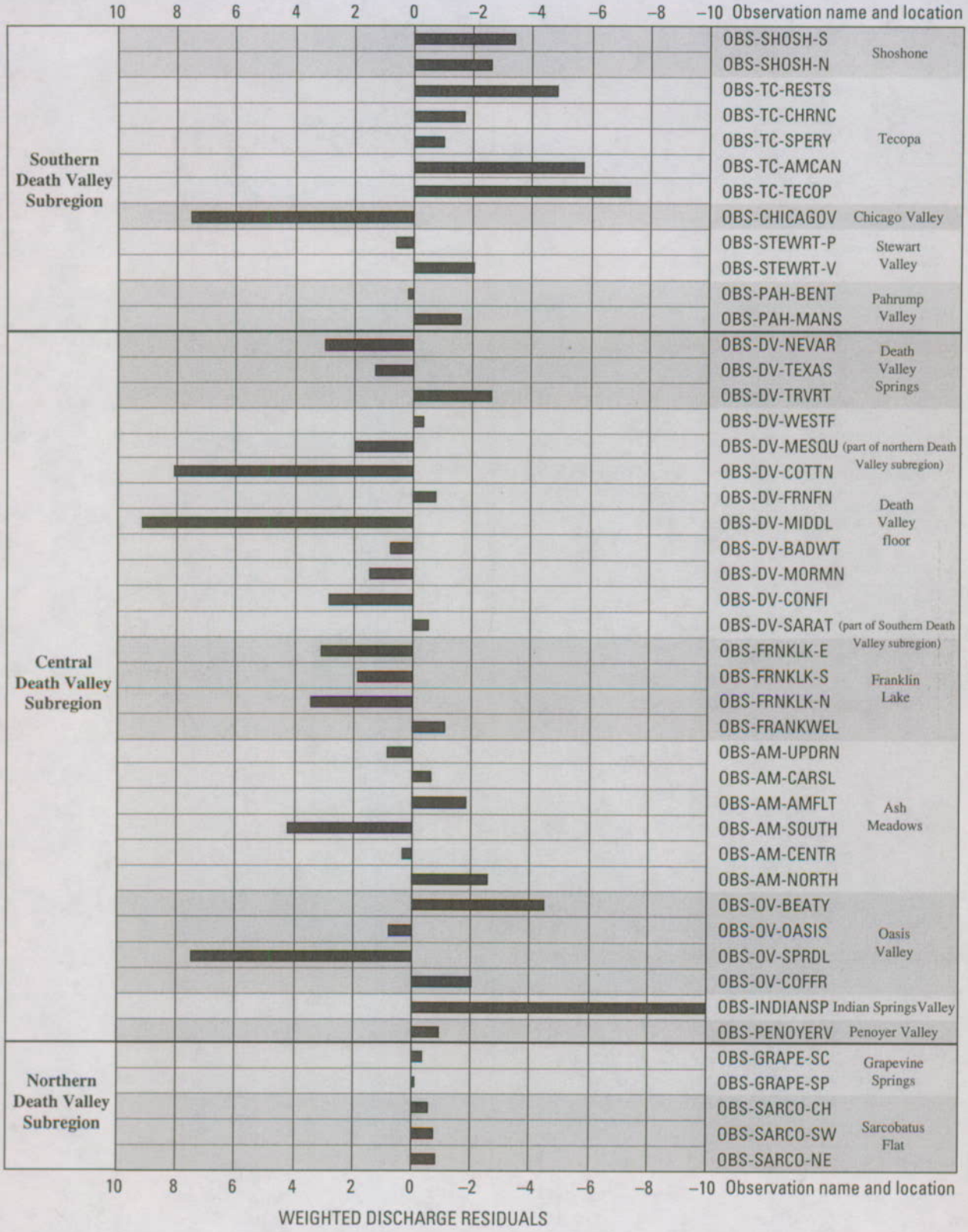

Figure F–43. Ground-water discharge weighted residuals (observed minus simulated).

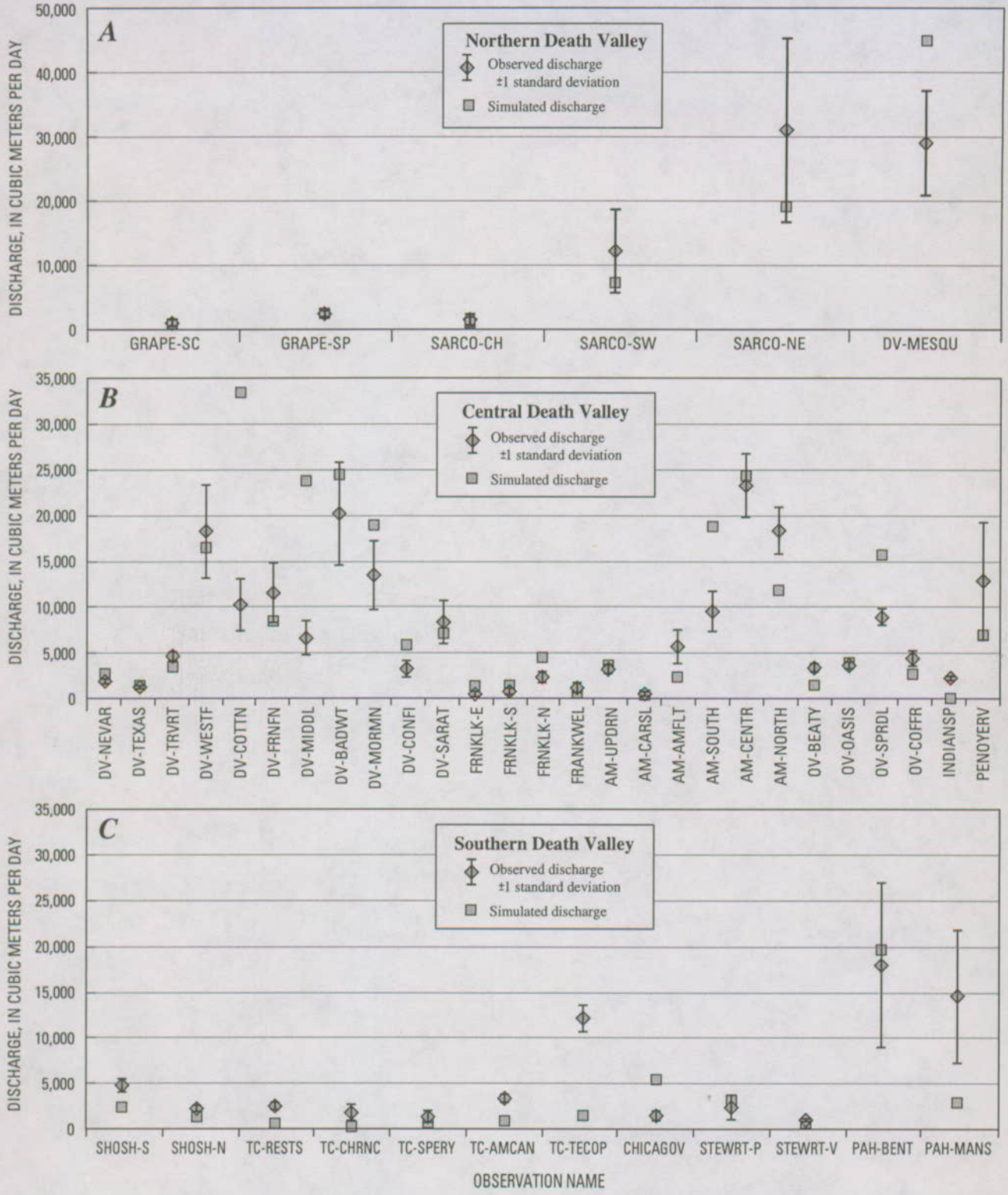

Figure F–44. Observed and simulated ground-water discharge by subregion: (*A*) Northern Death Valley, (*B*) Central Death Valley, and (*C*) Southern Death Valley with expected observed discharge variation.

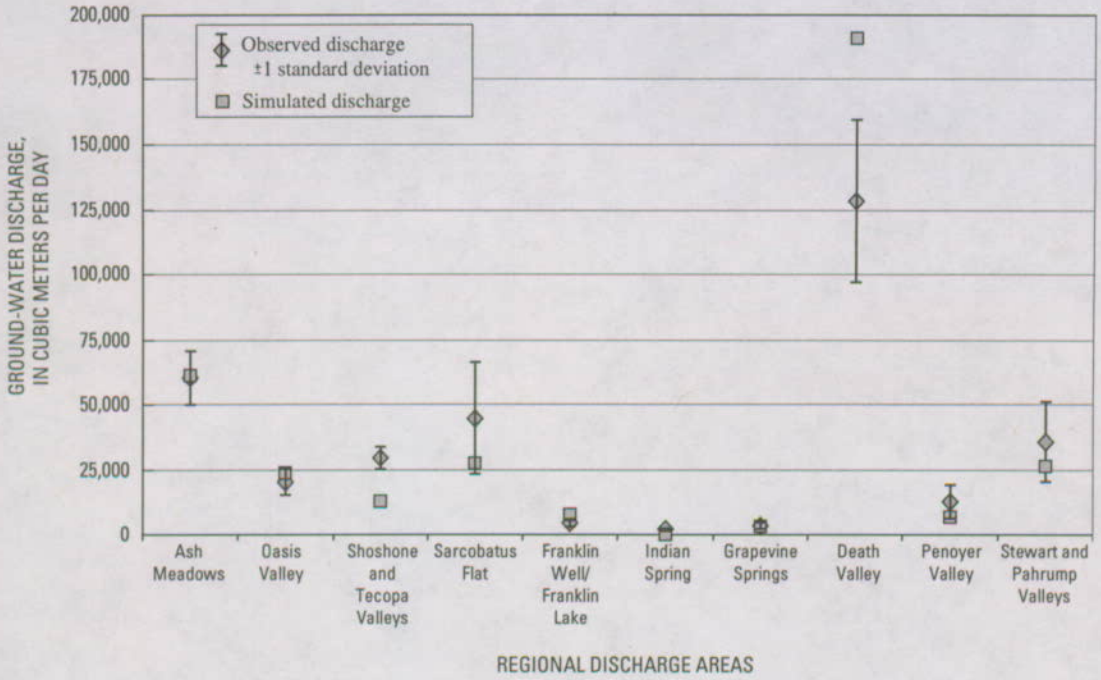

Figure F–45. Observed and simulated ground-water discharge observations by major discharge area with expected observation discharge variation.

Patterns in the spatial distribution of weighted residuals indicate a nonrandom distribution, indicating some model error (fig. F–47). In the northwestern part of the Amargosa Desert, weighted residuals are of moderate magnitude, but heads are consistently simulated lower than observations near the Bullfrog Hills and the slopes of the Funeral Mountains. Heads also are consistently simulated higher than in the northeastern arm of the Amargosa Desert and along the slopes of the southern part of the Funeral Mountains. Although a number of well-matched observations exist, weighted residuals also indicate that heads are simulated higher than observations at the northern part of Pahute Mesa and lower than observations on the southeastern part of Pahute Mesa (fig. F–47). There are four simulated head values of 2,500 m near the peak of the Spring Mountains; these simulated values are greater than observations, possibly indicating model bias. Where concentrated hydraulic-head observations are available for the remainder of the model domain, the distribution of the weighted residuals is random (fig. F–41*B*).

When plotted against simulated values, most of the weighted residuals for hydraulic heads vary randomly about a value of zero (fig. F–41*B*). However, 13 head-change weighted-residual values are greater than +8.2, which is three times the regression standard error of 2.7; 3 values are less than –8.2. Thirty-one hydraulic-head weighted-residual values are greater than 8.2; 26 values are less than –8.2. For normally distributed values, only 3 in 1,000 on average would be so different from the expected value. Here, out of about 4,900 observations, 57 are greater in absolute value than three times the standard error of the regression, with most of those being positive. Although this distribution is slightly biased, it is still largely random. Many of the head observations with large negative weighted residuals can be attributed to steep hydraulic gradients or potentially perched water levels (D'Agnese and others, 1997; D'Agnese and others, 2002). Many of the large positive weighted residuals are along the northern and southern parts of the model boundary, where considerable uncertainty exists in the hydrogeology.

Changes in Hydraulic Heads for the Transient Stress Periods

Changes in hydraulic heads for the transient stress periods were evaluated by assessing head residuals and by examining hydrographs. Weighted values of head change do not fall along a 1 to 1 line, indicating bias (fig. F–42*C*). Overall, the simulated head change is less than the observed head change, and not enough drawdown was simulated. Additionally, two outliers are located south of Beatty, Nev., where model-predicted drawdown is about 7 m, but 70 m or more of drawdown was observed. The clustering of head changes about the simulated model value of 0 is a result of generally underpredicting drawdown; many simulated head-change values are within about 5 m of observed head changes.

The simulated heads were compared with observed heads by using hydrographs from 869 of the wells in the model domain. Representative hydrographs (pl. 2) are, for the most part, grouped by wells from different pumping areas. In general, the simulated head changes match the observed head changes. Discrepancies between the simulated heads

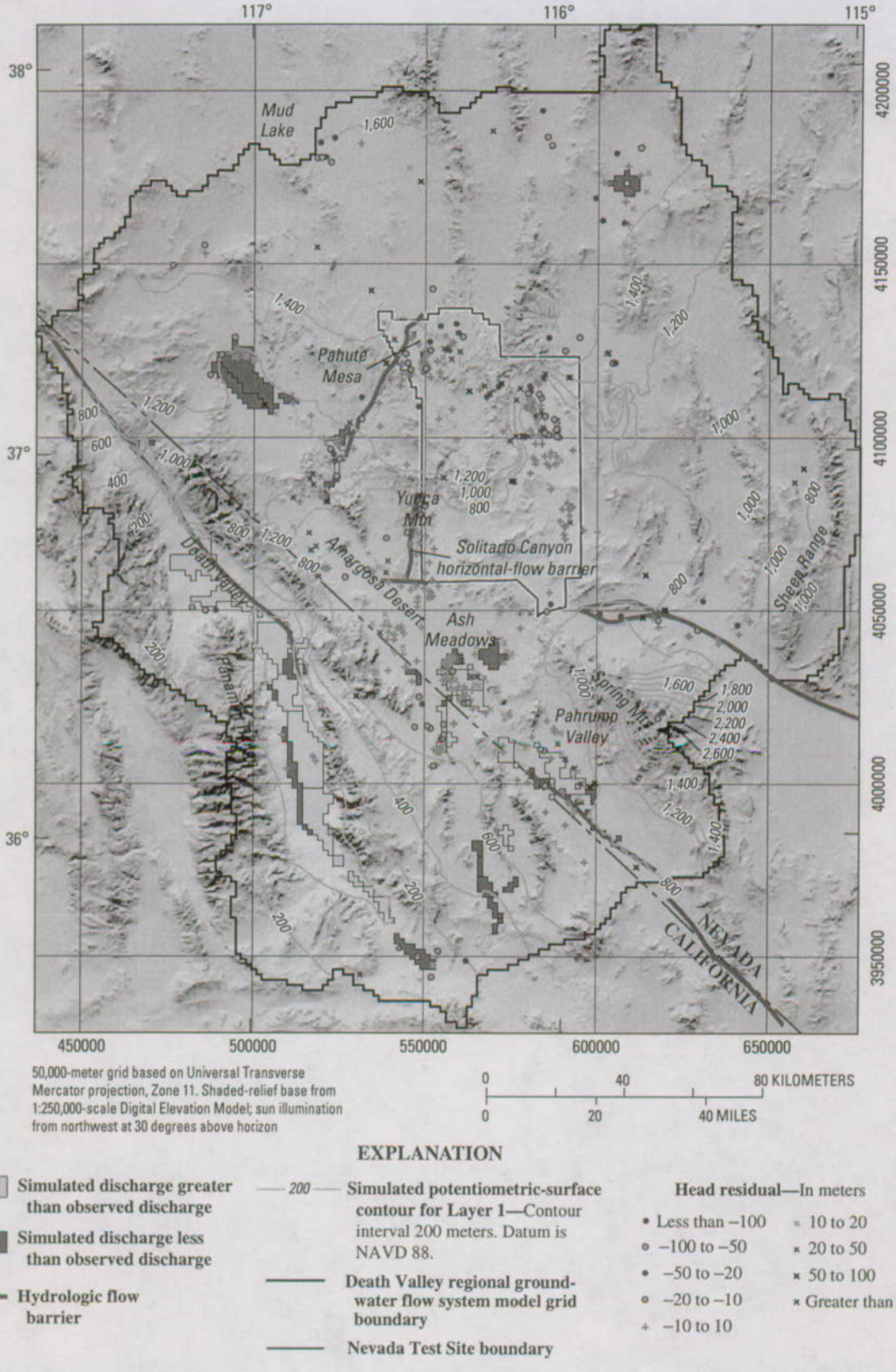

Figure F–46. Steady-state stress period hydraulic-head residuals (observed minus simulated) and simulated potentiometric surface for uppermost active model layer.

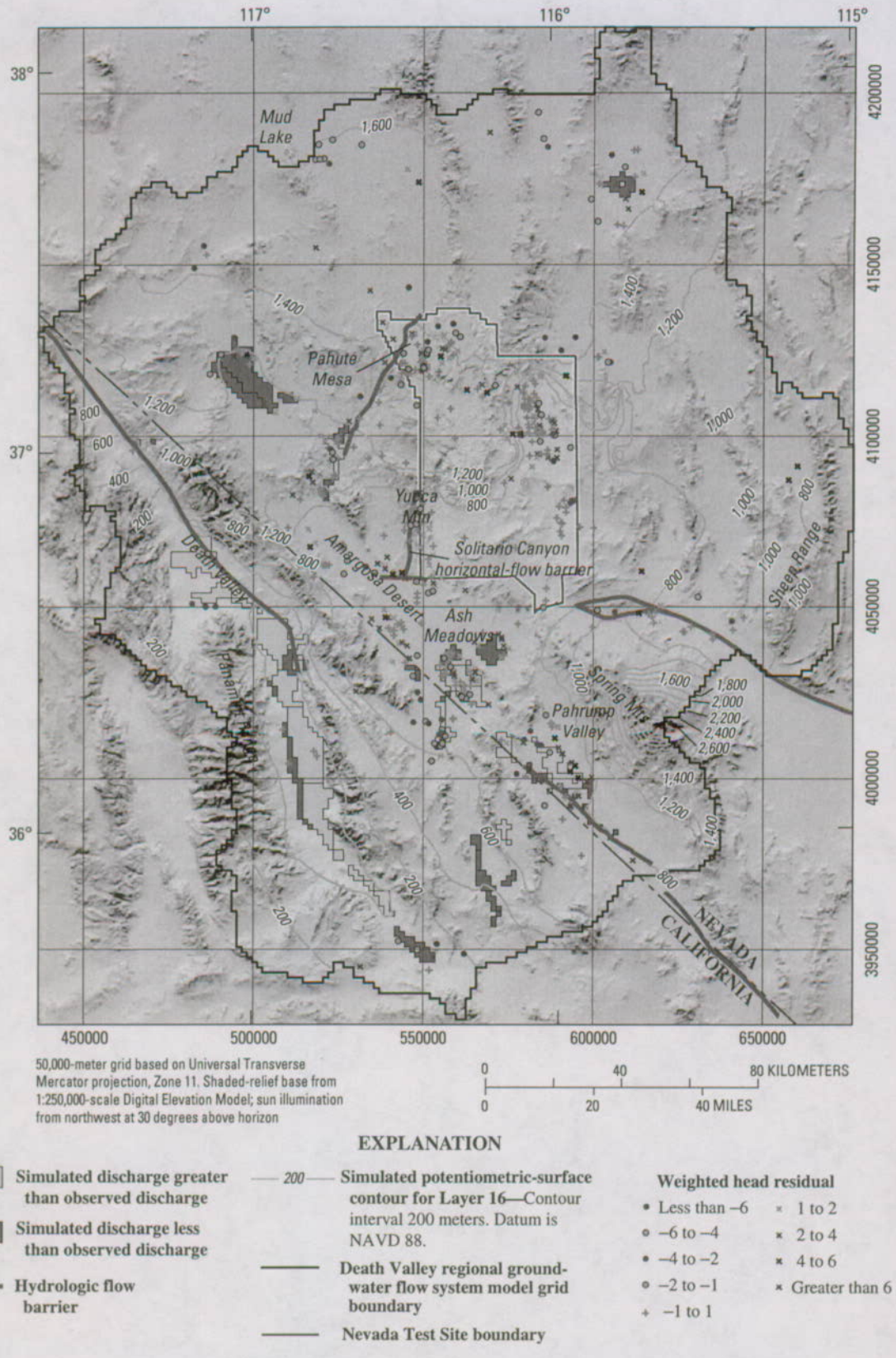

Figure F–47. Steady-state stress period hydraulic-head weighted residuals (observed minus simulated) and simulated potentiometric surface for uppermost active model layer 16.

and the observed heads may be caused, in part, by assuming that pumping is constant during each calendar year. For some areas, the match between simulated and observed values likely could be improved with better estimates of the quantity and temporal distribution of pumping.

For wells in the Amargosa Desert and Penoyer Valley, the observed heads began declining in the 1960's and 1970's, respectively (pl. 2), and these declines were generally matched by simulated heads. The hydrogeologic system at Pahrump Valley appears to be complicated as a result of large amount of pumpage over various time periods from various basin-fill units. Observed heads began to decline significantly in the 1960's and the declines continued, for most locations in Pahrump Valley, until the late 1980's. In some areas, heads are still declining, but in other areas, heads began to recover in the 1990's. Examination of the simulated hydrographs (pl. 2) shows that in some areas in Pahrump Valley these features are matched and in other areas they are not. Because of the complex hydrogeologic system in Pahrump Valley, a more detailed model would be needed to simulate head changes more accurately. The transient simulation is discussed in more detail in the "Evaluation of Hydrologically Significant Areas" section.

Normality of Weighted Residuals and Model Linearity

Linear confidence intervals on estimated parameters are valid only if the model correctly represents the system; that is, weighted residuals are normally distributed and the model is effectively linear. However, normal probability plots for the weighted residuals (not presented here) were not linear. The R^2_N statistic (Hill, 1998, p. 23) equaled 0.871, indicating that the normal probability plot is significantly nonlinear. Correlations among weighted residuals caused by the fitting of the simulated values to the observations could cause the deviation from a straight line. Model linearity was statistically tested using the modified Beale's measure (Cooley and Naff, 1990). The modified Beale's measure calculated for the transient simulation equals 212. This value indicates that the model is highly nonlinear (modified Beale's measure greater than 0.66). This lack of normality of the weighted residuals and the degree of nonlinearity of the model indicate that linear confidence intervals for parameter values may not be valid.

Evaluation of Estimated Parameter Values and Sensitivities

Most of the parameters estimated during model calibration were related to hydraulic conductivity (horizontal hydraulic conductivity, horizontal-flow barriers, drain conductances, vertical anisotropy, and depth decay). Of the 100 defined parameters, 23 were estimated in the steady-state simulation, and 32 were estimated in the transient simulation (fig. F–48 and tables F–8—F–11). The other defined parameters were not estimated because *CSS* and(or) *PCC* values indicate that there is inadequate information to estimate them. Compared to field-measured hydraulic-conductivity estimates (Belcher and others, 2001), estimated parameter values appeared realistic (figs. F–37 and F–38, tables F–8—F–11), revealing very little indication of model error.

Evaluation of Boundary Flows

Although simulated values of flow for each boundary segment (or subsegment) differ somewhat from those reported by Harrill and Bedinger (Appendix 2, this volume), except for the Silurian segment, the direction of flow is simulated accurately and the flows are generally matched well within their estimated error. For the Silurian segment, simulated flow is about 1,500 m^3/d out of the model domain, rather than an inflow of 500 m^3/d. Despite the generally low-permeability rocks along most of the western boundary, estimates indicate a potential for flow into the model domain across the Clayton, Eureka, Saline, Panamint, and, to a lesser degree, the Owlshead boundary segments (Appendix 2, this volume). The model simulates net flow greater than 1,000 m^3/d into the model domain at these segments. Net flow out of the model domain with a net flow greater than 1,000 m^3/d across the Las Vegas, Sheep Range, Pahranagat, and the Silurian boundary segments is simulated. The simulated flow out of the system at parts of the Pahranagat and Sheep Range boundary segments and the inflow across the Stone Cabin–Railroad boundary segment are much greater than estimated. These differences may result from inaccuracies in the HFM or in the boundary-flow estimates.

Evaluation of Hydrologically Significant Areas

The simulation of the conceptual hydrologic model presented in Chapter D (this volume) was evaluated in several hydrologically significant areas. These areas are: (1) the Sheep Range; (2) the Pahranagat Range; (3) northern Death Valley and Sarcobatus Flat; (4) the pumping centers of Pahrump Valley, Penoyer Valley, and the Amargosa Desert; and (5) the NTS area (including Yucca Mountain). Hydrochemical, isotopic, and thermal data (see Chapter D, this volume) were used, where possible, to help delineate the flow system and assess whether simulated flow paths were reasonable. These hydrochemical characteristics are used as qualitative information to help in the calibration of the flow model and to indicate where flow directions and magnitudes are reasonable.

Sheep Range

In the original conceptual model of the flow system, the boundary of the model was placed at the flow system boundary in the vicinity of the Sheep Range, which was assumed to coincide with the approximate trace of the Gass Peak thrust fault (fig. F–49 and Chapter D, this volume). On the basis of examination of the limited regional-potential data

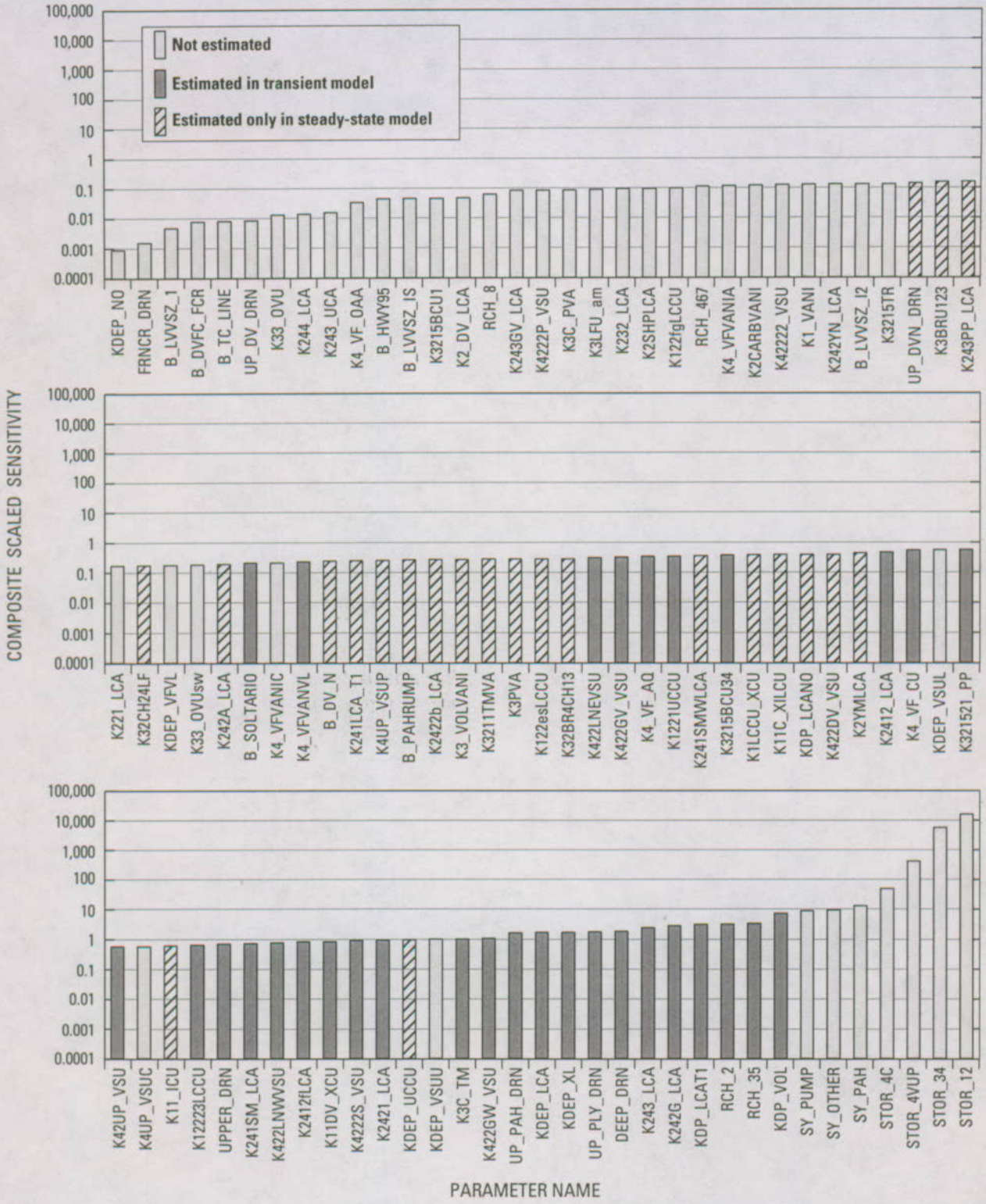

Figure F–48. Composite scaled sensitivities for all parameters. Parameter RCH_9 had a composite-sealed sensitivity of virtually zero and is not included in the figure.

Figure F–49. Model boundary and ground-water divide near Sheep Range with simulated potentiometric surface from model layers 1 and 16.

(Appendix 1, this volume), the flow system boundary actually may be west of the model boundary in the approximate location of the Desert Range (fig. F–49 and pl. 1), and flow east of this ground-water divide would be to the Colorado River ground-water flow system. In the upper layers of the model (layer 1, for example), the location of this ground-water divide is controlled primarily by topography and the presence of recharge areas (fig. F–49). Simulated recharge on the southern Sheep Range exits the model domain to the east.

The simulated ground-water divide is not a vertical plane, and in the deeper parts of the model, the position of the divide is controlled by geology and regional hydraulic gradients. The LCCU in the upper plate of the Gass Peak thrust is modeled in the HFM (Chapter E, this volume) thinner than previous geologic interpretations (Chapter B, this volume), indicating a less effective barrier to ground-water flow. Simulated head for the lower model layers representative of the deep regional system (layer 16, for example), indicates a ground-water divide in the general area of the regional ground-water divide estimated from regional potentiometric data (fig. F–49, pl. 1, and Appendix 1). Differences in the simulated ground-water divide with depth are owing to the scarcity of head data and the relatively large simulated vertical hydraulic conductivity in this area.

Pahranagat Range

Early studies describe the Ash Meadows ground-water basin as potentially receiving ground-water flow from the Pahranagat Range (fig. A–1, and Chapter D, this volume). On the basis of more recent studies (Chapter D, this volume), little to no flow is simulated from the Pahranagat Range to Ash Meadows. An overall net outflow is simulated along the Pahranagat boundary segment. Water enters the system along the Garden-Coal boundary segment and exits along the northern part of the Pahranagat boundary segment. Flow also is simulated entering the model domain across the Pahranagat boundary segment and exiting through the Sheep Range boundary segment.

Northern Part of Death Valley and Sarcobatus Flat

Although the observed heads and spring flow and flow across the Eureka Saline boundary segment appear to be adequately simulated, discharge from drains representing ET is simulated much higher than observed (figs. F–46 and F–47). The steep hydraulic gradient required to simulate discharge to Grapevine Springs and reasonable ET rates in northern Death Valley was maintained by specifying an HFB along the northern Death Valley fault zone. Although geologically reasonable, the extremely low permeability barrier required to produce the observed discharge from Grapevine Springs resulted in simulated heads that are above land surface on the floor of Death Valley and upgradient from this fault zone. Given the current HFM (Chapter E, this volume), this feature is required to simulate discharge at Grapevine Springs.

This HFB, however, could not simulate the observed discharge at Sarcobatus Flat, even with local recharge. Inflow along the northern model boundary (Stone Cabin–Railroad and Clayton boundary segments) in excess of that estimated (Appendix 2, this volume) was required to simulate heads and observed discharge at Sarcobatus Flat. The excess inflow, the configuration of the HFM, and the constant heads specified along the Stone Cabin–Railroad boundary segment resulted in heads being simulated above land surface at Mud Lake (fig. F–46 and F–47). The simulated discharge at Sarcobatus Flat was less than observed (figs. F–44—F–47).

Pahrump Valley

Although the general trends, heads, and drawdowns are approximated on a regional scale, the DVRFS model appears to lack sufficient detail to accurately simulate ground-water flow in the complex basin-fill system of Pahrump Valley (fig. A–1 in Chapter A, this volume). Heads respond differently to pumping over short distances, so that the heads are accurately simulated in some areas of Pahrump Valley but not in others (pl. 2).

Examination of selected hydrographs for Pahrump Valley (pl. 2, HG 11–17) shows the variable heads and drawdown. In general, trends are simulated; however, spikes are not. The pumping induces hydraulic gradients that increase and decrease with changes in pumping over the simulation period (pl. 2, HG 11,12, and 14). Pumping in this area appears to decrease from the 1950's on, while pumping in other areas, often in shallower wells, increases (pl. 2, HG 11–14). Plate 2 (HG 11, 13, and 16) shows that the simulated trends are matched fairly well and most of the effects in this area are in layers 1 and 2 (pl. 2, HG 11); however, the simulated trends are subdued (HG 12). A prominent feature of HG 12 is that head observations with the highest weights are matched well, and head observations with lower weights are matched less well, indicating that the lower weights may be contributing to the subdued nature of the hydrograph. In the northern part of Pahrump Valley, wells in model layer 1 are much less affected by pumping than wells in the deeper model layers, with maximum drawdown occurring in the 1990's. Because pumping occurs mostly in the eastern and central parts of the valley, there has been little effect from pumping in the western part of the valley (pl. 2, HG 15). The effect of some of the more recent, larger pumping rates in the eastern part of the valley can be seen on the map of head change (pl. 2) and on HG 13 (pl. 2). A small amount of drawdown in the southeastern part of Pahrump Valley is indicated by a long-term water-level record (pl. 2, HG 17). The simulated heads in this area are less than observed but replicate the small drawdown over time.

In order to simulate the change in natural discharge due to pumping in the Pahrump Valley (including both ET and spring flow), three values of discharge were estimated

from various data for Bennetts and Manse Springs areas (Chapter C, this volume). The discharge observations represent that the springs went dry prior to the end of the simulation period, although ET continued (fig. F–40). Simulated discharge and discharge observations are matched relatively well from 1959 to 1961; however, discharge prior to and after this period is not simulated as accurately. Although a general trend of decreasing simulated discharge with time is evident (fig. F–40), the decrease is not at the same rate as observed. Early-time discharge observations are simulated lower than expected, and late-time observations are simulated higher than expected.

Penoyer Valley

Little is known about the hydrogeology of Penoyer Valley (fig. A–1 in Chapter A, this volume). Given that many of the drains simulating ET in the valley are dry, and the discharge rate is greatly underestimated, the drain altitudes may be simulated higher than is reasonable or the hydrogeologic conditions may not be represented correctly. Most of the wells in the Penoyer Valley are shallow and some areas are affected by drawdown. Head observations (figs. F–46 and F–47) and hydrographs (pl. 2, HG 21–23) show that heads and general trends of head change are matched where pumping does and does not occur. In most areas, heads are matched within 10 m, while in isolated areas, the unweighted head residuals reach 20 m (fig. F–46 and pl. 2). As in other areas, abrupt changes in heads shown in the hydrographs are not simulated. Although this area is adjacent to the model boundary, flow across these boundary segments does not appear to be affected by the pumping. The proximity of the constant-head boundary may also be influencing the high head residuals in this area. To match these head observations, unrealistically low hydraulic conductivity values and high specific storage values were required.

Amargosa Desert

The Amargosa Desert has two main centers of pumping, Ash Meadows and Amargosa Farms. At Ash Meadows, heads generally are matched well in the shallow model layers (layers 1–3) and generally show a small upward hydraulic gradient (pl. 2, HG 1–3 and fig. F–46). In the deeper model layers (fig. F–47), such as those representing the carbonate-rock aquifer at Devils Hole (pl. 2, HG 27), heads are not matched as well and show a small downward hydraulic gradient. Despite the poor fit of simulated and observed head at Devils Hole (pl. 2, HG 27), a small amount of drawdown can be seen in the 1970's and some recovery in late 1970's to early 1980's, simulating the hydraulic connection between the basin-fill units, where pumping is occurring, and the LCA.

Except for a few wells, very little drawdown is seen in the hydrographs (pl. 2). Because of the numerous wells in the area (fig. F–9), most completed without casing, and the simulation of the hydraulic connection between layers with the MNW package, heads appear to begin to increase in model layer 1 in the 1980's) (pl. 2, HG 1). Because of the lack of information required to define the effects of the well-bore inflow, the simulation of flow from higher heads in deeper parts of the system through inactive well bores into lower heads in shallower parts of the system may be incorrect. Drawdown from pumping in nearby wells is superimposed on this increase.

In the Amargosa Farms area, there generally is a good match of simulated to observed heads (<10-m residuals, fig. F–46; pl. 1, HG 4–9), though the match is poor for some wells (pl. 2, HG 10). On the adjacent alluvial fans sloping up to the Funeral Mountains, simulated heads are somewhat lower than observations. Heads are also less well matched in the northwest arm of the Amargosa Desert (fig. F–46, pl. 2, HG 10). Pumping rates in this northwestern area are lower than in other areas in the Amargosa Desert, resulting in less drawdown with strong upward hydraulic gradients. In most areas, the trend of head changes resulting from changes in pumping is matched reasonably well in the model (pl. 2, HG 4–10). Spikes generally are not matched well (pl. 1, HG 8), but some small head changes (pl. 2, HG 5) appear to be local effects and are matched well.

Nevada Test Site and Yucca Mountain

At the NTS, recharge and discharge areas are represented by downward and upward hydraulic gradients in a number of the deeper wells (pl. 2, HG 18–20 and 28). Some heads are simulated higher than observed values, and others are simulated lower than observed values (fig. F–46; pl. 2, HG 18–20). There has been minimal pumping at the NTS, and, as a result, little drawdown is observed in simulated hydrographs (pl. 2, HG 18–20). Fenelon (2000) describes NTS wells in which pumping effects were evident, as is shown in HGs 18 and 28 (pl. 2). More than 10 m of drawdown is measured and simulated in some wells (pl. 2, HG 28).

At Yucca Mountain, simulated hydraulic gradients are generally upward from the carbonate-rock aquifer into the volcanic rocks (pl. 2, HG 26). The potentiometric surface at and to the east of Yucca Mountain is generally flat and the simulated heads are mostly within 10 m of the observations (fig. F–46; pl. 2, HG 25 and 26). The steep hydraulic gradient at the northern end of Yucca Mountain may be caused by perched water levels (Luckey and others, 1996). Because of this possibility, head observations in wells associated with this steep hydraulic gradient were given lower weights. Because of these lower weights and the inability of the model to simulate such a steep hydraulic gradient at a regional scale, a steep hydraulic gradient is simulated, but not as steep as observed. Heads are lower than observations to the north and higher than observations to the south (fig. F–46). A moderate hydraulic gradient on the western side of Yucca Mountain, likely associated with the Solitario Canyon fault (fig. F–46), was simulated by an HFB at the location of the fault. Although some pumping has

occurred periodically for water supply and tests associated with the hydrogeologic characterization of Yucca Mountain, little drawdown is observed at a regional scale.

Model Evaluation Summary

The evaluation of the DVRFS transient model described on the preceding pages indicates that the model simulates observed values reasonably well. The three-dimensional aspects of the flow system are simulated with downward hydraulic gradients in recharge areas and upward hydraulic gradients in discharge areas. Most wells are in discharge areas and as a result, observations and hydrographs are biased to show upward hydraulic gradients.

Pumping from both shallow and deeper layers of the model is imposed early in the transient simulation. Simulation of increased pumping, mostly from the shallow layers for stress periods corresponding to the 1950's and 1980's, resulted in local drawdown cones and reversals of hydraulic gradients. Since 1998, most of the pumpage has come from ground-water storage in the system. A small amount of flow comes from a decrease in discharge at ET areas and springs (mostly in Pahrump Valley). The model underestimates this decrease in natural discharge in Pahrump Valley.

Generally, the simulated boundary flows matched the estimated boundary flows well within their estimated error. Changes in flow across the model boundary segments are negligible, indicating that the effects of pumping have not reached the model boundary.

Evaluation of model fit on the basis of weighted residuals of heads and discharges reveals one or more types of model error: (1) large positive weighted residuals for some head observations in steep hydraulic-gradient areas indicate that simulated heads in these areas are significantly lower than the observations, (2) large negative weighted residuals for ground-water discharge rates in Death Valley indicate that the simulated discharge rate is greater than the observations, (3) large positive weighted residuals for ground-water discharge rates at Sarcobatus Flat indicate that the simulated discharge is smaller than the observations, and (4) positive weighted residuals for ground-water discharge rates in Pahrump Valley in the transient simulations indicate that the simulated discharge rates are greater than the observations.

Model Improvements

The transient model is based on up-to-date geologic and hydrogeologic framework models of the regional flow system. The models represent an intensive integration and synthesis of the available hydrogeologic data and interpretations for the DVRFS.

Data and Data Analysis

The DVRFS ground-water flow model described in this report reflects the current representation of hydrogeologic and hydrologic data for the region. This current understanding affects nearly every aspect of the flow system and improves the constraints on the conceptual and numerical flow models. Improvements in data and data analysis include:

- More detailed description and delineation of the basin-fill units over the entire DVRFS model domain, particularly in the Amargosa Desert,
- Increased understanding of the volcanic-rock stratigraphy at the NTS and Yucca Mountain based on recent drilling,
- Evaluation of recharge using surface-process modeling,
- More accurate and comprehensive measurement of natural ground-water discharge (ET and spring flow),
- More complete compilation and analysis of hydraulic-head and pumpage data, especially in areas not included in previous models, and
- Evaluation of boundary inflows and outflows, resulting in a more realistic depiction of the flow system than in previous conceptual models.

Model Construction and Calibration

In addition to advances in data collection, compilation, and analysis, the ways in which these data were applied in the modeling process also represent significant advances in simulating hydrogeologic systems. For example:

- The DVRFS model simulates transient, long-term regional-scale changes in hydraulic heads and discharges that result from pumpage.
- Using the HUF package allowed the HGUs to be defined independently of model layers, linking the HFM and the flow models more directly. This linkage facilitated testing many different conceptual models.

Model Limitations

All models are based on a limited amount of data and thus are necessarily simplifications of actual systems. Model limitations are a consequence of uncertainty in three basic aspects of the model, including inadequacies or inaccuracies in (1) observations used in the model, (2) representation of geologic complexity in the HFM, and (3) representation of the ground-water flow system in the flow model. It is important to understand how these characteristics limit the use of the model.

Observation Limitations

Observations of hydraulic-head and ground-water discharge, and estimates of boundary flows, constrain model calibration through parameter estimation. Uncertainty in these observations introduces uncertainty in the results of flow-model simulations. Although head and discharge observations were thoroughly analyzed prior to and throughout calibration, there was uncertainty regarding (1) the quality of the observation data, (2) appropriateness of the hydrogeologic interpretation, and (3) the representation of observations in the flow model.

Quality of Observations

The clustering of head observations limits the flow model because it results in the overemphasis of many observations in isolated areas, thus biasing those parts of the model. Outside the Yucca Mountain, NTS, Amargosa Desert, and Pahrump Valley areas, water-level data are sparse, both spatially and temporally. A method of better distributing weights for these situations would reduce model uncertainty.

Some hydraulic-head observations used in the steady-state calibration likely are affected by pumping. Many observations in agricultural areas represent measurements made in pumping wells. Because many of the wells in the Amargosa Desert and Pahrump Valley were drilled at the start of, or after, ground-water development, it is difficult to assess which of these observations best represents prepumping conditions.

The errors in estimates of the model boundary flow also affect the accuracy of the model. Any unknown, and thus unsimulated, flow diminishes model accuracy, and improving the boundary-flow estimates can reduce model uncertainty.

Interpretation of the Observations

It is difficult to assess whether certain head observations represent the regional saturated-zone or local perched-water conditions. Areas of steep hydraulic gradient, which are important features in the regional ground-water flow system, also may be an artifact of perched water levels. The uncertainty used to weight head observations in recharge areas commonly was increased because large head residuals indicated the possibility of perched water. Decreasing the number of observations, or reducing observation weights, increased model uncertainty. Further evaluation of potentially perched water levels in these areas may help to reduce model uncertainty.

Most discharge observations were computed on the basis of vegetated areas, and it is assumed that these areas are similar to their size prior to ground-water development. In some areas, such as Pahrump Valley, this assumption may not be entirely valid because local pumping already had lowered water levels and decreased the size of the discharge areas. The uncertainty in the discharge observations increases uncertainty in the flow model.

Representation of Observations

Because of the small distance affected and comparably large grid-cell size, simulating drawdowns near wells with small pumpage rates (less than 700 m^3/d) was difficult because the cones of depression are small relative to the size of the model grid. This limitation may be resolved by creating a higher resolution model, lowering the weights on the observations, or by removing these head-change observations from the model.

The altitude assigned to drains affected the ability of the model to simulate ground-water conditions accurately. The altitude of drains used to simulate discharge through ET and spring flow likely approximates the extinction depth for all discharge areas, particularly in areas with highly variable root depth of plants and discontinuous areas of capillary fringe. Penoyer Valley is an example of a discharge area that may have a zone of fairly extensive capillary effects contributing to ET. The observed heads are lower than the drain altitudes, and the Penoyer Valley drain, or any drain with similar relative heads, will not discharge if the heads are simulated accurately.

Incised drainages and other focused discharge areas are difficult to simulate accurately at a grid resolution of 1,500 m because in many cases, the hydraulic conductivity of the HGUs at the land surface controls the simulated discharge. In situations where this methodology does not control flow, a consistent method for assigning drain conductance needs to be used.

Hydrogeologic Framework Limitations

The accuracy of the ground-water flow model depends on the accuracy of the hydrogeologic conceptual model. Limitations exist in the ground-water flow model because of the difficulties inherent in the interpretation and representation of the complex geometry and spatial variability of hydrogeologic materials and structures in both the HFM and the flow model.

Complex Geometry

Geometric complexity of hydrogeologic materials and structures is apparent throughout the model domain. One notable example is the Las Vegas Valley Shear Zone (LVVSZ). Simulation of heads in this area is limited by the current understanding of fault-system geometry and the accuracy and resolution of its representation in the HFM and in the ground-water flow model.

Similarly, the steep hydraulic gradient that extends from the Groom Range through the Belted and Eleana Ranges to Yucca Mountain and the Bullfrog Hills is inadequately simulated because of an incomplete understanding of the complex geometries in this area. However, the steep hydraulic gradient also is simulated inadequately because of simplifications inherent in the HFM and ground-water flow model construction and discretization.

Complex Spatial Variability

The spatial variability of material properties of the HGUs and structures is represented to some degree in the model (Chapter B, this volume). Incorporating these features in the flow model substantially improved the simulation; however, the model remains a significantly simplified version of reality, resulting in imperfect matching of hydraulic gradients and heads affected by detailed stratigraphy not represented in the HFM. In the ground-water flow model, the assumption of homogeneity within a given HGU or hydraulic-conductivity zone removes the potential effects of smaller scale variability. A particularly noteworthy area where poor model fit exists is in the vicinity of Oasis Valley and the Bullfrog Hills. In this area, the observed effects of hydrothermal alteration are characterized incompletely by data and inadequately represented in the HFM and the ground-water flow model. Many of the inadequacies in the simulation of heads within the SWNVF are caused in part by the underrepresentation of local-scale hydrogeologic complexities in the HFM and the ground-water flow model.

Flow Model Limitations

Three basic limitations of the flow model are inherent in its construction. These inaccuracies are in (1) representation of the physical framework, (2) representation of the hydrologic conditions, and (3) representation of time.

Representation of Physical Framework

While the 1,500-m resolution of the flow model grid is appropriate to represent regional-scale conditions, higher resolution would improve simulation accuracy, particularly in areas of geologic complexity. The large grid cells tend to generalize important local-scale complexities that affect regional hydrologic conditions. To represent more local dynamics, smaller grid cells throughout the model (or local refinement around selected features or in critical areas in the model domain) would be required.

Representation of Hydrologic Conditions

The hydrologic conditions represented by the model are expressed as boundary conditions and include recharge, lateral boundary flows, discharge from ET and springs, and pumpage. Of these boundary conditions, the most significant is recharge. The main limitation in the representation of recharge is the inaccurate estimation of net infiltration that likely is owing in large part to the assumption that net infiltration results in regional recharge. The net-infiltration model likely overestimates recharge in many parts of the model domain because it is assumed that all infiltrating water that passes the root zone ultimately reaches the water table. This assumption ignores the possibility that infiltrating water could be intercepted and either diverted or perched by a lower permeability layer in the unsaturated zone, or the possibility of deep evaporation from the unsaturated zone. This limitation may be resolved by including in the flow model a means to account for deep, unsaturated zone processes that may act to reduce or redistribute infiltrating water.

Limitations in the definition of lateral boundary flow are the result of incomplete understanding of natural conditions. Because very little data exist in the areas defined as lateral flow-system boundary segments, all aspects of the assigned boundary conditions are poorly known. Despite these uncertainties, the data used to characterize these boundary flows have been thoroughly analyzed for this model. The model does not simulate the complex process of ET but accounts for the ground-water discharge attributed to ET through use of the Drain package for MODFLOW-2000. ET by native vegetation was studied extensively. Future revisions of the DVRFS model might be improved by using a more complex ET package instead of the Drain package. This package could incorporate spatially varying parameters to simulate direct recharge, soil moisture, and vegetative growth.

Representation of Time

The year-long stress periods simulated in the model limit its temporal applicability to dynamics that change over at least several years. Simulation of seasonal dynamics using shorter stress periods could be advantageous to account for the seasonal nature of irrigation pumpage. Such a simulation would require seasonal definition of hydrologic conditions.

Appropriate Uses of the Model

Because the DVRFS model was constructed to simulate regional-scale ground-water flow, it can be used to answer questions regarding ground-water flow issues at that scale. For example, interactions can be considered between hydraulic heads, discharge, pumping, and flow direction and magnitude on a regional scale.

The model can provide boundary conditions for the development of local-scale models, such as those being developed by the Department of Energy for both the NNSA/NSO and ORD programs. Consistency between regional and local models must be ensured. Advances in linking regional- and local-scale models may allow for simultaneous calibration and uncertainty analysis. Although regional scale by design, the DVRFS model includes many local-scale features and site-specific data. Local features include facies changes and pumpage from one or a few wells. In some circumstances the model could be used to evaluate the regional consequences of such local features. Yet, some regional consequences and all local consequences would be evaluated most effectively using local-scale models in combination with simulations from the regional model.

The model can be used to evaluate alternative conceptualizations of the hydrogeology that are likely to have a regional effect. These might include the effects of increased recharge caused by climate change, different interpretations of the extent or offset of faults, or other conceptual models of depositional environments that would affect the spatial variation of hydraulic properties.

The model also can be used to provide insight about contaminant transport. Flow direction and magnitude are appropriately represented using particle tracking methods as long as the particle paths are interpreted to represent regional, not local, conditions. The model may be a useful tool for evaluating advective-transport flow paths that are at least several times longer than the length of a 1,500-m model cell (Hill and others 2001; Tiedeman and others, 2003).

Increased urbanization in southern Nevada necessitates the development of ground-water resources. The model can be used for examining the effects of continued or increased pumpage on the regional ground-water flow system to effectively manage ground-water resources within conflicting land-use management policies.

Summary

The Death Valley regional ground-water flow system was simulated by a three-dimensional (3D) model that incorporates a nonlinear least-squares regression technique to estimate aquifer parameters. The model was constructed with MODFLOW-2000, a version of the U.S. Geological Survey 3D, finite-difference, modular ground-water flow model in which nonlinear regression may be used to estimate model parameters that result in the best fit to measured heads and discharges.

The model consists of 16 layers, on a finite-difference grid of 194 rows and 160 columns, and uniform, square model cells with a dimension of 1,500 meters (m) on each side. Model layers are simulated under confined flow conditions, so that the top of each layer and its thickness are defined. Although the top of the actual flow system is unconfined, the model accounts for the position of the simulated potentiometric surface in the top model layer to account for the thickness of the top layer and approximate unconfined flow conditions. Prepumping conditions were used as the initial conditions for the transient-state calibration of the model. Transmissivity is temporally constant and is spatially defined by hydrogeologic units (HGUs) and zones within some of these units. Storage properties were constant in time.

The model design was based on a 3D hydrogeologic framework model (HFM) that defines the physical geometry and composition of the surface and subsurface materials of 27 HGUs through which ground water flows. The HFM defines the geometry of the HGUs in the model domain (the area inside the model boundary).

Several conceptual models were evaluated during calibration to test the validity of various interpretations about the flow system. The evaluation focused on testing alternative hypotheses concerning (1) the location and type of flow system boundaries, (2) the definition of recharge areas, and (3) variations in interpretation of the hydrogeologic framework. For each conceptual model, a new set of parameters was estimated, and the resulting simulated hydraulic heads, drawdowns, ground-water discharges, and boundary flows were compared to observed values. Only those conceptual model changes contributing to a significant improvement in model fit were retained in the final calibrated model.

Ground-water flow into the model is from the simulation of infiltration of direct precipitation (recharge) and, to a lesser extent, from the simulation inflow across the model boundary. The distribution of simulated recharge varies spatially but is held at a constant rate for the entire simulation period. Ground-water flow out of the model primarily is through simulated ET, spring flow and pumping, and, to a lesser extent, by outflow across the model boundary. Observations of the combined discharge by ET and spring flow and estimated boundary flows were used to calibrate the model.

Boundary flows into and out of the model domain were simulated using head-dependent boundaries that were assigned the regional potentiometric surface altitude. Because previous models of the system generally used no-flow boundaries, the representation of inflow and outflow across the model boundary from adjacent systems are significantly different. In particular, ground-water flow from the north is simulated to sustain heads in the northern parts of the Nevada Test Site and, in particular, discharge around Sarcobatus Flat.

The final calibration was evaluated to assess the accuracy of simulated results by comparing measured and expected values with simulated values. The fit of simulated heads to observed hydraulic heads is generally good (residuals with absolute values less than 10 m) in most areas of nearly flat hydraulic gradients, and moderate (residuals with absolute values of 10 to 20 m) in the remainder of the areas of nearly flat hydraulic gradients. The poorest fit of simulated heads to observed hydraulic heads (residuals with absolute values greater than 20 m) is in steep hydraulic-gradient areas in the vicinity of Indian Springs, western Yucca Flat, and the southern Bullfrog Hills. Most of these inaccuracies can be attributed to (1) insufficient representation of the hydrogeology in the HFM, (2) misinterpretation of water levels, and (3) model error associated with grid cell size.

Ground-water discharge residuals are fairly random, with as many areas in which simulated discharges are less than observed discharges as areas in which simulated discharges are greater than observed. The largest unweighted ground-water discharge residuals are in Death Valley and Sarcobatus Flat (northeastern area). The two major discharge areas that contribute the largest volumetric error to the model are the Shoshone/Tecopa area and Death Valley. Positive

weighted residuals were computed in transient simulations of the Pahrump Valley that may indicate a poor definition of hydraulic properties and(or) discharge estimates, especially near Bennetts Spring.

Parameter values estimated by the regression analyses were reasonable—that is, within the range of expected values. As with any model, uncertainties and errors remain, but this model is considered an improvement on previous representations of the flow system.

The model is appropriate for evaluation of regional-scale processes. These include the assessment of boundary conditions of local-scale models, the evaluation of alternative conceptual models, the approximation of aspects of regional-scale advective transport of contaminants, and the analysis of the consequences of changed system stresses, such as those that would be imposed on the system by increasing pumpage.

Inherent limitations result from uncertainty in three basic aspects of the model: inadequacies or inaccuracies in observations used in the model, in the representation of geologic complexity in the HFM, and representation of the ground-water flow system in the flow model. It is important to understand how these characteristics limit the use of the model. These basic aspects of the model are represented at a regional scale, and the use of the model to address regional-scale issues or questions is the most appropriate use of the model.

References Cited

Anderman, E.R., and Hill, M.C., 2000, MODFLOW-2000, The U.S. Geological Survey modular ground-water flow model—Documentation of the hydrogeologic-unit flow (HUF) package: U.S. Geological Survey Open-File Report 00–342, 89 p.

Anderman, E.R., and Hill, M.C., 2003, MODFLOW-2000, The U.S. Geological Survey modular ground-water flow model—Three additions to the hydrogeologic-unit flow (HUF) package—Alternative storage for the uppermost active cells (STYP parameter type), flows in hydrogeologic units, and the hydraulic conductivity depth-dependence (KDEP) capability: U.S. Geological Survey Open-File Report 03–347, 36 p. Accessed April 14, 2004, at *http://water.usgs.gov/nrp/gwsoftware/modflow2000/modflow2000.html*

Anderman, E.R., Hill, M.C., and Poeter, E.P., 1996, Two-dimensional advective transport in ground-water flow parameter estimation: Ground Water, v. 34, no. 6, p. 1001–1009.

Anderson, M.P., and Woessner, W.W., 1992, Applied groundwater modeling—Simulation of flow and advective transport: San Diego, Calif., Academic Press, Inc., 381 p.

Bard, Jonathon, 1974, Nonlinear parameter estimation: New York, Academic Elsevier, 476 p.

Bedinger, M.S., Langer, W.H., and Reed, J.E., 1989, Groundwater hydrology, *in* Bedinger, M.S., Sargent, K.A., and Langer, W.H., eds., Studies of geology and hydrology in the Basin and Range Province, southwestern United States, for isolation of high-level radioactive waste—Characterization of the Death Valley region, Nevada and California: U.S. Geological Survey Professional Paper 1370–F, p. 28–35.

Belcher, W.R., Elliott, P.E., and Geldon, A.L., 2001, Hydraulic-property estimates for use with a transient ground-water flow model for the Death Valley regional ground-water flow system, Nevada and California: U.S. Geological Survey Water-Resources Investigations Report 01–4210, 28 p., accessed on September 1, 2004 at *http://water.usgs.gov/pubs/wri/wri014210/*

Cooley, R.L., and Naff, R.L., 1990, Regression modeling of ground-water flow: U.S. Geological Survey Techniques of Water-Resources Investigations, book 3, chap. B4, 232 p.

D'Agnese, F.A., Faunt, C.C., Turner, A.K., and Hill, M.C., 1997, Hydrogeologic evaluation and numerical simulation of the Death Valley regional ground-water flow system, Nevada and California: U.S. Geological Survey Water-Resources Investigations Report 96–4300, 124 p.

D'Agnese, F.A., Faunt, C.C., and Turner, A.K., 1998, An estimated potentiometric surface of the Death Valley region, Nevada and California, using geographic information systems and automated techniques: U.S. Geological Survey Water-Resources Investigations Report 97–4052, 15 p., 1 plate.

D'Agnese, F.A., O'Brien, G.M., Faunt, C.C., Belcher, W.R., and San Juan, Carma, 2002, A three-dimensional numerical model of prepumping conditions in the Death Valley regional ground-water flow system, Nevada and California: U.S. Geological Survey Water-Resources Investigations Report 02–4102, 114 p.

DeMeo, G.A., Laczniak, R.J., Boyd, R.A., Smith, J.L., and Nylund, W.E., 2003, Estimated ground-water discharge by evapotranspiration from Death Valley, California, 1997–2001: U.S. Geological Survey Water-Resources Investigations Report 03–4254, 27 p.

Fenelon, J.M., 2000, Quality assurance and analysis of water levels in wells on Pahute Mesa and vicinity, Nevada Test Site, Nye County, Nevada: U.S. Geological Survey Water-Resources Investigations Report 00–4014, 68 p.

Grasso, D.N., 1996, Hydrology of modern and late Holocene lakes, Death Valley, California: U.S. Geological Survey Water-Resources Investigations Report 95–4237, 53 p.

Halford, K.J., and Hanson, R.T., 2002, User guide for the drawdown-limited, multi-node well (MNW) package for the U.S. Geological Survey's modular three-dimensional finite-difference ground-water flow model, versions MODFLOW-96 and MODFLOW-2000: U.S. Geological Survey Open-File Report 02–293, 33 p.

Harbaugh, J.W., Banta, E.R., Hill, M.C., and McDonald, M.G., 2000, MODFLOW-2000, The U.S. Geological Survey's modular ground-water flow model—User guide to modularization concepts and the ground-water flow process: U.S. Geological Survey Open-File Report 00–92, 121 p.

Hevesi, J.A., Flint, A.L., and Flint, L.E., 2003, Simulation of net infiltration and potential recharge using a distributed parameter watershed model of the Death Valley region, Nevada and California: U.S. Geological Survey Water-Resources Investigations Report 03–4090, 91 p.

Hill, M.C., 1998, Methods and guidelines for effective model calibration: U.S. Geological Survey Water-Resources Investigations Report 98–4005, 90 p.

Hill, M.C., Banta, E.R., Harbaugh, A.W., and Anderman, E.R., 2000, MODFLOW-2000, The U.S. Geological Survey's modular ground-water flow model—User guide to the observation, sensitivity, and parameter-estimation procedures and three post-processing programs: U.S. Geological Survey Open-File Report 00–184, 209 p., accessed September 1, 2004, at *http://water.usgs.gov/nrp/gwsoftware/modflow2000/modflow2000.html*

Hill, M.C., Cooley, R.L., and Pollock, D.W., 1998, A controlled experiment in ground-water flow model calibration: Ground Water, v. 36, no. 3, p. 520–535.

Hill, M.C., Ely, M.D., Tiedeman, C.R., O'Brien, G.M., D'Agnese, F.A., and Faunt, C.C., 2001, Preliminary evaluation of the importance of existing hydraulic-head observation locations to advective-transport predictions, Death Valley regional flow system, California and Nevada: U.S. Geological Survey Water-Resources Investigations Report 00–4282, 82 p., accessed September 1, 2004, at *http://water.usgs.gov/pubs/wri/wri004282/*

Hill, M.C., and Tiedeman, C.R, 2003, Weighting observations in the context of calibrating ground-water models, *in* Kovar, Karel, and Zbynek, Hrkal, eds., Calibration and reliability in groundwater modeling, a few steps closer to reality: International Association Hydrological Sciences Publication 277, p. 196–203.

Hsieh, P.A., and Freckleton, J.R., 1993, Documentation of a computer program to simulate horizontal-flow barriers using the U.S. Geological Survey modular three-dimensional finite difference ground-water flow model: U.S. Geological Survey Open-File Report 92–477, 32 p.

IT Corporation, 1996, Underground Test Area subproject, Phase I data analysis task, volume IV, Hydrologic parameter data documentation package: Report ITLV/10972–181 prepared for the U.S. Department of Energy, 8 volumes, various pagination.

Laczniak, R.J., Smith, J.L., Elliott, P.E., DeMeo, G.A., Chatigyn, M.A., and Roemer, G.J., 2001, Ground-water discharge determined from estimates of evapotranspiration, Death Valley regional flow system, Nevada and California: U.S. Geological Survey Water-Resources Investigations Report 01–4195, 51 p.

Luckey, R.R., Tucci, Patrick, Faunt, C.C., Ervin, E.M., Steinkampf, W.C., D'Agnese, F.A., and Patterson, G.L., 1996, Status of understanding of the saturated-zone ground-water flow system at Yucca Mountain, Nevada as of 1995: U.S. Geological Survey Water-Resources Investigations Report 96–4077, 71 p.

Miller, G.A., 1977, Appraisal of the water resources of Death Valley, California-Nevada: U.S. Geological Survey Open-File Report 77–728, 68 p.

Moreo, M.T., Halford, K.J., La Camera, R.J., and Laczniak, R.J., 2003, Estimated ground-water withdrawals from the Death Valley regional flow system, 1913–1998, Nevada and California: U.S. Geological Survey Water-Resources Investigations Report 03–4245, 28 p.

Poeter, E.P. and Hill, M.C., 1997, Inverse modeling, a necessary next step in ground-water modeling: Ground Water, v. 35, no. 2, p. 250–260.

Potter, C.J., Sweetkind, D.S., Dickerson, R.P., Kilgore, M.L., 2002, Hydrostructural maps of the Death Valley regional flow system, Nevada and California: U.S. Geological Survey Miscellaneous Field Studies MF–2372, 2 sheets, 1:250,000 scale, 14 pages of explanatory text.

Prudic, D.E., Harrill, J.R., and Burbey, T.J., 1995, Conceptual evaluation of regional ground-water flow in the carbonate-rock province of the Great Basin, Nevada, Utah, and adjacent States: U.S. Geological Survey Professional Paper 1409–D, 102 p.

Rantz, S.E. (compiler), 1982, Measurement and computation of stream flow: U.S. Geological Survey Water-Supply Paper 2175, v. 1, p. 181–183.

Reiner, S.R., Laczniak, R.J., DeMeo, G.A., Smith, J.L., Elliott, P.E., Nylund, W.E., and Fridrich, C.J., 2002, Ground-water discharge determined from measurements of evapotranspiration, other available hydrologic components, and shallow water-level changes, Oasis Valley, Nye County, Nevada: U.S. Geological Survey Water-Resources Investigations Report 01–4239, 65 p.

Schaefer, D.H., and Harrill, J.R., 1995, Simulated effects of proposed ground-water pumping in 17 basins of east-central and southern Nevada: U.S. Geological Survey Water-Resources Investigations Report 95–4173, 71 p.

Sweetkind, D.S., and White, D.K, 2001, Facies analysis of Late Proterozoic through Lower Cambrian clastic rocks of the Death Valley regional ground-water system and surrounding areas, Nevada and California: U.S. Geological Survey Open-File Report 01–351, 13 p.

Thomas, J.M., Carlton, S.M., and Hines, L.B., 1989, Ground-water flow and simulated response to selected developmental alternatives in Smith Creek Valley, a hydrologically closed basin in Lander County, Nevada: U.S. Geological Survey Professional Paper 1409–E, 57 p.

Tiedeman, C.R., Hill, M.C., D'Agnese, F.A., and Faunt, C.C., 2003, Methods for using ground-water model predictions to guide hydrogeologic data collection with application to the Death Valley regional groundwater flow system: Water Resources Research, v. 39, no. 1, p. 5–1 to 5–17.

Van Denburgh, A.S., and Rush, F.E., 1974, Water-resources appraisal of Railroad and Penoyer Valleys, east-central Nevada: Nevada Department of Conservation and Natural Resources Ground-Water Resources—Reconnaissance Series Report 60, 61 p.

Waddell, R.K., 1982, Two-dimensional, steady-state model of ground-water flow, Nevada Test site and vicinity, Nevada-California: U.S. Geological Survey Water-Resources Investigations Report 84–4267, 72 p.

Regional Potential for Interbasin Flow of Ground Water

By M.S. Bedinger and J.R. Harrill

Appendix 1 of

Death Valley Regional Ground-Water Flow System, Nevada and California—Hydrogeologic Framework and Transient Ground-Water Flow Model

Edited by Wayne R. Belcher

Prepared in cooperation with the
U.S. Department of Energy
Office of Environmental Management, National Nuclear Security Administration, Nevada Site Office,
under Interagency Agreement DE–AI52–01NV13944, and
Office of Repository Development,
under Interagency Agreement DE–AI08–02RW12167

Scientific Investigations Report 2004–5205

U.S. Department of the Interior
U.S. Geological Survey

Contents

Figures

Tables

APPENDIX 1. Regional Potential for Interbasin Flow of Ground Water

By M.S. Bedinger and J.R. Harrill

Introduction

Quantitative analysis of regional and interbasin flows in the Death Valley regional ground-water flow system (DVRFS) region could be improved if hydraulic head values were available to develop a spatially interpolated contour map of the regional ground-water potential. Water-balance studies could be complemented and the direction of interbasin flows better discerned using such a contour map. The map could be used to delineate the areas outside the DVRFS model domain that contribute ground-water flow to the model, to estimate the regional hydraulic gradient on the lateral DVRFS model boundary, and to estimate the amount of flow by the Darcy method (Harrill and Bedinger, Appendix 2, this volume). The number of deep wells that can be measured, however, is insufficient for the spatial distribution of data points needed to map the regional potential of the DVRFS region. Because of the regional hydraulic continuity between deep and shallow flow in the DVRFS, additional data points for the regional ground-water potential can be inferred from flow-net relations with the shallow ground-water potential.

Regional Ground-Water Flow

The quantitative basis for regional ground-water flow in the Basin and Range physiographic province is grounded in the basin studies made under the U.S. Geological Survey and the State of Nevada cooperative ground-water program. Maxey and Eakin (1949), in attempting to quantify the available ground-water resources of basins, developed field methods for estimating basin recharge and discharge. They discovered, in evaluating ground-water budgets of closed basins, that many basins actually were not closed to ground-water transfer to or from adjacent basins. Early studies, such as those by Eakin and Winograd (1965), Eakin and Moore (1964), Mifflin (1968), Winograd and Thordarson (1975), and Mifflin and Hess (1979), recognized the importance of interbasin ground-water flow. In time, practically all basins in Nevada were studied, and estimates of recharge and discharge were established. Mifflin (1968) mapped the first set of regional potential contours from the surface altitudes of springs in Nevada issuing water at average temperatures of 27 degrees Celsius (80 degrees Fahrenheit) or greater, recognizing that thermal springs are surface manifestations of regional potential. Harrill and others (1988) used water-budget imbalances in their work in the Great Basin by showing arrows indicating interbasin flow and by mapping generalized contours of the regional ground-water potential in the Great Basin. Prudic and others (1995) used a digital model to analyze the regional aquifer system in the carbonate-rock province of Nevada, California, and adjacent States. This model simulated regional potential contours for both layers of the model and depicted regional flow potential from the higher basins in central Nevada to the terminal discharge areas of the Death Valley and the Colorado River regional ground-water flow systems.

Bredehoeft and others (1982) noted that the differences in topographic relief provide the principal driving force for regional flow. It follows that the potential for ground water to move from basin to basin is related to the relative altitudes of the individual basins. The DVRFS region is made up of a complex network of basins that range in altitude from greater than 3,400 m above sea level in the mountain recharge areas of Nevada and California to below sea level at the terminal discharge area at Death Valley in California (pl. 1). Many of the segments of the DVRFS model boundary are drawn along basin boundaries. For the most part, there are great altitude differences between these basins, indicating a difference in ground-water potential between adjacent basins. Where the rocks that form the boundary between such basins are sufficiently permeable, there will be flow into or out of the model area.

Identification of Regional Head

The number of wells deeper than 300 m that can be measured is insufficient to map the regional potential. A set of guidelines was developed that expresses relations between the regional ground-water potential and more readily observed surface and near-surface ground-water levels and hydrologic characteristics of ground-water basins. Topographic settings that express near-surface ground-water characteristics, such as shallow ground-water levels, recharge areas, discharging playas and phreatophyte areas, perennial streams and lakes,

and springs, can indicate that the regional potential is either greater than or less than the indicated altitude. These relations are broad generalizations; local geologic and hydrologic conditions can cause local variations in the applicability of the relations.

Examination of head and flow lines in several configurations of cross-sectional flow models (flow nets) of Freeze and Witherspoon (1967) and by Reed in Sargent and Bedinger (1985) is useful in visualizing the relations between regional potential and common topographic settings (figs. A1–1 and A1–2). Because there is regional hydraulic continuity between deep and shallow flow, the ground-water flow system has hydraulic heads at depth in the zone of regional flow that can be characterized by general relations to the hydraulic head in the upper part of the flow system (figs. A1–1 and A1–2). The general guidelines used for identifying regional head for mapping regional potential are:

1. The regional hydraulic head can be represented by shallow water levels in large areas of low topographic relief and virtually no recharge (fig. A1–1*A*).

2. The regional head is generally at or above areas of local discharge by evapotranspiration in basins (figs. A1–1*B* and A1–2*A*). The presence of regional springs at the lower altitudes in a basin indicates that the regional hydraulic head is higher than the basin-floor discharge areas. Deep regional springs are characteristically those that issue from depths well below the water table. Deep regional springs may issue from relatively great depths beneath the surface. Among the areas in Nevada exhibiting this characteristic are Railroad and Hot Creek Valleys; Columbus Marsh; Alkali Springs; Death, Pahrump, and Pahranagat Valleys; and Amargosa Desert; and in California, Deep Springs, Panamint, Saline, and Owens Valleys. Cross-sectional flow nets (fig. A1–2*B*) indicate that exceptions to this generalization may occur. Topographic, hydrologic, and geologic conditions in the Great Basin may indicate that a discharge area is above the regional potential.

3. The regional hydraulic head is above intermediate and terminal areas of regional discharge by evapotranspiration, regional springs, or ground-water discharge to major surface-water bodies, which are typically at lower altitudes in the flow system.

4. The regional hydraulic head is below the altitude of nondischarging dry playas. The regional head would be equal to or below the head in wells drilled to deep horizons beneath nondischarging basins.

5. The regional hydraulic head is lower than the water table in areas of recharge.

6. Shallow springs discharging at higher basin altitudes, well above the basin floors, generally are above the regional hydraulic head. They represent discharge from locally derived recharge and relatively short and shallow flow paths. These are commonly "cold" springs having temperatures near or only a few degrees above the ambient average air temperature.

7. Deep regional springs occur at the lower altitudes of basins, though commonly above the playa altitude. Deep regional springs, commonly originating from deep carbonate-rock aquifers, are typically large and the temperature of the water significantly greater than the ambient air temperature. These springs are inferred to represent discharge from deep and long flow paths.

These guidelines for identifying regional hydraulic head are supplemented by field observations of water-level measurements, springs, basin discharge areas, and intermediate and terminal discharge areas, coupled with concepts of how these near-surface hydrologic features are related to regional flow and potential. Specific hydrogeologic knowledge is used as control when applying the guidelines to a particular basin or set of basins. It is recognized that the general guidelines are drawn from flow nets computed for simplified geologic and hydrologic conditions. The control points may seem imprecise, but in designating the estimated regional potential "less than" and "greater than" the control potential, they provide a reasonable constraint on the estimate.

Regional Potential Map

The regional potential map (pl. 1) was constructed from a network of control points using water-level measurements and the guidelines given above (tables A1–1—A1–5). From a regional standpoint, these data points are well distributed and abundant. Water levels in wells for Nevada that are greater than 300 m deep are listed in table A1–1. The ground-water potential measured in these wells is assumed to be equal to or above the regional potential. Reference points for regional potential altitudes derived from surface-water features, ground-water levels, and topographic settings are listed in table A1–2 for California and table A1–3 for Nevada. As described in the guidelines, the regional potential is higher than the altitude of perennial surface-water features and higher than the water level of playas that discharge ground water by evapotranspiration. The regional potential is below valley floors of playas that do not discharge ground water by evapotranspiration. The altitudes of springs are listed in table A1–4 for California and table A1–5 for Nevada. The regional potential is above the altitude of regional springs and below the altitude of local springs. Most regional springs are thermal springs and discharge at low altitudes relative to valley floors. Local springs discharge well above the valley floors; their temperatures are cool, commonly no more than a few degrees above the average ambient air temperature. The reference points of tables A1–1 through A1–5 are plotted and identified by number on the regional potential map (pl. 1). The regional potential data were hand-contoured to produce the regional potential map shown on plate 1. The regional potential map then was used to estimate boundary flows for the DVRFS model (see Appendix 2, this volume).

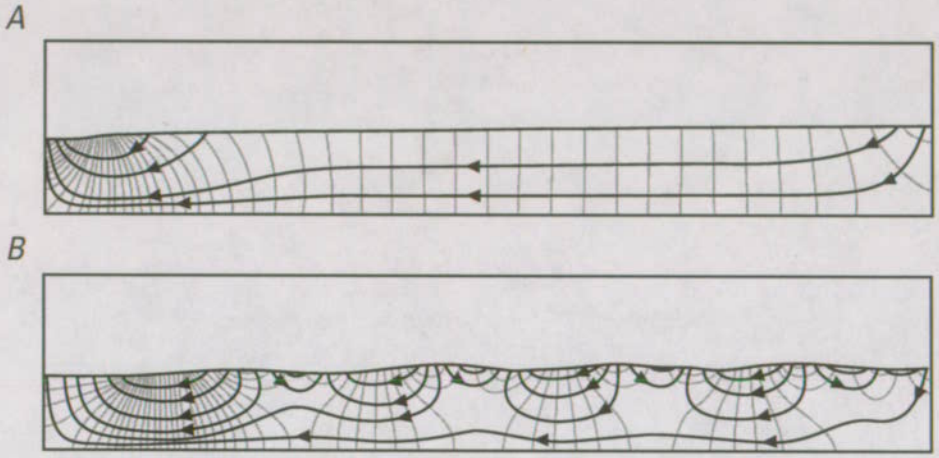

after Freeze and Witherspoon (1967)

Figure A1–1. Cross-sectional flow nets illustrating regional potential as represented by (*A*) shallow water levels in large areas of low topographic relief and (*B*) water levels at or above evapotranspiration areas.

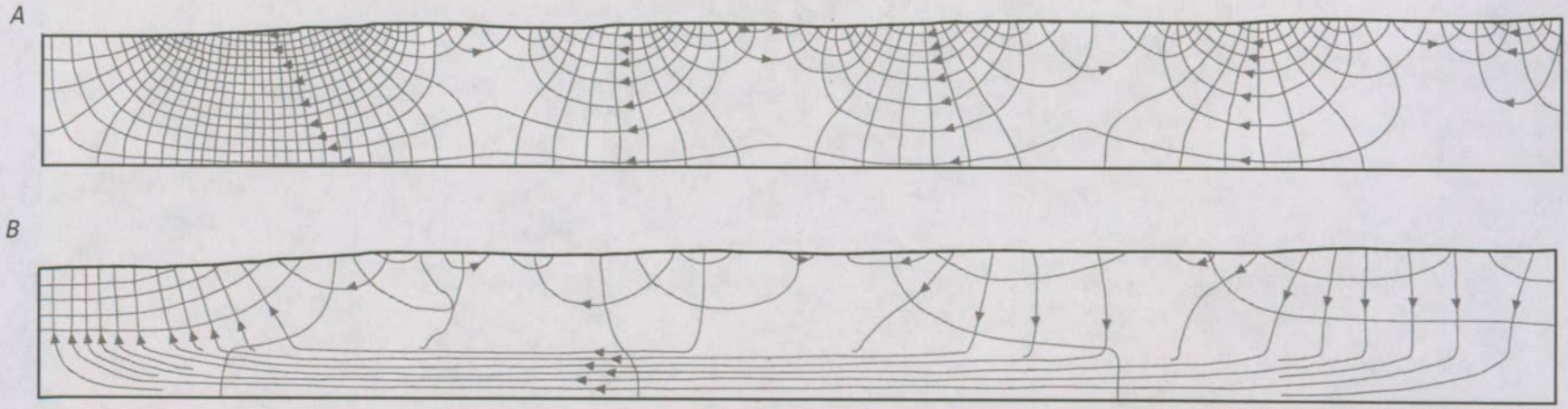

after Reed in Sargent and Bedinger (1985)

Figure A1–2. Cross-sectional flow nets illustrating regional potential as represented by (*A*) water levels at or above evapotranspiration areas and (*B*) water levels below discharge areas.

Table A1–1. Reference points for regional potential in wells deeper than 300 meters in Nevada.

[ID no, identification number; UTM, Universal Transverse Mercator projection, Zone 11, NAD27; vertical datum is NAVD88; --, no data; >, greater than]

Map ID no.	Well name[1]	UTM Easting (meters)	UTM Northing (meters)	Longitude	Latitude	Well depth (meters)	Land surface altitude (meters)	Date measured	Depth to water (meters)	Regional potential altitude (meters)	Reference
1	Army–6A	587780	4048190	116°01′08″	36°34′37″	382	1,050	1955	314	736	Harrill and Bedinger, 2000
3	Army–1	586128	4049310	116°02′14″	36°35′14″	593	961	10/15/87	239	722	Arteaga and others, 1991
5	TW–F	578870	4068350	116°06′59″	36°45′34″	1,036	1,263	01/14/86	529	734	Arteaga and others, 1991
6	TW–3	601939	4074020	115°51′26″	36°48′30″	565	1,060	01/11/80	337	723	Arteaga and others, 1991
7	UE25P#1	551501	4075660	116°25′21″	36°49′38″	1,805	1,114	10/12/84	362	752	Arteaga and others, 1991
8	MX CE–VF–2	682939	4082680	114°56′51″	36°52′27″	366	746	02/04/86	184	562	Berger and others, 1988
9	Well C	588208	4086130	116°00′35″	36°55′08″	518	1,195	10/18/75	471	725	Arteaga and others, 1991
10	Well C–1	588233	4086100	116°00′34″	36°55′07″	503	1,195	08/06/72	471	724	Arteaga and others, 1991
11	TW–D	582226	4103330	116°04′30″	37°04′28″	594	1,265	03/26/85	525	739	Arteaga and others, 1991
13	WW–2	581017	4113490	116°05′15″	37°09′58″	1,043	1,362	03/28/61	584	779	Arteaga and others, 1991
14	MX DL–DT–3	684597	4217900	114°53′42″	38°05′31″	730	1,643	02//1981	259	1,383	Bunch and Harrill, 1984
15	MX CV–DT–1	645075	4221640	115°20′41″	38°07′58″	560	1,695	04//1981	245	1,450	Bunch and Harrill, 1984
16	N7/55–28CA	605121	4254780	115°47′44″	38°26′13″	522	1,441	--	Flowing	>1,441	Van Denburgh and Rush, 1974
17	N7/56–2DAB	618772	4261440	115°38′17″	38°29′43″	3,085	1,435	--	Flowing	>1,435	Van Denburgh and Rush, 1974
18	MX SV–DT–2	686967	4310180	114°50′36″	38°55′21″	746	2,243	01//1981	130	2,195	Bunch and Harrill, 1984
19	Fad Shaft	587289	4373160	115°59′05″	39°30′20″	751	--	--	--	1,811	Thomas and others, 1986
21	SHV–1	685719	4047000	114°55′30″	36°33′08″	280	807	09/13/87	253	554	Berger and others, 1988
22	CC–1	646328	4048060	115°21′53″	36°34′07″	428	1,276	08/10/88	408	868	Schaefer and others, 1992
23	CF–2	539976	4071710	116°33′07″	36°47′32″	762	963	1985	184	779	Harrill and Bedinger, 2000
24	JF–1	554034	4078690	116°23′38″	36°51′16″	415	1,083	1991	354	729	Harrill and Bedinger, 2000
25	JF–2	553754	4075890	116°23′50″	36°49′45″	354	1,033	1984	304	729	Harrill and Bedinger, 2000
26	JF–2A	551501	4075660	116°25′21″	36°49′38″	1,805	1,114	1984	362	752	Harrill and Bedinger, 2000
27	J–11	563799	4071060	116°17′06″	36°47′06″	405	1,049	1960	317	732	Harrill and Bedinger, 2000
28	J–12	554444	4068770	116°23′24″	36°45′54″	347	953	1974	226	727	Harrill and Bedinger, 2000
29	J–13	562045	4073570	116°18′16″	36°48′28″	1,063	1,011	1964	283	728	Harrill and Bedinger, 2000
30	JF–3	554498	4067970	116°23′22″	36°45′28″	347	944	1992	216	728	Harrill and Bedinger, 2000
31	RV–1	562604	4054690	116°17′59″	36°38′15″	244	931	1972	206	725	Harrill and Bedinger, 2000
33	AD–1	536878	4060050	116°35′14″	36°41′14″	293	801	1986	82	719	Harrill and Bedinger, 2000
34	AD–2	553289	4055090	116°24′14″	36°38′30″	229	804	1987	99	706	Harrill and Bedinger, 2000
35	AD–6	569339	4023250	116°13′38″	36°21′13″	206	732	1967	12	720	Harrill and Bedinger, 2000
36	AD–10[2]	562652	4020760	116°18′07″	36°19′54″	332	668	1986 & 1987[3]	2	665	Harrill and Bedinger, 2000
37	AD–12	569353	4021430	116°13′38″	36°20′14″	482	741	1987	27	714	Harrill and Bedinger, 2000
39	MW–4	514842	4073270	116°50′01″	36°48′25″	360	927	1987	127	769	Harrill and Bedinger, 2000
40	MW–6	517461	4065140	116°48′16″	36°44′01″	573	829	1987	86	743	Harrill and Bedinger, 2000
41	MW–9	523893	4061950	116°43′57″	36°42′17″	579	824	1989	96	728	Harrill and Bedinger, 2000
42	CDH–61	516611	4081220	116°48′49″	36°52′43″	300	1,015	1988	208	806	Harrill and Bedinger, 2000
43	DR–1	641598	4046870	115°25′04″	36°33′31″	293	1,091	1989	249	842	Harrill and Bedinger, 2000

[1]From table 6 in Dettinger and others (1995).

[2]Well is in California.

[3]Average.

Table A1–2. Reference points for regional potential from topographic settings for California.

[ID no., identification number; UTM, Universal Transverse Mercator projection, Zone 11, NAD27; vertical datum is NAVD88; PLSS, Public Land Survey System section, township, range, S for San Bernardino principal meridian, M for Mount Diablo principal meridian; >, greater than; <, less than; ET, evapotranspiration; do., ditto; USGS, U.S. Geological Survey]

Map ID no.	UTM Easting (meters)	UTM Northing (meters)	Longitude	Latitude	Map feature	PLSS location	Regional potential altitude (meters)	Topographic setting	Reference
1	401523	3854800	118°04′37″	34°49′57″	Rosamond Lake	33/9N/11W/S	>686	Valley floor, ET	Langer and others, 1984
2	397454	3826990	118°07′05″	34°34′53″	Palmdale	24/6N/12W/S	<762	Basin floor, upper elevation	Langer and others, 1984
3	369461	3844170	118°25′33″	34°43′59″	Fairmont	38/8N/15W/S	<823	Basin floor, upper elevation	Langer and others, 1984
4	468547	3837260	117°20′36″	34°40′43″	Bryman	19/7N/4W/S	>762	Mojave River Valley	Langer and others, 1984
5	465701	3817710	117°22′25″	34°30′08″	US 395	21/5N/15W/S	<869	Basin floor, upper elevation	Langer and others, 1984
6	501275	3818660	116°59′10″	34°30′41″	Lucerne Lake	4/5N/1W/S	>853	Valley floor, ET	Langer and others, 1984
7	481403	3852290	117°12′12″	34°48′52″	Hodge	4/9N/3W/S	>701	Mojave River Valley	Langer and others, 1984
9	560494	3836420	116°20′23″	34°40′11″	Lavic Lake	27/7N/6E/S	>564	Valley floor, ET	Langer and others, 1984
10	564209	3843960	116°17′55″	34°44′15″	Lavic	36/8N/6E/S	>488	Basin floor, upper elevation	Langer and others, 1984
11	550940	3791700	116°26′48″	34°16′01″	W. of Landers	14/2N/5E/S	<914	Alluvial slope, upper elevation	Langer and others, 1984
12	620191	3778530	115°41′47″	34°08′33″	Dale Lake	25/1N/12E/S	>351	Valley floor, ET	Langer and others, 1984
13	668087	3792210	115°10′28″	34°15′33″	Danby Lake	14/2N/17E/S	>183	do.	Langer and others, 1984
14	643119	3798690	115°26′40″	34°19′17″	Cadiz Lake	18/3N/15E/S	>168	do.	Langer and others, 1984
15	616595	3816220	115°43′49″	34°28′58″	Bristol Lake	33/5N/12E/S	>183	do.	Langer and others, 1984
16	650701	3832430	115°21′22″	34°37′28″	Danby	7/6N/16E/S	<305	Valley floor, upper elevation	Langer and others, 1984
17	734426	3775900	114°27′32″	34°05′58″	Vidal	7/1S/24E/S	>91	Colorado River Valley	Langer and others, 1984
20	646170	3934510	115°23′15″	35°32′43″	Ivanpah Lake	5/16N/15E/S	<762	Valley floor, no ET	Langer and others, 1984
21	627938	3953550	115°35′08″	35°43′10″	Mesquite lake	4/18 1/2/13E/S	>777	Valley floor, ET	Langer and others, 1984
22	666065	3892450	115°10′36″	35°09′47″	Lanfair Valley	32/13N/17E/S	<1,067	Alluvial slope, upper elevation	Langer and others, 1984
24	590946	3987730	115°59′26″	36°01′54″	Pahrump Valley	22/22N/9E/S	>756	Valley floor, ET	Langer and others, 1984
25	496740	3899430	117°02′09″	35°14′23″	Superior Lake	2/31S/46E/M	<888	Valley floor, no ET	Langer and others, 1984
26	457298	3907320	117°28′11″	35°18′36″	Cuddeback Lake	22/30S/42E/M	<768	do.	Langer and others, 1984
27	420173	3910070	117°52′42″	35°19′57″	Koehn Lake	14/30S/38E/M	>578	Valley floor, ET	Langer and others, 1984
28	471517	3875660	117°18′44″	35°01′30″	Harper Lake	28/11N/4W/S	>579	do.	Langer and others, 1984
29	522392	3879160	116°45′16″	35°03′24″	Coyote Lake	10/11N/2E/S	>518	do.	Langer and others, 1984
31	418332	3940710	117°54′06″	35°36′31″	Freeman Junction	8/27S/38E/M	<762	Alluvial slope, upper elevation	Langer and others, 1984
32	423312	3866140	117°50′23″	34°56′12″	Rogers Lake	4/9N/9W/S	<686	Valley floor, no ET	Langer and others, 1984
33	440198	3825480	117°39′07″	34°34′16″	El Mirage	32/6N/7W/S	<884	Alluvial slope, upper elevation	Langer and others, 1984
34	442238	3866070	117°37′57″	34°56′14″	Kramer Junction	30/10N/7W/S	<762	do.	Langer and others, 1984

Table A1–2. Reference points for regional potential from topographic settings for California.—Continued

[ID no., identification number; UTM, Universal Transverse Mercator projection, Zone 11, NAD27; vertical datum is NAVD88; PLSS, Public Land Survey System section, township, range, S for San Bernardino principal meridian, M for Mount Diablo principal meridian; >, greater than; <, less than; ET, evapotranspiration; do., ditto; USGS, U.S. Geological Survey]

Map ID no.	UTM Easting (meters)	UTM Northing (meters)	Longitude	Latitude	Map feature	PLSS location	Regional potential altitude (meters)	Topographic setting	Reference
35	555729	3812050	116°23′36″	34°27′01″	Emerson Lake	7/4N/6E/S	<680	Valley floor, no ET	Langer and others, 1984
36	469096	3952440	117°20′30″	35°43′02″	Searles Lake	34/19N/43W/S	>493	Valley floor, ET	Langer and others, 1984
38	426780	4062100	117°49′11″	36°42′13″	Saline Lake	26/14S/38W/M	>323	do.	Langer and others, 1984
40	391880	4073260	118°12′43″	36°48′03″	Kearsarge	19/13S/35W/M	>1,189	Owens River Valley	Langer and others, 1984
41	419373	4148770	117°54′43″	37°29′03″	Oasis	27/5S/37E/M	>1,524	Valley floor, ET	Langer and others, 1984
42	355143	4196840	118°38′52″	37°54′34″	Adobe Valley	10/1N/30E/M	>1,951	do.	USGS topographic map
43	325311	4208220	118°59′23″	38°00′24″	Mono Lake	27/2N/27E/M	>1,952	Lake	USGS topographic map
44	520769	4009500	116°46′08″	36°13′55″	Badwater	33/19S/2E/S	>–71	Valley floor, ET	USGS topographic map
51	512341	4002580	116°51′46″	36°10′11″	Bennetts Well	22/20S/1E/S	>–40	do.	USGS topographic map
52	531346	4025210	116°39′02″	36°22′24″	Travertine Point	21/26N/3E/S	<649	Valley, no ET	National Park Service files
54	539387	4015970	116°33′41″	36°17′23″	AD–13	21/25N/4E/S	<710	Valley, upper elevation	National Park Service files
58	487675	4066300	117°08′17″	36°44′39″	Midway Well	18/14S/45E/M	>21	Valley floor, discharging well	National Park Service files
63	449418	4059320	117°33′58″	36°40′48″	Racetrack Playa	31/14S/41E/M	<1,119	Valley floor, no ET	USGS topographic map
64	598836	3777790	115°55′41″	34°08′17″	Twentynine Palms	27/1N/10E/S	<457	Valley, upper elevation	Langer and others, 1984
65	550675	3774390	116°27′02″	34°06′39″	Yucca Valley	3/1S/5E/S	<945	Valley floor, upper elevation	Langer and others, 1984
66	581031	3842580	116°06′54″	34°43′26″	Ludlow	2/7N/8E/S	<305	do.	Langer and others, 1984
67	662700	3849710	115°13′19″	34°46′42″	Essex	29/8N/17E/S	<457	do.	Langer and others, 1984
68	673121	3867460	115°06′16″	34°56′12″	Goffs	23/10N/18E/S	<610	do.	Langer and others, 1984
69	625306	3876970	115°37′35″	35°01′46″	Kelso	29/11N/13E/S	<518	do.	Langer and others, 1984
70	345781	4170400	118°44′55″	37°40′11″	Crowley Lake	22/3N/29E/M	>2,063	Stream level	Langer and others, 1984

Table A1–3. Reference points for regional potential from topographic settings for Nevada.

[ID no., identification number; UTM, Universal Transverse Mercator projection, Zone 11, NAD27; vertical datum is NAVD88; PLSS, Public Land Survey System section, township, range; >, greater than; <, less than; ET, evapotranspiration; do., ditto; USGS, U.S. Geological Survey]

Map ID no.	UTM Easting (meters)	UTM Northing (meters)	Longitude	Latitude	Map feature	PLSS location	Regional potential altitude (meters)	Topographic setting	Reference
1	686348	3921450	114°56′51″	35°25′15″	Searchlight	16/29S/63E	<914	Valley floor, no ET	Bedinger and others, 1984
2	687256	3914190	114°56′21″	35°21′19″	Searchlight	3/30S/63E	<701	do.	Bedinger and others, 1984
3	685866	3980440	114°56′21″	35°57′09″	Boulder City	11/23S/63E	<457	do.	Bedinger and others, 1984
4	658416	3961130	115°14′50″	35°46′60″	Jean Lake	10/25S/60E	<744	do.	Thomas and others, 1986
5	626984	3963990	115°35′40″	35°48′49″	Sandy	33/24S/57E	<792	do.	Thomas and others, 1986
6	658964	3986450	115°14′10″	36°00′41″	Arden	26/22S/60E	<671	do.	Bedinger and others, 1984
7	702843	3998640	114°44′47″	36°06′47″	Lake Mead	18/21S/65E	>372	Lake level	USGS topographic map
8	677568	3995350	115°01′40″	36°05′18″	East Las Vegas	26/21S/62E	<488	Valley floor, no ET	Bedinger and others, 1984
9	691971	4036560	114°51′28″	36°27′25″	Dry Lake	17/17S/64E	<549	do.	Bedinger and others, 1984
10	704373	4039870	114°43′07″	36°29′03″	California Wash	3/17S/65E	<518	do.	Bedinger and others, 1984
11	724452	4054930	114°29′25″	36°36′55″	Logan Dale	21/15S/67E	>427	Valley floor, ET	Bedinger and others, 1984
12	716330	4060520	114°34′46″	36°40′03″	Moapa	35/14S/66E	>457	do.	Bedinger and others, 1984
13	585629	4006750	116°02′51″	36°12′13″	Pahrump	20/20S/53E	>792	do.	Bedinger and others, 1984
14	652338	4017370	115°18′13″	36°17′28″	Hwy 99 -1	7/19S/60E	<732	Valley floor, no ET	Bedinger and others, 1984
15	644548	4028120	115°23′18″	36°23′21″	Hwy 99 - 2	17/18S/59E	<823	do.	Bedinger and others, 1984
16	639560	4036050	115°26′33″	36°27′41″	Hwy 99 - 3	23/17S/58E	<884	do.	Bedinger and others, 1984
17	754715	4073360	114°08′46″	36°46′25″	Bunkerville	26/13S/70E	>457	Virgin River	Bedinger and others, 1984
18	708321	4072100	114°39′57″	36°46′25″	Rox	26/12S/65E	>549	Meadow Valley Wash	Bedinger and others, 1984
19	657156	4086570	115°14′09″	36°54′50″	DDL–2	10/12S/60E	<924	Valley floor, no ET	Schaefer and others, 1992
20	660051	4091900	115°12′08″	36°57′41″	DDL–1	24/11S/60E	<929	do.	Schaefer and others, 1992
21	688985	4073710	114°52′55″	36°47′32″	Arrow Canyon	25/13S/63E	<555	do.	Schaefer and others, 1992
22	616614	4048290	115°41′48″	36°34′29″	Indian Springs	7/16S/56E	<975	Valley margin	Bedinger and others, 1984
24	643155	4044460	115°24′03″	36°32′12″	SBH-1	23/16S/58E	<882	do.	Schaefer and others, 1992
25	588923	4091130	116°00′04″	36°57′50″	Yucca Lake	24/11S/54E	<701	Valley floor, no ET	Bedinger and others, 1984
26	553211	4051670	116°24′18″	36°36′39″	Lathrop Wells	25/15S/49E	<701	do.	Bedinger and others, 1984
28	552095	4030830	116°25′08″	36°25′23″	Longstreet	35/17S/49E	<655	do.	Thomas and others, 1986
29	595439	4074620	115°55′48″	36°48′52″	Frenchman Flat	8/13S/54E	<732	do.	Thomas and others, 1986
30	584841	4103540	116°02′44″	37°04′34″	Yucca Flat	10/10S/53E	<732	do.	Thomas and others, 1986
31	521524	4086650	116°45′30″	36°55′39″	Beatty	7/12S/47E	>1,006	Amargosa River	Bedinger and others, 1984
32	522034	4080650	116°45′10″	36°52′24″	Beatty	19/12S/47E	>914	do.	Bedinger and others, 1984
33	529083	4068130	116°40′27″	36°45′37″	Beatty	36/13S/47E	<732	Valley floor, no ET	Bedinger and others, 1984
34	519285	4102730	116°46′59″	37°04′21″	Beatty	12/10S/46E	<1,189	do.	Bedinger and others, 1984
35	502761	4116490	116°58′08″	37°11′48″	Sarcobatus Flat	36/8S/44E	>1,204	Valley floor, ET	Bedinger and others, 1984
36	487959	4143120	117°08′10″	37°26′12″	Lida Valley	10/6S/43E	>1,311	do.	Bedinger and others, 1984

Table A1–3. Reference points for regional potential from topographic settings for Nevada.—Continued

[ID no., identification number; UTM, Universal Transverse Mercator projection, Zone 11, NAD27; vertical datum is NAVD88; PLSS, Public Land Survey System section, township, range; >, greater than; <, less than; ET, evapotranspiration; do., ditto; USGS, U.S. Geological Survey]

Map ID no.	UTM Easting (meters)	UTM Northing (meters)	Longitude	Latitude	Map feature	PLSS location	Regional potential altitude (meters)	Topographic setting	Reference
37	542166	4124390	116°31′28″	37°16′01″	Pahute Mesa	5/8S/49E	<1,280	Upland	Bedinger and others, 1984
38	551182	4132240	116°25′20″	37°20′14″	Pahute Mesa	4/7S/50E	<1,372	do.	Bedinger and others, 1984
39	608980	4127520	115°46′14″	37°17′23″	Groom Lake	31/7S/55 1/2E	<1,067	Valley floor, no ET	Bedinger and others, 1984
40	591715	4138840	115°57′50″	37°23′37″	Groom Lake	21/6S/54E	<1,341	do.	Bedinger and others, 1984
41	656156	4157370	115°13′56″	37°33′07″	Hiko	34/4S/60E	>1,158	White River	Bedinger and others, 1984
42	662520	4139420	115°09′51″	37°23′21″	Alamo	32/6S/61E	>1,067	do.	Bedinger and others, 1984
43	667563	4125960	115°06′37″	37°16′01″	Pahranagat Lakes	11/8S/61E	>1,006	do.	Bedinger and others, 1984
44	678395	4090260	114°59′48″	36°56′36″	Coyote Springs Valley	32/11S/63E	<770	Valley floor, no ET	Bedinger and others, 1984
45	677960	4101560	114°59′56″	37°02′43″	Coyote Springs Valley	31/10S/62E	<788	do.	Bedinger and others, 1984
46	686730	4087170	114°54′14″	36°54′50″	Coyote Springs Valley	10/12S/63E	<566	do.	Bedinger and others, 1984
47	723861	4111200	114°28′49″	37°07′20″	Meadow Valley Wash	?/9S/67E	>792	Stream	Bedinger and others, 1984
48	724410	4128550	114°28′08″	37°16′42″	Meadow Valley Wash	3/8S/67E	>853	do.	Bedinger and others, 1984
49	719206	4136180	114°31′31″	37°20′54″	Meadow Valley Wash	7/7S/67E	>1,036	do.	Bedinger and others, 1984
50	714557	4149390	114°34′26″	37°28′06″	Meadow Valley Wash	34/5S/66E	>1,189	do.	Bedinger and others, 1984
51	717965	4163790	114°31′52″	37°35′50″	Meadow Valley Wash	18/4S/67E	>1,311	do.	Bedinger and others, 1984
52	728802	4185460	114°24′06″	37°47′23″	Meadow Valley Wash	7/2S/68E	>1,433	do.	Bedinger and others, 1984
53	728250	4205280	114°24′06″	37°58′06″	Patterson Valley	1/1N/69E	<1,646	Valley floor, no ET	Bedinger and others, 1984
54	744990	4147200	114°13′51″	37°26′28″	Dry Valley Wash	21/1N/69E	<1,646	do.	Bedinger and others, 1984
55	762018	4119580	114°02′54″	37°11′16″	Bull Valley Wash	4/9S/71E	<945	do.	Bedinger and others, 1984
56	755771	4126920	114°06′58″	37°15′20″	Bull Valley Wash	13/8S/71E	<1,128	do.	Bedinger and others, 1984
57	694815	4174530	114°47′25″	37°41′57″	Dry Lake Valley	10/3S/64E	<1,280	do.	Bedinger and others, 1984
58	694789	4200410	114°47′01″	37°55′56″	Dry Lake Valley	22/1N/64E	<1,311	do.	Bedinger and others, 1984
59	610275	4167200	115°45′00″	37°38′50″	Sand Springs Valley	36/3S/55E	>1,448	Valley floor, ET	Bedinger and others, 1984
60	612604	4194090	115°43′10″	37°53′21″	Sand Springs Valley	31/1S/56E	<1,448	do.	Bedinger and others, 1984
61	511895	4193660	116°51′53″	37°53′32″	Stone Cabin Valley	31/1N/46E	<1,585	Valley floor, no ET	Bedinger and others, 1984
62	519848	4197590	116°46′27″	37°55′39″	Stone Cabin Valley	30/1N/47E	<1,615	do.	Bedinger and others, 1984
63	531195	4205150	116°38′41″	37°59′43″	Stone Cabin Valley	30/2N/48E	<1,646	do.	Bedinger and others, 1984
64	478773	4192850	117°14′29″	37°53′05″	Alkali Valley	2/1S/42E	>1,463	Valley floor, ET	Bedinger and others, 1984
65	468250	4187860	117°21′39″	37°50′22″	Alkali Valley	15/1S/41E	>1,463	do.	Bedinger and others, 1984
66	463040	4192380	117°25′13″	37°52′48″	Alkali Valley	6/1S/41E	>1,463	do.	Bedinger and others, 1984
67	443938	4178430	117°38′11″	37°45′12″	Clayton Valley	22/2S/39E	>1,311	do.	Bedinger and others, 1984
68	450293	4177160	117°33′51″	37°44′32″	Clayton Valley	29/2S/40E	>1,311	do.	Bedinger and others, 1984
69	455229	4184650	117°30′31″	37°48′36″	Clayton Valley	35/1S/40E	>1,311	do.	Bedinger and others, 1984
71	412964	4160640	117°59′09″	37°35′26″	Fish Lake Valley	20/4S/36E	>1,494	do.	Bedinger and others, 1984

Table A1–3. Reference points for regional potential from topographic settings for Nevada.—Continued

[ID no., identification number; UTM, Universal Transverse Mercator projection, Zone 11, NAD27; vertical datum is NAVD88; PLSS, Public Land Survey System section, township, range; >, greater than; <, less than; ET, evapotranspiration; do., ditto; USGS, U.S. Geological Survey]

Map ID no.	UTM Easting (meters)	UTM Northing (meters)	Longitude	Latitude	Map feature	PLSS location	Regional potential altitude (meters)	Topographic setting	Reference
72	407077	4171490	118°03′14″	37°41′16″	Fish Lake Valley	11/3S/35E	>1,463	Valley floor, ET	Bedinger and others, 1984
73	412240	4187060	117°59′50″	37°49′43″	Fish Lake Valley	20/1S/36E	>1,433	do.	Bedinger and others, 1984
74	414398	4201770	117°58′28″	37°57′41″	Fish Lake Valley	7/1N/36E	>1,433	do.	Bedinger and others, 1984
75	361486	4219330	118°34′48″	38°06′47″	Huntoon Valley	13/3N/30E	>1,695	do.	Bedinger and others, 1984
76	367284	4226790	118°30′55″	38°10′52″	Huntoon Valley	27/4N/31E	>1,695	do.	Bedinger and others, 1984
77	377944	4230140	118°23′39″	38°12′46″	Teels Marsh	10/4N/32E	>1,509	do.	Bedinger and others, 1984
78	386376	4225980	118°17′50″	38°10′35″	Teels Marsh	27/4N/33E	>1,509	do.	Bedinger and others, 1984
79	422549	4211990	117°52′58″	38°03′15″	Columbus Salt Marsh	8/2N/37E	>1,387	do.	Bedinger and others, 1984
80	414117	4221380	117°58′48″	38°08′17″	Columbus Salt Marsh	8/3N/36E	>1,387	do.	Bedinger and others, 1984
81	455180	4220160	117°30′41″	38°07′48″	Big Smoky Valley	8/3N/40E	>1,460	do.	Bedinger and others, 1984
83	427638	4244180	117°49′41″	38°20′41″	Dry Lake	35/6N/37E	>1,600	do.	Bedinger and others, 1984
84	483003	4275930	117°11′43″	38°38′01″	Big Smoky Valley	18/9N/43E	<1,737	Valley floor, no ET	Bedinger and others, 1984
85	466012	4248770	117°23′21″	38°23′18″	Big Smoky Valley	8/6N/41E	>1,524	do.	Bedinger and others, 1984
86	476943	4261860	117°15′52″	38°30′24″	Big Smoky Valley	33/8N/42E	>1,676	do.	Bedinger and others, 1984
87	492110	4192420	117°05′23″	37°52′52″	Mud Lake	6/1S/44E	<1,524	do.	Bedinger and others, 1984
88	492948	4229710	117°04′50″	38°13′02″	Ralston Valley	8/4N/44E	>1,737	Valley floor, ET	Bedinger and others, 1984
89	495725	4238500	117°02′56″	38°17′47″	Ralston Valley	15/5N/44E	>1,768	do.	Bedinger and others, 1984
90	503150	4257080	116°57′50″	38°27′50″	Ralston Valley	17/7N/45E	<1,859	Valley floor, high altitude	Bedinger and others, 1984
91	506512	4265400	116°55′31″	38°32′20″	Ralston Valley	16/8N/45E	<1.981	do.	Bedinger and others, 1984
92	520487	4281950	116°45′52″	38°41′16″	Monitor Valley	23/10N/46E	>2,103	do.	Bedinger and others, 1984
93	529243	4171020	116°40′06″	37°41′16″	Cactus Flat	15/1S/47E	<1,625	Valley floor, no ET	USGS topographic map
94	523634	4188320	116°43′53″	37°50′38″	Cactus Flat	12/3S/47E	<1,634	do.	USGS topographic map
95	553229	4150800	116°23′52″	37°30′16″	Gold Flat	16/5S/50E	<1,539	do.	USGS topographic map
96	568625	4150670	116°13′25″	37°30′08″	Kawich Valley	19/5S/52E	<1,621	do.	USGS topographic map
97	535811	4220540	116°35′29″	38°08′02″	Stone Cabin Valley	3/3N/48E	>1,676	Valley floor, ET	Bedinger and others, 1984
98	534485	4228980	116°36′22″	38°12′36″	Stone Cabin Valley	9/4N/48E	>1,707	do.	Bedinger and others, 1984
99	570284	4229000	116°11′50″	38°12′29″	Hot Creek Valley	13/4N/51E	>1,570	do.	Bedinger and others, 1984
100	565871	4248290	116°14′45″	38°22′56″	Hot Creek Valley	9/6N/51E	>1,585	do.	Bedinger and others, 1984
101	556791	4262800	116°20′55″	38°30′49″	Hot Creek Valley	33/8N/50E	>1,646	do.	Bedinger and others, 1984
102	583072	4274310	116°02′45″	38°36′55″	Big Sand Springs Valley	29/9N/53E	<1,631	Valley floor, no ET	Bedinger and others, 1984
103	590212	4282430	115°57′46″	38°41′16″	Big Sand Springs Valley	29/9N/53E	>1,585	do.	Bedinger and others, 1984
104	618922	4275780	115°38′02″	38°37′28″	Railroad Valley	24/9N/56E	>1,448	Valley floor, ET	Bedinger and others, 1984
105	604260	4244440	115°48′25″	38°20′38″	Railroad Valley	29/6N/55E	>1,448	do.	Bedinger and others, 1984
106	611163	4315100	115°43′00″	38°58′47″	Railroad Valley	7/13N, 56E	<1,676	Valley floor, high altitude	Bedinger and others, 1984

Table A1–3. Reference points for regional potential from topographic settings for Nevada.—Continued

[ID no., identification number; UTM, Universal Transverse Mercator projection, Zone 11, NAD27; vertical datum is NAVD88; PLSS, Public Land Survey System section, township, range; >, greater than; <, less than; ET, evapotranspiration; do., ditto; USGS, U.S. Geological Survey]

Map ID no.	UTM Easting (meters)	UTM Northing (meters)	Longitude	Latitude	Map feature	PLSS location	Regional potential altitude (meters)	Topographic setting	Reference
107	595769	4237800	115°54′18″	38°17′06″	Railroad Valley	22/5N/54E	>1,463	Valley floor, ET	Bedinger and others, 1984
108	607972	4231940	115°45′59″	38°13′51″	Railroad Valley	11/4N/55E	>1,463	do.	Bedinger and others, 1984
109	620441	4296890	115°36′46″	38°48′52″	Railroad Valley	18/11N/57E	>1,494	do.	Bedinger and others, 1984
110	633181	4216250	115°28′53″	38°05′10″	Garden Valley	32/3N/58E	<1,554	Valley floor, no ET	Bedinger and others, 1984
111	642084	4235270	115°22′34″	38°15′22″	Garden Valley	32/5N/59E	<1,615	do.	Bedinger and others, 1984
112	646271	4186010	115°20′18″	37°48′42″	Coal Valley	34/1S/59E	<1,305	do.	Thomas and others, 1986
113	656150	4214380	115°13′12″	38°03′56″	Coal Valley	3/2N/60E	>1,579	do.	Thomas and others, 1986
114	646558	4194620	115°19′60″	37°53′21″	Coal Valley	2/1S/59E	>1,500	do.	USGS topographic map
115	693529	4216450	114°47′37″	38°04′37″	Dry Lake Valley	34/3N/64E	<1,341	do.	Bedinger and others, 1984
116	679555	4211100	114°57′15″	38°01′54″	White River	18/2N/63E	>1,311	White River	Bedinger and others, 1984
117	677734	4214080	114°58′27″	38°03′32″	White River	2/2N/62E	>1,402	do.	Bedinger and others, 1984
118	669492	4223430	115°03′57″	38°08′41″	White River	7/3N/62E	<1,494	White River, no discharge	Bedinger and others, 1984
120	660481	4244340	115°09′50″	38°20′05″	White River	31/6N/61E	>1,554	White River	Bedinger and others, 1984
121	665909	4259100	115°05′54″	38°27′60″	White River	3/7N/61E	>1,585	do.	Bedinger and others, 1984
122	665484	4279630	115°05′54″	38°39′06″	White River	9/9N/61E	>1,615	do.	Bedinger and others, 1984
123	667978	4293250	115°03′59″	38°46′26″	White River	36/11N/61E	>1,646	do.	Bedinger and others, 1984
124	668775	4302310	115°03′18″	38°51′19″	White River	31/12N/62E	>1,676	do.	Bedinger and others, 1984
125	687817	4255510	114°50′54″	38°25′48″	Cave Valley	25/7N/63E	<1,737	Valley floor, no ET	Bedinger and others, 1984
126	691828	4272420	114°47′52″	38°34′53″	Cave Valley	4/8N/64E	<1,829	do.	Bedinger and others, 1984
127	686997	4285380	114°50′59″	38°41′57″	Cave Valley	25/10N/63E	<2,012	do.	Bedinger and others, 1984
128	711983	4244540	114°34′30″	38°19′33″	Lake Valley	4/5N/66E	>1,798	do.	Bedinger and others, 1984
129	710269	4280190	114°35′02″	38°38′50″	Lake Valley	9/9N/66E	>1,798	do.	Bedinger and others, 1984
130	720197	4294780	114°27′55″	38°46′34″	Spring Valley	33/11N/67E	>1,753	do.	Bedinger and others, 1984
131	753440	4292500	114°05′02″	38°44′48″	Snake Valley	11/10N/70E	>1,676	do.	Bedinger and others, 1984
132	581776	4206020	116°04′07″	38°00′00″	Railroad Valley	30/2N/53E	>1,463	do.	Bedinger and others, 1984
133	587801	4206080	116°00′00″	38°00′00″	Railroad Valley	27/2N/53E	>1,463	do.	Bedinger and others, 1984
134	437425	4284940	117°43′11″	38°42′46″	Ione Valley	21/10N/38E	<1,768	do.	Bedinger and others, 1984
135	440274	4294450	117°41′16″	38°47′55″	Ione Valley	22/11N/38E	<1,798	do.	Bedinger and others, 1984
136	442397	4310980	117°39′53″	38°56′52″	Ione Valley	11/12N/38E	<1,829	do.	Bedinger and others, 1984
137	420242	4303160	117°55′10″	38°52′32″	Gabbs Valley	27/12N/36E	>1,372	Valley floor, ET	Bedinger and others, 1984
138	396366	4307450	118°11′43″	38°54′42″	Gabbs Valley	7/12N/34E	>1,265	do.	Bedinger and others, 1984
139	401072	4257570	118°08′02″	38°27′46″	Soda Spring Valley	13/7N/34E	>1,340	do.	Bedinger and others, 1984
140	403676	4236050	118°06′04″	38°16′09″	Rhodes Salt Marsh	28/5N/35E	>1,340	do.	Bedinger and others, 1984
141	487186	4291210	117°08′51″	38°46′17″	Big Smoky Valley	33/11N/43E	>1,707	do.	Bedinger and others, 1984

Table A1–3. Reference points for regional potential from topographic settings for Nevada.—Continued

[ID no., identification number; UTM, Universal Transverse Mercator projection, Zone 11, NAD27; vertical datum is NAVD88; PLSS, Public Land Survey System section, township, range; >, greater than; <, less than; ET, evapotranspiration; do., ditto; USGS, U.S. Geological Survey]

Map ID no.	UTM Easting (meters)	UTM Northing (meters)	Longitude	Latitude	Map feature	PLSS location	Regional potential altitude (meters)	Topographic setting	Reference
142	499616	4334140	117°00′16″	39°09′30″	Big Smoky Valley	13/15N/44E	>1,707	Valley floor, ET	Bedinger and others, 1984
143	459595	4312970	117°27′59″	38°57′60″	Reese River Valley	27/13N/40E	>2,042	do.	Bedinger and others, 1984
144	465306	4325680	117°24′04″	39°04′53″	Reese River Valley	17/14N/41E	>1,951	do.	Bedinger and others, 1984
145	471632	4340970	117°19′43″	39°13′10″	Reese River Valley	26/16N/41E	>1,859	do.	Bedinger and others, 1984
146	513014	4359520	116°50′56″	39°23′13″	Big Smoky Valley	19/18N/46E	>1,707	do.	Bedinger and others, 1984
147	448317	4343620	117°35′56″	39°14′32″	Smith Creek Valley	21/16N/39E	>1,844	do.	Bedinger and others, 1984
148	459407	4373920	117°28′20″	39°30′57″	Smith Creek Valley	15/19N/40E	>1,844	do.	Bedinger and others, 1984
149	435965	4380610	117°44′44″	39°34′29″	Edwards Creek Valley	30/20N/38E	>1,569	do.	Bedinger and others, 1984
150	452878	4395750	117°32′59″	39°42′44″	Edwards Creek Valley	2/21N/39E	>1,569	do.	Bedinger and others, 1984
151	522066	4304790	116°44′44″	38°53′37″	Monitor Valley	6/12N/46E	>2,073	do.	Bedinger and others, 1984
152	530626	4333710	116°38′44″	39°09′14″	Monitor Valley	11/15N/47E	>1,981	do.	Bedinger and others, 1984
153	530507	4370330	116°38′43″	39°29′02″	Monitor Valley	26/19N/47E	>1,890	do.	Bedinger and others, 1984
154	562093	4361020	116°16′44″	39°23′54″	Antelope Valley	30/18N/51E	>1,891	do.	Bedinger and others, 1984
155	569891	4382180	116°11′10″	39°35′18″	Kobeh Valley	13/20N/51E	>1,829	do.	Bedinger and others, 1984
156	607934	4376080	115°44′39″	39°31′46″	Newark Valley	11/19N/55E	>1,783	do.	Bedinger and others, 1984
157	612490	4405780	115°41′10″	39°47′47″	Newark Valley	8/22N/56E	>1,783	do.	Bedinger and others, 1984
158	637624	4410440	115°23′30″	39°50′05″	Long Valley	25/23N/58E	>1,859	do.	Bedinger and others, 1984
159	658795	4394040	115°08′54″	39°41′00″	Butte Valley	18/21N/61E	>1,859	do.	Bedinger and others, 1984
160	689530	4391710	114°47′27″	39°39′22″	Steptoe Valley	26/21N/63E	>1,829	do.	Bedinger and others, 1984
161	546322	4057660	116°28′54″	36°39′55″	2DB	9/16S/49E	<682	Valley floor, no ET	Nye County files
162	548428	4036320	116°27′34″	36°28′22″	AD9	15/17S/49E	<674	Valley floor, no ET	USGS files
163	536230	4049080	116°35′42″	36°35′18″	AD3A	5/16S/48E	<696	Valley floor, no ET	USGS files

Table A1–4. Reference points for regional potential from springs for California.

[ID no., identification number; UTM, Universal Transverse Mercator projection, Zone 11, NAD27; vertical datum is NAVD88; PLSS, Public Land Survey System section, township, range, S for San Bernardino p ey]

Map ID no.	UTM Easting (meters)	UTM Northing (meters)	Longitude	Latitude	Spring name	PLSS location	Temperature (degrees Celsius)	Regional potential altitude (meters)	Reference
1	365174	4184370	118°31′53″	37°47′55″	Benton Hot Springs	2/2S/31E/M	57.2	>1,780	Waring, 1965
2	510810	4008800	116°52′47″	36°13′33″	Eagle Borax Spring	9/24N/1E/S	--	>–40	Miller, 1977
5	377472	4123940	118°22′54″	37°15′21″	Keough Hot Spring	17/8S/33E/M	54.4	>1,300	Waring, 1965; Bliss, 1976
6	469860	4098730	117°20′20″	37°02′10″	Stainінger Spring	6/9S/43E/M	26.1	<1,000	Steinkampf and Werrell, 2001
7	506056	4059300	116°55′56″	36°40′52″	Keene Wonder Spring	1/15S/46E/M	27–34	>375	Waring, 1965; Bliss, 1976; Steinkampf and Werrell, 2001
8	430662	3988830	117°46′11″	36°02′36″	Coso Hot Springs	4/22S/39E/M	60–boiling	1,120	Waring, 1965; Bliss, 1976
9	480652	3997330	117°12′54″	36°07′20″	Warm Sulphur Springs	10/21S/44E/M	26.7	>340	Waring, 1965; Bliss, 1976
10	567704	3970210	116°15′00″	35°52′32″	Tecopa Hot Spring	32/21N/8E/S	42–48	>439	Waring, 1965; Bliss, 1976; Steinkampf and Werrell, 2001
11	566337	3971860	116°15′54″	35°53′26″	Resting Spring	30/21N/8E/S	--	>539	Waring, 1965; Bliss, 1976
12	552278	3958050	116°25′18″	35°46′01″	Saratoga Springs	2/18N/5E/S	27.8	>94	Waring, 1965; Bliss, 1976; King and Bredehoeft, 1999; Steinkampf and Werrell, 2001
13	518116	3889410	116°48′04″	35°08′57″	Paradise Spring	8/12N/2E/S	28–42	<775	Waring, 1965; Bliss, 1976
14	581276	3889260	116°06′28″	35°08′41″	Soda Station Spring	10/12N/8E/S	23.9	>290	Waring, 1965; Bliss, 1976
15	528044	3853640	116°41′36″	34°49′35″	Newberry Spring	32/9N/3E/S	25.0	>560	Waring, 1965
16	483673	3799610	117°10′39″	34°20′22″	Unnamed (Deep Creek Spring)	15/3N/3W/S	27–38	>1,122	Waring, 1965
17	484926	3800100	117°09′50″	34°20′38″	Unnamed (Warm Spring)	14/3N/3W/S	27–39	>1,125	Waring, 1965
18	515110	4033460	116°49′53″	36°26′53″	Travertine Springs	23/27N1E/S	32–35	>125	Bliss, 1976; Steinkampf and Werrell, 2001
19	513839	4034690	116°50′44″	36°27′33″	Texas Spring	14/27N/1E/S	31.1	>110	Miller, 1977
20	515845	4039960	116°49′23″	36°30′24″	Nevares Spring	36/28N/1E/S	38.9	>275	Steinkampf and Werrell, 2001
21	503256	3981250	116°57′50″	35°58′39″	Warm Spring	5/23S/47E/M	34.4	<750	Steinkampf and Werrell, 2001
22	465833	4098500	117°23′03″	37°02′02″	Grapevine Spring	10/11S/42E/M	37.8	>840	Bliss, 1976; Steinkampf and Werrell, 2001
23	526632	3805640	116°42′37″	34°23′37″	Old Woman Spring	31/4N/3E/S	--	>899	USGS topographic map
24	703599	3863310	114°46′19″	34°53′37″	Spring	3/9N/21E/S	--	>280	USGS topographic map

Table A1–4. Reference points for regional potential from springs for California.—Continued

[ID no., identification number; UTM, Universal Transverse Mercator projection, Zone 11, NAD27; vertical datum is NAVD88; PLSS, Public Land Survey System section, township, range, S for San Bernardino p ey]

Map ID no.	UTM Easting (meters)	UTM Northing (meters)	Longitude	Latitude	Spring name	PLSS location	Temperature (degrees Celsius)	Regional potential altitude (meters)	Reference
25	466134	3966250	117°22′30″	35°50′30″	Bainter Spring	18/24S/43E/M	32.8	<799	Bliss, 1976
26	427924	3987560	117°48′00″	36°01′54″	Devils Kitchen Fumarole	7/22S/39E/M	97.2	1,311	Bliss, 1976
27	415517	4021810	117°56′29″	36°20′22″	Dirty Sox Spring (Well)	26/18S/37E/M	34.4	>1,094	Bliss, 1976
28	482968	4030930	117°11′24″	36°25′31″	Emigrant Spring	27/17S/44E/M	--	<1,173	Bliss, 1976
29	423744	4061110	117°51′13″	36°41′40″	Little Hunter Canyon Spring	28/14S/38E/M	--	>550	Bliss, 1976
30	432414	4074850	117°45′28″	36°49′08″	Burro Warm Spring	18/13S/39E/M	43.3	>450	Moyle, 1974
31	556884	3876780	116°22′35″	35°02′02″	Spring	19/11N/6E/S	--	>427	USGS topographic map
32	431564	4073870	117°46′02″	36°48′36″	Palm Spring	18/13S/39E/M	9.4	>430	Bliss, 1976; Mase and others, 1979; Moyle, 1974
33	564990	3981220	116°16′45″	35°58′30″	Shoshone Spring	30/22S/7E/S	--	>500	Steinkampf and Werrell, 2001
34	408081	4127040	118°02′13″	37°17′14″	Deep Springs	4/7S/36E/M	--	>1,503	Langer and others, 1984
35	527879	4026460	116°41′21″	36°23′05″	Navel Spring	13/26N/R2E	--	<640	Bliss, 1976
36	495477	4000570	117°03′01″	36°09′06″	Dripping Spring	12/19S/45E/M	--	<1,317	Bliss, 1976
38	565754	3942280	116°16′26″	35°37′26″	Salt Spring	20/18N/7E/S	--	<152	USGS topographic map
39	381495	3860060	118°17′48″	34°52′40″	Willow Springs	7/9N/13W/S	--	>771	USGS topographic map
40	411273	3996740	117°59′09″	36°06′47″	Spring	11/21S/37E/M	--	>1,097	USGS topographic map
41	511032	4010620	116°52′38″	36°14′32″	Tule Spring	28/25N/1E/S	--	>–40	USGS topographic map
42	498236	4049000	117°01′11″	36°35′18″	McLean Spring	7/16S/46E/M	--	>–49	National Park Service files
43	498236	4051010	117°01′11″	36°36′23″	Burnt Wagon Spring	31/15S/46E/M	--	>–46	National Park Service files
44	488268	4064570	117°07′53″	36°43′43″	Triangle Spring	19/14S/45E/M	--	>21	National Park Service files
45	467308	4090200	117°22′02″	36°57′33″	Mesquite Spring	26/11S/42E/M	--	>539	National Park Service files
46	452849	4113880	117°31′52″	37°10′19″	Little Sand Spring	17/9S/41E/M	--	>925	USGS topographic map
47	451873	4115640	117°32′32″	37°11′16″	Sand Spring	7/9S/41E/M	--	>955	USGS topographic map
49	329098	4168480	118°56′14″	37°38′58″	East of Mammoth	31/35/28E/M	--	>2,286	USGS topographic map

Table A1–5. Reference points for regional potential from springs for Nevada.

[ID no., identification number; UTM, Universal Transverse Mercator projection, Zone 11, NAD27; vertical datum is NAVD88; PLSS, Public Land Survey System section, township, range; >, greater than; <, less than; --, no data]

Map ID no.	UTM Easting (meters)	UTM Northing (meters)	Longitude	Latitude	Spring name	PLSS location	Regional potential altitude (meters)	Temperature (degrees Celsius)	Reference
1	704337	4066480	114°42′43″	36°43′26″	Warm (Muddy) Spring	16/14S/65E	>536	32	Mifflin, 1968
2	704142	4064230	114°42′53″	36°42′13″	Iverson (Warm) Spring	21/14S/65E	>536	32	Mifflin, 1968
3	729188	4028250	114°26′43″	36°22′26″	Rogers Spring	12/18S/67E	>488	27	Mifflin, 1968
4	730686	4031000	114°25′40″	36°23′54″	Blue Point Spring	6/18S/68E	>463	27	Mifflin, 1968
5	607601	4039420	115°47′55″	36°29′45″	Indian Springs	16/16S/55E	>975	26	Mifflin, 1968
6	610405	4030360	115°46′07″	36°24′50″	Willow Spring	2/18S/55E	<1,829	12	Mifflin, 1968
7	622889	4017740	115°37′53″	36°17′55″	Deer Creek Springs	18/19S/57E	<2,621	7	Mifflin, 1968
8	613804	4002820	115°44′05″	36°09′55″	Intermittent Spring	31/20S/56E	<1,414	14	Mifflin, 1968
9	612716	4310840	115°41′58″	38°56′28″	Big Warm Spring	32/13N/56E	>1,707	32	Mifflin, 1968
10	613171	4309330	115°41′40″	38°55′39″	Little Warm Spring	5/12N/56E	>1,707	32	Mifflin, 1968
11	661598	4273260	115°08′40″	38°35′42″	Mormon Spring	32/9N/61E	>1,615	37–38	Mifflin, 1968
12	670061	4278220	115°02′46″	38°38′17″	Immigrant Spring	19/9N/62E	>1,661	19	Mifflin, 1968
13	605462	4267540	115°47′23″	38°33′07″	Lockes Stockyard Spring	15/8N/55E	>1,481	32–34	Mifflin, 1968
14	605462	4267540	115°47′23″	38°33′07″	Lockes Big Spring	15/8N/55E	>1,481	37–38	Mifflin, 1968
15	605462	4267540	115°47′23″	38°33′07″	Reynolds Spring	15/8N/55E	>1,481	36–37	Mifflin, 1968
16	628430	4269640	115°31′33″	38°34′04″	Blue Eagle and Jacks Springs	11/8N/57E	>1,451	28	Mifflin, 1968
17	628430	4269640	115°31′33″	38°34′04″	Tom Spring	12/8N/57E	>1,451	22	Mifflin, 1968
18	626250	4265100	115°33′06″	38°31′38″	Butterfield Spring	27/8N/57E	>1,448	16	Mifflin, 1968
19	672058	4256150	115°01′43″	38°26′20″	Butterfield Springs	28/7N/62E	>1,600	--	Mifflin, 1968
20	672349	4253900	115°01′33″	38°25′07″	Flagg Springs	33/7N/62E	>1,600	--	Mifflin, 1968
21	640565	4248500	115°23′27″	38°22′32″	Forest Home Spring	18/6N/59E	<1,893	14	Mifflin, 1968
22	658921	4247090	115°10′52″	38°21′35″	Moon River Spring	25/6N/60E	>1,585	33	Mifflin, 1968
24	557974	4037890	116°21′10″	36°29′11″	Fairbanks Spring	9/17S/50E	>695	27	Mifflin, 1968
25	559726	4036390	116°19′60″	36°28′22″	Rogers Spring	15/17S/50E	>689	28–29	Mifflin, 1968
26	559486	4035130	116°20′10″	36°27′41″	Longstreet Spring	22/17S/50E	>701	27–28	Mifflin, 1968
27	564017	4031680	116°17′09″	36°25′48″	Devils Hole	36/17S/50E	>732	33	Mifflin, 1968
28	560517	4030140	116°19′30″	36°24′59″	Crystal Pool	3/18S/50E	>664	28	Mifflin, 1968
29	564488	4028660	116°16′51″	36°24′10″	Point-of-Rocks	7/18S/51E	>686	32–33	Mifflin, 1968
30	566068	4027160	116°15′48″	36°23′21″	Big Spring	19/18S/51E	>683	28	Mifflin, 1968
31	587314	4008030	116°01′43″	36°12′54″	Bennetts Springs	14/20S/53E	>805	24	Mifflin, 1968
32	598530	4001130	115°54′17″	36°09′06″	Manse Springs	3/21S/54E	>853	24	Mifflin, 1968

Table A1–5. Reference points for regional potential from springs for Nevada.—Continued

[ID no., identification number; UTM, Universal Transverse Mercator projection, Zone 11, NAD27; vertical datum is NAVD88; PLSS, Public Land Survey System section, township, range; >, greater than; <, less than; do., ditto; --, no data]

Map ID no.	UTM Easting (meters)	UTM Northing (meters)	Longitude	Latitude	Spring name	PLSS location	Regional potential altitude (meters)	Temperature (degrees Celsius)	Reference
33	692016	4278710	114°47′38″	38°38′17″	Cave Spring	16/9N/64E	<1,981	Cool	Mifflin, 1968
34	700920	4284460	114°41′24″	38°41′16″	Geyser Spring	4/9N/65E	<2,073	20	Mifflin, 1968
35	730392	4183750	114°23′03″	37°46′26″	Panaca Spring	4/2S/68E	>1,451	29–31	Mifflin, 1968
36	658210	4162930	115°12′28″	37°36′06″	Hiko Spring	14/4S/60E	>1,186	27	Mifflin, 1968
37	656261	4154380	115°13′54″	37°31′30″	Crystal Spring	10/5S/60E	>1,170	28	Mifflin, 1968
38	657840	4150120	115°12′53″	37°29′11″	Brownie Spring	26/5S/60E	>1,128	Warm	Mifflin, 1968
39	659136	4147900	115°12′02″	37°27′58″	Ash Spring	36/5S/60E	>1,100	32	Mifflin, 1968
40	583741	4347660	116°01′45″	39°16′34″	Fish Creek Springs	8/16N/53E	>1,838	19	Mifflin, 1968
41	634921	4347110	115°26′10″	39°15′53″	Illipah Spring	10/16N/58E	<2,304	Cool	Mifflin, 1968
42	624153	4330740	115°33′50″	39°07′08″	Green Springs	33/15N/57E	>1,853	17	Mifflin, 1968
43	618260	4326490	115°37′58″	39°04′53″	Big Bull Spring	14/14N/56E	>1,768	12	Mifflin, 1968
44	619065	4322490	115°37′27″	39°02′43″	Bull Creek Spring	25/14N/56E	>1,768	12	Mifflin, 1968
45	665895	4308540	115°05′12″	38°54′43″	Preston Big Spring	2/12N/61E	>1,737	21	Mifflin, 1968
46	667394	4308290	115°04′10″	38°54′34″	Cold Spring	12/12N/61E	>1,737	21	Mifflin, 1968
47	667394	4308290	115°04′10″	38°54′34″	Nicholas Spring	12/12N/61E	>1,737	22	Mifflin, 1968
48	667394	4308290	115°04′10″	38°54′34″	Arnoldson Spring	12/12N/61E	>1,737	22	Mifflin, 1968
49	639821	4308770	115°23′14″	38°55′07″	Currant Spring	18/12N/59E	<2,347	8	Mifflin, 1968
50	667982	4278170	115°04′12″	38°38′17″	West Immigrant Spring	13/9N/61E	>1,631	19	Mifflin, 1968
51	677583	4300990	114°57′14″	38°50′30″	Lund Spring	1/11N/62E	>1,707	12–13	Mifflin, 1968
52	673669	4291340	115°00′05″	38°45′20″	Six Mile Springs	4/10N/62E	>1,722	16	Mifflin, 1968
53	680459	4318700	114°54′58″	39°00′02″	Water Canyon Springs	8/13N/63E	<2,341	9	Mifflin, 1968
54	684612	4322250	114°52′02″	39°01′54″	Willow Creek Basin Springs	35/14N/63E	<2,195	13	Mifflin, 1968
55	680647	4345010	114°54′25″	39°14′15″	Murry Springs	20/16N/63E	>2,024	13	Mifflin, 1968
56	692583	4369670	114°45′42″	39°27′25″	McGill Spring	3/18N/64E	>2,024	24–29	Mifflin, 1968; Garside and Schilling, 1979
57	702659	4339010	114°39′14″	39°10′43″	Cave Springs	10/15N/65E	<2,316	Cool	Mifflin, 1968
58	711455	4336990	114°33′10″	39°09′30″	Bastian Spring	21/15N/66E	<2,024	12	Mifflin, 1968
59	725331	4353980	114°23′12″	39°18′28″	South Mulick Spring	25/17N/67E	>1,707	13	Mifflin, 1968

Table A1–5. Reference points for regional potential from springs for Nevada.—Continued

[ID no., identification number; UTM, Universal Transverse Mercator projection, Zone 11, NAD27; vertical datum is NAVD88; PLSS, Public Land Survey System section, township, range; >, greater than; <, less than; do., ditto; --, no data]

Map ID no.	UTM Easting (meters)	UTM Northing (meters)	Longitude	Latitude	Spring name	PLSS location	Regional potential altitude (meters)	Temperature (degrees Celsius)	Reference
60	741145	4321520	114°12′54″	39°00′41″	Rowland Spring	10/13N/69E	<1,920	9	Mifflin, 1968
61	751093	4309330	114°06′17″	38°53′56″	Spring Creek Spring	15/12N/70E	<1,865	12–13	Mifflin, 1968
62	725558	4302460	114°24′04″	38°50′38″	Shoshone Springs	1/11N/67E	>1,768	12	Mifflin, 1968
63	725609	4300700	114°24′04″	38°49′41″	Minerva Spring	12/11N/67E	>1,951	12	Mifflin, 1968
64	730357	4302590	114°20′45″	38°50′38”	Swallow Canyon Spring	4/11N/68E	>1,951	9	Mifflin, 1968
65	725807	4302220	114°23′54″	38°50′30”	Spring	5/11N/68E	>1,853	10	Mifflin, 1968
66	749805	4286610	114°07′40″	38°41′41”	Big Spring	33/10N/70E	>1,692	16	Mifflin, 1968
67	525068	4092700	116°43′06″	36°58′55″	Hick's Hot Spring	16/11S/47E	>1,097	38–43	Garside and Schilling, 1979
68	525068	4092700	116°43′06″	36°58′55″	Amargosa Hot Spring	16/11S/47E	>1,097	32–38	Garside and Schilling, 1979
69	524332	4090700	116°43′36″	36°57′50″	Burrell Hot Spring	21/11S/47E	>1,091	39	Garside and Schilling, 1979
70	522886	4085920	116°44′35″	36°55′15″	Beatty Municipal Spring	5/12S/47E	>1,045	24	Garside and Schilling, 1979
71	528769	4208430	116°40′20″	38°01′30″	Spring	14/2N/47E	<1,704	29	Garside and Schilling, 1979
72	553272	4204770	116°23′36″	37°59′27″	Pedro Spring	28/2N/50E	<1,963	25	Garside and Schilling, 1979
73	553272	4204770	116°23′36″	37°59′27″	Reveille Mill Spring	28/2N/50E	<1,963	29	Garside and Schilling, 1979
74	514800	4234750	116°49′51″	38°15′45″	Salisbury Spring	28/5N/46E	<1,993	24	Garside and Schilling, 1979
75	529690	4243080	116°39′37″	38°20′14″	Warm Spring	20/6N/47E	<1,899	26	Garside and Schilling, 1979
76	554357	4264540	116°22′35″	38°31′46″	Hot Creek Ranch Spring	29/8N/50E	>1,676	34–82	Garside and Schilling, 1979
87	457119	4186090	117°29′14″	37°49′23″	Pearl Hot Spring	25/1S/40E	>1,341	37	Garside and Schilling, 1979
88	469905	4185850	117°20′31″	37°49′17″	Alkali Spring	26/1S/41E	>1,524	49–60	Garside and Schilling, 1979
89	443759	4177200	117°38′18″	37°44′32″	Silver Peak Hot Springs	15/2S/39E	>1,326	21–48	Garside and Schilling, 1979
90	408438	4205630	118°02′34″	37°59′44″	Fish Spring	25/2N/35E	>1,463	24	Garside and Schilling, 1979
91	412682	4203300	117°59′39″	37°58′30″	Gap Spring	32/2N/36E	>1,413	23	Garside and Schilling, 1979
92	396615	4200500	118°10′36″	37°56′53″	Sand Spring	27/1N/34E	>1,676	23	Garside and Schilling, 1979
93	554709	4226870	116°22′31″	38°11′24″	Warm Spring	20/4N/50E	>1,695	63	Garside and Schilling, 1979

References Cited

Arteaga, F.E., Savard, C.S., Johnson, M.E., and Stone, J.C., 1991, Hydrogeologic data from selected wells and test holes in and adjacent to the Nevada Test Site, Nye County, Nevada, through 1986: U.S. Geological Survey Open-File Report 87–536, 23 p.

Bedinger, M.S., Harrill, J.R., Langer, William H., Thomas, J.M., and Mulvihill, Deborah A., 1984, Maps showing ground-water levels, springs, and depth to ground water, Basin and Range Province, Nevada: U.S. Geological Survey Water-Resources Investigations Report 83–4119–B, 2 sheets.

Berger, D.L., Kilroy, K.C., and Schaefer, D.H., 1988, Geophysical logs and hydrological data for eight wells in the Coyote Spring Valley area, Clark and Lincoln Counties, Nevada: U.S. Geological Survey Open-File Report 87–679, 59 p.

Bliss, J.D., 1976, California—Basic data for thermal springs and wells as recorded in Geotherm, Part B: U.S. Geological Survey Open-File Report 83–428–B, 108 p.

Bredehoeft, J.D., Back, W., and Hanshaw, B.B., 1982, Regional ground-water flow concepts in the United States—Historical perspective, *in* Narasimhan, T.N., Recent trends in hydrogeology: Geological Society of America, Special Paper 189, p. 297–316.

Bunch, R.L., and Harrill, J.R., 1984, Compilation of selected hydrologic data from the MX Missile-siting investigation, east-central Nevada and western Utah: U.S. Geological Survey Open-File Report 84–702, 123 p.

Dettinger, M.D., Harrill, J.R., Schmidt, D.L., and Hess, J.W., 1995, Distribution of carbonate-rock aquifers and the potential for their development, southern Nevada and parts of Arizona, California, and Utah: U.S. Geological Survey Water-Resources Investigations Report 91–4146, 100 p.

Eakin, T.E., and Moore, D.O., 1964, Uniformity of discharge of Muddy River Springs, southeastern Nevada, and relation to interbasin movement of ground water, *in* Geological Survey Research 1964, Chapter D: U.S. Geological Survey Professional Paper 501–D, p. D171–DI76.

Eakin, T.E., and Winograd, I.J., 1965, Interbasin movement of ground water in south-central Nevada—Some implications, *in* Abstracts for 1964: Geological Society of America Special Paper 82, p. 52.

Freeze, R.A., and Witherspoon, P.A., 1967, Theoretical analysis of regional groundwater flow; 2. Effect of water-table configuration and subsurface permeability variation: Water Resources Research, v. 3, no. 2, p. 623–634.

Garside, L.J., and Schilling, J.H., 1979, Thermal waters of Nevada: Nevada Bureau of Mines and Geology, Bulletin 91, 163 p.

Harrill, J.R., and Bedinger, M.S., 2000, Ground-water fluctuations in Devils Hole, 1962–1999, regional stresses and water-level changes in the Death Valley region: Prepared under contract to the National Park Service, 36 p., 20 figs., 6 appendices.

Harrill, J.R., Gates, J.S., and Thomas, J.M., 1988, Major ground-water flow systems in the Great Basin Region of Nevada, Utah, and adjacent States: U.S. Geological Survey Hydrologic Investigations Atlas HA–694–C, 2 sheets, map scale 1:1,000,000, with errata sheet.

King, M.J., Bredehoeft, J.D., 1999, Death Valley springs geochemical Investigation: Submitted to Inyo County Planning Department: Yucca Mountain Repository Oversight Program, 31 p.

Langer, W.H., Moyle, W.R., Woolfenden, L.R., and Mulvihill, D.A., 1984, Maps showing ground-water levels, springs, and depth to ground water, Basin and Range Province, Southern California: U.S. Geological Survey Water-Resources Investigations Report 83–4116–B, 7 p., 2 sheets.

Mase, C.W., Galanis, S.P., Jr., and Monroe, R.J., 1979, Near surface heat flow in Saline Valley, California: U.S. Geological Survey Open-File Report 79–1136, 52 p.

Maxey, G.B., and Eakin, T.E., 1949, Ground water in White River Valley, White Pine, Nye, and Lincoln Counties, Nevada: Nevada State Engineer, Water Resources Bulletin Number 8, 59 p.

Mifflin, M.D., 1968, Delineation of ground-water flow systems in Nevada: University of Nevada at Las Vegas, Center for Water Resources Research, Desert Research Institute, Water Resources Center, Technical Report Series H–W, Publication 4, 110 p.

Mifflin, M.D., and Hess, J.W., 1979, Regional carbonate flow systems in Nevada: Journal of Hydrology, v. 43, p. 217–237.

Miller, G.A., 1977, Appraisal of water resources of Death Valley, California-Nevada: U.S. Geological Survey Open-File Report 77–728, 68 p.

Moyle, W.R., Jr., 1974, Temperature and chemical data for selected thermal wells and springs in southeastern California: U.S. Geological Survey Water-Resources Investigations Report 33–73, 12 p.

Prudic, D.E., Harrill, J.R., and Burbey, T.J., 1995, Conceptual evaluation of regional ground-water flow in the carbonate-rock province of the Great Basin, Nevada, Utah, and adjacent States: U.S. Geological Survey Professional Paper 1409–D, 102 p.

Sargent, K.A., and Bedinger, M.S., 1985, Geologic and hydrologic characterization and evaluation of the Basin and Range Province relative to the disposal of high-level radioactive waste, Part II Geologic and hydrologic characterization: U.S. Geological Survey Circular 904–B, 30 p.

Schaefer, D.H., Morris, T.M., and Dettinger, M.D., 1992, Hydrologic and geophysical data for selected wells and springs in the Sheep Range area, Clark and Lincoln Counties, Nevada: U.S. Geological Survey Open-File Report 89–425, 26 p.

Steinkampf, W.C., and Werrell, W.E., 2001, Ground-water flow to Death Valley, as inferred from the chemistry and geohydrology of selected springs in Death Valley National Park, California and Nevada: U.S. Geological Survey Water-Resources Investigations Report 98–4114, 37 p.

Thomas, J.M., Mason, J.L., and Crabtree, J.D., 1986, Groundwater levels in the Great Basin region of Nevada, Utah, and adjacent States: U.S. Geological Survey Hydrologic Investigations Atlas HA–694–B, 2 sheets.

Van Denburgh, A.S., and Rush, F.E., 1974, Water-resources appraisal of Railroad and Penoyer Valleys, east-central Nevada: Nevada Division of Water Resources Reconnaissance Report 60, 61 p.

Waring, Gerald A., 1965, Thermal springs of the United States and other countries of the world—A summary: U.S. Geological Survey Professional Paper 492, 383 p.

Winograd, I.J., and Thordarson, William, 1975, Hydrogeologic and hydrochemical framework, south-central Great Basin, Nevada-California, with special reference to the Nevada Test Site: U.S. Geological Survey Professional Paper 712–C, 126 p.

Estimated Model Boundary Flows

By J.R. Harrill and M.S. Bedinger

Appendix 2 of

Death Valley Regional Ground-Water Flow System, Nevada and California—Hydrogeologic Framework and Transient Ground-Water Flow Model

Edited by Wayne R. Belcher

Prepared in cooperation with the
U.S. Department of Energy
Office of Environmental Management, National Nuclear Security Administration, Nevada Site Office,
under Interagency Agreement DE–AI52–01NV13944, and
Office of Repository Development,
under Interagency Agreement DE–AI08–02RW12167

Scientific Investigations Report 2004–5205

U.S. Department of the Interior
U.S. Geological Survey

Contents

Figures

Tables

APPENDIX 2. Estimated Model Boundary Flows

By J.R. Harrill and M.S. Bedinger

Introduction

Areas that contribute ground-water inflow to or receive outflow from the Death Valley regional ground-water flow system (DVRFS) model domain across the lateral boundary are called contributing areas and are defined by the gradient in the regional potential developed in Appendix 1. Estimates of the amount of lateral flow across the DVRFS model boundary from (or to) these contributing areas which will be used as components of the water budget for the calibration of the DVRFS model are presented here. The model boundary was divided into 12 segments, primarily on the basis of the hydrologic units in the contributing areas (figs. A2–1 and A2–2). Each segment of the model boundary was divided into subsegments to represent straight-line approximations of the boundary (fig. A2–3).

Approach

Two methods were used to estimate flow across segments of the lateral boundary of the DVRFS model: (1) calculations using Darcy's law, based on regional potential gradient, cross-sectional areas of each subsegment at the boundary, and hydraulic conductivities of hydrogeologic units at each subsegment cross section; and (2) calculations from water budgets of contributing areas.

Darcy's Law Estimates

Darcy's law was used to estimate boundary flow for each subsegment of the model boundary. Darcy's law (Freeze and Cherry, 1979, p. 28) states

$$Q = KiA,$$

where

Q is the flow (L^3/T),
K is the hydraulic conductivity (L/T),
i is the hydraulic gradient (L/L),

and

A is the cross-sectional area (L^2).

The cross-sectional flow areas were measured from cross sections prepared from the hydrogeologic framework model (HFM) (Chapter E, this volume) for each segment of the model boundary. The cross sections extend from land surface to 4,000 m below sea level, the base of the model; they are presented from the viewpoint of the model interior looking outward. The flow area of each cross section was estimated to be the area below the intersection of the regional potentiometric surface. Although ground-water flow occurs below accretion cells (mostly recharge mounds) that are present along much of the model boundary, this is considered to be a local phenomenon not associated with regional ground-water flow. The area of each hydrogeologic unit (HGU) below the regional potential was measured from each cross section.

The hydraulic gradient across each subsegment was estimated from the regional potentiometric map (fig. A2–1 and pl. 1) by calculating the hydraulic-head change over a distance measured between regional potentiometric contours. Flow lines were drawn through the ends of each subsegment to determine the flow width. If the direction of flow is not perpendicular to the subsegment, the cross-sectional area of the flow will be less than the cross-sectional area of the subsegment. The correction is calculated as the actual flow width divided by the width of the subsegment.

Hydraulic-conductivity values for each of the HGUs are based on data from Belcher and others (2001, 2002). Hydraulic conductivity values were adjusted in some areas by using professional judgment. Depth decay of hydraulic conductivity was not considered in these estimates.

Water Budget Estimates

Water budgets of hydrologic units in each contributing area (fig. A2–2, table A2–1) were used to estimate a water budget for each segment of the model boundary to calculate boundary flow (fig. A2–3). Water budgets were estimated for some of the contributing areas in California. For areas where boundaries of the contributing areas do not match exactly the hydrologic-unit boundaries for which water-budget information is available, the water-budget information is used only to indicate whether water is available to support the Darcy calculation of flow across the model boundary. For areas where water budgets are not available, the evapotranspiration (ET) areas were evaluated (based on professional judgment) to assess whether ET could account for the available recharge.

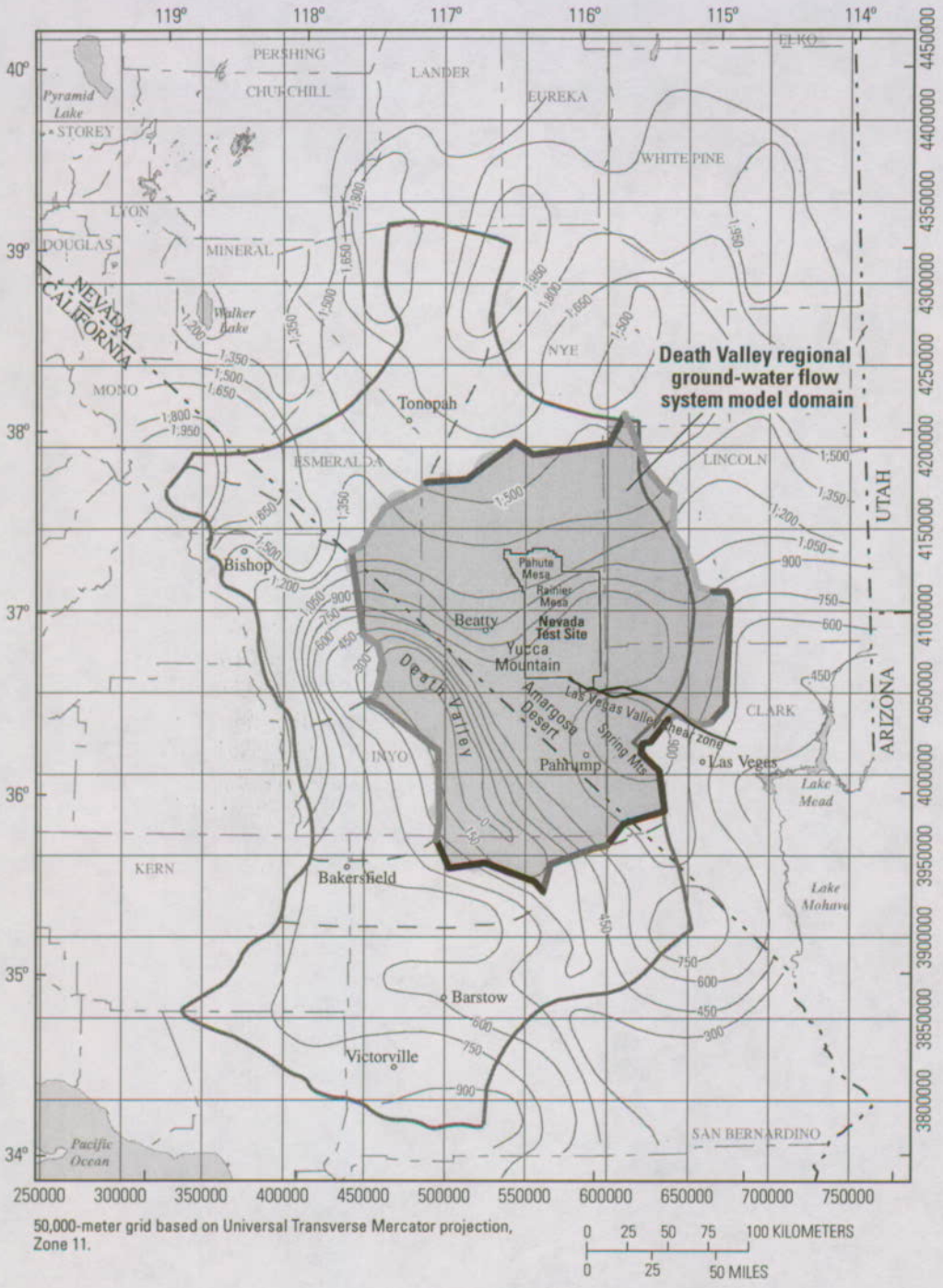

EXPLANATION

Area contributing flow to the Death Valley regional ground-water flow system, dashed line shows areas contributing flow to specific boundary segments (Bedinger and Harrill, Appendix 1, this volume)

Straight line segment that approximates model boundary. Segments are color coded—See figure A2–3 for segment names.

—750— **Potentiometric-surface contour**—Shows altitude of regional potential. Interval is 150 meters. Datum is sea level. (Bedinger and Harrill, Appendix 1, this volume)

Populated location

Figure A2–1. Death Valley regional ground-water flow system regional model domain, regional potential, and contributing areas.

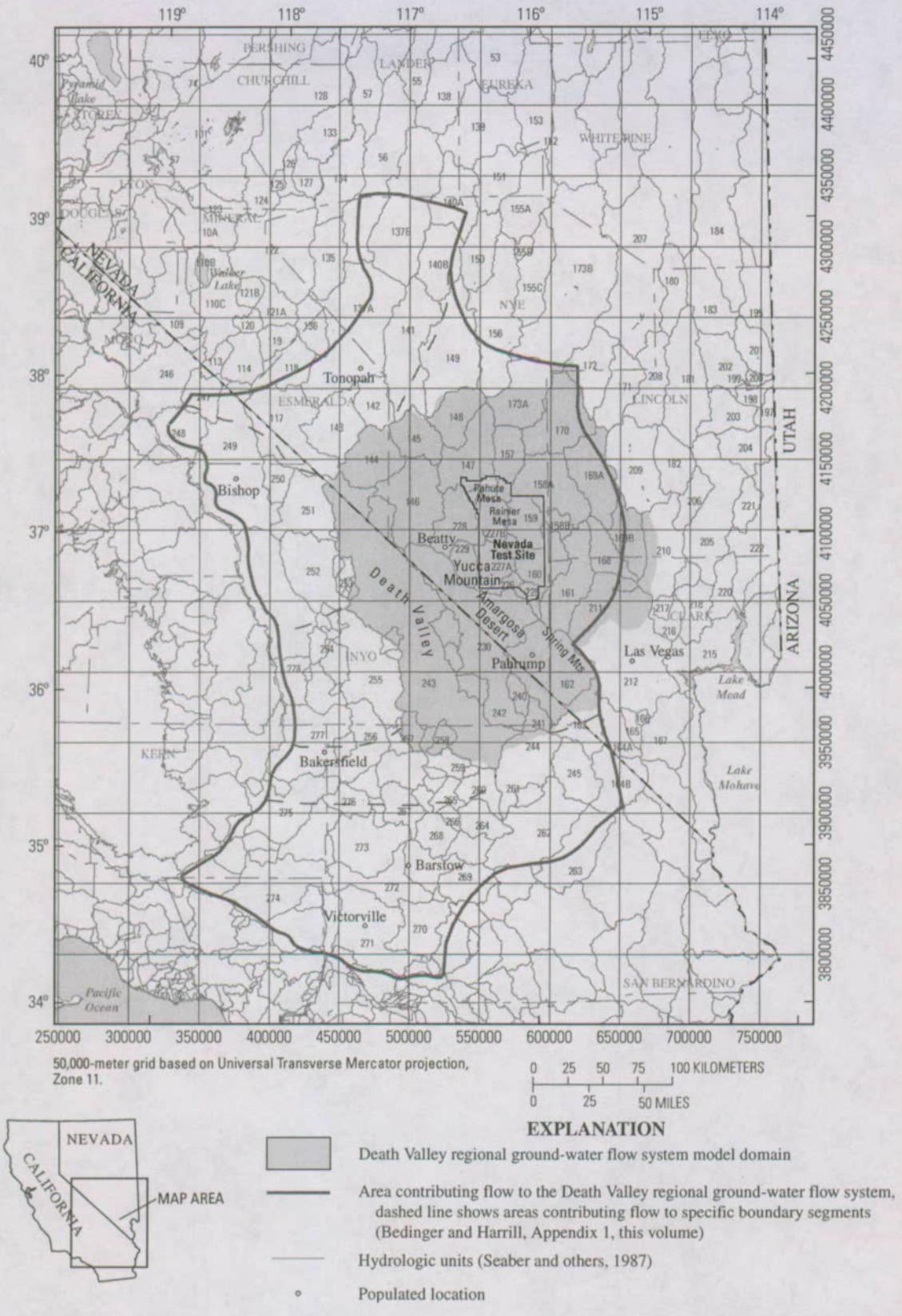

Figure A2–2. Death Valley regional ground-water flow system regional model domain, hydrologic units, and contributing areas.

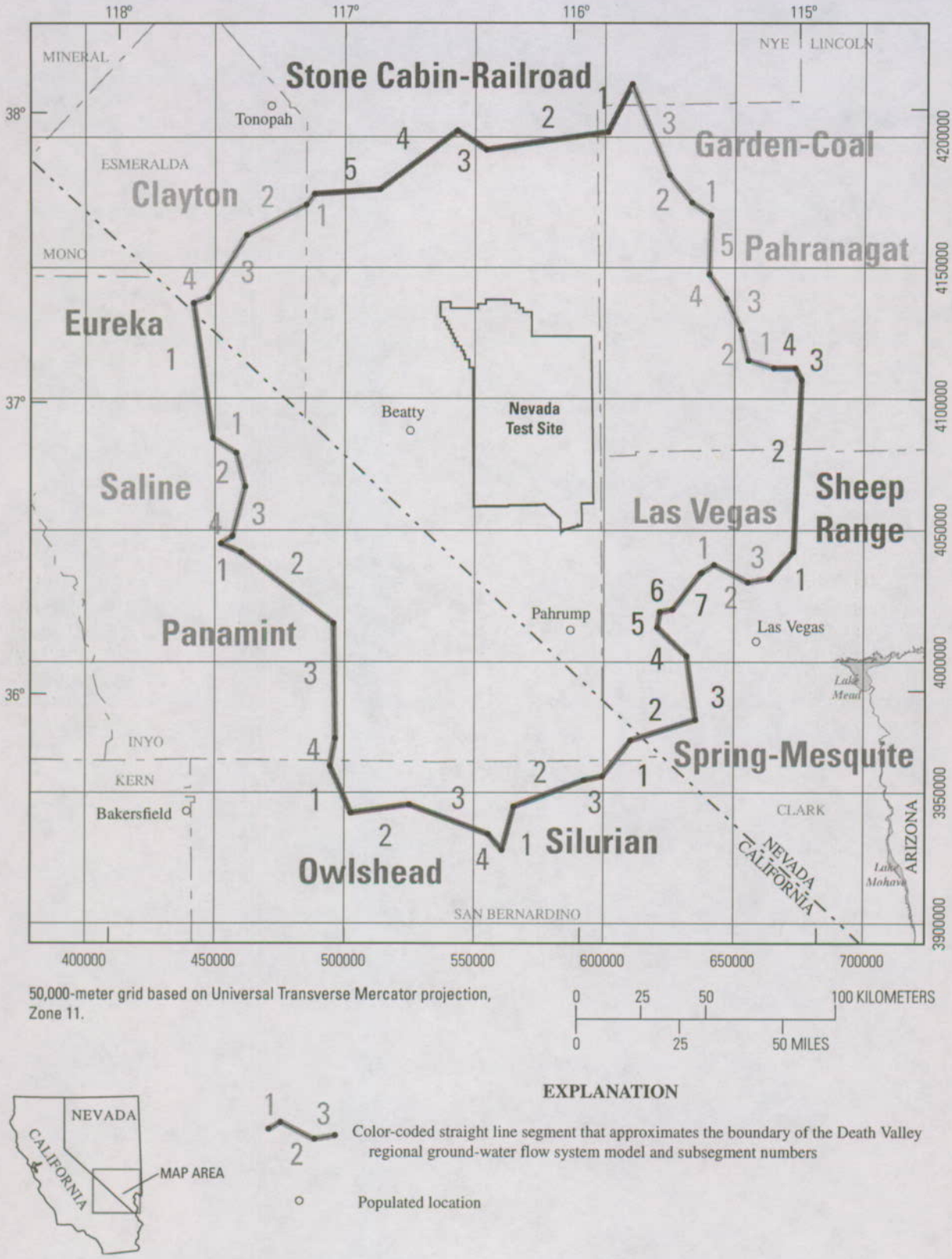

Figure A2–3. Death Valley regional ground-water flow system model boundary segments and subsegments.

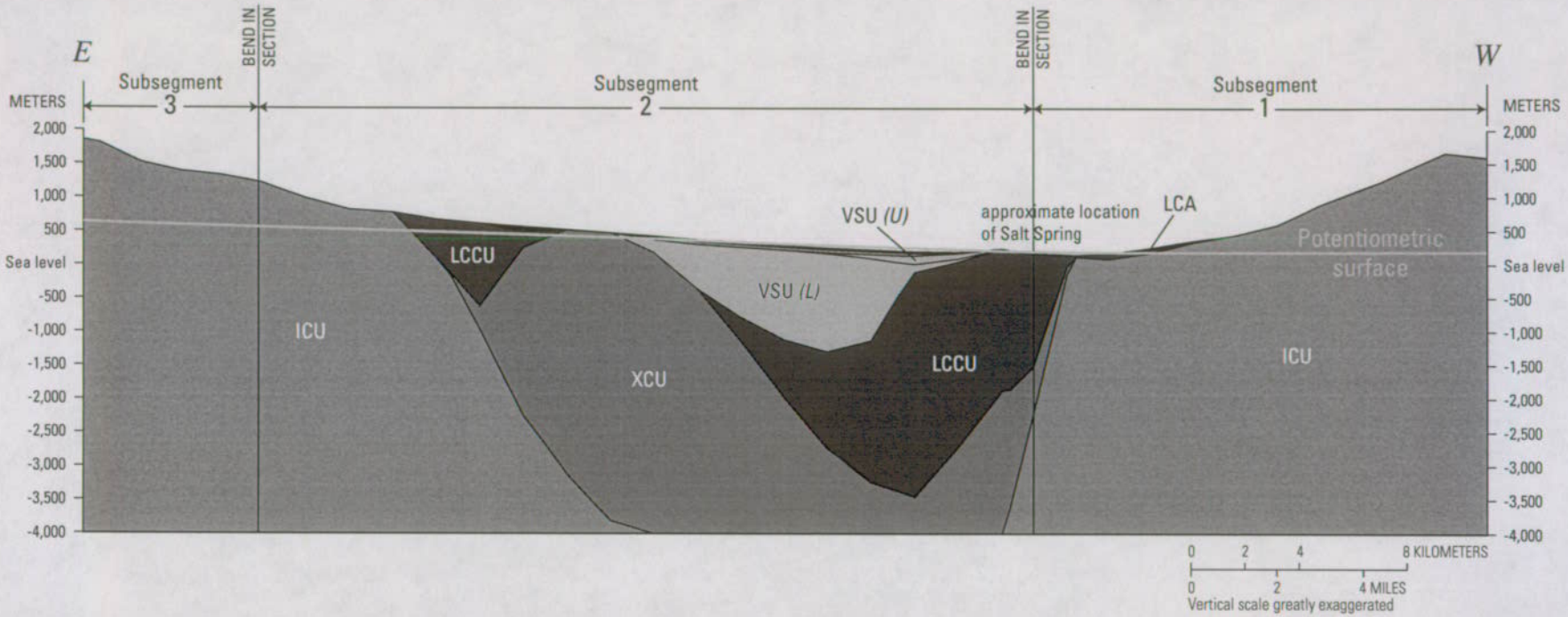

EXPLANATION OF HYDROGEOLOGIC UNITS

Not all units appear on all cross sections

YAA	Younger alluvial aquifer	VSU (U)	Upper volcanic- and sedimentary-rock unit	CFBCU	Crater Flat–Bullfrog confining unit	UCA	Upper carbonate-rock aquifer
YACU	Younger alluvial confining unit	TMVA	Thirsty Canyon–Timber Mountain volcanic-rock aquifer	CFTA	Crater Flat–Tram aquifer	UCCU	Upper clastic-rock confining unit
OAA	Older alluvial aquifer	PVA	Paintbrush volcanic-rock aquifer	BRU	Belted Range unit	LCA	Lower carbonate-rock aquifer
OACU	Older alluvial confining unit	CHVU	Calico Hills volcanic-rock unit	OVU	Older volcanic-rock unit	LCCU	Lower clastic-rock confining unit
LA	Limestone aquifer	WVU	Wahmonie volcanic-rock unit	VSU (L)	Lower volcanic- and sedimentary-rock unit	XCU	Crystalline-rock confining unit
LFU	Lava-flow unit	CFPPA	Crater Flat–Prow Pass aquifer	SCU	Sedimentary-rock confining unit	ICU	Intrusive-rock confining unit
YVU	Young volcanic-rock unit						

Figure A2–4. Hydrogeologic units of the Death Valley regional ground-water flow system model for the Silurian boundary segment.

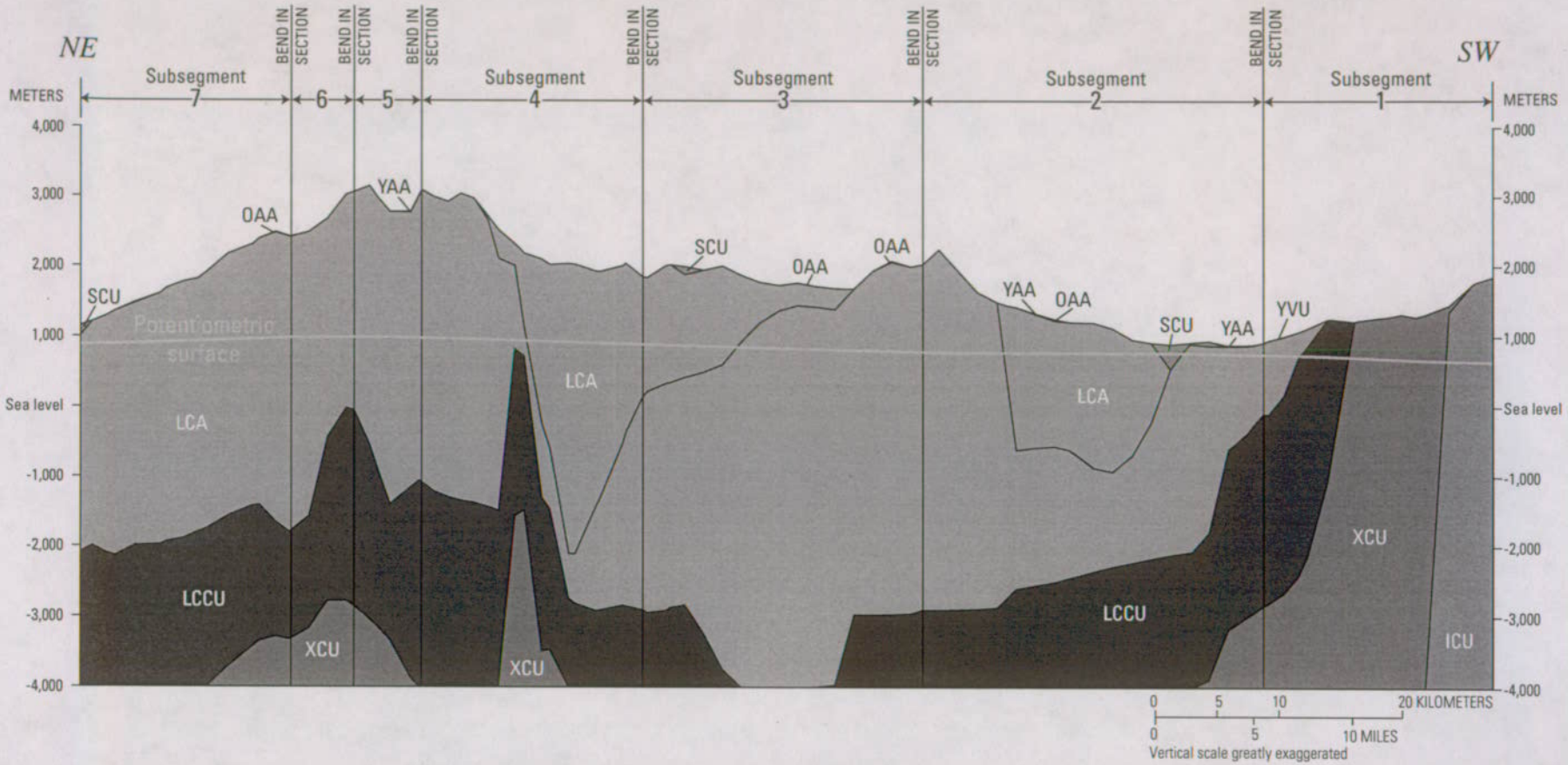

EXPLANATION OF HYDROGEOLOGIC UNITS

Not all units appear on all cross sections

YAA	Younger alluvial aquifer	VSU (U)	Upper volcanic- and sedimentary-rock unit	CFBCU	Crater Flat–Bullfrog confining unit	UCA	Upper carbonate-rock aquifer
YACU	Younger alluvial confining unit	TMVA	Thirsty Canyon–Timber Mountain volcanic-rock aquifer	CFTA	Crater Flat–Tram aquifer	UCCU	Upper clastic-rock confining unit
OAA	Older alluvial aquifer	PVA	Paintbrush volcanic-rock aquifer	BRU	Belted Range unit	LCA	Lower carbonate-rock aquifer
OACU	Older alluvial confining unit	CHVU	Calico Hills volcanic-rock unit	OVU	Older volcanic-rock unit	LCCU	Lower clastic-rock confining unit
LA	Limestone aquifer	WVU	Wahmonie volcanic-rock unit	VSU (L)	Lower volcanic- and sedimentary-rock unit	XCU	Crystalline-rock confining unit
LFU	Lava-flow unit	CFPPA	Crater Flat–Prow Pass aquifer	SCU	Sedimentary-rock confining unit	ICU	Intrusive-rock confining unit
YVU	Young volcanic-rock unit						

Figure A2–5. Hydrogeologic units of the Death Valley regional ground-water flow system model for the Spring–Mesquite boundary segment.

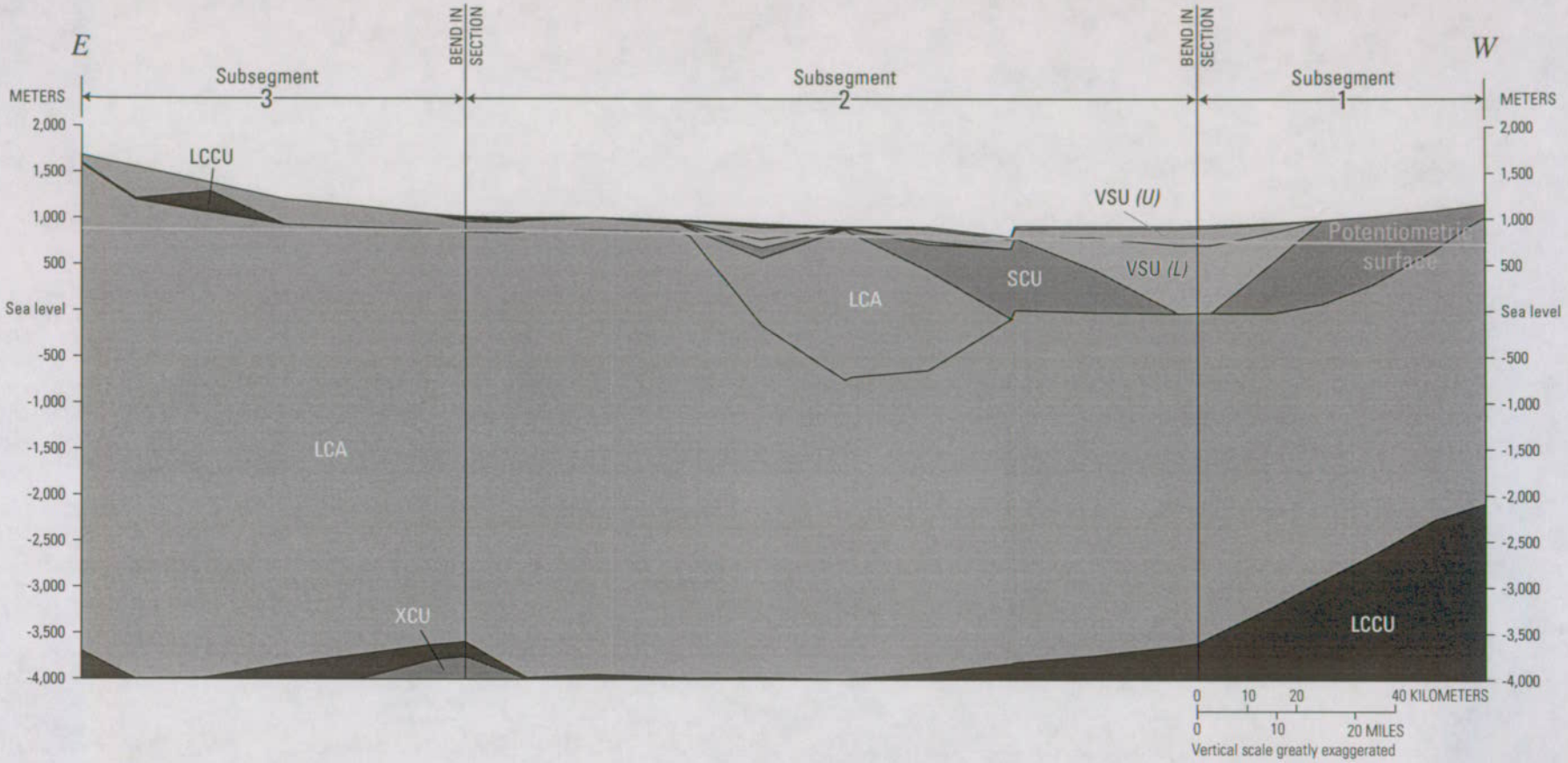

EXPLANATION OF HYDROGEOLOGIC UNITS

Not all units appear on all cross sections

YAA	Younger alluvial aquifer	VSU (U)	Upper volcanic- and sedimentary-rock unit	CFBCU	Crater Flat–Bullfrog confining unit	UCA	Upper carbonate-rock aquifer
YACU	Younger alluvial confining unit	TMVA	Thirsty Canyon–Timber Mountain volcanic-rock aquifer	CFTA	Crater Flat–Tram aquifer	UCCU	Upper clastic-rock confining unit
OAA	Older alluvial aquifer	PVA	Paintbrush volcanic-rock aquifer	BRU	Belted Range unit	LCA	Lower carbonate-rock aquifer
OACU	Older alluvial confining unit	CHVU	Calico Hills volcanic-rock unit	OVU	Older volcanic-rock unit	LCCU	Lower clastic-rock confining unit
LA	Limestone aquifer	WVU	Wahmonie volcanic-rock unit	VSU (L)	Lower volcanic- and sedimentary-rock unit	XCU	Crystalline-rock confining unit
LFU	Lava-flow unit	CFPPA	Crater Flat–Prow Pass aquifer	SCU	Sedimentary-rock confining unit	ICU	Intrusive-rock confining unit
YVU	Young volcanic-rock unit						

Figure A2–6. Hydrogeologic units of the Death Valley regional ground-water flow system model for the Las Vegas boundary segment.

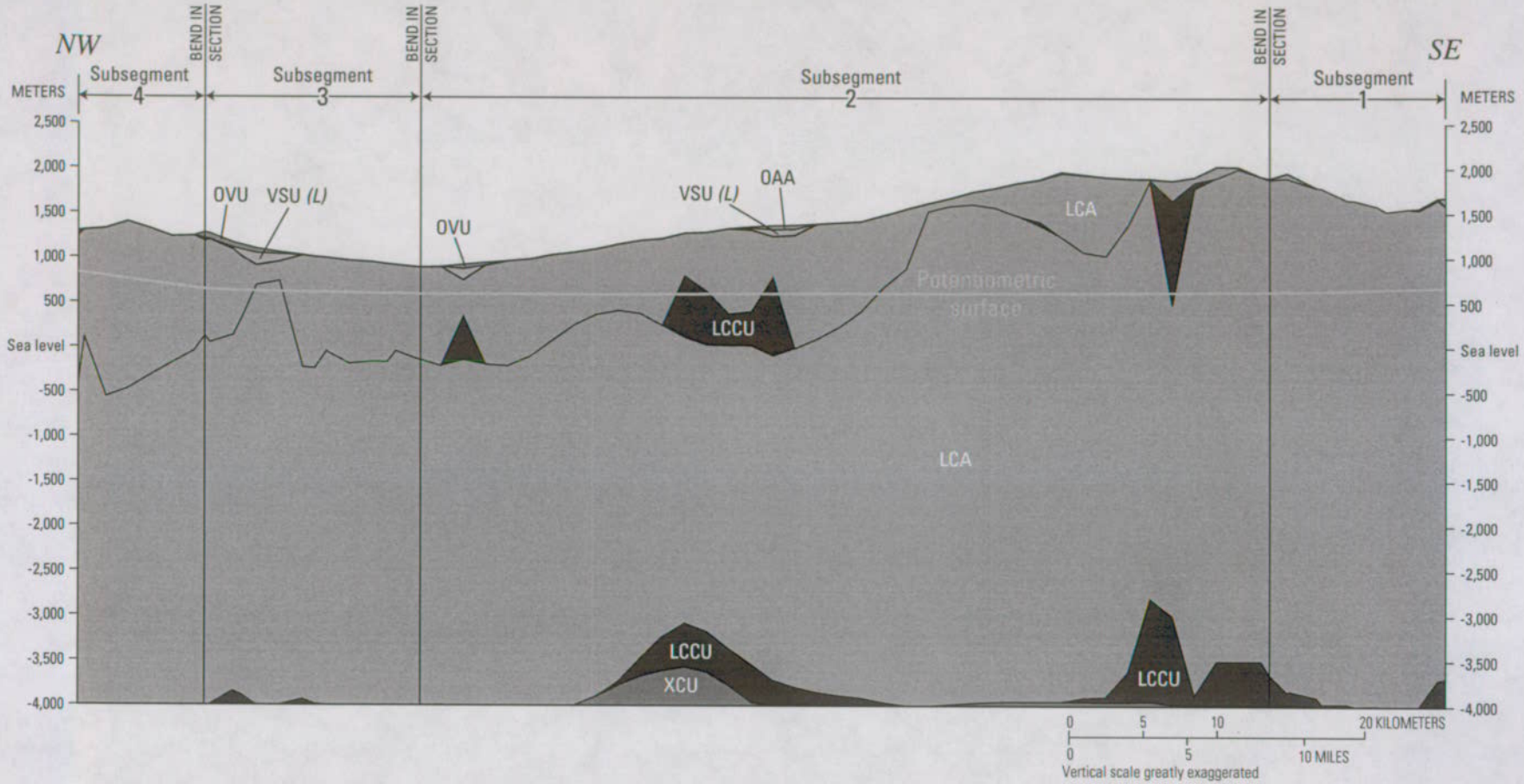

EXPLANATION OF HYDROGEOLOGIC UNITS

Not all units appear on all cross sections

YAA	Younger alluvial aquifer	VSU (U)	Upper volcanic- and sedimentary-rock unit	CFBCU	Crater Flat–Bullfrog confining unit	UCA	Upper carbonate-rock aquifer
YACU	Younger alluvial confining unit	TMVA	Thirsty Canyon–Timber Mountain volcanic-rock aquifer	CFTA	Crater Flat–Tram aquifer	UCCU	Upper clastic-rock confining unit
OAA	Older alluvial aquifer	PVA	Paintbrush volcanic-rock aquifer	BRU	Belted Range unit	LCA	Lower carbonate-rock aquifer
OACU	Older alluvial confining unit	CHVU	Calico Hills volcanic-rock unit	OVU	Older volcanic-rock unit	LCCU	Lower clastic-rock confining unit
LA	Limestone aquifer	WVU	Wahmonie volcanic-rock unit	VSU (L)	Lower volcanic- and sedimentary-rock unit	XCU	Crystalline-rock confining unit
LFU	Lava-flow unit	CFPPA	Crater Flat–Prow Pass aquifer	SCU	Sedimentary-rock confining unit	ICU	Intrusive-rock confining unit
YVU	Young volcanic-rock unit						

Figure A2–7. Hydrogeologic units of the Death Valley regional ground-water flow system model for the Sheep Range boundary segment.

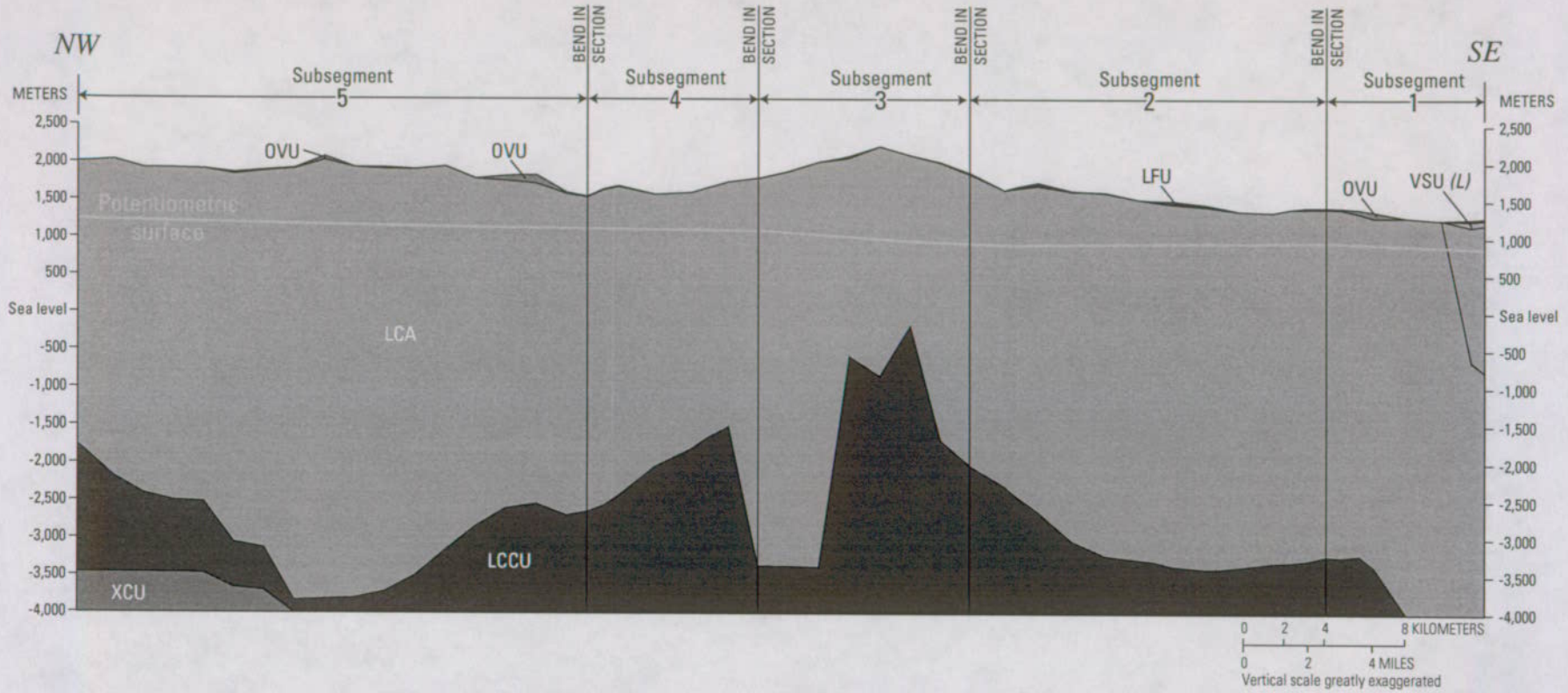

EXPLANATION OF HYDROGEOLOGIC UNITS

Not all units appear on all cross sections

YAA	Younger alluvial aquifer	VSU (U)	Upper volcanic- and sedimentary-rock unit	CFBCU	Crater Flat–Bullfrog confining unit	UCA	Upper carbonate-rock aquifer
YACU	Younger alluvial confining unit	TMVA	Thirsty Canyon–Timber Mountain volcanic-rock aquifer	CFTA	Crater Flat–Tram aquifer	UCCU	Upper clastic-rock confining unit
OAA	Older alluvial aquifer	PVA	Paintbrush volcanic-rock aquifer	BRU	Belted Range unit	LCA	Lower carbonate-rock aquifer
OACU	Older alluvial confining unit	CHVU	Calico Hills volcanic-rock unit	OVU	Older volcanic-rock unit	LCCU	Lower clastic-rock confining unit
LA	Limestone aquifer	WVU	Wahmonie volcanic-rock unit	VSU (L)	Lower volcanic- and sedimentary-rock unit	XCU	Crystalline-rock confining unit
LFU	Lava-flow unit	CFPPA	Crater Flat–Prow Pass aquifer	SCU	Sedimentary-rock confining unit	ICU	Intrusive-rock confining unit
YVU	Young volcanic-rock unit						

Figure A2–8. Hydrogeologic units of the Death Valley regional ground-water flow system model for the Pahranagat boundary segment.

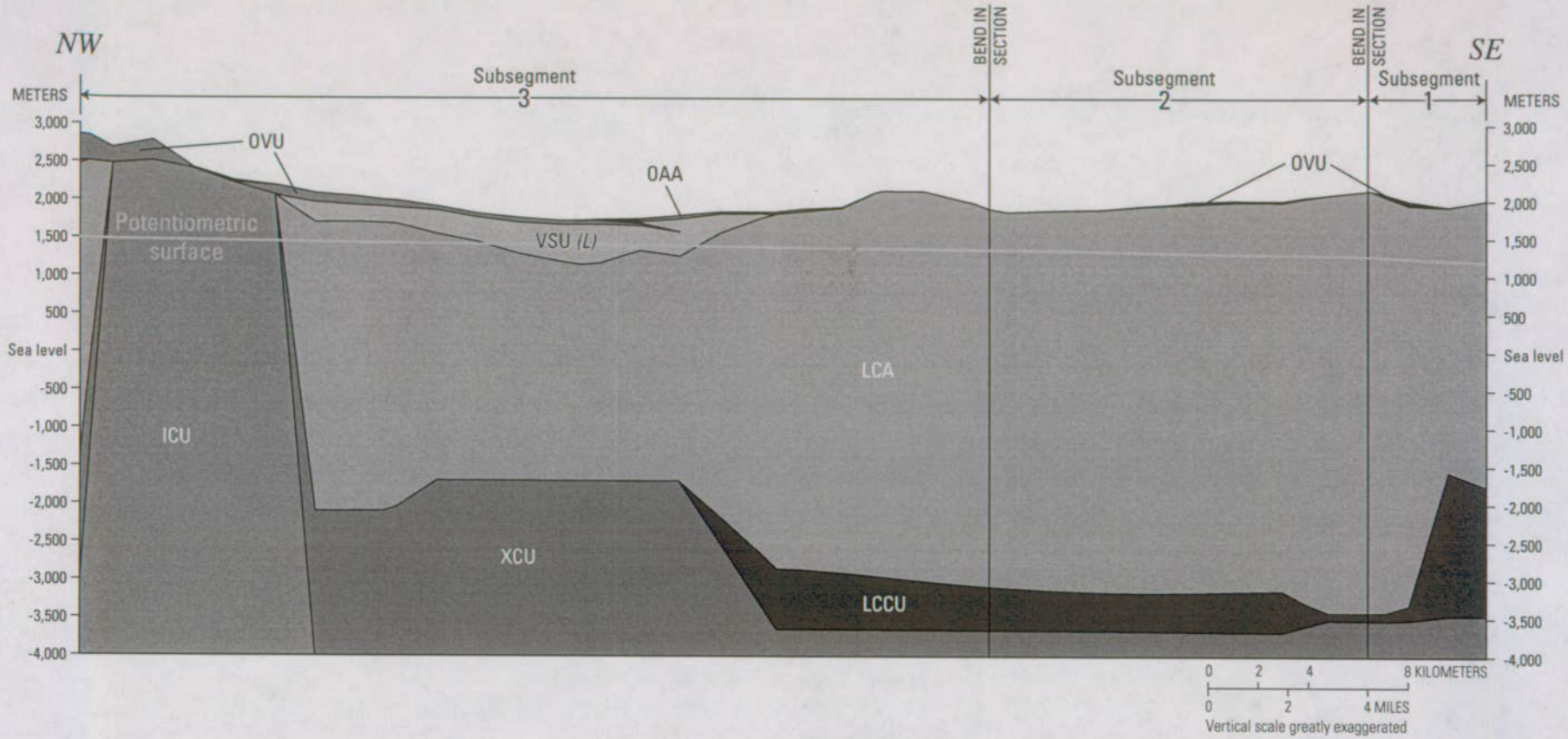

EXPLANATION OF HYDROGEOLOGIC UNITS

Not all units appear on all cross sections

YAA	Younger alluvial aquifer	VSU (U)	Upper volcanic- and sedimentary-rock unit	CFBCU	Crater Flat–Bullfrog confining unit	UCA	Upper carbonate-rock aquifer
YACU	Younger alluvial confining unit	TMVA	Thirsty Canyon–Timber Mountain volcanic-rock aquifer	CFTA	Crater Flat–Tram aquifer	UCCU	Upper clastic-rock confining unit
OAA	Older alluvial aquifer	PVA	Paintbrush volcanic-rock aquifer	BRU	Belted Range unit	LCA	Lower carbonate-rock aquifer
OACU	Older alluvial confining unit	CHVU	Calico Hills volcanic-rock unit	OVU	Older volcanic-rock unit	LCCU	Lower clastic-rock confining unit
LA	Limestone aquifer	WVU	Wahmonie volcanic-rock unit	VSU (L)	Lower volcanic- and sedimentary-rock unit	XCU	Crystalline-rock confining unit
LFU	Lava-flow unit	CFPPA	Crater Flat–Prow Pass aquifer	SCU	Sedimentary-rock confining unit	ICU	Intrusive-rock confining unit
YVU	Young volcanic-rock unit						

Figure A2–9. Hydrogeologic units of the Death Valley regional ground-water flow system model for the Garden–Coal boundary segment.

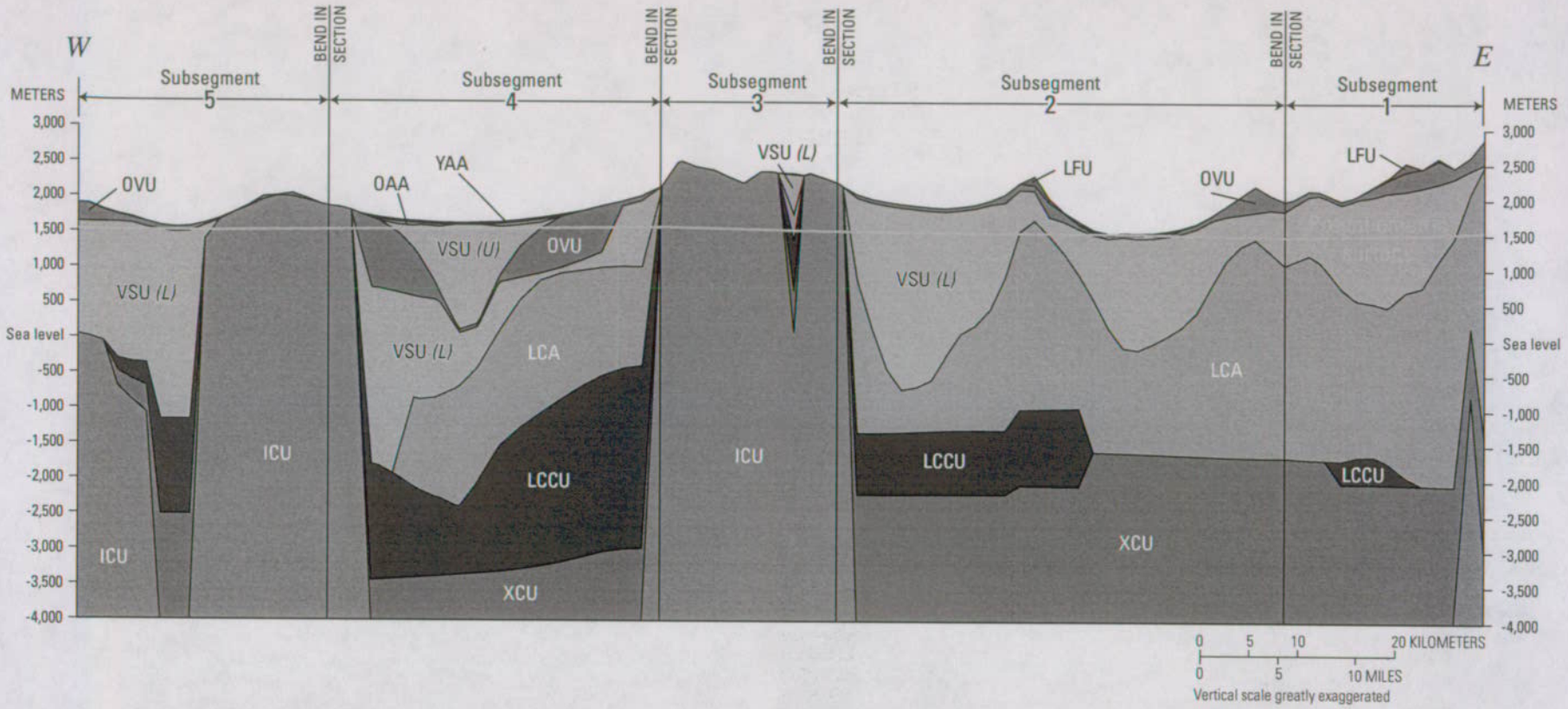

EXPLANATION OF HYDROGEOLOGIC UNITS

Not all units appear on all cross sections

YAA	Younger alluvial aquifer	VSU (U)	Upper volcanic- and sedimentary-rock unit	CFBCU	Crater Flat–Bullfrog confining unit	UCA	Upper carbonate-rock aquifer
YACU	Younger alluvial confining unit	TMVA	Thirsty Canyon–Timber Mountain volcanic-rock aquifer	CFTA	Crater Flat–Tram aquifer	UCCU	Upper clastic-rock confining unit
OAA	Older alluvial aquifer	PVA	Paintbrush volcanic-rock aquifer	BRU	Belted Range unit	LCA	Lower carbonate-rock aquifer
OACU	Older alluvial confining unit	CHVU	Calico Hills volcanic-rock unit	OVU	Older volcanic-rock unit	LCCU	Lower clastic-rock confining unit
LA	Limestone aquifer	WVU	Wahmonie volcanic-rock unit	VSU (L)	Lower volcanic- and sedimentary-rock unit	XCU	Crystalline-rock confining unit
LFU	Lava-flow unit	CFPPA	Crater Flat–Prow Pass aquifer	SCU	Sedimentary-rock confining unit	ICU	Intrusive-rock confining unit
YVU	Young volcanic-rock unit						

Figure A2–10. Hydrogeologic units of the Death Valley regional ground-water flow system model for the Stone Cabin-Railroad boundary segment.

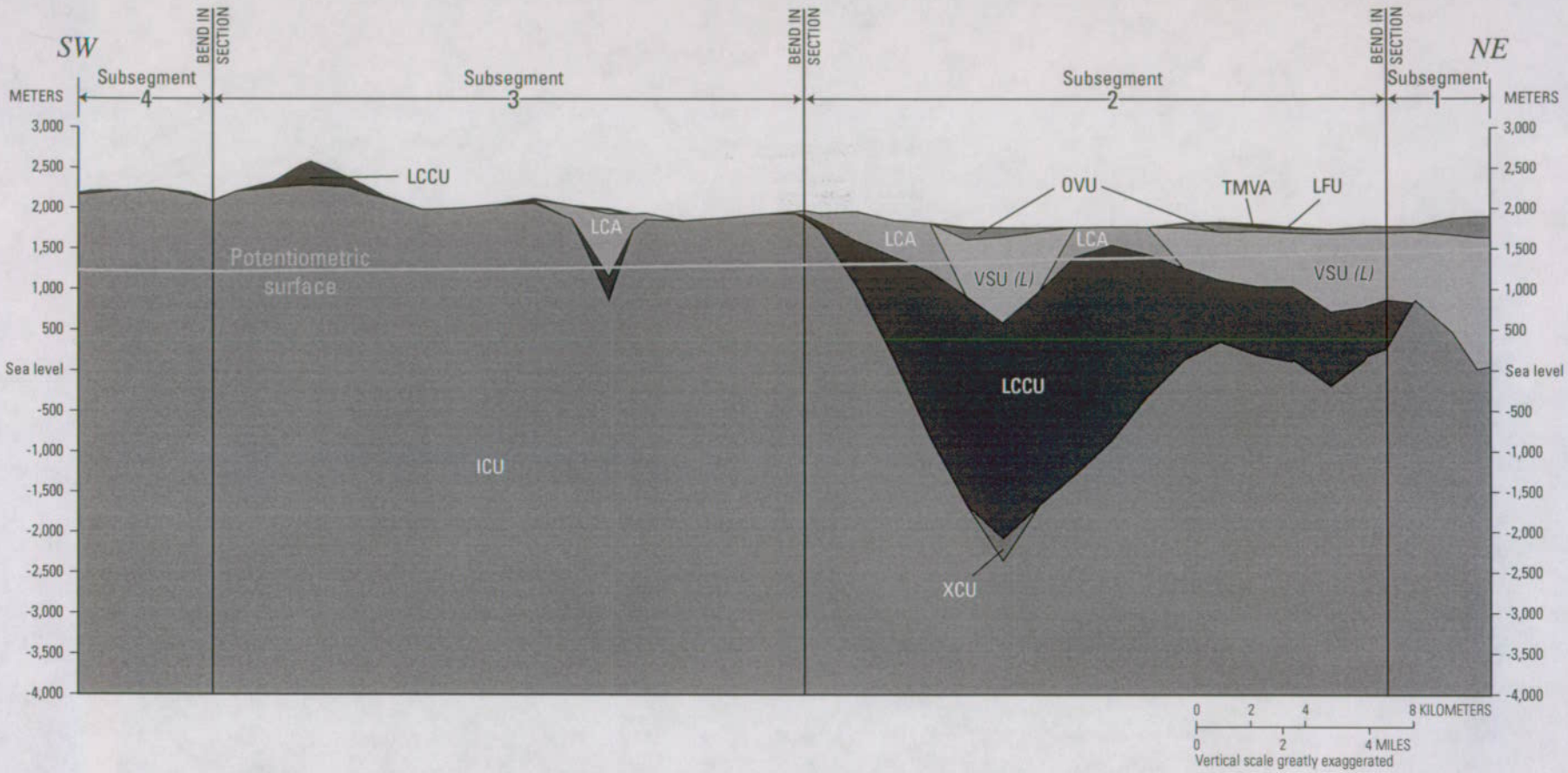

EXPLANATION OF HYDROGEOLOGIC UNITS

Not all units appear on all cross sections

YAA	Younger alluvial aquifer	VSU (U)	Upper volcanic- and sedimentary-rock unit	CFBCU	Crater Flat–Bullfrog confining unit	UCA	Upper carbonate-rock aquifer
YACU	Younger alluvial confining unit	TMVA	Thirsty Canyon–Timber Mountain volcanic-rock aquifer	CFTA	Crater Flat–Tram aquifer	UCCU	Upper clastic-rock confining unit
OAA	Older alluvial aquifer	PVA	Paintbrush volcanic-rock aquifer	BRU	Belted Range unit	LCA	Lower carbonate-rock aquifer
OACU	Older alluvial confining unit	CHVU	Calico Hills volcanic-rock unit	OVU	Older volcanic-rock unit	LCCU	Lower clastic-rock confining unit
LA	Limestone aquifer	WVU	Wahmonie volcanic-rock unit	VSU (L)	Lower volcanic- and sedimentary-rock unit	XCU	Crystalline-rock confining unit
LFU	Lava-flow unit	CFPPA	Crater Flat–Prow Pass aquifer	SCU	Sedimentary-rock confining unit	ICU	Intrusive-rock confining unit
YVU	Young volcanic-rock unit						

Figure A2–11. Hydrogeologic units of the Death Valley regional ground-water flow system model for the Clayton boundary segment.

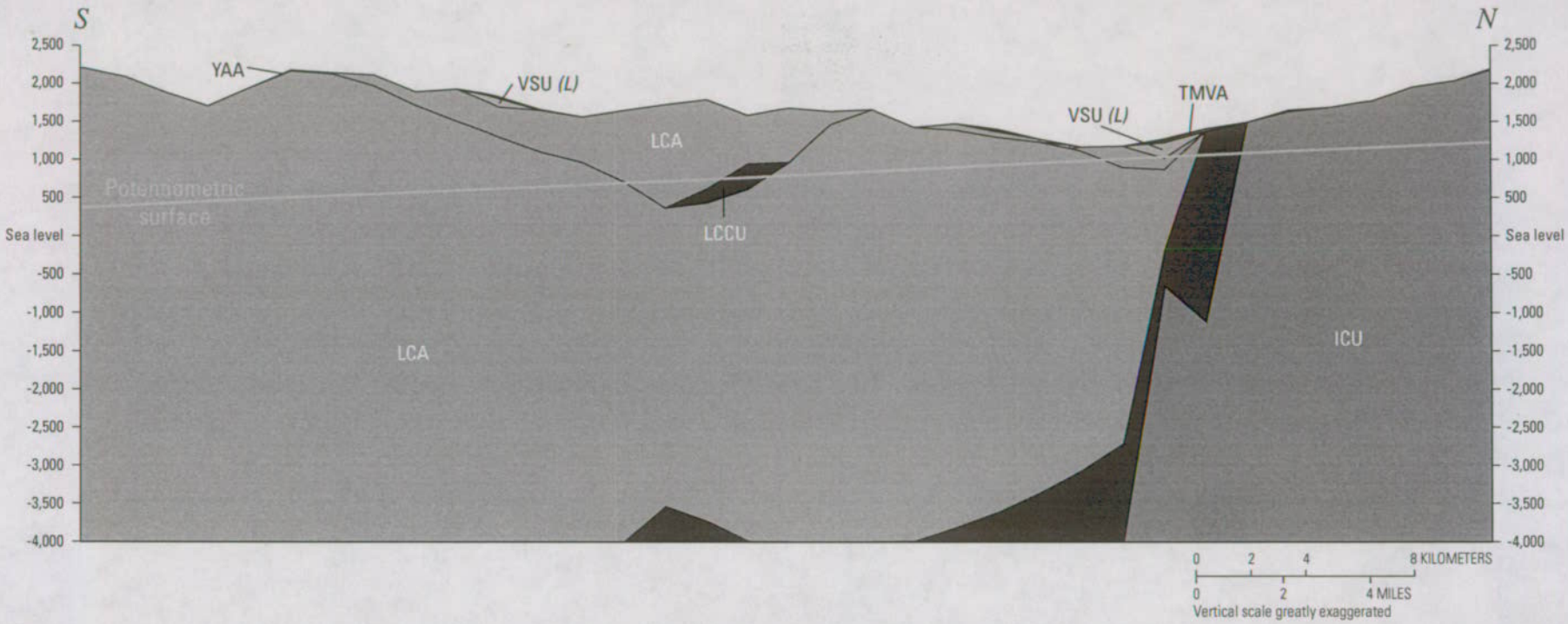

EXPLANATION OF HYDROGEOLOGIC UNITS

Not all units appear on all cross sections

YAA	Younger alluvial aquifer	VSU (U)	Upper volcanic- and sedimentary-rock unit	CFBCU	Crater Flat–Bullfrog confining unit	UCA	Upper carbonate-rock aquifer
YACU	Younger alluvial confining unit	TMVA	Thirsty Canyon–Timber Mountain volcanic-rock aquifer	CFTA	Crater Flat–Tram aquifer	UCCU	Upper clastic-rock confining unit
OAA	Older alluvial aquifer	PVA	Paintbrush volcanic-rock aquifer	BRU	Belted Range unit	LCA	Lower carbonate-rock aquifer
OACU	Older alluvial confining unit	CHVU	Calico Hills volcanic-rock unit	OVU	Older volcanic-rock unit	LCCU	Lower clastic-rock confining unit
LA	Limestone aquifer	WVU	Wahmonie volcanic-rock unit	VSU (L)	Lower volcanic- and sedimentary-rock unit	XCU	Crystalline-rock confining unit
LFU	Lava-flow unit	CFPPA	Crater Flat–Prow Pass aquifer	SCU	Sedimentary-rock confining unit	ICU	Intrusive-rock confining unit
YVU	Young volcanic-rock unit						

Figure A2–12. Hydrogeologic units of the Death Valley regional ground-water flow system model for the Eureka boundary segment.

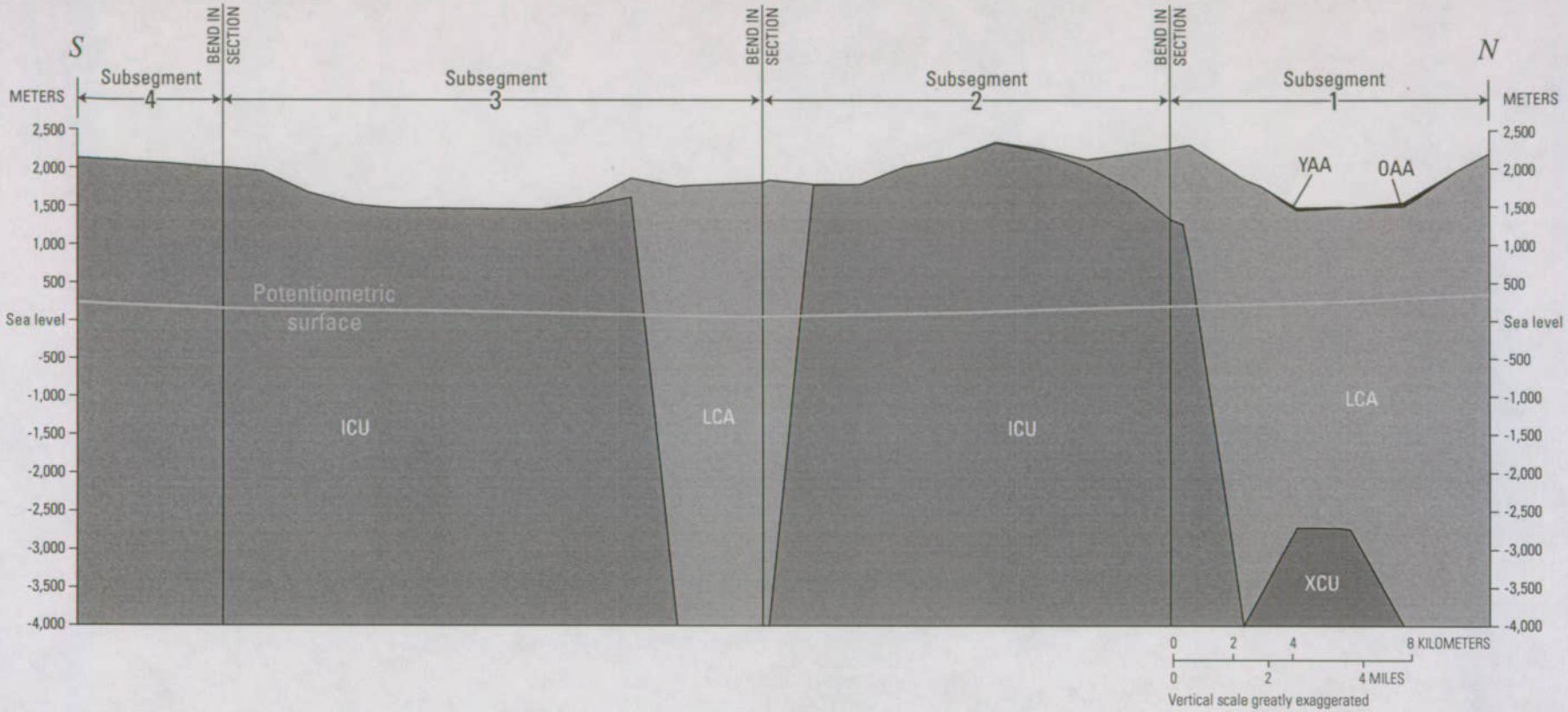

EXPLANATION OF HYDROGEOLOGIC UNITS

Not all units appear on all cross sections

YAA	Younger alluvial aquifer	VSU *(U)*	Upper volcanic- and sedimentary-rock unit	CFBCU	Crater Flat–Bullfrog confining unit	UCA	Upper carbonate-rock aquifer
YACU	Younger alluvial confining unit	TMVA	Thirsty Canyon–Timber Mountain volcanic-rock aquifer	CFTA	Crater Flat–Tram aquifer	UCCU	Upper clastic-rock confining unit
OAA	Older alluvial aquifer	PVA	Paintbrush volcanic-rock aquifer	BRU	Belted Range unit	LCA	Lower carbonate-rock aquifer
OACU	Older alluvial confining unit	CHVU	Calico Hills volcanic-rock unit	OVU	Older volcanic-rock unit	LCCU	Lower clastic-rock confining unit
LA	Limestone aquifer	WVU	Wahmonie volcanic-rock unit	VSU *(L)*	Lower volcanic- and sedimentary-rock unit	XCU	Crystalline-rock confining unit
LFU	Lava-flow unit	CFPPA	Crater Flat–Prow Pass aquifer	SCU	Sedimentary-rock confining unit	ICU	Intrusive-rock confining unit
YVU	Young volcanic-rock unit						

Figure A2–13. Hydrogeologic units of the Death Valley regional ground-water flow system model for the Saline boundary segment.

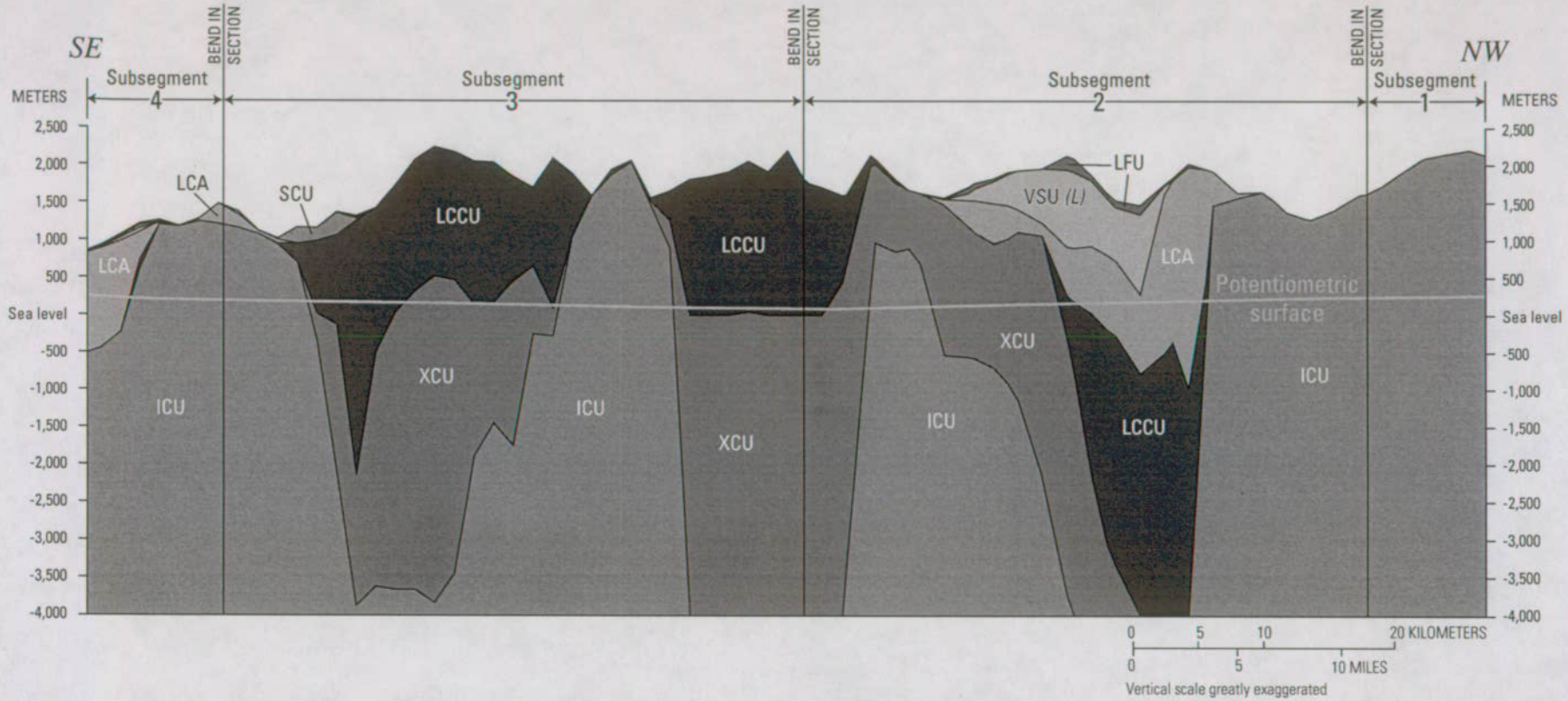

EXPLANATION OF HYDROGEOLOGIC UNITS

Not all units appear on all cross sections

YAA	Younger alluvial aquifer	VSU (U)	Upper volcanic- and sedimentary-rock unit	CFBCU	Crater Flat–Bullfrog confining unit	UCA	Upper carbonate-rock aquifer
YACU	Younger alluvial confining unit	TMVA	Thirsty Canyon–Timber Mountain volcanic-rock aquifer	CFTA	Crater Flat–Tram aquifer	UCCU	Upper clastic-rock confining unit
OAA	Older alluvial aquifer	PVA	Paintbrush volcanic-rock aquifer	BRU	Belted Range unit	LCA	Lower carbonate-rock aquifer
OACU	Older alluvial confining unit	CHVU	Calico Hills volcanic-rock unit	OVU	Older volcanic-rock unit	LCCU	Lower clastic-rock confining unit
LA	Limestone aquifer	WVU	Wahmonie volcanic-rock unit	VSU (L)	Lower volcanic- and sedimentary-rock unit	XCU	Crystalline-rock confining unit
LFU	Lava-flow unit	CFPPA	Crater Flat–Prow Pass aquifer	SCU	Sedimentary-rock confining unit	ICU	Intrusive-rock confining unit
YVU	Young volcanic-rock unit						

Figure A2–14. Hydrogeologic units of the Death Valley regional ground-water flow system model for the Panamint boundary segment.

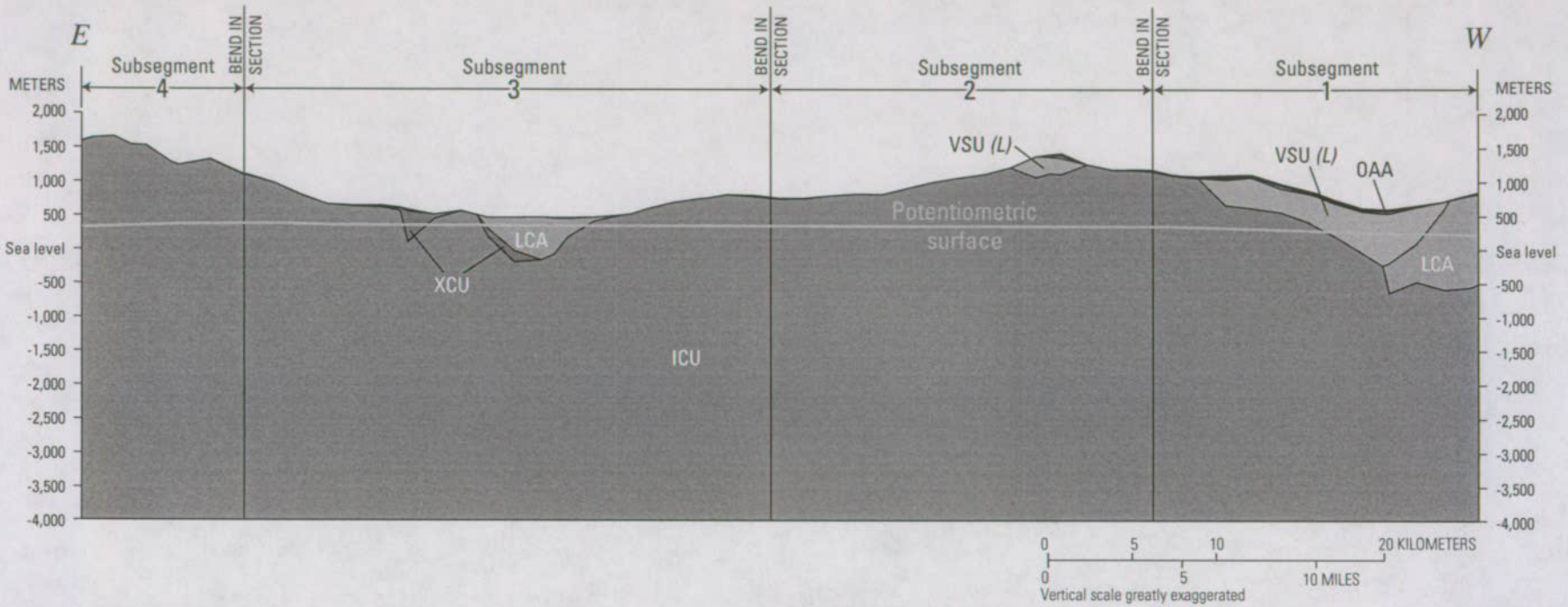

EXPLANATION OF HYDROGEOLOGIC UNITS

Not all units appear on all cross sections

YAA	Younger alluvial aquifer	VSU (U)	Upper volcanic- and sedimentary-rock unit	CFBCU	Crater Flat–Bullfrog confining unit	UCA	Upper carbonate-rock aquifer
YACU	Younger alluvial confining unit	TMVA	Thirsty Canyon–Timber Mountain volcanic-rock aquifer	CFTA	Crater Flat–Tram aquifer	UCCU	Upper clastic-rock confining unit
OAA	Older alluvial aquifer	PVA	Paintbrush volcanic-rock aquifer	BRU	Belted Range unit	LCA	Lower carbonate-rock aquifer
OACU	Older alluvial confining unit	CHVU	Calico Hills volcanic-rock unit	OVU	Older volcanic-rock unit	LCCU	Lower clastic-rock confining unit
LA	Limestone aquifer	WVU	Wahmonie volcanic-rock unit	VSU (L)	Lower volcanic- and sedimentary-rock unit	XCU	Crystalline-rock confining unit
LFU	Lava-flow unit	CFPPA	Crater Flat–Prow Pass aquifer	SCU	Sedimentary-rock confining unit	ICU	Intrusive-rock confining unit
YVU	Young volcanic-rock unit						

Figure A2–15. Hydrogeologic units of the Death Valley regional ground-water flow system model for the Owlshead boundary segment.

Table A2–1. Index of hydrologic units for areas contributing ground-water flow to the Death Valley regional ground-water flow system (after Seaber and others, 1987).

[Some hydrologic units have the same or similar names]

Code	Name	Code	Name	Code	Name
47	Huntington Valley	155C	Southern Little Smoky Valley	219	Muddy River Springs area
53	Pine Valley	156	Hot Creek Valley	220	Lower Moapa Valley
55	Carico Lake Valley	157	Kawich Valley	221	Tule Desert
56	Upper Reese River Valley	158A	Groom Lake Valley	222	Virgin River Valley
57	Antelope Valley	158B	Papoose Lake Valley	225	Mercury Valley
58	Middle Reese River Valley	159	Yucca Flat	226	Rock Valley
73B	Lovelock Valley	160	Frenchman Flat	227A	Jackass Flats
74	White Plains	161	Indian Springs Valley	227B	Buckboard Mesa
101	Carson Desert	162	Pahrump Valley	228	Oasis Valley
109	East Walker area	163	Mesquite Valley	229	Crater Flat
110A	Schurz subarea	164A	Northern Ivanpah Valley	230	Amargosa Desert
110B	Lake subarea	164B	Southern Ivanpah Valley	231	Grapevine Canyon
110C	Whiskey Flat-Hawthorne	165	Jean Lake Valley	232	Oriental Wash
113	Huntoon Valley	166	Hidden Valley	240	Chicago Valley
114	Teels Marsh Valley	167	Eldorado Valley	241	California Valley
117	Fish Lake Valley	168	Northern Three Lakes Valley	242	Lower Amargosa Valley
118	Columbus Salt Marsh	169A	Northern Tikaboo Valley	243	Death Valley
119	Rhodes Salt Marsh	169B	Southern Tikaboo Valley	244	Valjean Valley
120	Garfield Flat	170	Penoyer Valley	245	Shadow Valley
121A	Eastern Soda Spring Valley	171	Coal Valley	246	Mono Lake Valley
121B	Western Soda Spring Valley	172	Garden Valley	247	Adobe Lake Valley
122	Gabbs Valley	173A	Southern Railroad Valley	248	Long Valley
123	Rawhide Flats	173B	Northern Railroad Valley	249	Owens Valley
124	Fairwiew Valley	174	Jakes Valley	250	Deep Springs Valley
125	Stingaree Valley	175	Long Valley	251	Eureka Valley
126	Cowkick Valley	178	Butte Valley	252	Saline Valley
127	Eastgate Valley area	179	Steptoe Valley	253	Racetrack Valley area
128	Dixie Valley	180	Cave Valley	254	Darwin Plateau Basin
133	Edwards Creek Valley	181	Dry Lake Valley	255	Panamint Valley
134	Smith Creek Valley	182	Delamar Valley	256	Searles Valley
135	Lone Valley	183	Lake Valley	257	East Pilot Knob and Brown Mountain Valley
136	Monte Cristo Valley	184	Spring Valley	258	Lost Lake-Owl Lake Valley
137A	Tonopah Flat	185	Tippett Valley	259	Leach Valley
137B	Northern Big Smoky Valley	195	Snake Valley	260	Red Pass Valley
138	Grass Valley	197	Escalante Desert	261	Riggs Valley
139	Kobeh Valley	198	Dry Valley	262	Soda Lake Valley
140A	Northern Monitor Valley	199	Rose Valley	263	Kelso Valley
140B	Southern Monitor Valley	200	Eagle Valley	264	Cronise Valley
141	Ralston Valley	201	Spring Valley	265	Bicycle Valley
142	Alkali Spring Valley	202	Patterson Valley	266	Goldstone Valley
143	Clayton Valley	203	Panaca Valley	267	Superior Valley
144	Lida Valley	204	Clover Valley	268	Coyote Lake Valley
145	Stonewall Flat	205	Lower Meadow Valley Wash	269	Lower Mojave River Valley
146	Sarcobatus Flat	206	Kane Springs Valley	270	Lucerne Valley
147	Gold Flat	207	White River Valley	271	Upper Mojave River Valley
148	Cactus Flat	208	Pahroc Valley	272	Middle Mojave River Valley
149	Stone Cabin Valley	209	Pahranagat Valley	273	Harper Valley
150	Little Fish Lake Valley	210	Coyote Spring Valley	274	Antelope Valley
151	Antelope Valley	211	Southern Three Lakes Valley	275	Fremont Valley
152	Stevens Basin	212	Las Vegas Valley	276	Cuddleback Valley
153	Diamond Valley	215	Black Mountains area	277	Indian Wells Valley
154	Newark Valley	216	Garnet Valley	278	Rose Valley
155A	Northern Little Smoky Valley	217	Hidden Valley (north)		
155B	Central Little Smoky Valley	218	California Wash		

Estimates of Boundary Flow

Estimates of boundary flow from Darcy calculations and water budgets are summarized by model boundary segment. Results, special considerations, reliability of estimates, and the most representative value of boundary flow for each segment are discussed.

Silurian Boundary Segment

Ground-water inflow across the three subsegments from Lower Mojave River Valley (269) hydrologic unit was estimated by Darcy calculations. Figure A2–4 shows the cross section of the straight-line approximation of the Silurian boundary segment. The total Darcy estimate is 125 cubic meters per day (m^3/d) out of the flow-model domain (table A2–2).

The contributing area to the Silurian segment includes all or part of 18 hydrologic units (fig. A2–2). Most of the surface flow and ground-water recharge that is generated in the upgradient part of the contributing area is consumed before it reaches the boundary of the ground-water flow model. Consequently, only six hydrologic units in the lower part of the contributing area contribute flow and were evaluated in this estimate. Water budgets were calculated for the Valjean Valley (244), Shadow Valley (245), Mesquite Valley (163), Riggs Valley (261), Soda Lake Valley (262), and the lower part of the Lower Mojave River Valley (269) hydrologic units.

Inflow to Soda Lake Valley (262) hydrologic unit from the lower part of Lower Mojave River Valley (269) hydrologic unit includes streamflow at Afton Canyon and ground-water inflow (table A2–3). The ET from Soda Lake playa is an estimation of the maximum potential ET. The large negative balance for the Soda Lake Valley (262) hydrologic unit is an indication that all surface and ground-water inflow to Soda Lake playa is lost through ET.

The potential ET from the contributing area for the Silurian segment (table A2–3) is significantly greater than the ground-water recharge by infiltration of precipitation and stream inflow, indicating little or no inflow into the model domain. Low flow across the model boundary also is supported by the low recharge rate and the relatively flat regional hydraulic gradient. Water-budget estimates of net outflow across the Silurian segment is 11,400 m^3/d (table A2–3).

The Darcy estimate total (–125 m^3/d) and water budget estimate for the Silurian segment obviously do not agree. Recharge in Valjean Valley (244) and Shadow Valley (245) hydrologic units is not accounted for in the Darcy estimates. The regional potential contours (fig. A2–1) indicate that much of this water flows to the Soda Lake Valley (262) hydrologic unit; however, some probably flows toward Death Valley. Because of this, it was assumed, based on professional judgment, that only a small amount of ground-water inflow (about 500 m^3/d) occurs as underflow in the vicinity of Salt Spring at the junction of subsegments 1 and 2. This small inflow represents the estimated flow for the Silurian segment.

Spring–Mesquite Boundary Segment

Estimates of boundary flow for the Spring–Mesquite segment are based only on Darcy calculations because there is no water-budget information. Figure A2–5 shows the cross section of the straight-line approximation of the Spring–Mesquite boundary segment. Subsegments 3 through 7 are nearly parallel to divides and flow lines of the regional potential (fig. A2–1), so Darcy calculations of flow across subsegments 3 through 7 are zero. Subsegments 1 and 2 are subparallel to flow lines of the regional potential; inflow and outflow occur along these subsegments. Darcy calculations of outflow through subsegment 2 is 866 m^3/d. The inflow calculation for subsegment 1 is 84 m^3/d, which is considered insignificant. The net calculated flow across the Spring–Mesquite segment is about 800 m^3/d out of the model domain. The most reasonable estimate for boundary flow across the Spring–Mesquite segment, however is 0 m^3/d, because the flow in most of the segment is generally parallel to the boundary (table A2–9)

Las Vegas Boundary Segment

The Darcy estimate indicates an outflow of about 4,575 m^3/d across this segment (table A2–2), which is used as the most reasonable estimate (table A2–9). Figure A2–6 shows the cross section of the straight-line approximation of the Las Vegas boundary segment. The contributing areas to flow out of the model domain across the Las Vegas segment include a small part of the Spring Mountains and the southern part of the Sheep Range. Darcy calculations of outflow across subsegments 1 and 3 are about 900 and 3,600 m^3/d, respectively. No regional flow in or out of the model domain occurs across subsegment 2 because the regional hydraulic gradient is parallel to the subsegment, and the Las Vegas Valley shear zone (LVVSZ) is a relative barrier to flow (fig. A2–1). However, in the shallow part of the system a hydraulic gradient does exist across subsegment 2, and some outflow probably occurs in the shallow basin fill consisting of the upper and lower volcanic- and sedimentary-rock units (upper and lower VSU) (fig. A2–6) that was deposited after movement along the LVVSZ ceased.

Sheep Range Boundary Segment

Boundary flow across the Sheep Range segment was estimated from Darcy calculations. Figure A2–7 shows the cross section of the straight-line approximation of the Sheep Range boundary segment. The estimated hydraulic conductivities of carbonate rocks and confining-unit rocks are 0.02 and 0.00048 meters per day (m/d), respectively. Estimated outflow through subsegments 1, 2, and 3 is 24,674 m^3/d and estimated inflow across subsegment 4 is 5,927 m^3/d, which includes recharge from the east flank of the Sheep Range, giving a total estimated outflow of 18,747 m^3/d (table A2–2).

Table A2–2. Flow estimated using Darcy's law across the boundary for the Death Valley regional ground-water flow system model.

[Abbreviations: l, lower; K, hydraulic conductivity; LCA, lower carbonate-rock aquifer; OAA, older alluvial aquifer; OVU, older volcanic-rock rock unit; u, upper; VSU, volcanic- and sedimentary-rock unit; VSU-L, lower volcanic- and sedimentary-rock unit; VSU-U, upper volcanic- and sedimentary-rock unit; XXCU, combined crystalline-rock confining unit, lower clastic-rock confining unit, and intrusive-rock confining unit; m/d, meter per day; m^2, square meters; m^3/d, cubic meters per day. Rounding may produce difference between reported tottals for boundary flow and the sum of the subsegment flows]

Model boundary	Hydraulic conductivity (m/d) (Belcher and others, 2001)	Hydraulic gradient	Area (m^2)	Flow-width correction	Flow (m^3/d)	Remarks
Silurian segment						
Subsegment 1						
XXCU	0.00048	0.0081	70,462,242	0.58	159	
		Total subsegment 1			159	
Subsegment 2						
OAA	0.1	–0.0136	758,437	0.14	–144	
VSU	0.00101	–0.0136	10,175,910	0.14	–20	
XXCU	0.00048	–0.0136	114,724,294	0.14	–105	
		Total subsegment 2			–269	Flow approximately parallel to subsegment. Outflow may discharge at Salt Spring or flow back in through subsegment 1.
Subsegment 3						
XXCU	0.00048	–0.0054	30,194,944	0.19	–15	
		Total subsegment 3			–15	Flow approximately parallel to subsegment.
Estimated total					**–125**	
Spring–Mesquite segment						
Subsegment 1						
LCA	0.005	0.0053	1,574,606	0.32	13	
XXCU	0.00048	0.0053	86,531,361	0.32	70	
		Total subsegment 1			84	
Subsegment 2						
SCU	0.03	–0.0063	193,717	0.31	–11	
LCA	0.005	–0.0063	82,696,522	0.31	–808	
XXCU	0.00048	–0.0063	50,092,776	0.31	–47	Outflow.
		Total subsegment 2			–866	
Subsegments 3–7						
LCA	0.005	–0.0089	98,246,122	0	0	Flow nearly parallel to subsegment.
XXCU	0.00048	–0.0089	12,664,677	0	0	Flow nearly parallel to subsegment.
		Total subsegment 3			0	
Estimated total					**–782**	
Las Vegas segment						
Subsegment 1						
VSU	0.001	–0.0056	852,012	0.24	–1	
SCU	0.03	–0.0056	1,851,564	0.24	–75	
LCA	0.005	–0.0056	17,764,831	0.24	–119	
XXCU	0.08	–0.0056	6,946,448	0.24	–747	
		Total subsegment 1			–942	
Subsegment 2						
VSU	0.001	0.0056	178,038	0	0	
SCU	0.03	0.0056	2,832,562	0	0	
LCA	0.0219	0.0056	59,028,843	0	0	
XXCU	0.08	0.0056	2,774,777	0	0	
		Total subsegment 2			0	Flow parallel to subsegment.

Las Vegas segment—Continued

Table A2–2. Flow estimated using Darcy's law across the boundary for the Death Valley regional ground-water flow system model.—Continued

[Abbreviations: l, lower; K, hydraulic conductivity; LCA, lower carbonate-rock aquifer; OAA, older alluvial aquifer; OVU, older volcanic-rock rock unit; u, upper; VSU, volcanic- and sedimentary-rock unit; VSU-L, lower volcanic- and sedimentary-rock unit; VSU-U, upper volcanic- and sedimentary-rock unit; XXCU, combined crystalline-rock confining unit, lower clastic-rock confining unit, and intrusive-rock confining unit; m/d, meter per day; m², square meters; m³/d, cubic meters per day. Rounding may produce difference between reported tottals for boundary flow and the sum of the subsegment flows]

Model boundary	Hydraulic conductivity (m/d) (Belcher and others, 2001)	Hydraulic gradient	Area (m²)	Flow-width correction	Flow (m³/d)	Remarks
Subsegment 3						
LCA	0.0219	–0.008	36,409,119	0.5	–3,189	
XXCU	0.08	–0.008	1,385,261	0.5	–443	
		Total subsegment 3			–3,633	
Estimated total					**–4,575**	
Sheep Range segment						
Subsegment 1						
LCA-l	0.02	–0.005	55,094,466	0.8	–4,408	K est. by authors.
XXCU-l	0.00048	–0.005	836,217	0.8	–2	K est. by authors.
		Total subsegment 1			–4,410	Includes recharge from east flank of Sheep Range.
Subsegment 2						
LCA-u	0.02	–0.0139	3,238,033	0.92	–828	K est. by authors.
XXCU-u	0.00048	–0.0139	12,462,155	0.92	–76	K est. by authors.
LCA-l	0.02	–0.0033	236,813,520	0.92	–14,379	K est. by authors.
XXCU-l	0.00048	–0.0033	14,320,554	0.92	–21	K est. by authors.
		Total subsegment 2			–15,305	Includes recharge from east flank of Sheep Range.
Subsegment 3						
LCA-u	0.02	–0.0104	6,364,626	0.36	–477	K est. by authors.
XXCU-u	0.00048	–0.0104	1,622,942	0.36	–3	K est. by authors.
LCA-l	0.02	–0.0104	59,820,756	0.36	–224	K est. by authors.
XXCU-l	0.00048	–0.0104	284,208	0.36	–1	K est. by authors.
		Total subsegment 3			–4,959	Includes recharge from east flank of Sheep Range.
Subsegment 4						
LCA-u	0.02	0.0104	8,658,770	0.69	1,234	K est. by authors.
XXCU-l	0.00048	0.0104	116,074	0.69	0	K est. by authors.
LCA-l	0.02	0.0104	3,2636,808	0.69	4,684	K est. by authors.
		Total subsegment 4			5,927	Includes recharge from east flank of Sheep Range.
Estimated total					**–18,747**	
Pahranagat segment						
Subsegment 1						
LCA	0.012	0.008	35,095,853	0.54	1,819	K est. by authors.
XXCU	0.00048	0.008	3,716,562	0.54	8	
		Total subsegment 1			1,827	
Subsegment 2						
LCA	0.012	–0.0075	71,737,048	0.36	–2,324	K est. by authors.
XXCU	0.00048	–0.0075	16,456,431	0.36	–21	
		Total subsegment 2			–2,346	

Pahranagat segment—Continued

Table A2–2. Flow estimated using Darcy's law across the boundary for the Death Valley regional ground-water flow system model.—Continued

[Abbreviations: l, lower; K, hydraulic conductivity; LCA, lower carbonate-rock aquifer; OAA, older alluvial aquifer; OVU, older volcanic-rock rock unit; u, upper; VSU, volcanic- and sedimentary-rock unit; VSU-L, lower volcanic- and sedimentary-rock unit; VSU-U, upper volcanic- and sedimentary-rock unit; XXCU, combined crystalline-rock confining unit, lower clastic-rock confining unit, and intrusive-rock confining unit; m/d, meter per day; m², square meters; m³/d, cubic meters per day. Rounding may produce difference between reported tottals for boundary flow and the sum of the subsegment flows]

Model boundary	Hydraulic conductivity (m/d) (Belcher and others, 2001)	Hydraulic gradient	Area (m²)	Flow-width correction	Flow (m³/d)	Remarks
Subsegment 3						
LCA	0.012	–0.0055	30,087,908	0.05	–99	
XXCU	0.00048	–0.0055	22,904,328	0.05	–3	
		Total subsegment 3			–102	
Subsegment 4						
LCA	0.012	0.0055	28,026,698	0.19	351	
XXCU	0.00048	0.0055	16,030,089	0.19	8	
		Total subsegment 4			359	
Subsegment 5						
LCA	0.012	–0.004	106,150,918	0.49	-2,497	
XXCU	0.00048	–0.004	26,311,596	0.49	–25	
		Total subsegment 5			–2,521	Outflow.
Estimated total					**–2,783**	Net outflow.
Garden–Coal segment						
Subsegment 1						
LCA	0.012	0.0108	18,067,657	0.42	983	
XXCU	0.00048	0.0108	6,964,906	0.42	15	
		Total Subsegment 1			999	
Subsegment 2						
LCA	0.012	0.0067	17,409,087	0.56	784	
XXCU	0.00048	0.0067	12,222,297	0.56	22	
		Total Subsegment 2			806	
Subsegment 3						
LCA	0.012	0.0032	102,792,919	0.57	2,250	
XXCU	0.00048	0.0032	96,263,253	0.57	84	
		Total Subsegment 3			2,334	
Estimated total					**4,139**	
Stone Cabin–Railroad segment						
Subsegment 1						
LCA	0.012	–0.0031	64,588,868	0.31	–745	
XXCU	0.00048	–0.0031	49,333,073	0.31	–23	
		Total Subsegment 1			–768	Returns through subsegment 2.
Subsegment 2						
VSU	0.05465	0.0028	8,938,182	0.84	1,149	
LCA	0.012	0.0028	120,772,098	0.84	3,409	
XXCU	0.00048	0.0028	124,674,096	0.84	141	
		Total Subsegment 2			4,698	
Subsegment 3						
LCA	0.006	0.0047	22,363	0.27	0	
XXCU	0.00048	0.0047	102,013,424	0.27	62	
		Total Subsegment 3			62	

Stone Cabin–Railroad segment—Continued

Table A2–2. Flow estimated using Darcy's law across the boundary for the Death Valley regional ground-water flow system model.—Continued

[Abbreviations: l, lower; K, hydraulic conductivity; LCA, lower carbonate-rock aquifer; OAA, older alluvial aquifer; OVU, older volcanic-rock rock unit; u, upper; VSU, volcanic- and sedimentary-rock unit; VSU-L, lower volcanic- and sedimentary-rock unit; VSU-U, upper volcanic- and sedimentary-rock unit; XXCU, combined crystalline-rock confining unit, lower clastic-rock confining unit, and intrusive-rock confining unit; m/d, meter per day; m^2, square meters; m^3/d, cubic meters per day. Rounding may produce difference between reported tottals for boundary flow and the sum of the subsegment flows]

Model boundary	Hydraulic conductivity (m/d) (Belcher and others, 2001)	Hydraulic gradient	Area (m^2)	Flow-width correction	Flow (m^3/d)	Remarks
Subsegment 4						
VSU-U	0.05465	0.004	10,336,774	0.79	1,785	
OVU	0.0013	0.004	11,093,052	0.79	46	
VSU-L	0.05465	0.004	25,914,727	0.79	4,475	
LCA	0.006	0.004	40,719,263	0.79	772	
XXCU	0.00048	0.004	103,662,840	0.79	157	
		Total subsegment 4			7,235	
Subsegment 5						
VSU	0.0133	0.0036	25,690,839	0.87	1,070	
XXCU	0.00048	0.0036	118,258,401	0.87	178	
		Total subsegment 5			1,248	
Estimated total					**12,476**	
Clayton segment						
Subsegment 1						
VSU	0.00101	0.0077	4,427,844	0.24	8	
XXCU	0.00048	0.0077	21,701,252	0.24	19	
		Total subsegment 1			28	
Subsegment 2						
VSU	0.00101	0.0077	6,401,160	0.34	17	
LCA	0.16	0.0077	469,502	0.34	197	K est. by authors.
XXCU	0.00048	0.0077	138,460,787	0.34	174	
		Total subsegment 2			388	
Subsegment 3						
LCA	0.16	0.0044	37,886	0.19	5	Flow parallel to northern half of segment. K est. by authors.
XXCU	0.00048	0.0044	144,638,324	0.19	58	Flow parallel to northern half of segment.
		Total subsegment 3			63	
Subsegment 4						
XXCU	0.00048	0.0119	32,892,612	1	188	
		Total subsegment 4			188	
Estimated total					**667**	
Eureka segment						
Subsegment 1						
LCA	0.16	0.0176	177,125,504	0.04	19,951	K est. by authors
XXCU	0.00048	0.0176	70,931,206	0.04	24	
Estimated total					**19,975**	
Saline segment						
Subsegment 1						
LCA	0.003	–0.0186	34,724,150	0.38	–736	
XXCU	0.00048	–0.0186	11,942,934	0.38	–41	
		Total subsegment 1			–777	
Subsegment 2						
LCA	0.003	0.0186	3,069,221	0.72	123	
XXCU	0.00048	0.0186	54,681,421	0.72	352	
		Total subsegment 2			475	

Saline segment—Continued

Table A2–2. Flow estimated using Darcy's law across the boundary for the Death Valley regional ground-water flow system model.—Continued

[Abbreviations: l, lower; K, hydraulic conductivity; LCA, lower carbonate-rock aquifer; OAA, older alluvial aquifer; OVU, older volcanic-rock rock unit; u, upper; VSU, volcanic- and sedimentary-rock unit; VSU-L, lower volcanic- and sedimentary-rock unit; VSU-U, upper volcanic- and sedimentary-rock unit; XXCU, combined crystalline-rock confining unit, lower clastic-rock confining unit, and intrusive-rock confining unit; m/d, meter per day; m^2, square meters; m^3/d, cubic meters per day. Rounding may produce difference between reported tottals for boundary flow and the sum of the subsegment flows]

Model boundary	Hydraulic conductivity (m/d) (Belcher and others, 2001)	Hydraulic gradient	Area (m^2)	Flow-width correction	Flow (m^3/d)	Remarks
Subsegment 3						
LCA	0.003	0.0091	14,482,916	0.9	356	
XXCU	0.00048	0.0091	62,051,113	0.9	244	
		Total subsegment 3			600	
Subsegment 4						
XXCU	0.00048	0.0017	21,136,287	0	0	
		Total subsegment 4			0	Flow parallel to subsegment.
Estimated total					**898**	
Panamint segment						
Subsegment 1						
XXCU	0.00048	0.0121	381,663,383	0.96	2,128	
		Total subsegment 1			2,128	
Subsegment 2						
LCA	0.16	0.013	5,337,688	0.88	9,770	K est. by authors.
XXCU	0.00048	0.013	174,846,484	0.88	960	
		Total subsegment 2			10,730	
Subsegment 3						
XXCU	0.00048	0.0123	185,428,139	0.91	996	
		Total subsegment 3			996	
Subsegment 4						
LCA	0.001	0.0117	1,710,262	0.75	15	
XXCU	0.00048	0.0117	42,840,019	0.75	180	
		Total subsegment 4			195	
Estimated total					**14,050**	
Owlshead segment						
Subsegment 1						
VSU	0.00101	0.0076	1,264,971	0.96	9	
LCA	0.001	0.0076	3,622,217	0.96	26	
XXCU	0.00048	0.0076	76,641,484	0.96	268	
		Total subsegment 1			304	
Subsegment 2						
XXCU	0.00048	0.0112	97,960,865	0.64	337	
		Total subsegment 2			337	
Subsegment 3						
LCA	0.001	0.0261	1,534,492	0.98	39	
XXCU	0.00048	0.0261	133,817,769	0.98	1,643	
		Total subsegment 3			1,682	
Subsegment 4						
XXCU	0.00048	0.0093	41,474,680	0.32	59	
		Total subsegment 4			59	
Estimated total					**2,382**	

Table A2–3. Estimated water budget for the Silurian boundary segment of the Death Valley regional ground-water flow system model.

[m^3/d, cubic meters per day; --, no data]

Hydrologic unit name and code (fig. A2–2)	Recharge (m^3/d)	Inflow (m^3/d)	Evapotranspiration (m^3/d)	Flow[1] (m^3/d)	Reference
Valjean (244)	1,400	0	0	1,400	Harrill and others, 1988
Shadow (245)	4,100	0	0	4,100	Harrill and others, 1988
Mesquite (163)	4,730	2,360	7,430	–340	Glancy, 1968
[2]Riggs (261)	--	--	--	--	Estimated by authors
Soda Lake (262)	1,400	[3]15,000	[4]34,000	–17,600	Estimated by authors
Lower Mojave River (269)	--	1,000	--	1,000	
Total (rounded)	**11,600**	**18,400**	**41,400**	**–11,400**	

[1]Flow estimate is the sum of recharge, inflow, and evapotranspiration. Negative values indicate flow out of the model domain; positive values indicate flow into the model domain.

[2]Budget components not estimated in this study, but no sign of significant evapotranspiration was observed during the field reconnaissance. Riggs hydrologic unit (261) may transmit small amounts of underflow to Valjean Valley hydrologic unit (244).

[3]Surface-water inflow (Mojave River) at Afton Canyon.

[4]Maximum potential evapotranspiration from the playa of Soda Lake Valley hydrologic unit (262).

The Sheep Range segment is in a part of the DVRFS model domain that is in the Colorado River flow system. Flow from Pahranagat subsegment 1 (1,827 m^3/d) and Sheep Range subsegment 4 (5,927 m^3/d) enters the flow model domain and exits through the rest of the Sheep Range segment (–18,747 m^3/d) (table A2–4). The net outflow from the Sheep Range segment is derived from inflow across these two subsegments and recharge to the Sheep Range. Based on these relations, these flow volumes appear reasonable.

Pahranagat Boundary Segment

The Darcy calculations show no significant gain or loss to the model domain from the combined inflow from the Garden–Coal segment (4,139 m^3/d) and subsegments 2 through 5 of the Pahranagat segment (–4,610 m^3/d). Figure A2–8 shows the cross section of the straight-line approximation of the Pahranagat boundary segment. The Darcy calculations show an inflow of 1,827 m^3/d across the Pahranagat subsegment 1.

Subsegments 2 through 5 of the Pahranagat segment generally are near and parallel to the boundary of the Death Valley and Colorado River flow systems. The net outflow from these subsegments is derived from inflows to the model domain across the adjacent Garden–Coal segment to the north. Flow enters the Garden-Coal segment and exits through the Pahranagat segment (table A2–4).

Garden–Coal Boundary Segment

The total inflow to the model domain across the Garden–Coal segment calculated by the Darcy method is 4,139 m^3/d, which is considered the best available estimate of inflow to the model domain for this segment. Figure A2–9 shows the cross section of the straight-line approximation of the Garden–Coal boundary segment. The inflow to this segment is the major source of ground water that moves out of the model domain through the Pahranagat segment, discussed previously (table A2–4).

Small areas of Southern Railroad Valley (173A), Garden Valley (172), and Coal Valley (171) hydrologic units contribute to flow across the Garden–Coal segment. Recharge to the Garden Valley (172) and Coal Valley (171) hydrologic units totals 40,500 m^3/d, and ET of ground water is 6,750 m^3/d (Eakin, 1963).

Table A2–4. Summary of inflow and outflow of ground water across the Sheep Range, Paharanagat, and Garden–Coal boundary segments of the Death Valley regional ground-water flow system model.

[m^3/d, cubic meters per day]

Segment	Subsegment (fig. A2–3)	Inflow (m^3/d)	Outflow (m^3/d)
Sheep Range	1		4,409
	2		15,305
	3		4,959
	4	5,927	
Pahranagat	1	1,827	
	2		2,346
	3		102
	4	359	
	5		2,521
Garden–Coal	1	999	
	2	806	
	3	2,334	
Subtotal		12,252	29,642
Total			**17,390**

Stone Cabin–Railroad Boundary Segment

The Darcy calculations (table A2–2) show a net inflow across the Stone Cabin–Railroad segment of about 12,500 m^3/d. Figure A2–10 shows the cross section of the straight-line approximation of the Stone Cabin–Railroad boundary segment. The Darcy calculated inflow is accepted as the most reasonable estimate of inflow across the boundary.

The contributing areas to this segment (fig. A2–1) include relatively small parts of the Southern Railroad Valley (173A), Hot Creek Valley (156), Stone Cabin Valley (149), Southern Monitor Valley (140B), and Ralston Valley (141) hydrologic units. The water budgets given in table A2–5 show an excess of recharge over ground-water discharge through ET. The water budgets, however, are for the entire basins and are not amenable to separation of the flows that actually cross the Stone Cabin–Railroad segment.

Clayton Boundary Segment

The Darcy calculation of flow across the segment (table A2–2) shows a net inflow to the model domain of about 667 m^3/d. Figure A2–11 shows the cross section of the straight-line approximation of the Clayton boundary segment. The flat gradient across the boundary segment and the small water balance from the basins in the contributing area indicate that the inflow across the model boundary is small.

The contributing area to the Clayton segment (fig. A2–3) includes all or parts of the Clayton Valley (143), Alkali Spring Valley (142), Fish Lake Valley (117), Ralston Valley (141), Adobe Lake Valley (247), Tonopah Flat (137A), Upper Reese River Valley (56), Northern Big Smoky Valley (137B), and Southern Monitor Valley (140B) hydrologic units and the Owens Valley ground-water basin. This is a large area that contains not only significant recharge areas but also large areas of ET. Table A2–6 lists water-budget information for the most significant contributing basins. As noted, the total area of these basins is not coincident with the contributing area of the Clayton segment. The water budgets for these basins show that although there is a great amount of recharge to basins in the contributing area, about 99 percent of this recharge is consumed by ET.

As discussed previously, the flat gradient and the small water budget indicate very little flow across the Clayton segment. Because of this, the Darcy estimate of 667 m^3/d into the model domain is accepted as the most reasonable.

Eureka and Saline Boundary Segments

The Darcy calculations show the net flow into the model from the Eureka and Saline segments is about 20,900 m^3/d (table A2–2). Figures A2–12 and A2–13 shows the cross sections of the straight-line approximation of the Eureka and Saline boundary segments. This estimated inflow appears to be sensitive to the estimated hydraulic-conductivity (0.16 m/d) of the carbonate rocks. This estimated inflow should be used with caution because of the uncertain nature of the estimate.

The regional ground-water potential map (fig. A2–1; Appendix 1) shows that the contributing basins are Saline Valley (252), Eureka Valley (251), Deep Springs Valley (250), Racetrack Valley (253), and Long Valley (248) hydrologic units, and parts of the Owens Valley (249) and Darwin Plateau Basin (254) hydrologic units. Water-budget calculations for Saline Valley (252), Eureka Valley (251), Racetrack Valley (253), and Deep Springs Valley (250) hydrologic units (table A2–7) show an excess of ground water of about 15,600 m^3/d (J.R. Harrill, written commun., 2003). It is estimated that the inflow from Owens Valley (249), Long Valley (248), and the Darwin Plateau Basin (254) hydrologic units is less than 1,000 m^3/d based on the order of magnitude Darcy calculations. The boundary flow across these segments is into the model domain except for flow out of the model in subsegment 1 of the Saline segment.

An inflow from the Saline and Eureka segments of 15,100 m^3/d is used as the most reasonable estimate on the basis of the water budget and order of magnitude Darcy estimates of inflow from the Owens Valley (249) hydrologic unit. An inflow of about 27,000 m^3/d from Saline Valley (252) and possibly part of the Panamint Valley (255) hydrologic units

Table A2–5. Estimated water budget for the Stone Cabin–Railroad boundary segment of the Death Valley regional ground-water flow system model.

[m^3/d, cubic meters per day]

Hydrologic unit and code (fig. A2–2)	Recharge (m^3/d)	Evapotranspiration (m^3/d)	Balance[1] (m^3/d)	Reference
Southern Railroad (173A)	18,600	675	17,925	Van Denburgh and Rush (1974)
Hot Creek (156)	23,600	15,500	8,100	Rush and Everett (1966)
Stone Cabin (149)	16,900	5,100	11,800	Rush (1968)
Ralston (141)	16,900	8,400	8,500	Rush (1968)
Monitor South (140B)	50,700	31,100	19,600	Rush and Everett (1966)
Total (rounded)	**126,700**	**60,800**	**65,900**	

[1]Flow estimate is the sum of recharge, inflow, and evapotranspiration.

previously was estimated by Harrill (1995, p. 91) primarily based on the focused discharge in and adjacent to Mesquite Flat (fig. A–1) in Death Valley.

Panamint Boundary Segment

The regional ground-water potential slopes rather uniformly across the Panamint segment with a gradient of about 0.01. Although there are carbonate rocks in the cross section, most of these rocks are above the zone of regional ground-water flow and do not contribute ground water from the contributing area across the Panamint segment. Figure A2–14 shows the cross section of the straight-line approximation of the Panamint boundary segment. The Darcy flow calculated through this segment to the model domain of about 14,050 m^3/d is obtained by assuming a hydraulic-conductivity value of 0.16 m/d for the lower carbonate-rock aquifer in subsegment 2.

Contributing basins to this segment include Panamint Valley (255), Rose Valley (278), and parts of Owens Valley (249), Darwin Plateau Basin (254), Indian Wells Valley (277), Searles Valley (256), and East Pilot Knob–Brown Mountain Valley (257) hydrologic units (fig. A2–2 and table A2–1). The major contribution of flow to the model domain is from the Panamint Valley (255) hydrologic unit. An estimated water budget for Panamint Valley (J.R. Harrill, written commun., 2003) includes recharge of 56,000 m^3/d and ET of 42,000 m^3/d (table A2–8). The balance of ground-water flow, 14,000 m^3/d, is tributary to the Death Valley (243) hydrologic unit in the model domain. The greatest part of

Table A2–6. Estimated water budget for the Clayton boundary segment of the Death Valley regional ground-water flow system model.

[m^3/d, cubic meters per day; --, no data]

Hydrologic unit and code (fig. A2–2)	Recharge (m^3/d)	Evapotranspiration (m^3/d)	Balance[1] (m^3/d)	Reference
Clayton (143)	5,100	81,100	–76,000	Rush (1968)
Alkali Spring (142)	330	1,350	–1,020	Rush (1968)
Fish Lake (117)	111,000	81,000	30,000	Rush and Katzer (1973)
Tonopah Flat (137A)	40,500	20,300	20,200	Rush and Schroer (1970)
Ralston (141)	16,900	8,400	8,500	Rush (1968)
Northern Big Smoky Valley (137B)	220,000	216,000	4,000	Rush and Schroer (1970)
Monitor South (140B)	50,700	31,100	19,600	Rush and Everett (1966)
Owens (249)	--	--	--	--
Total (rounded)	**445,000**	**439,000**	**6,000**	

[1]Flow estimate is the sum of recharge, inflow, and evapotranspiration. Negative values indicate flow out of the model domain; positive values indicate flow into the model domain.

Table A2–7. Estimated water budget for the Eureka and Saline boundary segments of the Death Valley regional ground-water flow system.

[m^3/d, cubic meters per day; --, no data; <, less than]

Hydrologic unit and code (fig. A2–2)	Recharge (m^3/d)	Evapotranspiration (m^3/d)	Balance[1] (m^3/d)	Reference
Deep Springs (250)	29,000	25,000	4,000	J.R. Harrill, written commun., 2003
Eureka (251)	13,000	0	13,000	Estimated by authors
Saline (252)	79,000	86,000	–7,000	Estimated by authors
Racetrack (253)	4,600	0	4,600	Estimated by authors
Owens (249) and Long Valleys (248), and Darwin Plateau Basin (254)	--	--	[2]<1,000	Estimated by authors
Total (rounded)			**14,600 to 15,600**	

[1]Flow estimate is the sum of recharge, inflow, and evapotranspiration. Negative values indicate flow out of the model domain; positive values indicate flow into the model domain.

[2]Based on order of magnitude Darcy calculations.

this 14,000 m^3/d is from the Panamint Valley (255) hydrologic unit where the most precipitation falls and recharges the ground-water system. The inflow from basins upgradient from Panamint Valley (255) and Darwin Plateau Basin (254) hydrologic units is estimated by Darcy calculations to be less than 2,000 m^3/d. Thus, the estimated flow from Panamint Valley (255) into the model domain is 14,000 to 16,000 m^3/d.

Given the uncertainty of both the Darcy flow estimate and the water budget estimate, there is good agreement between the two methods. The most reasonable estimate, based on both the Darcy flow calculations and the water budget estimate, is 15,000 m^3/d for the boundary flow across the Panamint segment.

Owlshead Boundary Segment

Darcy calculations yield an inflow across this boundary segment of about 2,400 m^3/d (table A2–2). Figure A2–15 shows the cross section of the straight-line approximation of the Owlshead boundary segment. Almost all of this calculated inflow (97 percent) is through a large area of confining-unit rocks.

The contributing area includes parts of Indian Wells Valley (277), Fremont Valley (275), Cuddleback Valley (276), Searles Valley (256), East Pilot Knob and Brown Mountain Valley (257), Superior Valley (267), Goldstone Valley (266), Bicycle Valley (265), Leach Valley (259), Lost Lake–Owl Lake Valley (258), and Harper Valley (273) hydrologic units (fig. A2–2). Considering that the contributing area for this segment is an area of low precipitation and recharge and that ET areas are present in Searles Valley (256) and Indian Wells Valley (277) hydrologic units, the Darcy calculation is considered to yield a maximum value for flow across this segment and is used as the most reasonable estimate.

Summary of Flow Estimates

Flow estimates presented herein for the boundary segments are summarized in table A2–9. These estimates were developed on the basis of Darcy calculations and water-budget calculations where adequate information was available. These estimates were used to support some aspects of the model calibration.

Table A2–8. Estimated water budget for the Panamint boundary segment of the Death Valley regional ground-water flow system.

[m^3/d, cubic meters per day; <, less than]

Hydrologic unit and code (fig. A2–2)	Recharge (m^3/d)	Inflow (m^3/d)	Evapotranspiration (m^3/d)	Balance[1] (m^3/d)	Reference
Panamint (255), Darwin Plateau Basin (254), and East Pilot Knob–Brown Mountain (257)	56,000	<2,000	42,000	14,000 to 16,000	Estimated by authors
Total				**14,000 to 16,000**	

[1]Flow estimate is the sum of recharge, inflow, and evapotranspiration.

Table A2–9. Summary of boundary flow estimates for the Death Valley regional ground-water flow system model.

[m^3/d, cubic meters per day]

Model boundary segment and subsegment (fig. A2–3)	Flow estimated by Darcy method (table A2–2) (m^3/d)	Flow estimated by water-budget method (m^3/d)	Source of water-budget estimate	Most reasonable estimate of flow (m^3/d)	Basis of most reasonable estimate	Remarks
Silurian						
1	159					
2	–269					
3	–15					
Total	–125	–11,400	Table A2–3	500	Darcy, water budget (see text)	Most water consumed in areas upgradient from boundary (table A2–3).
Spring–Mesquite						
1	84					
2	–866					
3	0					
4	0					
5	0					Flow is generally parallel to boundary. No significant flow overall, even though flow was estimated across subsegments 1 and 2.
6	0					
7	0					
Total	–782	No data		0	See text	
Las Vegas						
1	–942					
2	0					
3	–3,633					
Total	–4,575	No data		–4,575	Darcy (table A2–2)	
Sheep Range						
1	–4,410					
2	–15,305					
3	–4,959					
4	5,927					
Total	–18,747	No data		–18,747	Darcy (table A2–2)	Net value (table A2–4 and text).
Pahranagat						
1	1827					
2	–2,345					
3	–102					
4	359					
5	–2,521					
Total	–2,783	No data		–2,783	Darcy (table A2–2)	Inflow and outflow (table A2–4).
Garden–Coal						
1	999					
2	806					
3	2,234					
Total	4,139	No data		4,139	Darcy (table A2–2)	
Stone Cabin–Railroad						
1	768					
2	4,698					
3	62					
4	7,235					
5	1,248					
Total	12,476	65,900	Table A2–5	12,476	Darcy (table A2–2; see text)	Recharge exceeds discharge (table A2–5)

Table A2–9. Summary of boundary flow estimates for the Death Valley regional ground-water flow system model.—Continued

[m^3/d, cubic meters per day]

Model boundary segment and subsegment (fig. A2–3)	Flow estimated by Darcy method (table A2–2) (m^3/d)	Flow estimated by water-budget method (m^3/d)	Source of water-budget estimate	Most reasonable estimate of flow (m^3/d)	Basis of most reasonable estimate	Remarks
Clayton						
1	28					
2	388					
3	63					
4	188					
Total	667	6,000	Table A2–6	667	Darcy (see text)	Most recharge consumed by evapotranspiration (table A2–6)
Eureka and Saline						
Eureka						
1	19,975					
Saline						
1	–777					
2	475					
3	600					
4	0					
Subtotal	898					
Combined total	20,873	14,600 to 15,600	Table A2–7	15,100	Darcy, water budget	
Panamint						
1	2,128					
2	10,730					
3	996					
4	195					
Total	14,050	14,000 to 16,000	Table A2–8	15,000	Darcy, water budget (table A2–8, see text)	
Owlshead						
1	304					
2	337					
3	1,682					
4	59					
Total	2,382	No data		2,382	Darcy (table A2–2)	Maximum value

References Cited

Belcher, W.R., Elliott, P.E., and Geldon, A.L., 2001, Hydraulic-property estimates for use with a transient ground-water flow model for the Death Valley regional ground-water flow system, Nevada and California: U.S. Geological Survey Water-Resources Investigations Report 01–4210. Accessed September 1, 2004 at *http://water.usgs.gov/pubs/wri/wri014210*

Belcher, W.R., Sweetkind, D.S., and Elliott, P.E., 2002, Probability distributions of hydraulic conductivity for the hydrogeologic units of the Death Valley regional ground-water flow system, Nevada and California: U.S. Geological Survey Water-Resources Investigations Report 02–4212, 18 p. Accessed September 1, 2004 at *http://water.usgs.gov/pubs/wri/wrir024212*

Eakin, T.E., 1963, Ground-water appraisal of Garden and Coal Valleys, Lincoln and Nye Counties, Nevada: Nevada Department of Conservation and Natural Resources, Ground-Water Resources Reconnaissance Report 18, 29 p.

Freeze, R.A. and Cherry, J.A., 1979, Groundwater: Englewood Cliffs, New Jersey, Prentice-Hall, 604 p.

Glancy, P.A., 1968, Water resources appraisal of Mesquite–Ivanpah Valley area, Nevada and California: Nevada Division of Water Resources, Reconnaissance Report 46, 57 p.

Harrill, James R., 1995, A conceptual model of the Death Valley ground-water flow system, Nevada and California: Prepared for National Park Service by Pal Consultants Inc., San Jose, Calif., 98 p.

Harrill, J.R., Gates, J.S., and Thomas, J.M., 1988, Major ground-water flow systems in the Great Basin region of Nevada, Utah, and adjacent States: U.S. Geological Survey Hydrologic Investigations Atlas HA–694–C, 2 sheets.

Rush, F.E., 1968, Water resources appraisal of Clayton Valley-Stonewall Flat area, Nevada and California: Nevada Department of Conservation and Natural Resources, Water Resources, Reconnaissance Report 47, 61 p.

Rush, F.E., and Everett, D.E., 1966, Water resources appraisal of Little Fish Lake, Hot Creek, and Little Smoky Valleys, Nevada: Nevada Department of Conservation and Natural Resources, Reconnaissance Report 38, 39 p.

Rush, F.E., and Katzer, T.L., 1973, Water resources appraisal of Fish Lake Valley, Nevada and California: Nevada Division of Water Resources, Reconnaissance Report 58, 70 p.

Rush, F.E., and Schroer, C.V., 1970, Water resources of Big Smoky Valley, Lander, Nye, and Esmeralda Counties, Nevada, with special reference to the water-use period, 1953–72: Nevada Division of Water Resources, Bulletin 41, 84 p.

Seaber, P.R., Kapinos, F.P, Knapp, G.L., 1987, Hydrologic unit maps: U.S. Geological Survey Water-Supply Paper 2294, 63 p., 1 plate.

Van Denburgh, A. S., and Rush, F. E., 1974, Water resources appraisal of Railroad and Penoyer Valleys, east-central Nevada: Nevada Department Conservation and Natural Resources, Water Resources-Reconnaissance Series Report 60, 61 p.

Manuscript approved for publication September 27, 2004.

Prepared by the USGS Water Resources Discipline, Colorado District.

Edited by Pamela B. Daddow and Mary A. Kidd

Graphics by Nancy A. Damar, Laurel L. Rogers, Larry G. Schneider, and Rudolph R. Contreras

USGS publishing staff—Joy K. Monson, Robert J. Olmstead, Margo J. VanAlstine, Sharon M. Powers, Alene J. Brogan, Loretta J. Ulibarri, Carol L. Anderson, and Betty B. Palcsak

Prepared in cooperation with the
U.S. DEPARTMENT OF ENERGY
OFFICE OF ENVIRONMENTAL MANAGEMENT,
NATIONAL NUCLEAR SECURITY ADMINISTRATION, NEVADA SITE OFFICE,
under Interagency Agreement DE-AI52-01NV13944, and
OFFICE OF REPOSITORY DEVELOPMENT,
under Interagency Agreement DE-AI08-02RW12167

USGS U.S. DEPARTMENT OF THE INTERIOR
U.S. GEOLOGICAL SURVEY

SCIENTIFIC INVESTIGATIONS REPORT 2004-5205
Regional potential for interbasin flow of ground water in the Death Valley regional ground-water flow system area, Nevada and California—Plate 1
Bedinger, M.S., ed., Death Valley regional ground-water flow system, Nevada and California — Hydrogeologic framework and transient ground-water flow model

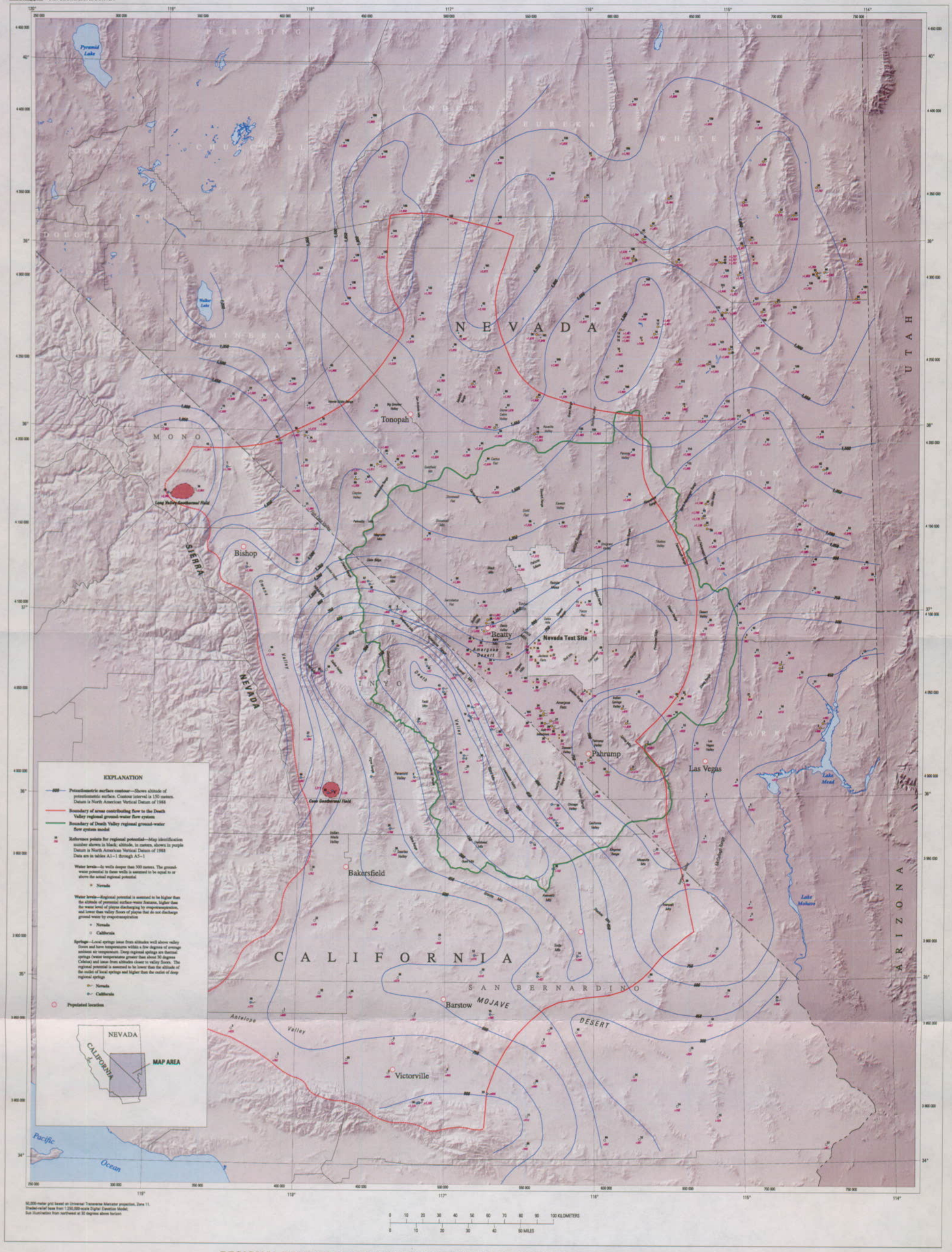

REGIONAL POTENTIAL FOR INTERBASIN FLOW OF GROUND WATER IN THE DEATH VALLEY REGIONAL GROUND-WATER FLOW SYSTEM AREA, NEVADA AND CALIFORNIA

By M.S. Bedinger and J.R. Harrill

2004

Prepared in cooperation with the
U.S. DEPARTMENT OF ENERGY
OFFICE OF ENVIRONMENTAL MANAGEMENT,
NATIONAL NUCLEAR SECURITY ADMINISTRATION, NEVADA SITE OFFICE,
under Interagency Agreement DE-AI52-01NV13944, and
OFFICE OF REPOSITORY DEVELOPMENT,
under Interagency Agreement DE-AI08-02RW12167

USGS U.S. DEPARTMENT OF THE INTERIOR
U.S. GEOLOGICAL SURVEY

SCIENTIFIC INVESTIGATIONS REPORT 2004–5205
Simulated ground-water response to pumping in the
Death Valley ground-water flow system—**Plate 2**
Belcher, W.R., ed., Death Valley regional ground-water flow system,
Nevada and California — Hydrogeologic framework and transient ground-water flow model

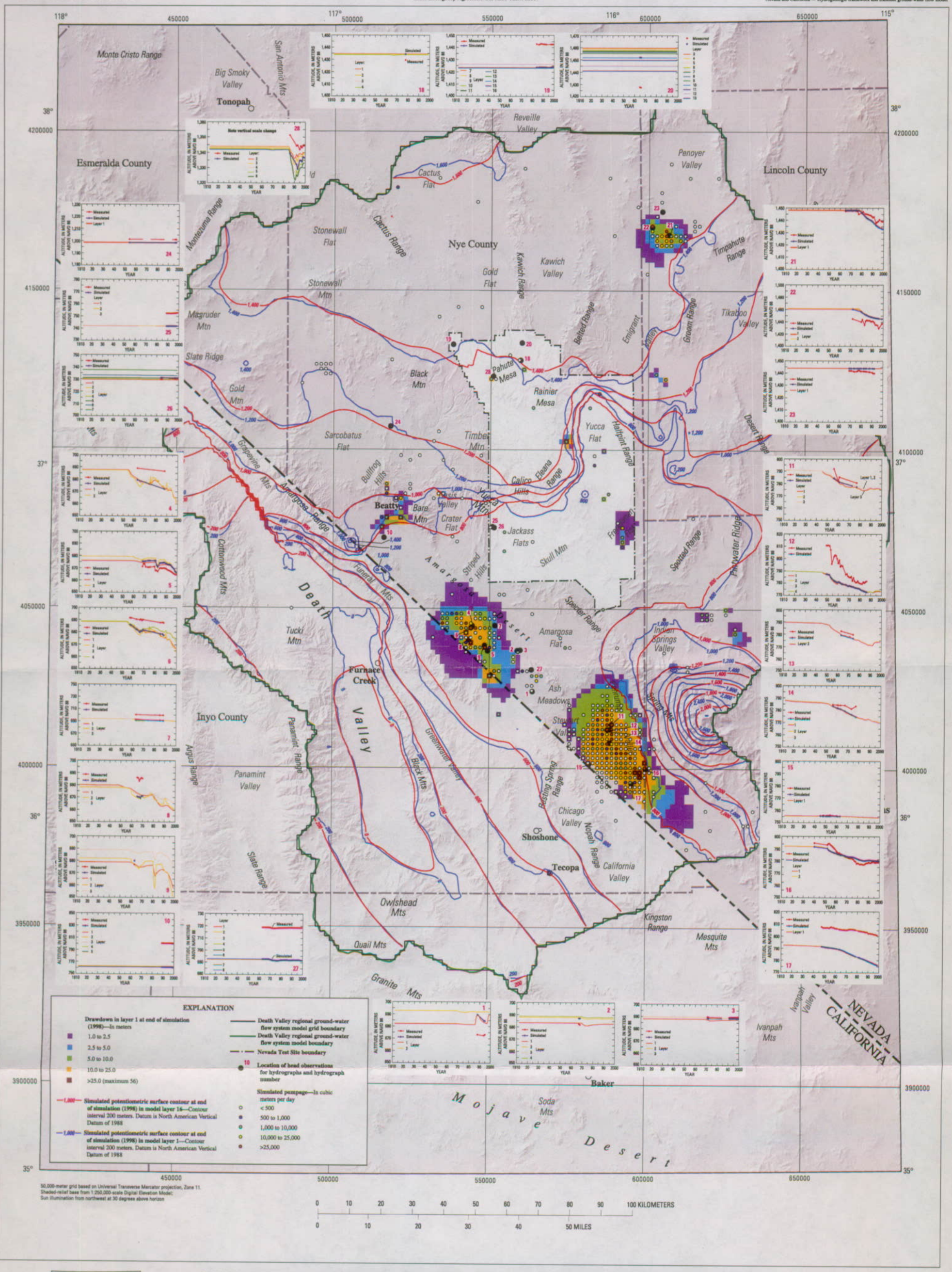

SIMULATED GROUND-WATER RESPONSE TO PUMPING IN THE DEATH VALLEY REGIONAL GROUND-WATER FLOW SYSTEM AREA, NEVADA AND CALIFORNIA

By Claudia C. Faunt, Joan B. Blainey, Mary C. Hill, Frank A. D'Agnese, and Grady M. O'Brien

2004